

Evaluation of the Cone Penetrometer
for Liquefaction Hazard Assessment

Geoffrey R. Martin
and
Bruce J. Douglas

Fugro, Inc.
3777 Long Beach Boulevard
Long Beach, California 90807

USGS CONTRACT NO. 14-08-0001-17790
Supported by the EARTHQUAKE HAZARDS REDUCTION PROGRAM

OPEN-FILE NO.81-284

U.S. Geological Survey
OPEN FILE REPORT

This report was prepared under contract to the U.S. Geological Survey and has not been reviewed for conformity with USGS editorial standards and stratigraphic nomenclature. Opinions and conclusions expressed herein do not necessarily represent those of the USGS. Any use of trade names is for descriptive purposes only and does not imply endorsement by the USGS.



October 3, 1980

Mr. Gordon Greene
U.S. Department of the Interior
Geological Survey
345 Middlefield Road
Menlo Park, California 94025

Dear Mr. Greene:

This letter serves to transmit our final Technical Report for U.S.G.S. Contract No. 14-08-0001-17790. We are submitting fifteen copies of our report as per contract requirements. The report is titled, "Evaluation of the Cone Penetrometer for Liquefaction Hazard Evaluation". In addition, we are submitting five copies of our final Management Report to the Contracting Officer.

We have enjoyed working on this most interesting and valuable project and appreciate the flexibility shown by the U.S.G.S regarding project schedules. We hope this report serves to increase the present capabilities for definition of earthquake induced hazards.

Should you have any questions regarding our report, please contact me.

Sincerely,

ORIGINAL SIGNED BY

Bruce J. Douglas
Project Engineer.

BD:mv

Enclosures

EVALUATION OF THE CONE PENETROMETER
FOR LIQUEFACTION HAZARD ASSESSMENT

Prepared for:

U.S. Department of the Interior
Geological Survey
Menlo Park, California 94025

Prepared by:

Fugro, Inc.
Consulting Engineers and Geologists
3777 Long Beach Boulevard
Long Beach, California 90807

Principal Investigators:

Geoffrey R. Martin
Associate and Director of Engineering

Bruce J. Douglas
Project Engineer, and Manager In-Situ Testing

October, 1980

CONTRACT NO. 14-08-0001-17790

TABLE OF CONTENTS

	<u>Page</u>
1. <u>INTRODUCTION</u>	1-1
1.1 CURRENT METHODS OF LIQUEFACTION POTENTIAL ASSESSMENT	1-1
1.1 MICROZONATION OF EARTHQUAKE HAZARDS	1-3
1.3 FACTORS AFFECTING LIQUEFACTION POTENTIAL, SPT, CPT	1-5
1.4 SCOPE OF RESEARCH	1-8
2. <u>FIELD AND LABORATORY INVESTIGATIONS</u>	2-1
2.1 INTRODUCTION	2-1
2.2 PROCEDURES	2-1
2.3 SITE DESCRIPTIONS	2-4
2.3.1 <u>San Diego, California</u>	2-4
2.3.2 <u>Salinas, California</u>	2-6
2.3.3 <u>Moss Landing, California</u>	2-8
2.3.4 <u>Sunset Beach, California</u>	2-9
2.3.5 <u>San Jose, California</u>	2-10
2.3.6 <u>Edmond, Oklahoma</u>	2-11
2.4 CONCLUSIONS	2-13
3. <u>DATA ANALYSES</u>	3-1
3.1 INTRODUCTION	3-1
3.2 PREVIOUS INVESTIGATIONS	3-2
3.2.1 <u>SPT Research</u>	3-2
3.2.2 <u>CPT Research</u>	3-5
3.2.2.1 CPT Versus Soil Type	3-5
3.2.2.2 CPT Versus Overburden Pressure	3-9

TABLE OF CONTENTS (Cont.)

	<u>Page</u>
3.2.2.3 CPT Versus SPT	3-10
3.3 CURRENT INVESTIGATIONS	3-14
3.3.1 <u>CPT Classification of Soil Type</u> . . .	3-14
3.3.2 <u>Correlation of CPT Measurements for Overburden Pressure</u>	3-21
3.3.3 <u>Correlation of q_c to N</u>	3-25
3.3.3.1 q_c/N Range Comparisons . . .	3-26
3.3.3.2 q_c/N Versus Depth	3-28
3.3.3.3 q_c/N Versus N	3-31
3.3.3.4 q_c/N Versus q_c	3-32
3.3.3.5 q_c/N Versus Friction Ratio. .	3-34
3.3.3.6 q_c/N Versus Median Grain Size	3-35
3.3.3.7 q_c/N Versus N	3-36
3.3.3.8 Comparison of N and Side Friction	3-42
3.3.3.9 Summary of q_c/N Relations . .	3-42
4. <u>SUMMARY AND CONCLUSIONS</u>	4-1
4.1 SUMMARY	4-1
4.2 CONCLUSIONS	4-3
4.3 RESEARCH SUGGESTIONS	4-7
5. <u>REFERENCES</u>	5-1

APPENDICES

Appendix No.

A	(Under Separate Cover)
B	(Under Separate Cover)

LIST OF FIGURES

Chapter 2

Figure No.

- 2.1 Electric Friction Cone Penetrometer
- 2.2 Mechanical Trip Hammer (Pilcon Engineering)
- 2.3 San Diego Site Location
- 2.4 San Diego Site Layout
- 2.5 San Diego Site, CPT Profile
- 2.6 San Diego Site, Composite Site Profile
- 2.7 Moss Landing/Salinas, Site Locations
- 2.8 Salinas Site Layout
- 2.9 Salinas Site, CPT Profile
- 2.10 Salinas Site, Composite Site Profile
- 2.11 Moss Landing Site Layout
- 2.12 Moss Landing Site, CPT Profile
- 2.13 Moss Landing Site, Composite Site Profile
- 2.14 Sunset Beach Site Location
- 2.15 Sunset Beach Site Layout
- 2.16 Sunset Beach Site, CPT Profile
- 2.17 San Jose Site Locations: Coyote Creek North and Coyote Creek South
- 2.18 Coyote Creek North and South Site Layout
- 2.19 San Jose Site: Coyote North, CPT Profile
- 2.20 San Jose Site: Coyote North, Composite Site Profile
- 2.21 San Jose Site: Coyote South, CPT Profile
- 2.22 San Jose Site: Coyote South, Composite Site Profile
- 2.23 Edmond, Oklahoma Site Location

LIST OF FIGURES (Cont.)

Chapter 2 (Cont.)

Figure No.

- 2.24 Oklahoma Site, CPT layout
- 2.25 San Diego Site, Composite \bar{N} profile and \bar{N}_S/\bar{N}_T
- 2.26 Salinas Site, Composite \bar{N} profile and \bar{N}_S/\bar{N}_T
- 2.27 Moss Landing Site, Composite \bar{N} Profile and \bar{N}_S/\bar{N}_T
- 2.28 San Jose Sites: Coyote North and South, Composite \bar{N} Profiles and \bar{N}_S/\bar{N}_T
- 2.29 Effect of Borehole on Subsequent Adjacent CPT Soundings - Salinas Site

Chapter 3

- 3.1 C_N Factors Versus Effective Overburden Pressure
- 3.2 Effects of Rod Length on SPT Blowcounts
- 3.3 CPT Soil Classification, Begemann Method
- 3.4 CPT Soil Classification, After Schmertmann (1978)
- 3.5 Effective Overburden Pressure Versus $C_p=q_c$ @ $1Tsf/q_c$
- 3.6 Comparison of C_p , C_N and Rod Length
- 3.7 Previous Correlations: $q_c = F(SPT)$, For Pure Sands (After de Mello, 1971)
- 3.8 Previous Correlations: $q_c = F(SPT)$, For Sands (After Sangerlat, 1972)
- 3.9 Composite: All Sites, q_c vs Friction Ratio, Soil Classification Chart
- 3.10 Continuous Trace Method, Edmond Site, CPT Probe 119
- 3.11 Soil Type Classifications Using the CPT Continuous Trace Method
- 3.12 Soil Type Classifications Using the CPT Continuous Trace Method

LIST OF FIGURES (Cont.)

Chapter 3 (Cont.)

Figure No.

- 3.13 Limited Trace Method; Coyote North Site
- 3.14 Selected Points - Edmond Site, Liquidity Index vs q_c and Friction Ratio
- 3.15 Trends in CPT Soil Classification
- 3.16 q_c vs σ_v' for CPT Measurements in Sands (After Treadwell, 1975)
- 3.17 Composite: All Sites, σ_v' vs C_{p1} , Standard Hammer
- 3.18 Composite: All Sites, σ_v' vs C_{p1} , Trip Hammer
- 3.19 Composite: All Sites, σ_v' vs C_{p1} , by Layer Average, Standard Hammer
- 3.20 Composite: All Sites, σ_v' vs C_{p1} by Layer Average, Trip Hammer
- 3.21 Select Points: All Sites, σ_v' vs C_{p1} , Standard Hammer
- 3.22 Select Points: All Sites, σ_v' vs C_{p1} , Trip Hammer
- 3.23 San Diego Site: q_c/N Range Comparison, Standard Hammer
- 3.24 Salinas Site: q_c/N Range Comparisons, Standard Hammer
- 3.25 Moss Landing Site: q_c/N Range Comparison, Standard Hammer
- 3.26 San Jose Site: Coyote North and South, q_c/N Range Comparisons, Standard Hammer
- 3.27 San Diego Site: NAS North Island, q_c/N Range Comparisons, Trip Hammer
- 3.28 Salinas Site: q_c/N Range Comparisons, Trip Hammer
- 3.29 Moss Landing Site: q_c/N Range Comparisons, Trip Hammer
- 3.30 San Jose Site: Coyote North and South, q_c/N Range Comparisons, Trip Hammer
- 3.31 Composite Blowcount vs Depth, San Diego: North Island
- 3.32 Composite Blowcount vs Depth, Salinas Site

LIST OF FIGURES (Cont.)

Chapter 3 (Cont.)

Figure No.

- 3.33 Composite Blowcount vs Depth, Moss Landing Site
- 3.34 Composite Blowcount vs Depth, San Jose Site:
Coyote North
- 3.35 Composite Blowcount vs Depth, San Jose Site:
Coyote South
- 3.36 Composite: All Sites, \bar{q}_C/\bar{N} vs Depth by Layer
Averages
- 3.37 q_C/N vs Effective Overburden Pressure
(After Schmertmann, 1978)
- 3.38 Composite: All Sites, q_C/N vs Depth, Standard
Hammer
- 3.39 Composite: All Sites, q_C/N vs Depth, Trip Hammer
- 3.40 Composite: All Sites, \bar{q}_C/\bar{N} vs N , by Layer Averages
- 3.41 Composite: All Sites, q_C/N vs N , Standard Hammer
- 3.42 Composite: All Sites, q_C/N vs N , Trip Hammer
- 3.43 Composite: All Sites, q_C/N vs N , for Selected
Points, Standard Hammer
- 3.44 Composite: All Sites, q_C/N vs N for
Selected Points, Trip Hammer
- 3.45 Composite: All Sites, \bar{q}_C/\bar{N} vs \bar{q}_C , by Layer Averaging
- 3.46 Composite: All Sites, q_C/N vs q_C , Standard Hammer
- 3.47 Composite: All Sites, q_C/N vs q_C , Trip Hammer
- 3.48 Composite: All Sites, q_C/N vs q_C , for
Select Points, Standard Hammer
- 3.49 Composite: All Sites, q_C/N vs q_C , for
Select Points, Trip Hammer
- 3.50 Comparison of End Bearing of Mechanical vs Electric
Cone (After Schmertmann, 1978)
- 3.51 Composite: All Sites, \bar{q}_C/\bar{N} vs Friction Ratio, by
Layer Averages

LIST OF FIGURES (Cont.)

Chapter 3 (Cont.)

Figure No.

- 3.52 Composite: All Sites, q_c/N vs Friction Ratio, Standard Hammer
- 3.53 Composite: All Sites, q_c/N vs Friction Ratio, Trip Hammer
- 3.54 Composite: All Sites, q_c/N vs Friction Ratio, for Select Points, Standard Hammer
- 3.55 Composite: All Sites, q_c/N vs Friction Ratio, for Select Points, Trip Hammer
- 3.56 Composite: All Sites, q_c/N vs D_{50} , Standard Hammer
- 3.57 Composite: All Sites, q_c/N vs D_{50} , Trip Hammer
- 3.58 Composite: All Sites, \bar{q}_c vs \bar{N} by Layer Averages
- 3.59 Composite: All Sites, q_c vs N , Standard Hammer
- 3.60 Composite: All Sites, q_c vs N , Trip Hammer
- 3.61 Composite: All Sites, q_c vs N , for Select Points, Standard Hammer
- 3.62 Composite: All Sites, q_c vs N , for Selected Points, Trip Hammer
- 3.63 Comparison of q_c vs N , Standard Hammer and Schmertmann Relation
- 3.64 Comparison of q_c vs N , Trip Hammer and Schmertmann Relation
- 3.65 Comparison of q_c vs N , Trip Hammer and COE Trip Hammer
- 3.66 Penetration Resistance in Layered Media (after Treadwell (1975))
- 3.67 Composite: Average Corrected Blowcount vs Plasticity Indices, Edmond Site
- 3.68 Edmond Site, Range of Average CPT End Bearing for Friction Ratio Bands

LIST OF FIGURES (Cont.)

Chapter 3 (Cont.)

Figure No.

- 3.69 Comparison of Edmond Site, SPT with $PI < 3$ and CPT with Friction Ratio = 0.8 to 2.25%
- 3.70 Edmond Site, SPT N to LI, All Borings with Adjacent CPT Soundings
- 3.71 Composite: All Soundings: Edmond Site, Corrected q_c vs Depth for Sand Zone
- 3.72 Composite: All Soundings and Borings, Edmond Site, q_c/N vs Depth for CPT Sand Zones and Blowcounts with $PI < 3$
- 3.73 Composite: All Sites, CPT Side Friction vs N, Standard Hammer
- 3.74 Composite: All Sites, CPT Side Friction vs N, Trip Hammer
- 3.75 Composite: All Sites, Frequency Histograms by Layer Average
- 3.76 Composite: All Sites, Frequency Histogram, q_c/N vs Friction Ratio, Standard Hammer
- 3.77 Composite: All Sites, Frequency Histogram, q_c/N vs Friction Ratio, Trip Hammer
- 3.78 Composite: All Sites, Frequency Histogram, q_c/N

Chapter 4

- 4.1 Composite: All Sites, N vs q_c vs Friction Ratio, Standard Hammer
- 4.2 Composite: All Sites, N vs q_c vs Friction Ratio, Trip Hammer
- 4.3 Predicted vs Measured N Value Profile: Edmond Site: Boring 120

LIST OF APPENDICES

APPENDIX A

Appendix No.

A.1 - A.10	Cone Penetrometer Tests, San Diego
A.11 - A.18	Log of Borings, San Diego
A.19 - A.33	Cone Penetrometer Tests, Salinas Site
A.34 - A.41	Log of Borings, Salinas Site
A.42 - A.50	Cone Penetrometer Tests, Moss Landing Site
A.51 - A.58	Log of Borings, Moss Landing Site
A.59 - A.61	Cone Penetrometer Tests, Sunset Beach
A.62 - A.73	Cone Penetrometer Tests, San Jose: Coyote North
A.74 - A.83	Cone Penetrometer Tests, San Jose: Coyote South
A.84 - A.89	Log of Borings, San Jose: Coyote North
A.90 - A.93	Log of Borings, San Jose: Coyote South

APPENDIX B

B.1	San Diego Site: \bar{q}_C/\bar{N} vs Depth by Layer Averages
B.2	Salinas Site, \bar{q}_C/\bar{N} vs Depth by Layer Averages
B.3	Moss Landing Site, \bar{q}_C/\bar{N} vs Depth by Layer Averages
B.4	San Jose Site: Coyote North and South, \bar{q}_C/\bar{N} vs Depth by Layer Averages
B.5	San Diego Site q_C/N vs Depth, Standard Hammer
B.6	Salinas Site, q_C/N vs Depth, Standard Hammer

LIST OF APPENDICES

APPENDIX B (Cont.)

Appendix No.

- | | |
|------|--|
| B.7 | Moss Landing Site, q_C/N vs Depth, Standard Hammer |
| B.8 | San Jose Site: Coyote North and South, q_C/N vs Depth, Standard Hammer |
| B.9 | San Diego Site q_C/N vs Depth, Standard Hammer |
| B.10 | Salinas Site, q_C/N vs Depth, Trip Hammer |
| B.11 | Moss Landing Site, q_C/N vs Depth, Trip Hammer |
| B.12 | San Jose Site: Coyote North and South, q_C/N vs Depth, Trip Hammer |
| B.13 | San Diego Site, \bar{q}_C/\bar{N} vs \bar{N} by Layer Averages |
| B.14 | Salinas Site, \bar{q}_C/\bar{N} vs \bar{N} by Layer Averages |
| B.15 | Moss Landing Site, \bar{q}_C/\bar{N} vs \bar{N} by Layer Averages |
| B.16 | San Jose Sites: Coyote North and South, \bar{q}_C/\bar{N} vs \bar{N} by Layer Averages |
| B.17 | San Diego Site, q_C/N vs N , Standard Hammer |
| B.18 | Salinas Site, q_C/N vs N , Standard Hammer |
| B.19 | Moss Landing Site, q_C/N vs N , Standard Hammer |
| B.20 | San Jose Site: Coyote North and South, q_C/N vs N , Standard Hammer |
| B.21 | San Diego Site, q_C/N vs N , Trip Hammer |
| B.22 | Salinas Site, q_C/N vs N , Trip Hammer |
| B.23 | Moss Landing, q_C/N vs N , Trip Hammer |
| B.24 | San Jose Site: Coyote North and South, q_C/N vs N , Trip Hammer |
| B.25 | San Diego: \bar{q}_C/\bar{N} vs \bar{q}_C by Layer Average |
| B.26 | Salinas Site, \bar{q}_C/\bar{N} vs \bar{q}_C by Layer Average |

LIST OF APPENDICES

APPENDIX B (Cont.)

Appendix No.

- B.27 Moss Landing, \bar{q}_C/\bar{N} vs \bar{q}_C , by Layer Average
- B.28 San Jose Site: Coyote North and South,
 \bar{q}_C/\bar{N} vs \bar{q}_C , by Layer Average
- B.29 San Diego Site, q_C/N vs q_C , Standard Hammer
- B.30 Salinas Site, q_C/N vs q_C , Standard Hammer
- B.31 Moss Landing Site, q_C/N vs q_C , Standard Hammer
- B.32 San Jose Site: Coyote North and South,
 q_C/N vs q_C , Standard Hammer
- B.33 San Diego Site, q_C/N vs q_C , Trip Hammer
- B.34 Salinas Site, q_C/N vs q_C , Trip Hammer
- B.35 Moss Landing Site, q_C/N vs q_C , Trip Hammer
- B.36 San Jose Site: Coyote North and South,
 \bar{q}_C/\bar{N} vs \bar{q}_C , Trip Hammer
- B.37 San Diego Site, \bar{q}_C/\bar{N} vs Friction Ratio, by Layer Averages
- B.38 Salinas Site, \bar{q}_C/\bar{N} vs Friction Ratio, by Layer Averages
- B.39 Moss Landing, \bar{q}_C/\bar{N} vs Friction Ratio, by Layer Averages
- B.40 San Jose: Coyote North and South, \bar{q}_C/\bar{N} vs Friction Ratio by Layer Averages
- B.41 San Diego Site q_C/N vs Friction Ratio, Standard Hammer
- B.42 Salinas Site, q_C/N vs Friction Ratio, Standard Hammer
- B.43 Moss Landing Site, q_C/N vs Friction Ratio, Standard Hammer

LIST OF APPENDICES

APPENDIX B (Cont.)

Appendix No.

- | | |
|------|---|
| B.44 | San Jose Site: Coyote North and South, q_C/N vs Friction Ratio, Standard Hammer |
| B.45 | San Diego Site, q_C/N vs Friction ratio, Trip Hammer |
| B.46 | Salinas Site, $q_C N$ vs Friction Ratio, Trip Hammer |
| B.47 | Moss Landing Site, q_C/N vs Friction Ratio, Trip Hammer |
| B.48 | San Jose Site: Coyote North and South, q_C/N vs Friction Ratio, Trip Hammer |
| B.49 | San Diego Site: NAS North Island, \bar{q}_C vs \bar{N} , by Layer Averages |
| B.50 | Salinas Site, \bar{q}_C vs \bar{N} by Layer Averages |
| B.51 | Moss Landing Site, \bar{q}_C vs \bar{N} by Layer Averages |
| B.52 | San Jose Site: Coyote North and South, \bar{q}_C vs \bar{N} by Layer Averages |
| B.53 | San Diego, q_C vs N , Standard Hammer |
| B.54 | Salinas Site, q_C vs N , Standard Hammer |
| B.55 | Moss Landing Site, q_C vs N , Standard Hammer |
| B.56 | San Jose: Coyote North and South, q_C vs N , Standard Hammer |
| B.57 | San Diego Site, q_C vs N , Trip Hammer |
| B.58 | Salinas Site, q_C vs N , Trip Hammer |
| B.59 | Moss Landing Site, q_C vs N , Trip Hammer |
| B.60 | San Jose Site: Coyote North and South, q_C vs N , Trip Hammer |

1. INTRODUCTION

This report describes the activities and results of the investigations of the correspondence between Cone Penetrometer Tests (CPT) and Standard Penetration Tests (SPT) performed under USGS Contract No. 14-08-0001-17780. The program involved performance of CPTs and SPTs at several sites in California and at one site in Oklahoma. The comparison of the correspondence between those test results has as a primary goal the development of a data base facilitating the use of the CPT for use in liquefaction potential assessments. The scope of investigations was defined in proposal P78-310 in response to USGS RFP 460W.

1.1 CURRENT METHODS OF LIQUEFACTION POTENTIAL ASSESSMENT

Current methods of liquefaction potential assessment are in general limited to either extensive field sampling, laboratory testing, and dynamic analyses, or rely upon the simplified, empirical SPT-based method developed by Seed (1979). The former method has the disadvantages of high cost and time commitment, the need for field borings and sophisticated laboratory equipment, and advanced computational capabilities. In addition, taking high-quality samples of liquefiable soils (loose, saturated, sands and silts) is a difficult procedure, and almost invariably results in changed sample structure and density.

In addition, the idealization of the soil profile based upon lab test results usually requires selection of some average or bounding properties for use in subsequent analyses. It

is never known which properties are most important for transmission of shear waves and, therefore, parametric studies usually need be performed.

The second routine method, the Standard Penetration Test (SPT), avoids the extreme costs of the more analytical approach, yet still suffers from the need for expensive field operations and some laboratory work. Although the test is dynamic, and should therefore provide some direct indication of dynamic soil properties, the results can be taken as only general indications of site conditions.

It is well known in the geotechnical industry how error-plagued is the SPT, with some 30 different error sources having been defined (Fletcher, F. A., 1965; Kovacs, et al, 1975). A survey of equipment and procedures in use throughout the U.S. reveals that not only equipment but also procedure suffers from lack of standardization. Efforts by many, notably Schmertmann (1976) and Kovacs (1978), to standardize the test have met with only limited success. One of the major impediments to standardization results from the importance of maintaining the SPT data base that has been developed in the last forty years. This data base is found in publications as well as in design guidelines for use at national or local levels. Further, most practitioners have developed a "feeling" for SPT results, and are able to make valid engineering judgments from such results. Many of these practitioners feel that by standardization (such as using controlled-energy, or velocity, mechanical hammers) the data

base developed over the years will be invalidated. This is a realistic concern, and several researchers have responded by instituting a nationwide program of hammer-energy measurements. Once such measurements have been made, it should be possible to correlate the average energies represented by any particular data base with the energy of the standardized hammer (Kovacs, 1978).

1.2 MICROZONATION OF EARTHQUAKE HAZARDS

In recent years there has been an effort, in response to recognized need, to develop procedures for regional-level microzonation of earthquake hazards, in particular with respect to liquefaction potential. With regard to liquefaction hazard assessment, the usual method involves qualitative definition of two necessary conditions: a sufficient driving source and susceptible soils (Youd, et al, 1978; Youd and Perkins, 1977; Kennedy, et al, 1977). Ignoring the delineation of zones having potential to receive sufficient strong motion shaking, the delineation of susceptible soil zones has been based upon existence of high ground water levels (liquefaction is primarily of concern in the upper 40 feet of a soil profile) in cohesionless, young (Holocene age) soils. The delineation of water levels is usually through records of ground water investigations, and provides adequate information for regional assessments. Site specific investigations still need more accurate definition of water level, but this factor is relatively easily determined.

The delineation of susceptible soils (young, cohesionless) has been through recourse to published data. These data are usually either geologic or soils maps, or boring information from previous investigations. The shortcoming of using geologic maps is their overly generalized nature. Certainly such generalization is necessary for microzonation efforts covering hundreds of square miles of land surface; however, the method provides only an indication of actual extent of susceptible materials. On a regional basis, it is possible to define zones of clearly nonsusceptible materials, such as clays or gravels, as differentiated from susceptible materials such as beach or river sand. The primary difficulty arises in those intermediate and mixed soils: silts, silty sands, clayey sands, sands, sandy silts, and even silty and sandy clays. The liquefaction potential of a soil depends, for a given driving energy, upon the grain size and distribution, and the amount and activity of any clay size components. In addition, the in-situ stress conditions and soil density have a significant influence on liquefaction potential. Although some qualitative estimates of stress state and density can be made on the basis of geologic history, it becomes difficult to attach any quantitative information to such estimates.

The difficulty in quantifying microzonation delineations reinstates the need for some field measurement. The cost and time associated with a boring-type measurement likely becomes prohibitive. This is where the Cone Penetrometer Test (CPT) is seen to be of value. The test is very rapid, with up to

800 feet of measurements being made in a single day, as compared to a maximum of about 100 feet of comparable SPT measurements in a like time. Further, the CPT is standardized, is not operator or technique dependent, and provides a repeatable set of continuous measurements of soil resistance.

The primary concern in using CPT for microzonation efforts is establishing some correlation between CPT results and liquefaction potential. Such correlation exists for SPT results (Seed, 1979). The SPT-liquefaction potential correlation is based upon SPT measurements made at sites which subsequently liquefied during earthquake shaking. The correlation was extended through use of "shaking-table" tests. Knowledge of the magnitude and acceleration characterizing the actual or artificial earthquake allowed development of a set of values, for any specific earthquake, bounding the soil cyclic strength dividing liquefiable from non-liquefiable soils. The soil cyclic strength was then represented by a normalized SPT blowcount.

Because no extensive data base of this type exists for CPT measurements, a possible approach is to first compare the CPT to liquefaction potential through the intermediate use of the SPT data base. Thus the current program is designed to further study correspondence between the CPT and SPT as a step toward the eventual goal of a CPT-liquefaction potential correlation.

1.3 FACTORS AFFECTING LIQUEFACTION POTENTIAL, SPT, CPT

Several questions arise when considering such a correlation program. First, for any empirical "index" to be valid for

prediction of some other property, such as liquefaction potential, the index and the property should be similarly dependent upon the same variables. Typical variables include soil type, stress state and stress history, soil density, and soil structure. Given the range in parameter variation in-situ, it is not sensible to try to account for the effect of variations producing only a small change in the correlation. Rather, major changes should be investigated. The variables accepted as having major affect upon liquefaction potential are: soil type, degree of saturation, effective overburden pressure, density or relative density, lateral stress, and soil structure or fabric. It is assumed that location of permanent ground water can be established, thus eliminating degree of saturation from concern. This leaves, as of primary importance, the influences of soil type, structure, and density and effective stress history.

These variables are not easily rated in terms of their effect upon either liquefaction potential or SPT measurements. First, it is in general true that increasing clay content results in decreased liquefaction potential and decreased blowcounts. Increased sand content results in increased blowcount and increased liquefaction potential as compared to clayey soils. However, for a given soil, an increase in blowcount results in decrease of liquefaction potential. Further, the effect of intermediate fines content upon liquefaction potential is not known. It is generally assumed that some value of Plasticity Index (PI) can divide susceptible from nonsusceptible soils (Donovan and Singh, 1976). This value has been assumed

at from 5 to 12 percent. It is unlikely, however, that the SPT varies inversely proportional to liquefaction potential as fines content increases up to this point of low PI. Further, there is no certainty that the criteria is applicable on other than a case-by-case level.

The same type of arguments can be advanced relating liquefaction potential to median grain size (D_{50}). Although the trend in the relation between D_{50} and liquefaction potential holds for comparison of extremes, it is not valid for comparisons within the range most commonly of concern: sands and silts.

A second primary factor, effective overburden and lateral pressures, is likewise difficult to assess. The cyclic strength of a soil (or liquefaction potential) certainly varies with the effective stress in the soil in that increased driving energy is required to generate sufficient shear strains to result in increased porewater pressure at increased confining pressures. Thus for a sand at a constant relative density, the blowcount measured would non-linearly vary proportional to the effective pressure at the location of the blowcount. In order to eliminate the influence of this variable, both cyclic strength and blowcounts are normalized by either the effective vertical stress or some measure of that stress. For blowcounts, the measure is the factor C_N , which is intended to normalize a blowcount to that which would be obtained at an effective overburden pressure of one ton per square foot. This factor is appropriate for normally consolidated soils only.

being of different ages. In particular, the correlations are examined as dependent upon soil type, resistance, and overburden pressure, as these are the primary, presently quantifiable, factors affecting liquefaction potential.

Considerable attention is placed upon the method of data comparison. The primary reason for this attention is the essential difference between the data of the CPT and SPT. The CPT provides continuous, repeatable measurements, while the SPT provides point data dependent upon equipment and method. The variability of SPT measurements is clearly evidenced in examination of the data presented in this report. Such variability further emphasizes the need for SPT hammer energy measurements, as discussed previously. This need, as well as other research needs related to field methods of liquefaction potential assessment, are further discussed in Chapter 4, Summary and Conclusions.

2. FIELD AND LABORATORY INVESTIGATIONS

2.1 INTRODUCTION

Field investigations supported under this research program included Standard Penetration Tests and electric Cone Penetrometer Tests performed at several sites in California. In addition, data from other projects are also included, in particular, from a project in Oklahoma. Samples taken from California sites during the SPT program were returned to the Long Beach soils laboratory for classification testing. All classification data and SPT measurements from the Oklahoma site were developed and provided by the Tulsa District U.S. Army Corps of Engineers, who also allowed use of the CPT data from the site. A summary of field investigations is given in Table 2.1.

2.2 PROCEDURES

The testing procedures used in this program were in general accordance with those procedures recommended by the ASTM. Applicable standards used in the program are: D1586 for SPT procedures, D3441-75T for CPT procedures, and D422 for laboratory grain size analyses. Corps of Engineers field and laboratory tests were performed in accordance with U.S. Army Corps of Engineers Testing Standards.

The CPT soundings were performed using a truck-mounted electric cone penetrometer. The electric CPT system consists of a 40,000 pound truck equipped with a hydraulic loading system capable of applying 40,000 pounds of force onto the end of 1.4 inch diameter, hollow "sounding" rods. The electric

friction cone tip is mounted on the end of the rod string with an electrical cable threaded from the cone, through the trailing rods, and into the electronics located in the truck.

The electric friction cone tip essentially consists of a strain-gage-instrumented body enclosed within a cylindrical friction sleeve of 150 square centimeters surface area, and capped with a 60-degree apex angle conical tip of 10 square centimeters projected surface area. An inclinometer is located within the cylindrical body. A description of this friction cone and the general CPT methodology is given by de Ruiter (1971); a schematic diagram of the electric friction cone is shown in Figure 2.1.

The sounding rods with attached friction cone are pushed into the soil at a constant rate of two cm/sec in one-meter runs. At the end of each one-meter run, an additional one-meter length of rod is added, and the sounding continued. This process is repeated until reaching refusal or a specified depth. Additional information about the general procedures used for CPT site investigations are described elsewhere (Sangerlat, 1972).

A continuous analog record of the forces on the end (cone end bearing, q_c) and friction sleeve (side friction) of the cone is taken on a strip-chart recorder located in the penetrometer truck. The chart recorder is driven by an optical encoder controlled by the advance of the sounding rods; the length of the cone record is directly and exactly proportional to the length of extended sounding rods. Inclinometer readings (taken

during rod breaks) showed inclinations of no more than 3 degrees during any of the sounding.

The Standard Penetration Tests at California sites were performed using Failing 750 drill rigs and drill pipe having an I.D. of 1.5 inches and an O.D. of 2.375 inches with a weight of 55 pounds per 10.5 foot long rod section. Drill bits were 5-7/8" fishtails baffled to prevent any jetting-induced soil disturbance. Particular care was taken to thoroughly flush the hole prior to slow removal of the drill bit. Drilling mud was maintained at ground surface in all borings.

SPT hammers were of two types: a rope-around-the-cathead "donut" hammer provided by the drillers (total weight of 225 pounds), and a "free-fall", mechanical trip hammer (total weight of 210 pounds) manufactured by Pilcon Engineering (Figure 2.2). The trip hammer uses a rocker arm cam release system which provides a constant hammer drop height of 30± 1 inches. No measurements of the energies delivered by these hammers were obtained.

Sampling spoons were newly constructed following ASTM guidelines with the exception that space for liners was provided, but liners were not used. Schmertmann (1976, 1979) notes that liner samplers used without liners is the common practice, and represents a de facto change to ASTM D2586.

The Corps of Engineers SPT procedures follow ASTM guidelines with the exception of hammer type. The hammer used in this

program is of the type described by Marcuson and Bieganousky (1977) and is a free-fall hammer with hydraulic drive. More information about the effects of such free fall hammers is given in later sections. The rate of application of hammer blows with this device was about five per minute, while the rates with both the standard and the Pilcon mechanical hammer were about 40 blows per minute.

2.3 SITE DESCRIPTIONS

The sites investigated during this program were generally selected on the basis of having saturated, cohesionless soils. Sites were located in San Diego, Seal Beach, Salinas, Moss Landing, and San Jose, California, and Edmond, Oklahoma. The following sections provide brief description of site geology and soil profiles based upon the boring, sounding, and laboratory investigations.

2.3.1 San Diego, California

The site is located at the Naval Air Station near San Diego, on artificial fill emplaced between North Island and Coronado Island to connect the islands across the old Spanish Bight. North Island and Coronado Island are probably remnants of the Quaternary Nestor or lower marine terrace (Ellis and Lee, 1919). Surficial terrace deposits are chiefly silts and sands. In the Spanish Bight area, hydraulic fill, principally sand silty sand, and silt dredged from San Diego Bay, occurs at the surface (Forrest and Ferritto, 1976). Fill in this zone was placed in 1945.

Bedrock beneath terrace deposits and artificial fill consists of Cretaceous and Tertiary marine, lagoonal, and fluviatile clastic rocks, chiefly sandstone, conglomerate, and shale (Kennedy, 1973). These rocks dip gently northeast on the northeast flank of a northwest trending anticline with axis off the coast of San Diego. Planation of these dipping beds has resulted in removal of upper (Eocene-Pliocene) units beneath North Island with occurrence of progressively younger rocks to the east (Kennedy, 1973). Only the Cretaceous Rosario Group occurs beneath North Island. In the vicinity of the Spanish Bight and Coronado Island, rocks of the Eocene La Jolla Group overlie Cretaceous rocks in the subsurface (Kennedy, 1973). Further east, marine Pliocene deposits of the San Diego Formation overlie these Eocene rocks, and may extend into the test site area (Forrest and Ferritto, 1976).

Basement in the area consists of Cretaceous and older metamorphic and intrusive rocks (Kennedy, 1973; Forrest and Ferritto, 1976). The Rose Canyon fault is postulated to occur just west of the test site forming the eastern edge of North Island (Forrest and Ferritto, 1976), although others place the southern extension of this fault along the east side of San Diego Bay (Ziony, 1973). Movement on this fault has probably occurred during late Pleistocene and may be as recently as early Holocene (Ziony, 1973).

Nine Cone Penetrometer Tests and eight Standard Penetration Tests were performed at the San Diego site. The location of

the site and of each sounding and boring is given in Figures 2.3 and 2.4. The sounding logs are shown summarized in Appendix A in Figure A.1, and individually in Figures A.2 through A.10, and the boring logs in Figures A.11 through A.18. Site profiles were drawn based on the CPT results, and the SPT logs and laboratory classification results. These two profiles are shown in Figures 2.5 and 2.6. It should be noted that all of the CPT profile-series logs have been smoothed, that is, averaged over a vertical distance of one foot. The effect of such smoothing can be seen by comparison of the profile-series logs of Figure 2.5 with the individual logs of Figures A.2 through A.10.

Examination of the profiles shown in Figures 2.5 and 2.6 reveals that essentially identical profiles result using either CPT or SPT methods. The SPT results revealed changes in color indicative of a layer transition, while the CPT, being essentially a strength measurement, shows virtually no layering. However, the CPT continuous record does reveal the presence of lenses or pockets of dissimilar materials not found with the SPT method.

2.3.2 Salinas, California

The Salinas site is on the southwest bank of the Salinas River near the mouth of El Toro Creek. Sediments in the area consist chiefly of interbedded fluvial silty sand and sand deposited by the Salinas River, with interbeds of sand and gravel from the El Toro Creek alluvial fan. These fluvial deposits are Holocene age and extend to depths of 10-20 m (Tinsley, 1980,

personal communication). They are underlain by delta and estuarine sediments deposited during higher stands of sea level when the sea transgressed up the Salinas Valley into the area. Estuarine deposits are chiefly black muds (organic silty clays) of Holocene age. These fine-grained deposits interfinger with delta/fluviol sandy deposits, and generally do not persist to depths exceeding 30 m (Tinsley, 1980, personal communication). At these depths, deposits are again predominantly fluvial in origin and are Pleistocene in age. Beneath these Pleistocene-age Salinas River fluvial deposits is the Plio-Pleistocene nonmarine Paso Robles Formation, generally at depths greater than 300 feet (Tinsley, 1980, personal communication).

Dibblee (1976) has mapped and named the Rinconada-Reliz fault along the northeastern flank of the Sierra de Salinas, forming the southwestern edge of the Salinas Valley. The fault would project very close to the site, between it and the mountain front 1/4 mile to the west. Movement along the fault was right-lateral during late Pleistocene times, but has since shifted to predominantly reverse-slip during Holocene time (Tinsley, 1980, personal communication).

Fifteen CPTs and eight SPTs were performed at the Salinas site. The locations of the site and each sounding and boring are given in Figures 2.7 and 2.8. The sounding and boring logs are shown in Appendix A Figures A.19 through A.33 and A.34 through A.41, respectively. It should be noted that some of the soundings were performed using an oversized cone

(15 square centimeter projected end area). These soundings are also shown in Appendix A (identified as F15CKE) along with the rest of the Salinas soundings. The final site profiles, again as based on CPT and SPT and laboratory test data are shown in Figures 2.9 and 2.10.

Comparison of the logs shown in Figures 2.9 and 2.10 reveals the expected differences. The SPT method provides information regarding soil grain size, while the CPT method implicitly provides strength data and more detailed stratigraphic data than possible using the SPT method.

2.3.3 Moss Landing, California

The site at Moss Landing is underlain by beach sands to probable depths of ten meters or more. Eolian sands, derived from reworking of beach sands, form a thin cover at the surface and may occur interbedded with beach deposits at depth. Other deposits in areas adjacent to the site are part of a late Holocene transgressive sequence consisting of relatively thick sands offshore and estuarine and fluvial deposits onshore (Tinsley, 1980, personal communication). The site is near the mouths of the Salinas and Pajaro Rivers which empty into Monterey Bay. Sloughs (Elkhorn, Moro Cojo) and tidal channels occur just east of Moss Landing, forming an area of modern fine-grained estuarine deposits which thin to the east. These types of deposits occur at depth near Moss Landing, interbedded and underlain by sandy fluvial deposits (Tinsley, 1980, personal communication), and contain gravel lenses, particularly at the

base of the Holocene section which extends to about 100 to 180 feet below the surface (Tinsley, 1980, personal communication). In the immediate site vicinity, deposits are principally littoral, i.e., deposited in the shoreline environment within the zone of tidal fluctuation. Sands predominate with some interbedded silts and clays.

Nine CPTs and eight SPTs were performed at the Moss Landing site. The site and boring and sounding locations are shown in Figures 2.10 and 2.11. The sounding logs are given in Figures A.42 through A.50 of Appendix A, and boring logs in Figures A.51 through A.58. The final site profile for Moss Landing based upon the CPT and the SPT and laboratory classification data is shown in Figures 2.12 and 2.13, respectively.

2.3.4 Sunset Beach, California

The Sunset Beach site lies east of Anaheim Bay along the principal tidal inlet into Sunset Bay. Sunset Bay is a tidal marshland which has been closed off by a barrier beach. The site is on the landward side of the barrier beach adjacent to the marshlands. Surface materials consist of beach sands (U.S. Department of Agriculture, 1978), probably reworked to some extent by man during modification of the beach. Beach sands at the site probably overlies and interfinger with tidal marsh deposits (organic sands, silts, and clays) derived from both marine and continental sources. Immediately inland from the beach, Holocene deposits generally do not extend to depths greater than 20 feet (Poland, et al, 1956). Along the beach,

deposits may be somewhat thicker, consisting of unconsolidated sand, silt and clay with no known gravels in the area (Poland et al, 1956; Poland, 1959). Holocene deposits are underlain by the Pleistocene Lakewood and San Pedro Formations, which extend to depths greater than 500 feet consisting of loosely to moderately consolidated sandstone, claystone, siltstone, and marl (California Department of Water Resources, 1968; Poland et al, 1956).

Three CPTs were performed at the Sunset Beach site (Figure 2.14) at the locations shown in Figure 2.15. No SPTs were performed as the site was selected primarily because the uniformity of the site soils facilitates estimation of the effect of depth (or pressure) on cone penetrometer readings. The results of the soundings are shown in Appendix A in Figures A.59 through A.61 and the interpreted profile is shown in Figure 2.16.

2.3.5 San Jose, California

Two different sites in the Coyote Creek vicinity near San Jose were investigated. These sites occur in the gently sloping alluvial plain of the Santa Clara Valley six to seven miles south of the southern tip of San Francisco Bay. The surficial material at the sites is predominantly medium-grained alluvium (fine sand, silt, and clayey silt) of Holocene age (Helley and Brabb, 1971; Helley, et al, 1979). This alluvium was derived from sources to the east and south along the Coyote Creek drainage. Natural levees deposited during flood stage

occur along the banks of Coyote Creek in which test sites are located. The site areas are near the southern limit of modern bay mud and may be underlain at shallow depths by thin bay muds deposited when the bay extended further southward as recently as 125 years ago (Helley and others, 1979). At greater depths, Pleistocene alluvium and Pleistocene bay mud interfinger, but alluvial deposits probably predominate beneath the site area. No known faults traverse or underlie the area, although the historically active Hayward fault occurs about 5 kilometers to the east. Holocene and Pleistocene beds underlying the area are generally undeformed, dipping slightly northward toward the bay in original depositional position.

The locations of the two Coyote Creek sites are shown in Figure 2.17. The north site had eleven CPT soundings (two with the oversized cone) and six borings, while the south site had ten soundings (two with oversized cone) and four borings. The locations of the borings and soundings are shown in Figure 2.18. The sounding logs are presented in Appendix A in Figures A.62 through A.73 and A.74 through A.83 for the north and south sites, and the boring logs in Figures A.84 through A.89 and A.90 through A.93 for north and south sites, respectively. The site profiles based on these data are given in Figures 2.19 and 2.20 for the north site, and in Figures 2.21 and 2.22 for the south site.

2.3.6 Edmond, Oklahoma

The Oklahoma site lies in the valley of the Deep Fork River

northeast of Oklahoma City (Figure 2.23). The area is on the east flank of the Anadarko Basin, characterized by gently west-dipping Permian-age sedimentary rocks. The rocks in the site vicinity are principally sandstone of the Garber Sandstone and Wellington Formations of Lower Permian age (Wood and Burton, 1968). These two formations are lithologically similar, consisting of lenticular beds of cross-bedded sandstone interbedded with shale, generally sandy to silty. Sands are fine- to very fine-grained, and are poorly cemented (Wood and Burton, 1968). The site lies essentially along the gradational contact between the two formations (Bingham and Moore, 1975).

The site is underlain by modern alluvium of the Deep Fork River Valley. Alluvium consists of sand, silt and clay with lenticular beds of gravel (Bingham and Moore, 1975). The thickness of alluvium in the valley overlying the Permian bedrock varies from several feet to more than 50 feet (Wood and Burton, 1968; Bingham and Moore, 1975). At the dam centerline, the alluvium is about 83 feet thick, but upstream 300 feet it is only 14.5 feet thick (U.S. Army Corps of Engineers, 1978). Valley bottom alluvium is Holocene age and is unconsolidated.

Twenty-three CPTs and twenty-four SPTs were performed at the Arcadia site at locations shown in Figure 2.24. Because of the extremely complex nature of the site profile, significant changes in soil type or resistance were found over distances

of only a few feet in either horizontal or vertical directions. For this reason, some of the data analyses (discussed in subsequent sections) were performed upon average CPT and SPT results. Likewise, only a generalized profile could be developed. This profile covers several hundred feet both along the dam centerline and in the upstream-downstream axis and is not shown in this report. For more information about the characteristics of this site, the Corps of Engineers Design Memorandum may be consulted. The complete set of boring and sounding logs from the Arcadia site are available in that memorandum. Select information about site characteristics is discussed in a subsequent section of this report.

2.4 CONCLUSIONS

Primary conclusions that can be drawn based upon the field investigations focus upon testing procedures, data consistency, data interpretation, and the degree to which the test methods provide data representative of site conditions. In regard to testing procedures, it was noted during the field program that constant attention was required to keep repeatability of SPT method, although only one driller was used. The tendency was for the rope-around-the-cathead method hammer-drop height to decrease with increasing number of blowcounts. Further, as the focus of measurements was on sandy soils, after the first boring was complete and the location of significant clay layers known, the driller tended to assume layer continuity without actually checking the clay layer extent encountered in subsequent borings.

The effect of this assumption can be seen in comparison of the CPT and SPT profiles where thin interlayers of sands and silts are apparent in the CPT records but missing from the SPT records.

Further comparison of the CPT-SPT profiles reveals that greater evidence of spatial variability of soil types and layering is visible with the CPT method. This includes the definition of interlayers as well as thickness and extent of more massive layers. However, the CPT method primarily reveals changes in material type via the intermediary of changes in strength using the tip measurement and the sleeve measurement, and no visual evidence of material change is obtained. At the sites investigated, this lack of sample presented no difficulties, but materials were in general fairly common, well behaved sands, silts, and mixes. One notable shortcoming is that the CPT profiles presented in previous sections reveal no information allowing definition of water table depth.

The potential for use of the piezometric cone penetrometer to define water levels was to be investigated in this program. However, due to equipment fabrication problems and because the location of sensing elements within the tip and the interpretation of measured data are areas of current controversy, no such investigations were performed. Subsequent investigations in which the piezometric cone has been used indicate that if the porous element is saturated with a high viscosity fluid, then penetration through a dry layer overlying a saturated layer will not result in loss of saturation to a degree eliminating pore pressure response upon entering the saturated layer.

Another interesting phenomenon observed during the field program was the apparent "smoothing" of layer resistances during SPT penetration using the higher energy free-fall hammer. Figures 2.25 through 2.28 show average blowcount versus depth profiles for each hammer type at each site. The average blowcount values were calculated over three-foot intervals where layer continuity was present. Also shown in those figures are the ratios of average blowcounts using the two hammers.

Further examination of the blowcount ratios by material type reveals a trend toward increase in blowcount ratio with increasing blowcount. A possible explanation for this trend revolves around the question of the extension wave reflected from the "free" end of the rod string. As the soil hardens, the free end becomes progressively more fixed, allowing more of the available energy to be transmitted by the rod string. The trip hammer is of a type having a large diameter anvil which acts as a wave trap, in particular for the free end condition. Thus with increasing fixity, the trapped energy is more fully transmitted, with resultant reduction in trip hammer blowcount as compared with standard hammer blowcounts. This trend is more fully discussed by Schmertmann (1979b).

As a final examination of field data, a series of CPT soundings is presented in Figure 2.29. These soundings were performed adjacent to and after a boring had been placed to determine how close a sounding could be without showing any effects of

the nearby boring. In Figure 2.29 it can be seen that the sounding placed one and one-half foot from the boring shows one anomalously low end-bearing zone. Whether or not this reduction resulted from the nearby boring cannot be certain with only one test series; however, based upon this result, the few soundings performed after a boring was completed were placed at a distance of from six to twelve feet from the nearest boring, a distance which is close enough to allow a high degree of horizontal uniformity without being close enough to sense any effect of the boring.

SITE	SPT			CPT	
	DATE	TYPE	NUMBER	NUMBER	DATE
SAN DIEGO: NAS NORTH ISLAND	10/10-12/79	STANDARD TRIP	4 5	9	4/18-19/79
SALINAS SOUTH	11/6-9,12-13/79	STANDARD TRIP	4 4	15	11/12,14-15/79
MOSS LANDINGS	11/13-15/79	STANDARD TRIP	4 4	9	11/12-13/79
SUNSET BEACH	—	—	—	3	3/17/80 7/11/80
SAN JOSE: COYOTE NORTH	11/16-17, 20-21/79	STANDARD TRIP	3 3	11	11/5-16,19/79
SAN JOSE: COYOTE SOUTH	11/19-20/79	STANDARD TRIP	2 2	10	11/17-19/79
ARCADIA:* EDMOND, OKLAHOMA	1/20-5/8/80	STANDARD TRIP	24	23	3/28-4/3/80

*ALL SPT's PERFORMED BY U.S. ARMY
CORPS OF ENGINEERS, TULSA, OKLAHOMA,
DISTRICT

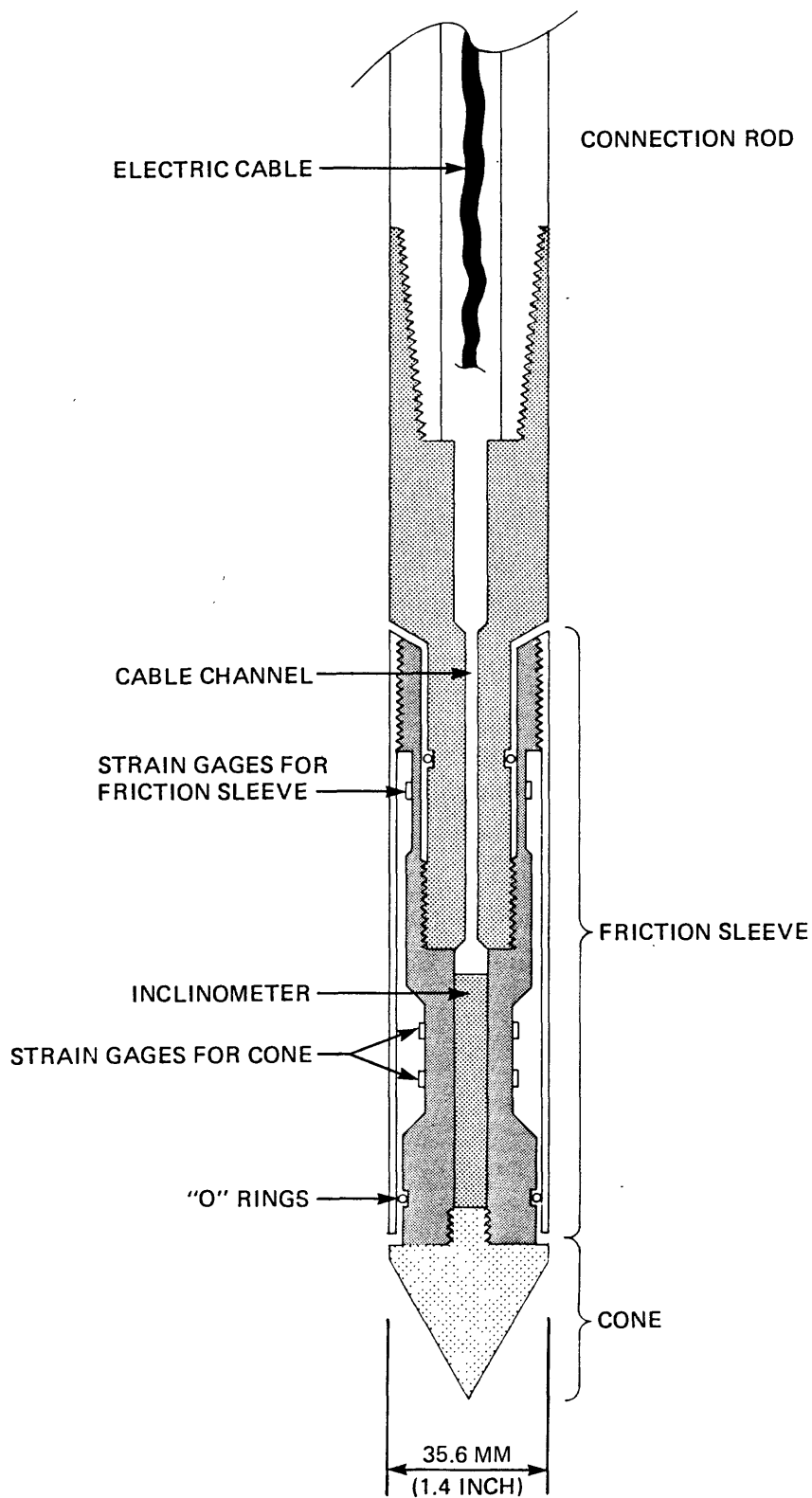


PROJECT NO:

79-153

USGS

SUMMARY OF FIELD WORK

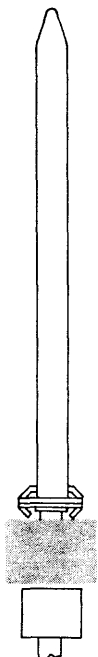


PROJECT NO.:

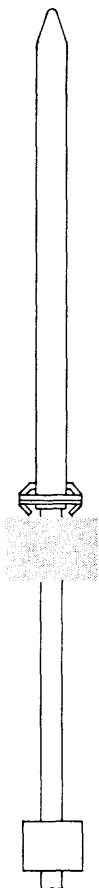
79-153

USGS CPT-SPT

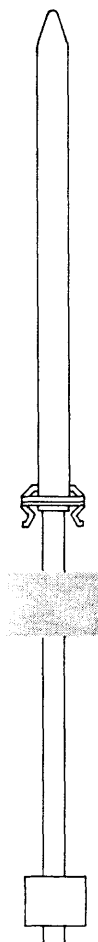
ELECTRIC FRICTION CONE PENETROMETER



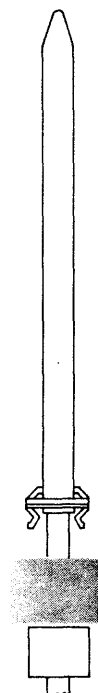
1. THE WHOLE ASSEMBLY IS SHACKLED TO THE WINCH ROPE, HOISTED ON TO THE ROD OR PIPE CONNECTION AND SCREWED HOME



2. THE LOCKING PIN IS THEN REMOVED AND THE OUTER TUBE ASSEMBLY - CARRYING WITH IT THE MONKEY - IS RAISED BY THE WINCH



3. ON REACHING A HEIGHT OF 30", THE TRIP CAM OPERATES THE PAWLS, RELEASING THE MONKEY TO DROP FREELY ON THE ANVIL



4. THE OUTER TUBE IS LOWERED TO RE-ENGAGE THE HAMMER



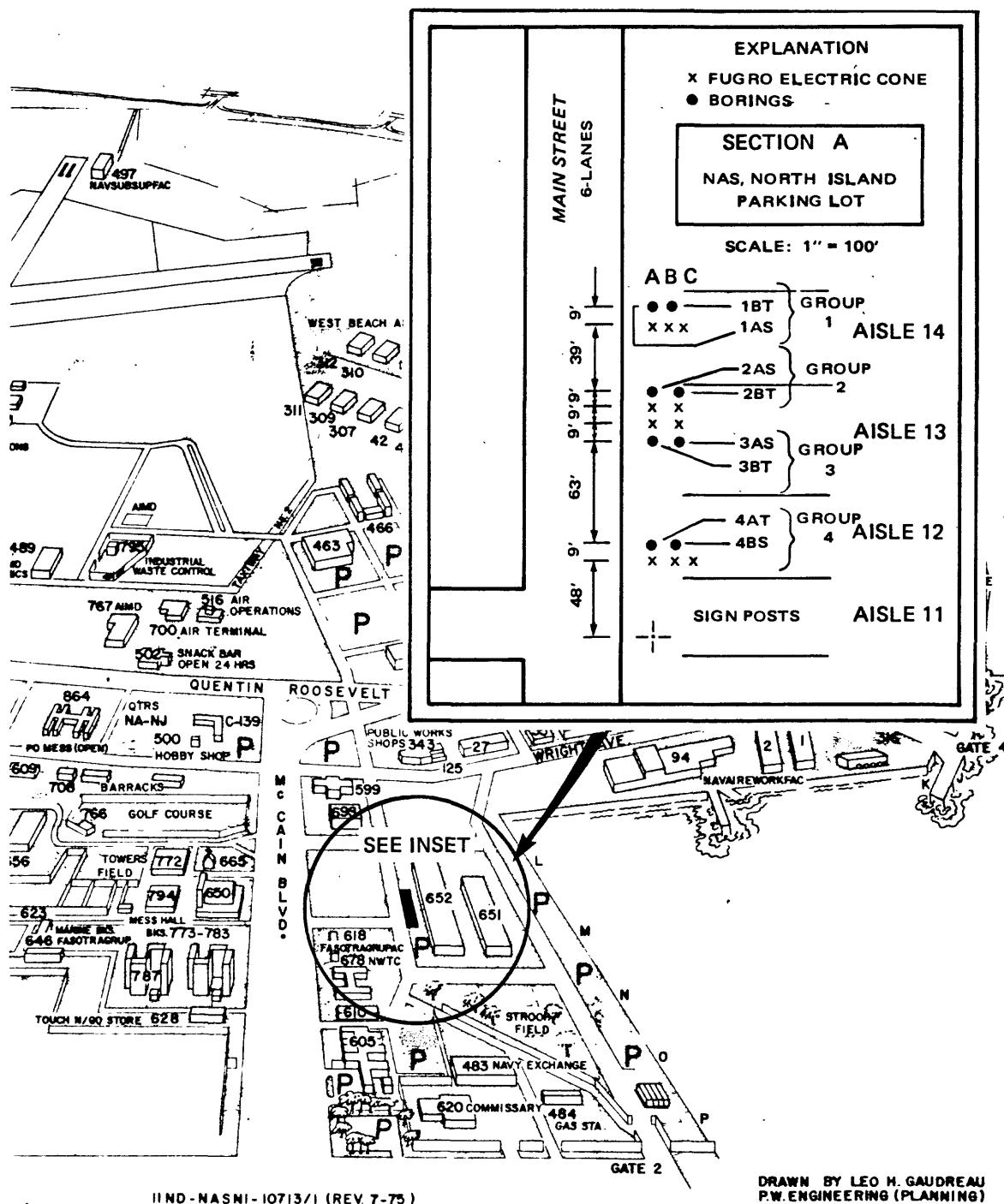
PROJECT NO.:

79-153

USGS CPT-SPT

MECHANICAL TRIP HAMMER
(PILCON ENGINEERING)

APPROVED BY
CHECKED BY
DRAWN BY
COMPILED BY



REFERENCE NAVAL AIR STATION, NORTH ISLAND, CA 1975

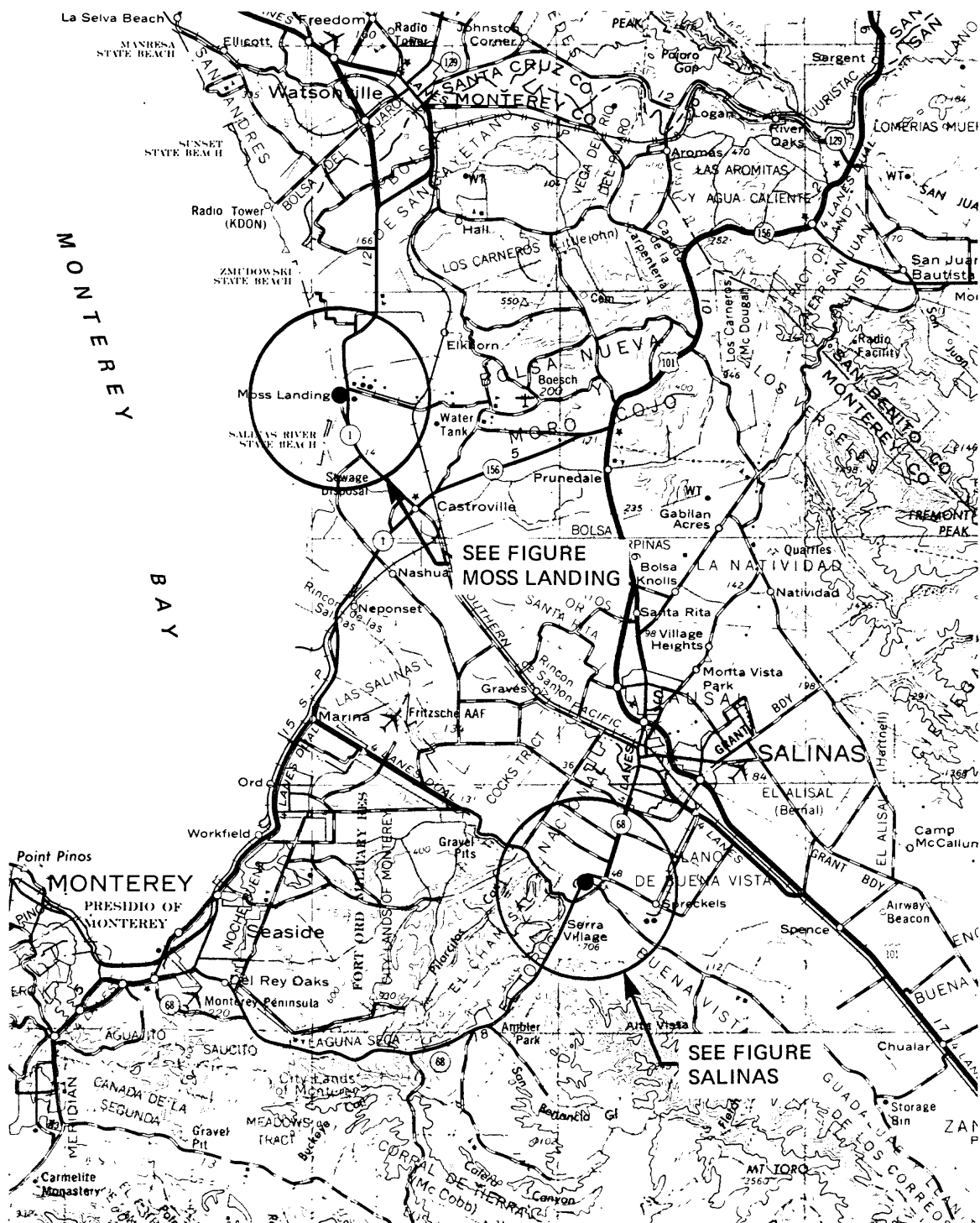


PROJECT NO.:

79-153

USGS CPT-SPT

NORTH ISLAND SITE LAYOUT



FROM USGS 2° TOPOGRAPHIC MAP OF
SANTA CRUZ, CA. 1965



PROJECT NO.:

79-153

USGS CPT-SPT

MOSS LANDING/SALINAS
SITE LOCATIONS

Approved by

Checked by

Drawn by LESHER, D.

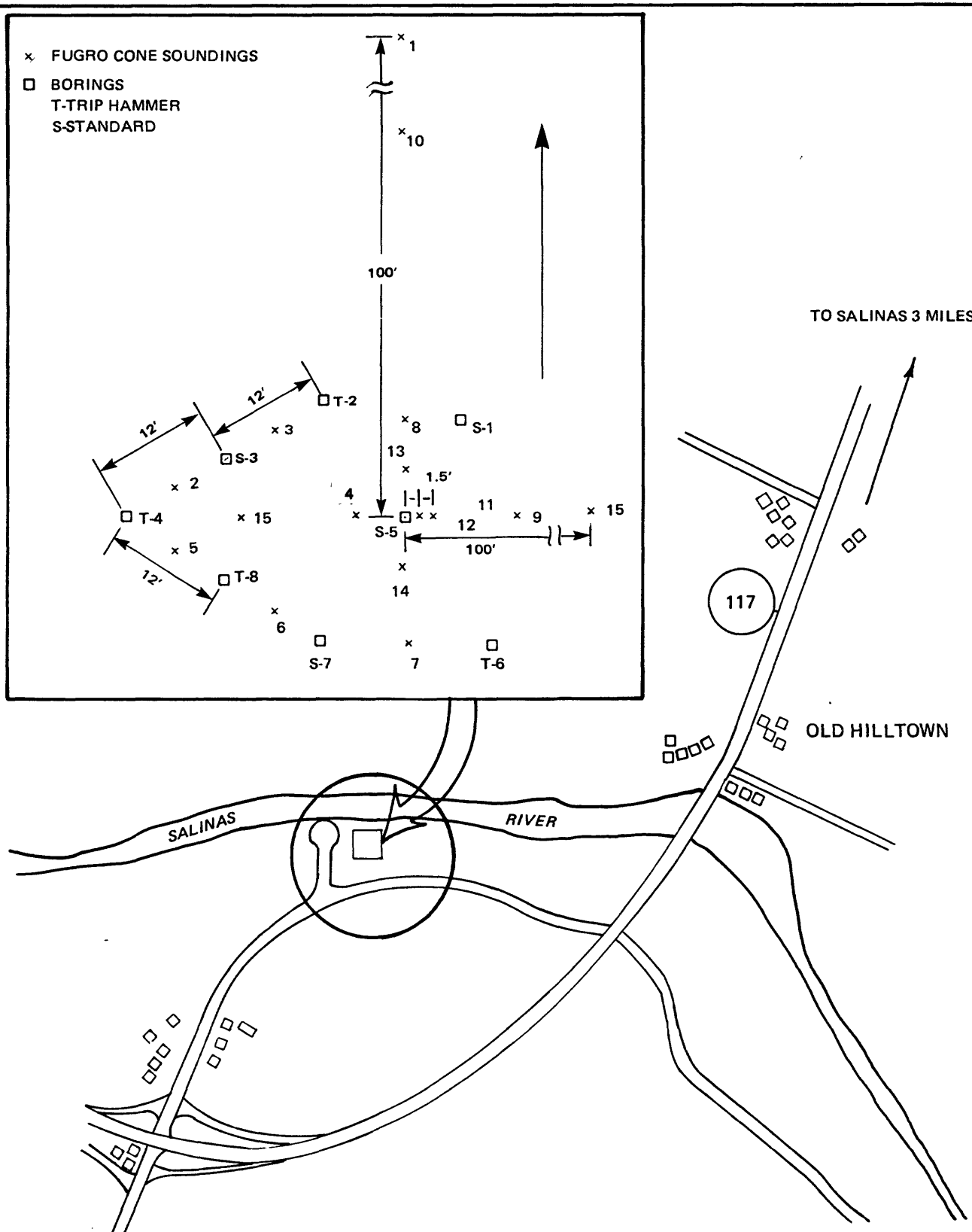
Compiled by

x FUGRO CONE SOUNDINGS

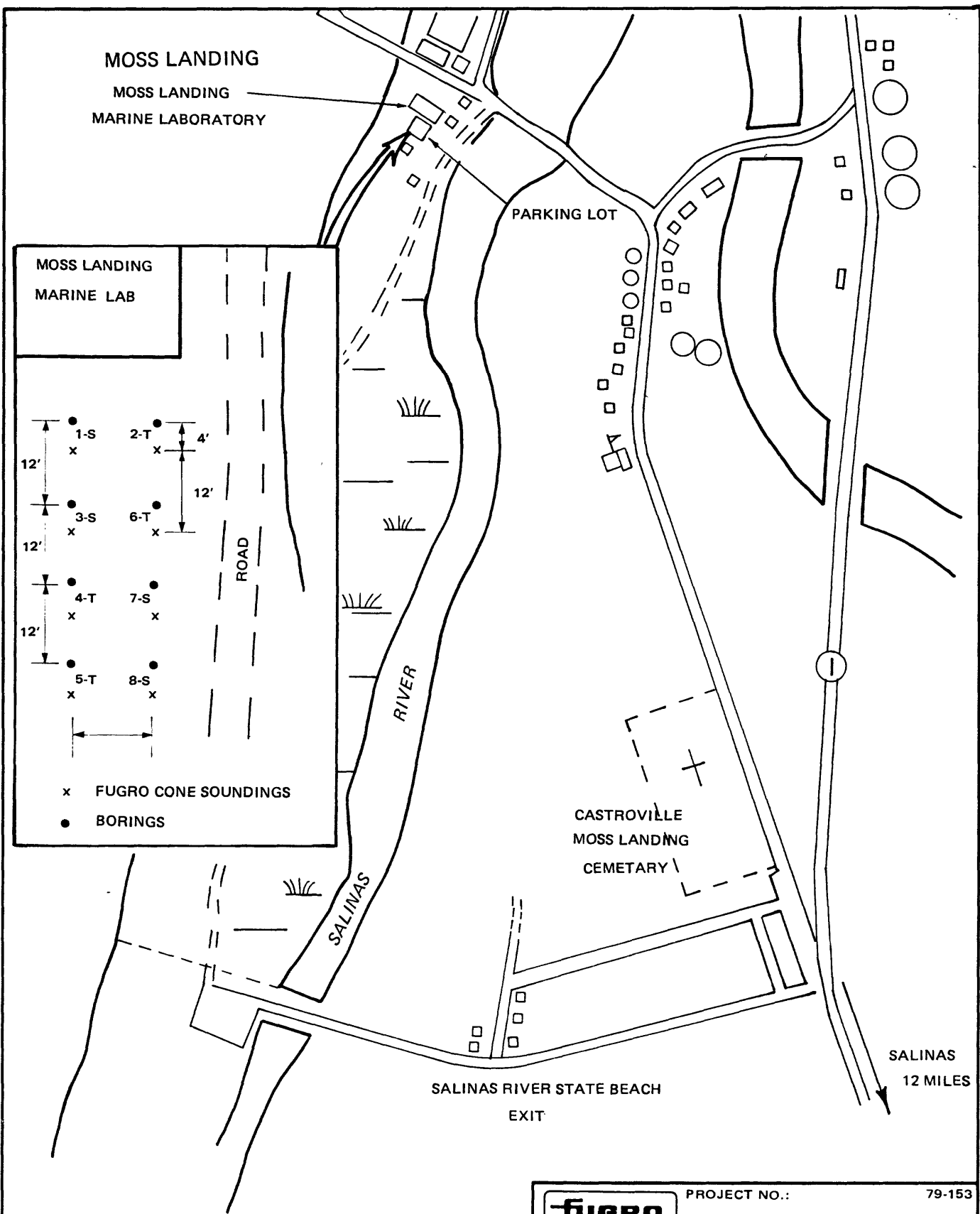
□ BORINGS

T-TRIP HAMMER

S-STANDARD



Compiled by _____
Drawn by LESHER, J.D.
Checked by _____
Approved by _____



4X ENLARGEMENT ADAPTED FROM USGS 7 1/2" TOPOGRAPHIC MAP OF MOSS LANDING, CA 1954, PHOTOREVISED 1968

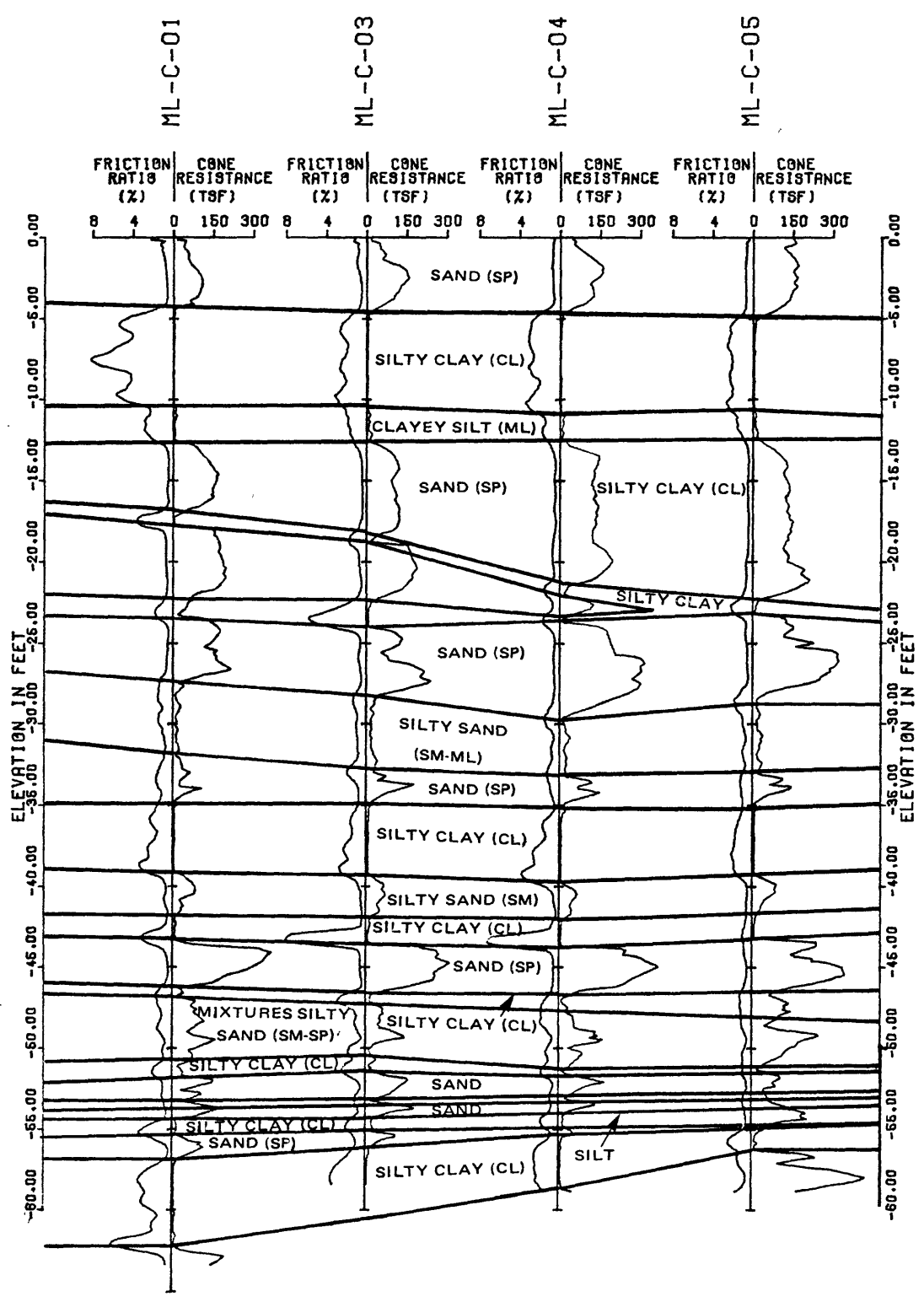



PROJECT NO.: 79-153

USGS CPT-SPT

MOSS LANDING SITE LAYOUT

Approved by _____
Checked by _____
Drawn by _____
Compiled by _____





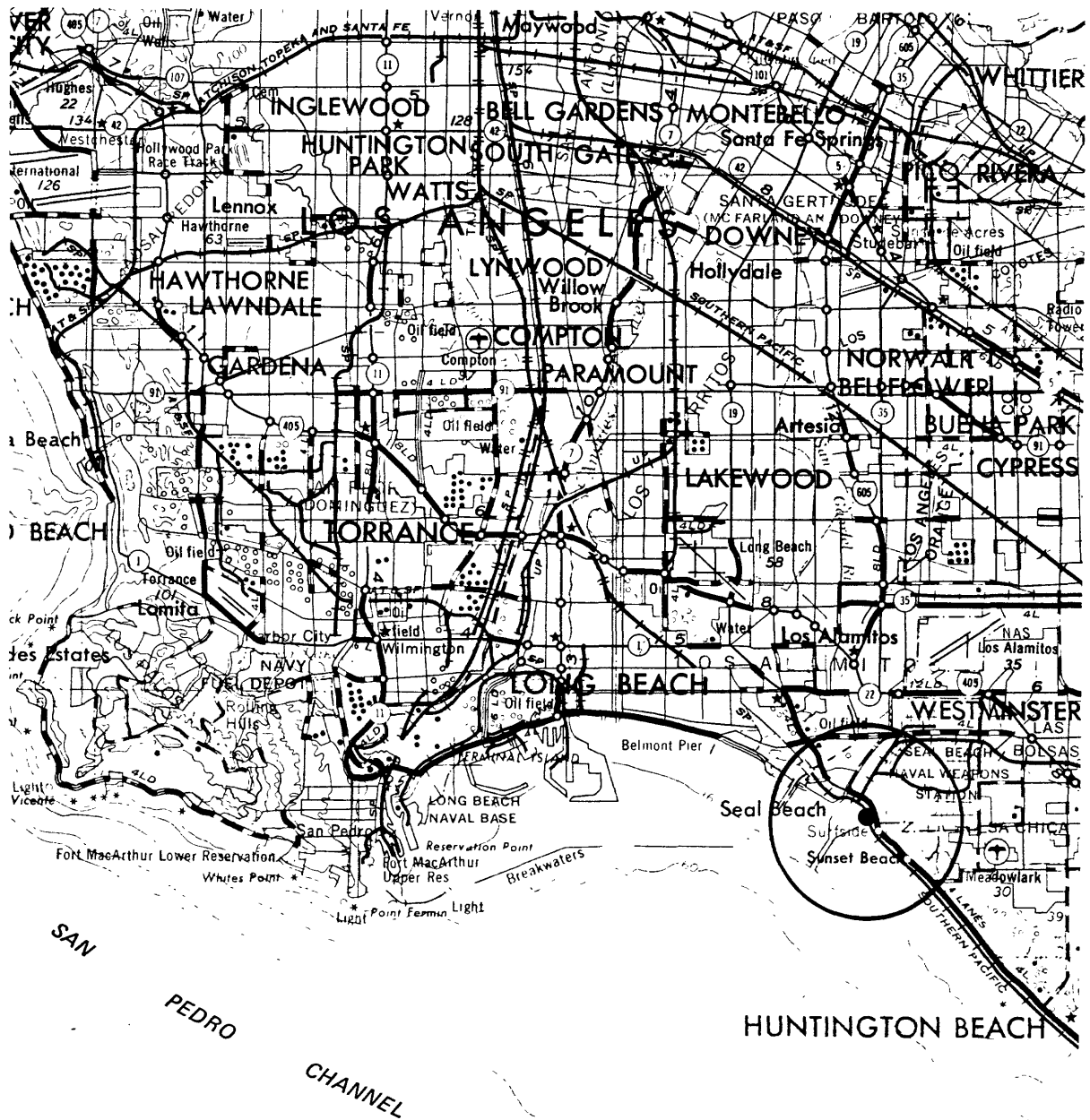
PROJECT NO.: 79-153

USGS CPT-SPT

MOSS LANDING SITE
CPT PROFILE

9-80

FIGURE 2.12



FROM USGS 2° TOPOGRAPHIC MAP OF
LONG BEACH, CA 1957, REVISED 1970



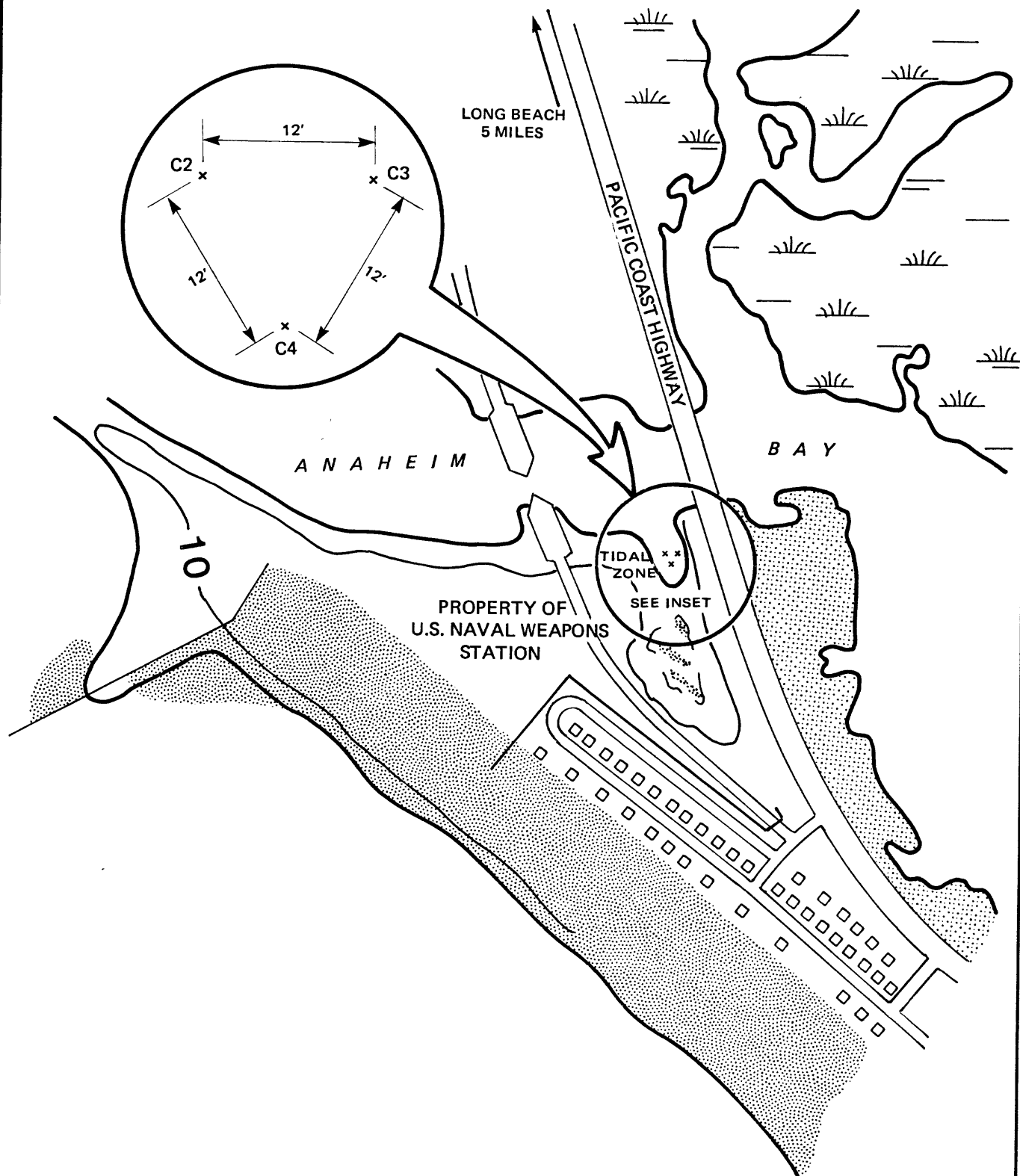
PROJECT NO.:


79-153

USGS CPT-SPT

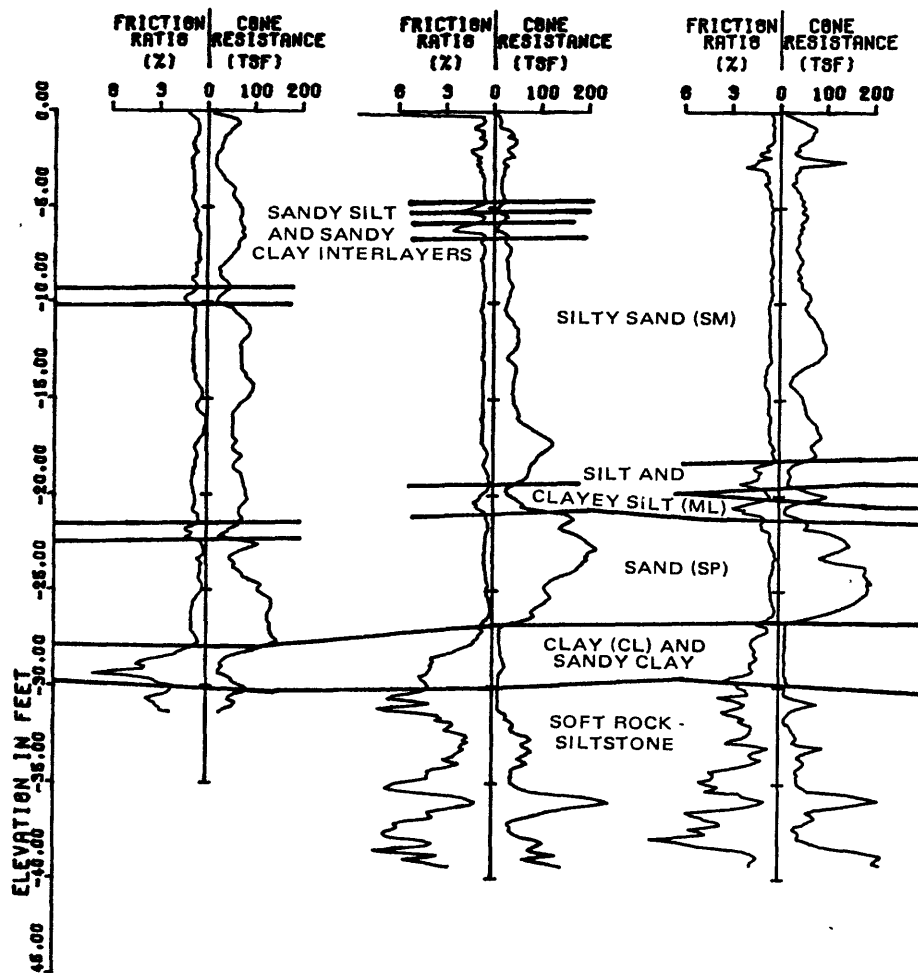
SUNSET BEACH SITE LOCATION

Compiled by _____
Drawn by H. J. [signature]
Checked by _____
Approved by _____



	PROJECT NO.:	79-153
	USGS CPT-SPT	
SUNSET BEACH SITE LAYOUT		
9-80	FIGURE 2.15	

5X ENLARGMENT ADAPTED FROM USGS 7½" TOPOGRAPHIC MAP OF SEAL BEACH, CA. 1965, PHOTOREVISED, 1972.

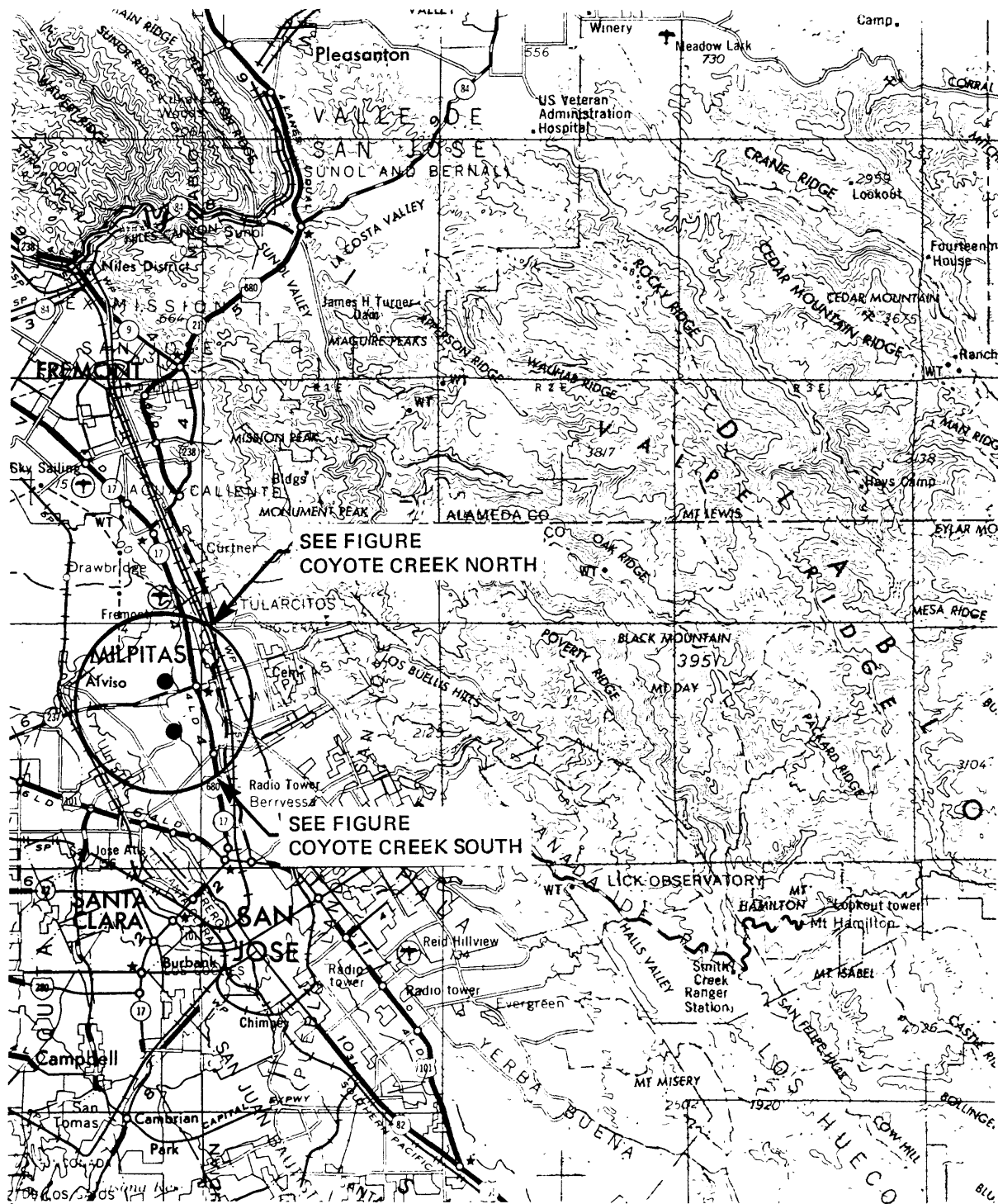


PROJECT NO.:

79-153

USGS CPT-SPT

SUNSET BEACH SITE
CPT PROFILE



FROM USGS 2° TOPOGRAPHIC MAP OF
SAN JOSE, CA. 1962, REVISED 1969



PROJECT NO.:

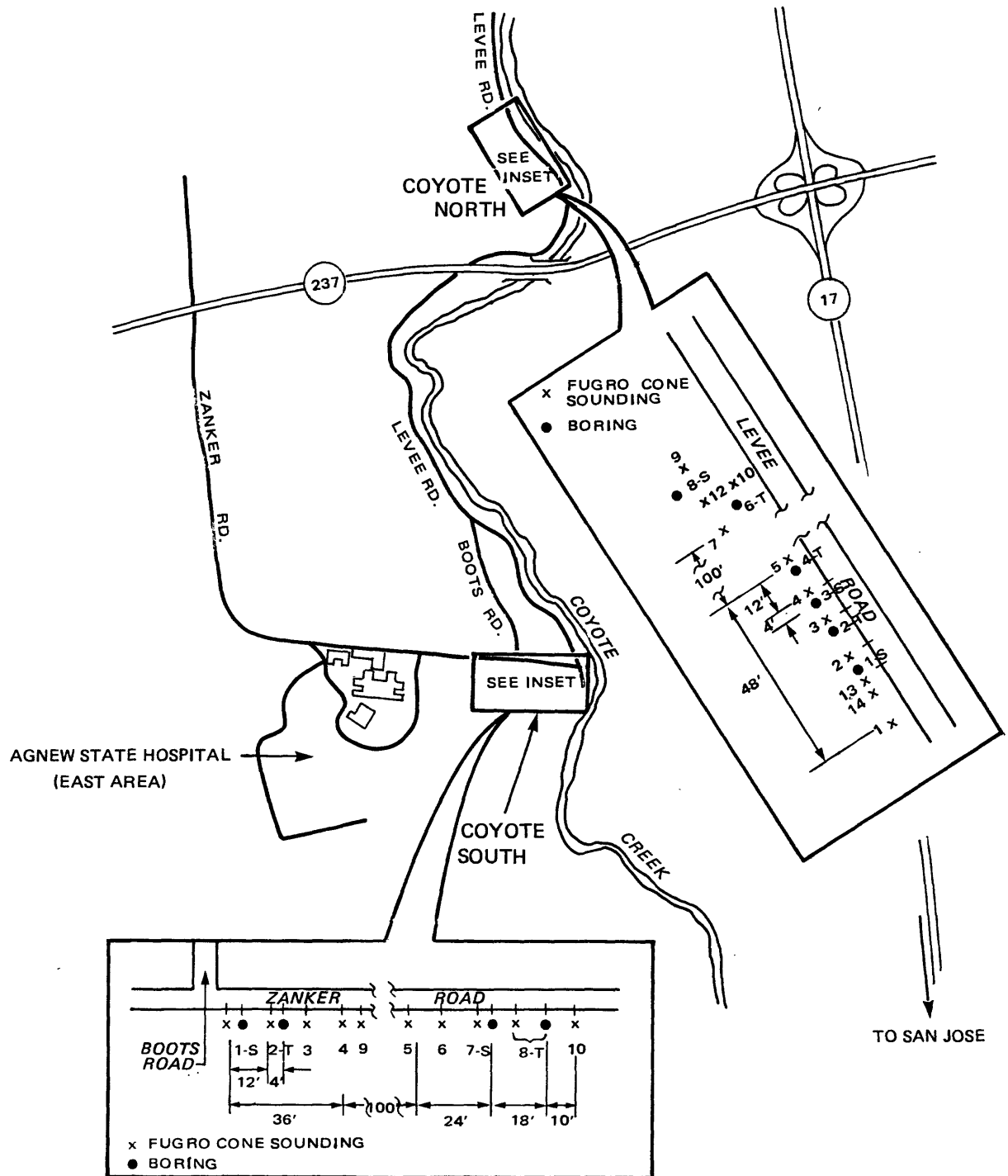
79-153

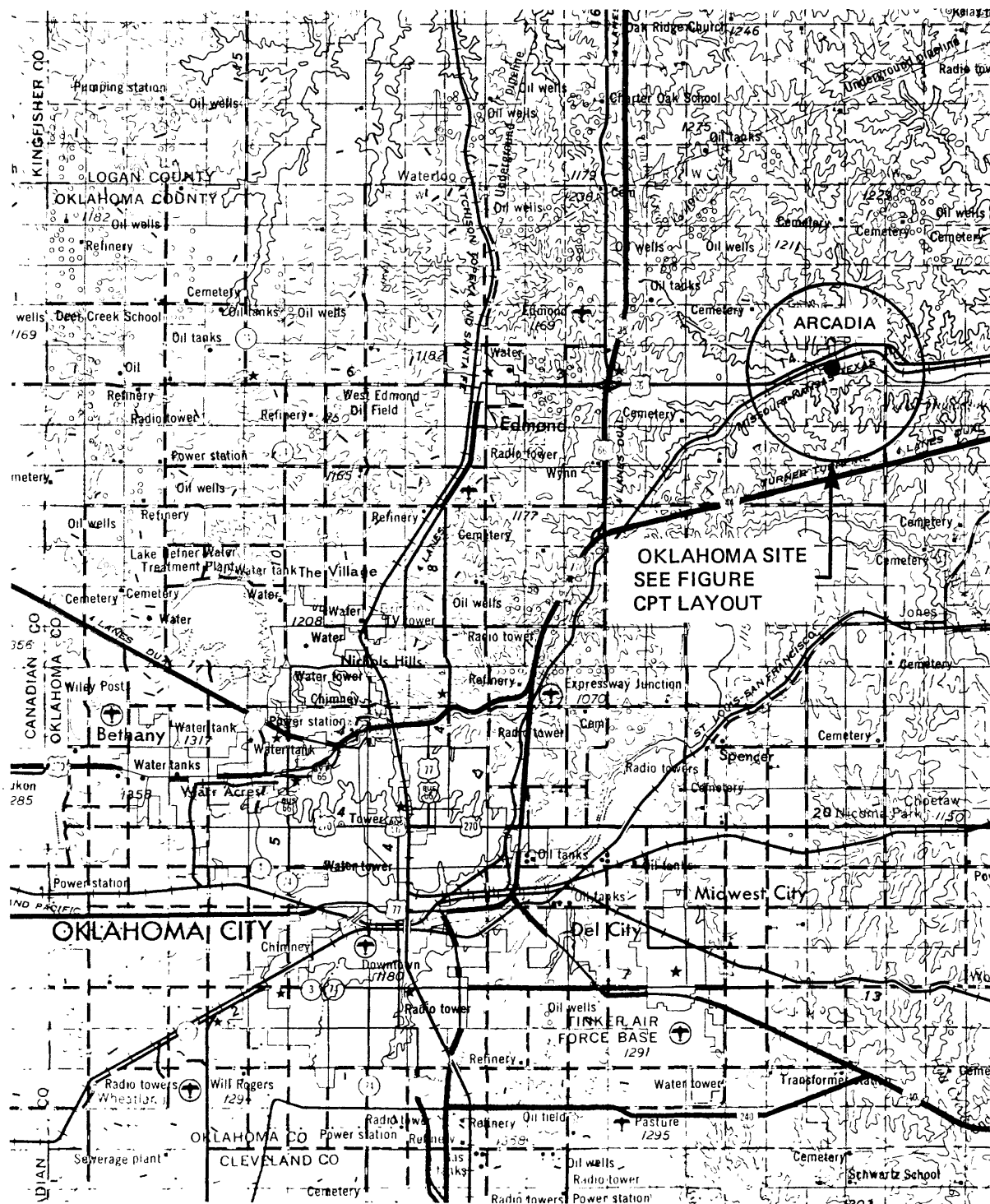
USGS CPT-SPT

SAN JOSE SITE LOCATIONS:
COYOTE CREEK NORTH AND
COYOTE CREEK SOUTH

9-80

FIGURE 2.17





FROM USGS 2° TOPOGRAPHIC MAP OF
OKLAHOMA CITY, OK. 1957, LIMITED REVISION 1968



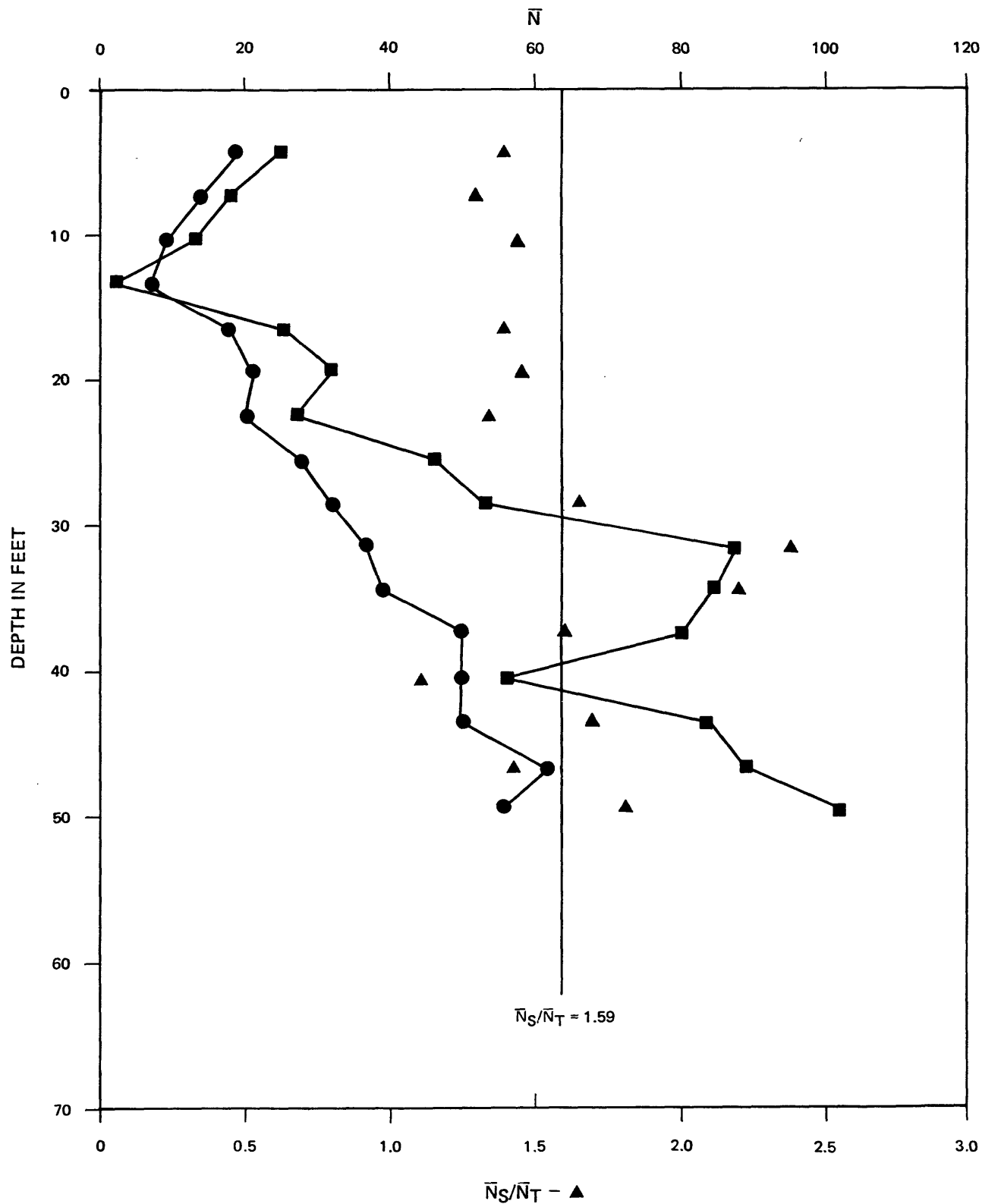
PROJECT NO.:

79-153

USGS CPT-SPT

EDMOND, OKLAHOMA SITE LOCATION

Compiled by _____ Drawn by _____ Checked by _____ Approved by _____

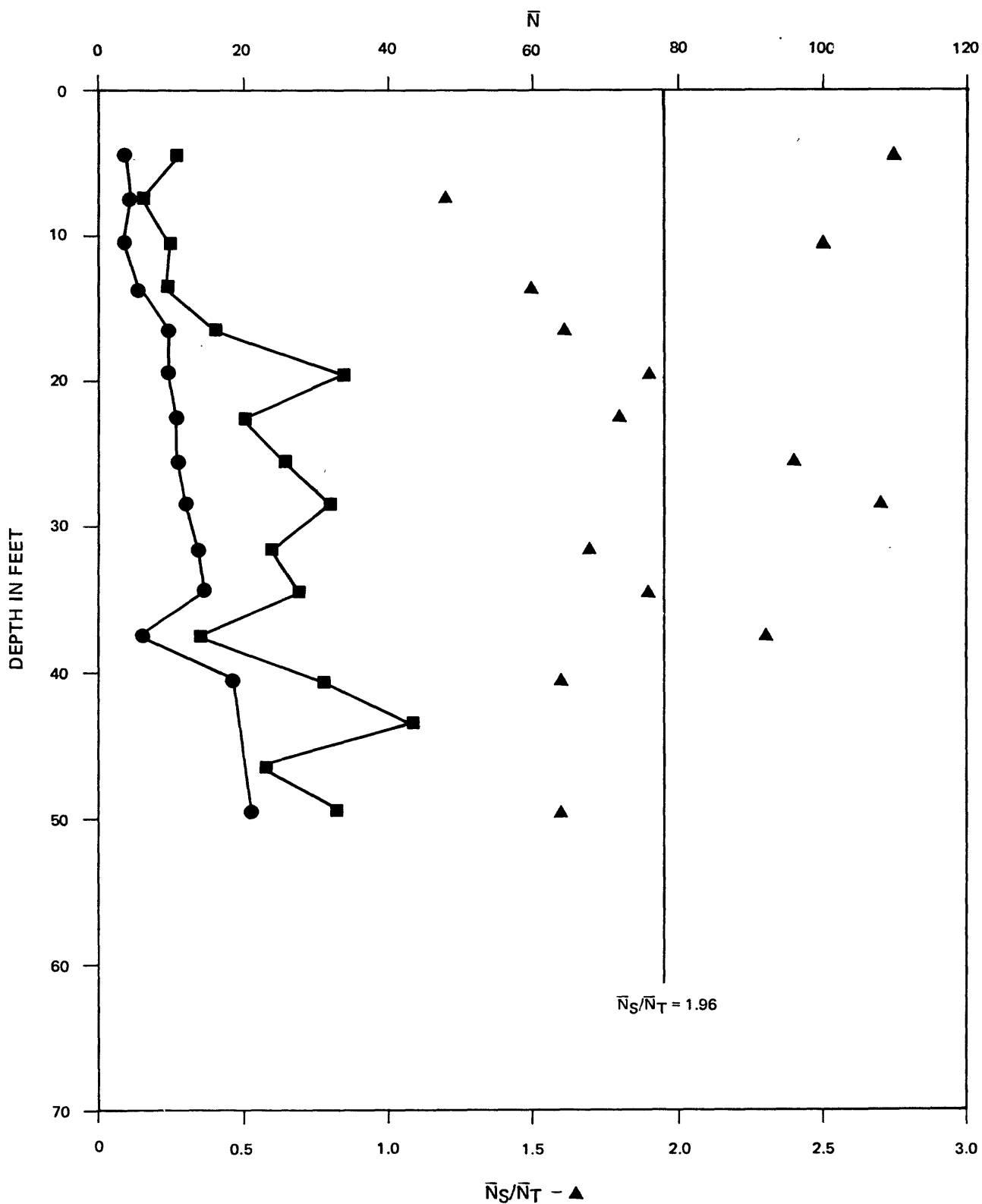


Approved by

Checked by

Drawn by

Compiled by



- \blacksquare STANDARD - \bar{N}_S
 \bullet TRIP - \bar{N}_T
 \blacktriangle - \bar{N}_S/\bar{N}_T



PROJECT NO.:

79-153

USGS CPT-SPT

SALINAS SITE
COMPOSITE \bar{N} PROFILES AND \bar{N}_S/\bar{N}_T

9-80

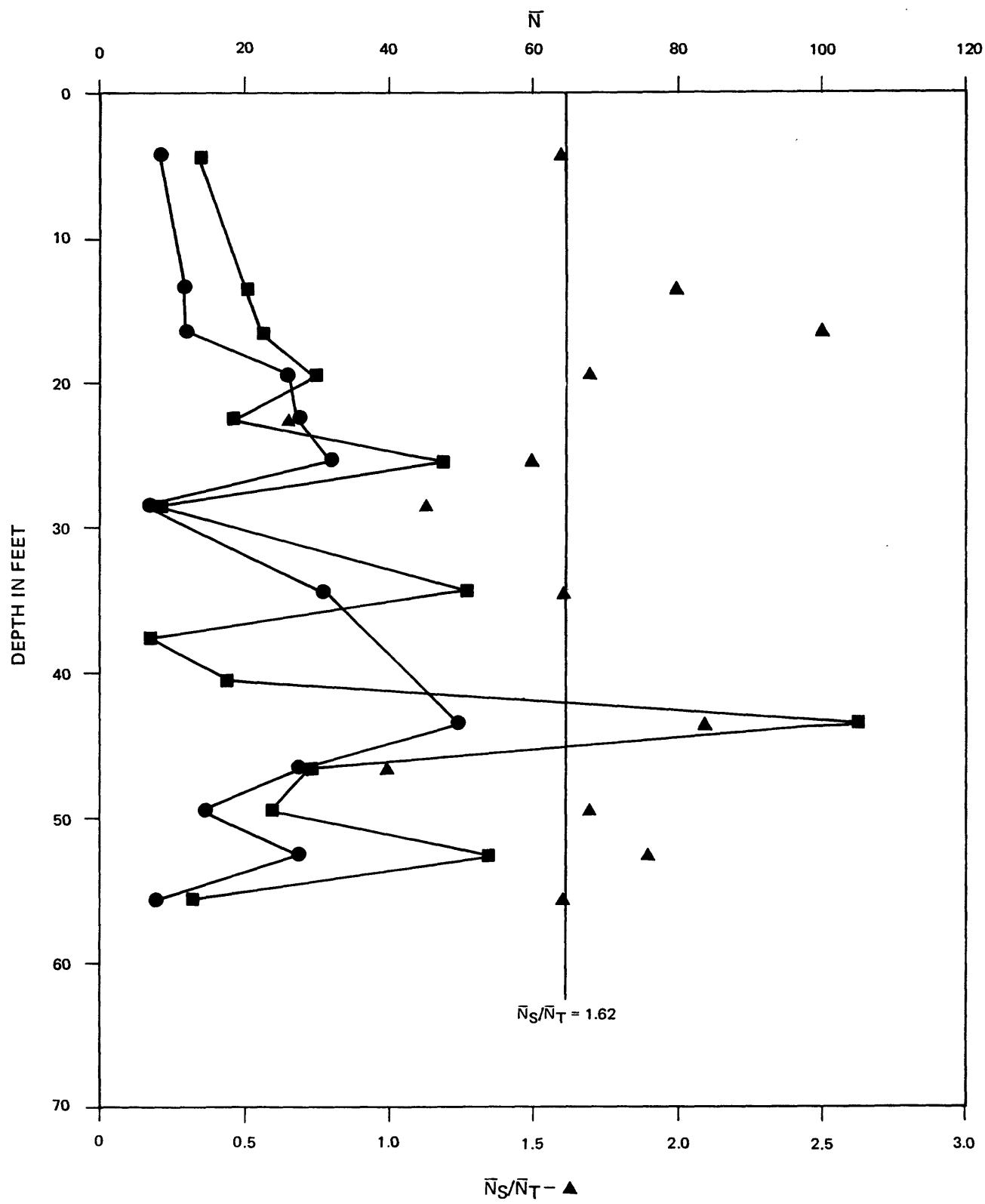
FIGURE 2.26

Approved by _____


Checked by _____

Drawn by _____

Compiled by _____



- STANDARD - \bar{N}_S
- TRIP - \bar{N}_T
- ▲ - \bar{N}_S/\bar{N}_T



PROJECT NO.: 79-153

USGS CPT-SPT

MOSS LANDING SITE
COMPOSITE N PROFILES AND \bar{N}_S/\bar{N}_T

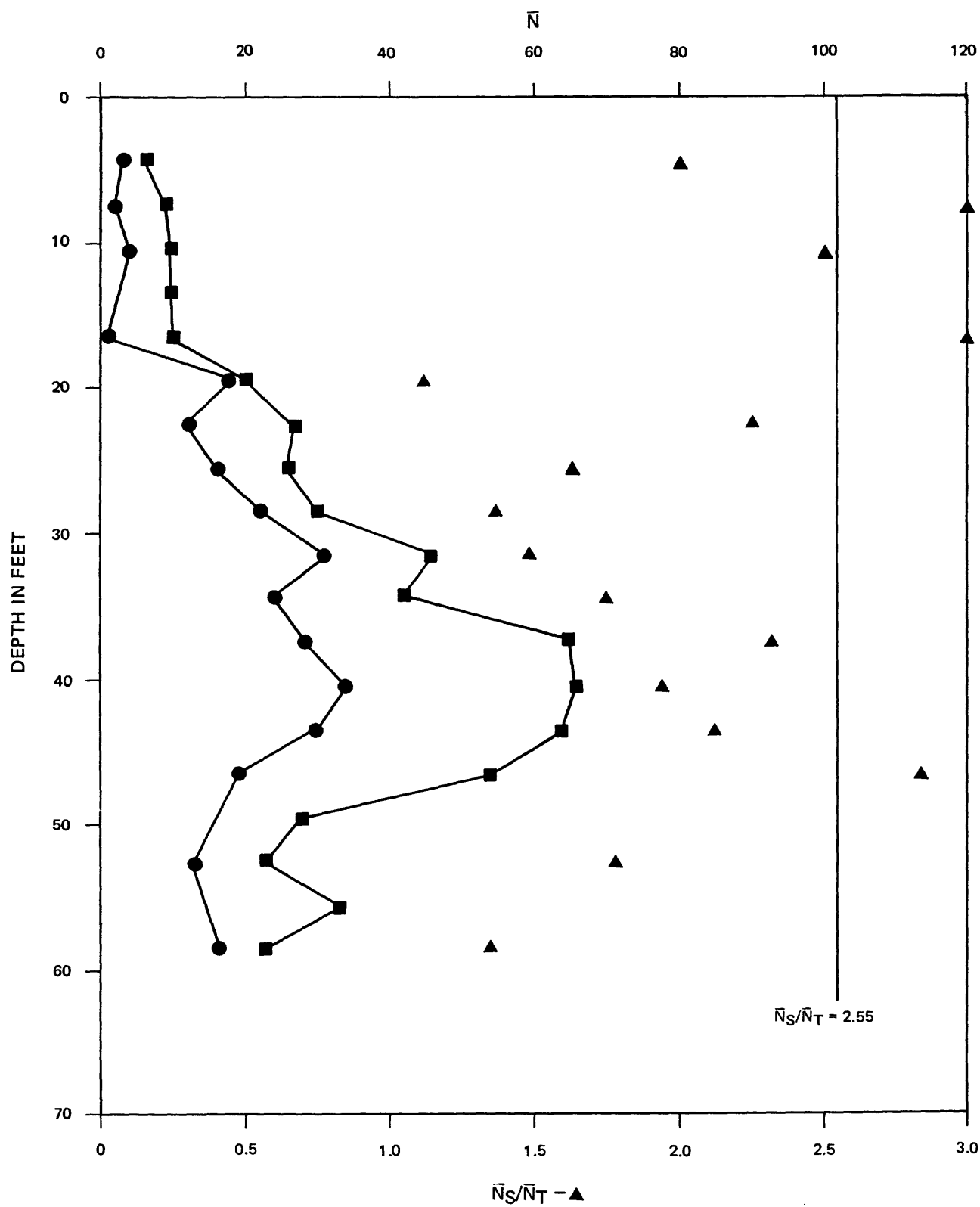
9-80 FIGURE 2.27

Approved by

Checked by

Drawn by

Compiled by



- STANDARD - \bar{N}_S
- TRIP - \bar{N}_T
- ▲ - \bar{N}_S/\bar{N}_T



PROJECT NO.: 79-153

USGS CPT-SPT

SAN JOSE SITES:
COYOTE NORTH & SOUTH
COMPOSITE \bar{N} PROFILES AND \bar{N}_S/\bar{N}_T

3. DATA ANALYSES

3.1 INTRODUCTION

Because the primary purpose of this research was to investigate the correspondence between CPT and SPT, facilitating use of CPT for liquefaction potential assessments, the investigations were directed mainly at definition of the form of CPT-SPT correspondence for soils in which the blowcount method of assessment is applicable (sands with less than about 30 percent fines). However, the correlations were examined for all natural soils encountered. These soils ranged from medium sized clean sands, to clayey fine sands possessing structural sensitivity. Only occasionally were pure clays encountered. The reason for examining these other soils is not only to allow prediction of particular SPT values but, more importantly, to allow increased certainty in the assessment of types of soils encountered in-situ. That is, without being able to differentiate soil types, it would never be clear when the CPT-SPT conversions would be valid and, therefore, when the CPT use for simplified liquefaction potential assessments would be valid.

The second requisite for use of the simplified method of liquefaction potential evaluation is a means to normalize CPT data in a manner eliminating the effect of overburden pressure. Such normalization would be directly comparable to the blowcount correction factor, C_N , which is used to adjust a blowcount to that expected for the soil if confined under an effective overburden pressure of one ton per square foot. The blowcount correction factor, C_N , or its equivalent for CPT

measurements, C_p , is a function of effective overburden pressure and, therefore, soil unit density and location of phreatic surface must be determined or reliably estimated.

Finally, the relation between CPT end bearing, q_c , and SPT blowcount, N , must be determinable from CPT measurements alone. Although a more satisfying approach to the estimation of liquefaction potential from CPT measurements would be through some strength or compressibility related factor, it is currently necessary to use the already-existing blowcount relation. Although such correlation may not be satisfactory for site-specific liquefaction potential assessments for critical structures, certainly the method is applicable to regional zonation or site specific screening to the extent of defining the existence or lack of a problem requiring more detailed site investigation.

Because the SPT is so widespread in U.S. application, and because the SPT is recognized as an uncertain measurement, several researchers have investigated the test, from equipment and procedures to theory and usage. Likewise, the relation between SPT and CPT has been investigated, and the CPT alone has been the subject of controlled studies. It is informative to review some of those studies.

3.2 PREVIOUS INVESTIGATIONS

3.2.1 SPT Research

When investigating use of an in-situ tool the greatest need is to establish a reference against which the measurements made

with the tool may be evaluated. For investigation in sands the most common reference is the SPT. Thus, not only the CPT and CPT-SPT correlations need be studied, but also the SPT alone.

The question of repeatability of the SPT as a result of natural in-situ spatial variability of soil properties or vagaries of equipment and procedure has been discussed at length by several authors (de Mello, 1971; Tavenas, 1971; Fletcher, 1965; Schmertmann, 1976; Kovacs, 1978). The message contained in these works is that although the SPT is beset with equipment and procedural difficulties, the test does provide useful information. Some 20 potential error sources are mentioned, and some results are cited showing up to a ± 100 percent error in SPT measurements under controlled conditions. Such errors tend to be largest at shallow depths. When such lack of repeatability is compounded by the use of different hammer energies (Kovacs, 1978; Schmertmann, 1976), and different C_N adjustments for depth (effective overburden), it is clear that use of any particular set of N values with the Seed blowcount method requires considerable caution. For example, Kovacs notes that the combinations of rope age, sheave speed, and driller effort also significantly affect the hammer-delivered energy, while Schmertmann (1976) shows that average energies delivered to the sampler by the common rope-around-the-cathead method are about 55 percent of the theoretical amount and that the actual energy entering the rods depends not only upon the hammer system but also the rod type and length.

Following this question of the effect of rod length, and hence, depth, upon entering and delivered energy is of interest in that the CPT measurements should depend upon effective overburden pressure but not upon rod length. Several researchers have examined the N - effective pressure relation (C_N) proposed by Gibbs and Holtz (1957) and have presented modifications. Notable among these are Bazarra (1967), Seed (1976), Peck, et al (1973), and Marcuson and Bieganousky (1977). These authors have identified soil type, relative density, and overburden and lateral pressure as the primary variables influencing blowcount, although other variables such as soil structure have been considered. In Figure 3.1, a plot is shown comparing the C_N relations suggested by these authors. The wide range in values at any pressure precludes certainty in selection of an appropriate N value correction factor. Further, it is of interest that the curves presented by Marcuson and Bieganousky developed using a free fall hammer with laboratory sands show reasonable agreement with those developed empirically. The Marcuson-Bieganousky studies did not include rod length as a control variable, yet Schmertmann (1976) showed rod length to have a significant effect upon hammer-rod system efficiency and, presumably, upon blowcount. In Figures 3.2(A) through 3.2(D) a progression is shown based upon the Schmertmann (1976) data whereby rod length is related through energy measurements to N values. The final figure, 3.2(D) shows a C_N curve for rod length alone (C_{RL}) in which it is noted that because of the lesser delivered energies at shallow depths, the blowcounts must be adjusted

downward rather than upward as is the usual case for C_N adjustments. It should also be noted that some research appears to disagree with the Schmertmann data (Steiger, 1980), and that perhaps the apparent rod length effects are primarily inertial and may be cancelled by other losses such as stress wave attenuation or joint energy losses. In summary, it is found that the overburden correction factor depends upon more factors than effective overburden pressure, and that published values of C_N factors constitute a range precluding precision.

3.2.2 CPT Research

The two primary factors relating to CPT measurements that are of concern to this study are the influence of soil type and overburden pressure upon the CPT measurements.

3.2.2.1 CPT versus Soil Type

The CPT provides two distinct indicators of soil type: the end bearing record (q_c) and the ratio of side friction to end bearing expressed as a percentage (friction ratio). Prior to development of friction cones, the end bearing record alone was used to identify soil types: high readings indicated sands and low readings, clays. In addition, the variation of the curve provided information about soil type and layering. However, the ability to predict soil types was greatly increased with the development of the Begemann (1964) friction cone penetrometer. Data compiled by Begemann formed the basis of the soil differentiation charts shown in Figure 3.3. In Figure 3.4 is a composite of the classification and blowcount versus CPT relations

developed by Schmertmann following Begemann and modified by data measured in Florida.

Schmertmann (1978) notes that his chart is appropriate primarily for the mechanical friction cone and that local correlations are preferable. Further, he notes that structural sensitivity can produce values not corresponding with the presented delineations, and that friction ratios are undependable at low values of end bearing.

Alperstein and Leifer (1976) present data in general agreement with the Begemann-Schmertmann relations, again developed with the mechanical friction cone. Campanella, et al, (1979) also show general agreement with those classification guidelines.

It should be noted that disagreement should be encountered when comparing data measured with the electric friction cone penetrometer to the mechanical cone penetrometer classification chart. Several factors contribute to such disagreement. First, the mechanical cone is not continuously penetrated; rather, the tip is advanced and then the sleeve is advanced. Second, the mechanical friction sleeve has a beveled leading edge which adds some contribution from end bearing to the measured sleeve values. Although it is widely recognized that the Schmertmann-Begemann chart is not entirely appropriate for use with the electric cone, no applicable charts or recognized relations exist, and so, the mechanical-cone-based chart is usually used.

Because the CPT is essentially dependent upon strength and compressibility of a given soil, information about soil type is only indirectly known. Soil type is inferred based upon the two different measurements provided by the electric CPT, and upon the relation between these measurements. The usual comparatives are end bearing and friction ratio, equal to ratio of sleeve resistance to end resistance. To understand the classification of soils using these factors, the measurements themselves must be fully understood.

The cone resistance increases in value for sands and gravel with increasing values of friction angle, in-situ relative density, or overburden and lateral stress. The relative density depends primarily upon stress history and method of deposition while friction angle depends upon mineral type, particle size and distribution, and relative density. Further, cone resistance in sands increases approximately as an exponential function of the friction angle. Although the sleeve friction depends upon the same factors, its resistance increases roughly as a linear function of the friction angle. Therefore, the friction ratio for sands should decrease with increased values of friction angle.

The cone resistance in clays is dependent on the clay type, in-situ strength, overburden stress and stress history. The sleeve resistance is dependent on the same items as the cone with special importance on the in-situ lateral stress (K_0 , which depends on the stress history, soil type and soil activity,)

and sensitivity. The resistance of the cone and sleeve are both generally related to a linear function of soil strength and should, therefore, show an essentially constant friction ratio with increasing strength.

Further complicating the understanding of penetration resistances is the existence of the so called limiting depth, and the controversy regarding basic failure mechanisms as evidenced by the use of both bearing capacity and cavity expansion theories. In addition, cone and sleeve measurements in soil types such as silts, clayey silts, sandy silts, sandy clays, and silty clays are even harder to understand because of the number of variables acting simultaneously. For example, the intergranular soil matrix in sands has a large effect upon the behavior of the cone and sleeve. Depending on the condition of the soil matrix and gradation of the coarse fraction, several conditions can occur, including dilation, structural breakdown, pore water pressure generation, transmission of penetration resistance from sand structure to soil matrix, and grain crushing.

During penetration of the cone, soil in a zone extending several cone diameters in front of the tip experience compressive stresses resulting in some pore pressure generation depending on soil permeability and the speed of cone advancement. Soil closer to the front of the cone experiences high shear strains as it is translated from in front of the cone to the side of the shaft. Such large deformations result in

rearrangement of the near-field soil structure. If the soil structure was initially loose and of high permeability, a denser zone develops in front of the tip. This zone then carries greater stresses until finally the zone fails and the cone resistance drops to the lower values indicative of the underlying non-densified soil, and the process begins anew.

Most of these questions of mixed soil-penetrometer interaction have been avoided, with research being directed at understanding of behavior of purer soils (Levadoux and Baligh, 1980; Mitchell and Lunne, 1978; Yong and Chen, 1976; Janbu and Senneset, 1974). Such research has resulted in clearer understanding of the penetration mechanics, particularly with respect to end bearing behavior. What is notably lacking is research into the significance and interpretation of side friction.

3.2.2.2 CPT versus Overburden Pressure

Little information is available quantifying the effect of increased overburden upon CPT results. What little information is available relates primarily to end bearing, and the constancy of friction ratio with increasing overburden is assumed (Schmertmann, 1976). Treadwell (1975) examined the effect of gravity (or force) upon the CPT penetration including evaluation of the work of Vesic, while Schmertmann (1976) empirically found a set of summary curves of q_c versus overburden pressure for normally consolidated, recent, SP sands. By normalizing his curves (q_c at 1 tsf divided by q_c at any pressure) a C_p curve is obtained. This curve is shown in Figure 3.5, where it can be compared to the more common C_N curves shown in Figure 3.1.

From examination of Figures 3.1 and 3.5, it can be noted that the C_p relation is within the band of C_N relations presented previously. However, assuming that the C_N curve does include the effect of rod length as well as pressure, the final curve of Figure 3.2 relating rod length to $C_N(C_{RL})$ can be used to adjust the Seed et al. (1976) C_N relation. The resultant quotient of these two curves is shown in Figure 3.6 where it is noted that, perhaps coincidentally, good agreement is obtained with the C_p developed from the work of Schmertmann. Such comparisons are of interest, but do not serve to adjust any actual C_N curves, as the effects of relative density and soil type are certainly larger than that of rod length. At this time no quantitative data appears available describing the effects of soil type, density and stress conditions upon the C_p appropriate for use with CPT measurements.

3.2.2.3 CPT Versus SPT

Penetrometers of numerous varieties have been used and correlation between the types studied (Sangerlat, 1972; Sangerlat, 1974). An early compilation of research results was provided by de Mello (1971) and is presented in Figure 3.7. A summary provided by Sangerlat (1972) is shown in Figure 3.8. Alperstein and Leifer compiled and extended existing comparative data as shown in Table 3.1. The comparisons found by Campanella, et al. (1979) are shown added to those of Table 3.1. It should be noted that many of these tabulations are based upon mechanical CPT results and that indicated soil types are often defined by visual classification only.

TABLE 3.1

SUMMARY OF REPORTED q_c/N VALUES
(from Campanella, et al., 1979)

Soil Type	Campanella, et al.	Alperstein and Leifer	Schmertmann	Simons	LaCroix and Horn
Micaceous silty coarse to fine sand, some clay	0-1.5	10	2	4	4-6
Micaceous fine sand, trace to some silt	1.5-3.5	5.5	3-4	4	4-6
Coarse to fine sand, trace to some gravel	3.5-7.0	9	5-6	4	4-6

The summation of these results shows that the ratio of q_c to N (for constant equipment and procedures) increases when moving from plastic (ductile) to nonplastic materials and with grain size in the latter case. Further, the above-mentioned authors all note that the q_c/N values are not universal and depend upon site specific characteristics. How much of this range results from variability in the SPT and how much from soil conditions is not known. Further, the mechanical CPT data usually provides only an average soil resistance over about six inches, while the electric CPT provides point data representing some weighted influence of a few inches of soil ahead and behind the cone. None of the available research defines whether or not the data was averaged.

The most complete summary of factors affecting the q_c -N comparisons is given by Schmertmann (1976) in which theoretical considerations of penetration energy are used to relate the components of penetration resistances for the different tests. Through consideration of the role of side and tip resistance in penetration through any soil, an equation relating the components of resistance was developed (Schmertmann, 1971):

$$N = (A+B*FR\%) * q_c$$

where N equals SPT blowcount, A and B are constants, FR is friction ratio, and q_c is end bearing in tsf. The equation can be converted to:

$$q_c/N = n = 1/(A+B*FR\%),$$

in which the dependence of the ratio q_c/N on friction ratio is clearly seen. A further modification proposed by Schmertmann (1976) gives:

$$q_c = N^a / (A+B*FR\%),$$

in which form nonlinearity is incorporated to better fit data obtained in low resistance soils. Schmertmann gives values for the various parameters as follows: $a=4/3$, $A=0.641$, $B=0.224$ for the case of fifty percent of the theoretical energy available in the SPT. A set of curves showing these relations is given in Figure 3.63 of a later section. The curves are also shown, in different form, as contours of constant N value in Figure 3.4.

The brief preceding discussion is not intended to represent a thorough review of the state-of-the-art of static and dynamic penetration. The discussion is designed to illustrate what specific CPT-SPT research has been performed. Further information can be found in the 1976 Schmertmann reference. This reference provides the most complete examination of the q_c -N relations available, and provides theoretical as well as empirical examinations. Further, some information is available regarding the relative influences of side friction and end bearing of the CPT and SPT on the measured results. This is of great importance in any but the most uniform, artificial soil deposits. This importance can be seen when examining what is actually occurring in each test. The SPT sampler is driven six inches into the soil. The blows required for the next twelve inches of penetration are the recorded blowcount. At the start of the final twelve inches of penetration, the sampler is already subjected to six inches of side friction. By the end of the test, eighteen inches of side friction are resisting sampler penetration. The electric CPT on the other hand, has a constant area throughout the penetration. The situation is further complicated when the zone of measurement passes through a change in soil type or resistance. In such case a weighting of the CPT resistances would probably result in better comparison with the automatic weighting that occurs naturally during the SPT. It appears that only little research has been directed at such non-uniform conditions, although such conditions are invariably the rule rather than the exception in-situ.

3.3 CURRENT INVESTIGATIONS

The following sections provide examination of all of the data measured during this investigation. The data is subdivided into three sections: CPT Classification of Soil Type; Correction of CPT Measurements for Overburden Pressure; and Correlation of q_c to N .

3.3.1 CPT Classification of Soil Type

The sites selected for investigation were primarily sand sites. Further, only a limited number of samples were obtained when clayey layers were encountered. For these reasons, the classification data described in the following sections is heavily weighted toward definition of saturated sand zones by use of the CPT measurements. As mentioned previously, the CPT provides two measurements, both of which are predominantly influenced by soil strength and compressibility. Research has shown strength of soils dependent upon density or relative density, stress level, soil structure, grain size shape and distribution, and physico-chemical characteristics. As combinations of these numerous variables exist in-situ, and because such combinations may vary rapidly, strength-based classifications may not always agree with other classifications such as those of the Unified Soil Classification System (USCS). However, soil classification is usually used as an index to define potential problems and their magnitude. These goals of soil classification are to large degree determinable by the CPT method.

The program of CPT soil type (or, more appropriately, soil-behavior type) classification was based, in large part, upon idealization of the profiles encountered in-situ. After preliminary idealization was complete, laboratory grain size analyses were performed upon select representative samples. During this phase two factors became apparent. First, the boring logs represent an oversimplified view of in-situ conditions and, second, the classification names are not necessarily good indicators of soil behavior. For example, a sand with 95 percent of the material lying between the number 100 and 200 sieve sizes is classified as a SP, while a sand having 95 percent of the material just finer than the number 200 sieve is classified ML.

Certainly the behavior of these two materials would not be expected to greatly differ. Further, a mixture of 45 percent sand, 45 percent silt (or sand finer than the number 200 sieve), and 10 percent of an active clay is classified as CL, while a soil having 60 percent material in the clay size range with low Activity is also classified as CL. For this case, it is expected that significant differences in behavior should occur.

Three different approaches were used to examine the effect of changing material type upon the CPT measurements. First, all SPT samples were classified, either in the laboratory or visually with reference to adjacent samples that had been classified in the laboratory. The laboratory classifications have been compiled in the boring logs shown in Appendix A.

Next, the CPT end bearing and friction ratio from an adjacent sounding were averaged over the length of the SPT sample. The points were then plotted, as shown in Figure 3.9. In that figure some attempt was made to divide the most troublesome classification, SM, into two groups: SM, having fines content between 12 and 30 percent, and SM-ML having fines content between 30 and 60 percent. Examination of the data in Figure 3.9 shows some fairly well defined zones of differing soil types. It should be recalled that anomalous points may easily result from spatial variability in-situ, or from the presence of an interface which would significantly affect the CPT measurements but may not be reflected in the retrieved sample.

Another method of comparison involved calculation of average properties and CPT measurements by zone within more or less well defined layers. This approach was selected to define trends in data, not the boundaries between soil types. As the averaging was also used for estimation of the q_c/N relation, those plots are shown in a later section. However, it may be seen that the indicated soil classification trends fall within the boundaries shown in Figure 3.9.

Because of the rapid variation in CPT measurements in-situ, some investigations of measurement variance were performed to facilitate selection of comparison points in well defined zones. Variance can be shown by plotting a continuous CPT sounding on the q_c -FR plot. A typical plot of this type is shown in Figure 3.10. The numbers on the sounding trace

represent depth in feet. By examination of the boring logs for depths at which the CPT trace stays in a small zone of the q_c -FR plot, soil classification information can be attached to those q_c -FR zones. Examples of classification by these zones are shown in Figures 3.11 and 3.12. Again, these zones compare well with the boundaries shown in Figure 3.9. To define the complete boundaries of different soil types using the continuous trace-zone method, several large layers of different uniform soils at different densities and pressures would have to be encountered. At present, no such collection of data is available.

A modification of the continuous trace method is to have the continuous record traced on the q_c -FR plots only over depths at which a sample was obtained. The behavior of the soil during CPT penetration is then immediately apparent. An example of this method is shown in Figure 3.13. In that figure it can be seen that some depths tend to have CPT measurements staying in a small zone of the q_c -FR plot, while other SPT depths show extreme changes in CPT. The logic is that comparison of points in which the CPT is radically varying will be futile. An average value calculated for a limited trace ranging from sand to clay zones would show some intermediate classification, such as sandy clay. If, for example, the Schmertmann (1976) method of computing an equivalent CPT side friction and end bearing from incremental measurements of the SPT penetration was used with resultant similarity in behavior to the CPT trace, then neglecting the differences between

static and dynamic behavior would allow comparison of the two measurements.

The approach used in the limited trace method was to select for comparison only SPT values where the adjacent CPT measurement stayed within a small zone. The implicit assumption is that the SPT measurement would show similar constancy if treated using the incremental method. As with the layer-average method, the data from the limited-trace method is also used in comparison of the q_c/N ratio and, therefore, data plots are presented in subsequent sections. Review of that data does show agreement with the zones and boundaries shown in Figure 3.9.

As an extension of the classification data already presented, some select data obtained from the Edmond, Oklahoma site is presented. The reason for presentation of select data only is the heterogeneity of the site. Initial attempts at profiling of the site showed only the most generalized layers: from zero to about twenty feet are sandy clays, from twenty to about 60 feet are mixed soils (clay, silt, sand in varying percentages), and from 60 to about 80 feet is relatively clean sand with occasional lenses or stringers of sandy or clayey silt.

However, at any particular depth, a soil encountered in one boring or sounding may not be encountered in a second boring or sounding at the same depth at a distance of only a few horizontal feet. Even when the same soils are encountered, the penetration resistances are often quite different.

The CPT sounding logs usually evidenced the most disagreement with boring logs in the twenty to sixty foot depth zone. The most common material in which traditional CPT classification differed from the boring logs was a soil mixture consisting of about sixty to seventy percent fines with ten to twenty percent being clay-sized particles with a PI of about four to fifteen. Further examination of the CPT logs in these soils showed uniformly low friction ratios (one-half to one percent) with the smooth end bearing usually associated with plastic soils. It was noted that the soils typically had water contents close to the measured liquid limits, thus having a Liquidity Index (water content - Plastic Limit divided by Plasticity Index) close to unity.

A plot of the Liquidity Index of these CL-ML and CL soils is shown against measured q_c and FR in Figure 3.14. It can be noted that the apparent trend is for increasing Liquidity Index with decreasing cone side friction or, with decreasing end bearing and friction ratio. This fact is particularly important when recalling that friction ratios this low are generally associated with clean sands. Also of interest is the location of the boundary of the zone in which these soils having measurable Liquidity Index exist. A sand, not having a PI, has an undefined Liquidity Index. The boundary of soils found to have a Liquidity Index is very similar to the SM to SM-ML boundary shown in Figure 3.9.

Examination of the data in Figures 3.9 through 3.14 shows that general trends in soil type classification using the CPT method

seem to follow lines of constant side friction as well as of end bearing and friction ratio. That is, soils with a high specific volume (volume per unit mass) (clays) occupy the zone of high friction ratio, with increased overburden stresses (or depth) resulting in higher side friction and slightly increased friction ratio. Intermediate specific volume soils occupy the range between the clay zone and the sand zone, again with increasing side friction and friction ratio resulting from increased overburden stress. In this zone anomalous behavior can result because of the different compressibilities of the coarse and fine fractions. For soils in which the sand content is high enough (40 percent?) to form a continual interlocked structure, the application of overburden stress results in essentially sand-like compression of the structure, leaving the interstitial clay fraction in an psuedo-underconsolidated state. The application of large amplitude undrained shear strains collapses the sand skeleton, with resultant increase in pore pressure response and decrease in effective stresses, particularly with respect to the friction sleeve. This behavior causes the reduction in friction ratio observed for soundings in a given material as Liquidity Index increases. This use of Liquidity Index is as a measure of soil structural sensitivity. Sensitivity in clays is known to reduce friction ratios (Schmertmann, 1978). As lines of constant side friction are followed into zones of higher end bearing, sands of decreasing relative density are encountered, again with increasing overburden causing increasing side friction. A summary of these expected

trends is given in Figure 3.15. It should be emphasized that these trends are hypothesized on the basis of limited amounts of data, and do not rigorously account for the effect of interaction of all the shown variables.

3.3.2 Correction of CPT Measurements for Overburden Pressure

Comparison of CPT data with other CPT or SPT data requires some normalization to account for the effect of overburden stress on the measurements. Current methods of adjusting SPT blowcounts make use of the C_N factor. This factor is the subject of continuing research and, at present, is only poorly defined (that is, a wide range of values have been proposed as appropriate at any particular pressure). Because it is intended to relate CPT to SPT, a possible approach is to convert CPT to the corrected SPT value: $N_1 = N C_N$. The use of a particular C_N relation to adjust CPT data would be appropriate if the relation of q_c to N was constant with increasing overburden. In the next section it is shown that the relation is not constant and, therefore, a different correction must be used.

Examining the range of C_N shown in Figure 3.1 reveals that C_N uncertainty precludes certainty in prediction of the CPT correction factor, C_p . Although it is known that relative density, soil type, stress history, and structural anisotropy and sensitivity all affect such corrections, the appropriate weighting to account for each variable is not known.

Three methods were selected for examination of the C_p relation with increasing overburden. The simplest was simply a

modification of the existing C_N curves by quantitative removal of the influence of rod length. This has been discussed previously. The second approach was to select a site of constant material type with constant depositional history, thus leaving effective overburden pressure as the only variable. The third approach was to correct all N values to the 1 tsf overburden using a standard C_N relation, and to then divide each corrected blow-count by the uncorrected CPT end bearing, resulting in the parameter needed to equate q_c and N_1 . This parameter (C_{p1}) is equal to an overburden correction to CPT readings (C_p) divided by a constant q_c/N relation.

Three sites were selected as being most appropriate for examination of the C_p relations: the San Diego Site at North Island, the Salinas site, and the Sunset Beach site. Although all of these sites are of essentially constant material type, examination of the CPT records (Appendix A) shows lack of uniformity of penetration resistance. However, by comparison of select points an indication of the implicit in-situ C_p behavior is evidenced.

In Figure 3.16 plots are shown of the q_c -effective overburden pressure relation proposed by Schmertmann (1976) as well as those developed by Treadwell (1975) and Vesic (1972). Superimposed on that plot are the average relations found at the Sunset Beach, Salinas and San Diego sites. It is seen that no relation of the type found by other researchers completely fits the in-situ measurements. The data in Figure 3.16 suggests that either Relative Density is constantly changing, or that

the material type is constantly changing. In either case, it appears that none of the investigated sites had complete uniformity of soil type and/or density. The normalization of the curves shown in Figure 3.16 by the value of end bearing at an effective overburden pressure of 1 tsf produces a C_p curve differing from that presented by Schmertmann, as would be expected if Relative Density is constantly changing.

The next method of C_p investigation is based upon the concept that the q_c/N relation is a function of confining stress. This variance in q_c/N is discussed more fully in subsequent sections. At this point the variance is assumed and a factor to account for such variance is advanced. If C_p were equal to C_N , then q_c/N would be constant for constant soil conditions. The appropriate relation is:

$$N \cdot C_N = (q_c \cdot C_p) / n$$

where C_N , n , and C_p are all functions of confining stress. Carrying the relation one step further allows definition of an equivalent C_{p1} by which an equivalent N_1 may be estimated:

$$N \cdot C_N = N_1 = q_c \cdot C_p / n = q_c C_{p1}, \text{ or}$$

$$C_{p1} = \frac{N_1}{q_c},$$

where $C_{p1} = C_p / n$

In Figures 3.17 and 3.18, plots are shown of N_1/q_c where q_c is the average end bearing measured over the one-foot depth interval at which the blowcount was recorded in an adjacent

boring. Likewise, the friction ratios shown in those figures are the average over the one-foot interval. The trend lines shown in the figures represent the behavior of material with an average friction ratio less than 2.0 percent (essentially sandy soils). The scatter in C_{p1} with pressure is a probable result of the variation in relative density at constant pressure, as was seen in Fig. 3.16.

It is of interest to note that although the trend of the relation based upon the trip-hammer measurements is similar to that of the standard hammer, the scatter seems greatly diminished, a result possibly caused by the inherent "smoothing" of variable resistance layers when using the higher energy trip hammer. As the hammer total weights are similar, as were rate of application of blows, inertial effects or pore pressure effects were discarded as causative factors.

In hopes of reducing the data scatter, two variants of the above method were included: the use of average end bearing and N values selected from well defined layers only, and the use of points selected on the basis of uniformity of CPT record as described previously. The results of these investigations are shown in Figures 3.19 through 3.22. The indicated trends reveal the increased scatter using the standard hammer, but also reveal the constancy of the trend regardless of method used. The trip hammer curves also show the similarity of trend regardless of method. In addition, the trip hammer curves are relatively well defined. The comparison of the C_{p1} relation

to C_p needs estimation of the trend of q_c/N with increasing overburden. Thus, such comparisons are relegated to a subsequent section.

The practical significance of the data scatter is small when compared against the scatter that normally results from the spatial variability of soil type and relative density in-situ. With such consideration, it is clear that selection of an overburden correction factor, C_p or C_N , must invariably produce only a rough estimate of the actual normalization factor appropriate for any particular soil.

3.3.3 Correlation of q_c to N

The precise correlation of CPT end bearing to SPT blowcount requires that measurements be performed under similar conditions of soil type, stress state, density and fabric, and particle size, shape, and distribution. Most of these similarities will only generally be found in an in-situ comparative program. For example, Tavenas (1971) shows the range of N values obtained at single, supposedly uniform site using a single crew with equipment and procedure carefully controlled. His explanation for the N value scatter is advanced denying the repeatability of the test under even ideal conditions, an explanation which ignores the natural spatial variability of penetration resistance in even the most uniform of sites. Review of the CPT logs of Appendix A further reveals this natural variability, for the CPT is a carefully controlled test in which equipment, crew, and procedure have been eliminated as error sources.

In fact, the careful elimination of error sources has provided even more proof of spatial variability in-situ. Any of the sounding logs presented in Appendix A reveal the presence of pockets or lenses of dissimilar materials within supposedly homogeneous layers. This heterogeneity is particularly evident when examining the sounding traces on the soil classification chart as presented in Section 3.2.2.1. Further, such inter-layering can produce arching stresses resulting in non-uniformity of vertical stresses. As any penetration measurement is dependent upon soil type, density, and overburden stress, as well as stress history and age of the deposit, it is difficult to isolate the effect of a change in any single variable in-situ.

Several methods of data presentation are used in the q_c/N comparisons in order to well define the trends with changes in different variables. The range in q_c/N possible within any layer at a site was first examined. Next were comparisons of all measured N values with corresponding CPT measurements at the same depths in adjacent soundings. Average values of N and q_c by layer were compared and, finally, the comparisons were made for select depths at which the end bearing and friction ratio trace showed constant soil conditions. Using each method, several variables are isolated: q_c/N versus friction ratio; q_c/N versus N ; q_c/N versus q_c ; and q_c/N versus depth.

3.3.3.1 q_c/N Range Comparisons

With a goal of using the CPT for the equivalent blowcount method of liquefaction potential assessment, it is informative

to examine the range in q_c/N that could possibly be encountered at any site. The blowcount method is not a continuous test in that samples are usually taken at a maximum frequency of 3.0 feet and the results represent a weighted average of between 18 and 12 inches of soil resistance. Thus any particular horizontal and vertical location within a site boundary selected for testing can have a significantly different resistance than any other area selected.

The procedure used to investigate this range was to divide the profile into three foot thick layers and to tabulate the upper and lower bound of all SPT and CPT measurements made in each layer. By comparison of the maximum CPT with the minimum SPT a maximum q_c/N is obtained. Likewise, the minimum CPT and maximum SPT gives the minimum possible q_c/N . Comparison of maximum CPT with maximum SPT, and minimum SPT with minimum CPT bound the probable range. "Probable" is based upon the assumption that the most significant resistance variations within any horizontal layer occur at the widest horizontal separation of measurements, and that site investigations using either method will probably have similar horizontal distribution of measurements.

The results of these range comparisons are shown in Figs. 3.23 through 3.26 and 3.27 through 3.30 for standard hammer and trip hammer measurements, respectively. Also shown in those figures are the soil layers that show continuity of depth and general material type across the entire site. However, it should be noted that the layers do include a range of materials within a general soil classification such as sand or clay.

It can be seen in Figs. 3.23 through 3.30 that the probable range for sandy soils using the standard hammer is about 2 to 5 and about 3 to 10 for the trip hammer. This large range for the trip hammer is surprising in that it would be expected that because sampling energy is more controlled, the comparisons would show reduced scatter. However, in this program the standard hammer measurements were also carefully controlled with respect to drop height, frequency, rod inclination and rope obstruction. Composite plots of all blowcounts measured with each hammer at each site are shown in Figs. 3.31 through 3.35 where the greater variability of the standard hammer measurements is apparent. Further, examination of the average blowcount versus depth profiles of Section 2.4 reveals that the standard hammer profiles show better general agreement with the CPT profiles than do the trip hammer profiles. The higher energy of the trip hammer appears to extend the zone of influence in front of the sampler as compared to the lower energy standard hammer. This would result in an averaging of thin variations in penetration resistance. Such an averaging would be much less pronounced for the CPT measurements, producing the wider q_c/N range for the trip hammer comparisons.

3.3.3.2 q_c/N Versus Depth

Examination of the ranges in q_c/N versus depth (or effective overburden pressure) presented in the preceding section indicates the need for further refinement. As a first step in such refinement, the comparisons were performed for average measurements within each layer identified as continuous. Thus, if a

layer was dipping in cross section, the averaging procedure would exclude those zones bounded by the dipping-layer interface.

Figures B.1 through B.4 of Appendix B show q_c/N versus depth for each site, and Figure 3.36 presents a composite of all such data. Again the standard hammer qualitatively shows less scatter than the trip, and it is apparent that the q_c/N ratio tends to decrease with depth for constant friction ratio materials. Examination of the behavior of friction ratio with increasing depth for constant grain size and distribution materials shows slight increases with depth. However, such an effect is small for constant materials, and does not appear to be the cause of the reduction in q_c/N with depth (or more appropriately, with increasing effective overburden pressure). The scatter in values is not particularly well tracked by the friction ratio; however, recall that horizontal and vertical averaging was used within each layer and that the resultant average friction ratios probably are not weighted in a manner equivalent to the averaging of the N values.

It is of interest to compare the q_c/N versus depth relation with that predicted by the Schmertmann relations. In Figure 3.37 the effect of increasing effective overburden pressure on the q_c/N ratio is shown for soils having friction ratios indicative of sands for which Relative Density is an appropriate parameter. These data are drawn from a variety of measurements and, therefore, the portrayed behavior should be regarded qualitatively. It is seen that in all cases the

q_c/N relation rapidly increases with increasing pressure, a trend not supported by the data measured in this program.

Examination of the effect of increasing overburden on q_c/N may also be through comparison of q_c/N versus depth plots for all blowcount measurements. Such an approach will, of course, produce significant scatter because of the inherent spatial nonhomogeneity of natural soils. However, trends should be apparent. In Figures B.5 through B.8 are shown the comparisons for the standard hammer measurements, and in Figures B.9 through B.12 for the trip hammer measurements. Examination of those figures reveals the same trends as noted previously: the q_c/N ratio decreases with increasing depth.

Finally, the effect of overburden on the q_c/N ratio can be through examination of the behavior evidenced by points selected on the basis of the uniformity of the CPT record over the blowcount depth interval. This approach depends completely on the assumption of horizontal uniformity of soil type and resistance. The criteria by which uniformity of CPT measurement is defined has been described in Section 3.3.2.

The composite plots of q_c/N versus depth for select points from all sites are shown in Figs. 3.38 and 3.39 for standard and trip hammer measurements, respectively. It can be seen that as in the other plots, the q_c/N ratio decreases with depth and, therefore, with increasing effective overburden pressure. The decrease seems to hold for all materials (as represented by constant friction ratio) and, again, trends

are better defined for the standard hammer than for the trip hammer.

In summary, it has been shown by a variety of comparisons that the q_c/N ratio decreases with depth, and that the tendency for increasing friction ratio with depth is not large enough to account for such decreases. This observation is directly contrary to the relations suggested by Schmertmann (1976). However, as discussed in subsequent sections, there are equipment differences that may account for such discrepancies between the Schmertmann data and the data presented herein.

3.3.3.3 q_c/N versus N

As described in preceding sections, the influence of the N value upon the q_c/N ratio was investigated through examinations of layer average values, of all individual measurements, and of select points. Figures B.13 through B.16 of Appendix B show the layer average data from each site, and Figure 3.40 shows the composite of all such comparisons. Also shown in Figure 3.40 is the apparent qualitative trend line through the data, showing a decrease in q_c/N with increasing N .

The presentation of all individual measurements of q_c/N versus N is in Figures B.17 through B.20 and B. 21 through B.24 for standard and trip hammer, respectively, for each site and the data is summarized in Figure 3.41 for standard hammer measurements and Figure 3.42 for trip hammer measurements. Again the trend line is shown and it is apparent that the standard hammer comparisons show less scatter than do the trip

hammer results for the same reasons as discussed previously, and that the q_c/N ratio decreases for sands with increasing blowcount.

Finally, the results of the q_c/N versus N comparisons for all sites using select CPT measurements are presented in Figs. 3.43 and 3.44 for standard and trip hammer measurements respectively. Again, the trend lines are indicated in the figures, and show generally decreasing ratios with increasing N value.

In summary, the qualitative trends show consistent disagreement with the Schmertmann (1976) relations in which q_c/N increases with increasing N value. The disagreement between the data presented herein and the Schmertmann data is expected based upon the disagreement in trend of q_c/N with depth as noted in the previous section. The correspondence of increasing N with increasing depth forces such concurrence. However, by examining the relation as dependent upon different variables, more certainty is obtained that the trends are not just coincidental to any one set of comparisons. Again, a reason for such disagreement is advanced in the following section.

3.3.3.4 q_c/N versus q_c

The results of the same set of comparative measurements as used previously but applied to q_c/N versus q_c are shown for layer averages in Figures B.25 through B.28 and summarized in Figure 3.45; for all individual measurements in Figures B.29 through B.36 and summarized in Figures 3.46 and 3.47 for standard and trip hammer measurements, respectively; and in Figures 3.48 and

3.49 for select points with standard and trip hammer measurements, respectively. The qualitative trend lines of individual comparisons all show essentially the same behavior:

q_c/N remains essentially constant with increasing q_c using the standard hammer, and increases slightly when using the trip hammer. Comparison of these summary trends with the Schmertmann (1976) relation again shows general disagreement, as would be expected based upon the previous comparisons. However, in this case Schmertmann shows a definite increase in q_c/N with q_c , while the data presented herein shows either a constant relation or one slightly increasing with increasing q_c . Again, it is expected that as depth increases, the blowcounts and end bearing should also increase. However, the values don't necessarily increase at the same rate. In fact, examination of the C_N and C_p curves of Figure 3.6 shows that q_c will increase faster than N , particularly at the low effective pressures studied in this program.

As a further explanation of differences between the data presented herein and that presented by Schmertmann, Figure 3.50 shows a relation presented by Schmertmann (1978) between end bearing of a mechanical cone penetrometer and an electric cone penetrometer. It can be noted that at low values of end bearing, and hence at shallow depths and low N values, the mechanical cone shows higher resistance than the electric cone, and that at higher end bearing values the electric cone measurements are higher than the mechanical. Thus, because the

Schmertmann data is primarily based on the mechanical cone, it follows that his q_c/N ratios would be higher than presented herein at shallow depths, and lower at greater depths.

3.3.3.5 q_c/N versus Friction Ratio

As discussed in Section 3.2.2.3, previous research has shown q_c/N to be a function of Friction Ratio. Essentially, as side friction (and thus, friction ratio) increases at a constant end bearing, the total penetration resistance, either SPT or CPT, also increases. Therefore, the dependence of q_c/N on friction ratio is actually just the result of the equality of total penetration resistance when measured with either the SPT or CPT. That is, the SPT N value represents total resistance, while both the CPT end bearing and sleeve friction must be used to represent total resistance.

The results of the comparisons of q_c/N with friction ratio using the layer average method are shown in Figures B.37 through B.40 of Appendix B, and are summarized in Figure 3.51. Likewise, the results of the individual point method are shown in Figures B.41 through B.48 and are summarized in Figures 3.52 and 3.53 for the standard and trip hammer, respectively. Finally, the results of the select point method are shown in Figures 3.54 and 3.55 for standard and trip hammer measurements, respectively. The summary qualitative trends show essentially the same behavior as indicated by Schmertmann (1978) with differences probably due primarily to the different cones used in this study (electric) and by Schmertmann (mechanical). Of

primary concern regarding this data is the scatter evidenced using either the standard or trip hammer measurements. Again, however, it must be emphasized that the natural heterogeneity of the investigated sites precludes certainty that adjacent CPT and SPT measurements are made in identical soils. Therefore, the average q_c/N versus friction ratio measurements probably do represent a good indication of the behavior that would be expected if the measurements were made in identical soils.

3.3.3.6 q_c/N Versus Median Grain Size

As was discussed previously, the classification of soil types using the USCS system is not particularly appropriate for CPT investigations. The primary reason is that the USCS methodology divides soils by grain size and distribution and by a more or less arbitrary set of laboratory strength measurements. Often, but not always, these indices do provide information about expected in-situ performance of the soils. However, examination of the behavior of soils around a penetrometer indicates that other factors are of importance. In an attempt to provide some means by which the standard classifications could be subdivided, median grain size was examined for its effect upon the q_c/N ratio.

Plots of median grain size, D_{50} , against q_c/N are shown in Figures 3.56 and 3.57 for standard and trip hammer measurements, respectively. Essentially, no relation is apparent for non-clay soils other than that the trip hammer laboratory tests tended to be performed on a more constant grain size material

than used for the standard hammer laboratory tests. It is not particularly surprising that D_{50} is poorly related to q_c/N , in that it has been shown that q_c/N varies primarily with stress level, soil type, and equipment types. D_{50} relates only to soil types, and then is only useful for extremes, providing no information helping to define differences between similar soils such as SM and ML. It is probable that some combination of grain size information could help distinguish soil types. Such a combination could be D_{50} and the coefficient of uniformity (C_u), or perhaps, a combination of sphericity, D_{10} , and C_u or Coefficient of Curvature. cursory examination of these factors as a part of the investigations described herein identified no predictive trends.

3.2.1.7 q_c versus N

The most fundamental comparison of the correspondence between CPT and SPT measurements is necessarily the comparison of q_c to N as a function of friction ratio or side friction. However, as this relation is the primary goal of the research program, it is best presented after the trends of the relation with other factors have been estimated. The summary plots of the preceding four sections have, in effect, defined the expected behavior of the q_c versus N relation as N, q_c , friction ratio, and depth (or overburden) are varied.

The q_c versus N plots for layer averages are shown in Figures B.49 through B.52 of Appendix B, and a composite summary is shown in Figure 3.58. The qualitative best fit to the data is

also shown in Figure 3.58. It should be noted that where ambiguities exist, the trends from previous sections have been used to guide the curve fitting.

Following the same methods as used previously, the individual data comparisons of q_c versus N are shown in Figures B.53 through B.60 and are summarized in Figures 3.59 and 3.60. Again, data trends are indicated in the figures. Finally, the select point comparisons are presented in Figures 3.61 and 3.62 for standard and trip hammer measurements, respectively.

It can be seen in Figures 3.59 and 3.60 that the expected relation between q_c , N and FR is well defined for the standard hammer but shows some unexpected trends for the trip hammer comparisons. In Figure 3.63 the average q_c versus N relations for the standard hammer are shown compared against the Schmertmann (1976) relation. The trends are similar with differences probably resulting from differences in cone and hammer types, as discussed previously. In Figure 3.64 a plot of the trip hammer q_c versus N results is shown. Several factors of interest emerge in examination of these figures. First, the ratio of blowcounts for the trip and standard hammers at a specific q_c is not constant but increases with friction ratio and increasing soil strength. Second, the trip hammer curves show the same general trend toward decreasing q_c/N with increasing N as do the standard hammer curves. However, in the low friction ratio zone (less than 2.0 percent) the trip hammer curves show two curvature reversals, suggesting

either a reduction of q_c or an increase in N in the zone of q_c less than about 75 tsf. As no such anomaly is seen in the q_c versus N for the standard hammer, it follows that the N values are the anomalous data.

Following this trend of trip hammer behavior, q_c versus N comparisons were made for select points from the Edmond, Oklahoma site. The results of these comparisons are shown in Fig. 3.65, where it is seen that the Corps of Engineers hydraulically driven trip hammer provides higher energy than the Pilcon trip hammer and that again some trend for double curvature of the q_c versus N relation exists.

The use of a high energy hammer probably is the cause of many of the difficulties in data comparison. As was discussed previously, it is probable that the greater the hammer energy, the greater volume of soil ahead of the sampler which will influence the resistance to penetration. Thus the higher the hammer energy, the more each measurement represents an average of soil characteristics in the vertical plane. An indication of this effect can be seen for the lower energy penetrometer data presented by Treadwell (1975) in Fig. 3.66. Based upon the behavior shown on Figure 3.66, it was considered that the CPT data could be iteratively averaged over successively larger vertical extents until continuity of q_c versus N was obtained. However, it is probable that the CPT vertical averaging would need include some weighting function, requiring more information about the interrelation of dynamics of the SPT failure mechanism and the CPT failure mechanism than is presently known.

As a further attempt to relate q_c and N for the heterogeneous Edmond site, data was compared using Plasticity Index (PI) and FR as control variables. The COE Design Memorandum (1980) for the Edmond site shows blowcounts tabulated by range of Plasticity Index. The average corrected blowcount versus depth relations for ranges in PI are shown in Figure 3.67. It can be noted that no distinct trends are evident. However, the PI of a soil is basically a measure of strength potential and may not indicate anything about the actual strength of the sample under field conditions.

Next, the CPT measurements were compiled by elevation and then averaged by friction ratio bands. Thus, the averaging process excluded all measurements having friction ratios outside of the range of interest. Preliminary examination of the CPT data revealed extremely low side friction measurements concurrent with end bearing behavior indicative of plastic soils. A computer run was performed segregating the CPT values into average profiles for friction ratio bands of 0 to 0.5, 0.5 to 0.8, 0.8 to 2.25, 2.25 to 3.25, and greater than 3.25. Examination of the range averages shown in Figure 3.68 reveals maximum and minimum ranges of end bearing for each select friction ratio band increasing with friction ratio, behavior contrary to usual. It can be noted in Figure 3.68 that in the 0.0 to 0.5 friction ratio band the average profile has a very low magnitude of end bearing. Thus for soils supposedly non-plastic, extremely low strengths are evidenced. However, for friction ratios in the 0.8 to 2.25 range (still typically sands based upon the literature)

the end bearing values increase substantially. Thus, it appears that this FR range best compares with the blowcounts taken in the non-plastic soils. However, when examining the q_c (adjusted for overburden pressure) over N_1 ratio for this friction ratio band and blowcounts in materials of PI less than 3, only an ill defined ratio is found, as shown in Figure 3.69.

Further examination of the blowcount data revealed a trend in blowcount and side friction for a given material as a function of increasing Liquidity Index (LI). The effect of LI on side friction was shown in Figure 3.14. The trend of N_1 versus LI is shown for select points in Figure 3.70. Note, however, that the LI of a sandy soil with only 10 to 20 percent clay sized particles may not always be a good indicator of in-situ strength. Further, as shown previously, it appears the LI increases for constant end bearing and decreasing side friction. Thus, it would be expected that low side friction soils would have high structural sensitivity. Because the LI of a soil essentially indicates degree of consolidation, and because these data points were in general from a depth of 30 to 60 feet, it follows that the clay size interstitial material is underconsolidated, being prevented from fully consolidating by the sand fraction skeleton, which in turn is supported by the clay particles against any vibration induced densification. However, when sheared to large strains by the passage of a cone or split spoon sampler, the interstitial underconsolidated, high water content soils allow overriding shear of the granular phase without the sliding and interlocking resistance encountered

in cleaner sands. This behavior, then, is similar to the flowing of cleaner sands after the onset of liquefaction.

Examination of soil grain size distribution corresponding to high LI revealed some pattern. Typically, all material was finer than the number 40 sieve, was classed as CL-ML or CL with PI about 4 to 15, had about 60 to 80 percent material finer than the number 200 sieve, and had about 10 to 25 percent clay sized particles. However, no boundary was found for grain size distribution figures dividing "flowing" and nonflowing mixed soils.

The existence of soils with PI as high as 20 in the zero to 2.0 percent friction ratio band invalidates the comparison of N values for PI less than 3 soils with end bearings for the 0.8 to 2.25 percent friction ratio band. Rather, the classification of soil types by combinations of end bearing and friction ratio is necessary. This is in agreement with the classification boundaries shown previously in Figure 3.9. These criteria were then used to select sands and the CPT data again segregated by bands of q_c and FR. This average corrected end bearing curve, Figure 3.71, was then compared against the less than PI equal 3 blowcounts. The results of these comparisons are shown in Figure 3.72. It can be seen in that figure that the scatter in q_c/N is reduced. However, it is still apparent that the q_c/N relation is erratic, particularly in the deep-sands zone. Recall that the indicated reduction in q_c/N for these high resistance sands was noted in examination of the double curvature

and resultant decrease in q_c/N shown previously in Figure 3.65, and may be the result of transition between compressive and dilative-structure with resultant pore water pressure effects.

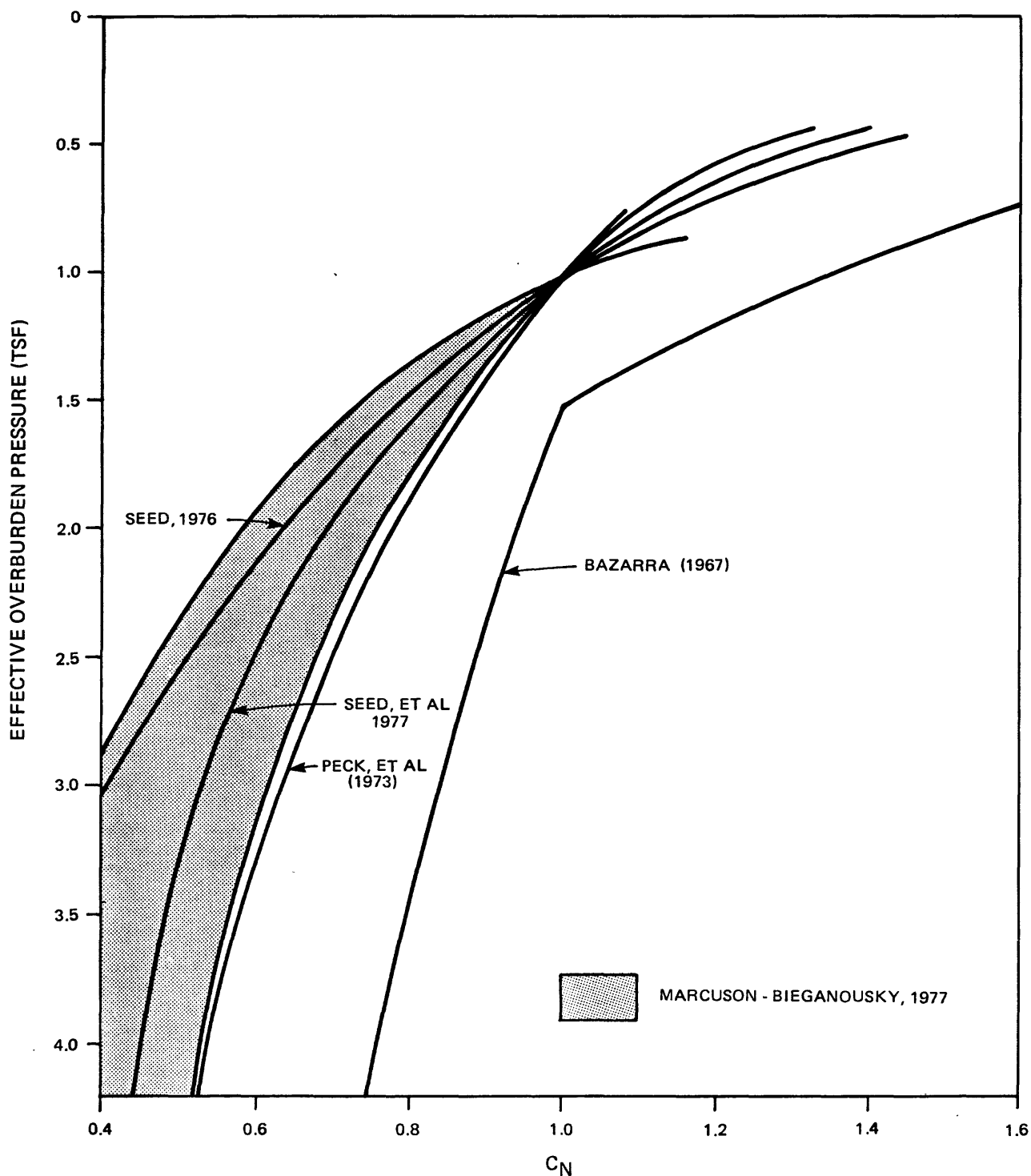
3.3.3.8 Comparison of N and CPT Side Friction

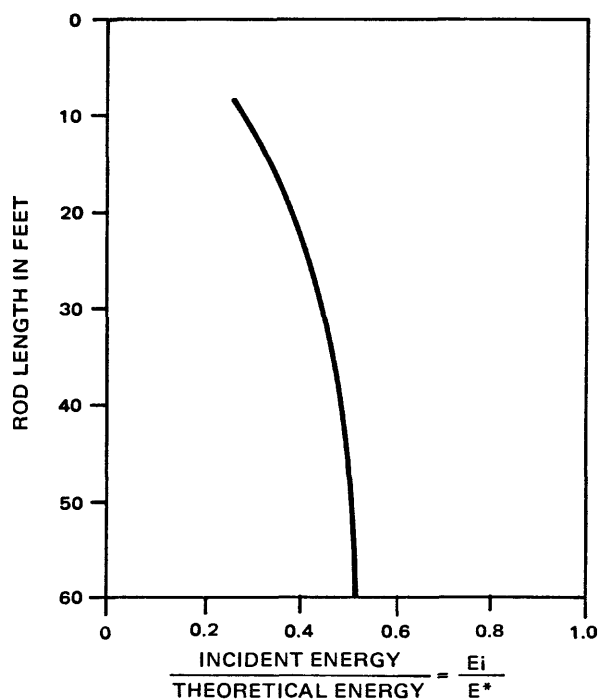
As a final comparison, all N values were plotted against the average side friction measured in an adjacent CPT sounding at the same depth. The results of this comparison are shown in Figures 3.73 and 3.74 for standard and trip hammer measurements, respectively. The trend in N with increasing side friction is apparent in both measurements; however, no attempt was made to refine the correlation through cross plots of side friction and q_c or FR versus N value.

3.3.3.9 Summary of q_c/N Relations

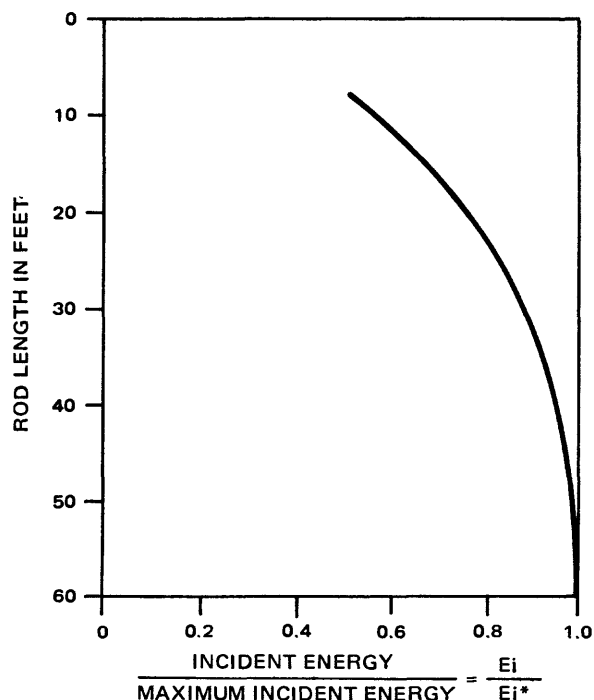
In order to examine the total range of q_c/N values described in the preceding sections, frequency histograms were prepared, as shown in Figures 3.75 through 3.78. In Figure 3.75 the layer-average data is presented for trip and standard hammer measurements. In Figure 3.76 and 3.77 the compilation of all individual comparisons is by hammer type and friction ratio band, while in Figure 3.77 all data is composited by hammer type alone.

Approved by _____
Checked by _____
Drawn by _____
Compiled by _____

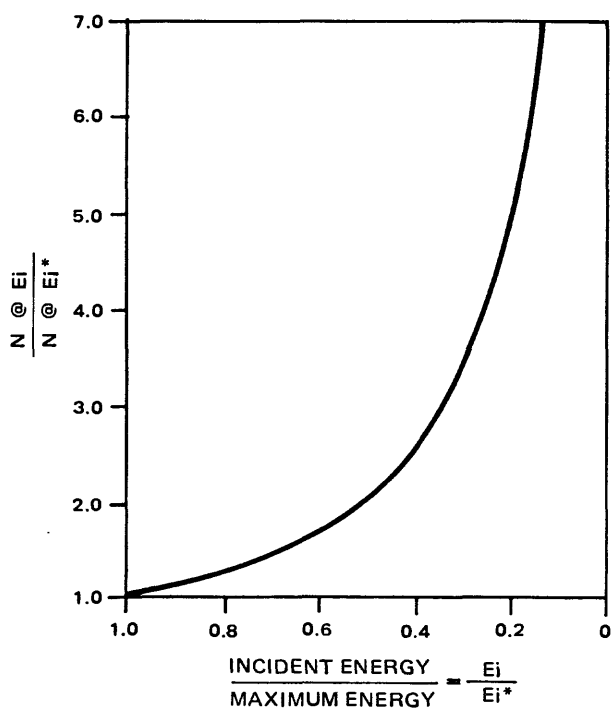




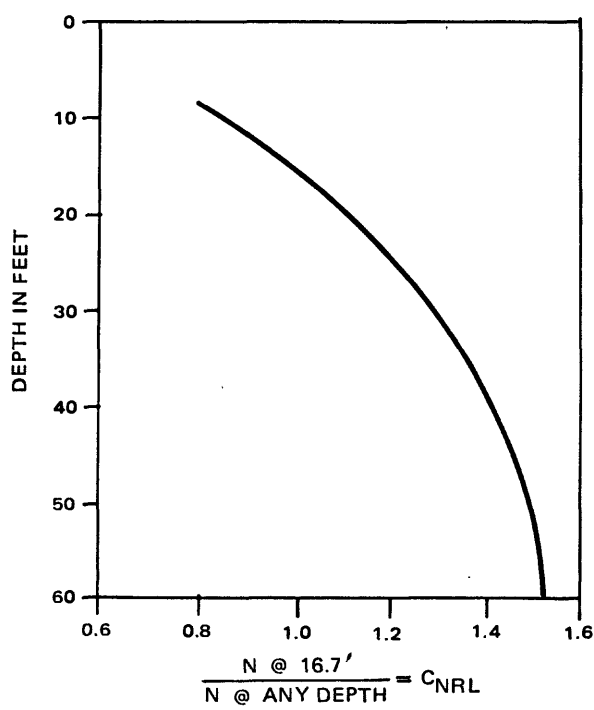
(A)



(B)



(C)



(D)

FROM SCHMERTMAN (1976)



PROJECT NO :

79-153

USGS CPT-SPT

EFFECT OF ROD LENGTH ON SPT BLOWCOUNTS

Compiled by _____
Drawn by _____
Checked by _____
Approved by _____

PERCENT PARTICLES < 16 μ

0 5 15 25 35 45 65 85 95

END BEARING (TSF)

100

10

1

COARSE SAND WITH GRAVEL
FINE SAND

SILTY SAND

SILT, CLAY, SAND

LOAM

CLAY LOAM

CLAY

1

2

3

4

5

6

FRICTION RATIO, %



PROJECT NO.:

79-153

USGS CPT-SPT

CPT SOIL CLASSIFICATION
BEGEMAN METHOD

9-80

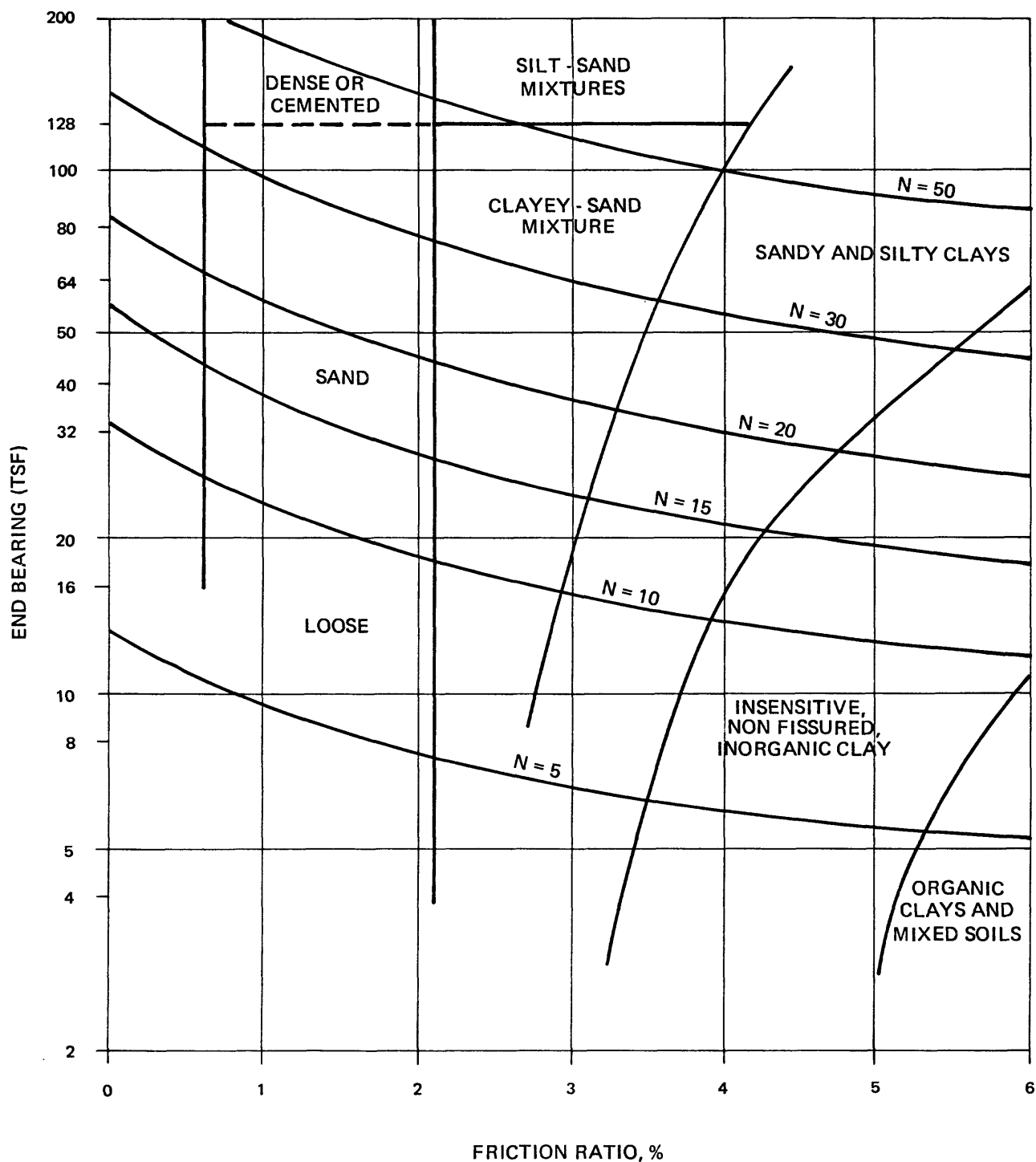
FIGURE 3.3

Approved by

Checked by

Drawn by

Compiled by



PROJECT NO.:

79-153

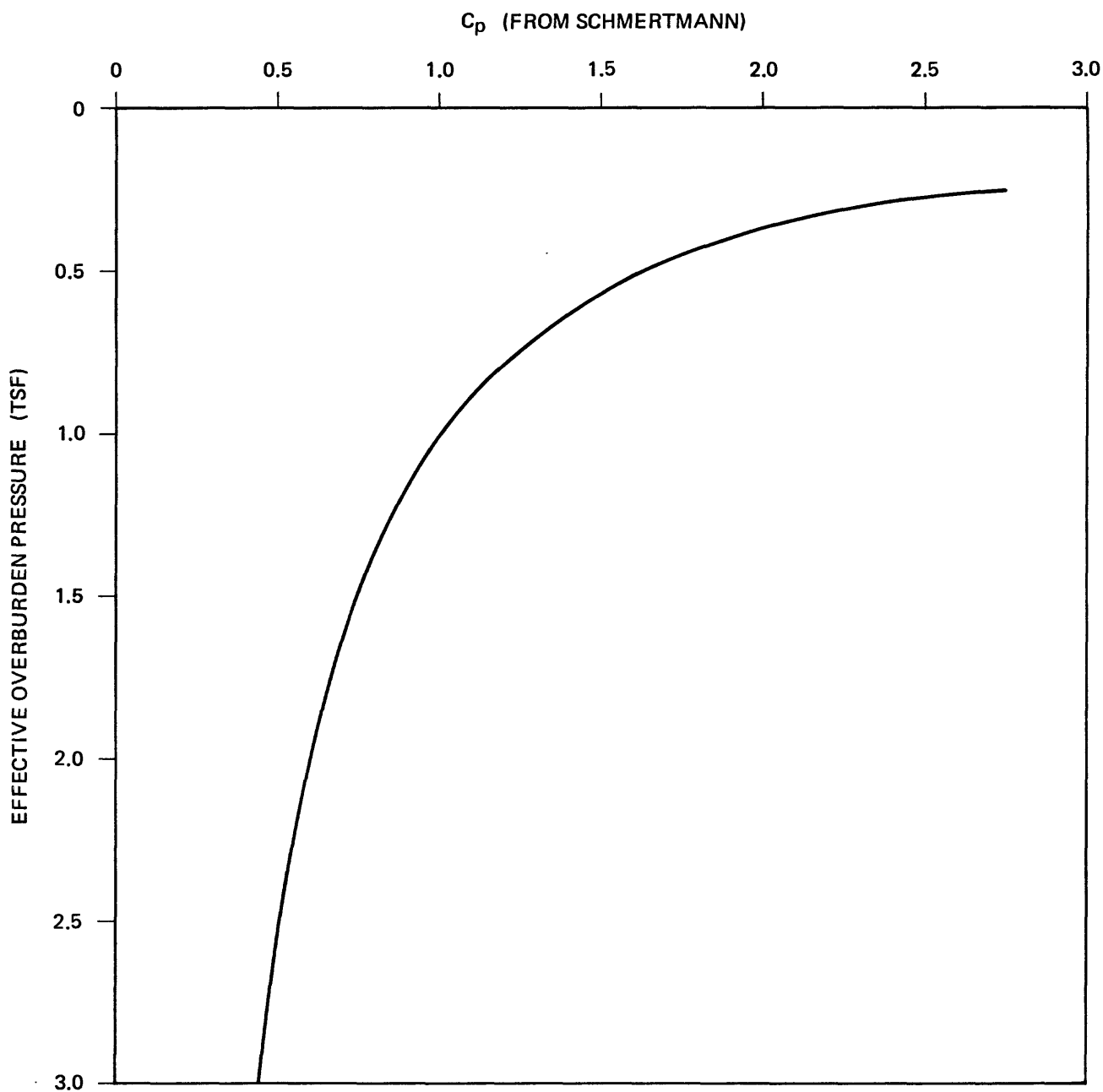
USGS CPT-SPT

CPT SOIL CLASSIFICATION
AFTER SCHMERTMANN (1978)

9-80

FIGURE 3.4

Compiled by _____
Drawn by _____
Checked by _____
Approved by _____



FROM SCHMERTMANN (1976)



PROJECT NO.:

79-153

USGS CPT-SPT

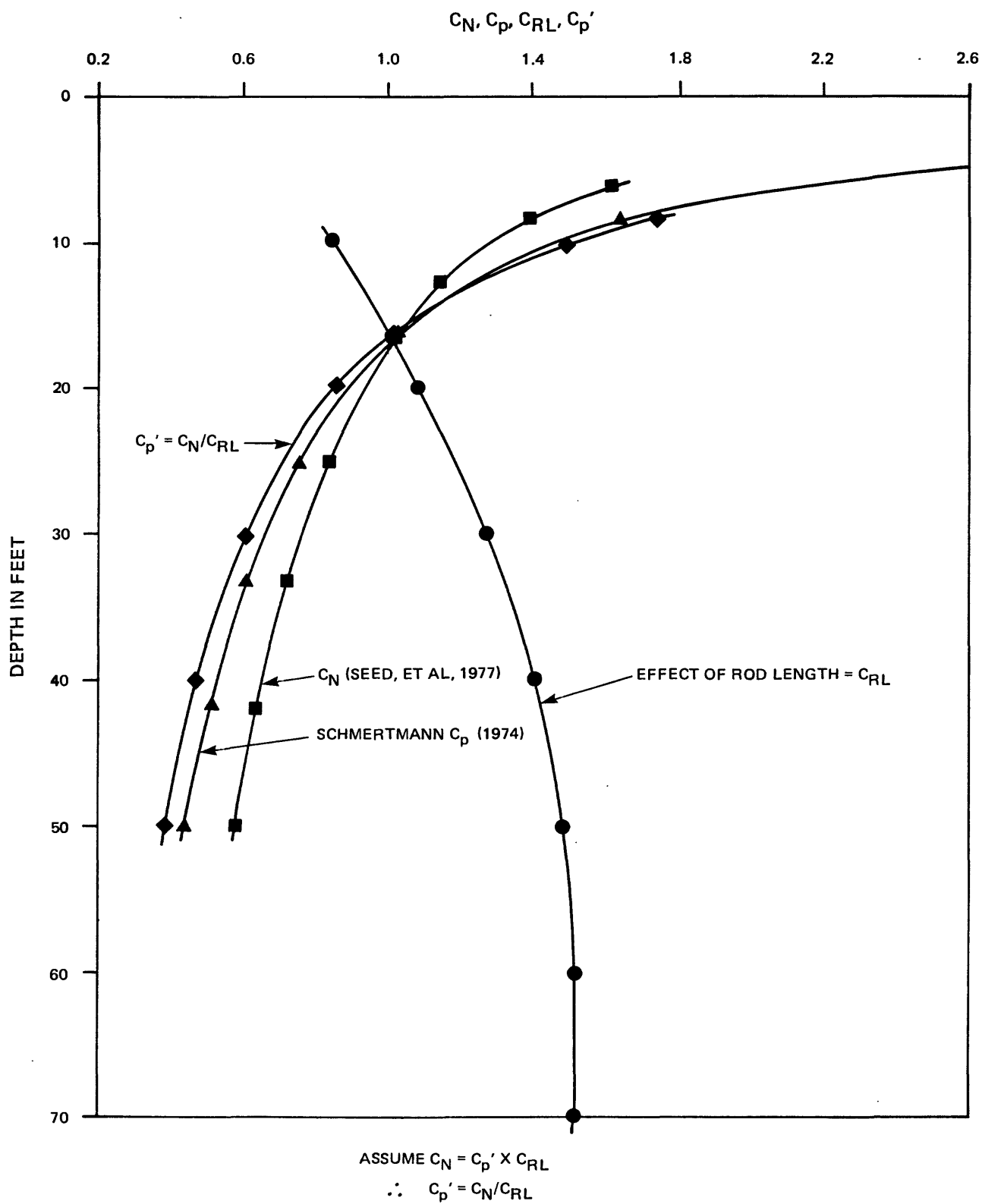
EFFECTIVE OVERBURDEN PRESSURE
VERSUS

$C_p = q_c @ 1 \text{ TSF}/q_c$

9-80

FIGURE 3.5

Compiled by _____
 Drawn by _____
 Checked by _____
 Approved by _____



ASSUMES UNSATURATED SITE



PROJECT NO.:

79-153

USGS CPT-SPT

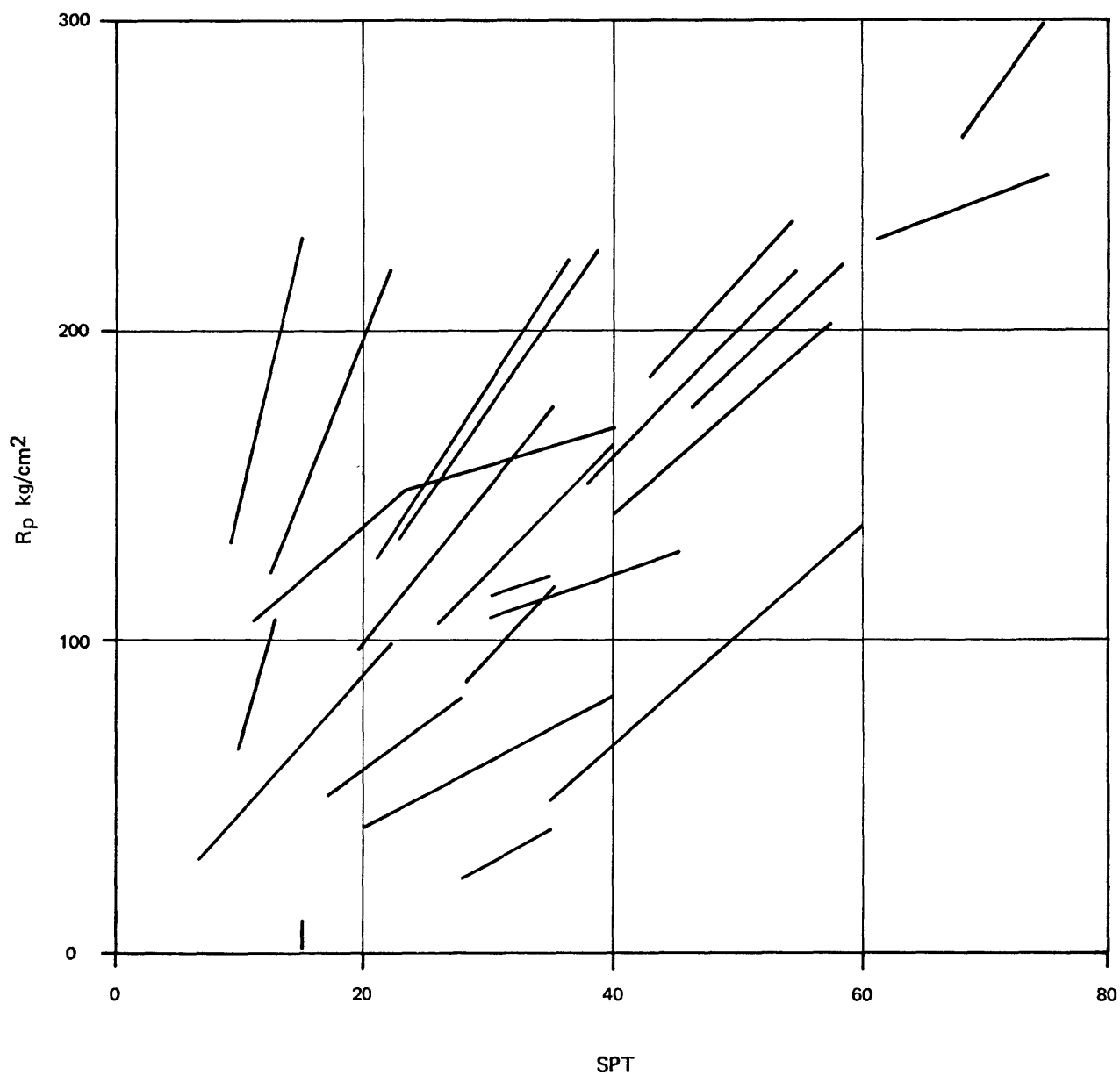
COMPARISON OF C_p, C_N
 AND ROD LENGTH

Approved by

Checked by

Drawn by

Computed by



PROJECT NO.:

79-153

USGS CPT-SPT

PREVIOUS CORRELATIONS: $q_c = f(\text{SPT})$
FOR PURE SANDS
(AFTER de MELLO, 1971)

9-80

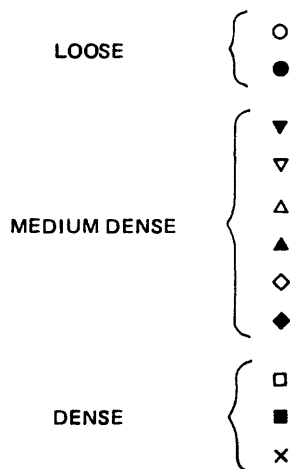
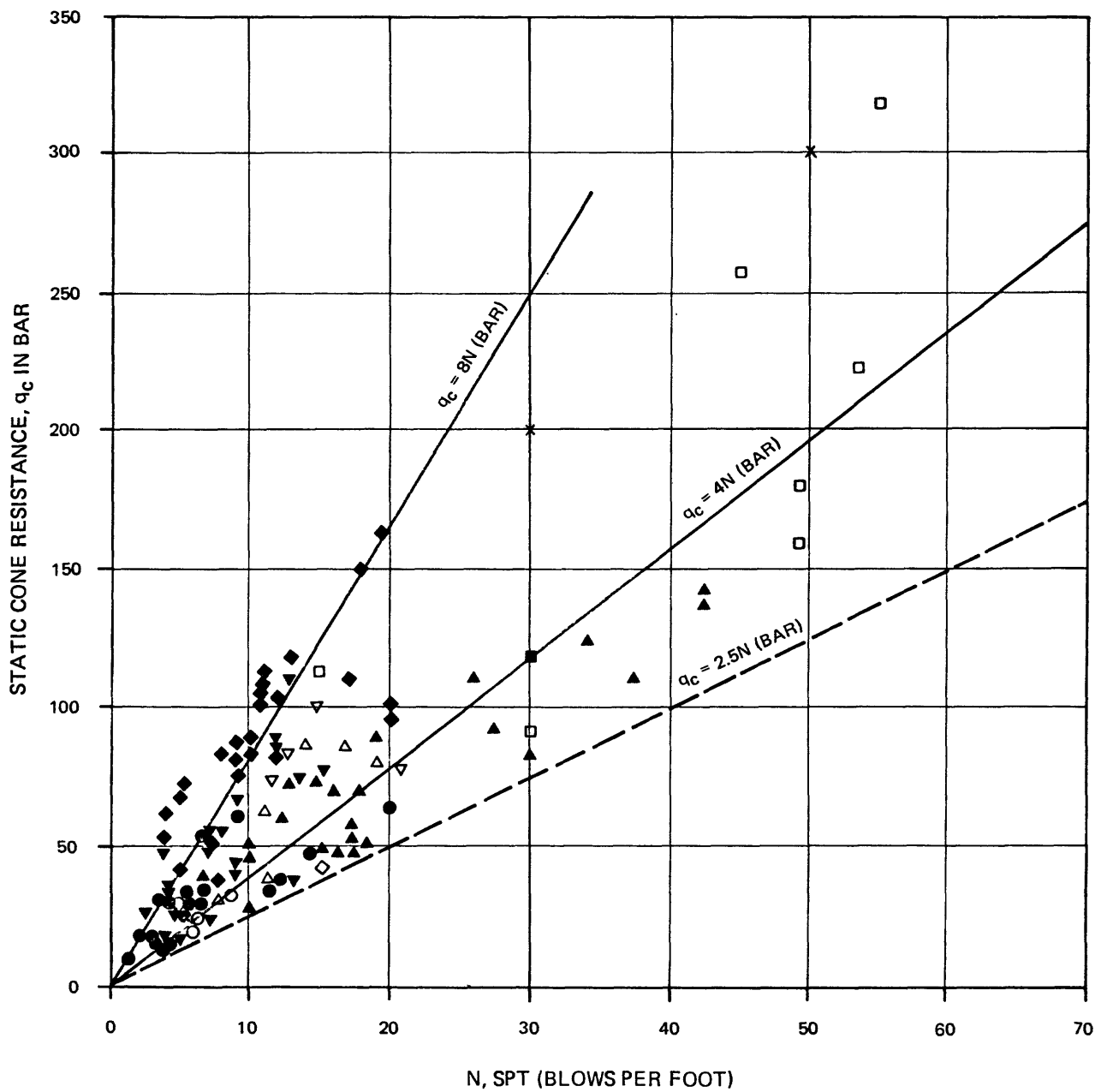
FIGURE 3.7

Approved by

Checked by

Drawn by

Compiled by



PROJECT NO.:

79-153

USGS CPT-SPT

PREVIOUS CORRELATIONS: $q_c = f$ (SPT)
FOR SANDS (AFTER SANGERLAT, 1972)

9-80

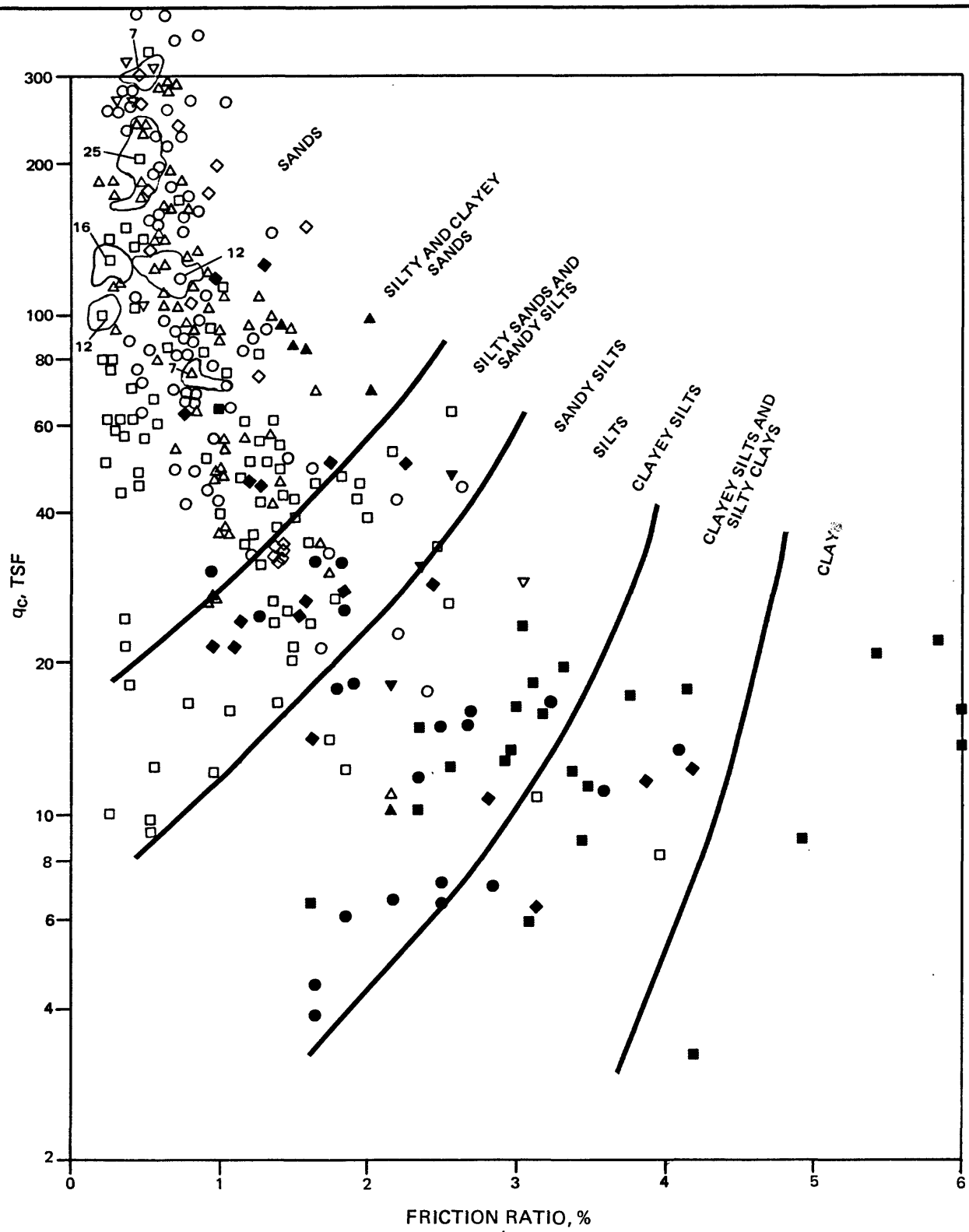
FIGURE 3.8

Approved by

Checked by

Drawn by

Compiled by



- | | |
|-------------------|------------------------|
| ◇ GP | ◆ SM-ML (30-60% FINES) |
| ▽ SP-GP | ● ML (> 60% FINES) |
| ○ SP | ■ CL |
| △ SP-SM | ▲ SC |
| □ SM (30% FINES) | ▼ ML-CL |

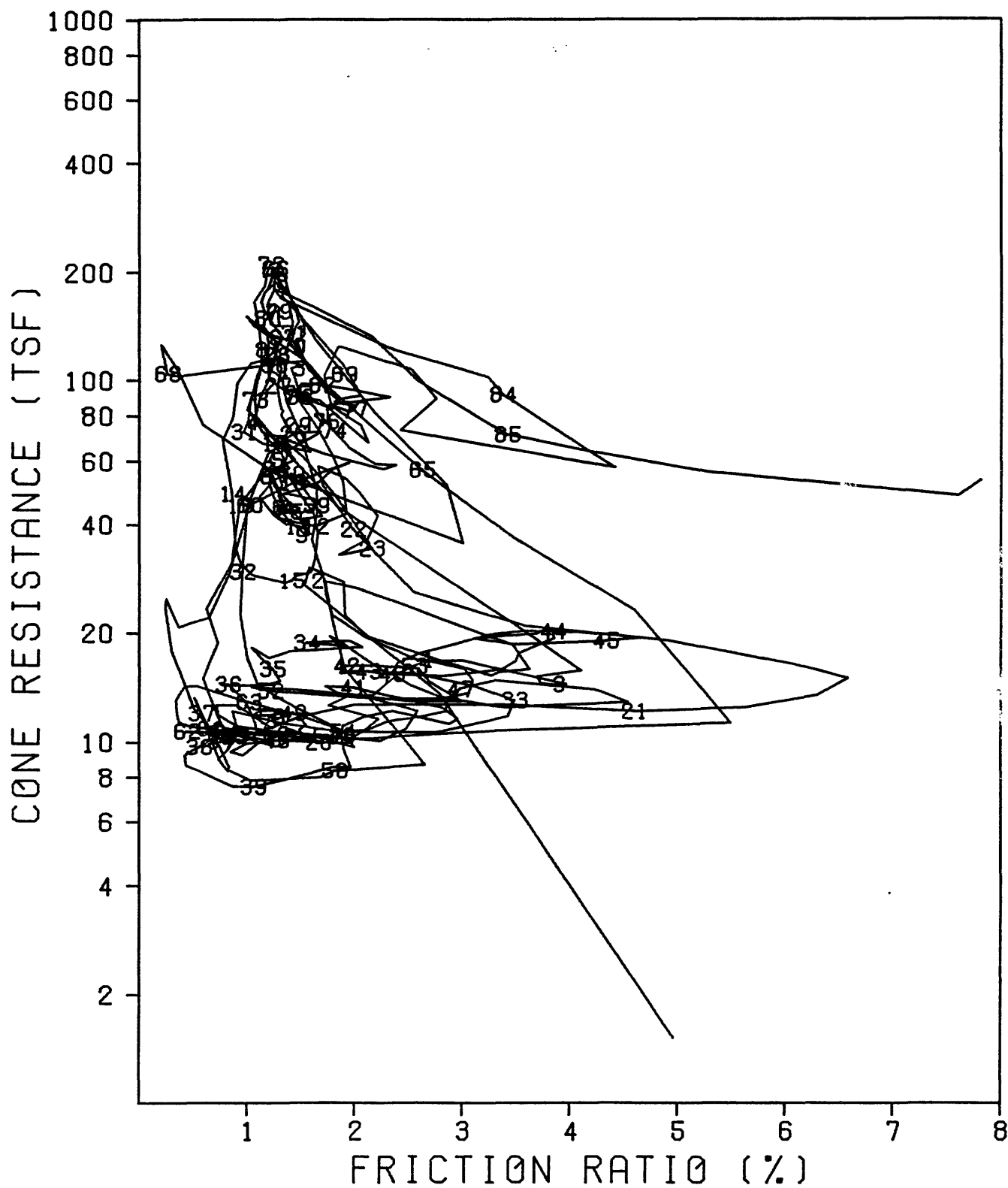
NUMBERS ON SYMBOLS INDICATE NUMBER OF OBSERVATIONS



PROJECT NO.: 79-153

USGS CPT-SPT

COMPOSITE: ALL SITES
 q_c VS FRICTION RATIO
SOIL CLASSIFICATION CHART



NUMBERS INDICATE DEPTH OF SOUNDING



PROJECT NO.:

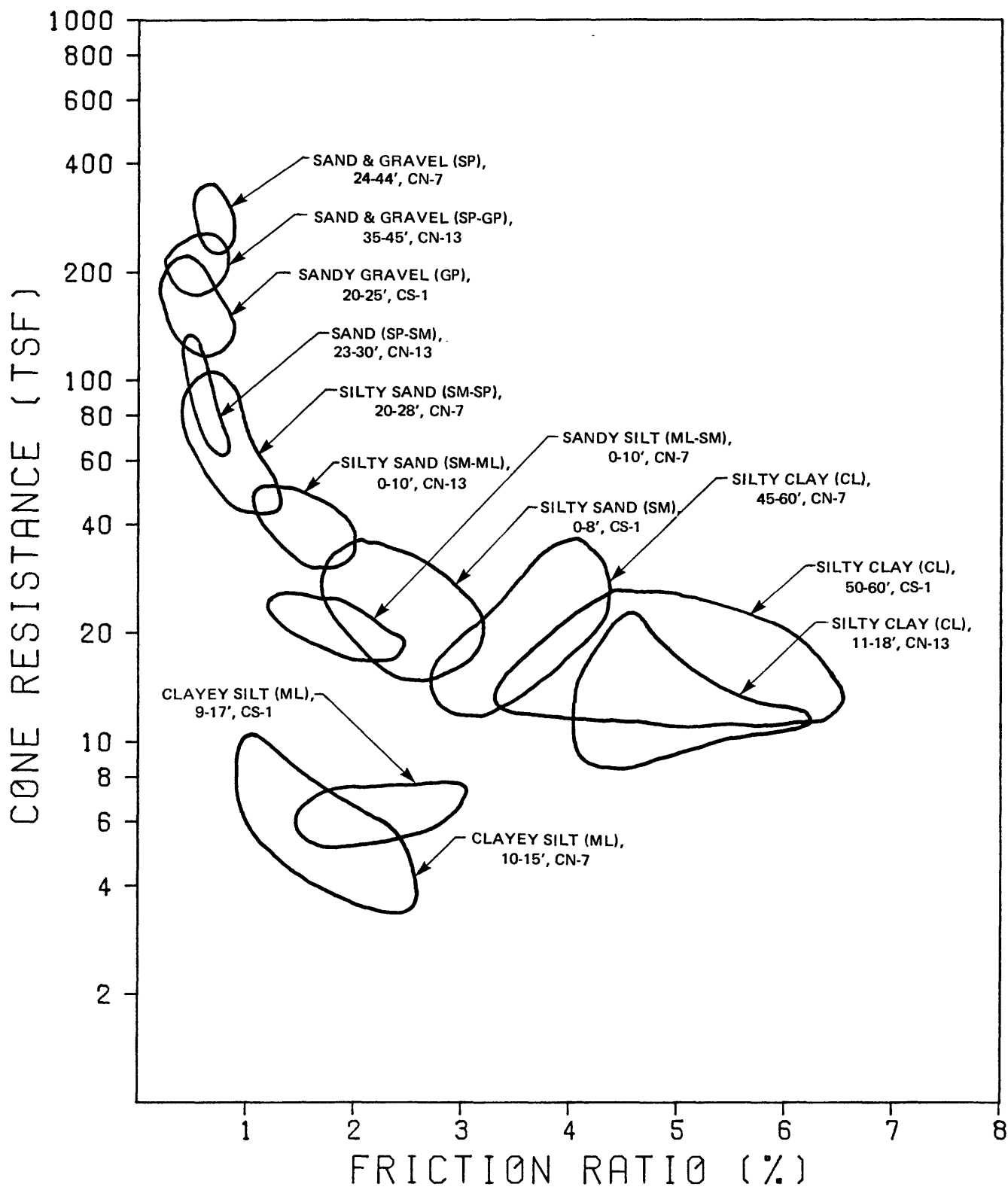
79-153

USGS CPT-SPT

CONTINUOUS TRACE METHOD
ARCADIA DAM CPT PROBE 119

9-80

FIGURE 3.10

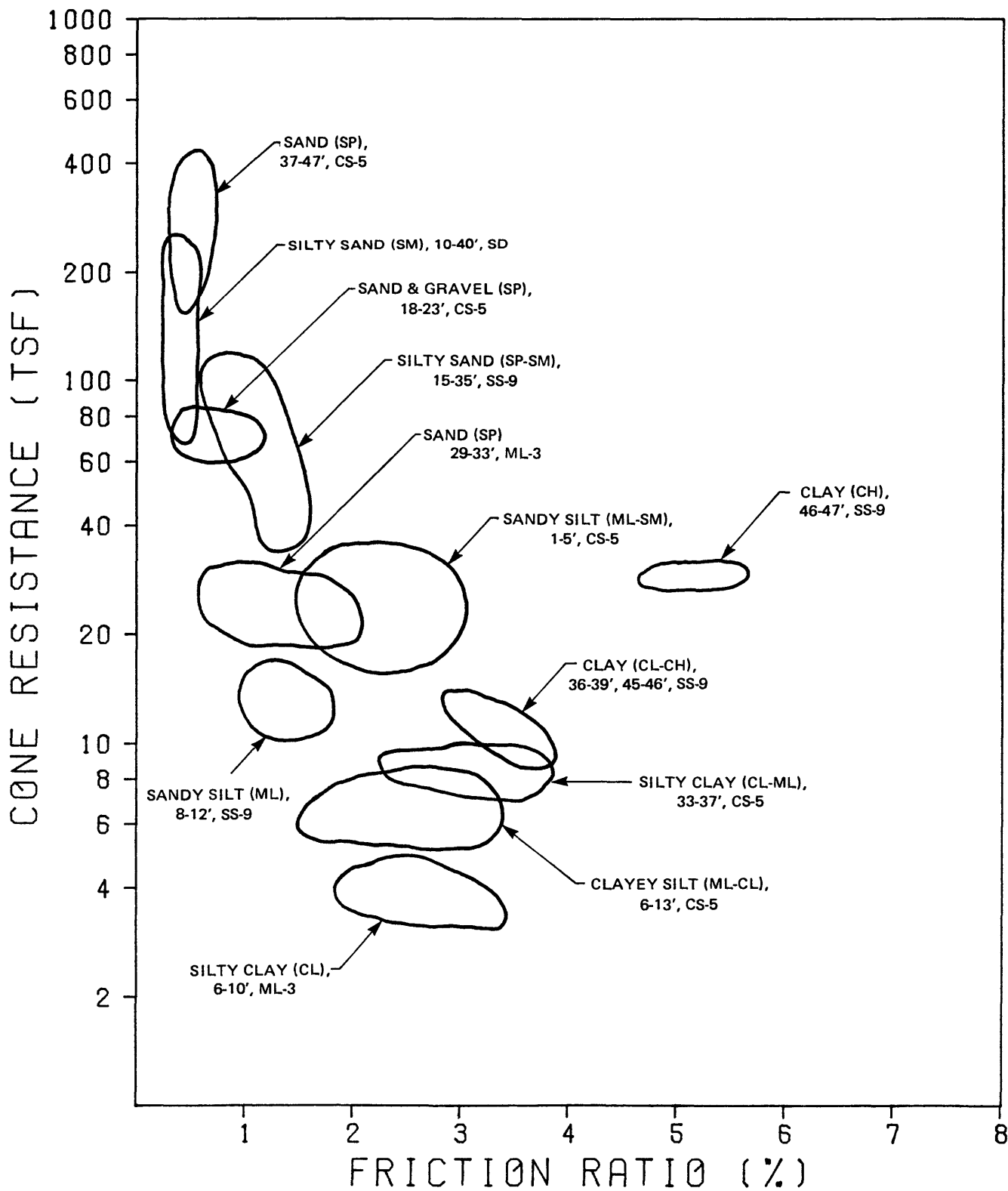


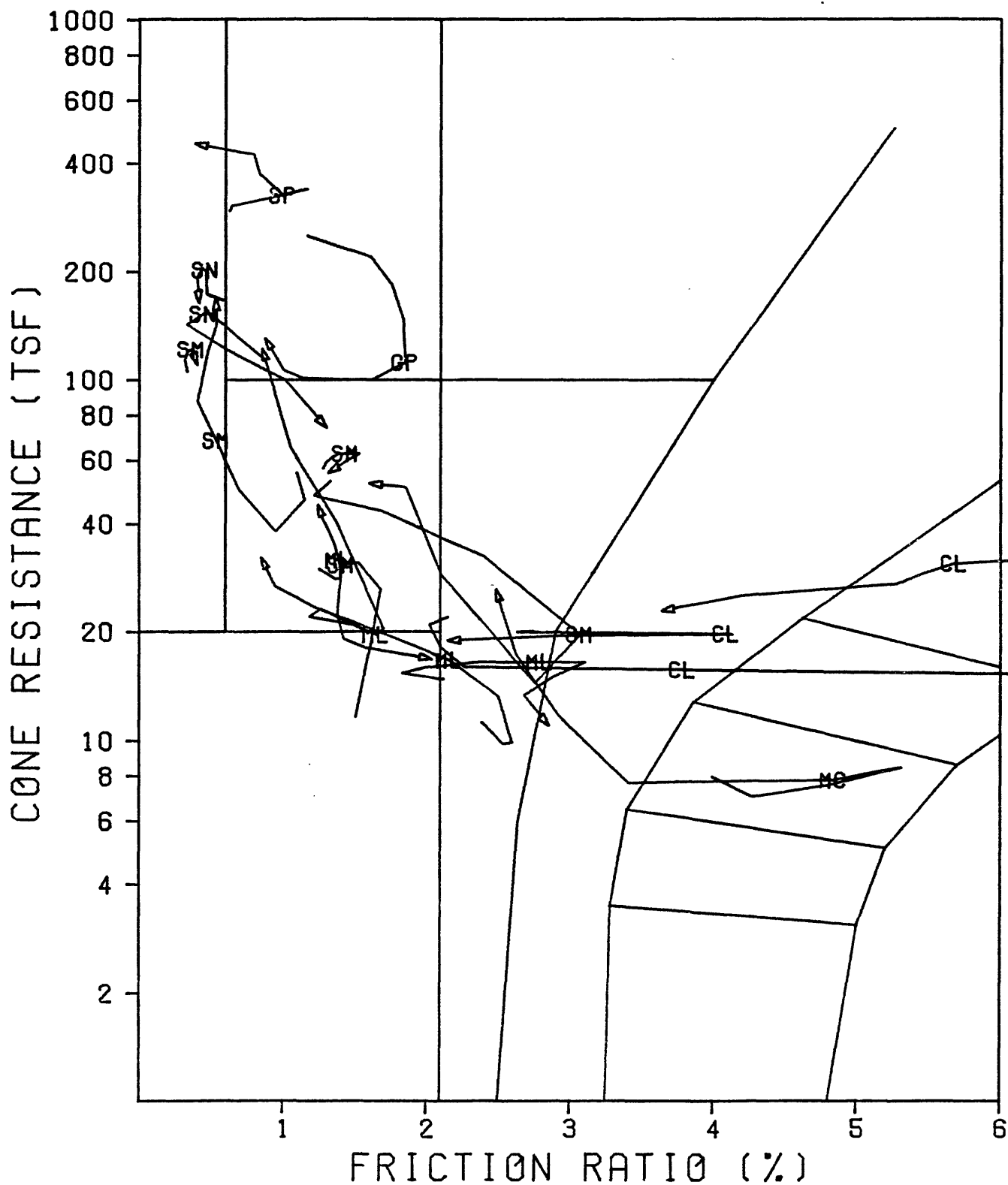
PROJECT NO.:

79-153

USGS CPT-SPT

SOIL TYPE CLASSIFICATIONS USING THE
CPT CONTINUOUS TRACE METHOD





SYMBOLS INDICATE LABORATORY CLASSIFICATION
BASED ON SIEVE SIZE ANALYSIS WITH THE LINE
INDICATING THE q_c TO FRICTION RATIO TRACE FOR 1'

SN = SP-SM
MC = ML-CL



PROJECT NO.:

79-153

USGS CPT-SPT

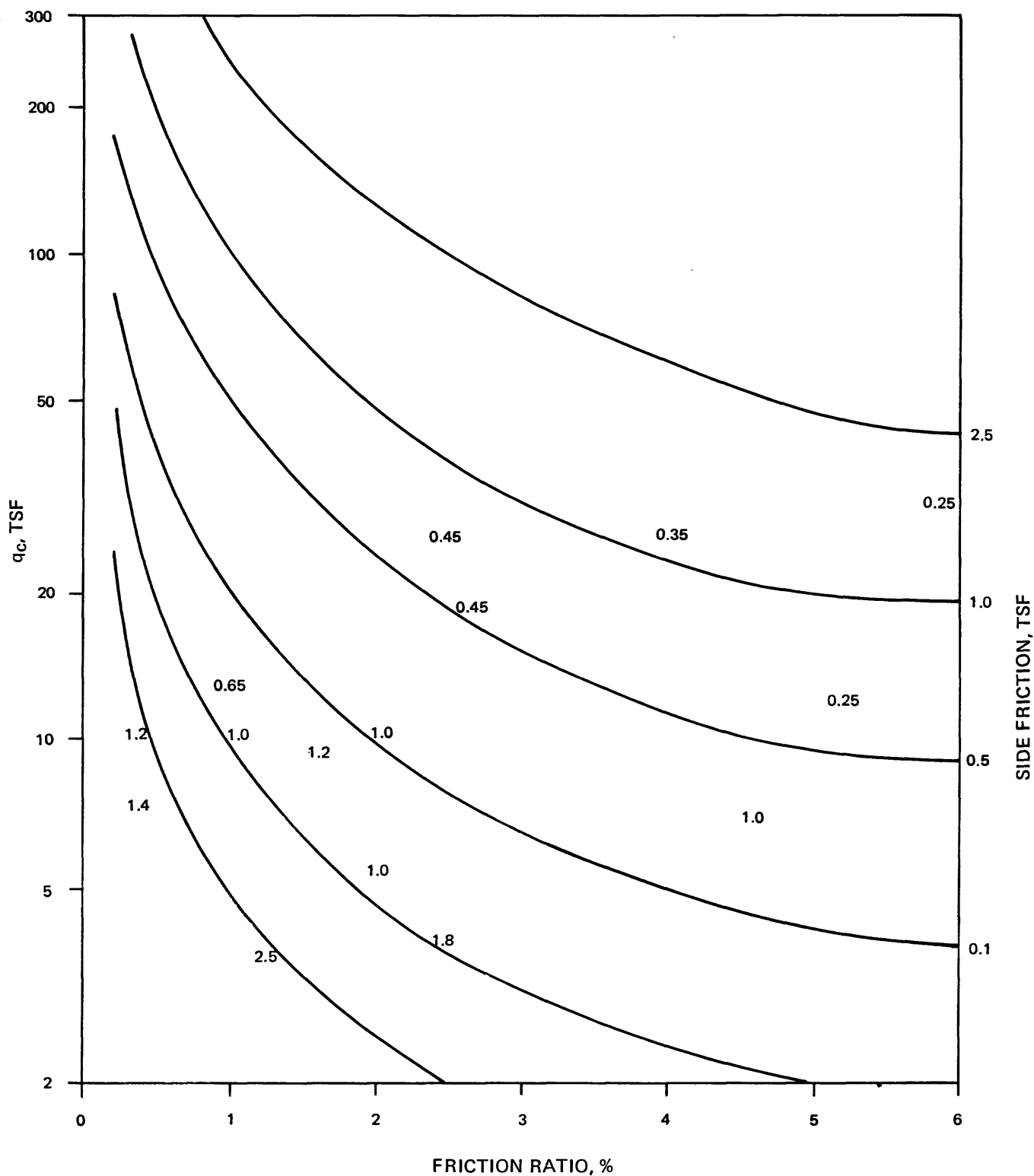
LIMITED TRACE METHOD
COYOTE NORTH SITE

Approved by _____

Checked by _____

Drawn by _____

Compiled by _____



NUMBERS REPRESENT VALUES OF LIQUIDITY INDEX



PROJECT NO.:

79-153

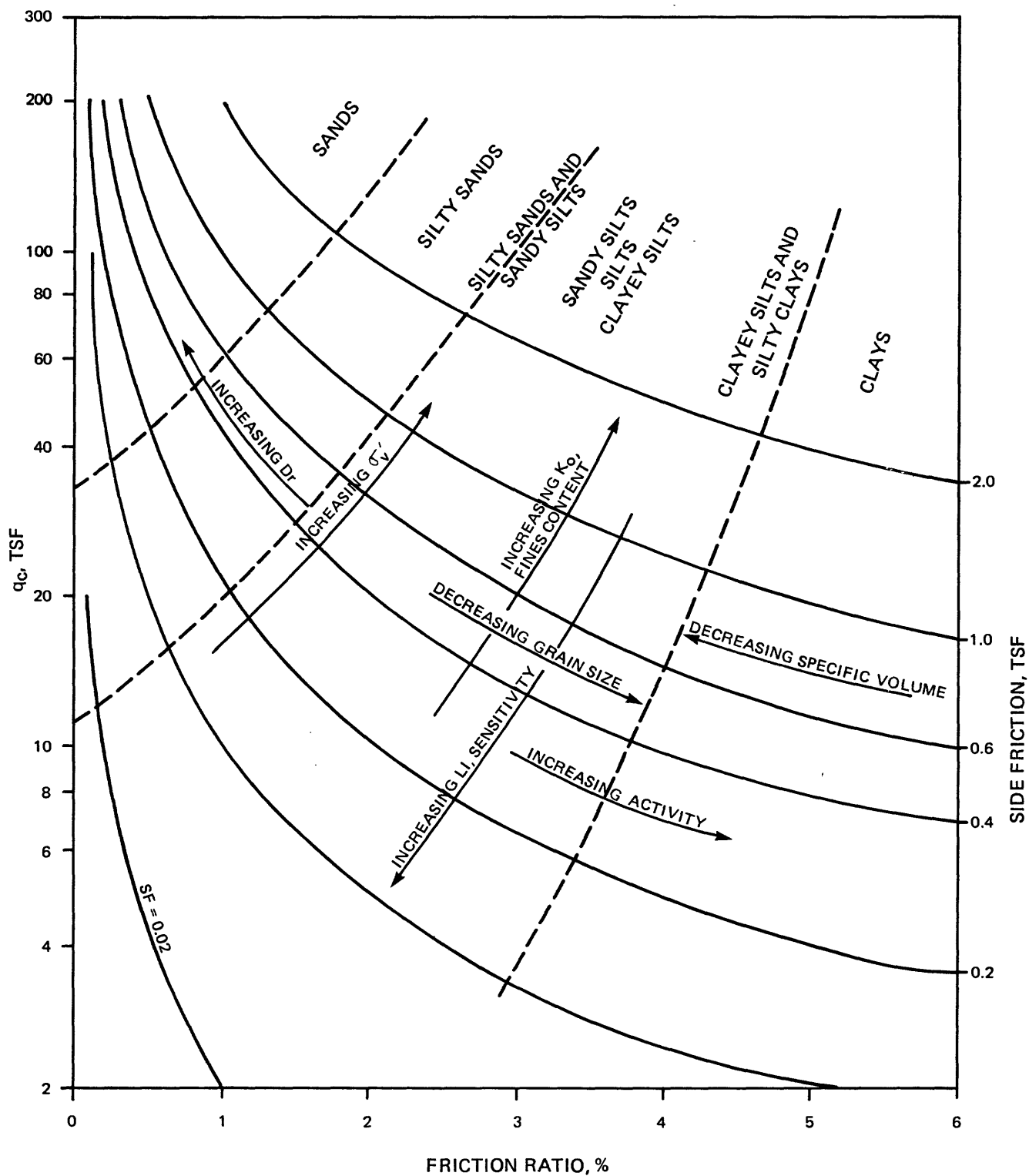
USGS CPT-SPT

SELECT POINTS - EDMOND SITE
LIQUIDITY INDEX VS q_c
AND FRICTION RATIO

9-80

FIGURE 3.14

Compiled by _____ Drawn by _____ Checked by _____ Approved by _____



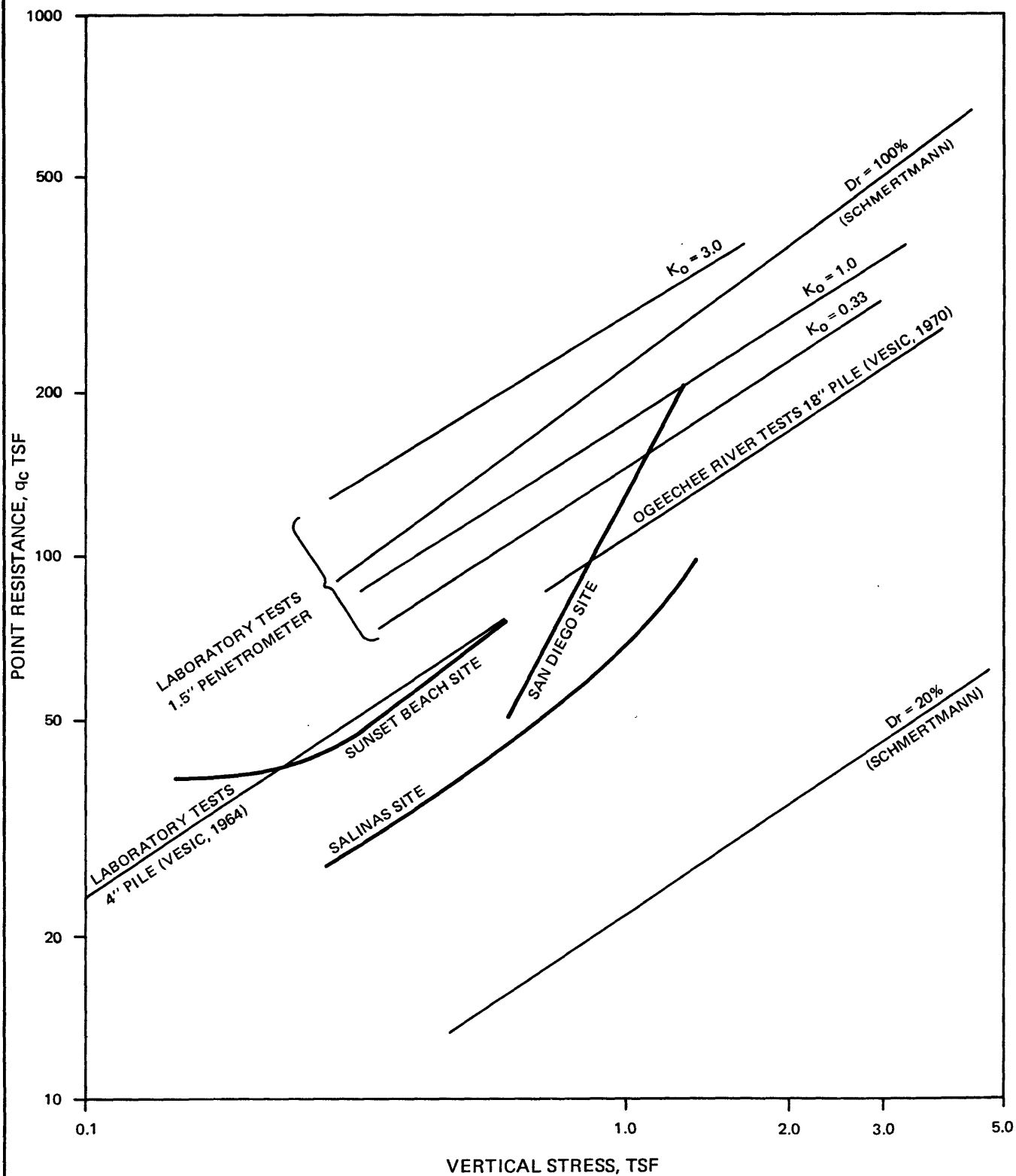
PROJECT NO.:

79-153

USGS CPT-SPT

TRENDS IN CPT SOIL CLASSIFICATION

Approved by _____
Checked by _____
Drawn by _____
Compiled by _____



PROJECT NO.: 79-153

USGS CPT-SPT

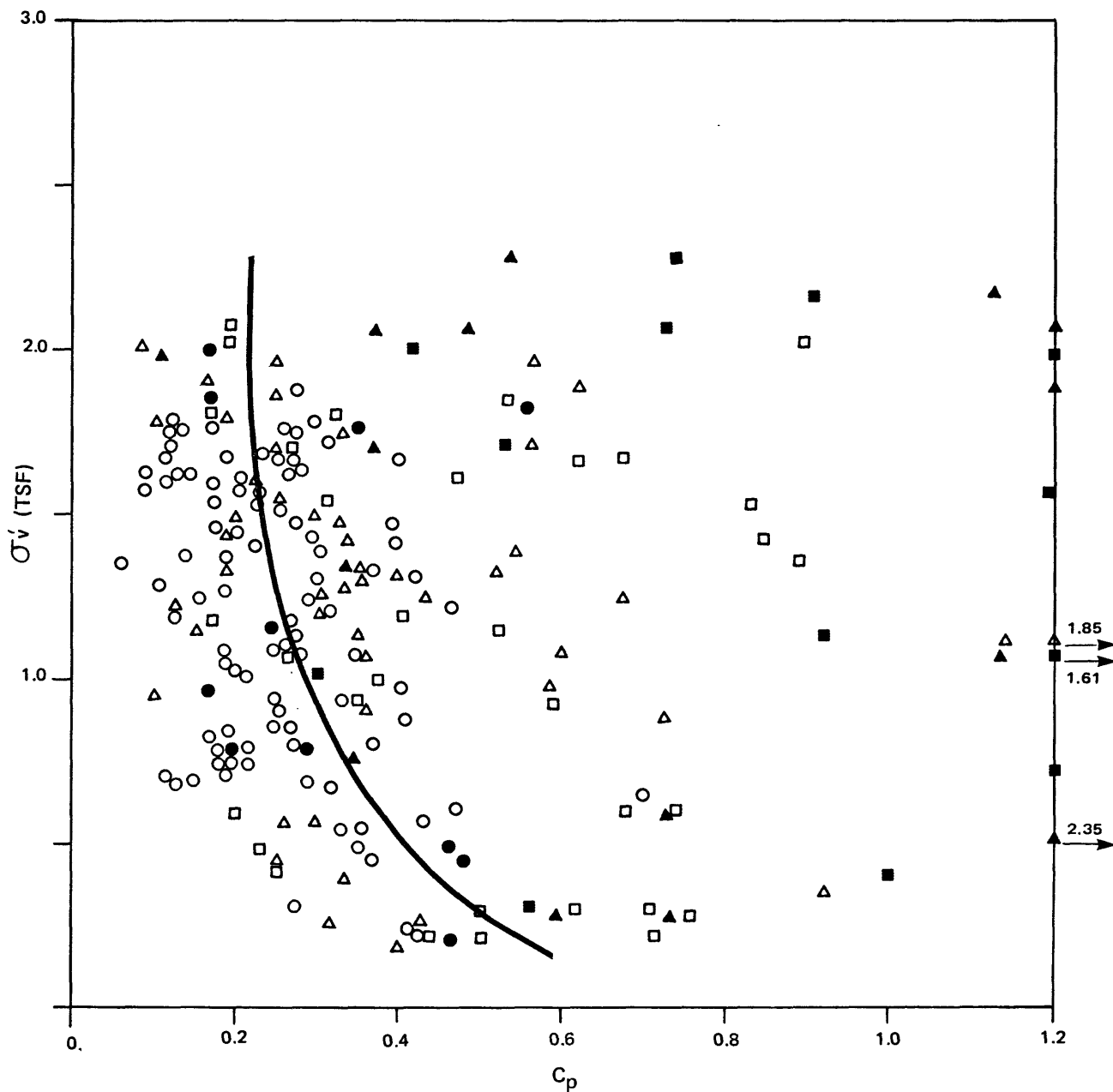
q_c VS σ'_v
FOR CPT MEASUREMENT IN SANDS
(AFTER TREADWELL, 1975)

Approved by

Checked by

Drawn by

Compiled by



- FRICITION RATIO, %
- < 0.75
 - △ 0.75 - 1.25
 - 1.25 - 1.75
 - 1.75 - 2.25
 - ▲ 2.25 - 3.25
 - 3.25 <



PROJECT NO.:

79-153

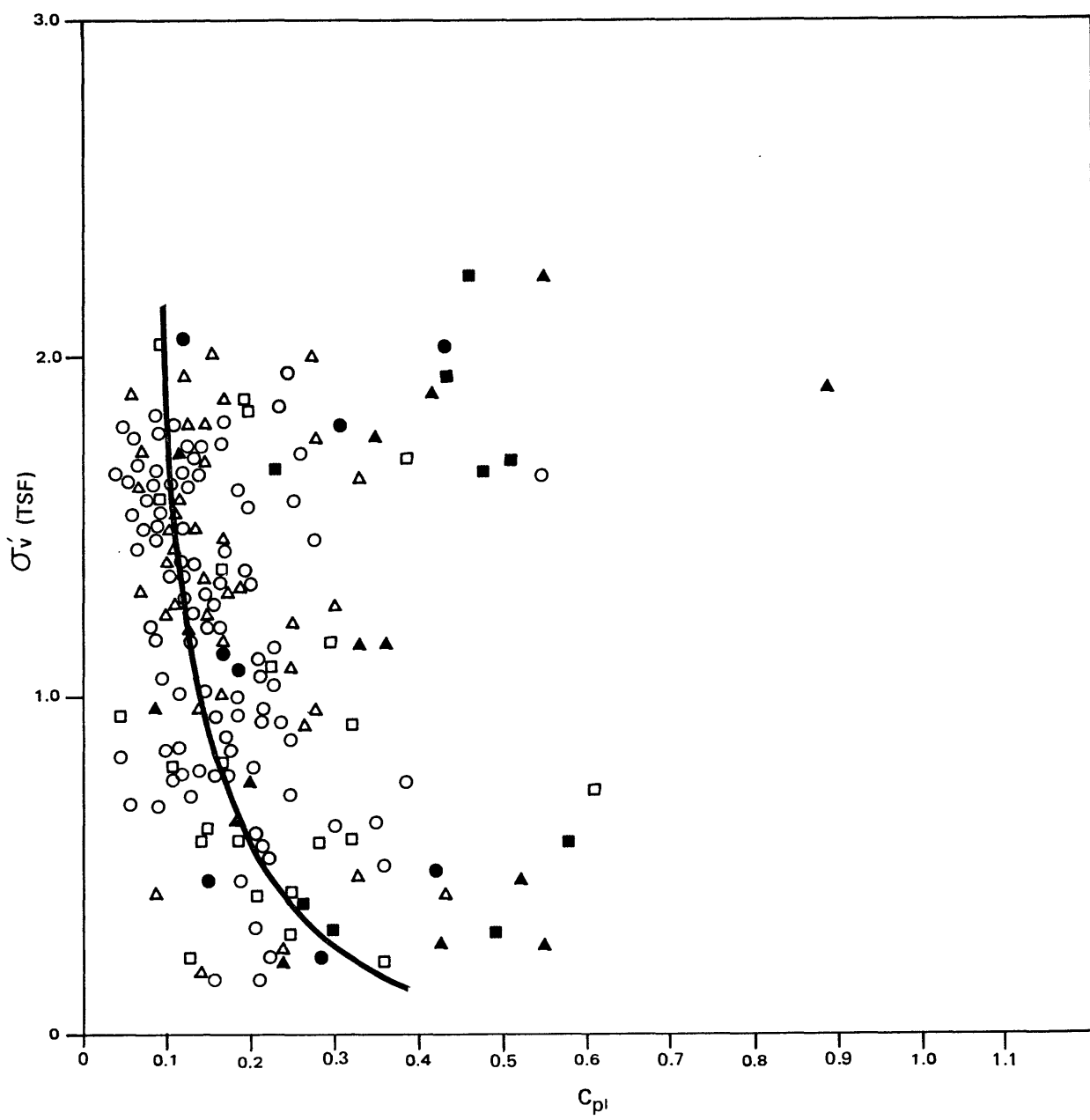
USGS CPT-SPT

COMPOSITE: ALL SITES
 σ'_v VS C_p
 STANDARD HAMMER

9-80

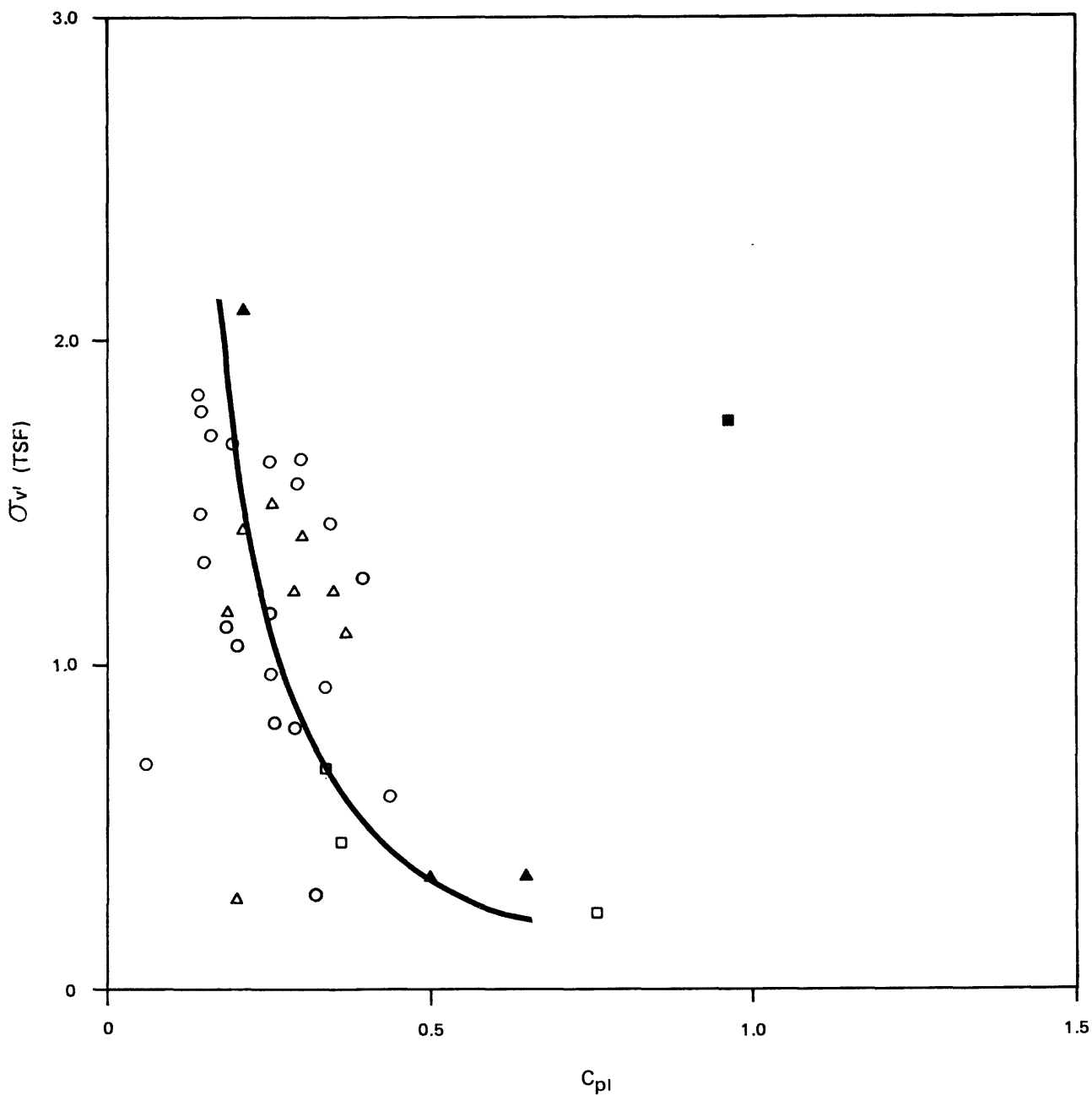
FIGURE 3.17

Approved by _____
 Checked by _____
 Drawn by _____
 Compiled by _____



- FRICTION RATIO, %
- < 0.75
 - △ 0.75 - 1.25
 - 1.25 - 1.75
 - 1.75 - 2.25
 - ▲ 2.25 - 3.25
 - 3.25 <

	PROJECT NO.: 79-153
	USGS CPT-SPT
COMPOSITE: ALL SITES σ'_v VS C_{pl} TRIP HAMMER	
9-80	FIGURE 3.18



- FRICTION RATIO, %
- < 0.75
 - △ 0.75 - 1.25
 - 1.25 - 1.75
 - 1.75 - 2.25
 - ▲ 2.25 - 3.25
 - > 3.25



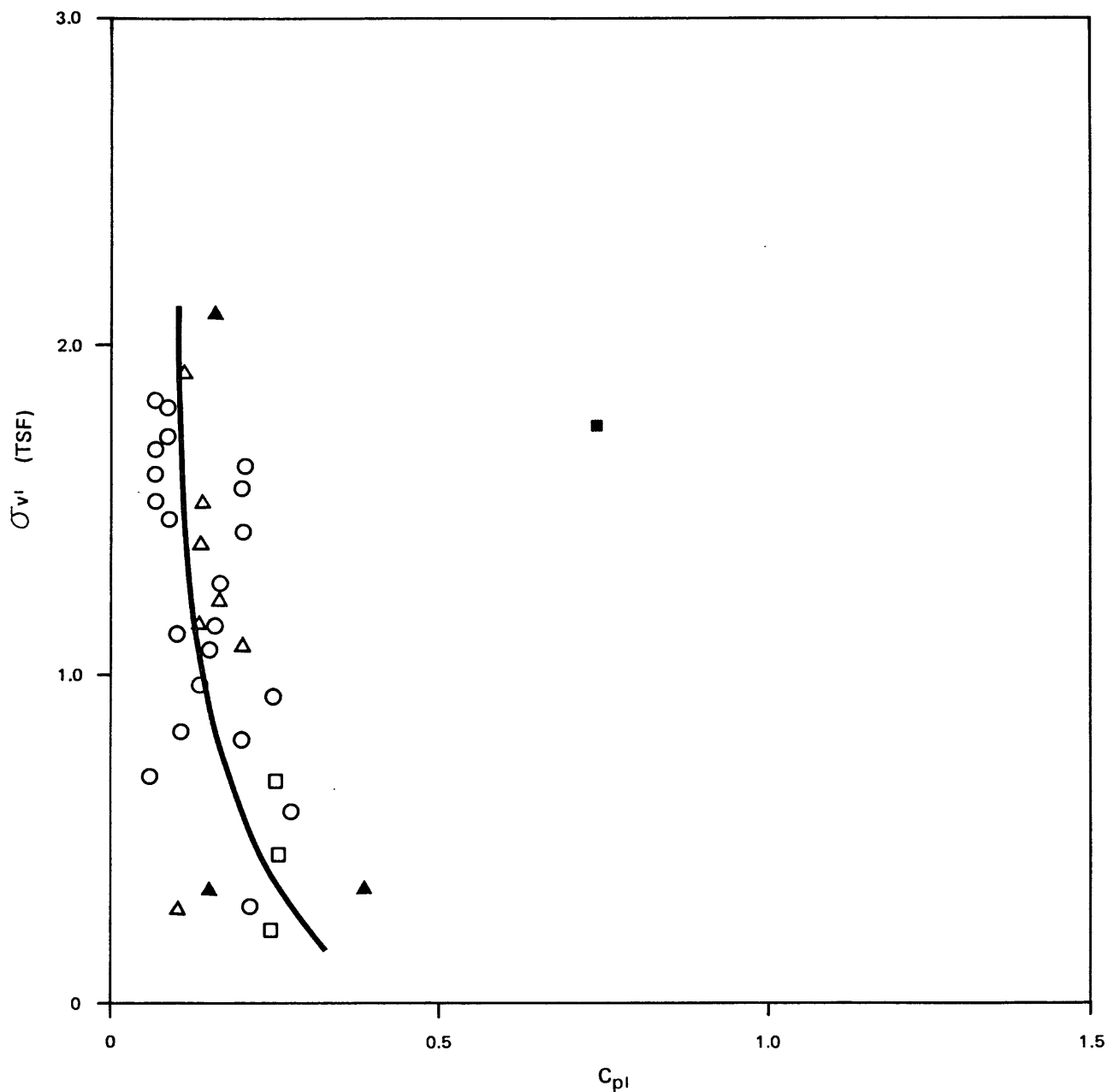
PROJECT NO.:

79-153

USGS CPT-SPT

COMPOSITE: ALL SITES
 σ_v VS C_{pl} BY LAYER AVERAGE
STANDARD HAMMER

Approved by _____
 Checked by _____
 Drawn by _____
 Compiled by _____



- FRICITION RATIO, %
- < 0.75
 - △ 0.75 - 1.25
 - 1.25 - 1.75
 - 1.75 - 2.25
 - ▲ 2.25 - 3.25
 - > 3.25

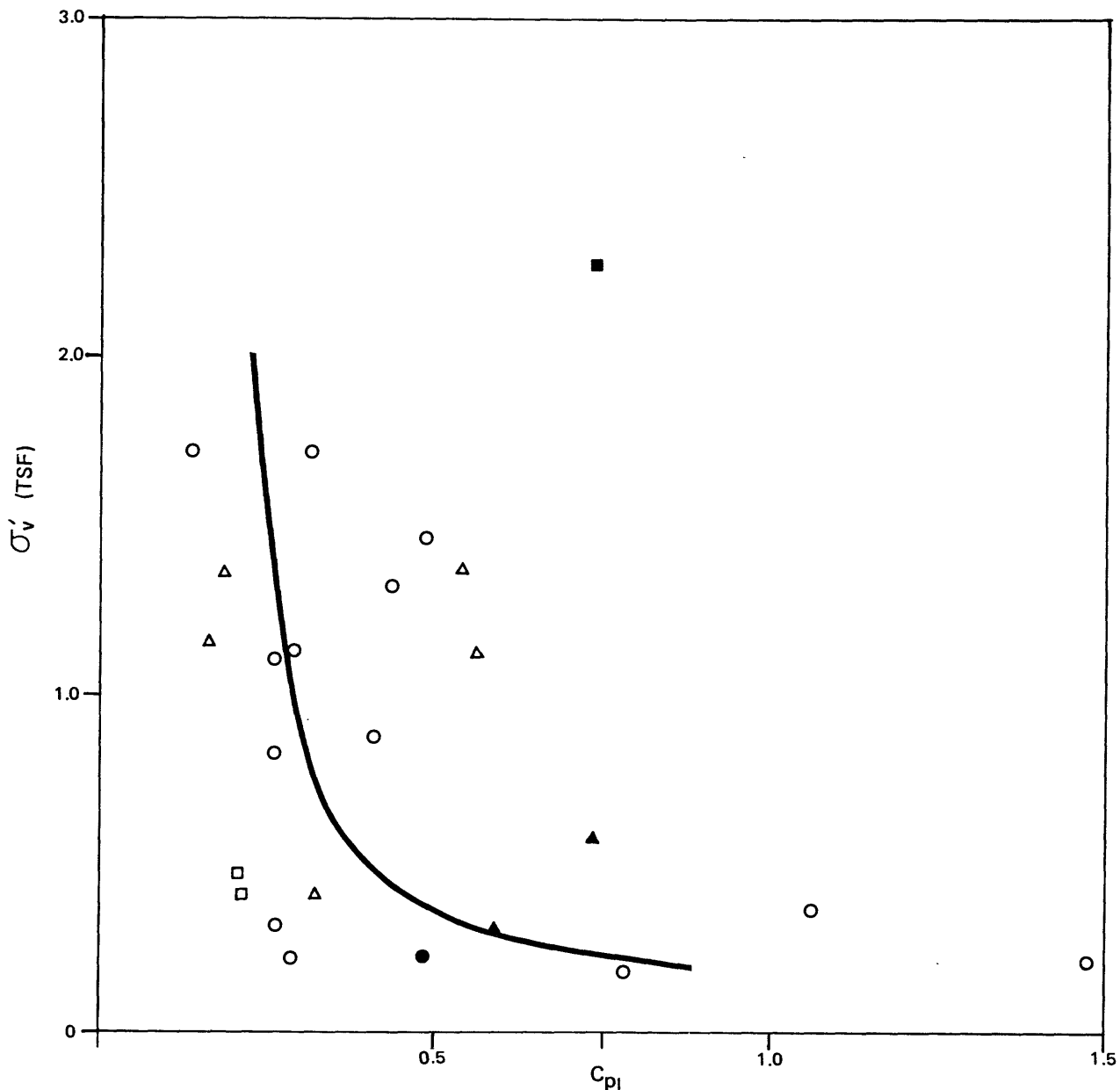


PROJECT NO.: 79-153

USGS CPT-SPT

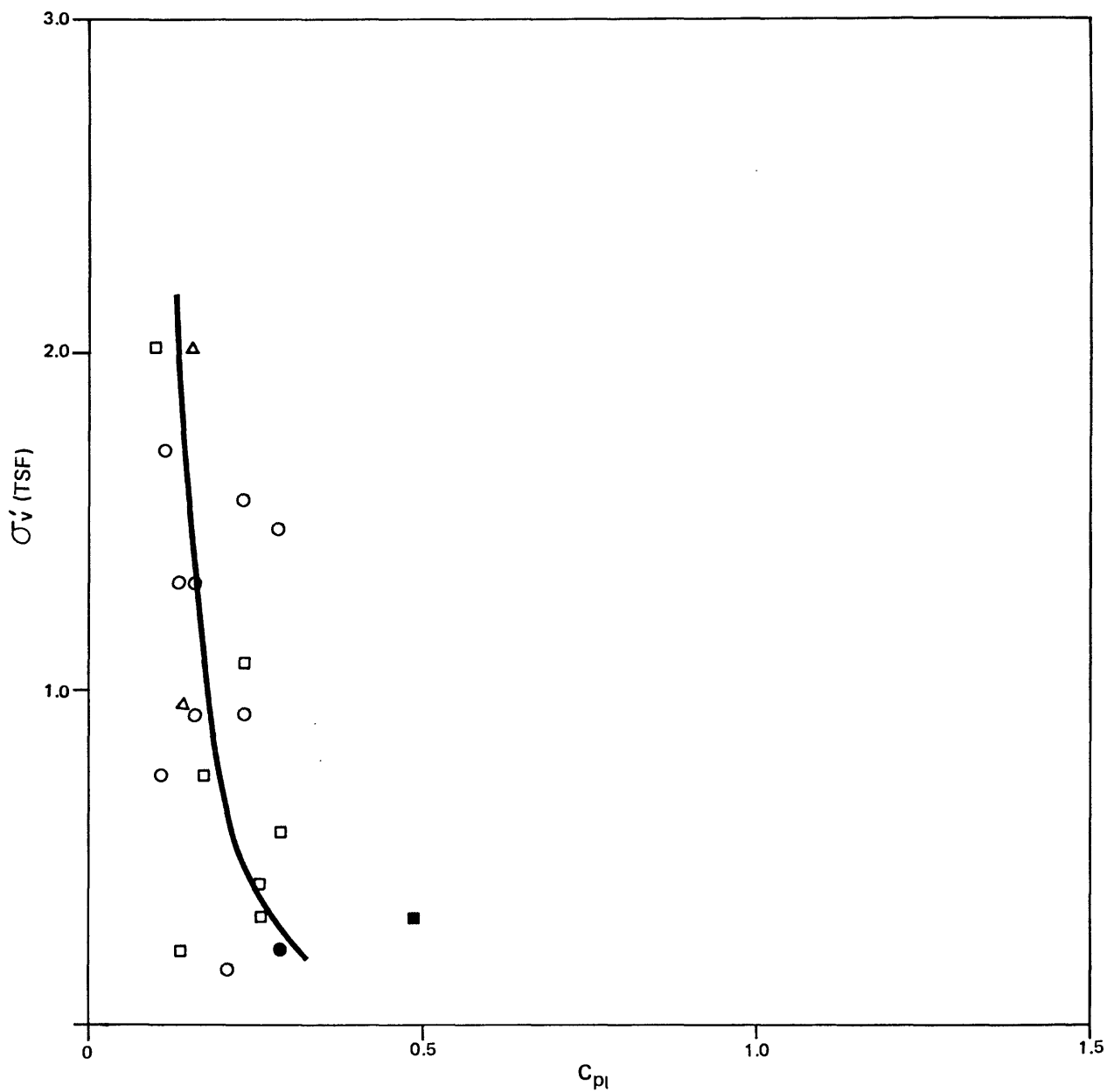
COMPOSITE: ALL SITES
 $\bar{\sigma}_{v'}$ VS C_{pl} BY LAYER AVERAGE
 TRIP HAMMER

Approved by _____
 Checked by _____
 Drawn by _____
 Compiled by _____



- FRICTION RATIO, %
- < 0.75
 - △ 0.75 - 1.25
 - 1.25 - 1.75
 - 1.75 - 2.25
 - ▲ 2.25 - 3.25
 - > 3.25

	PROJECT NO.:	79-153
	USGS CPT-SPT	
<p>SELECT POINTS: ALL SITES</p> <p>σ'_v VS C_p</p> <p>STANDARD HAMMER</p>		
9-80	FIGURE 3.21	



- FRICION RATIO, %
- < 0.75
 - △ 0.75 - 1.25
 - 1.25 - 1.75
 - 1.75 - 2.25
 - ▲ 2.25 - 3.25
 - > 3.25



PROJECT NO.:

79-153

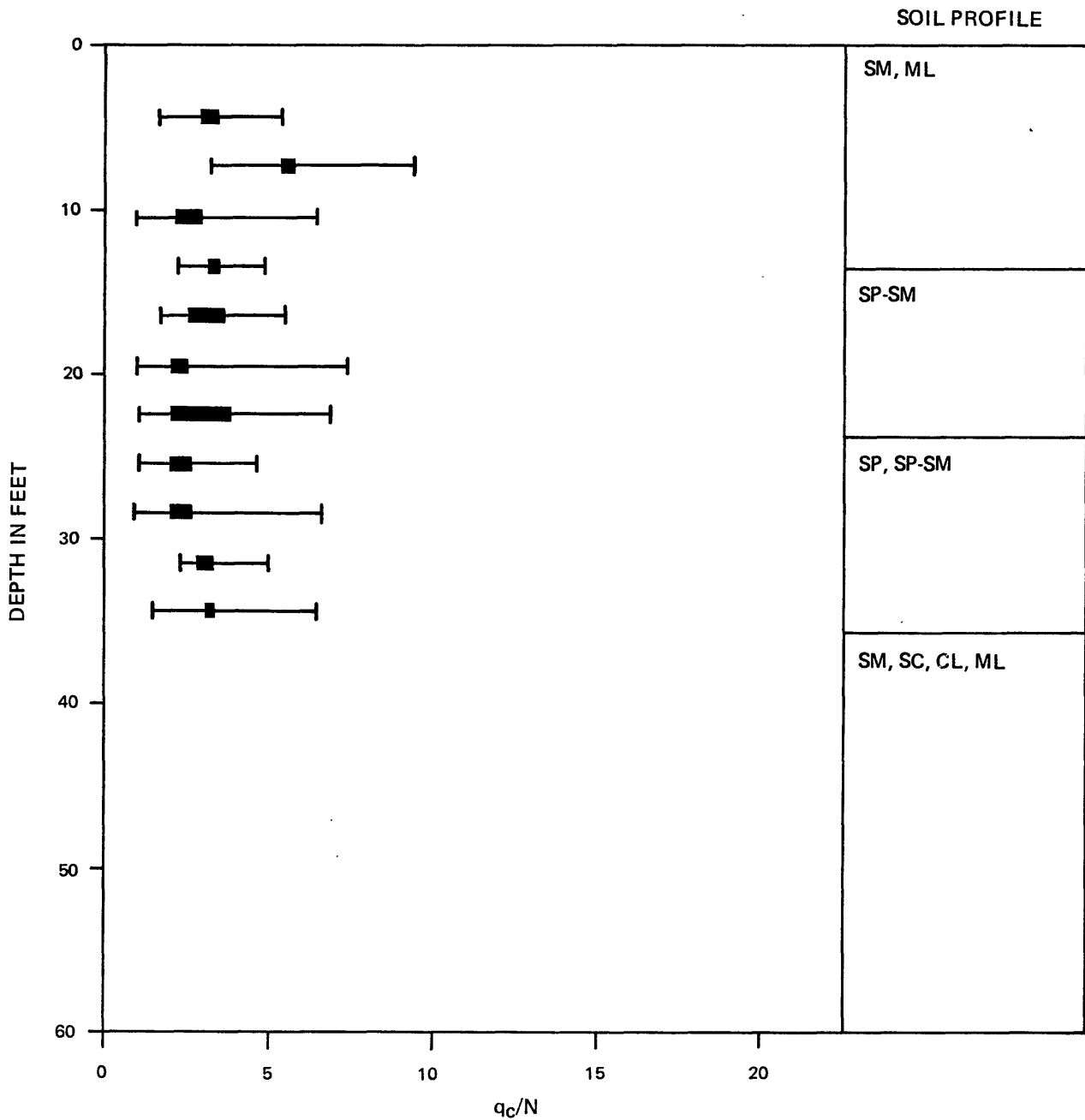
USGS CPT-SPT

SELECT POINTS: ALL SITES

σ'_v VS C_{pl}

TRIP HAMMER

Approved by _____
 Checked by _____
 Drawn by _____
 Compiled by _____



PROBABLE RANGE
 POSSIBLE RANGE

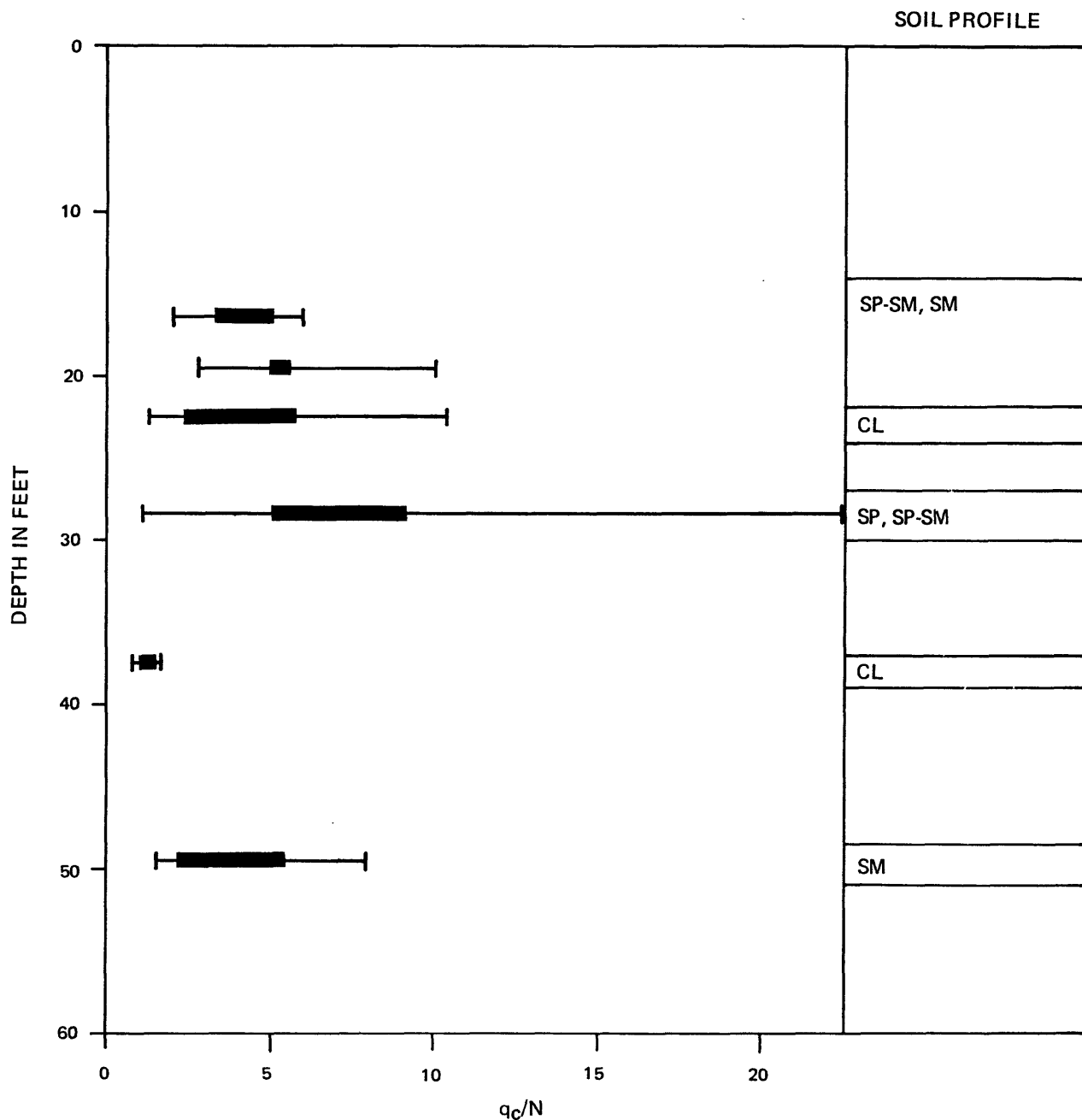
	PROJECT NO.:	79-153
	USGS CPT-SPT	
SALINAS SITE q_c/N RANGE COMPARISONS STANDARD HAMMER		
9-80	FIGURE 3.24	

Approved by

Checked by

Drawn by

Compiled by



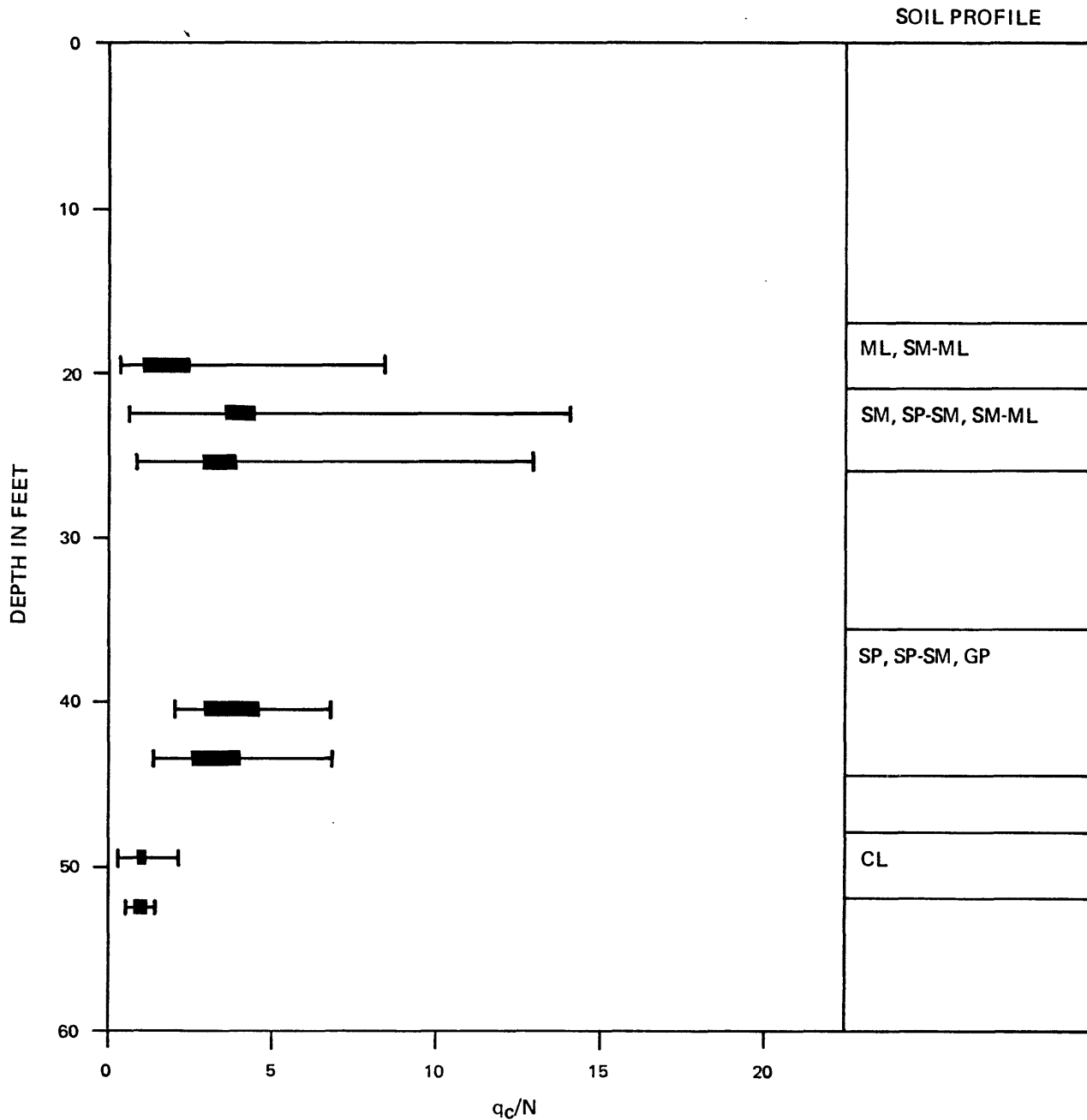
PROJECT NO.:

79-153

USGS CPT-SPT

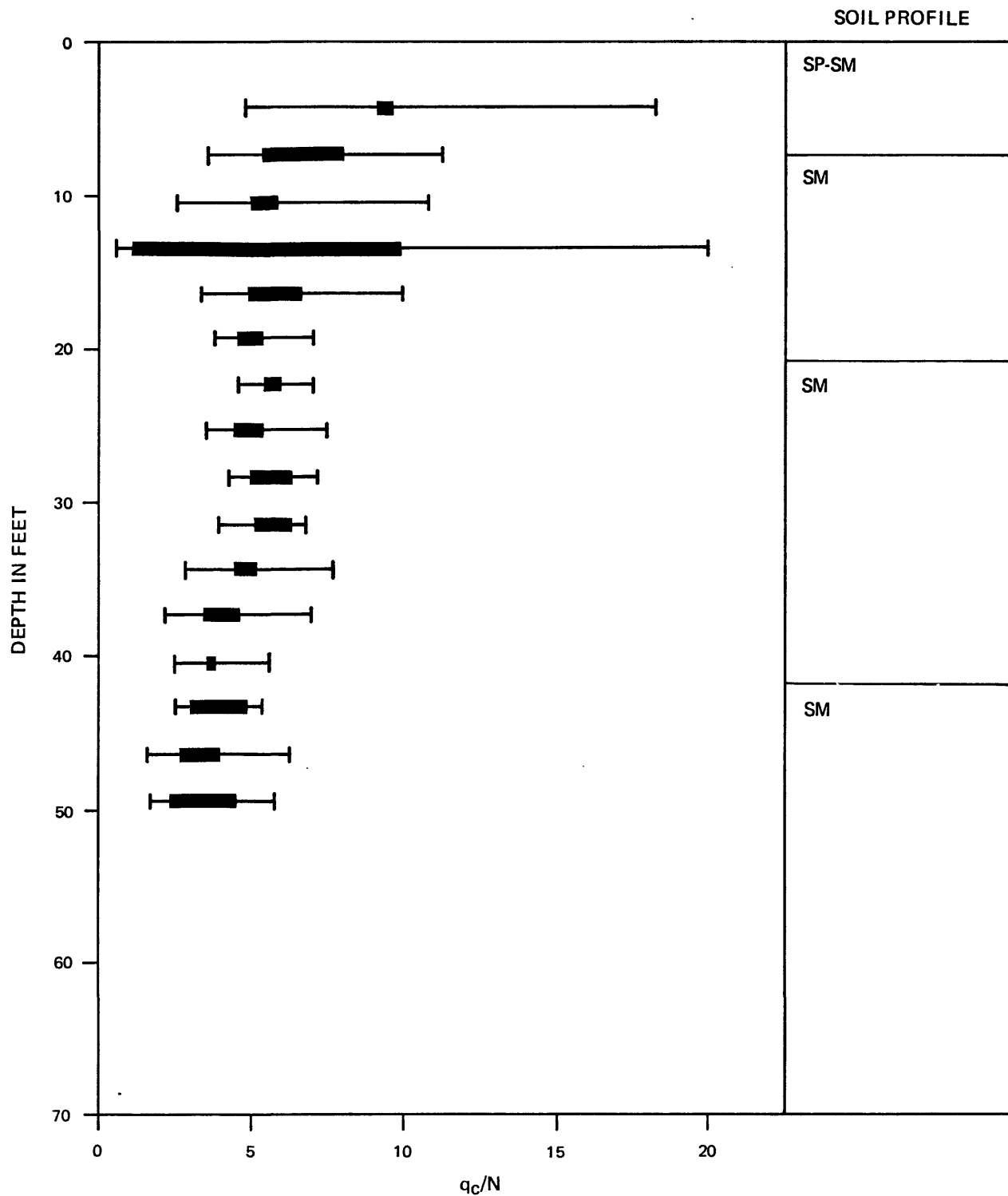
MOSS LANDING SITE
q_C/N RANGE COMPARISONS
STANDARD HAMMER


Approved by _____
 Checked by _____
 Drawn by _____
 Compiled by _____

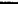


PROBABLE RANGE
 POSSIBLE RANGE

	PROJECT NO.:	79-153
	USGS CPT-SPT	
SAN JOSE SITE: COYOTE NORTH & SOUTH q_c/N RANGE COMPARISONS STANDARD HAMMER		
9-80	FIGURE 3.26	



 PROBABLE RANGE

 POSSIBLE RANGE

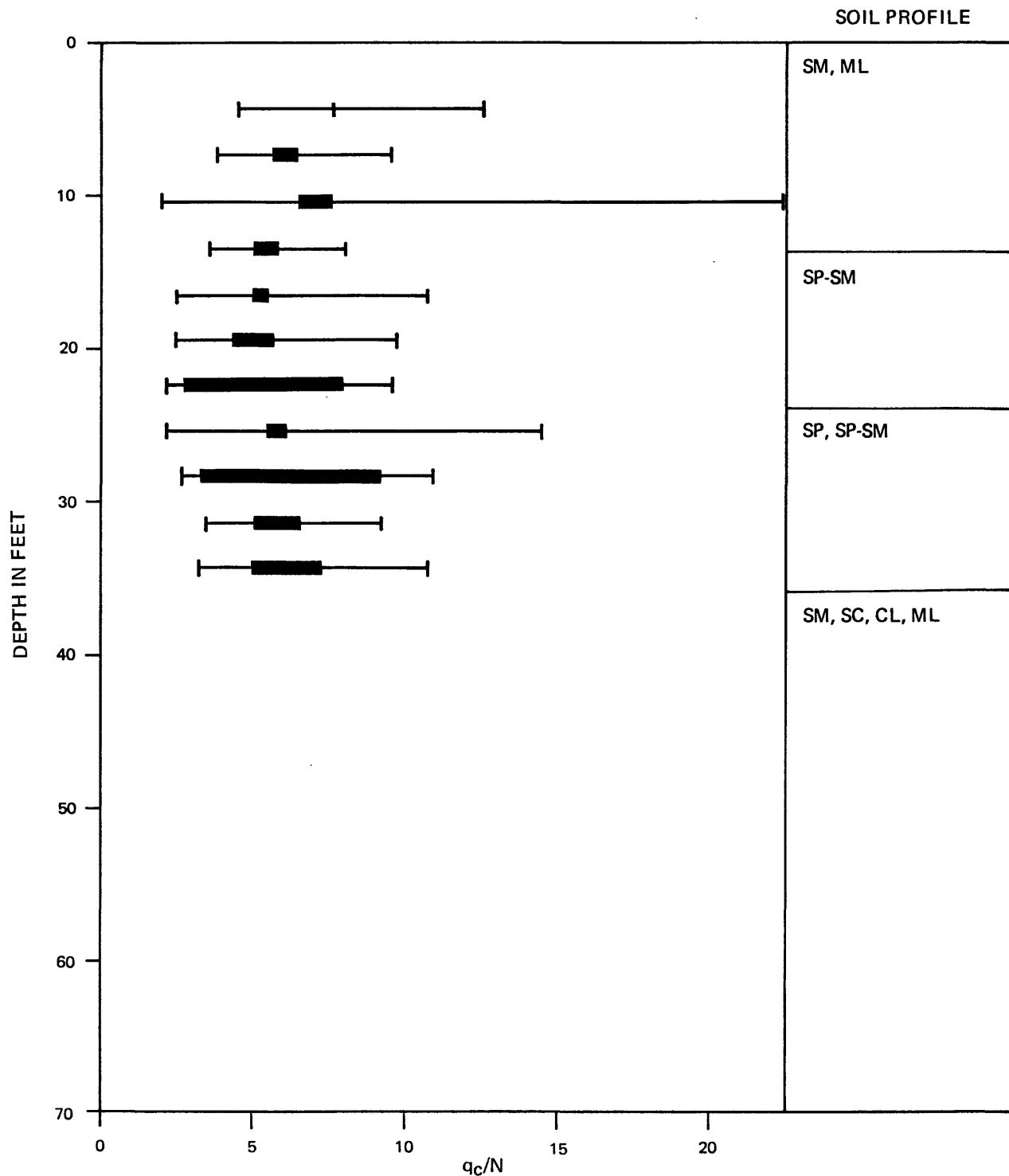


PROJECT NO.: 79-153

USGS CPT-SPT

SAN DIEGO SITE: NAS NORTH ISLAND
qC/N RANGE COMPARISONS
TRIP HAMMER

Approved by _____
Checked by _____
Drawn by _____
Compiled by _____



■ PROBABLE RANGE
— POSSIBLE RANGE



PROJECT NO.:

79-153

USGS CPT-SPT

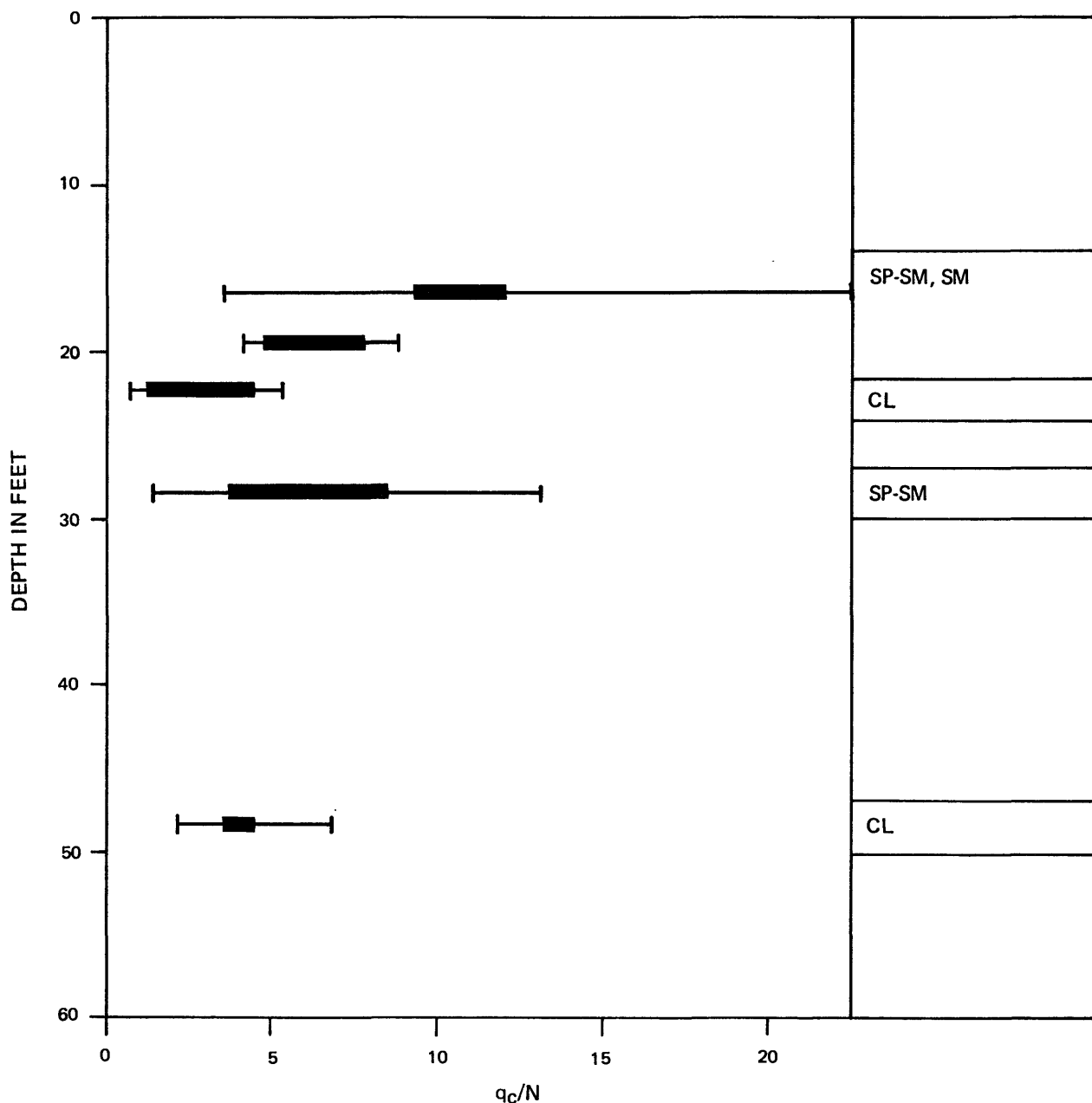
SALINAS SITE
 q_c/N RANGE COMPARISONS
TRIP HAMMER

9-80


FIGURE 3.28

Compiled by _____ /
 Drawn by _____ /
 Checked by _____ /
 Approved by _____ /

SOIL PROFILE



PROBABLE RANGE
POSSIBLE RANGE

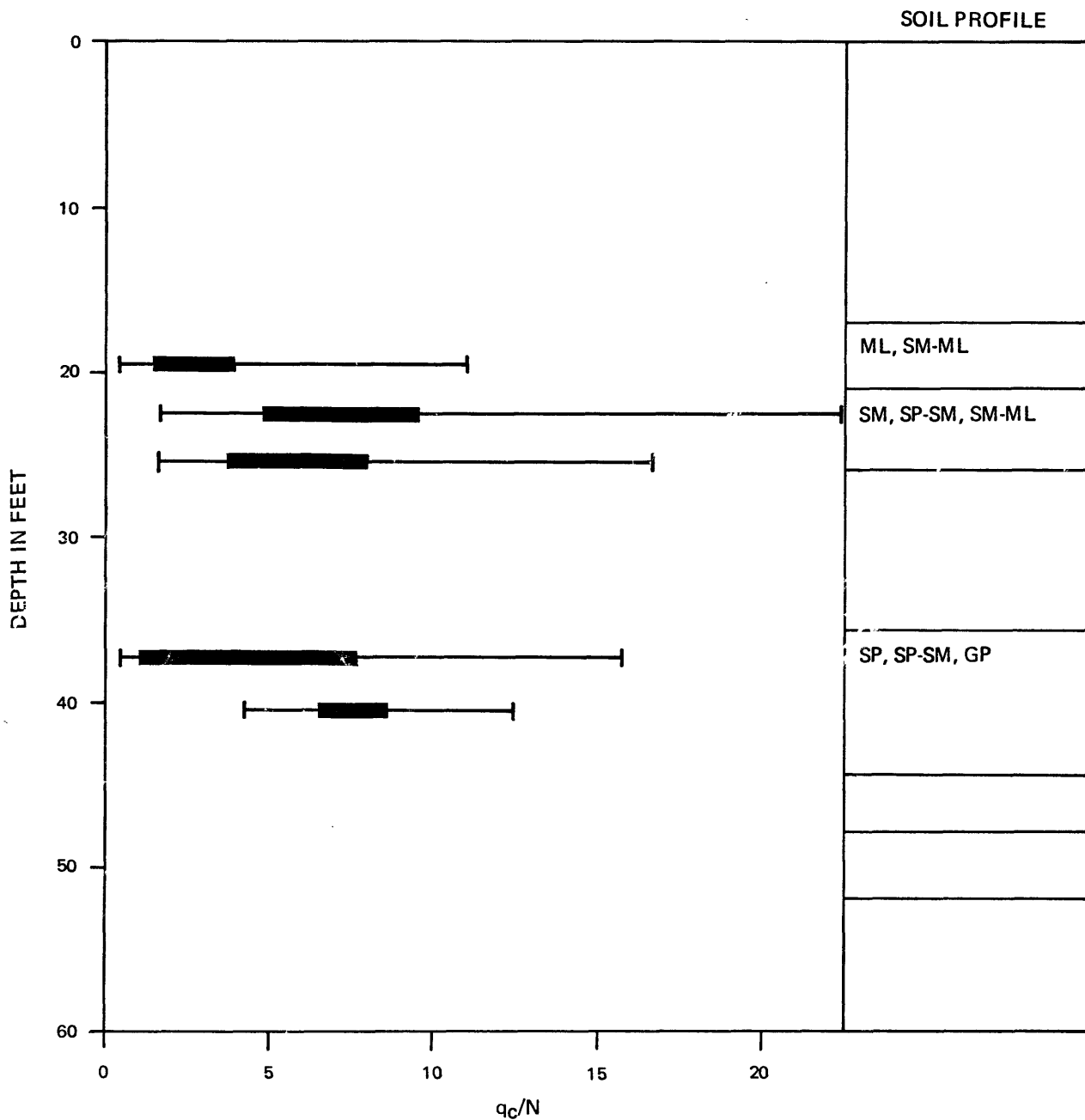


PROJECT NO.: 79-153
 USGS CPT-SPT

MOSS LANDING SITE
 qc/N RANGE COMPARISONS
 TRIP HAMMER

9-80
 FIGURE 3.29

Approved by _____
Checked by _____
Drawn by _____
Compiled by _____



■ PROBABLE RANGE
┌─┐ POSSIBLE RANGE



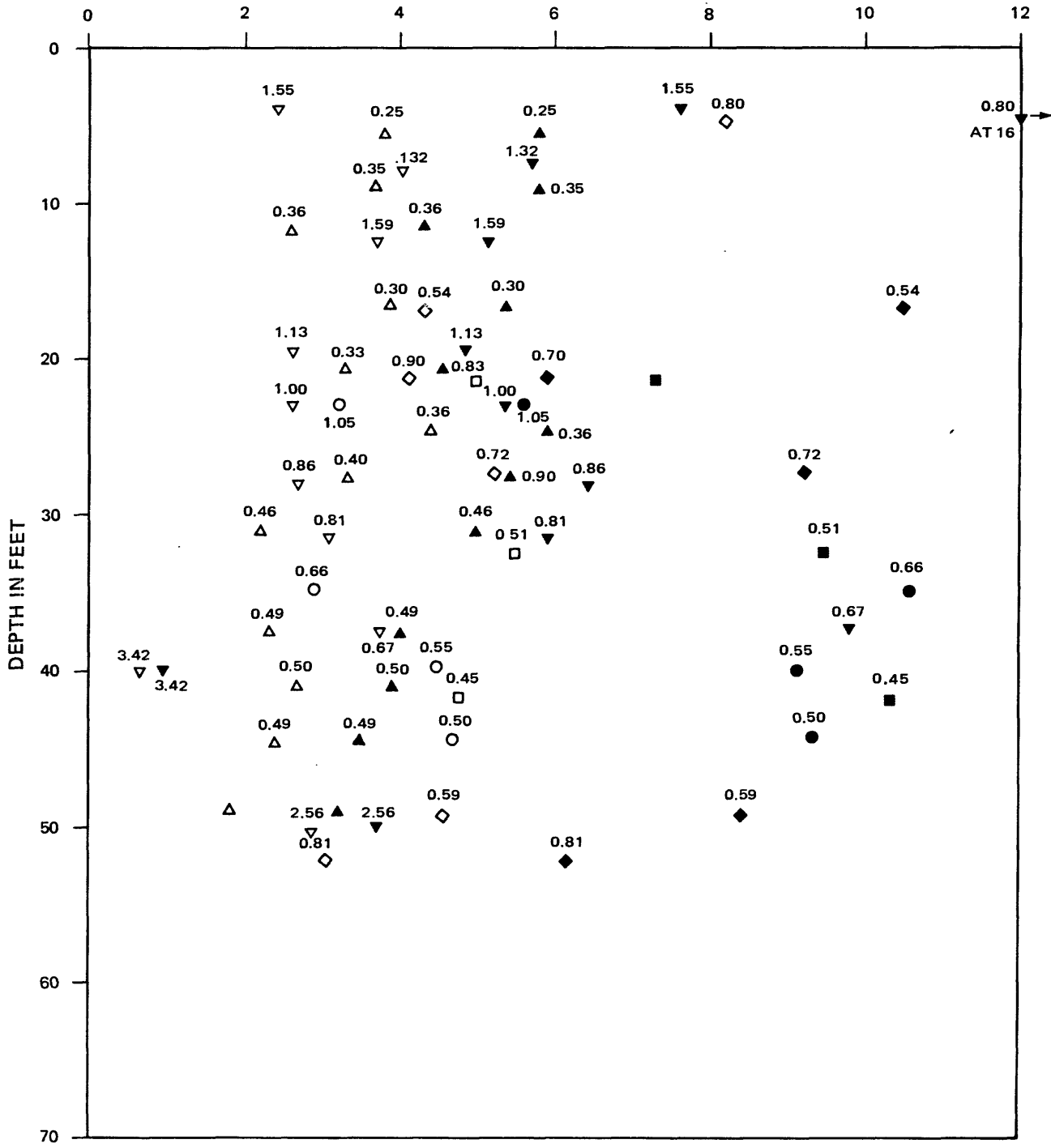
PROJECT NO.: 79-153

USGS CPT-SPT

SAN JOSE SITE: COYOTE NORTH & SOUTH
 q_c/N RANGE COMPARISONS
TRIP HAMMER


Approved by _____
Checked by _____
Drawn by _____
Compiled by _____

$$\bar{q}_c/\bar{N}$$



- | | | |
|--------------|---|----------|
| COYOTE SOUTH | ○ | STANDARD |
| | ● | TRIP |
| COYOTE NORTH | □ | STANDARD |
| | ■ | TRIP |
| MOSS LANDING | ◇ | STANDARD |
| | ◆ | TRIP |
| SAN DIEGO | △ | STANDARD |
| | ▲ | TRIP |
| SALINAS | ▽ | STANDARD |
| | ▼ | TRIP |

NUMBERS ON POINTS REPRESENT FRICTION RATIO, %



PROJECT NO.: 79-153

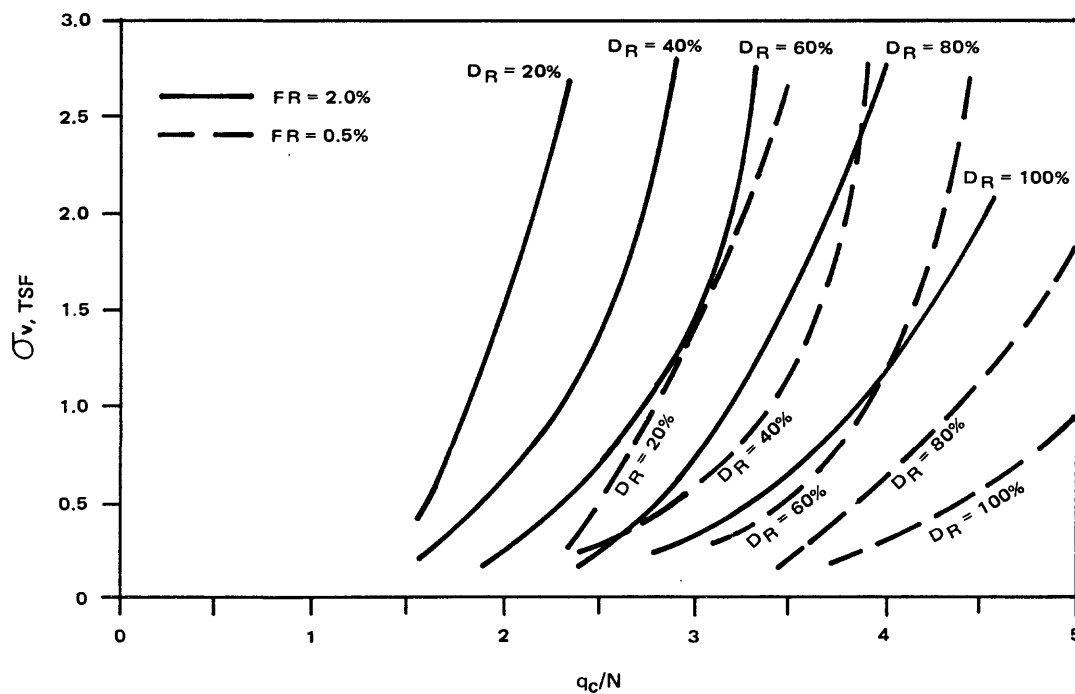
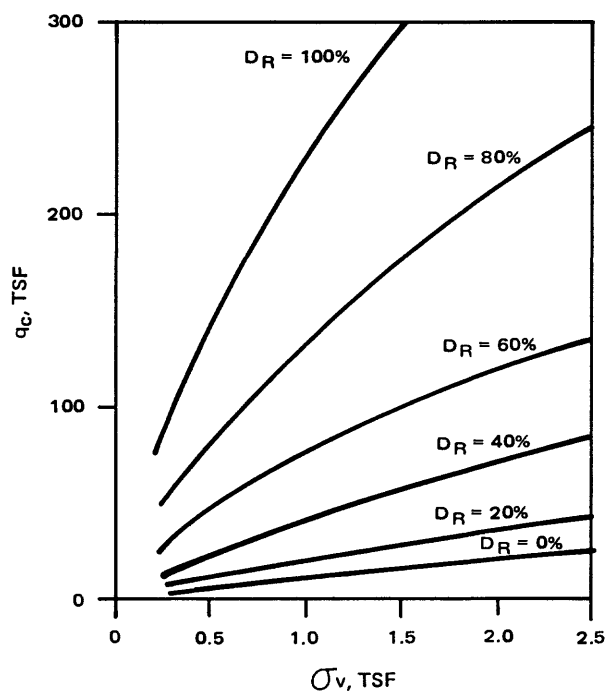
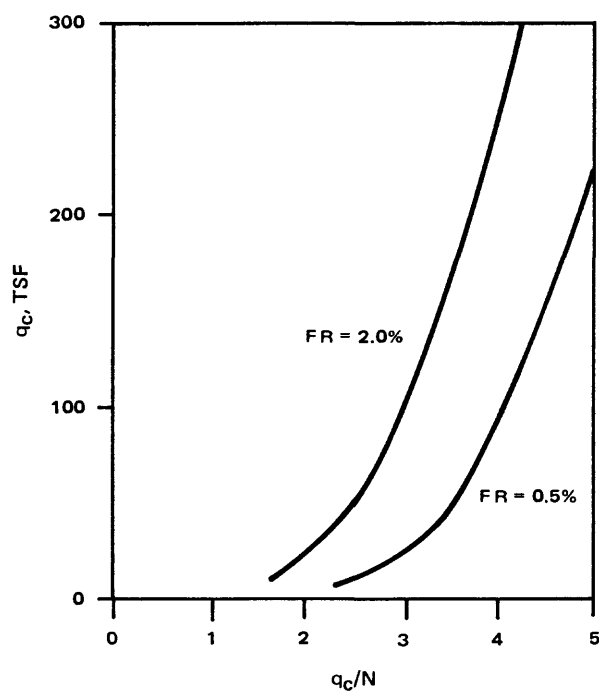
USGS CPT-SPT

COMPOSITE: ALL SITES
 \bar{q}_c/\bar{N} VS DEPTH BY LAYER AVERAGES

9-80

FIGURE 3.36

Approved by _____
Checked by _____
Drawn by _____
Compiled by _____



PROJECT NO.:

79-153

USGS CPT-SPT

q_c/N VS EFFECTIVE
OVERBURDEN PRESSURE
(AFTER SCHMERTMANN, 1978)

9-80

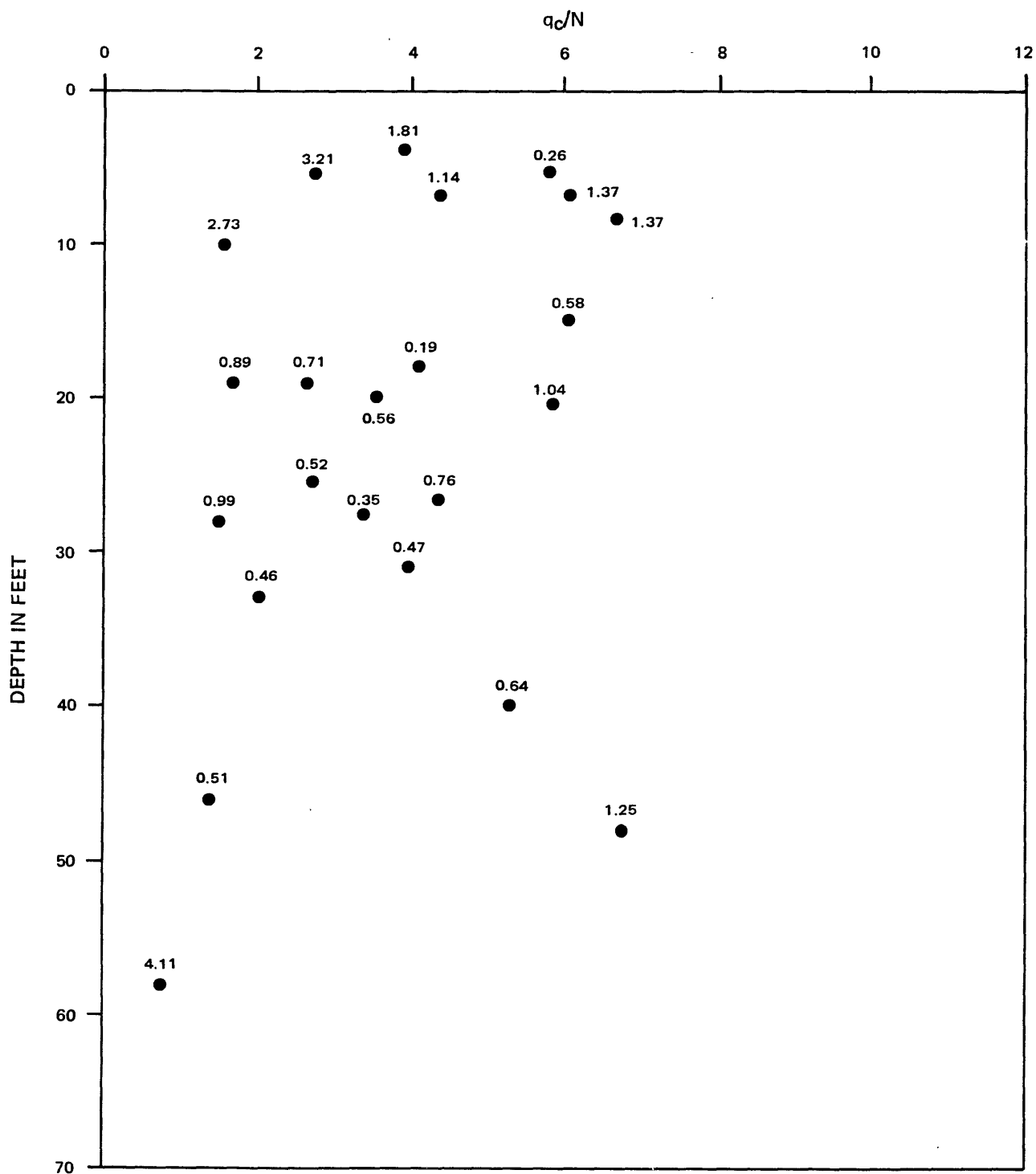
FIGURE 3.37

Approved by _____

Checked by _____

Drawn by _____

Compiled by _____



NUMBERS ON POINTS REPRESENT FRICTION RATIO, %



PROJECT NO.:

79-153

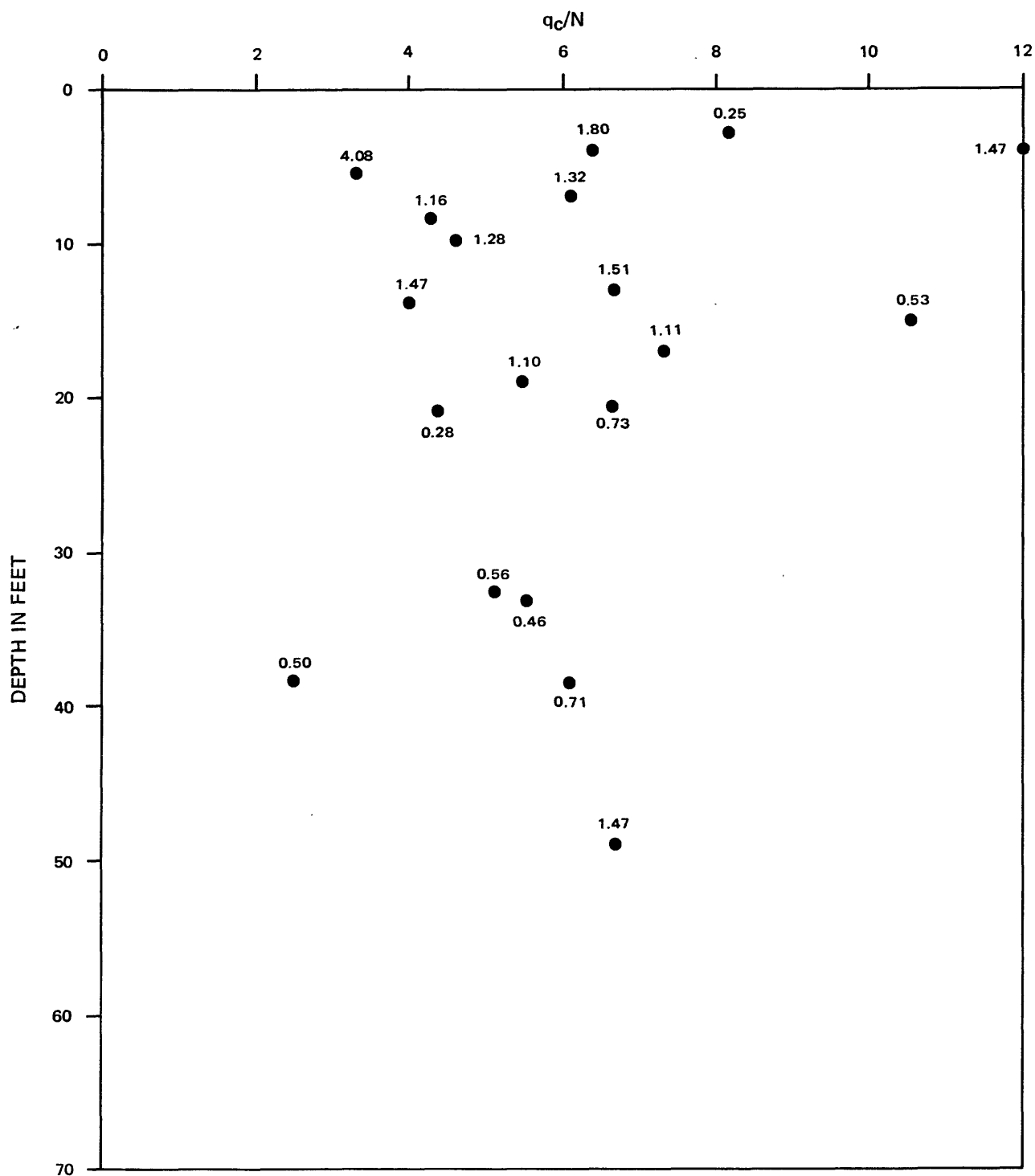
USGS CPT-SPT

COMPOSITE: ALL SITES
 q_c/N VS DEPTH FOR SELECT POINTS
 STANDARD HAMMER

9-80

FIGURE 3.38

Approved by /
Checked by /
Drawn by /
Compiled by /



NUMBERS ON POINTS REPRESENT FRICTION RATIO, %



PROJECT NO.:

79-153

USGS CPT-SPT

COMPOSITE: ALL SITES
 q_c/N VS DEPTH FOR SELECT POINTS
TRIP HAMMER

9-80

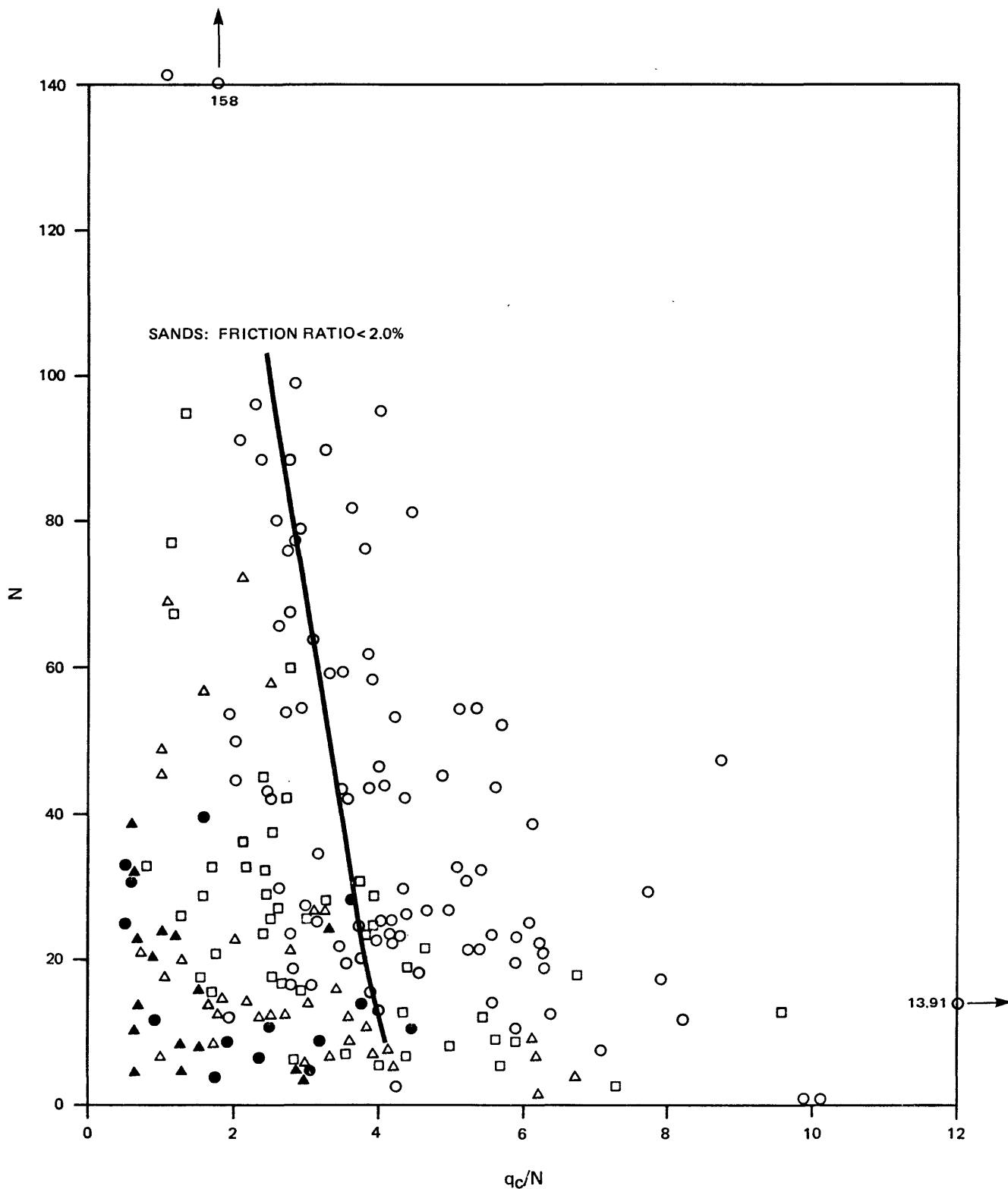
FIGURE 3.39

Approved by

Checked by

Drawn by

Compiled by



FRICTION RATIO, %

- < 0.75
- 0.75 - 1.25
- △ 1.25 - 2.0
- 2.0 - 3.0
- ▲ > 3.0



PROJECT NO.:

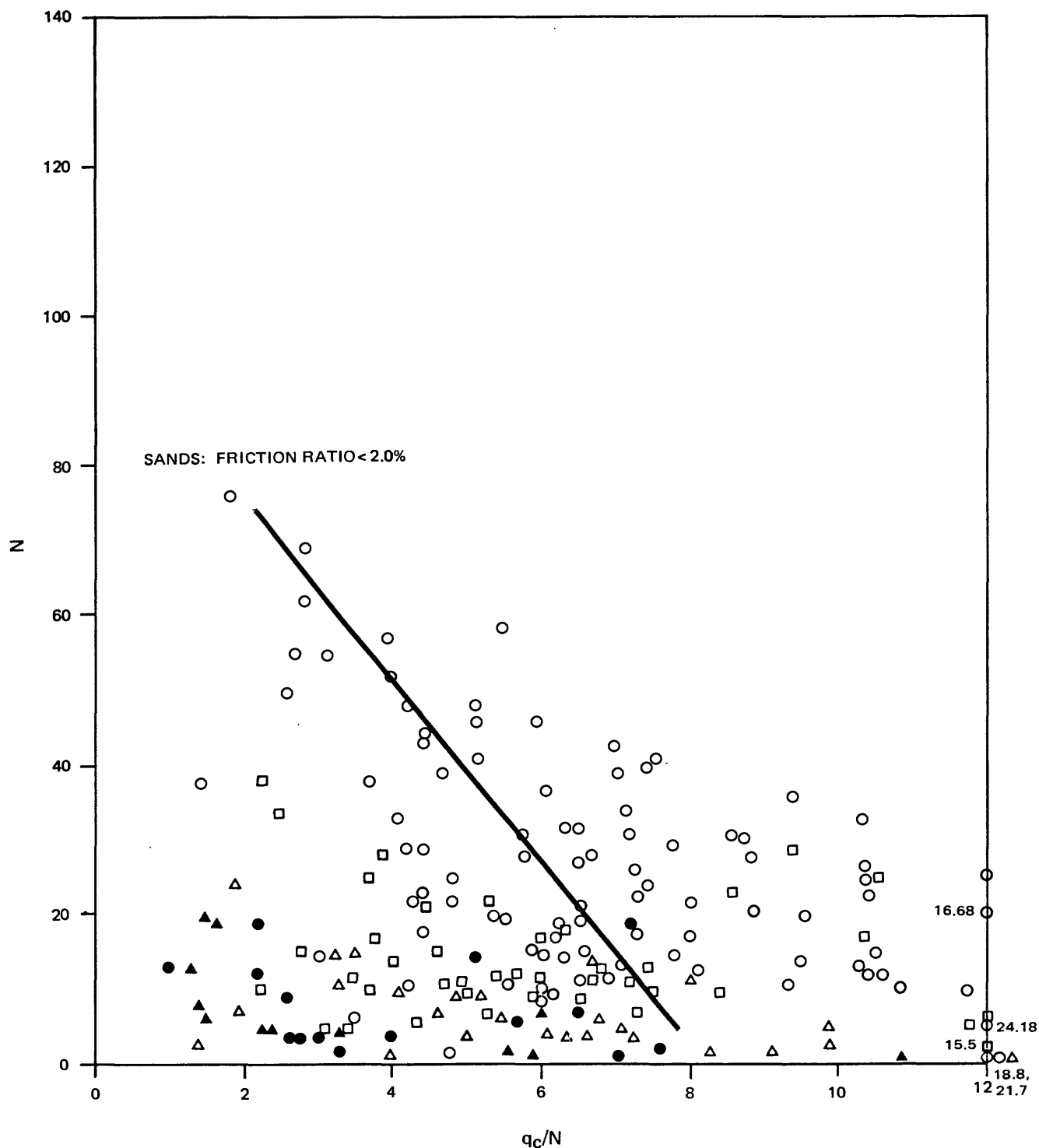
79-153

USGS CPT-SPT

COMPOSITE: ALL SITES
 q_c/N VS N
STANDARD HAMMER

9-80

FIGURE 3.41



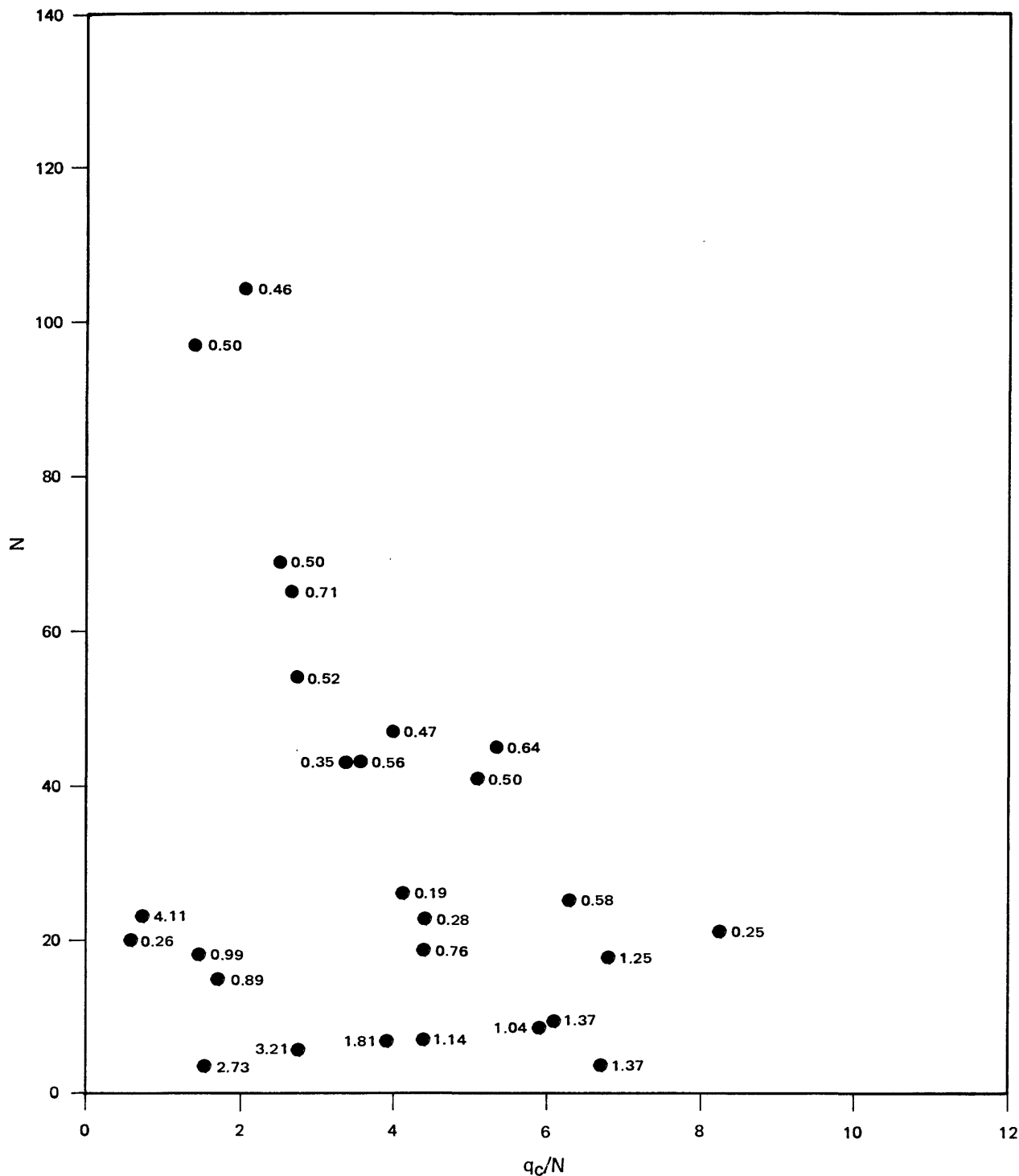
PROJECT NO.:

79-153

USGS CPT-SPT

COMPOSITE: ALL SITES
 q_c/N VS N
 TRIP HAMMER

Approved by _____
Checked by _____
Drawn by _____
Compiled by _____



NUMBERS ON POINTS REPRESENT FRICTION RATIO, %

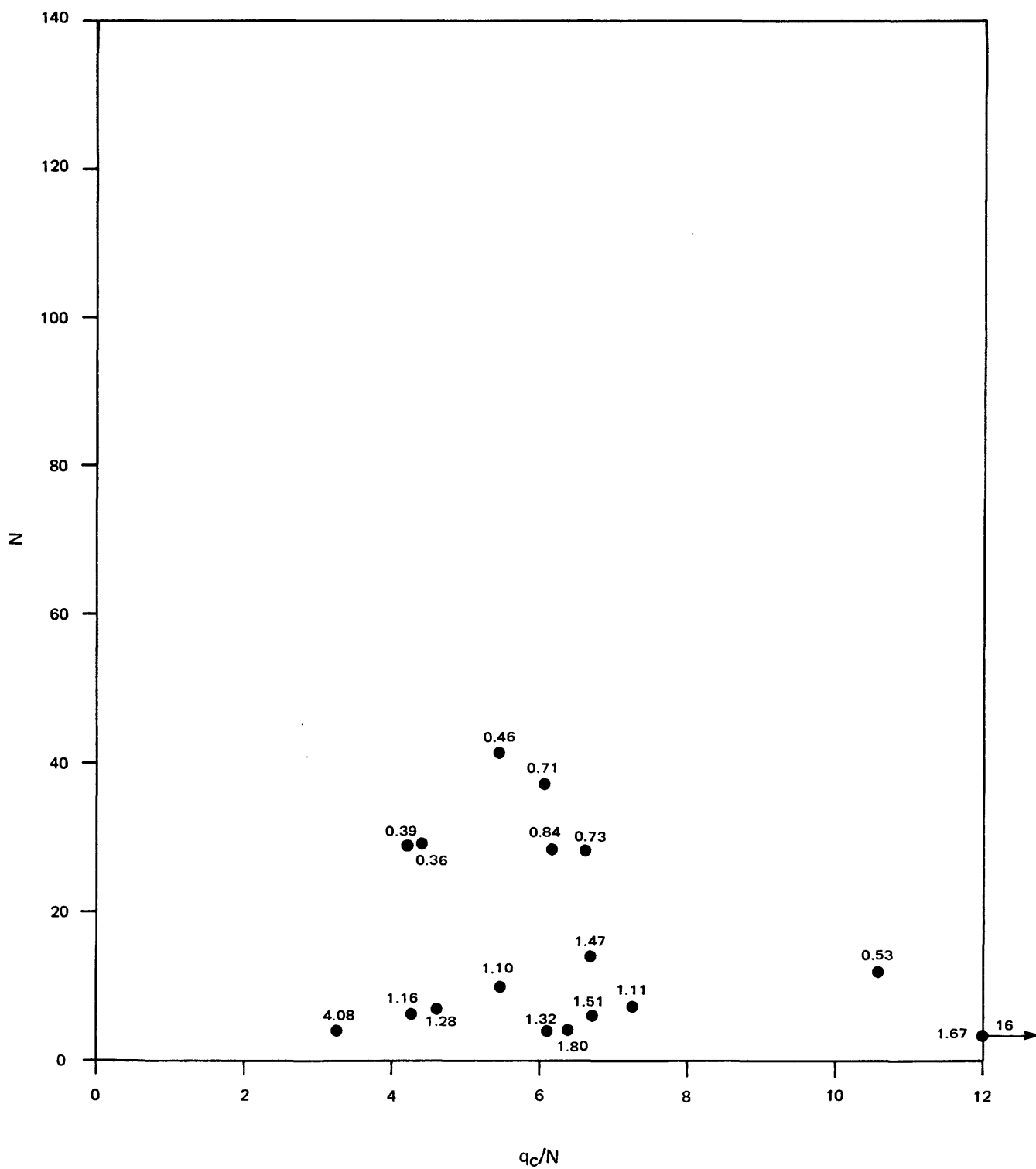


PROJECT NO.:

79-153

USGS CPT-SPT

COMPOSITE: ALL SITES
 q_c/N VS N FOR SELECT POINTS
STANDARD HAMMER



NUMBERS ON POINTS REPRESENT FRICTION RATIO, %



PROJECT NO.:

79-153

USGS CPT-SPT

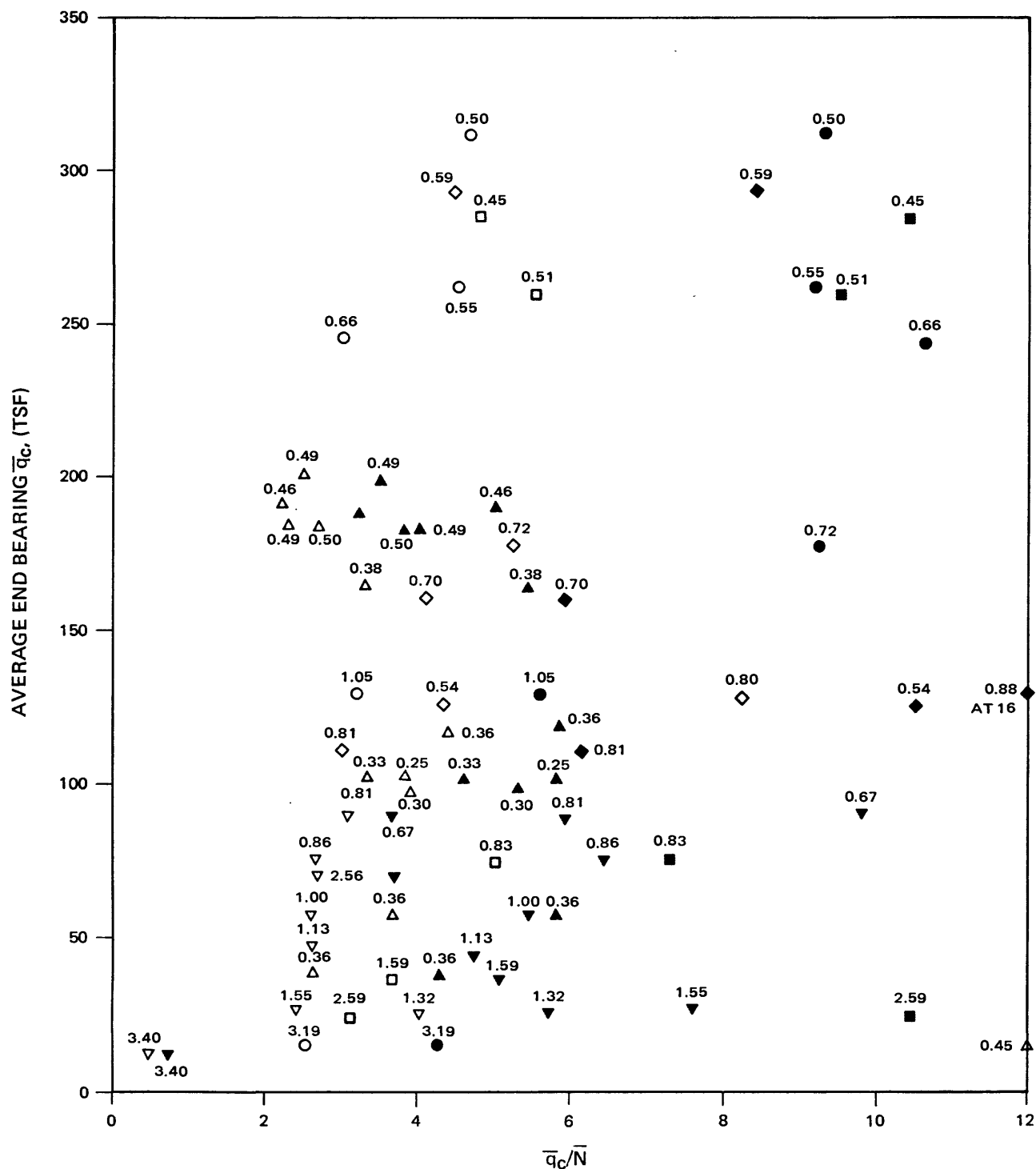
COMPOSITE: ALL SITES
 q_c/N VS N FOR SELECT POINTS
 TRIP HAMMER

Approved by

Checked by

Drawn by

Compiled by



COYOTE SOUTH

○ STANDARD

COYOTE NORTH

● TRIP

MOSS LANDING

□ STANDARD

SAN DIEGO

■ TRIP

SALINAS

◇ STANDARD

▲ TRIP

▼ STANDARD

▼ TRIP

NUMBERS ON POINTS REPRESENT FRICTION RATIO, %



PROJECT NO.:

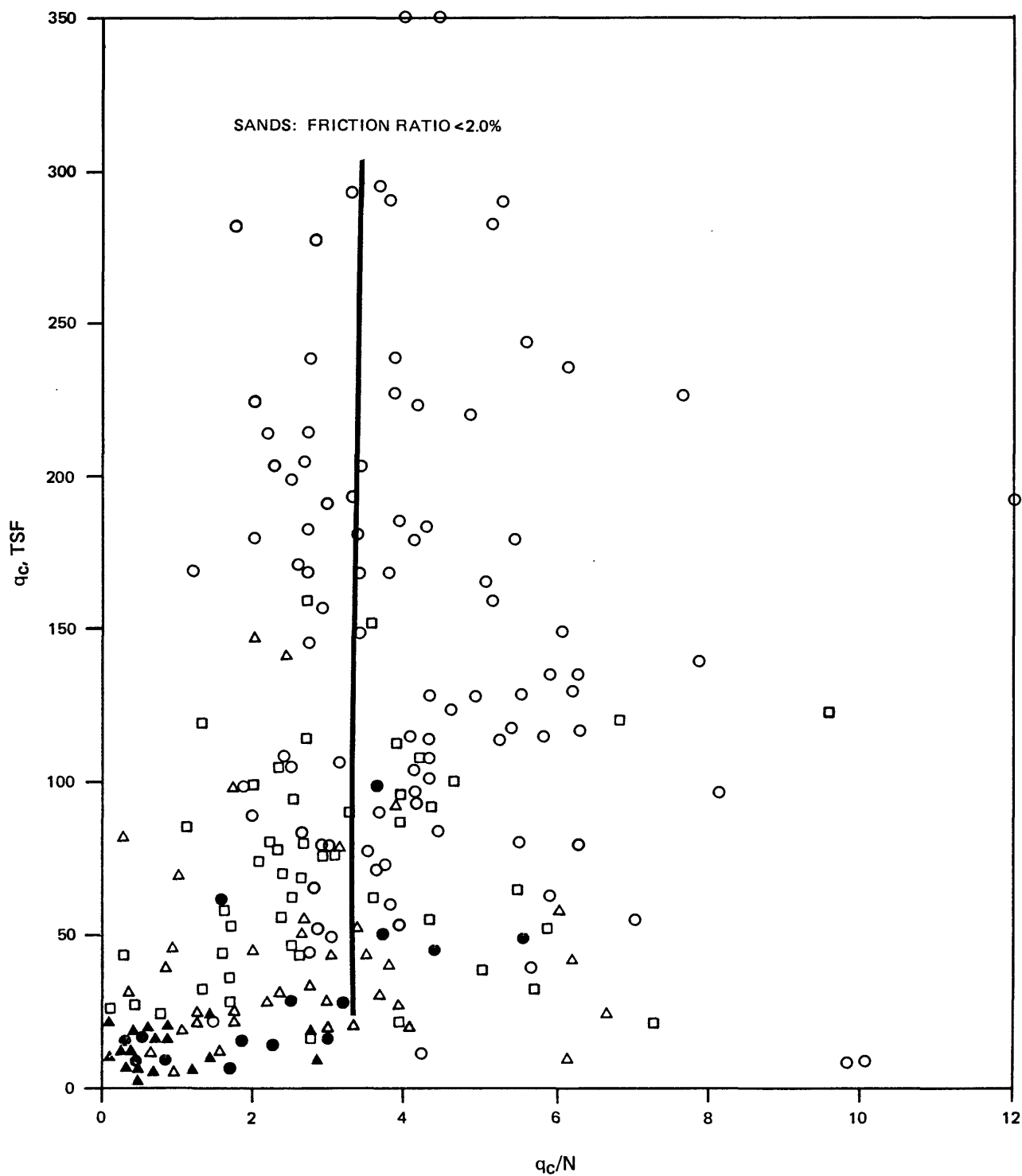
79-153

USGS CPT-SPT

COMPOSITE: ALL SITES
 \bar{q}_c/\bar{N} VS \bar{q}_c
 BY LAYER AVERAGES

9-80

FIGURE 3.45



FRICTION RATIO, %

- < 0.75
- 0.75 - 1.25
- △ 1.25 - 2.0
- 2.0 - 3.0
- ▲ > 3.0



PROJECT NO.:

79-153

USGS CPT-SPT

COMPOSITE: ALL SITES
 q_c/N VS q_c
 STANDARD HAMMER

9-80

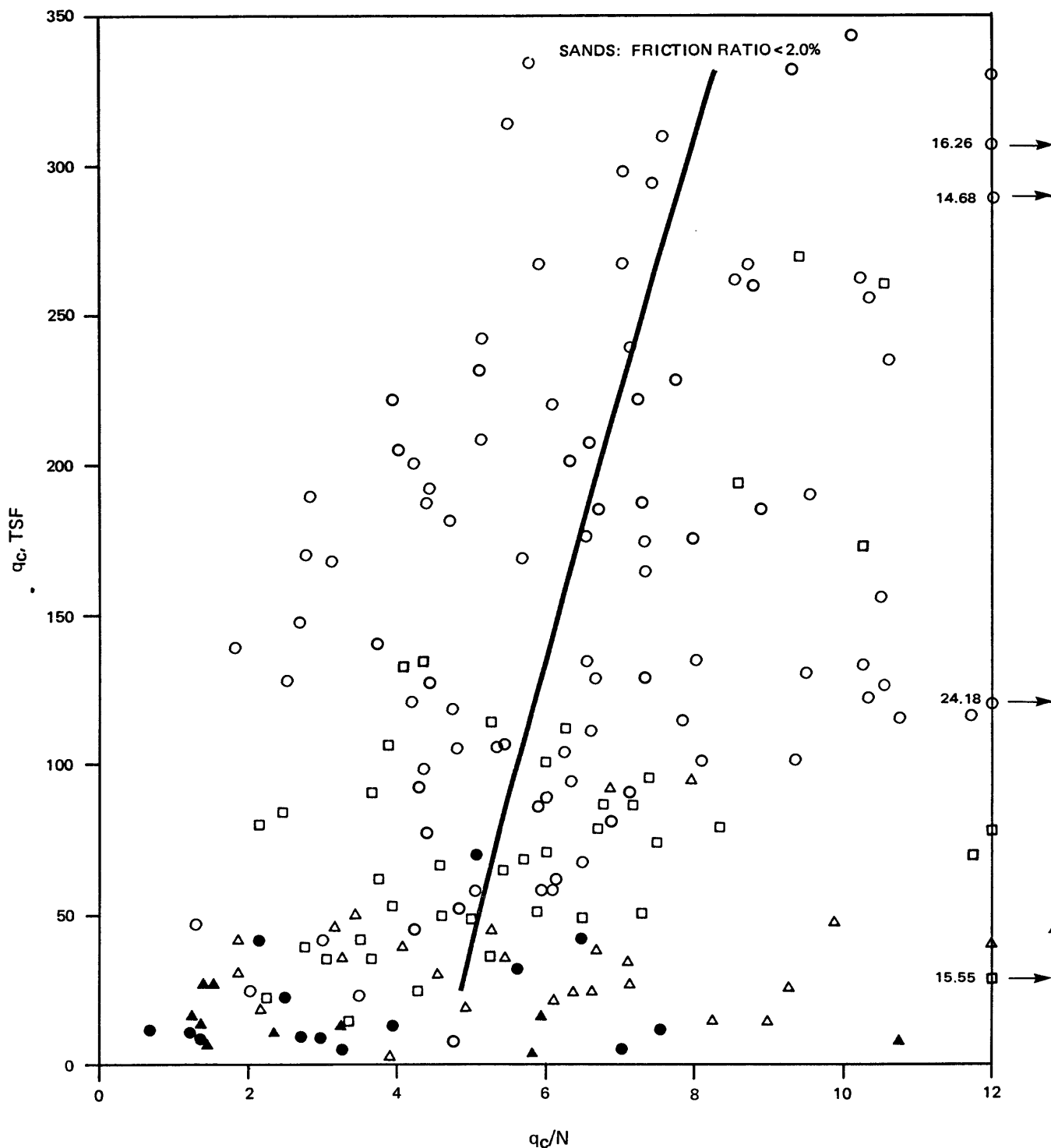
FIGURE 3.46

Approved by _____

Checked by _____

Drawn by _____

Compiled by _____



- FRICITION RATIO, %
- < 0.75
 - 0.75 - 1.25
 - △ 1.25 - 2.0
 - 2.0 - 3.0
 - ▲ > 3.0



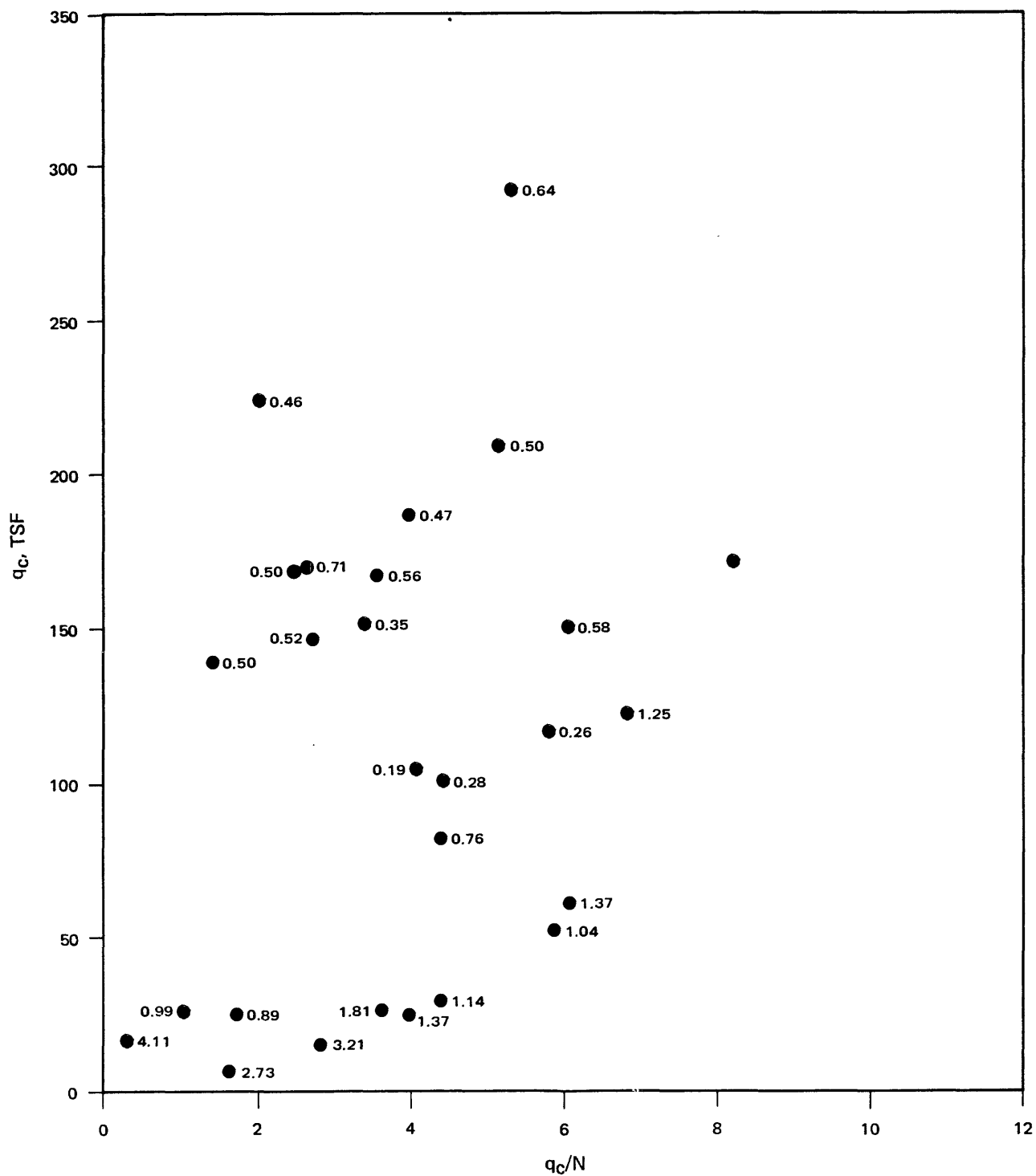
PROJECT NO.:

79-153

USGS CPT-SPT

COMPOSITE: ALL SITES
qc/N VS qc
TRIP HAMMER

Approved by _____
Checked by _____
Drawn by _____
Compiled by _____



NUMBERS ON POINTS REPRESENT FRICTION RATIO, %



PROJECT NO.:

79-153

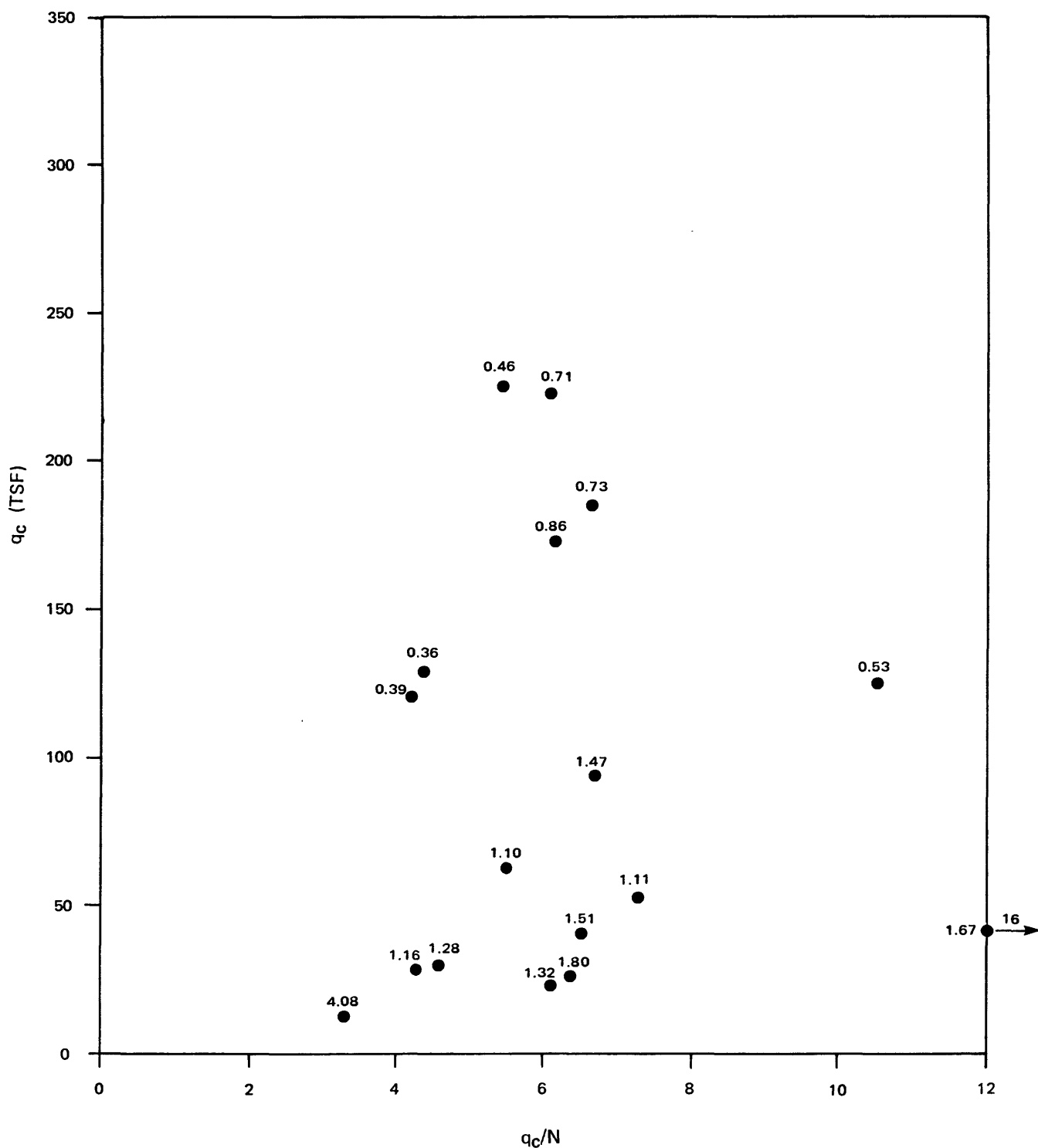
USGS CPT-SPT

COMPOSITE: ALL SITES
 q_c/N VS q_c FOR SELECT POINTS
STANDARD HAMMER

9-80

FIGURE 3.48

Approved by _____
Checked by _____
Drawn by _____
Compiled by _____



NUMBERS ON POINTS REPRESENT FRICTION RATIO, %



PROJECT NO.:

79-153

USGS CPT-SPT

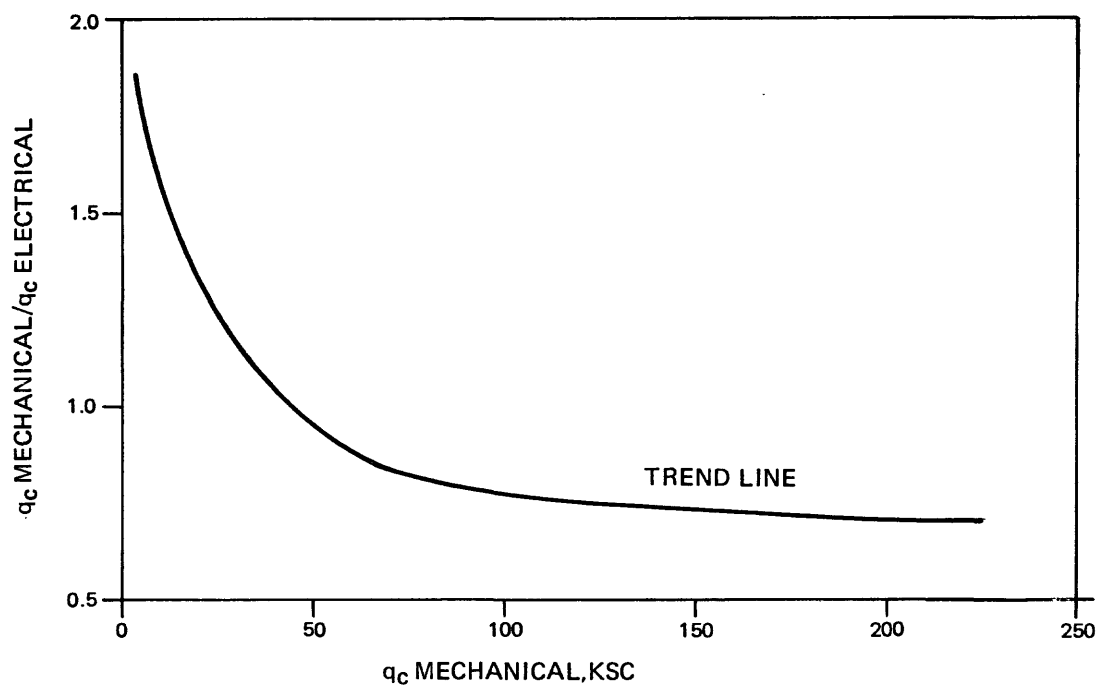
COMPOSITE: ALL SITES
 q_c/N VS q_c FOR SELECT POINTS
TRIP HAMMER

Approved by

Checked by

Drawn by

Compiled by



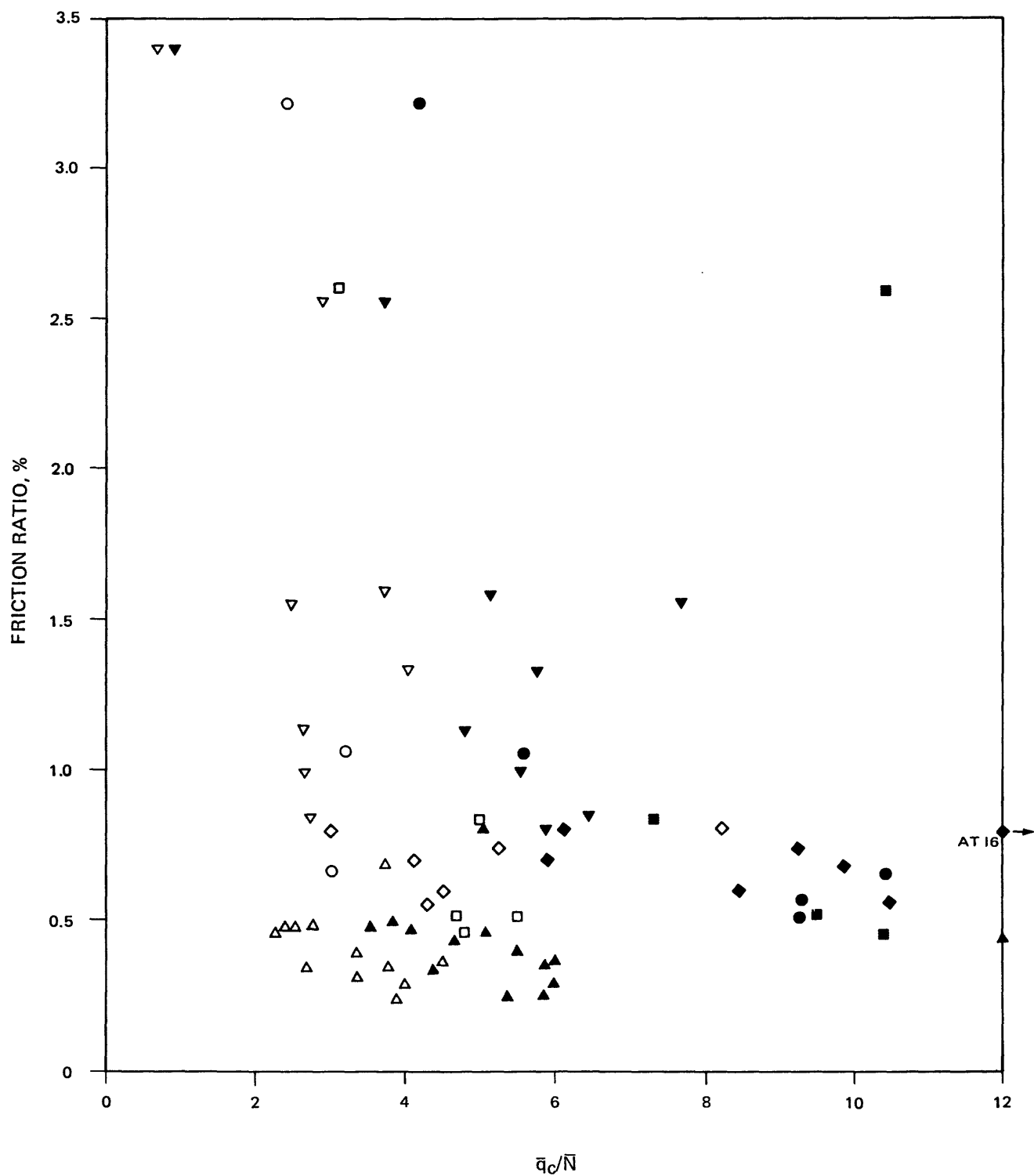
PROJECT NO.:

79-153

USGS CPT-SPT

COMPARISON OF END BEARING
OF MECHANICAL VS ELECTRIC CONE
(AFTER SCHMERTMANN, 1978)

Approved by _____
Checked by _____
Drawn by _____
Compiled by _____



- | | | |
|--------------|---|----------|
| COYOTE SOUTH | ○ | STANDARD |
| | ● | TRIP |
| COYOTE NORTH | □ | STANDARD |
| | ■ | TRIP |
| MOSS LANDING | ◇ | STANDARD |
| | ◆ | TRIP |
| SAN DIEGO | △ | STANDARD |
| | ▲ | TRIP |
| SALINAS | ▽ | STANDARD |
| | ▼ | TRIP |

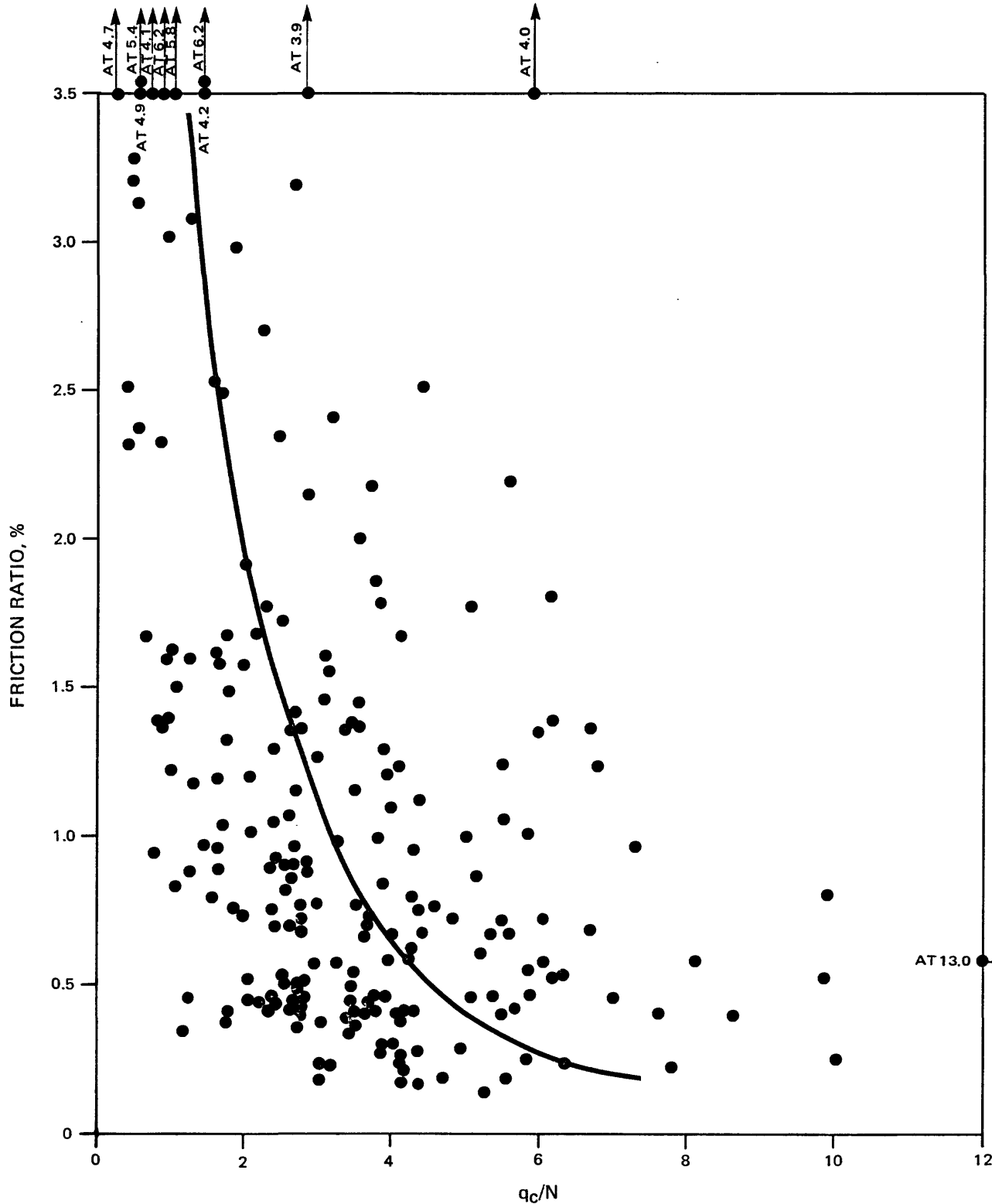


PROJECT NO.:

79-153

USGS CPT-SPT

COMPOSITE: ALL SITES
 \bar{q}_c/\bar{N} VS FRICTION RATIO
BY LAYER AVERAGES



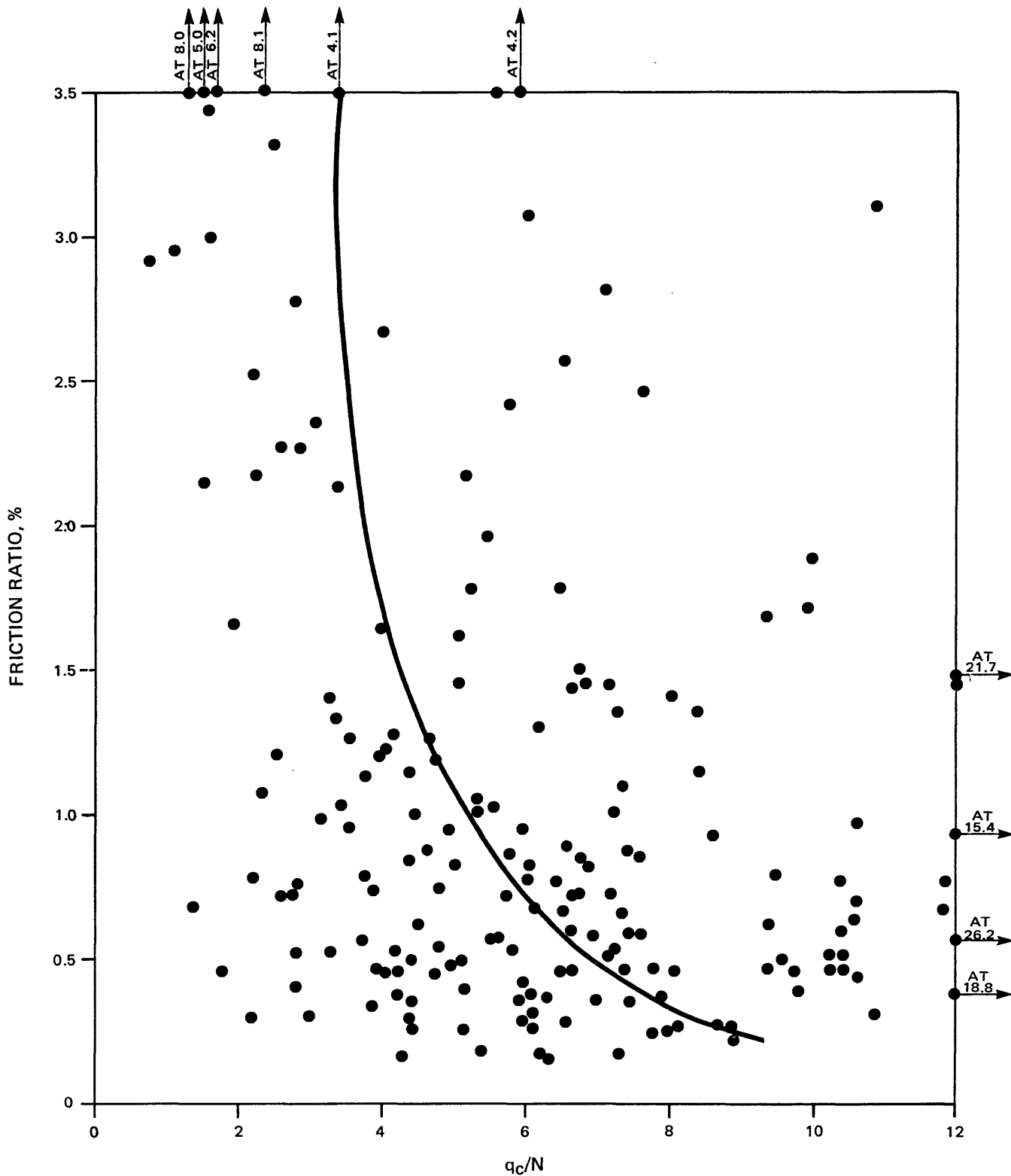
PROJECT NO.:


79-153

USGS CPT-SPT

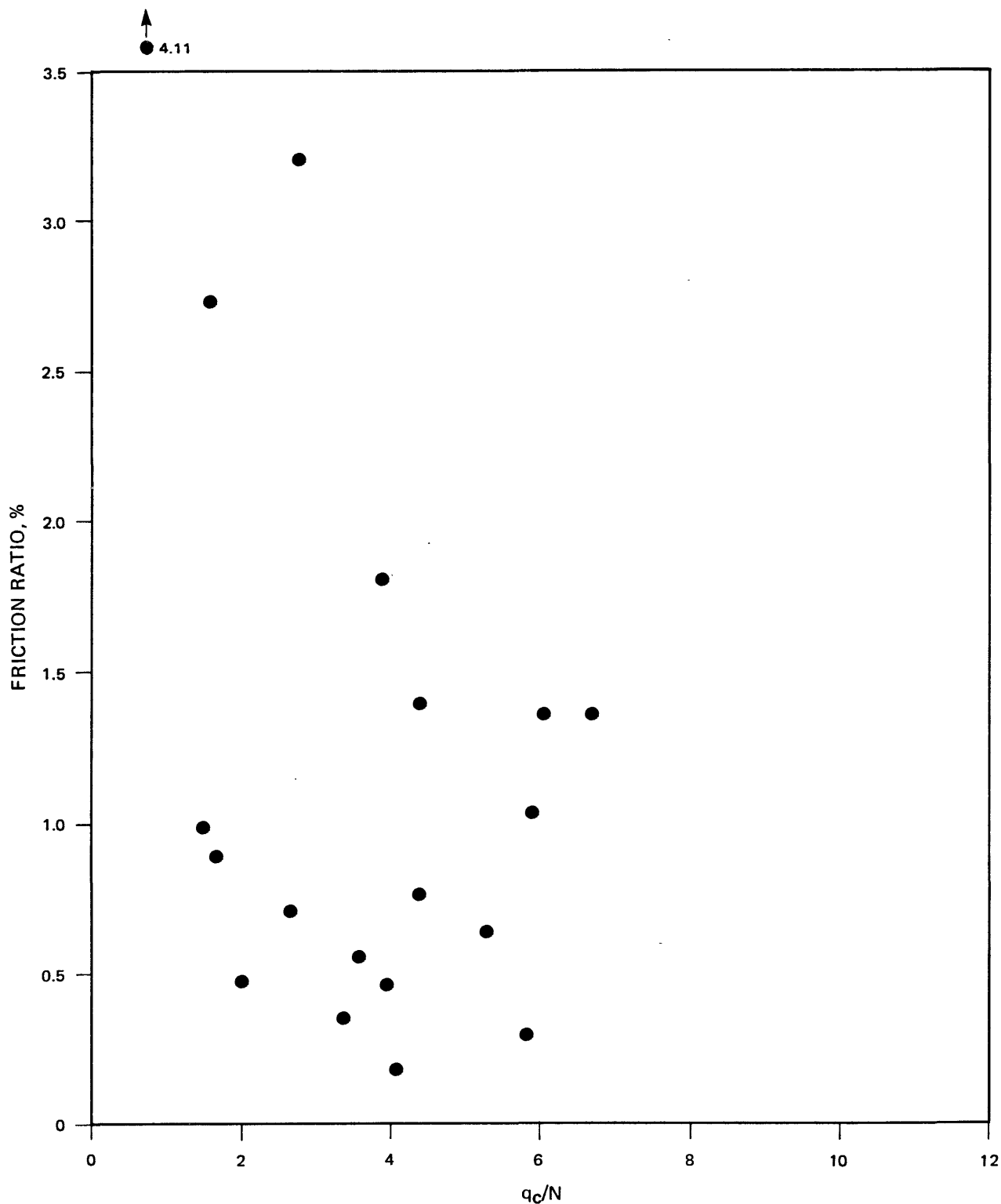
COMPOSITE: ALL SITES
 q_c/N VS FRICTION RATIO
 STANDARD HAMMER

Compiled by _____ /
Drawn by _____ /
Checked by _____ /
Approved by _____ /



	PROJECT NO.:	79-153
	USGS CPT-SPT	
COMPOSITE: ALL SITES q_c/N VS FRICTION RATIO TRIP HAMMER		
FIGURE 3.53		

Compiled by _____ Drawn by _____ Checked by _____ Approved by _____



PROJECT NO.:

79-153

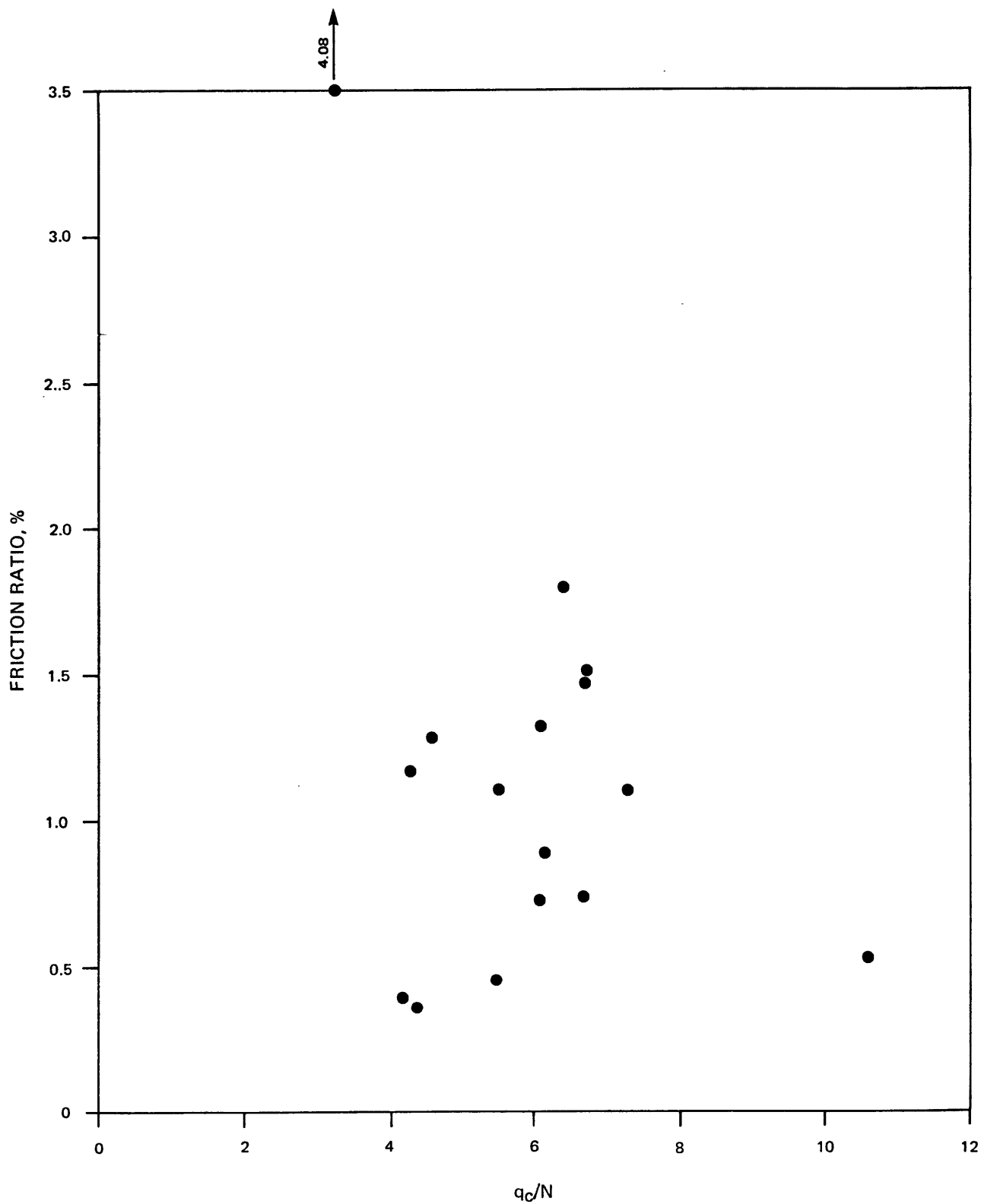
USGS CPT-SPT

COMPOSITE: ALL SITES
 q_c/N VS FRICTION RATIO
FOR SELECT POINTS
STANDARD HAMMER

9-80

FIGURE 3.54

Compiled by _____
Drawn by _____
Checked by _____
Approved by _____

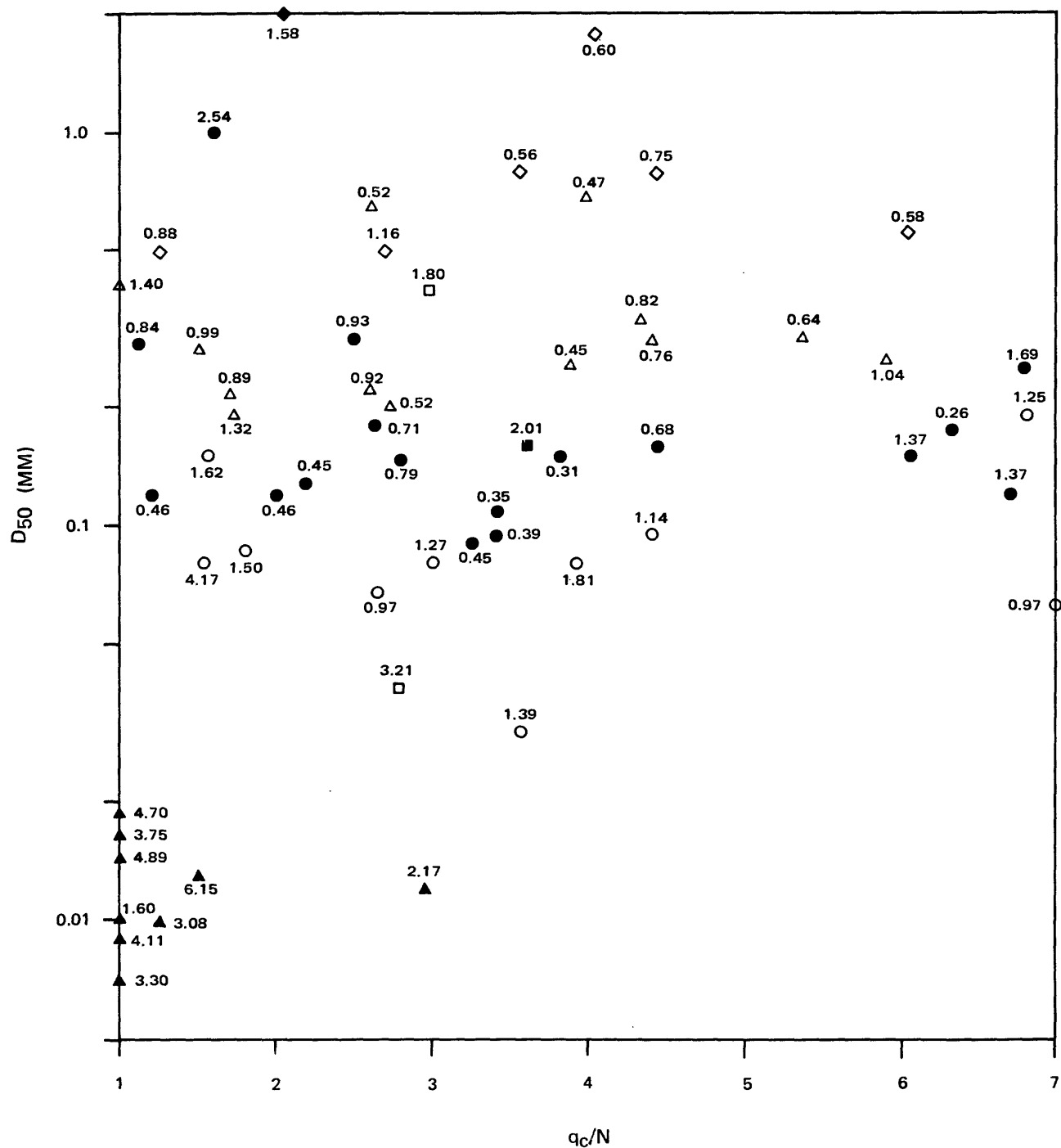


PROJECT NO.: 79-153

USGS CPT-SPT


COMPOSITE: ALL SITES
 q_c/N VS FRICTION RATIO
FOR SELECT POINTS
TRIP HAMMER

Approved by _____
 Checked by _____
 Drawn by _____
 Compiled by _____



- SM
- SM-ML
- SC
- ML
- ◆ GP
- ◇ SP
- ▲ CL
- △ SP-SM

NUMBERS ON POINTS REPRESENT FRICTION RATIO, %

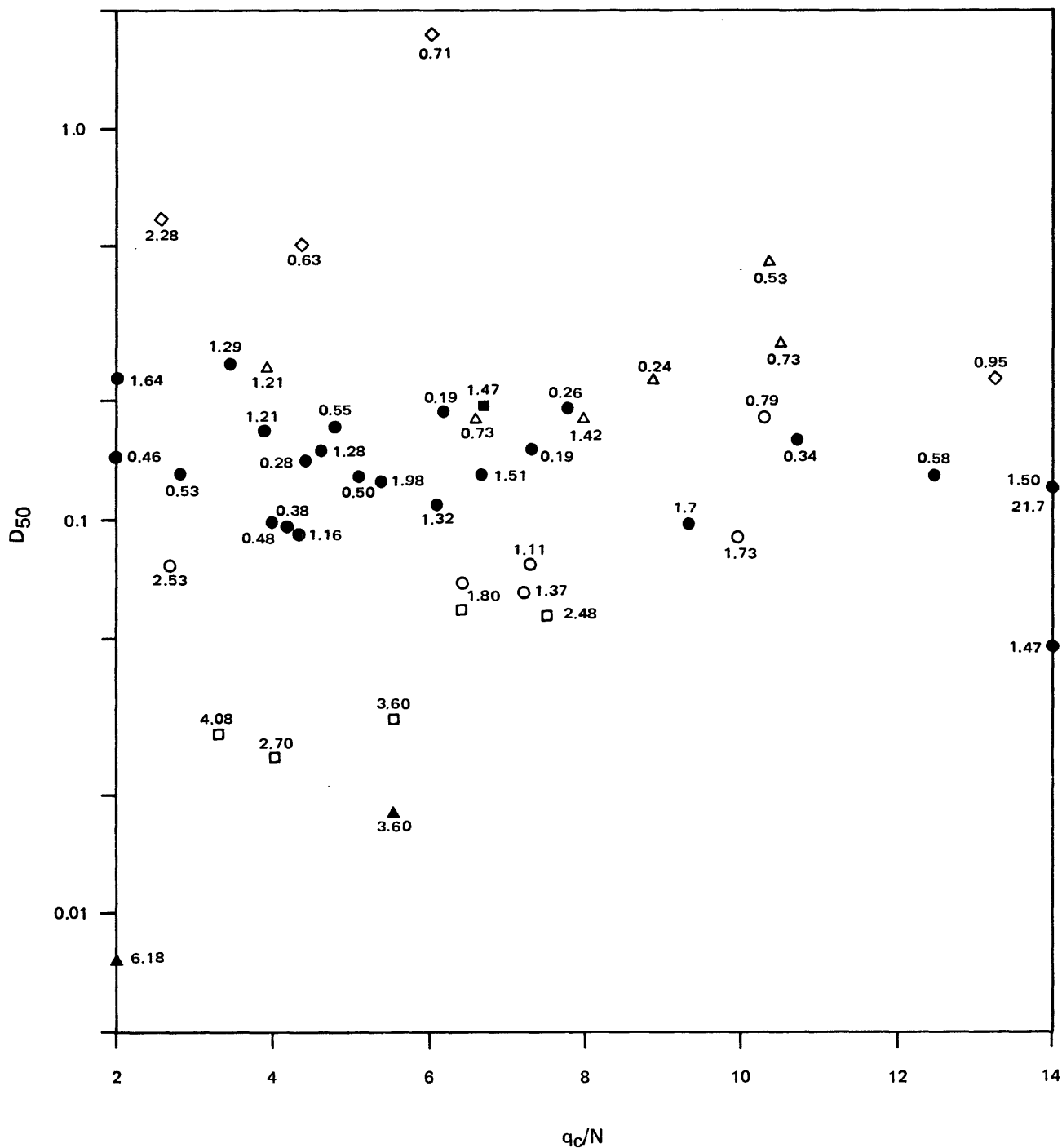
	PROJECT NO.:	79-153
	USGS CPT-SPT	
COMPOSITE: ALL SITES q_c/N VS D_{50} STANDARD HAMMER		
9-80	FIGURE 3.56	

Approved by

Checked by

Drawn by

Compiled by



- SM
- SM-ML
- SC
- ML
- ◆ GP
- ◇ SP
- ▲ CL
- △ SP-SM

NUMBERS ON POINTS REPRESENT FRICTION RATIO, %



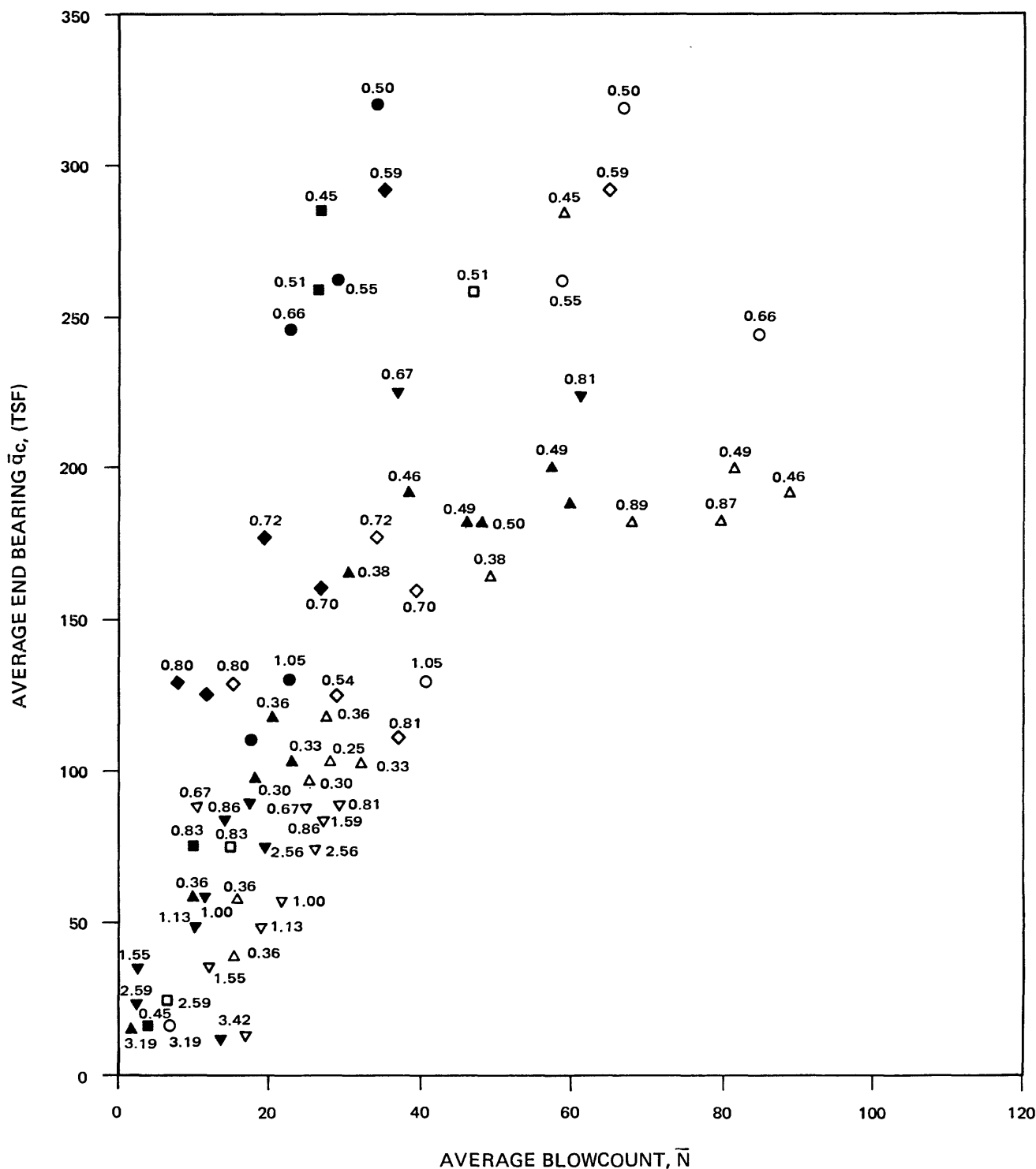
PROJECT NO.:

79-153

USGS CPT-SPT

COMPOSITE: ALL SITES
 q_c/N VS D_{50}
 TRIP HAMMER

Approved by _____
 Checked by _____
 Drawn by _____
 Compiled by _____

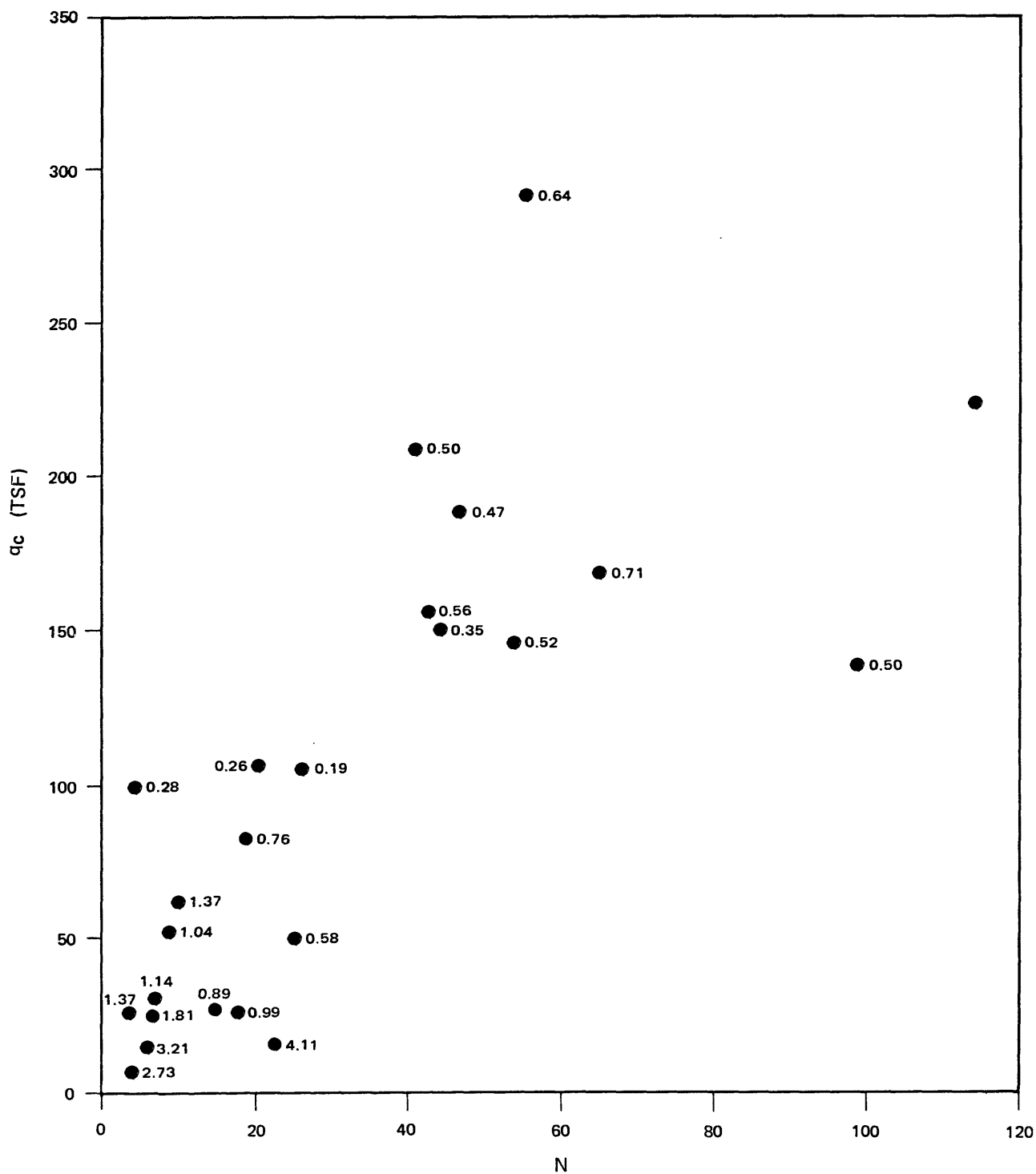


COYOTE SOUTH	○	STANDARD
	●	TRIP
COYOTE NORTH	□	STANDARD
	■	TRIP
MOSS LANDING	◇	STANDARD
	◆	TRIP
SAN DIEGO	△	STANDARD
	▲	TRIP
SALINAS	▽	STANDARD
	▼	TRIP

NUMBERS ON POINTS REPRESENT FRICTION RATIO, %

	PROJECT NO.: 79-153
	USGS CPT-SPT
COMPOSITE: ALL SITES \bar{q}_c VS \bar{N} BY LAYER AVERAGES	
9-80	FIGURE 3.58

Approved by _____
Checked by _____
Drawn by _____
Compiled by _____



NUMBERS ON POINTS REPRESENT FRICTION RATIO, %



PROJECT NO.:

79-153

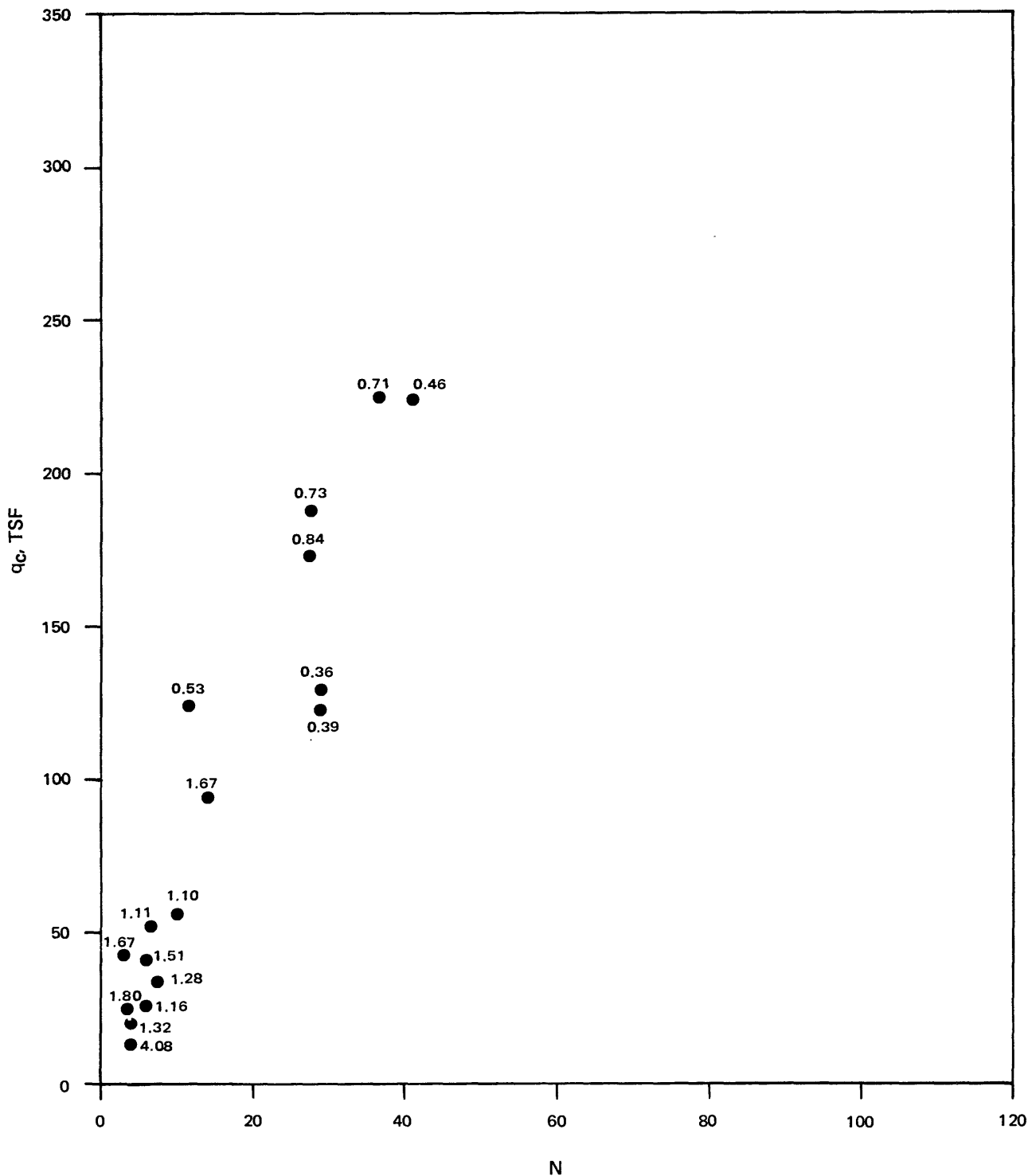
USGS CPT-SPT

COMPOSITE: ALL SITES
 q_c VS N FOR SELECT POINTS
STANDARD HAMMER

9-80

FIGURE 3.61

Approved by _____
Checked by _____
Drawn by _____
Compiled by _____



NUMBERS ON POINTS REPRESENT FRICTION RATIO, %



PROJECT NO.:

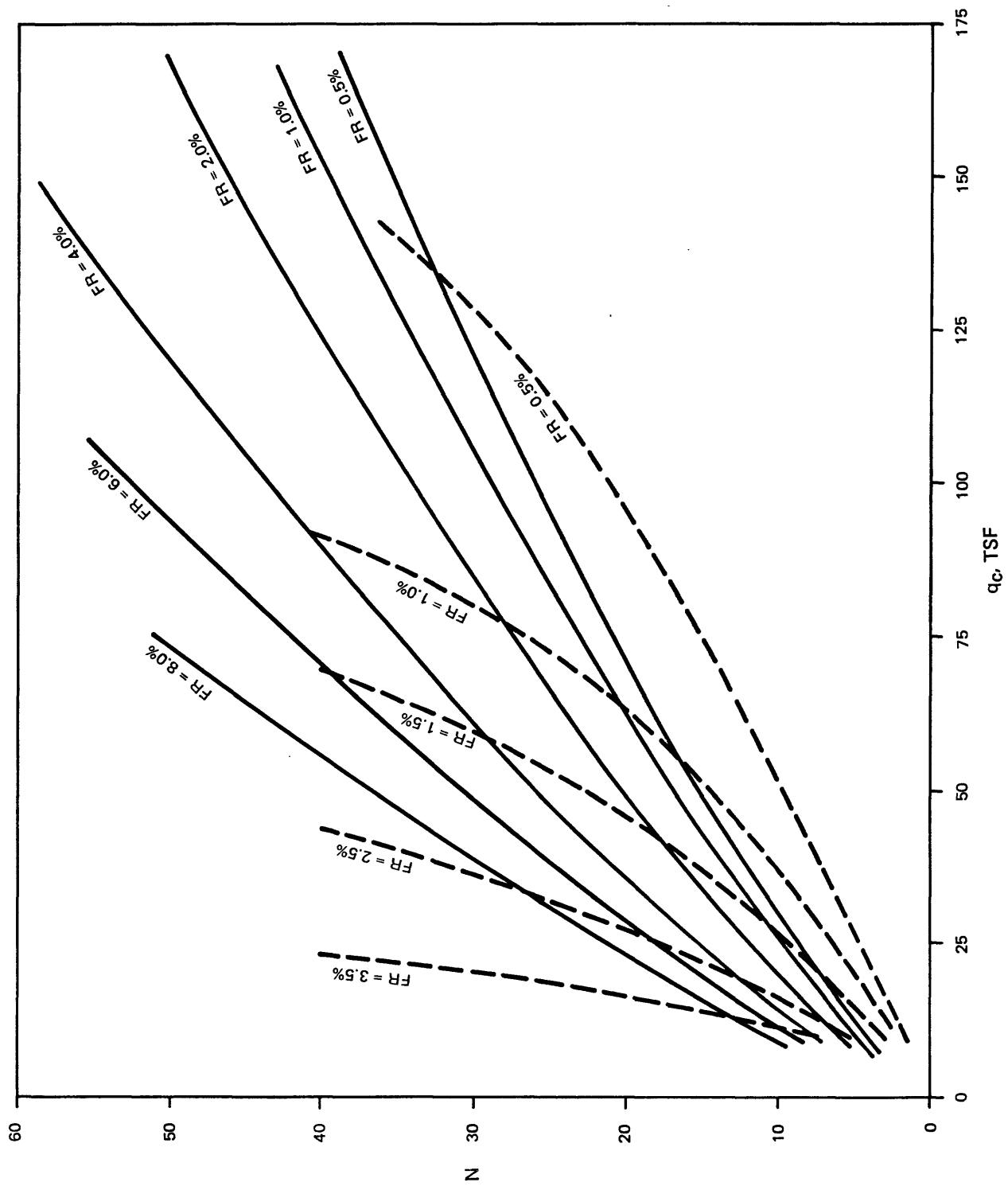
79-153

USGS CPT-SPT

COMPOSITE: ALL SITES
 q_c VS N FOR SELECT POINTS
TRIP HAMMER

9-80

FIGURE 3.62



— USGS STANDARD HAMMER
 --- SCHMERTMANN (1976)



PROJECT NO.:

79-153

USGS CPT-SPT

COMPARISON OF q_c VS N
 STANDARD HAMMER AND
 SCHMERTMANN RELATION

9-80

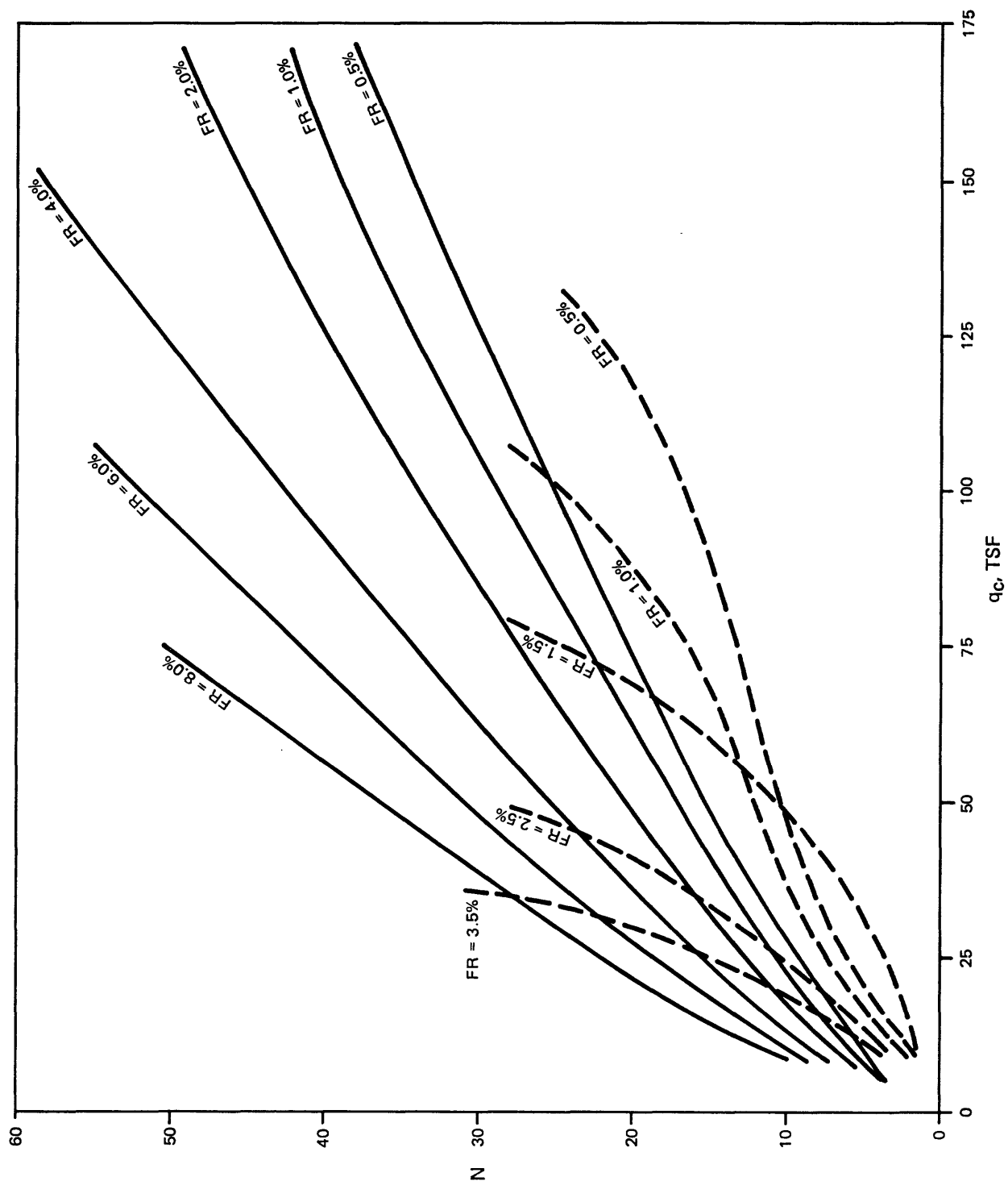
FIGURE 3.63

Approved by

Checked by

Drawn by

Compiled by



— USGS TRIP HAMMER
 - - - SCHMERTMANN (1976)

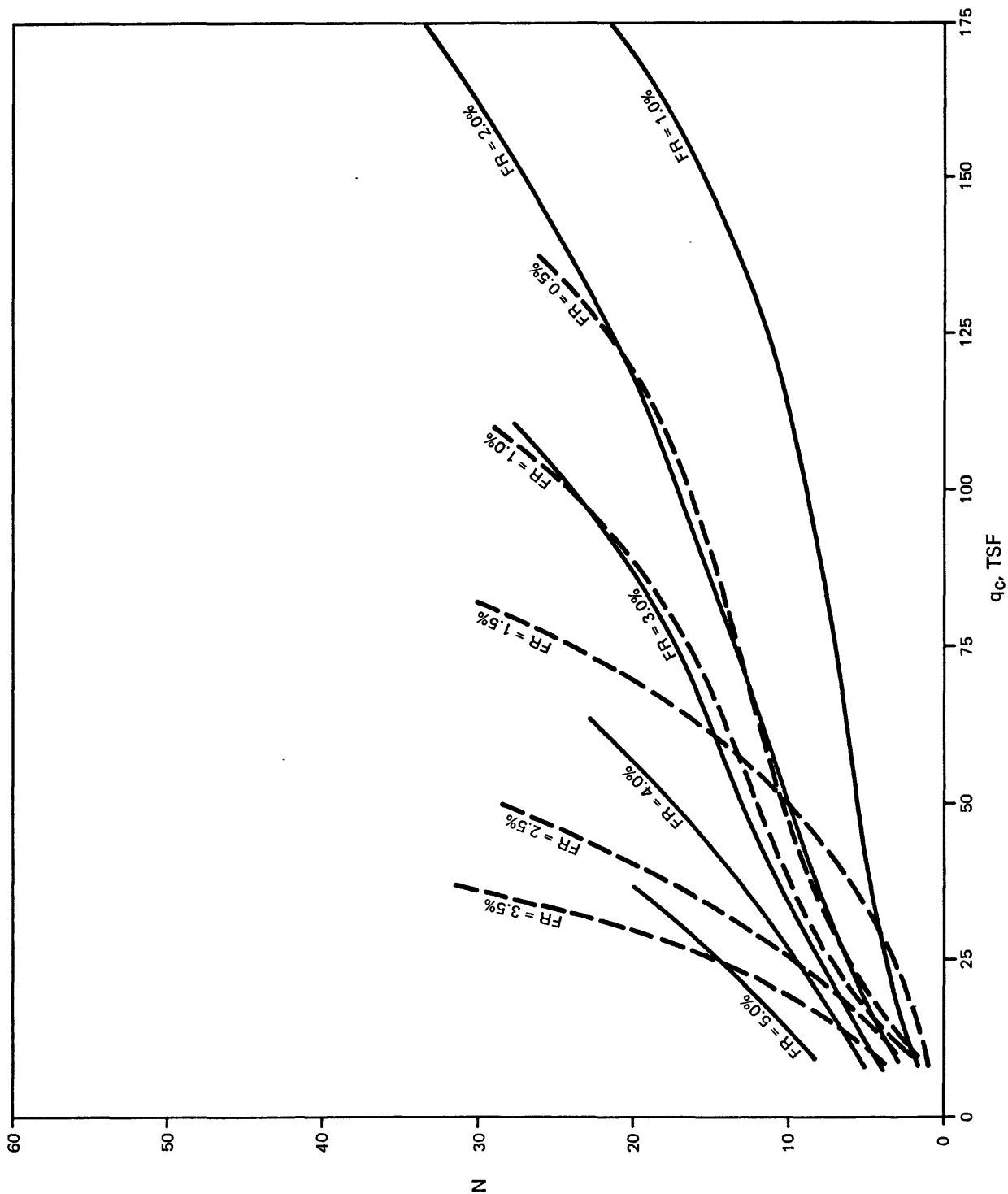


PROJECT NO.:

79-153

USGS CPT-SPT

COMPARISON OF q_c VS N
 TRIP HAMMER AND
 SCHMERTMANN RELATION



— USGS TRIP HAMMER
 - - - EDMOND, OKLAHOMA TREND (TRIP HAMMER)



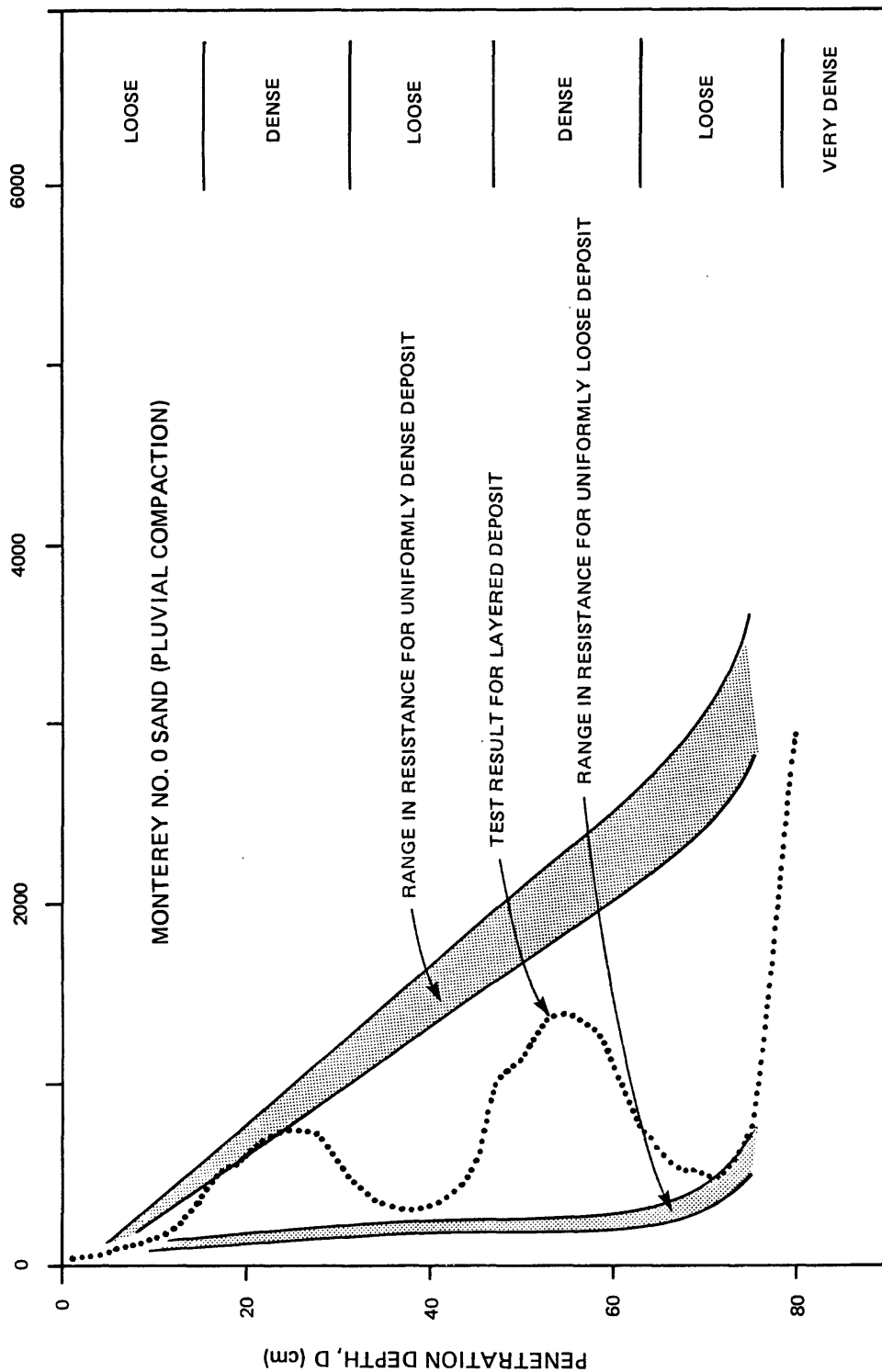
PROJECT NO.:

79-153

USGS CPT-SPT

COMPARISON OF q_c VS N
 TRIP HAMMER AND
 COE TRIP HAMMER

UNIT PENETRATION RESISTANCE, q_f (kN/m²)



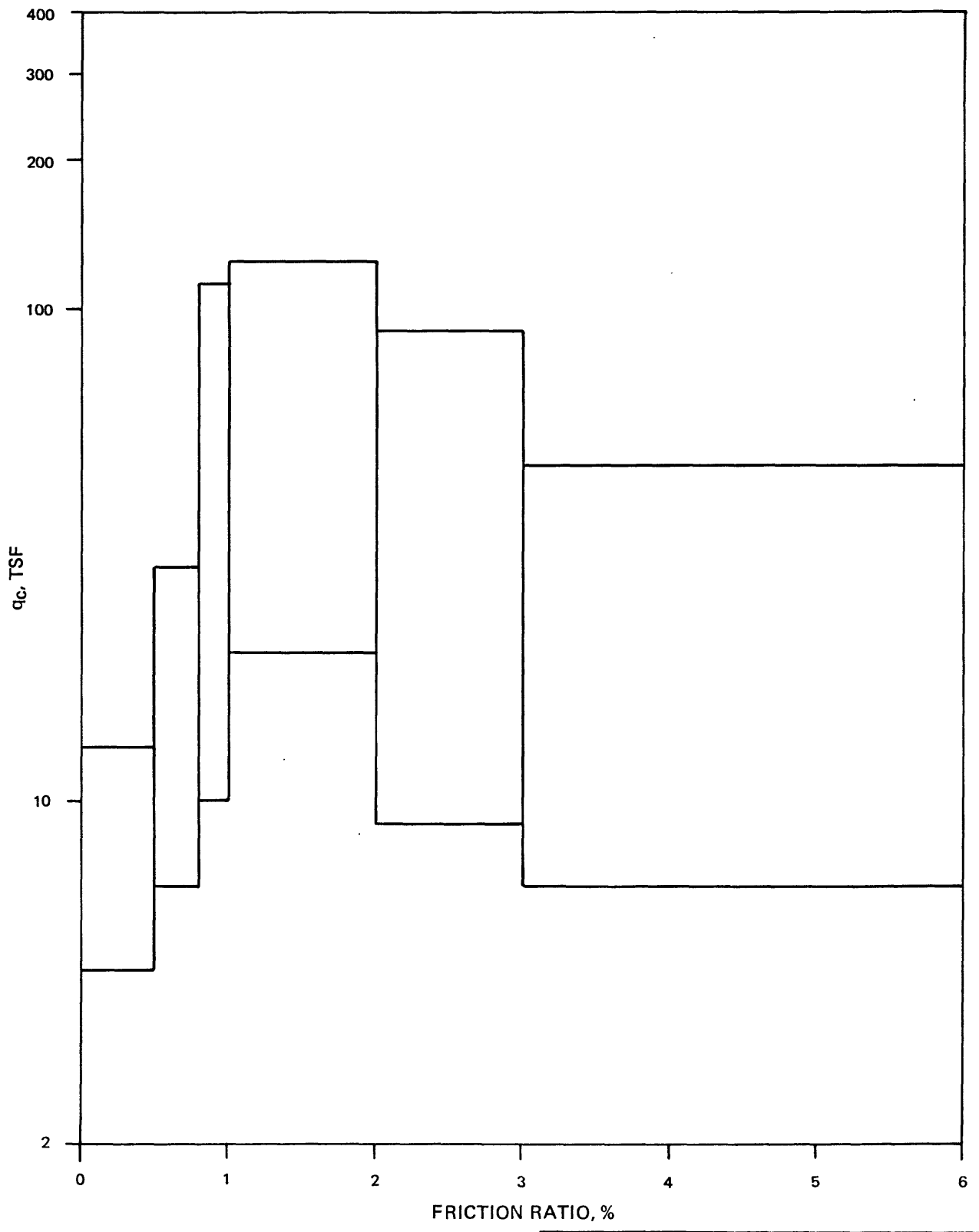
PROJECT NO.:


79-153

USGS CPT-SPT

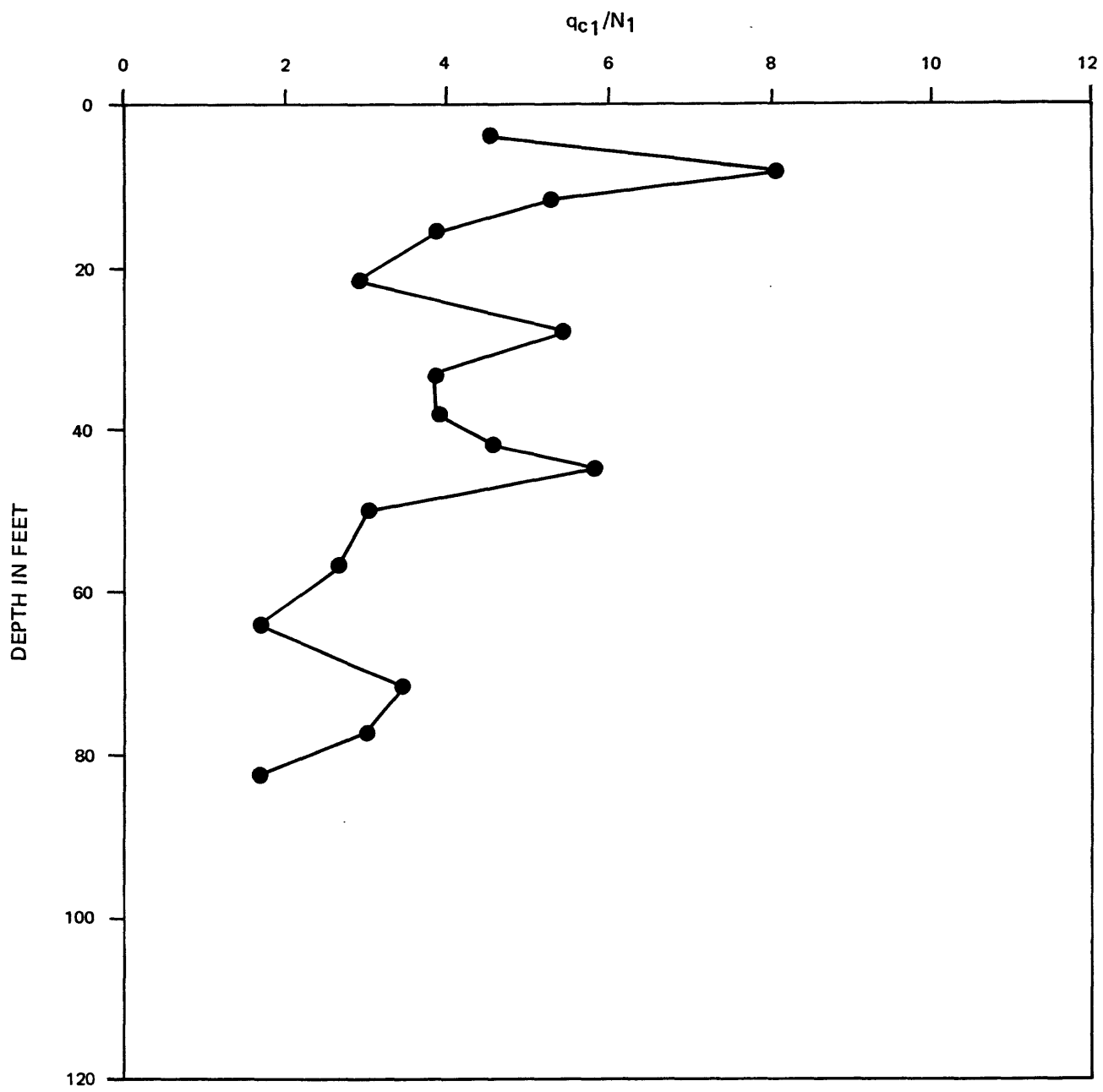
PENETRATION RESISTANCE
IN LAYERED MEDIA
(AFTER TREADWELL 1975)


Compiled by _____ Drawn by _____ Checked by _____ Approved by _____

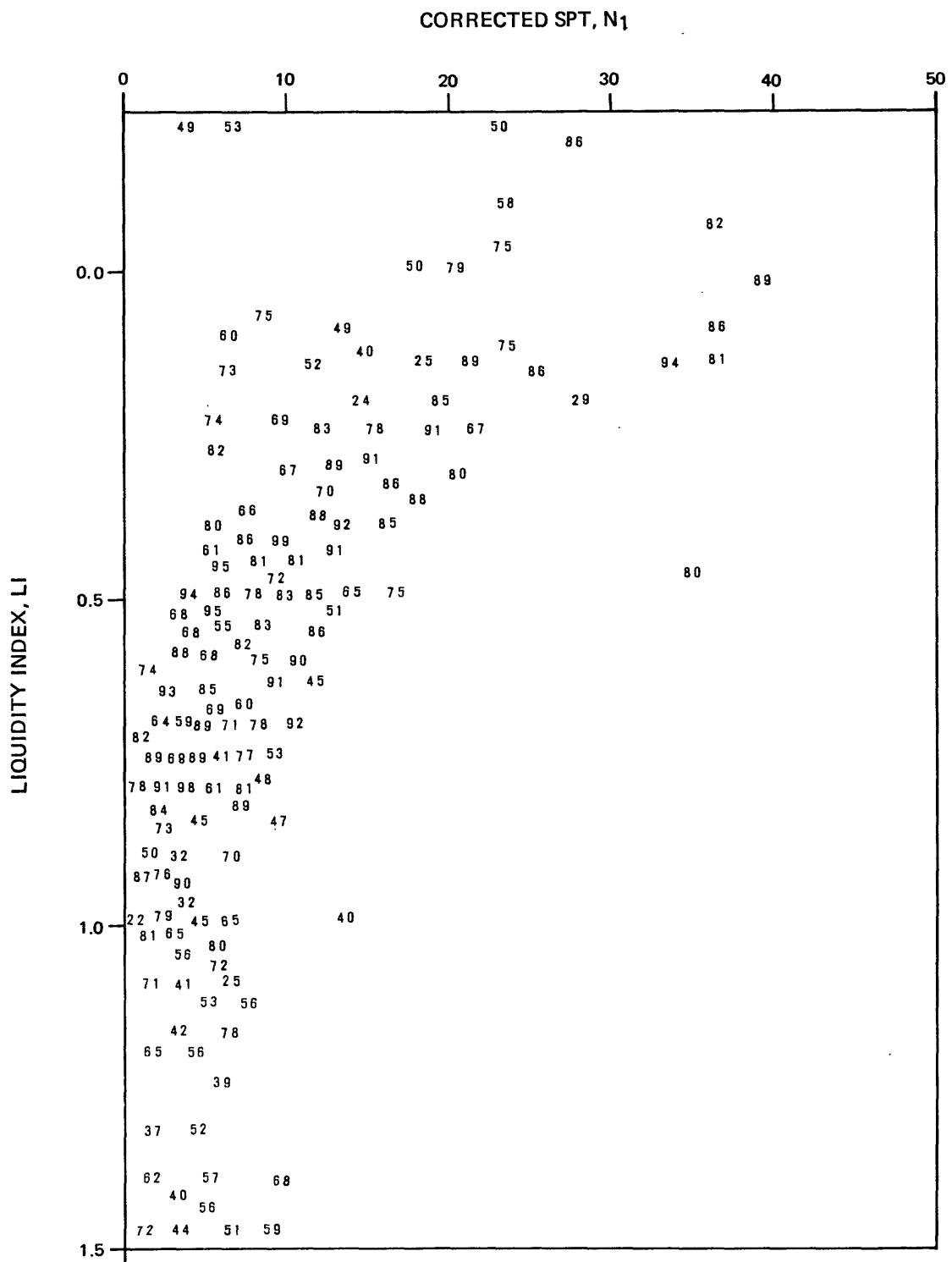


	PROJECT NO.:	79-153
	USGS CPT-SPT	
EDMOND SITE RANGE OF AVERAGE CPT END BEARING FOR FRICTION RATIO BANDS		
9-80	FIGURE 3.68	

Compiled by _____
Drawn by _____
Checked by _____
Approved by _____



	PROJECT NO.:	79-153
	USGS CPT-SPT	
COMPARISON OF EDMOND SITE SPT WITH $P_i < 3$ AND CPT WITH FRICTION RATIO = 0.8 TO 2.25%		
9-80		FIGURE 3.69



NUMBERS REPRESENT % < NO. 200 SIEVE



PROJECT NO.:

79-153

USGS CPT-SPT

EDMOND SITE
SPT N TO LI ALL BORINGS WITH
ADJACENT CPT SOUNDINGS

9-80

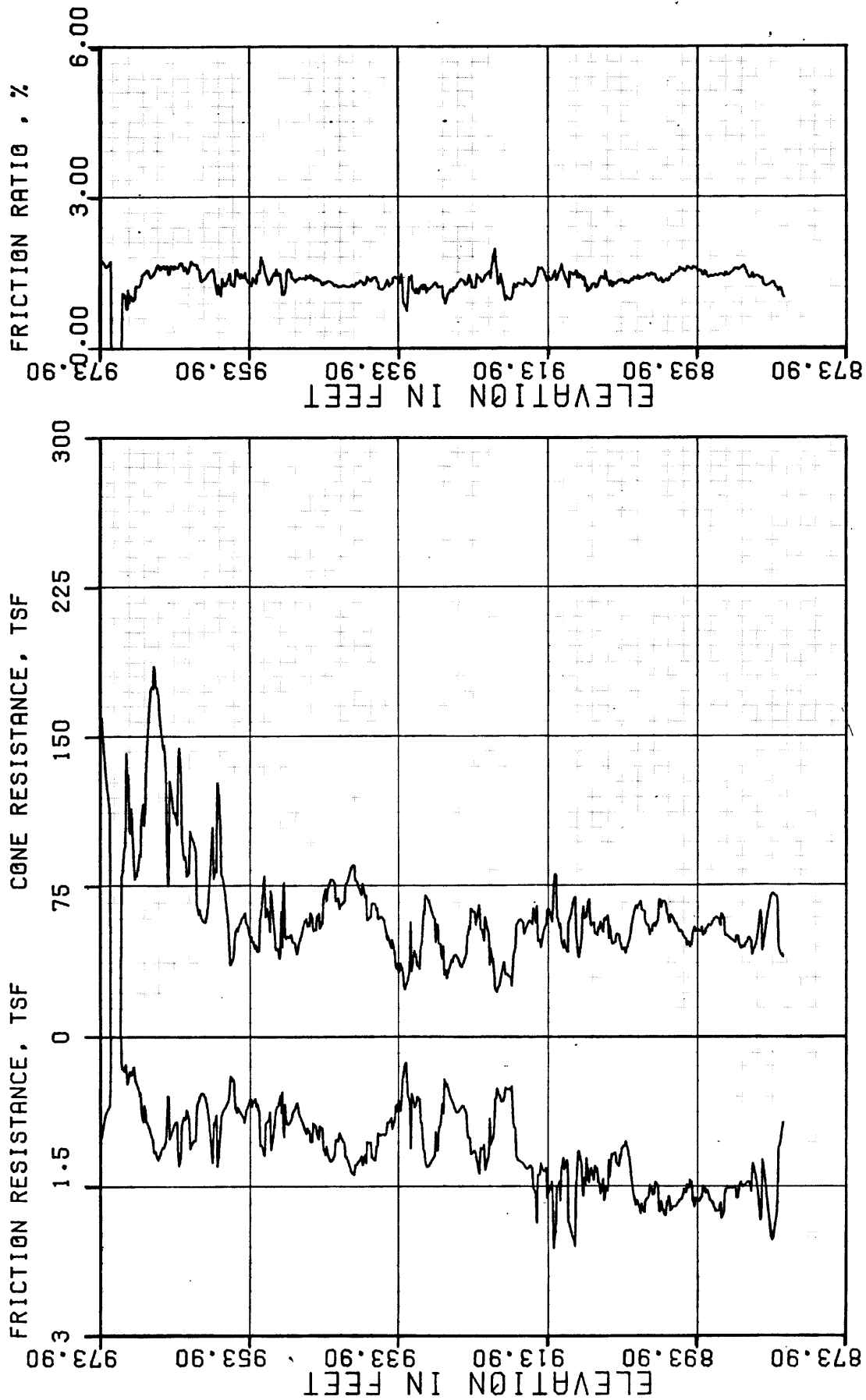
FIGURE 3.70

Approved by

Checked by

Drawn by

Compiled by



PROJECT NO.:

79-153



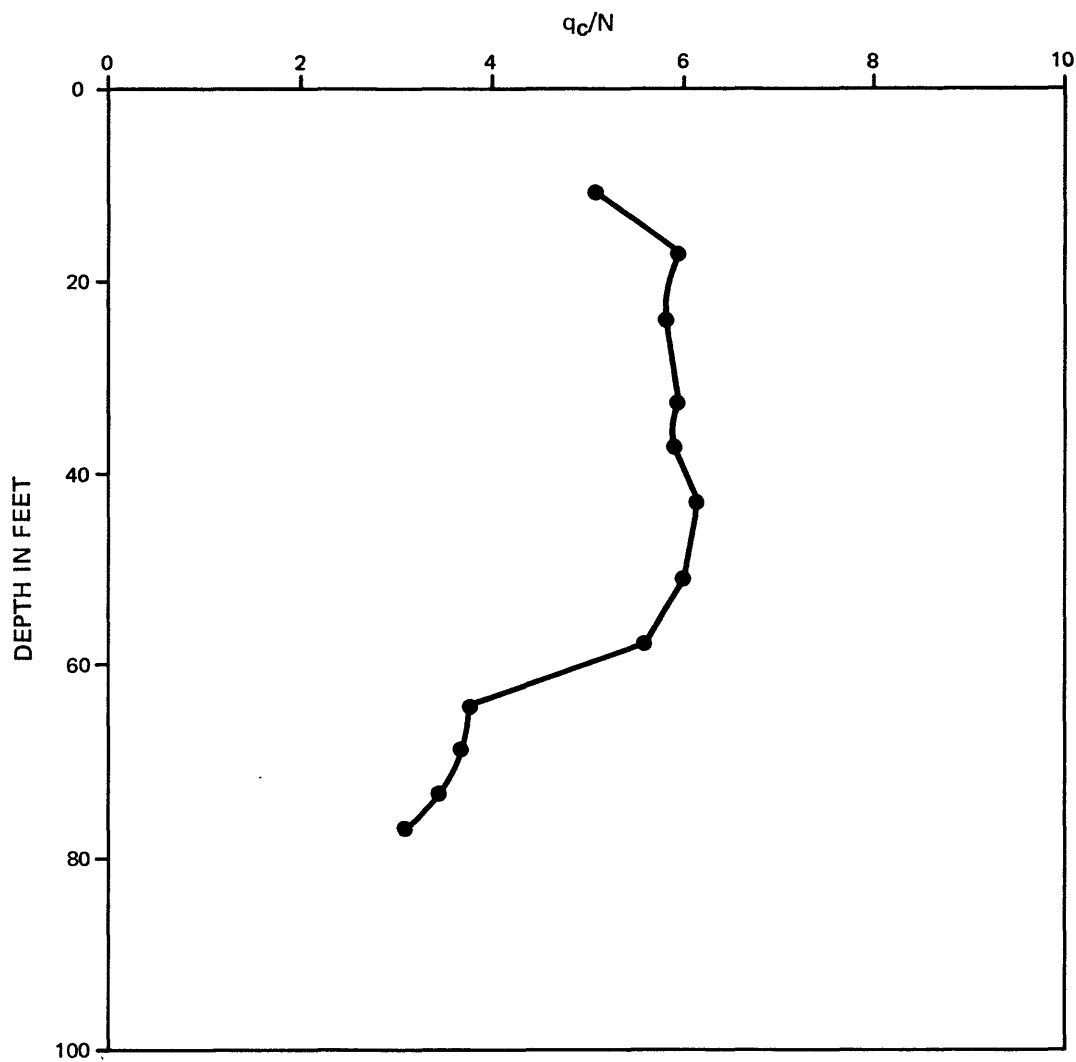
USGS CPT-SPT

PROFILE AVERAGE
 COMPOSITE: ALL SOUNDINGS
 EDMOND SITE CORRECTED
 qc VS DEPTH FOR SAND ZONE

INSTRUMENT:

SOUNDING:

FIGURE 3.71



PROJECT NO.:

79-153

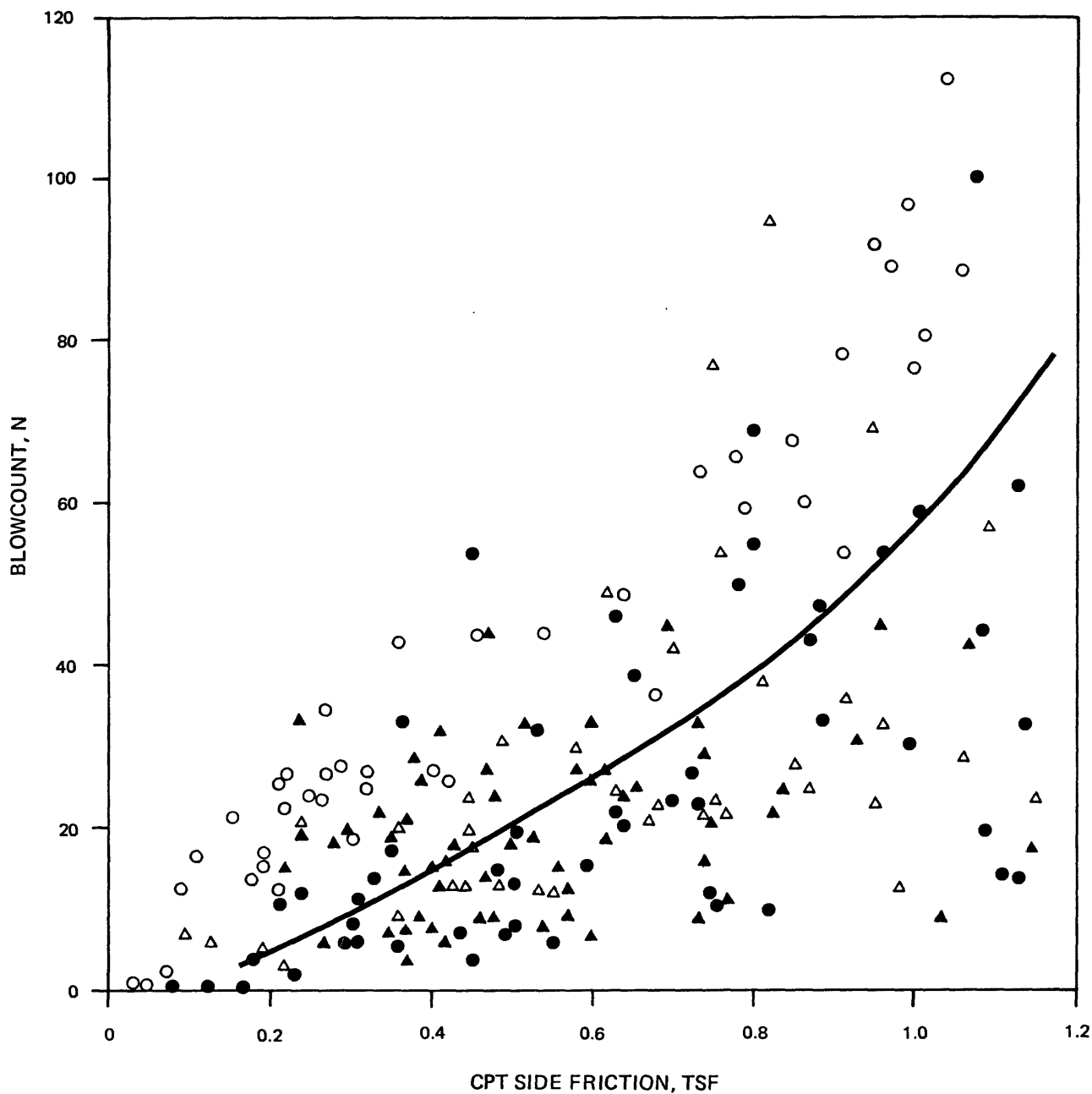
USGS CPT-SPT

COMPOSITE: ALL SOUNDINGS & BORINGS
EDMOND SITE q_c/N VERSUS
DEPTH FOR CPT SAND ZONES
AND BLOWCOUNTS WITH $P_i < 3$

9-80

FIGURE 3.72

Approved by _____
Checked by _____
Drawn by _____
Compiled by _____



SITES

- SAN DIEGO
- △ MOSS LANDING
- COYOTE NORTH & SOUTH
- ▲ SALINAS



PROJECT NO.:

79-153

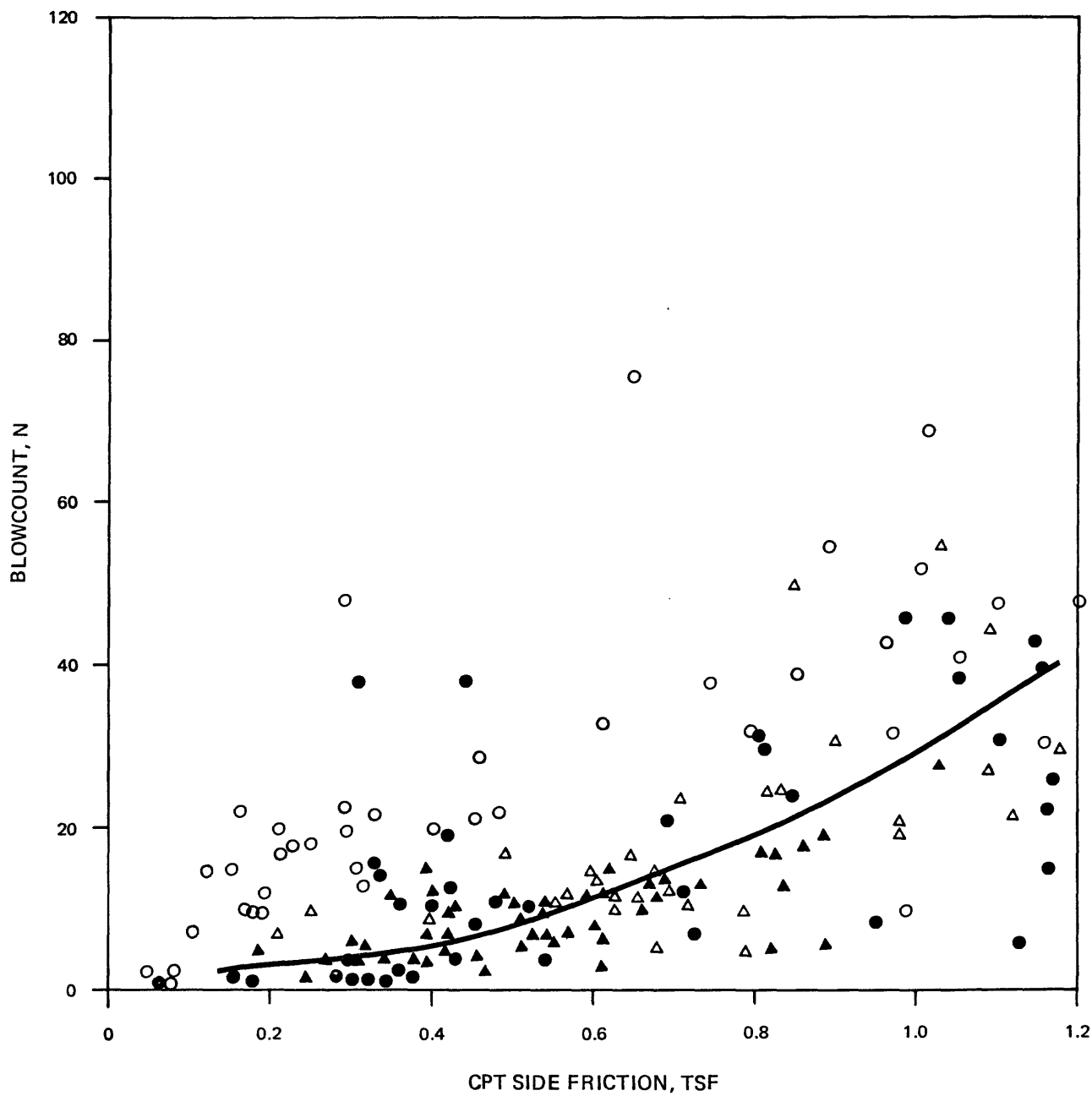
USGS CPT-SPT

COMPOSITE: ALL SITES
CPT SIDE FRICTION VS N
STANDARD HAMMER

9-80

FIGURE 3.73

Compiled by _____
Drawn by _____
Checked by _____
Approved by _____



SITES

- SAN DIEGO
- △ MOSS LANDING
- ▲ COYOTE NORTH & SOUTH
- SALINAS



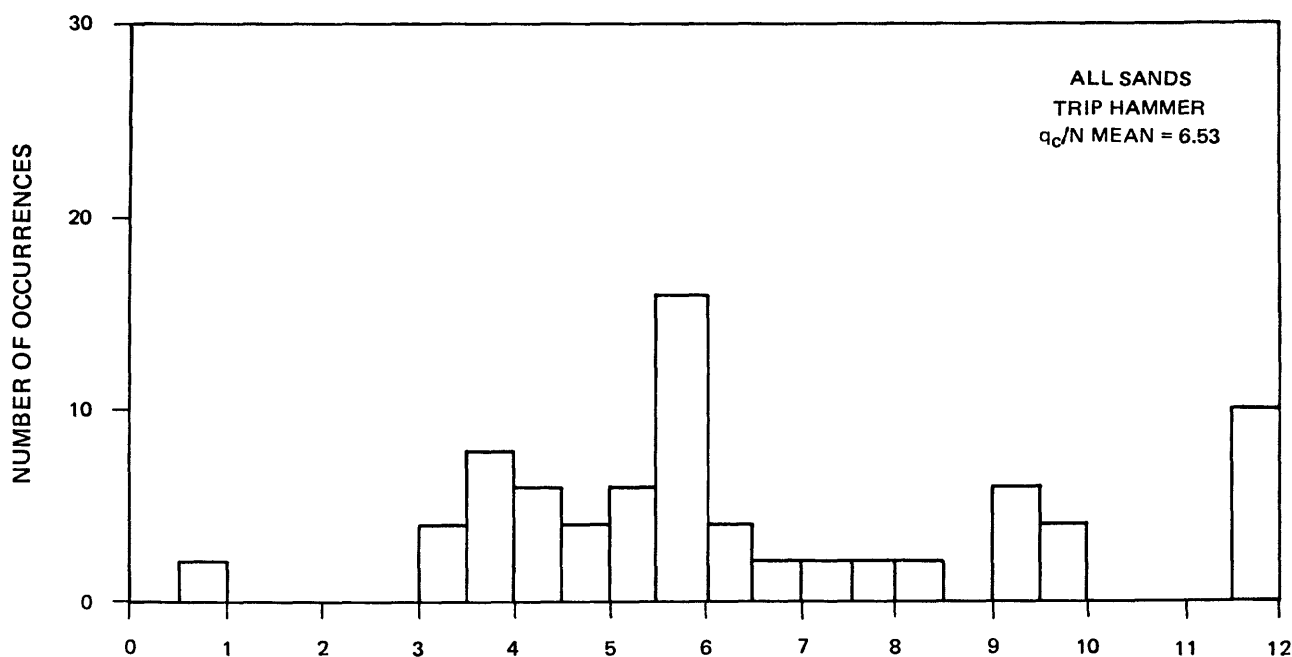
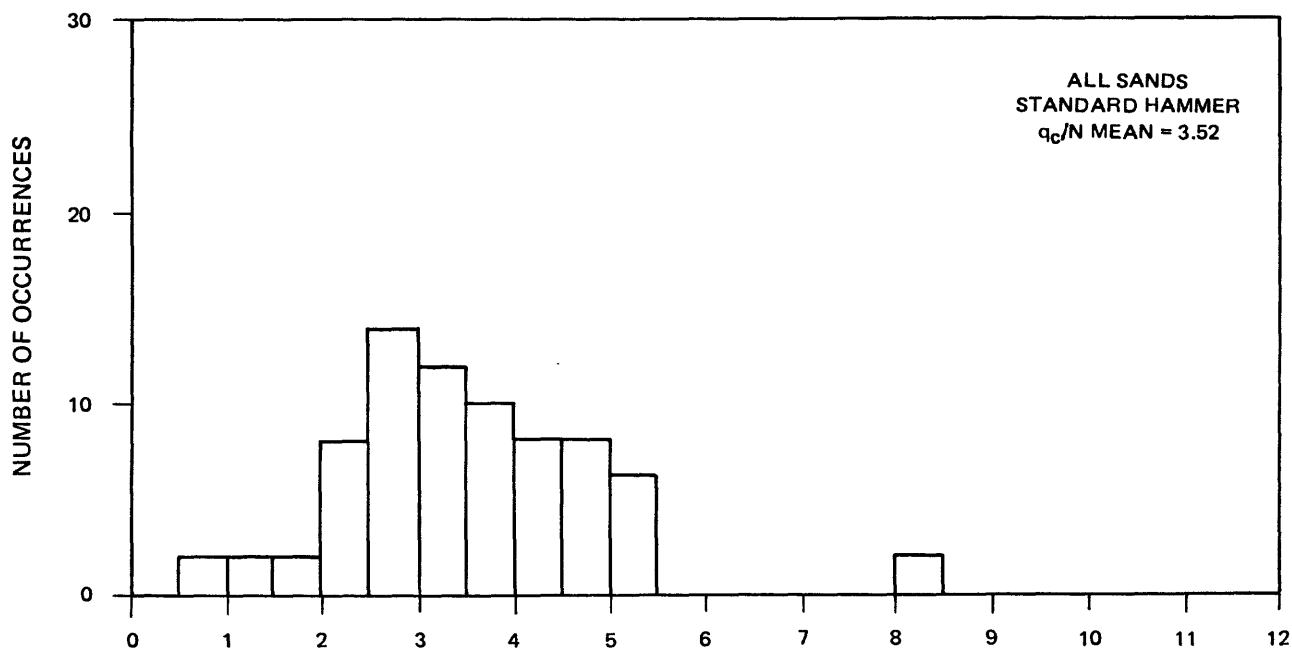
PROJECT NO.:

79-153

USGS CPT-SPT

COMPOSITE: ALL SITES
CPT SIDE FRICTION VS N
TRIP HAMMER

Approved by _____
Checked by _____
Drawn by _____
Compiled by _____



PROJECT NO.:

79-153

USGS CPT-SPT

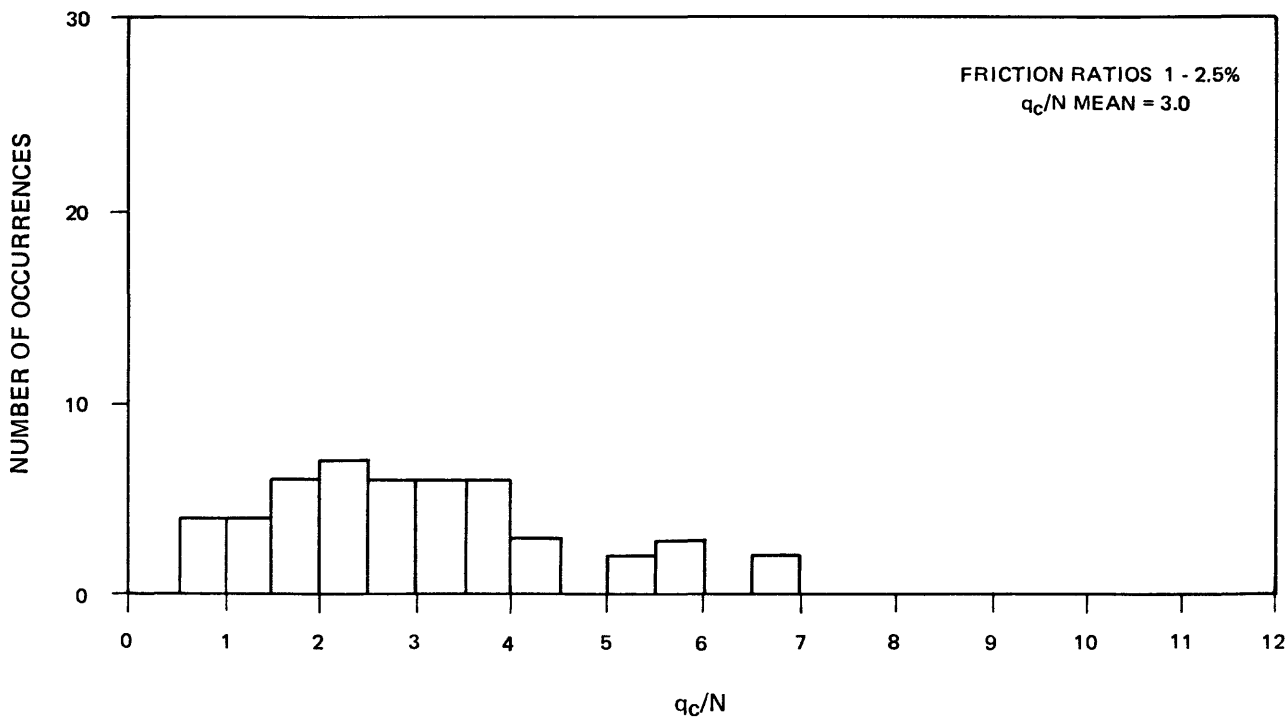
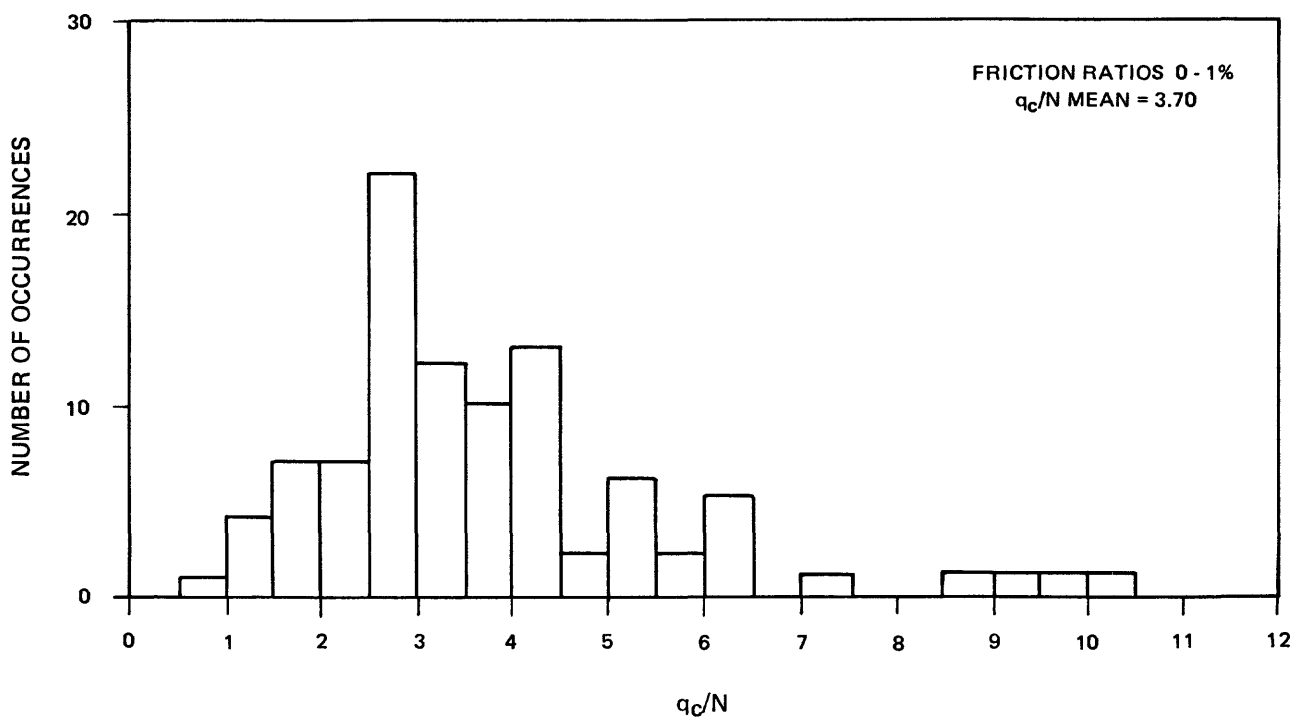
COMPOSITE: ALL SITES
FREQUENCY HISTOGRAMS
BY LAYER AVERAGES

Approved by

Checked by

Drawn by

Compiled by



PROJECT NO.:

79-153

USGS CPT-SPT

COMPOSITE: ALL SITES
 FREQUENCY HISTOGRAMS
 q_c/N VS FRICTION RATIO
 STANDARD HAMMER

9-80

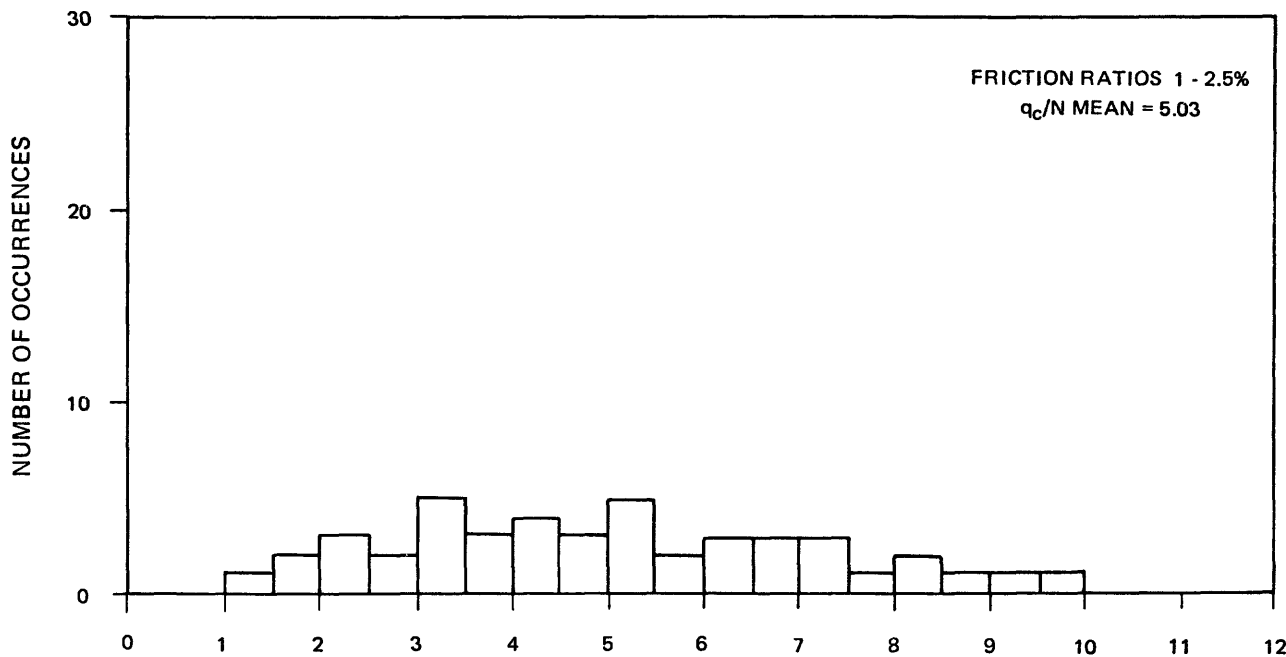
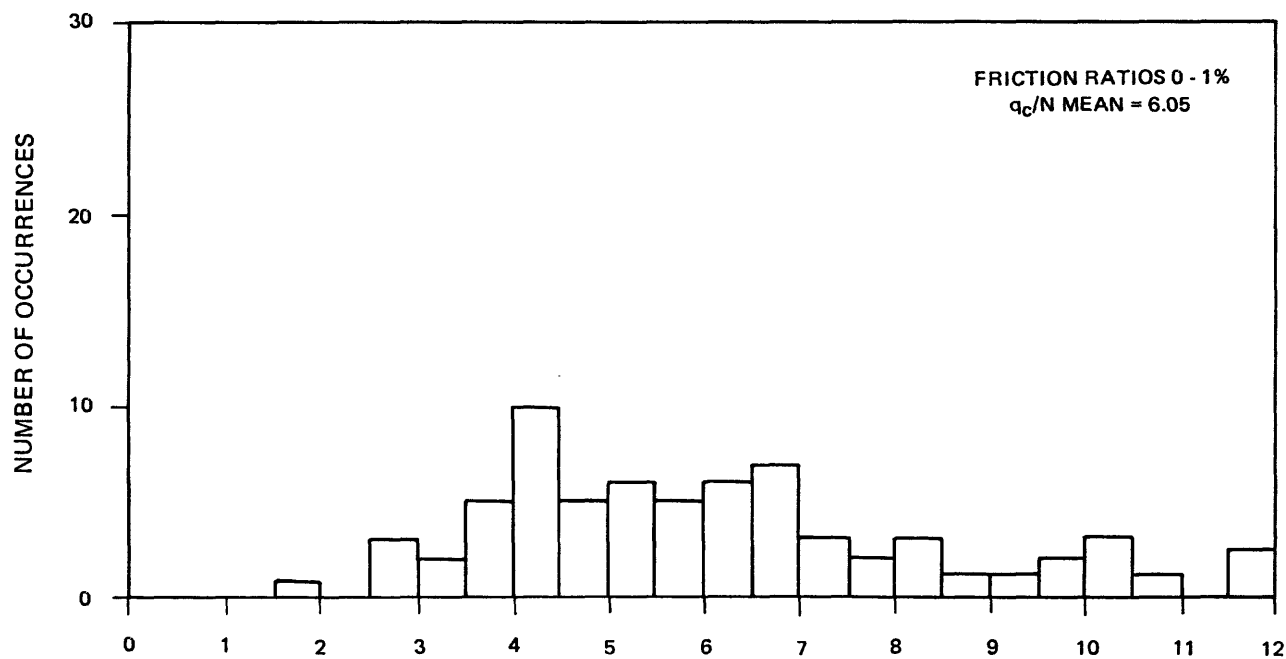
FIGURE 3.76

Approved by _____

Checked by _____

Drawn by _____

Compiled by _____



PROJECT NO.:

79-153

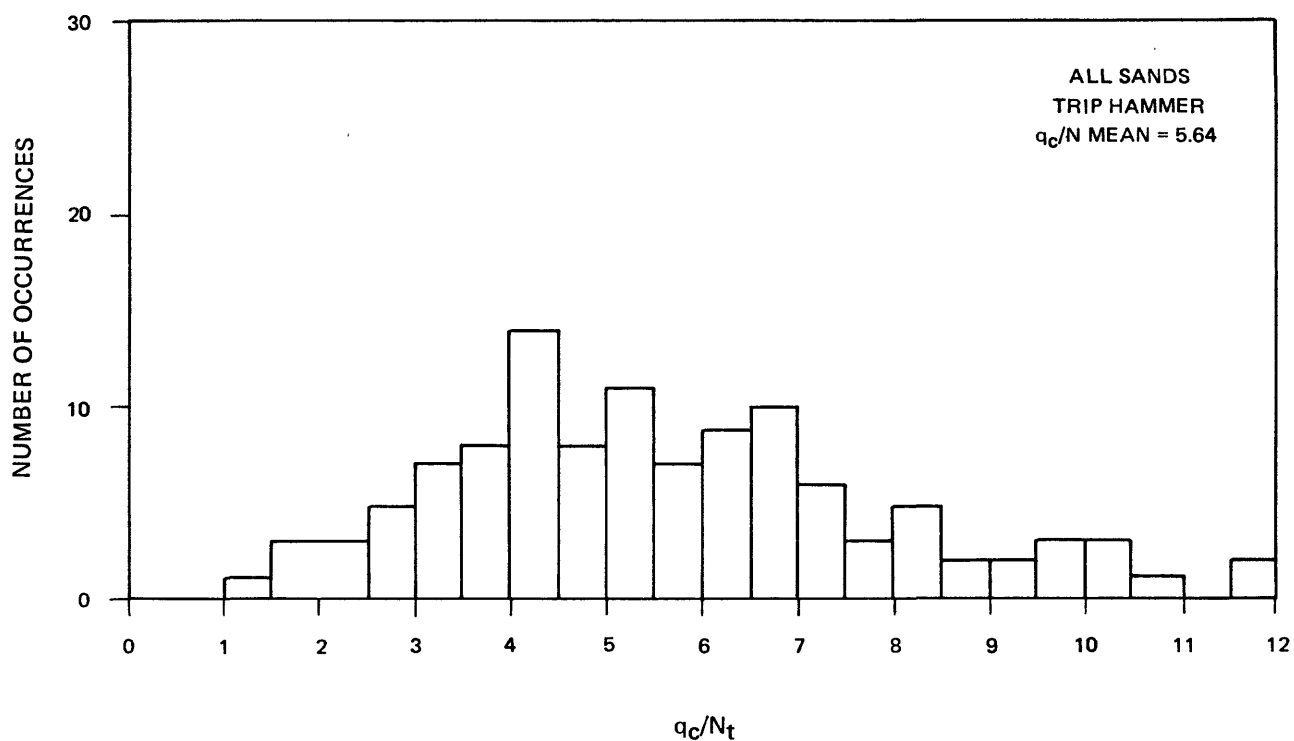
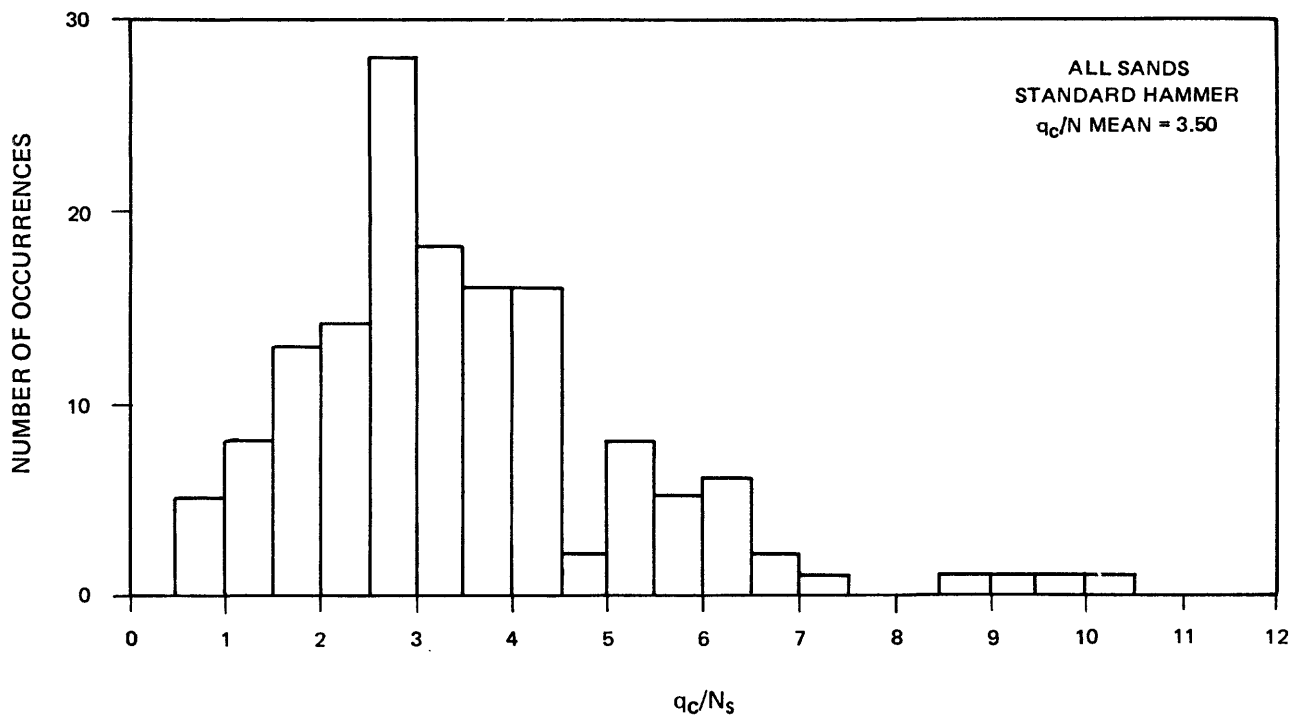
USGS CPT-SPT

COMPOSITE: ALL SITES
 FREQUENCY HISTOGRAMS
 q_c/N VS FRICTION RATIO
 TRIP HAMMER

9-80

FIGURE 3.77

Approved by _____
Checked by _____
Drawn by _____
Compiled by _____



PROJECT NO.: 79-153

USGS CPT-SPT

COMPOSITE: ALL SITES
FREQUENCY HISTOGRAMS
 q_c/N

4. SUMMARY AND CONCLUSIONS

The goal of this section is to summarize the findings of this research, to provide some conclusions regarding the reliability of CPT-SPT correlation for use in liquefaction potential analyses, and to suggest some needs for additional research.

4.1 SUMMARY

The data presented in the previous sections has been organized to meet the three basic requirements for use of a CPT-SPT-liquefaction potential assessment. These needs are the estimation of liquefiable soils, the normalization of CPT measurements, and the conversion of CPT measurements into SPT measurements. As no direct rule is available regarding when the SPT can be used to provide information for the empirical method, it is assumed that the SPT is valid for sands and a small range of silty sands, with fines content up to about 30 percent. An estimated boundary between the zone of 30 percent fines content and the 30 to 60 percent zone was shown in Figure 3.9. Also shown in that figure are the boundaries for other soil categories as interpreted from the data presented in the preceding sections. Although it is seen that friction ratio alone does not completely define soil-type boundaries, for the purposes of providing conservative estimates of susceptible soils it is acceptable to select a constant friction ratio as the boundary. Soft CL and CL-ML soils may also fall in the band, but such soft or sensitive soils may present their own hazard under earthquake loading. A suggested friction ratio band for use with the electric cone penetrometer is zero to 2.25 percent.

It was shown in Section 3.3.3.2 that a C_p relation to account for the effect of overburden pressure upon field investigations shows a considerable degree of scatter. Development of a parameter, C_{p1} , by which CPT measurements could be directly converted to corrected equivalent blowcounts was also described. C_{p1} could be defined for a particular friction ratio band, such as the sand range. The q_c/N versus depth relation could then be defined for the same band, and by multiplication of the two relations, a new C_p relation would be found. This C_p could then be used as an adjustment on the basis of constant material type with associated assumption of a constant q_c/N for that material. The trend in C_p would then automatically include the effect of the variable q_c/N relation. Because these field-based C_{p1} methods rely to large degree upon the particular C_N relation selected, and because the scatter in C_N relations is large and encompasses available C_p relations determined under controlled circumstances, it is most appropriate to use the available C_p relation shown in Figure 3.5.

Finally, the most appropriate means to convert q_c and FR into equivalent N values is discussed. It has been shown that q_c/N is primarily a function of soil type and in-situ stress conditions. Thus, the conversion of q_c to N for liquefaction potential assessments must also depend upon these factors. In Figures 4.1 and 4.2 are shown plots of N value ranges on the q_c -FR charts for standard and trip hammer measurements, respectively. Lines showing conservative definition of the constant N value trends are also shown on those figures. It

can be seen that those lines are essentially just the relations shown in previous section. For example, the q_c/N relation decreases with increasing N , but begins to show rapid increases with q_c at end bearing pressures above 100 tsf. The effect of changing soil type on q_c/N is also clearly visible.

4.2 CONCLUSIONS

Conclusions regarding the use of a CPT-SPT conversion with subsequent use of the SPT-liquefaction potential relation focus upon the method of CPT data analysis and the reliability of the CPT-SPT correlation.

Figures 3.9 and 4.1 and 4.2 present composite plots of CPT versus soil type and CPT versus N value data. Likewise, Figure 3.15 presents a summary of the classification trends as based upon CPT data. It is noted that the Friction Ratio is a primary variable used in all of the plots. Although many of the trends in Figure 3.15 are speculative, it can be seen that estimation of soil characteristics is dependent upon both of the primary CPT measurements: end bearing and side friction. Thus, although the normalized form of the data as represented by friction ratios is convenient, the actual measured side frictions should be routinely analyzed when using CPT data. The importance of side friction is also seen in Figures 4.1 and 4.2. These figures reveal the similarity of constant N value lines and lines of constant side friction. Such agreement suggests that graphical relations between the desired soil characteristic and end bearing

and side friction may be preferable to the use of friction ratio relations, and should be further investigated.

Although friction ratio indirectly accounts for side friction, there are difficulties in its practical use. For example, the end bearing penetration behavior in layered media was previously shown to depend upon some weighted average of soil resistance within several diameters in front and back of the tip. The effect of layers on sleeve measurements is different, and it appears that the influence of underlying layers is felt by the sleeve much later than the influence is felt by the cone tip. This often results in erratic calculated friction ratios in the near vicinity of layer interfaces.

This rapid fluctuation in friction ratio is not as apparent with the mechanical CPT as used by most previous researchers. The reason is that the typical mechanical cone procedure automatically averages measurements over the depth of the sounding increments. Thus, the rapid changes in resistance leading to erratic friction ratios are not as pronounced. However, by the same reasoning, it is apparent that this use of the mechanical penetrometers leads to an inability to distinguish the occurrence of sudden resistance changes as caused by a changed material type, and that resistances measured in thin layers will represent average values or may be entirely in error, as in the usual determination of side friction in a zone of rapidly increasing or decreasing end bearing.

Several methods of smoothing the friction ratio curve were investigated. These included moving averages of either of or both the end bearing and sleeve measurements, variable adjustments of the lead distance between sleeve zone of influence and tip zone of influence, and filtering of high frequency components of the friction ratio record. Although such devices are of use for investigation of the phase difference in response of the tip and sleeve, it appears that direct use of the sleeve measurement itself holds more promise than artificial adjustment of the friction ratio. Although the sleeve readings are erratic when passing through dense or interlayered soils, they are smoother than the calculated friction ratios. Further, soil types, stress conditions, and index characteristics and N values seem to bear a closer relationship to sleeve readings than to friction ratios.

Because little research has been focused on direct use of sleeve measurements, current methods still must rely upon the friction ratio method. That method as applied to N value prediction has been well explained by Schmertmann. A major concern, however, is still related to equipment. It has been shown that different hammer energies not only produce different N values, but also produce different shapes of the q_c versus N curve. Further, it appears that the ratio of N values relating two different hammer energies is not necessarily constant, but varies depending upon soil type and/or resistance. It is also known that the use of electrical versus mechanical cones results in different q_c versus N relations.

Therefore, in order to advance a set of q_c versus N relations, it is necessary to make an accurate assessment of the "average" hammer energy represented in the blowcount method. It is also necessary to specify the type of cone penetrometer for which the relations are valid. It should be noted that this problem of equipment standardization is everpresent but usually ignored in routine use of the N value method.

A set of functional relations between q_c , N , friction ratio and overburden pressure is not presented in this report. Until the standardization of SPT methods and equipment is complete, or until the SPT hammer energy implicit in the blowcount method is defined, the presentation of another set of equations for use by practitioners unaware of the inherent assumptions that must be accepted to use the equations seems inappropriate.

This is not to suggest that the CPT method is not valid for prediction of N values or liquefaction potential, for it certainly is. The profiling of a site using the CPT provides more information, faster, more reliably and at a lower cost than any other method now available. Likewise, the qualitative determination of strength variation throughout the site profile is immediately obtained from the field records. Further, the scatter in the CPT relation with another test measurement, such as the SPT, stems primarily from the scatter in the other test results or from the finite measurement intervals of the other test as compared to the essentially continuous CPT measurements. Even with the scatter in comparative relations,

the CPT method is so rapid that a large statistical data base can be developed, allowing precise definition of average site characteristics.

An example of CPT estimation of SPT blowcounts can be drawn from the Edmond site data. The q_c versus N relations for that site (Figure 3.65) were simplified (double curvature removed), and fit with equations relating to q_c and FR . The relations were then applied to the CPT records from the site. A plot of CPT predicted, corrected N value for a typical sounding is shown in Figure 4.3 compared against the corrected N value measured at the same location, wherein the accuracy of the CPT prediction is self-evident. However, it must be recalled that a hammer-specific blowcount is predicted in that figure, and it is not known how well that hammer compares with the hammers implicit in the empirical blowcount method. Thus, considering the variability of SPT measurements, the use of precise correlations of CPT and SPT measurements may be of little use. That is, the precision of the CPT-SPT correlation should be of the same order as the precision of the SPT and SPT-liquefaction potential correlation.

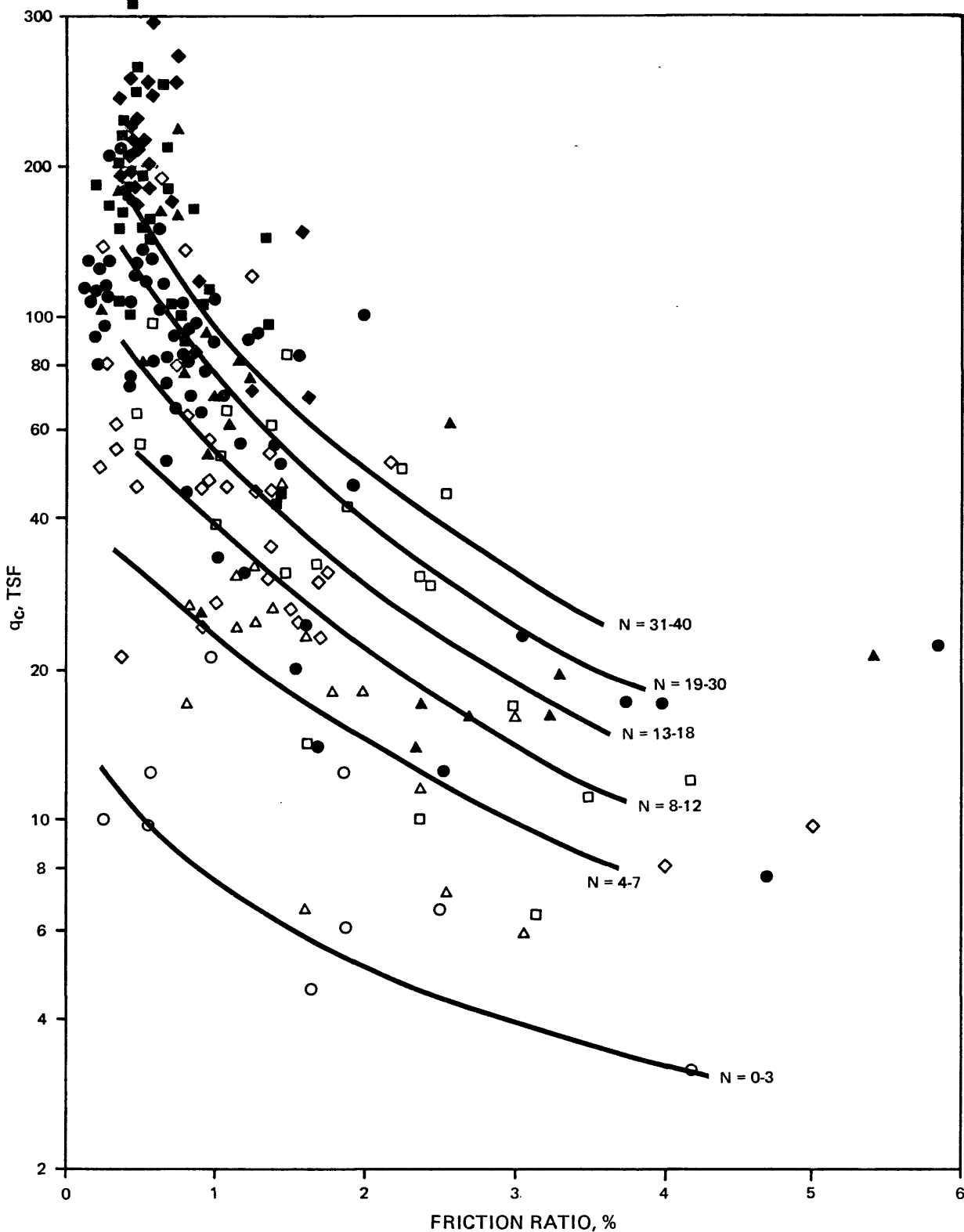
4.3 RESEARCH SUGGESTIONS

Three areas of needed research are suggested by this report. These areas deal with standardization of the SPT, analysis of the CPT, and further investigation of relations between the CPT and liquefaction potential.

The standardization of the SPT has been underway for many years and the only specific concern indicated in this report is the selection of standardization energy. It appears that resolution of soil type changes depends upon the energy delivered to the sampler per blow of the hammer.

Needs in analysis of the CPT are many, and include research into failure mechanism and the measurement process. Regarding the measurement process, it appears that the value of direct use of side friction measurements may be facilitated by relocation of the side friction sleeve to a location in which the pore pressure field is less variable than at its present location immediately behind the cone tip. In addition, some reanalysis of CPT data in terms of side friction and end bearing without dependence upon friction ratio may yield worthwhile results.

The use of the CPT for liquefaction potential analyses requires several related investigations. In the indirect approach, such as presented in this report, measurements of SPT hammer energy should be made. In fact, the hammers used in this study should be so calibrated. Direct approaches to the problem of CPT-liquefaction potential evaluations should be pursued. These include the use of piezometric (pore pressure measuring) cones, and the performance of cone penetrometer tests at previously liquefied sites.



BLOWCOUNT SYMBOLS	○	0 - 3
	△	4 - 7
	□	8 - 12
	◇	13 - 18
	●	19 - 30
	▲	31 - 40
	■	41 - 60
	◆	60 <



PROJECT NO.:

79-153

USGS CPT-SPT

COMPOSITE: ALL SITES
N VS q_c VS FRICTION RATIO
STANDARD HAMMER

9-80

FIGURE 4.1

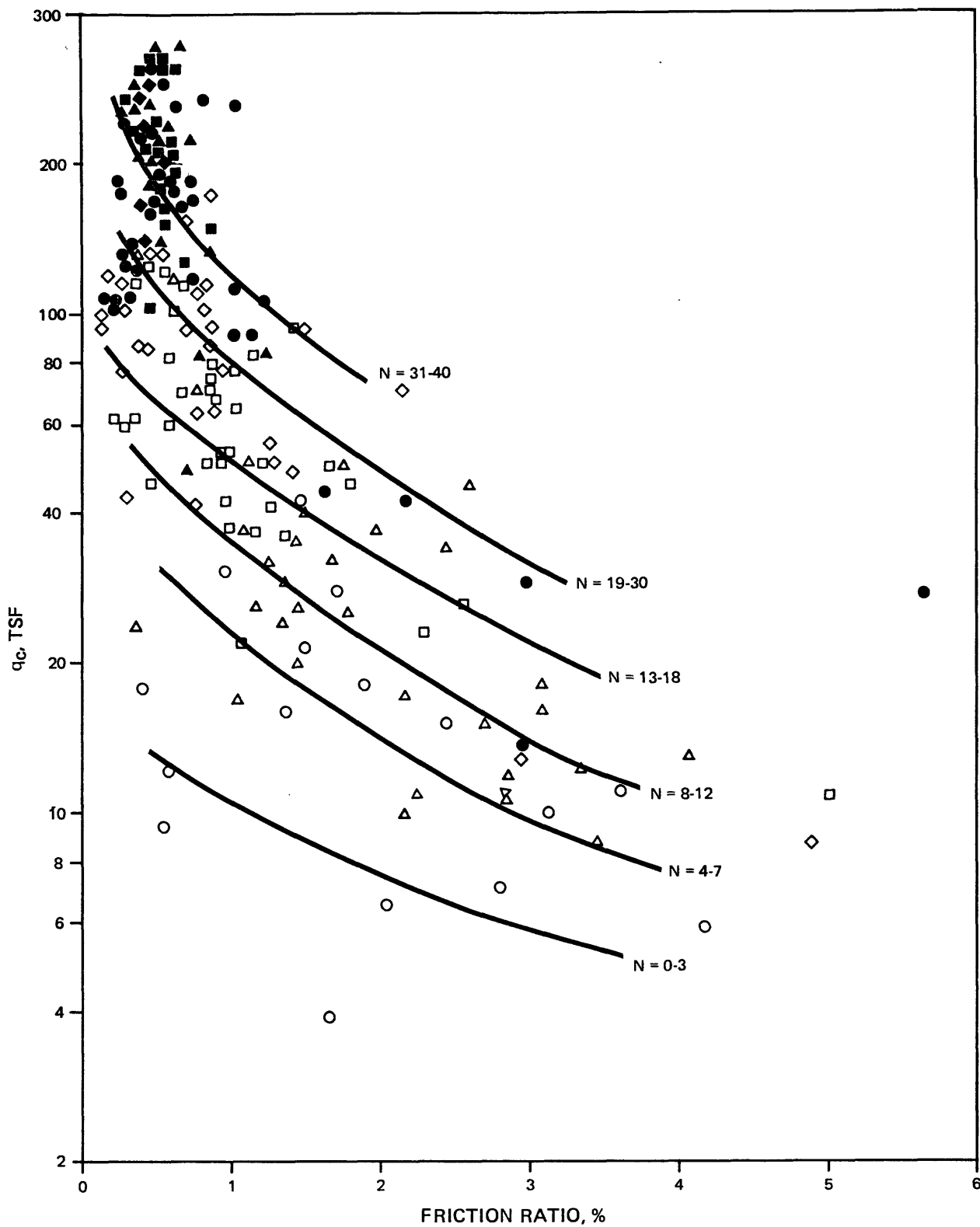
Approved by

Checked by

Drawn by

Compiled by

Approved by /
Checked by /
Drawn by /
Compiled by /



BLOWCOUNT SYMBOLS	○	0 - 3
	△	4 - 7
	□	8 - 12
	◇	13 - 18
	●	19 - 30
	▲	31 - 40
	■	41 - 60
	◆	60 <



PROJECT NO.:

79-153

USGS CPT-SPT

COMPOSITE: ALL SITES
N VS q_c VS FRICTION RATIO
TRIP HAMMER

9-80

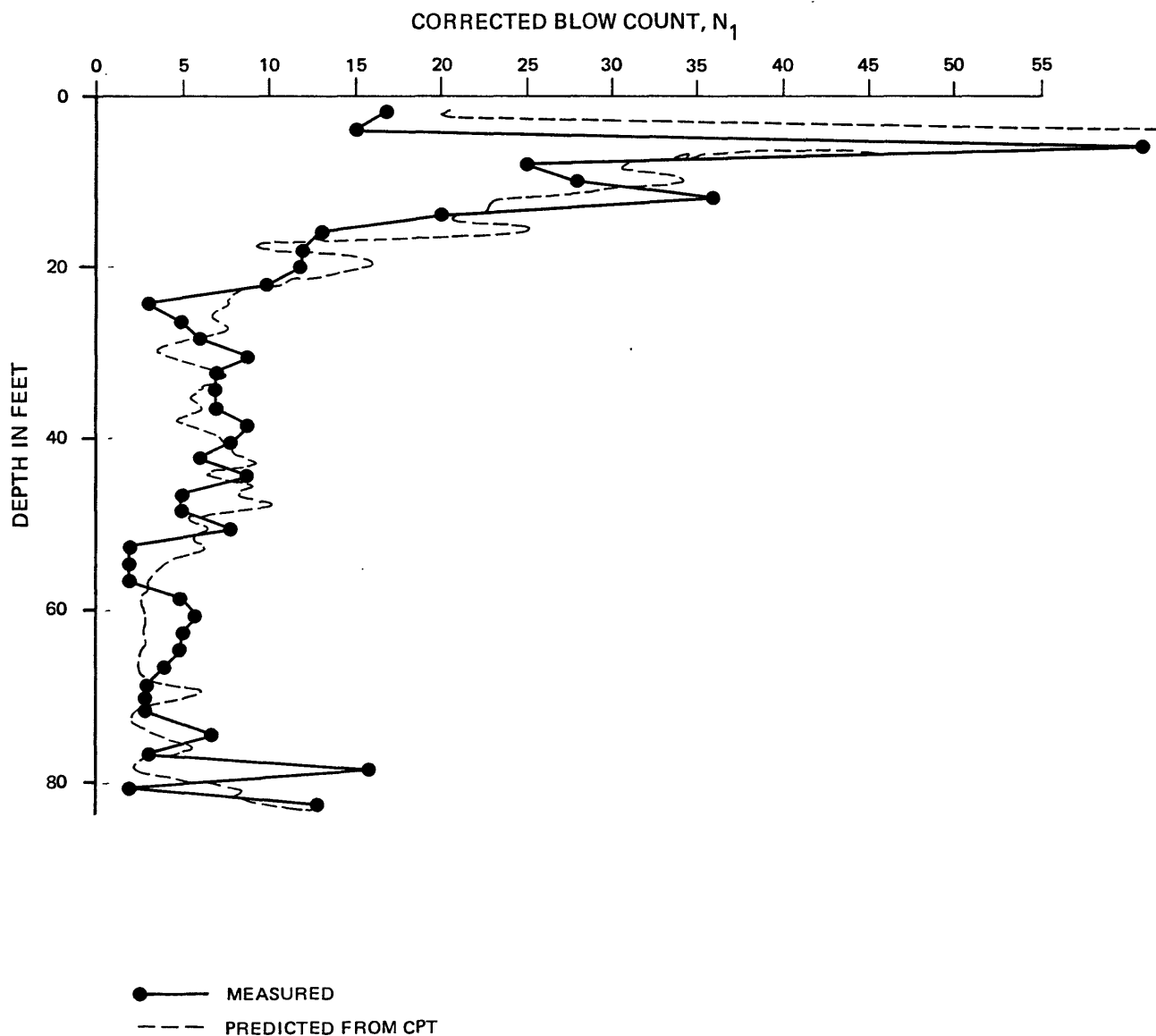
FIGURE 4.2

Approved by

Checked by

Drawn by

Compiled by



PROJECT NO.:

79-153

USGS CPT-SPT

PREDICTED VS MEASURED
N VALUE PROFILE
EDMOND SITE: BORING 120

9-80

FIGURE 4.3

5. REFERENCES

- Alperstein, R., and Leifer, S. A., 1976, "Site Investigation with Static Cone Penetrometer," Journal of the Geotechnical Engineering Division, ASCE, GT5, May.
- American Society for Testing and Materials, 1975, "Deep Quasi-static, Cone and Friction-Cone Penetration Tests of Soil," ASTM Tentative Standards, Part 19, Designation: D3441-75T, December, and ASTM D 1586, D422 and D1586.
- U.S. Army Corps of Engineers, Tulsa District, 1978, "General Design, Phase II, Project Design: Arcadia Lake Design Memorandum #3."
- Bazaraa, A.R.S.S., 1967, "Use of the Standard Penetration Test for Estimating Settlements of shallow foundations on sand," Ph.D. Thesis, Univ. of Illinois, Urbana.
- Begemann, H. K., 1965, "The Friction Jacket Cone as an Aid in Determining the Soil Profile," Proc. 6th International Conference of Soil Mechanics and Foundation Engineering, Volume 1, pp. 17-20.
- Bingham, R. H., and Moore, R. L., 1975, "Reconnaissance of the Water Resources of the Oklahoma City Quadrangle, Central Oklahoma," U.S. Geol. Survey and Oklahoma Geological Survey, Hydrologic Atlas 4 (HA-4).
- California Department of Water Resources, 1968, Bolsa-Sunset Area, Orange County: CDWR Bull. 63-2.
- Campanella, R. G., Berzins, W. E., and Shields, D. H., 1979, "A Preliminary Evaluation of Menard Pressuremeter, Cone Penetrometer, and Standard Penetration Tests in the Lower Mainland, British Columbia," Soil Mechanics Series No. 40, Department of Civil Engineering, The University of British Columbia, Vancouver, B.C., Canada, VGT 1W5, May.
- de Mello, Victor F. B., 1971, "The Standard Penetration Test," 4th Pan American Conference on Soil Mechanics and Foundation Engineering, San Juan, Puerto Rico, Vol. I, p. 43.
- de Ruiter, J., 1971, "Electric Penetrometer for Site Investigations," Journal of the Soil Mechanics and Foundation Division, ASCE, SM-2, February.
- Dibblee, J. W., Jr., 1976, "Rinconada and Related Faults in the Southern Coast Ranges, California, and Their Tectonic Significance," U.S. Geol. Survey Professional Paper 981, 55 p.

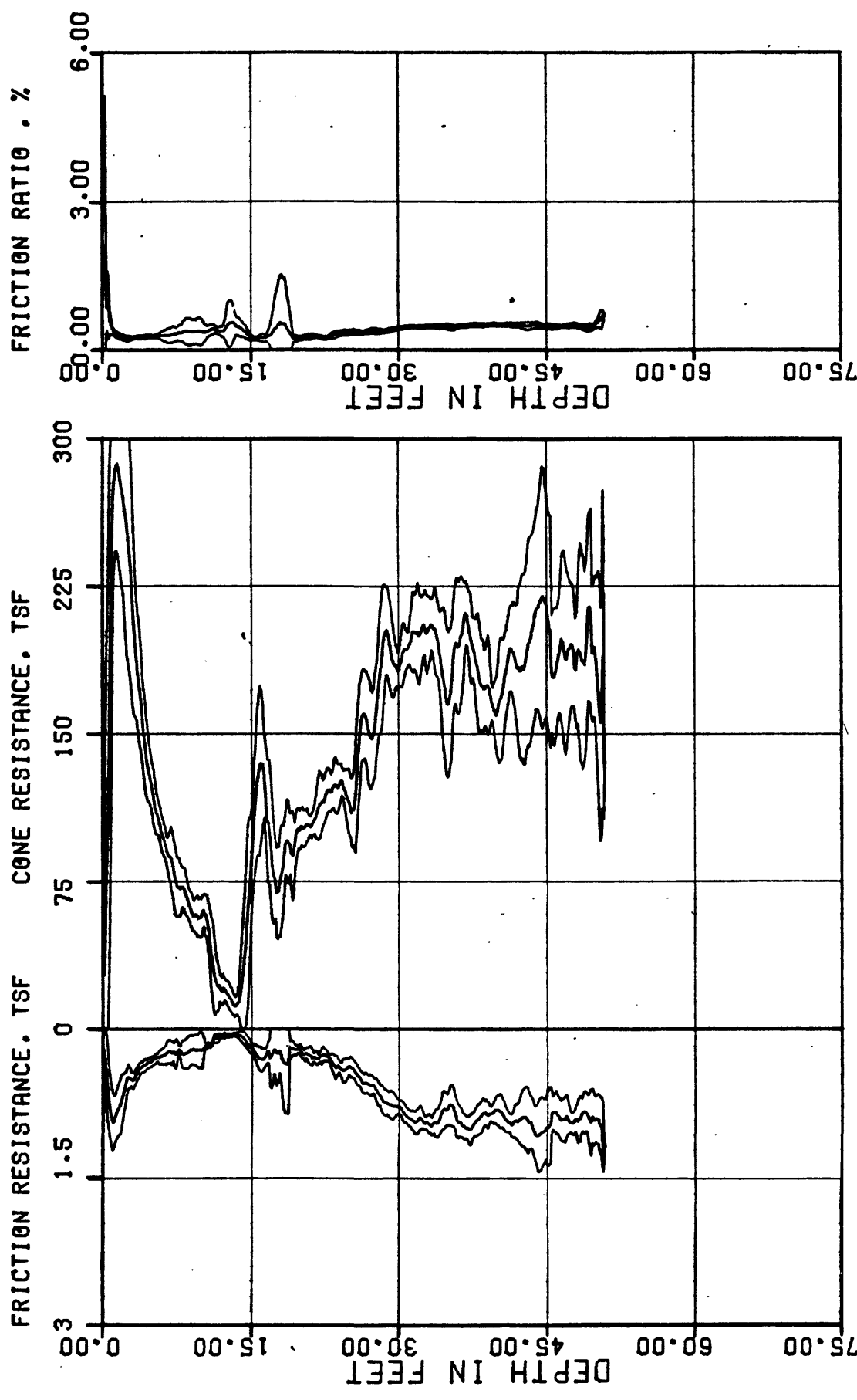
- Donovan, N. C., and Singh, S., 1976, "Liquefaction Criteria for the Trans-Alaska Pipeline," ASCE National Convention, Sept. 27-Oct. 1, Philadelphia, PA., pp. 139-168.
- Ellis, A. J., and Lee, C. H., 1919, "Geology and Ground Waters of the Western Part of San Diego County, CA," U.S. Geol. Survey Water-Supply Paper 446, 321 p.
- Forrest, J., and Ferritto, J., 1976, "An Earthquake Analysis of the Liquefaction Potential at the Naval Air Station, North Island," Port Hueneme, California, Civil Engineering Lab, Technical Report R847.
- Fletcher, G. F. A., 1965, "SPT: It's Uses and Abuses," ASCE Journal of the Soil Mechanics and Foundations Division, July.
- Gibbs, H. J., and Holtz, W. H., 1957, "Research on Determining the Density of Sands by Spoon Penetration Testing," 4th ICSMFE, London, Vol. I.
- Helley, E. J., and Brabb, E. E., 1971, "Geologic Map of Late Cenozoic Deposits, Santa Clara County, California," U.S. Geol. Survey Misc. Field Invest. Map MF-335.
- Helley, E. J., LaJoie, K. R., Spangle, E. E., and Blair, M. L., 1979, "Flatland deposits of the San Francisco Bay Region, California - Their Geology and Engineering Properties, and Their Importance to Comprehensive Planning," U.S. Geol. Survey Prof. Paper 943, 88 p.
- Janbu and Senneset, 1974, "Effective Stress Interpretation of In Situ Static Penetration Test," European Symposium on Penetration Testing, Stockholm, June, Vol. 2.2.
- Kennedy, M. P., Welday, E. E., Borchardt, G., Chase, G. W., and Chapman, R. H., 1977, "Studies on Surface Faulting and Liquefaction as Potential Earthquake Hazards in Urban San Diego, California," Final Technical Report, California Division of Mines and Geology (CDMG) Sacramento, California, October.
- Kennedy, M. P., 1973, "Bedrock Lithologies, San Diego area, California," in Ross, A., and Dowlen, R. J. (eds.), Studies on the geology and geologic hazards of the greater San Diego Area, California: San Diego Association of Geologists.
- Kovacs, William D., 1975, "A Comparative Investigation of the Mobile Drilling Company's Safe-T-Driver with the Standard Cathead with Manila Rope for the Performance of the Standard Penetration Test."

- Kovacs, William D., 1978, "An Alternative to the Cathead and Rope for the Standard Penetration Test," ASTM, GTJODJ, Vol. 1, No. 2. June.
- Levadoux, J. N., and Baligh, M. M., 1980, "Pore Pressure During Penetration in Clays," Publication No. R80-15, Massachusetts Institute of Technology, Department of Civil Engineering, Constructed Facilities Division, April.
- Marcuson, William F. III, and Bieganousky, Wayne A., 1977, "SPT and Relative Density in Coarse Sands," ASCE, GTJ, Vol. 1302, No. GT 11 November.
- Mitchell, J. K., and Lunne, T. A., 1978, "Cone Resistance as a Measure of Sand Strength," Journal of the Geotechnical Engineering Division, ASCE, GT-7, July.
- Peck, R. B., Hanson, W., E., Thornburn, T. H., 1973, Foundation Engineering, 2nd Ed., John Wiley & Sons, Inc., New York, New York, 514 p.
- Poland, J. F., 1959, "Hydrology of the Long Beach-Santa Ana Area, California," U.S. Geol. Survey Water-Supply Paper 1471, 257 p.
- Poland, J. F., Piper, A. M., and others, 1956, "Ground-Water Geology of the Coastal Zone, Long Beach-Santa Ana Area, California," U.S. Geol. Survey Water-Supply Paper 1109, 162 p.
- Sangerlat, G., 1972, The Penetrometer and Soil Exploration, Elsevier Publishing Company, New York.
- Sangerlat, G., 1974, "European Symposium on Penetration Testing," Stockholm, June, Vol. 2.2, State-of-the-Art Reports.
- Schmertmann, J. H., "Discussion of the Standard Penetration Test," 4th Pan American Conference on Soil Mechanics and Foundation Engineering, San Juan, Puerto Rico, Vol. III.
- Schmertmann, J. H., 1976, "Predicting the q_c/N Ratio," Final Report D-636, Engineering and Industrial Experiment Station, Department of Civil Engineering, University of Florida, Gainesville, October.
- _____, 1978, "Guidelines for Cone Penetration Test Performance and Design," U.S. Department of Transportation, Federal Highway Administration Report No. FHWA-TS-78-209.

- Schmertmann, J. H., 1979, "Statics of SPT," Journal of the Geotechnical Engineering Division, ASCE, GT5, May.
- _____, 1979b, "Energy Dynamics of SPT," Journal of the Geotechnical Engineering Division, ASCE, GT 8, August.
- Seed, Bolton H., 1976, "Evaluation of Soil Liquefaction Effects on Level Ground During Earthquakes," ASCE National Convention, Sept. 27-Oct.1, Philadelphia, PA.
- Seed, H. B., Mori, K., Chan, C. K., 1977, "Influence of Seismic History on Liquefaction of Sands," ASCE, GT Vol. 103, No. GT4, April.
- Seed, H. B., 1979, "Soil Liquefaction and Cyclic Mobility Evaluation for Level Ground During Earthquakes," Journal of the Geotechnical Engineering Division, ASCE, GT2, February.
- Steiger, F., 1979, "A Technical Report on the SPT Workshop Held During ASTM's June 1979 Committee Week," Geotechnical Testing Journal, ASTM, Volume 2, Number 3, September.
- Tavenas, F. A., 1971, "Discussion of the Standard Penetration Test," 4th Pan American Conference on Soil Mechanics and Foundation Engineering, San Juan, Puerto Rico, Vol. III.
- Tinsley, J. C. III, 1975, "Quaternary Geology of Northern Salinas Valley, Monterey County, California," Unpub. Ph.D. Dissertation, Stanford University.
- Treadwell, Donald D. 1975, "The Influence of Gravity, Pre-stress, Compressibility, and Layering on Soil Resistance to Static Penetration," Dissertation for Ph.D. in Engineering, Graduate Division of the University of Calif. Berkeley.
- U.S. Department of Agriculture, Soil Conservation Service, 1978, Soil Survey of Orange County and western part of Riverside County, California.
- Vesic, A. S., 1963 "Bearing Capacity of Deep Foundations in Sand," Highway Research Board, Highway Research Record No. 39.
- Wood, P. R., and Burton, L. C., 1968, "Ground-Water Resources, Cleveland and Oklahoma Counties," Oklahoma Geologic Survey Circular 71.
- Yong, R. N., and Chen, C. K., 1976, "Cone Penetration of Granular and Cohesive Soils," Journal of the Engineering Mechanics Division, ASCE, No. EM2, April.

- Youd, T. L., and Perkins, D. M., 1977, "Mapping of Liquefaction Potential Using Probability Concepts," Annual Convention of the ASCE, Oct., San Francisco, California.
- Ziony, J. I., 1973, "Recency of Faulting in the Greater San Diego Area, California," in Ross, A., and Dowlen, R. J. (eds.), "Studies on the Geology and Geologic Hazards of the Greater San Diego Area, California," San Diego Association of Geologists, p. 68-75.

APPENDIX A



PROFILES REPRESENT AVERAGE AND + ONE STANDARD DEVIATION.



PROJECT NO.:

79-153

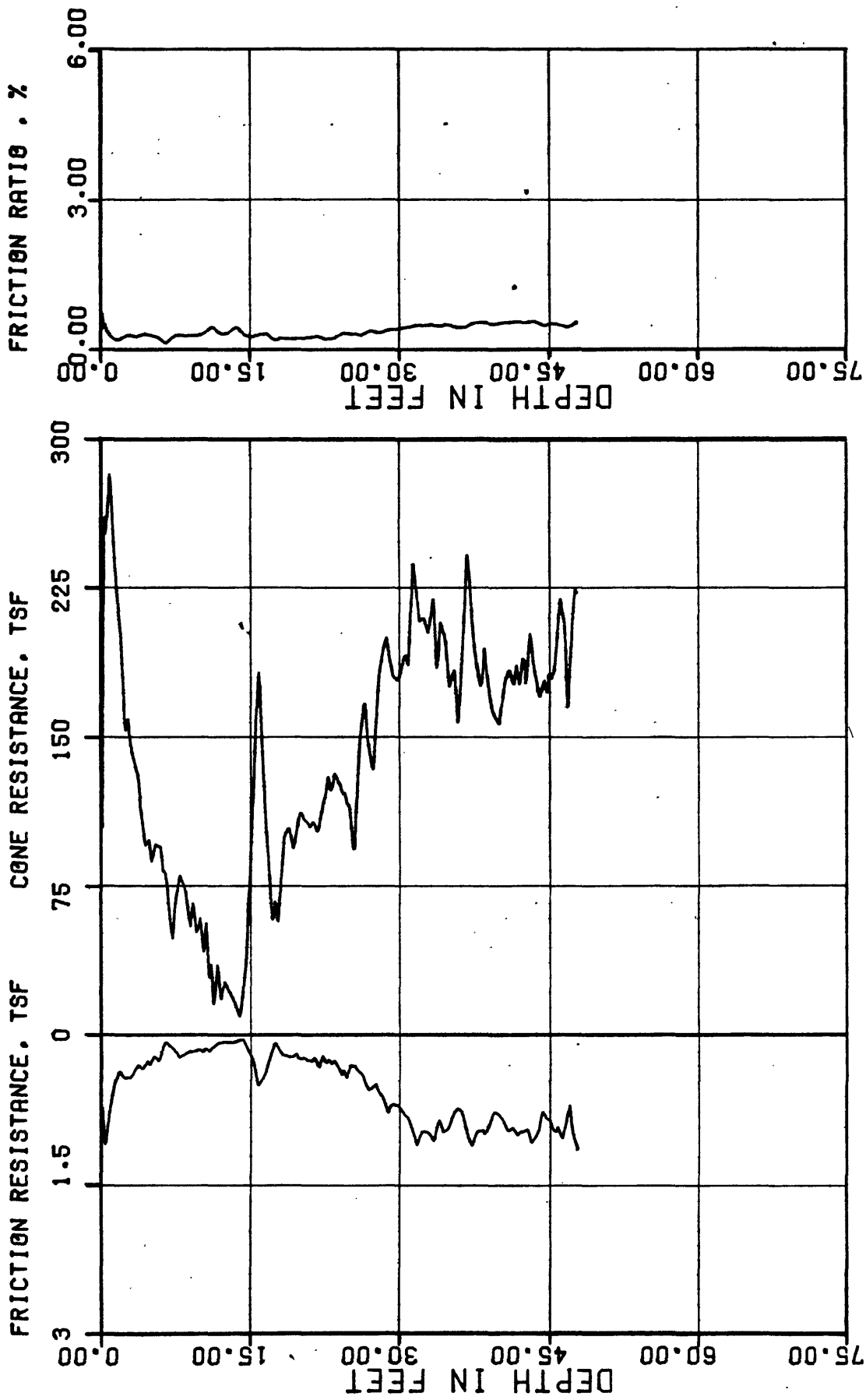
USGS CPT-SPT

PROFILE AVERAGE
CONE PENETROMETER TEST

INSTRUMENT:

SOUNDING: SAN DIEGO

FIGURE A.1



PROJECT NO.:

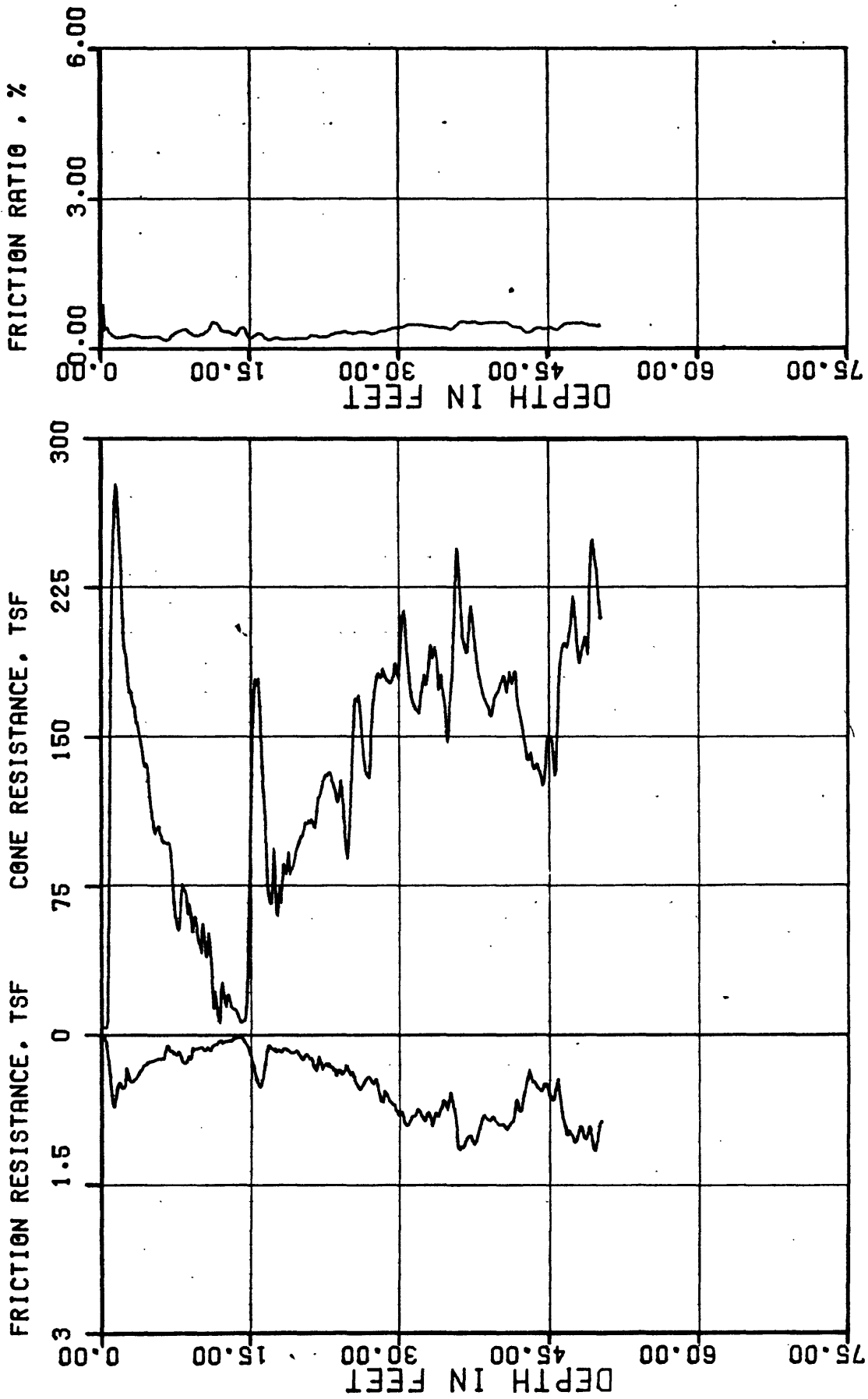
79-153

USGS CPT-SPT

CONE PENETROMETER TEST

INSTRUMENT: F5KC2-40 SOUNDING: SD-C-1A

FIGURE A.2



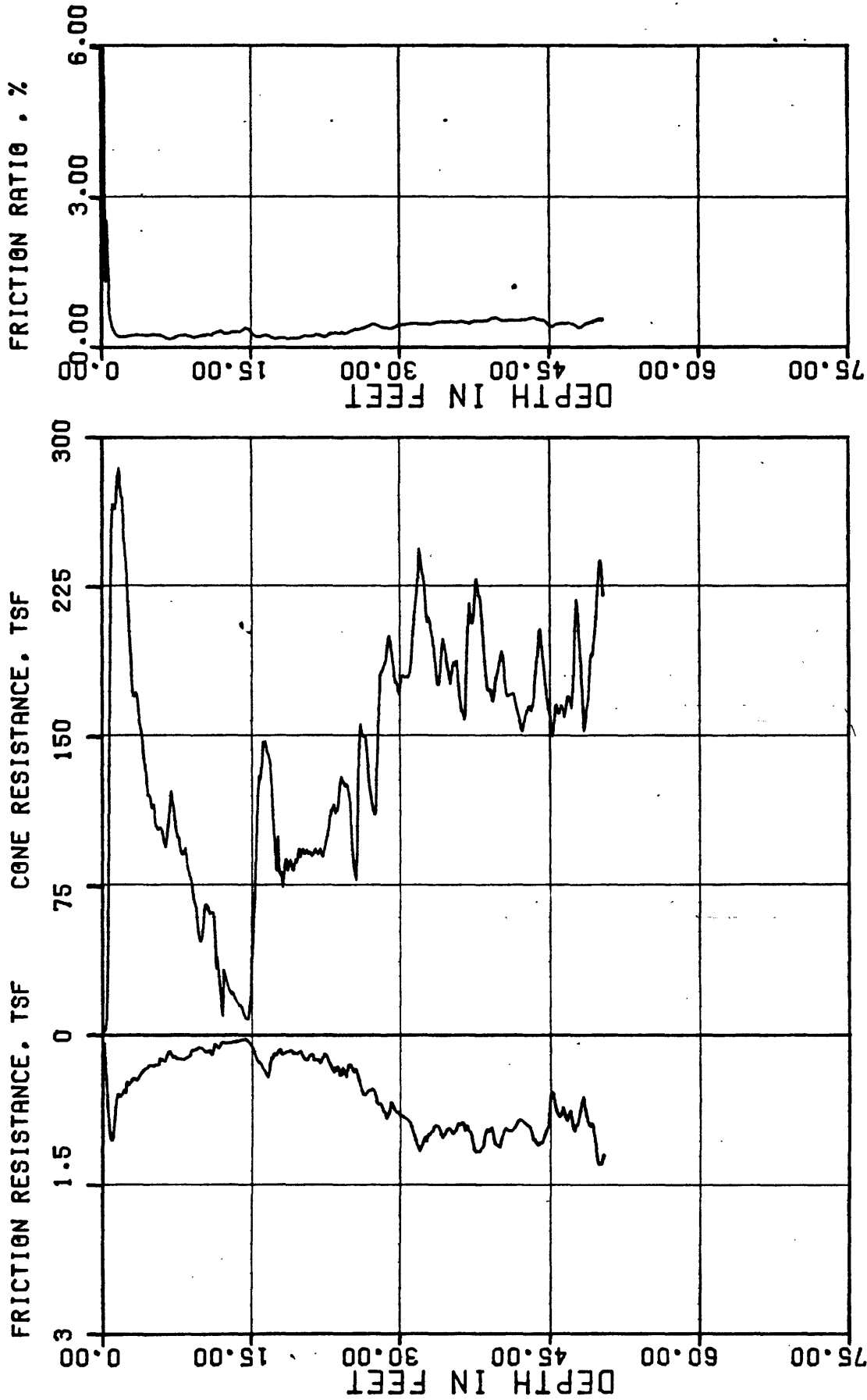
PROJECT NO.:

79-153

USGS CPT-SPT

CONE PENETROMETER TEST

INSTRUMENT: F5KC2-40 SOUNDRING: SD-C-1B FIGURE A.3

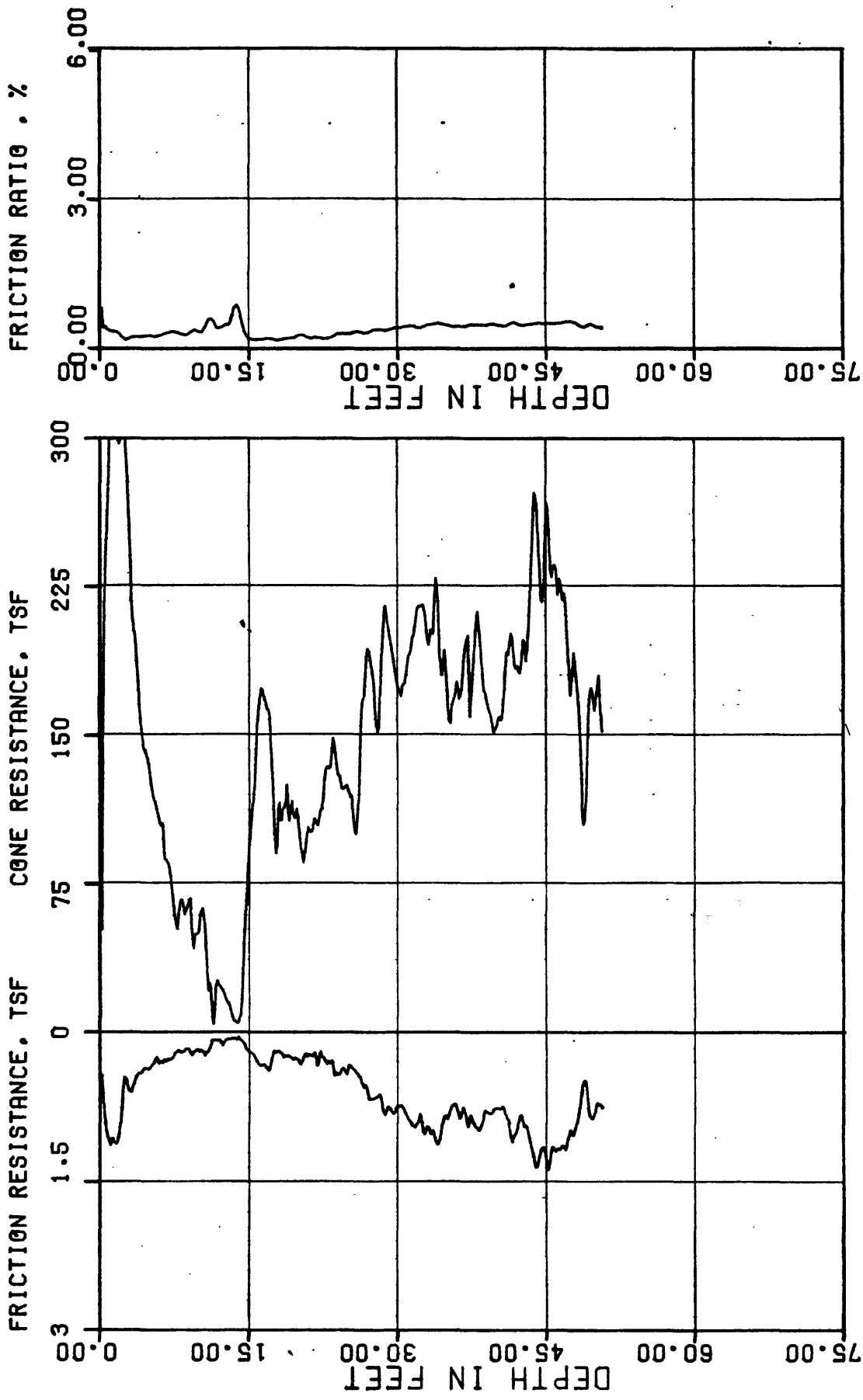


PROJECT NO.: 79-153

USGS CPT-SPT

CONE PENETROMETER TEST

INSTRUMENT: F5KC2-40 SOUNDING: SD-C-1C FIGURE A.4



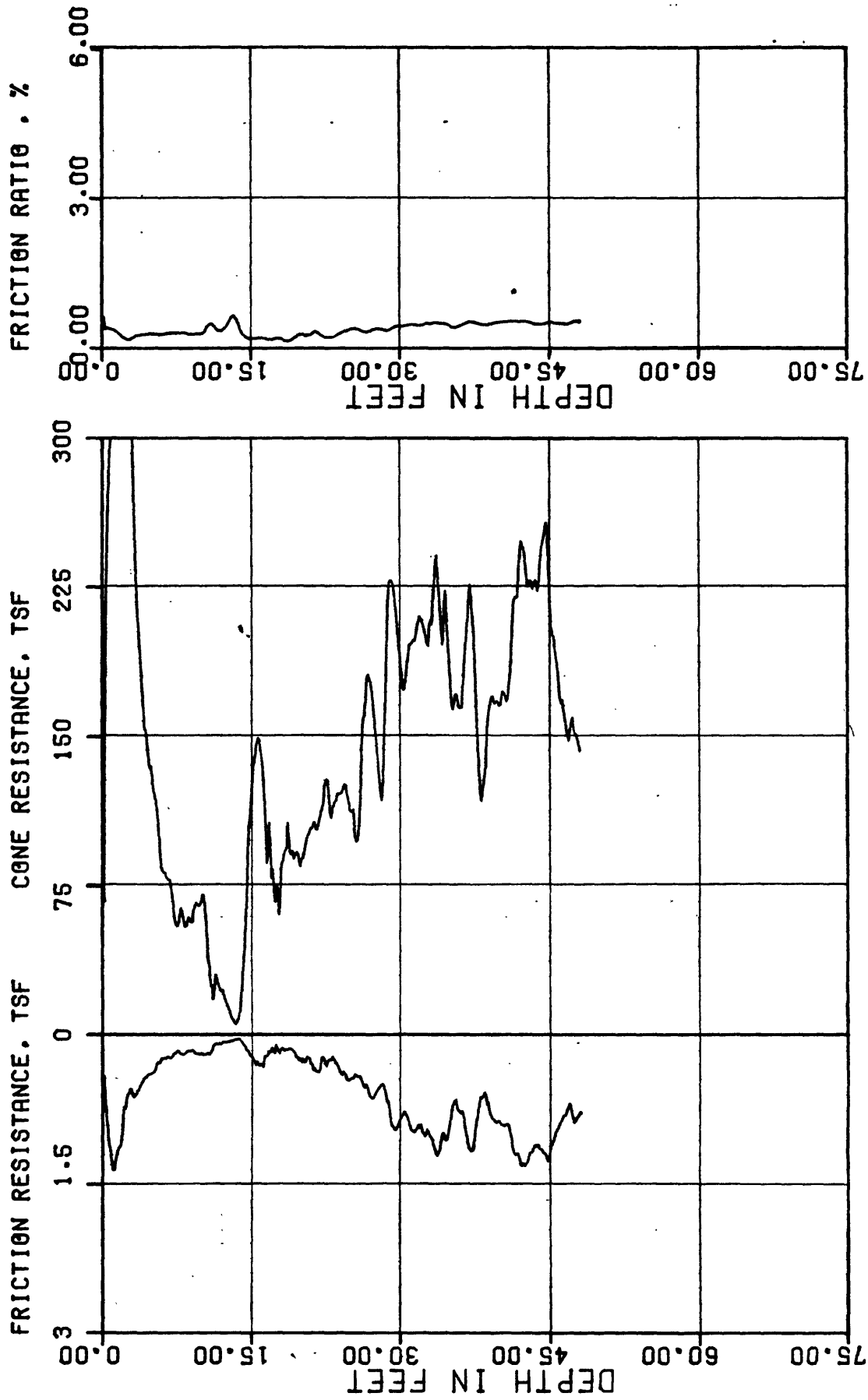
PROJECT NO.:

79-153

USGS CPT-SPT

CONE PENETROMETER TEST

INSTRUMENT: F5KC2-40 SOUNDING: SD-C-2A FIGURE A.5



PROJECT NO.:

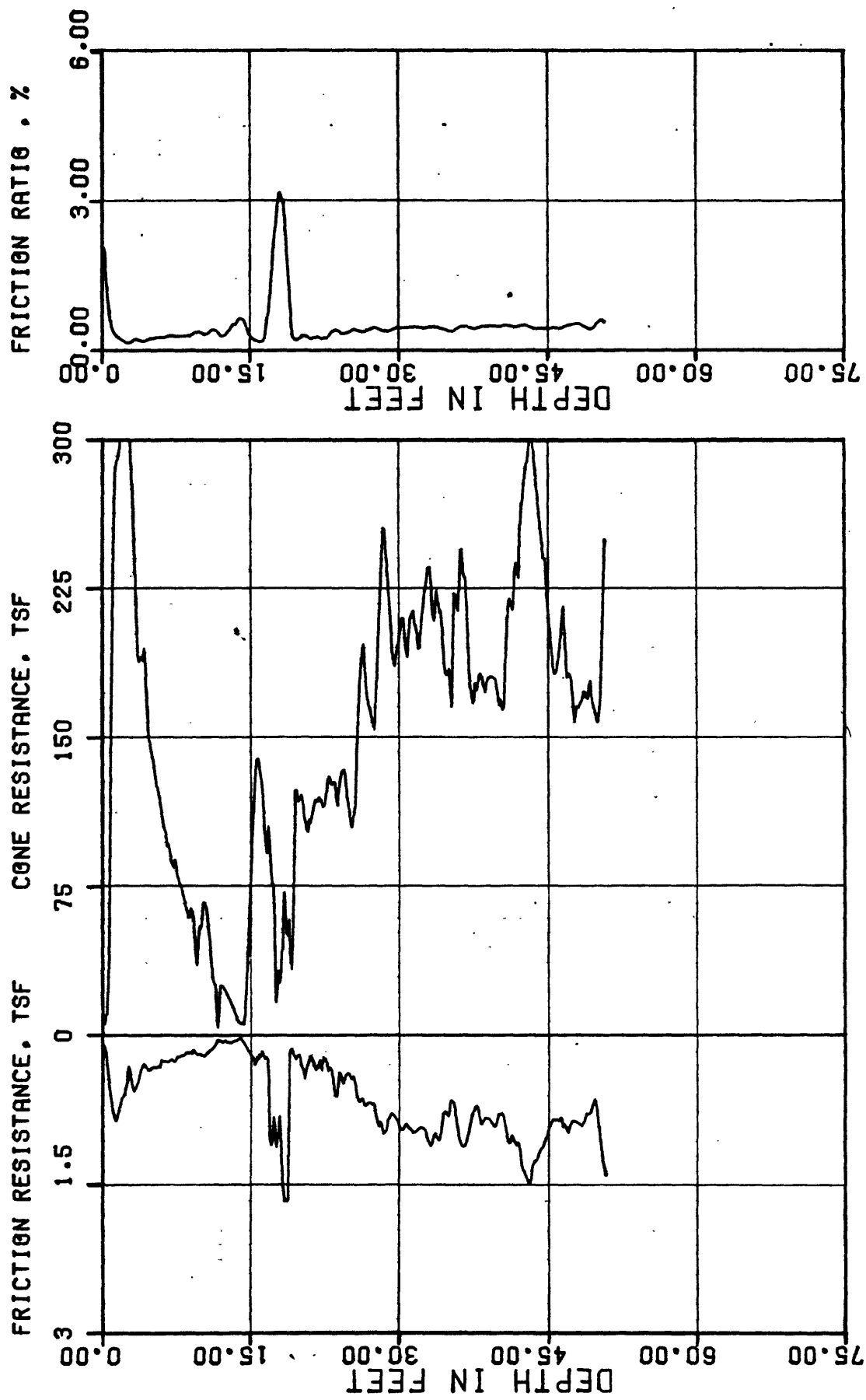
79-153

USGS CPT-SPT

CONE PENETROMETER TEST

INSTRUMENT: F5KC2-40 SOUNDING: SD-C-3A

FIGURE A.6



PROJECT NO.:

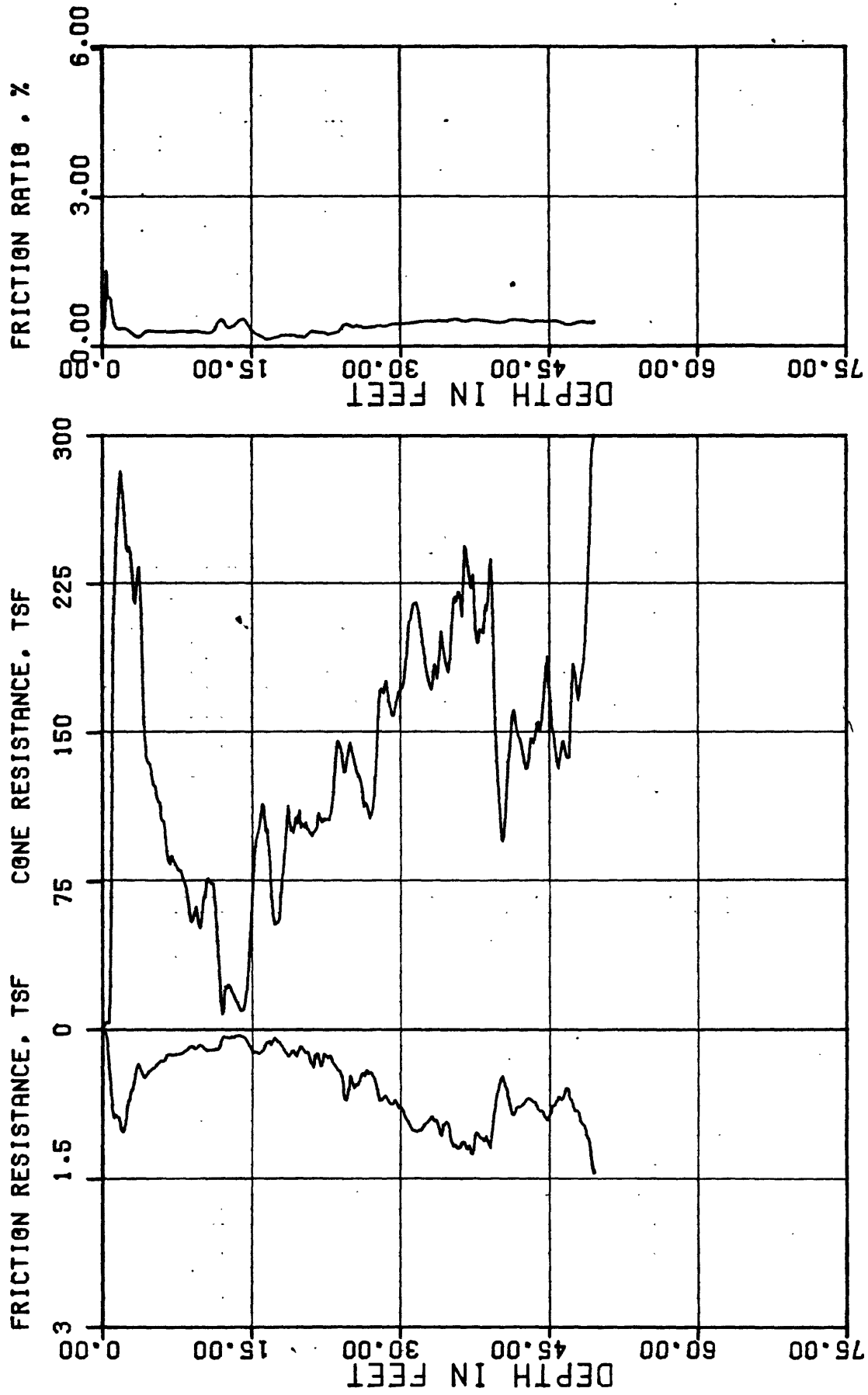
79-153

USGS CPT-SPT

CONE PENETROMETER TEST

INSTRUMENT: F5KC2-40 SOUNDING: SD-C-38

FIGURE A.7



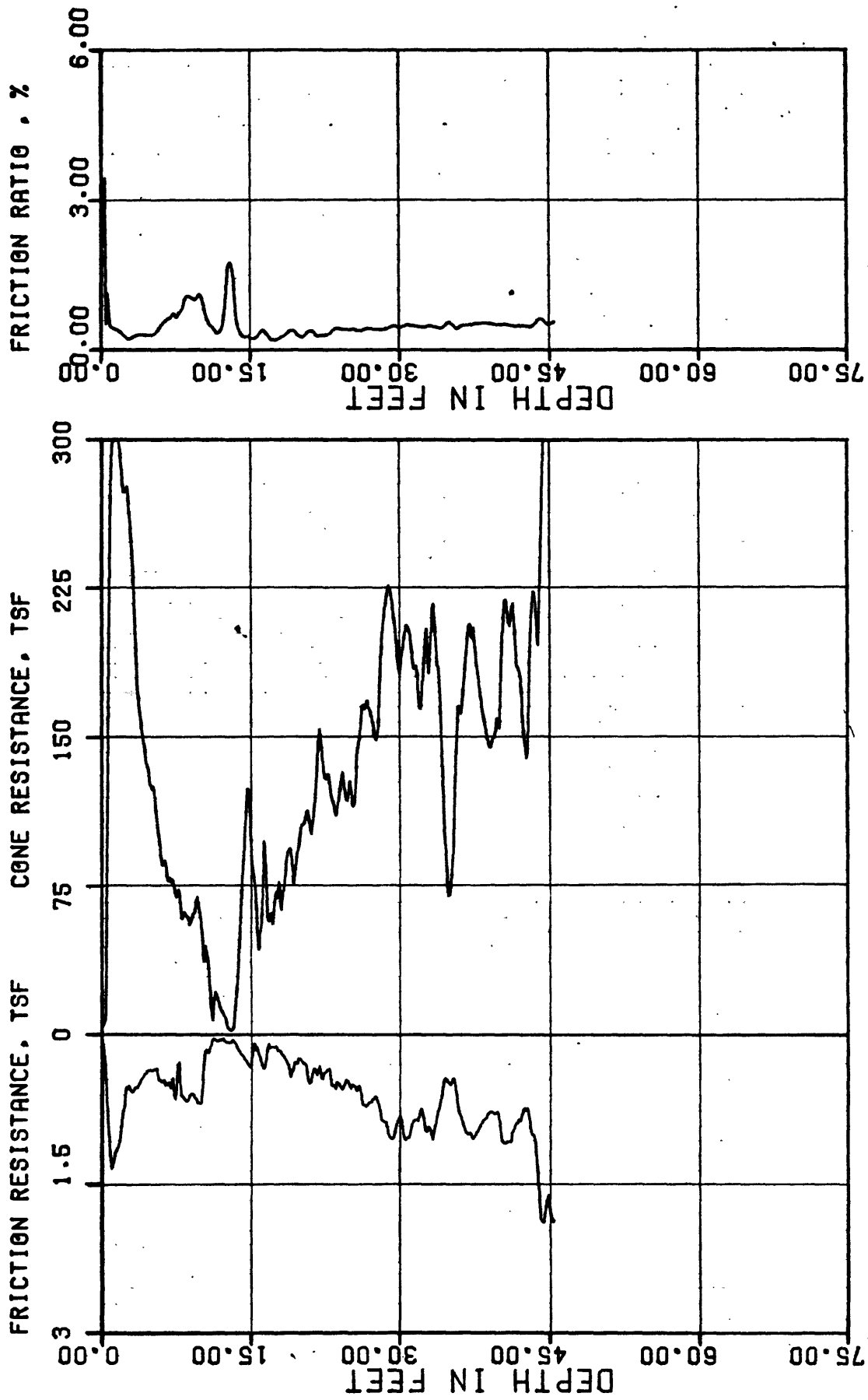
PROJECT NO.:

79-153

USGS CPT-SPT

CONE PENETROMETER TEST

INSTRUMENT: F5KC2-40 SOUNDING: SD-C-4A FIGURE A.8



PROJECT NO.:

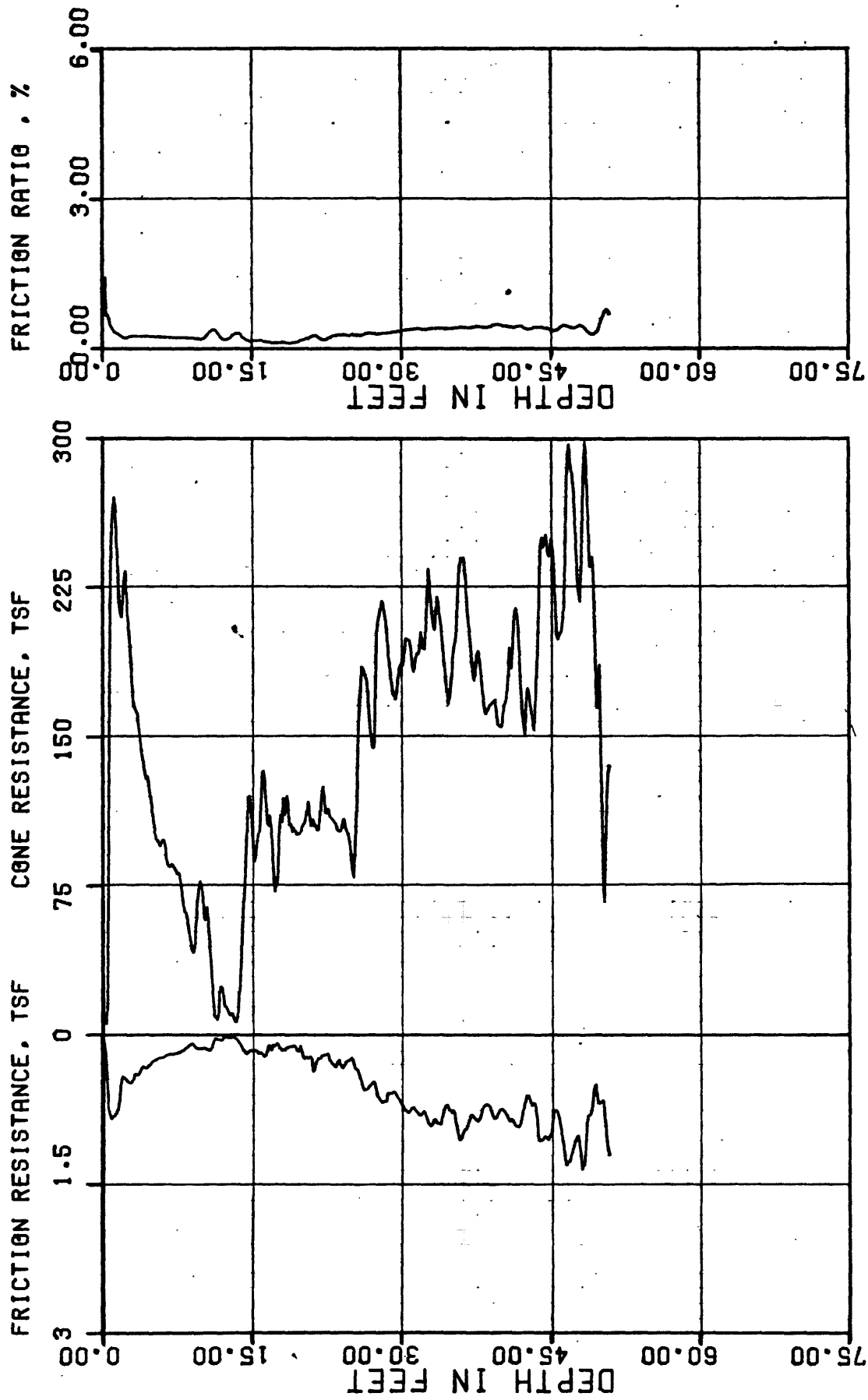
79-153

USGS CPT-SPT

CONE PENETROMETER TEST

INSTRUMENT: F5KC2-40 SOUNDRING: SD-C-48

FIGURE A.9



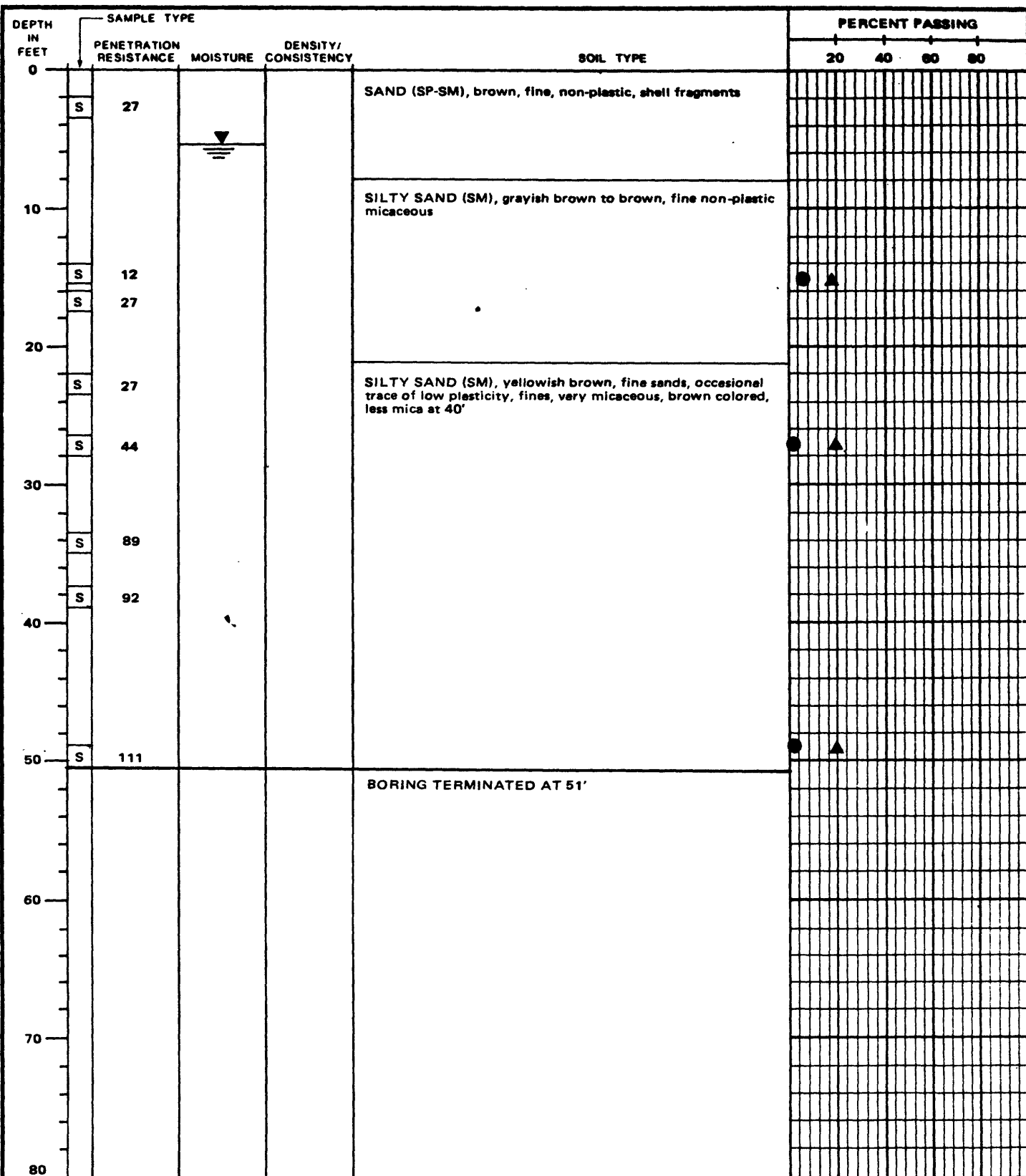
PROJECT NO.:

79-153

USGS CPT-SPT

CONE PENETROMETER TEST

INSTRUMENT: F5K2C-40 SOUNDING: SD-C-4C FIGURE A.10



ELEVATION: DATE DRILLED: 10-12-79
 EQUIPMENT USED: 5 7/8" ROTARY WASH
 WATER LEVEL: 5'

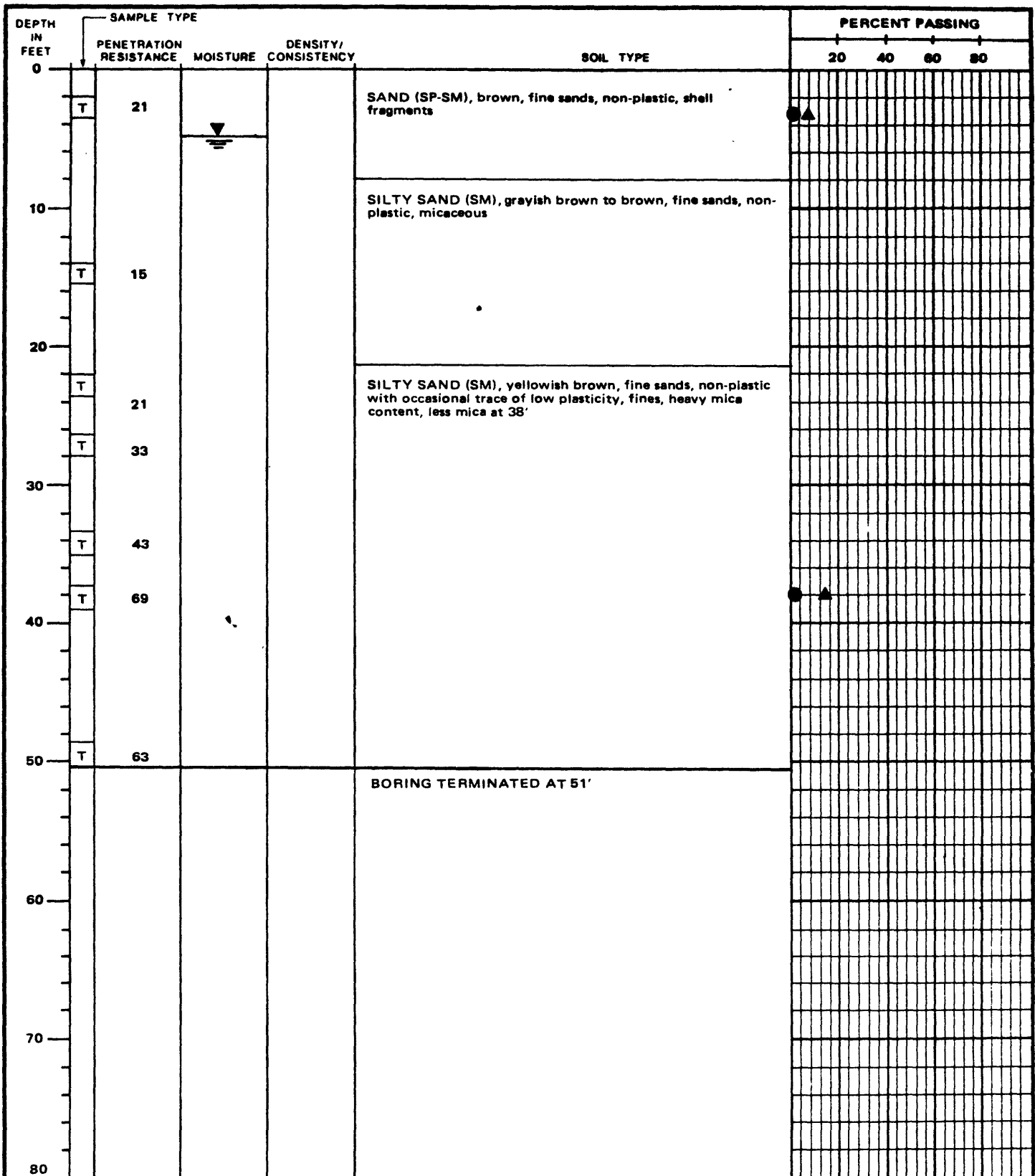
[S] STANDARD HAMMER SPLIT SPOON SAMPLE ▲ #200 SIEVE
 [T] TRIP HAMMER SPLIT SPOON SAMPLE ● 0.002 mm



PROJECT NO.: 79-153

USGS CPT-SPT

LOG OF BORING NO. 1A
 SAN DIEGO SITE: NAS NORTH ISLAND



ELEVATION: DATE DRILLED: 10-12-79
 EQUIPMENT USED: 5 7/8" ROTARY WASH
 WATER LEVEL: 5'

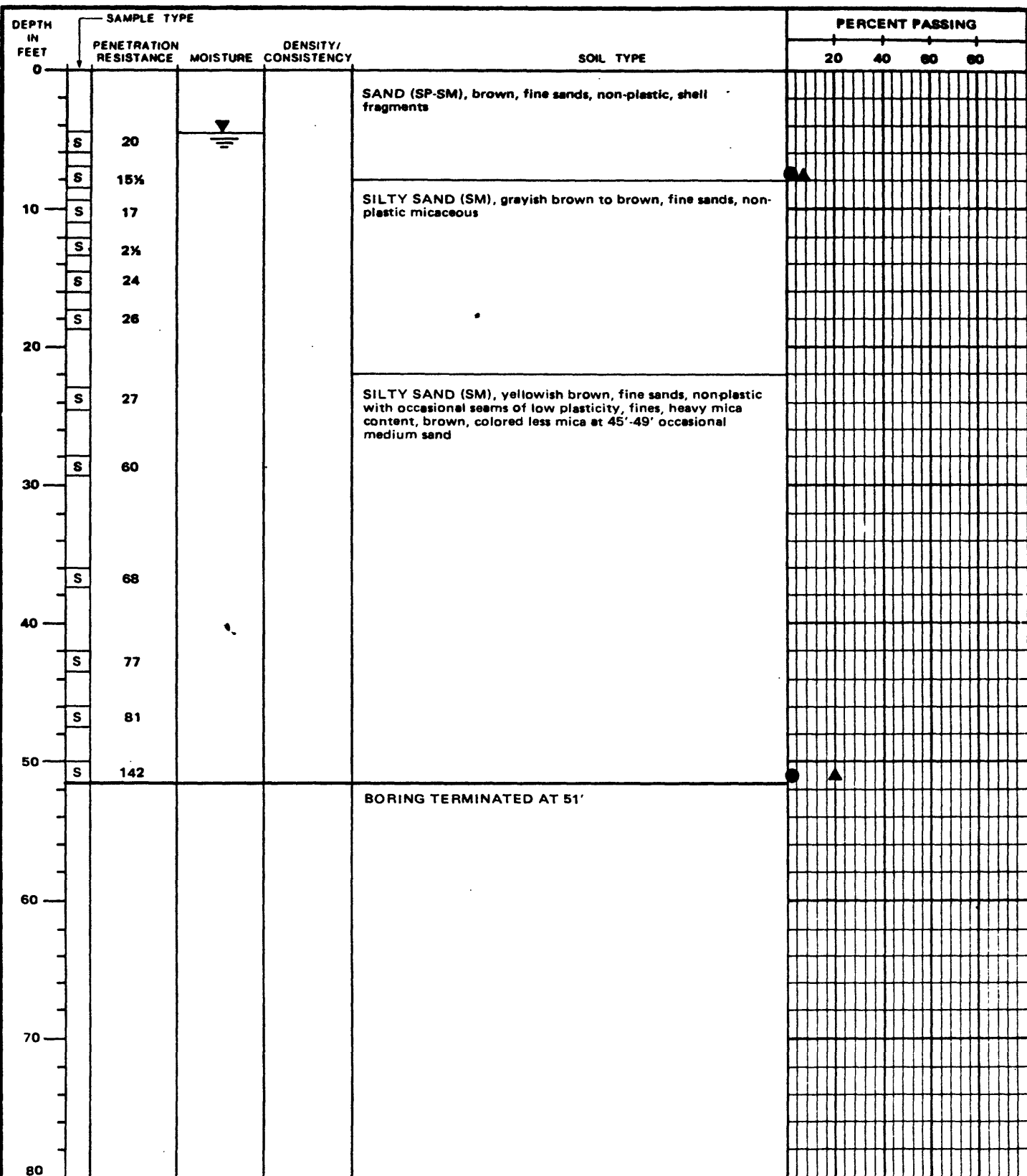
[S] STANDARD HAMMER SPLIT SPOON SAMPLE ▲ #200 SIEVE
 [T] TRIP HAMMER SPLIT SPOON SAMPLE ● 0.002 mm



PROJECT NO.: 79-153

USGS CPT-SPT

LOG OF BORING NO. 1B
 SAN DIEGO SITE: NAS NORTH ISLAND



ELEVATION: DATE DRILLED: 10-11-79
 EQUIPMENT USED: 5 7/8" ROTARY WASH
 WATER LEVEL: 5'

[S] STANDARD HAMMER SPLIT SPOON SAMPLE ▲ #200 SIEVE
 [T] TRIP HAMMER SPLIT SPOON SAMPLE ● 0.002 mm

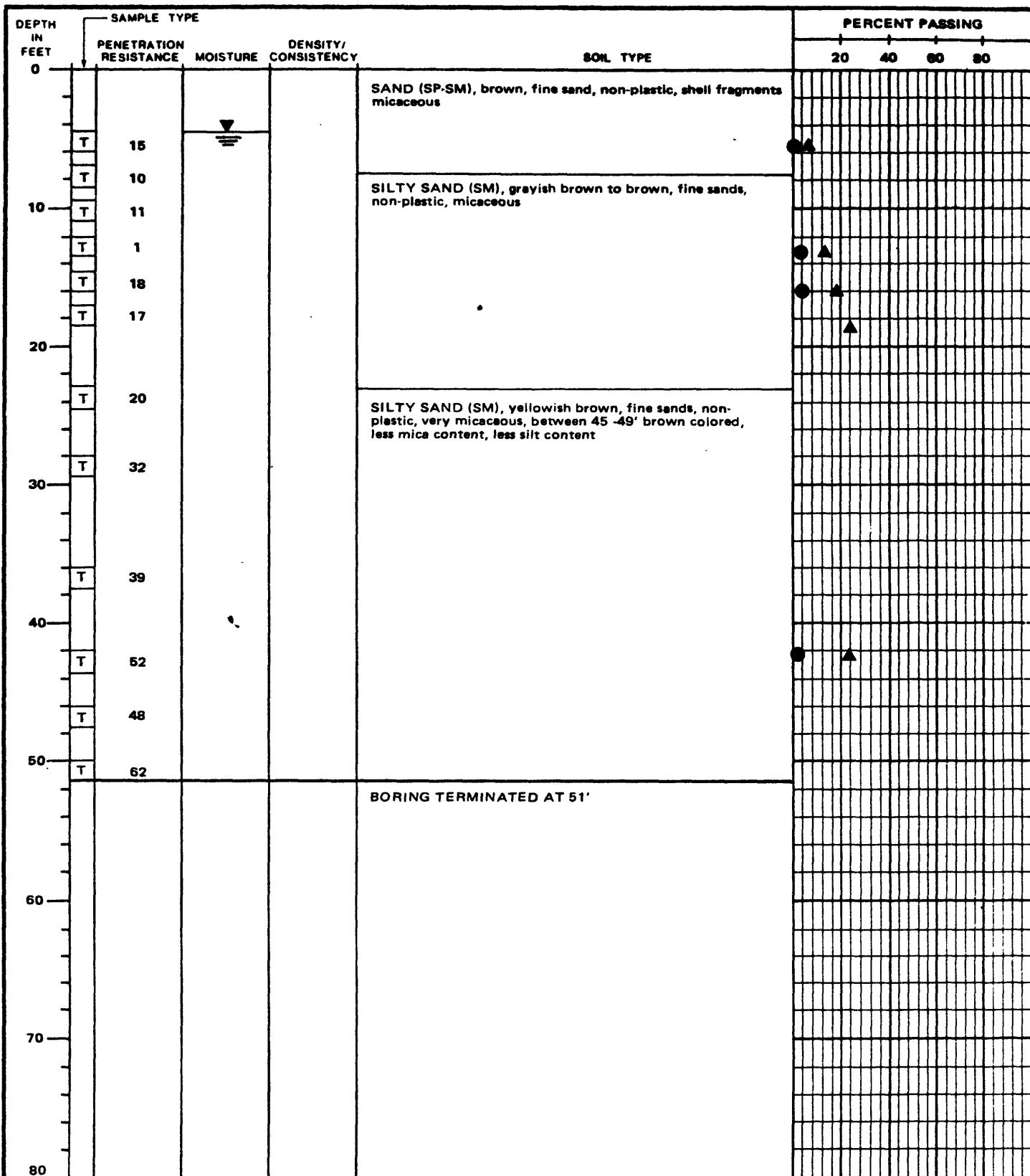


PROJECT NO.:

79-163

USGS CPT-SPT

LOG OF BORING NO. 2A
 SAN DIEGO SITE: NAS NORTH ISLAND



ELEVATION: DATE DRILLED: 10-12-79
EQUIPMENT USED: 5 7/8" ROTARY WASH
WATER LEVEL: 5'

[S] STANDARD HAMMER SPLIT SPOON SAMPLE ▲ #200 SIEVE
[T] TRIP HAMMER SPLIT SPOON SAMPLE ● 0.002 mm



PROJECT NO.:

79-153

USGS CPT-SPT

LOG OF BORING NO. 2B
SAN DIEGO SITE: NAS NORTH ISLAND

DEPTH IN FEET	SAMPLE TYPE			SOIL TYPE	PERCENT PASSING			
	PENETRATION RESISTANCE	MOISTURE	DENSITY/ CONSISTENCY		20	40	60	80
0				SAND (SP-SM), brown, fine to medium, micaceous with shell fragments				
S 43				SILTY SAND (SM), brown to grayish brown, fine sands, non-plastic, mica				
S 24								
S 14								
S 13								
S 1								
S 26								
S 37								
S 28				SILTY SAND (SM), dark brown to yellow brown, fine sands, non-plastic, locally having mica content				
S 49								
S 112								
S 55				SILTY SAND (SM), brown, fine sands, occasional medium sands, mica, non-plastic				
S 89								
S 66								
50	BORING E BORING TERMINATED AT 50'							
60								
70								
80								

ELEVATION: DATE DRILLED: 10-11-79

EQUIPMENT USED: 5 7/8" ROTARY WASH

WATER LEVEL: 5'

☐ STANDARD HAMMER SPLIT SPOON SAMPLE ▲ #200 SIEVE

☐ TRIP HAMMER SPLIT SPOON SAMPLE ● 0.002 mm

PROJECT NO.: 79-153

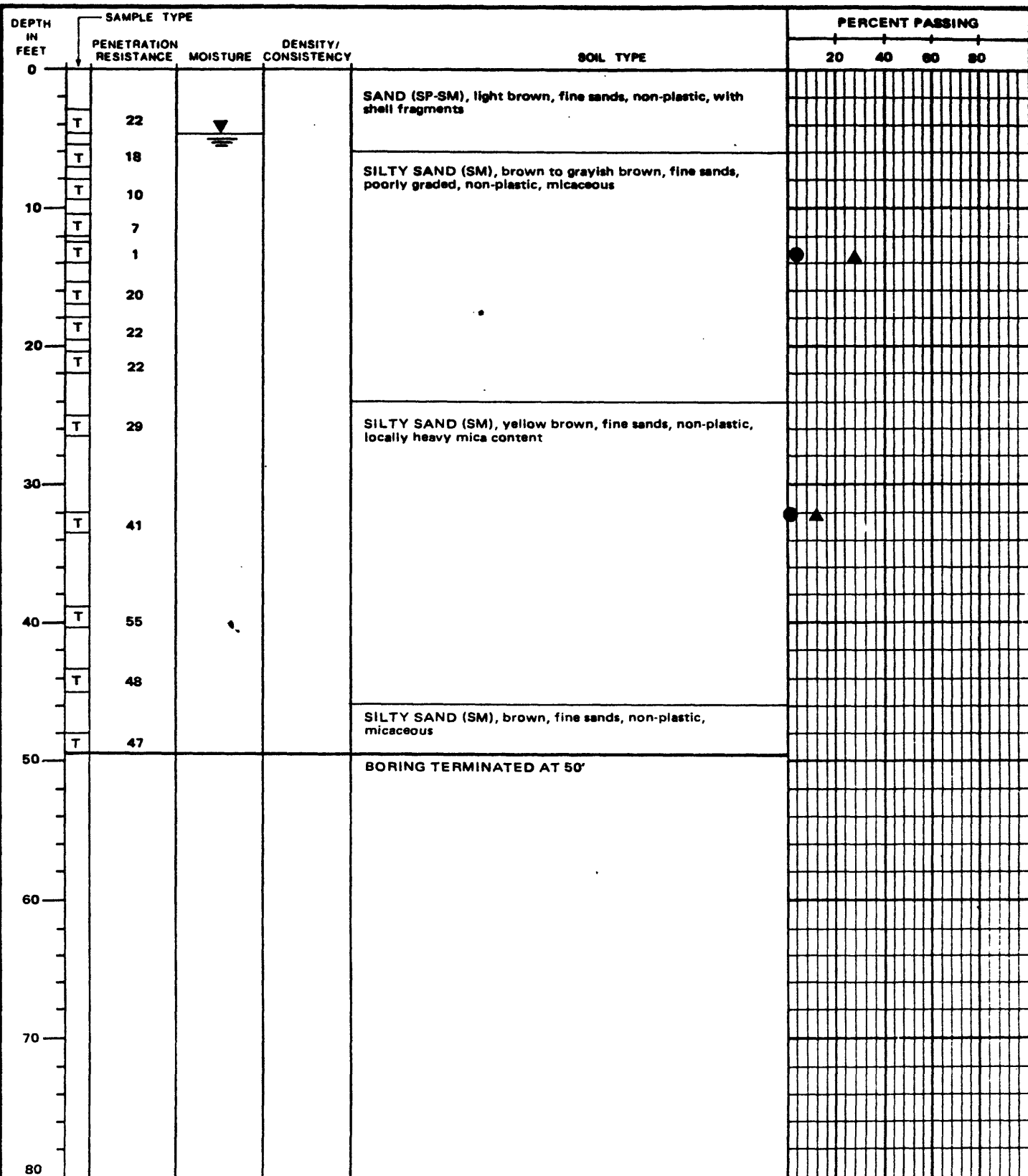
USGS CPT-SPT

LOG OF BORING NO. 3A

SAN DIEGO SITE: NAS NORTH ISLAND

9-80

FIGURE A.15



ELEVATION: DATE DRILLED: 10-11-79
 EQUIPMENT USED: 5 7/8" ROTARY WASH
 WATER LEVEL: 5'

[S] STANDARD HAMMER SPLIT SPOON SAMPLE ▲ #200 SIEVE
 [T] TRIP HAMMER SPLIT SPOON SAMPLE ● 0.002 mm

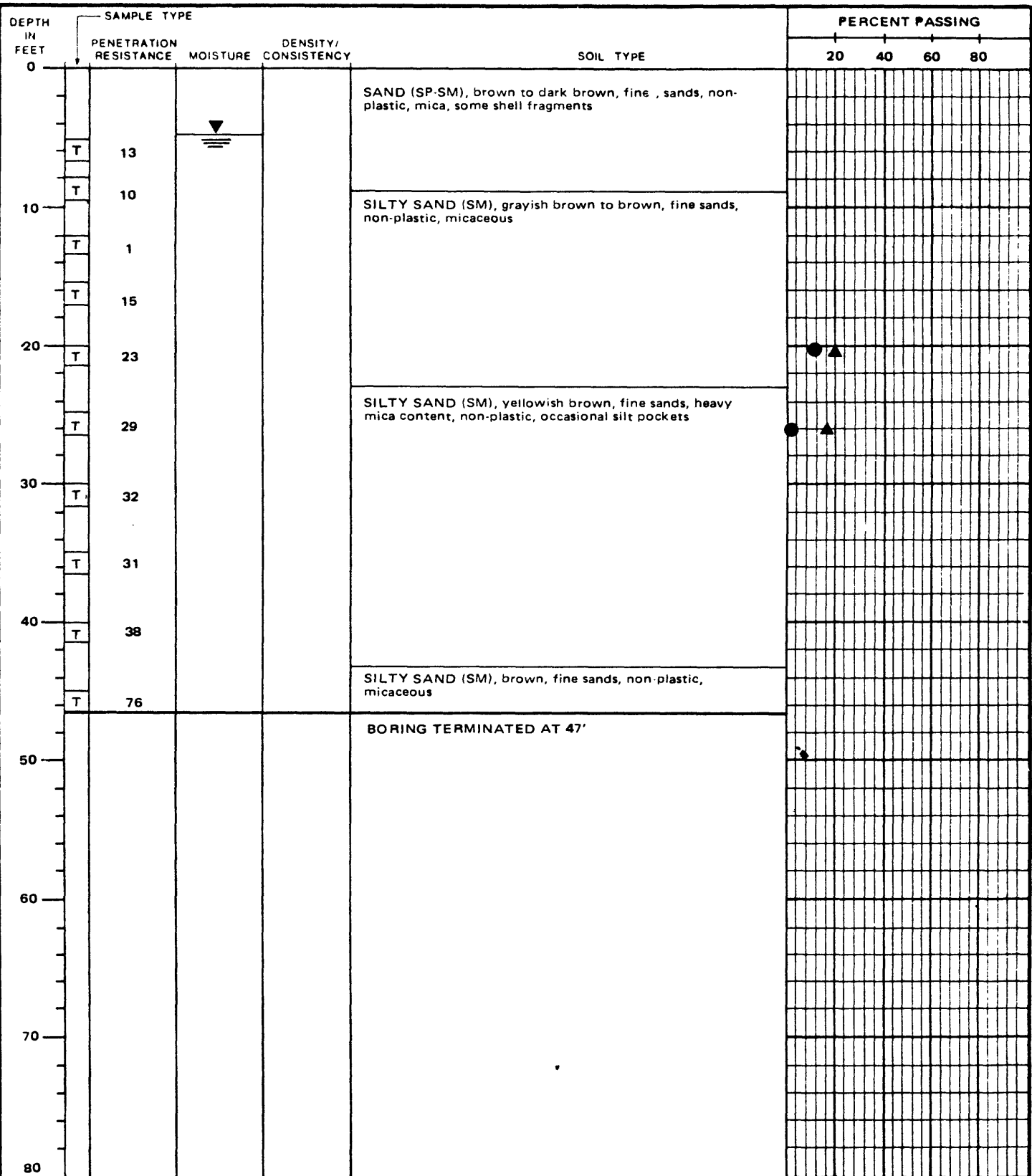


PROJECT NO.:

79-153

USGS CPT-SPT

LOG OF BORING NO. 3B
 SAN DIEGO SITE: NAS NORTH ISLAND



ELEVATION: DATE DRILLED: 10-10-79
 EQUIPMENT USED: 5 7/8" ROTARY WASH
 WATER LEVEL: 5'

[S] STANDARD HAMMER SPLIT SPOON SAMPLE ▲ #200 SIEVE
 [T] TRIP HAMMER SPLIT SPOON SAMPLE ● 0.002 mm



PROJECT NO.:

79-153

USGS CPT-SPT

LOG OF BORING NO. 4A
 SAN DIEGO SITE: NAS NORTH ISLAND

DEPTH IN FEET	SAMPLE TYPE			SOIL TYPE	PERCENT PASSING			
	PENETRATION RESISTANCE	MOISTURE	DENSITY/ CONSISTENCY		20	40	60	80
0				SAND (SP-SM), brown, fine sands, nonplastic, micaceous, shell fragments				
23	S							
17	S							
1	S			SILTY SAND (SM), grayish brown to brown, fine sands, nonplastic, micaceous				
22	S							
35	S							
44	S			SILTY SAND (SM), yellowish brown, fine sands, nonplastic, heavy mica content				
64	S							
79	S							
60	S							
97	S			SILTY SAND (SM), brown, fine sands, nonplastic, micaceous				
BORING TERMINATED AT 46'								
50								
60								
70								
80								

ELEVATION: DATE DRILLED: 10-10-79

EQUIPMENT USED: 5 7/8" ROTARY WASH

WATER LEVEL: 5'

S STANDARD HAMMER SPLIT SPOON SAMPLE

T TRIP HAMMER SPLIT SPOON SAMPLE

▲ #200 SIEVE

● 0.002 mm

PROJECT NO.: 79-153

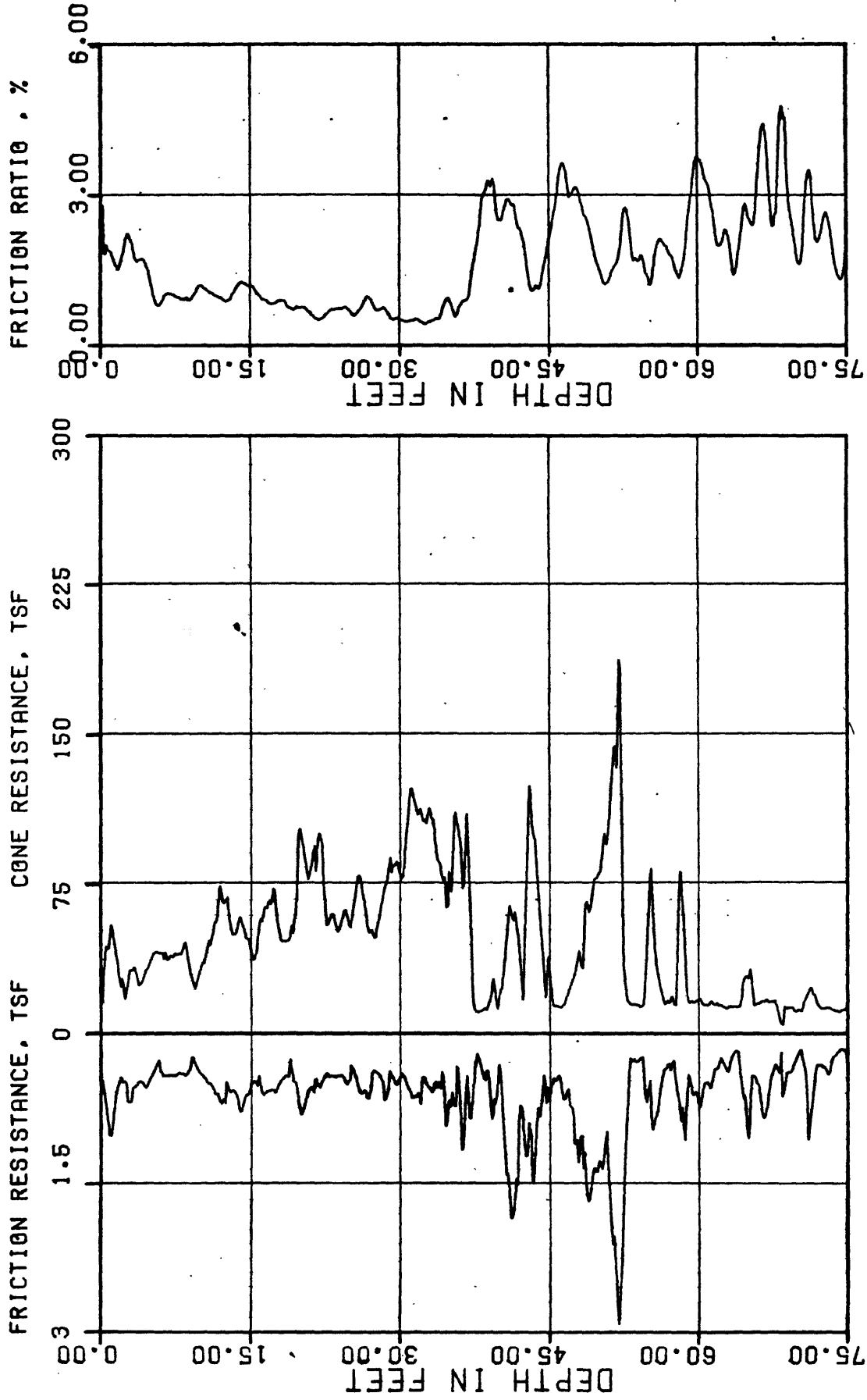
fugro

USGS CPT-SPT

LOG OF BORING NO. 4B

SAN DIEGO SITE: NAS NORTH ISLAND

9-80
FIGURE A.18



PROJECT NO.:

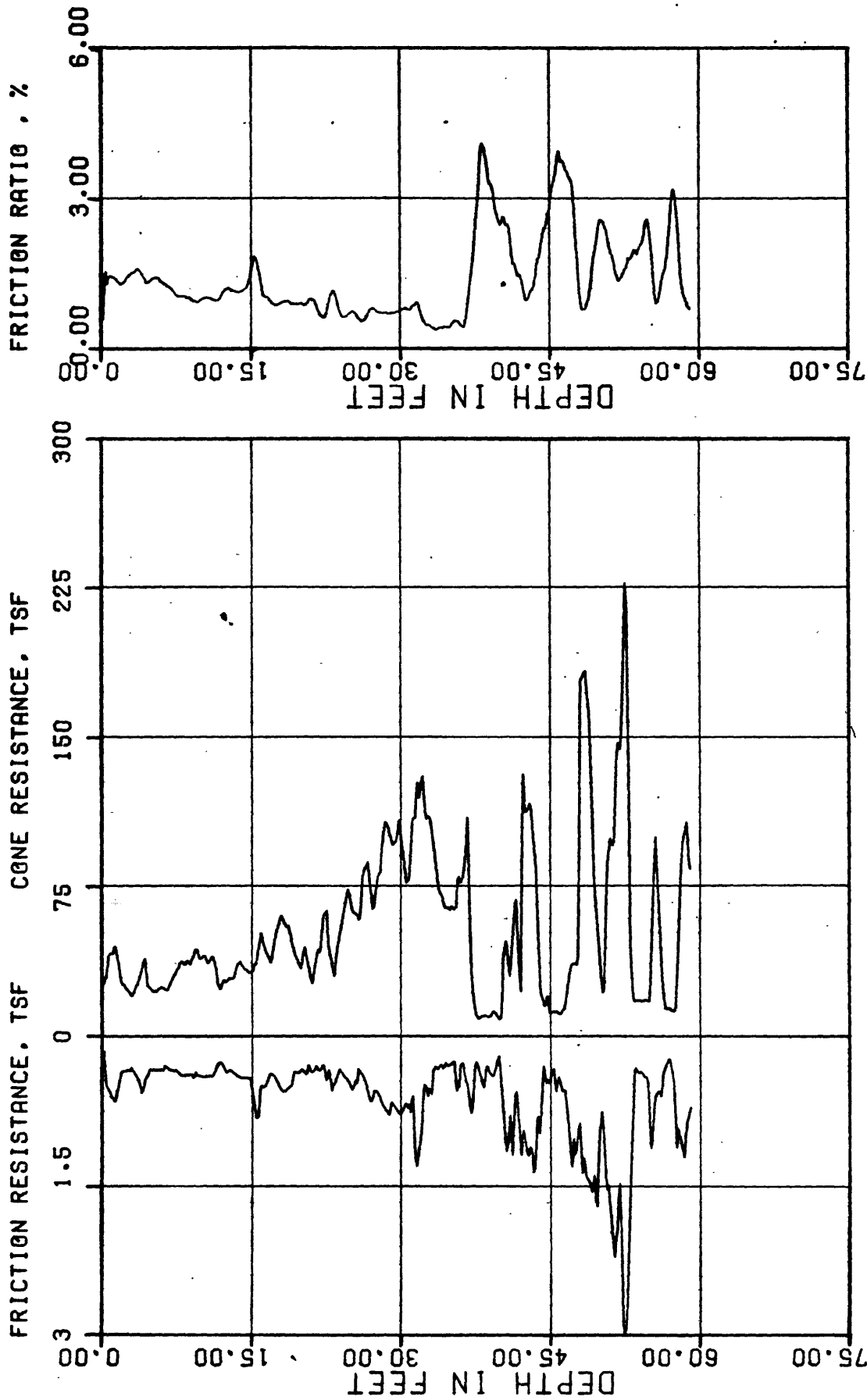
79-153

USGS CPT-SPT

CONE PENETROMETER TEST

INSTRUMENT: F5CK-230 SOUNDING: SS-C-1

FIGURE A.19



PROJECT NO.:

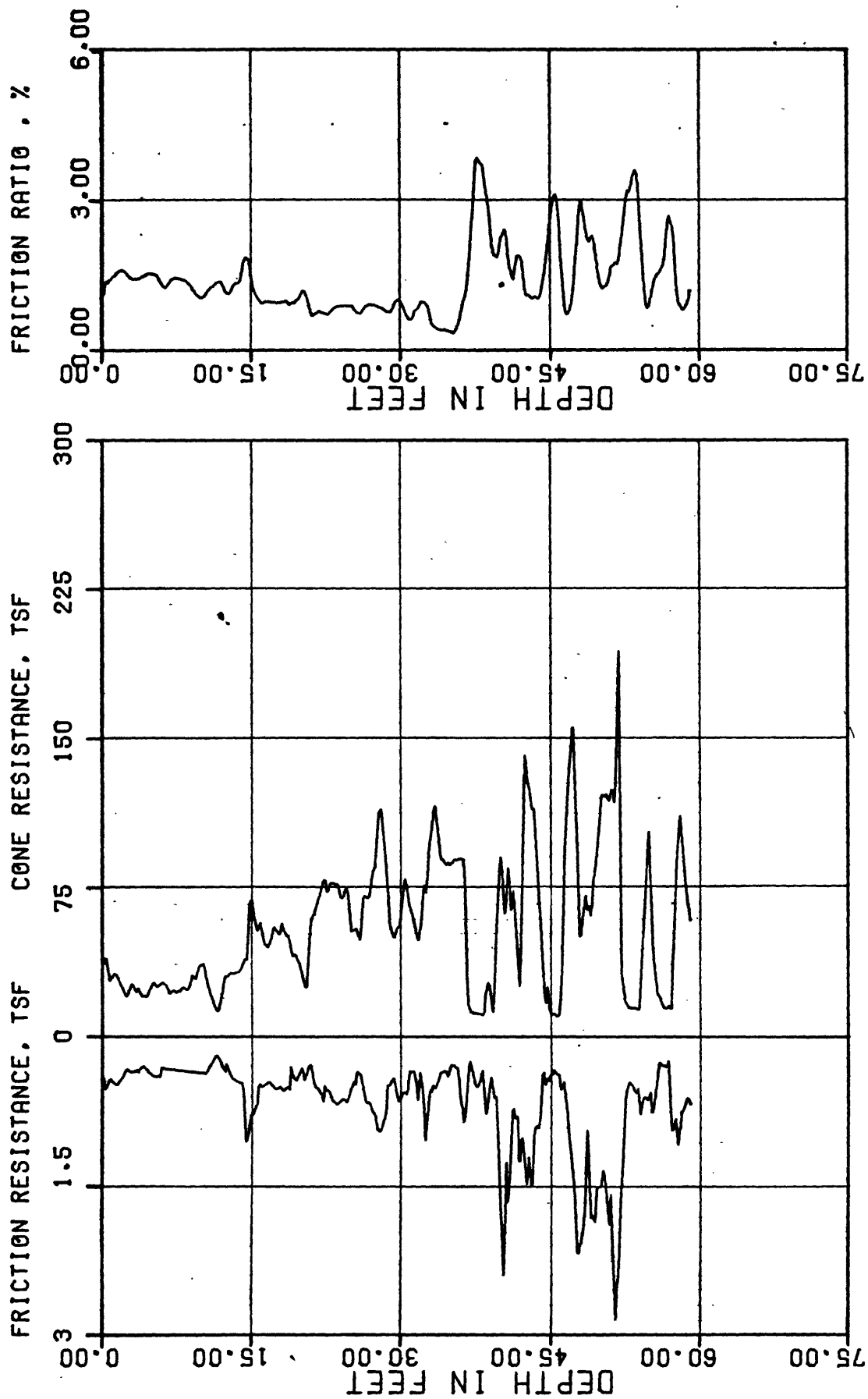
79-163

USGS CPT-SPT

CONE PENETROMETER TEST

INSTRUMENT: F5CK-230 SOUNDING: SS-C-2

FIGURE A.20



PROJECT NO.:

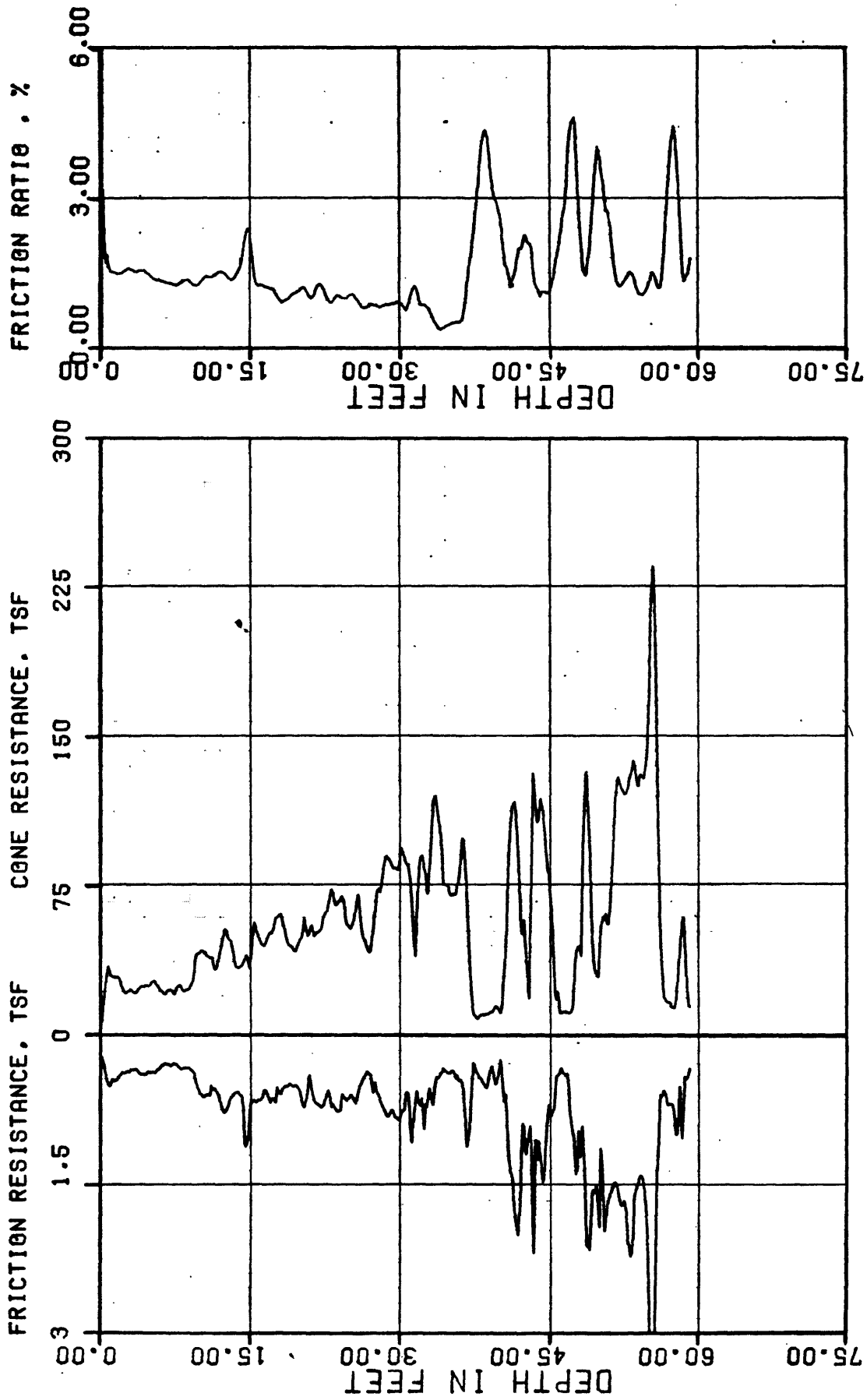
79-153

USGS CPT-SPT

CONE PENETROMETER TEST

INSTRUMENT: F5CK-230 SOUNDING: SS-C-3

FIGURE A.21



PROJECT NO.:

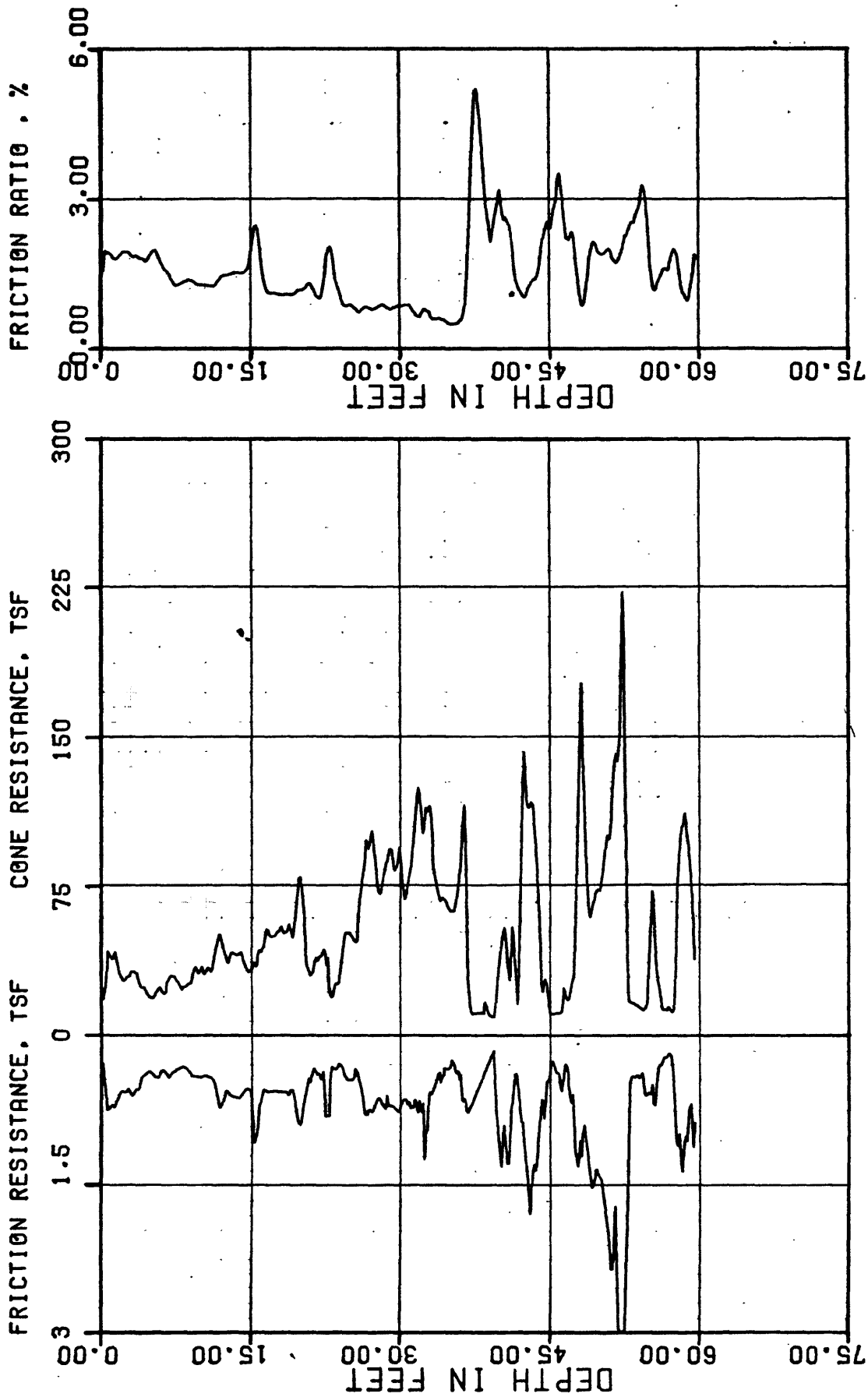
79-153

USGS CPT-SPT

CONE PENETROMETER TEST

INSTRUMENT: F15CKE-070 SOUNDING: SSC-4

FIGURE A.22



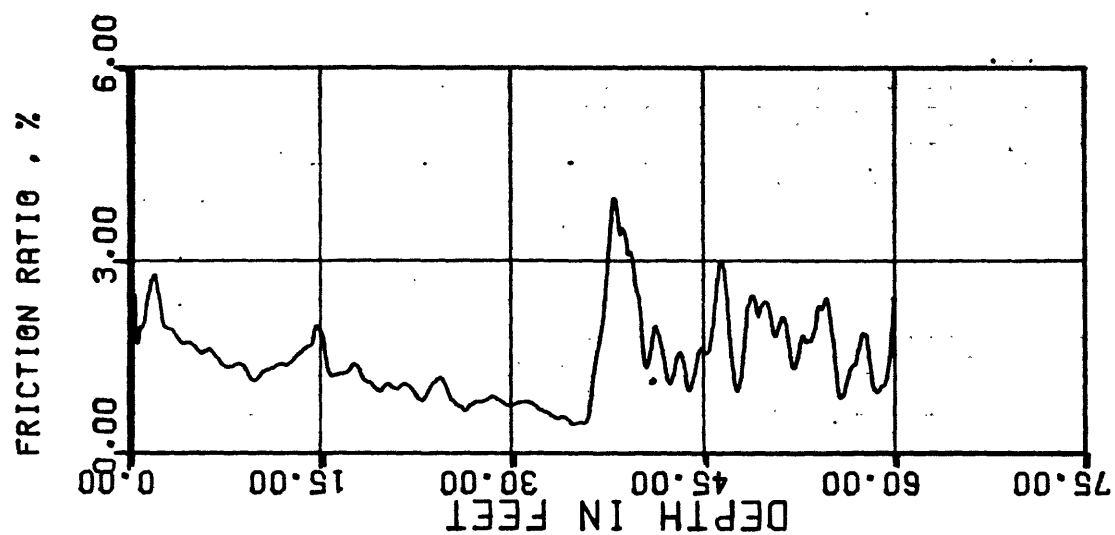
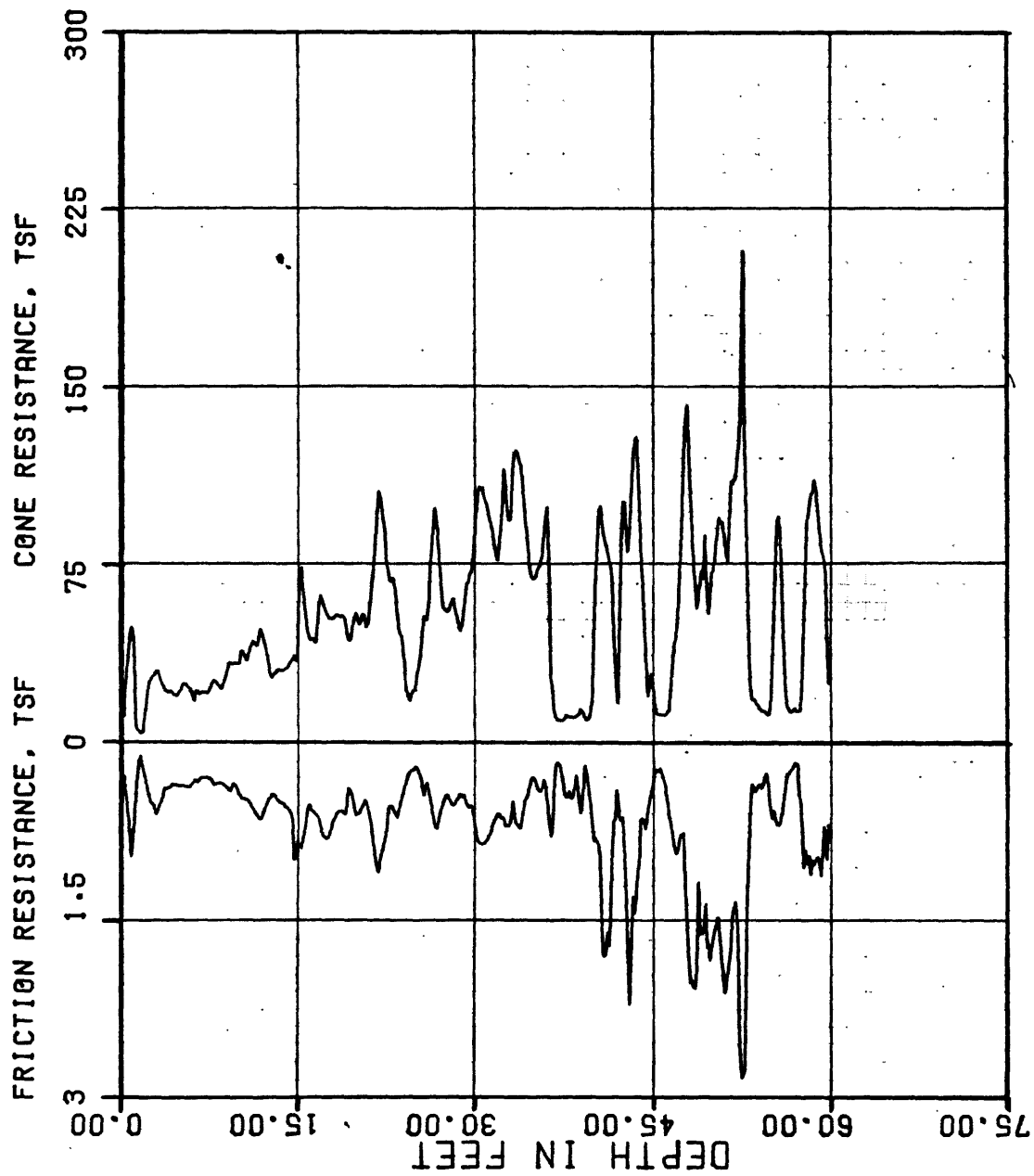
PROJECT NO.:

79-153

USGS CPT-SPT

CONE PENETROMETER TEST

INSTRUMENT: F5CK-230 SOUNDING: SS-C-5 FIGURE A.23



PROJECT NO.:

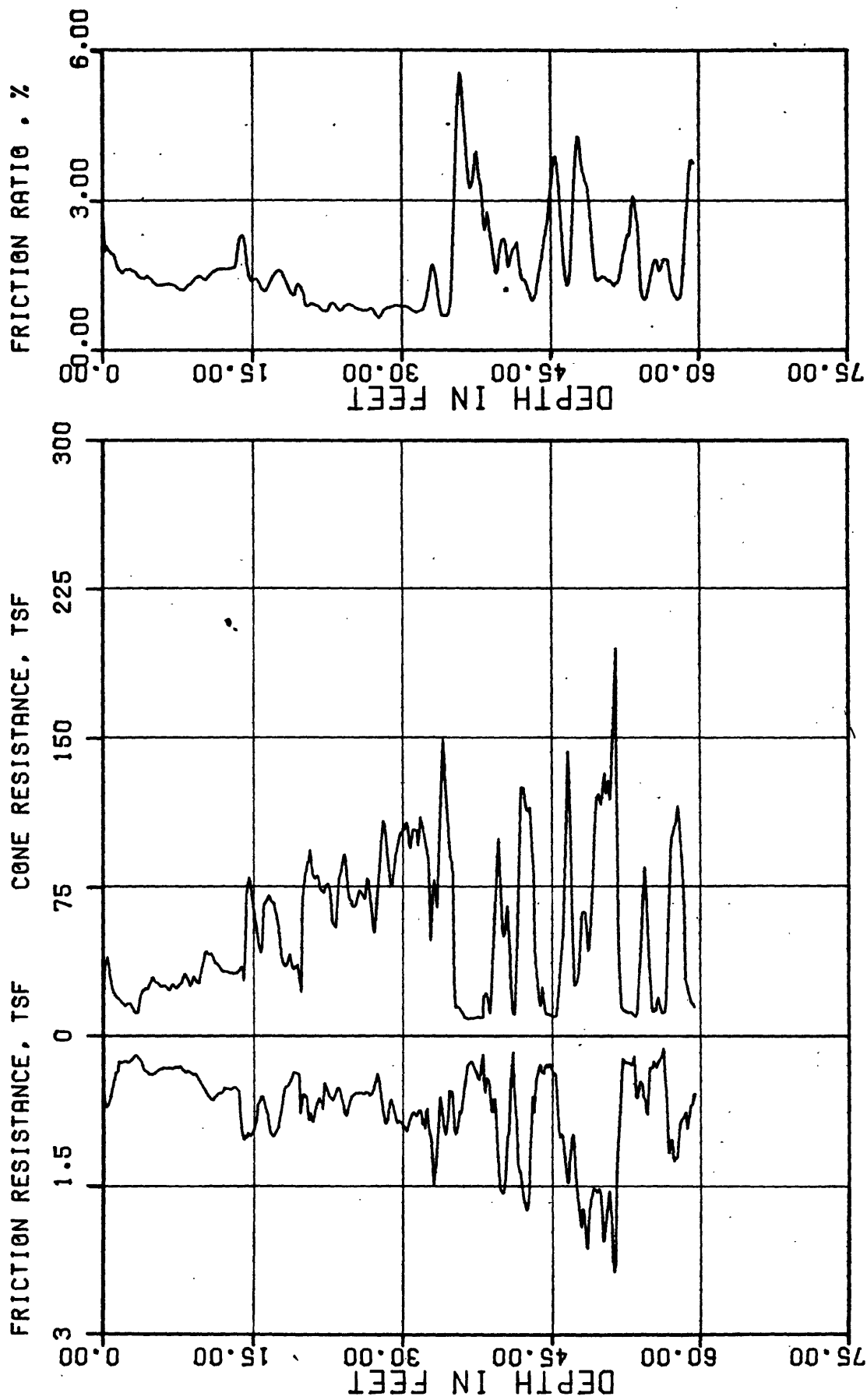
79-153

USGS CPT-SPT

CONE PENETROMETER TEST

INSTRUMENT: F5CK-230 SOUNDING: SSC-8

FIGURE A.24



PROJECT NO.:

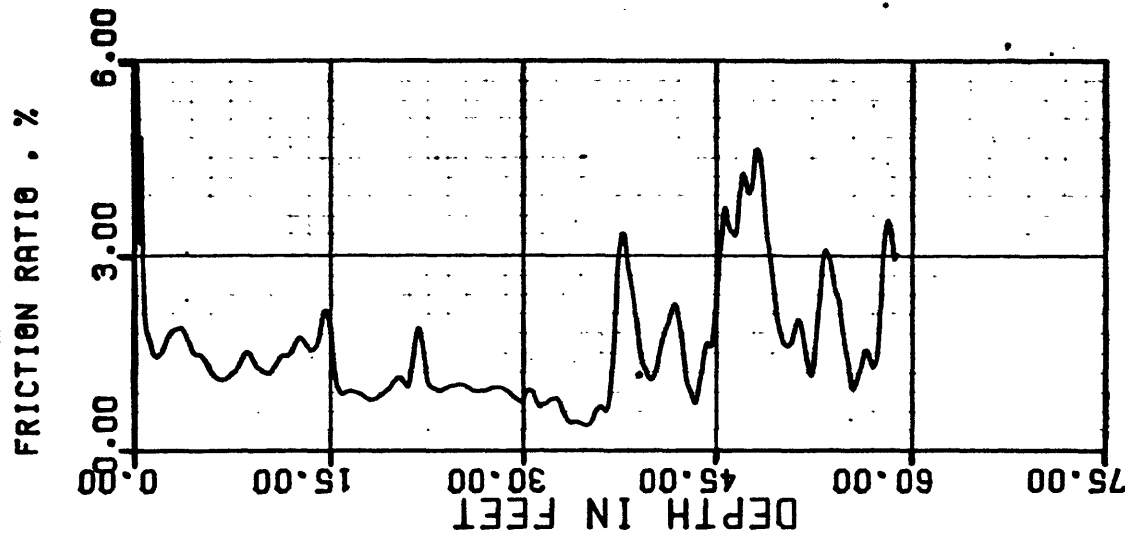
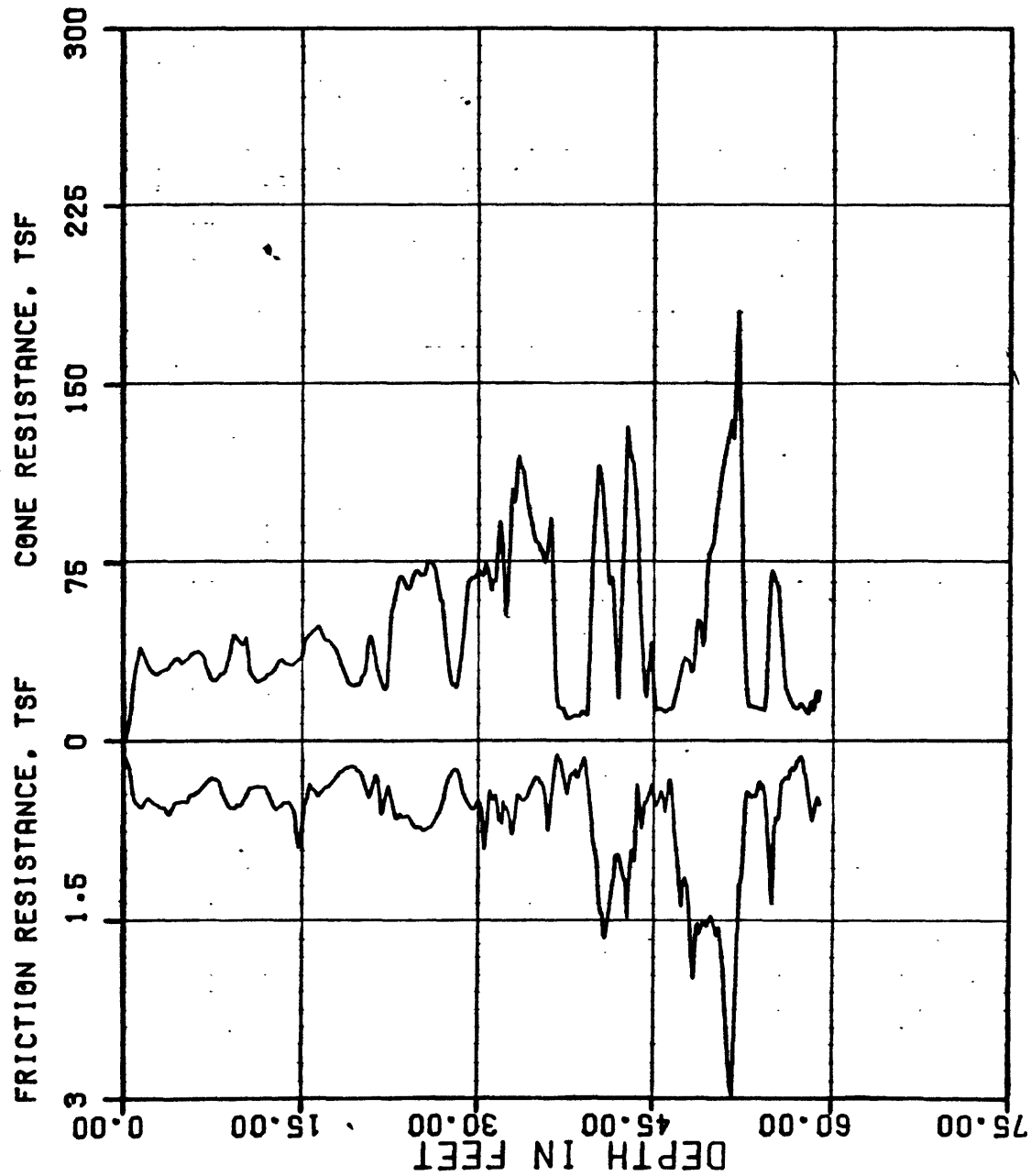
79-153

USGS CPT-SPT

CONE PENETROMETER TEST

INSTRUMENT: F5CK-230 SOUNDING: 89-C-7

FIGURE A.26



PROJECT NO.:

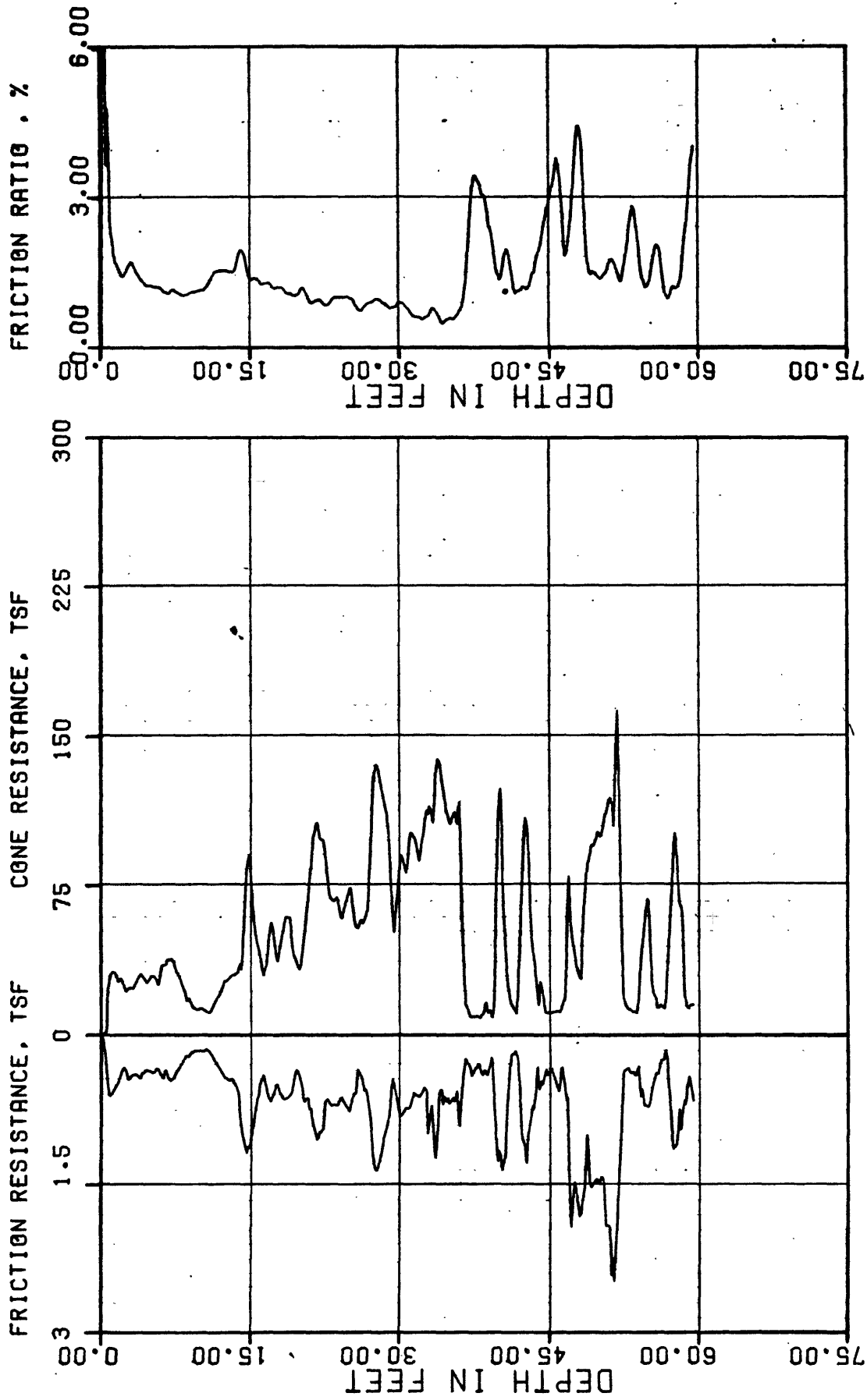
79-153

USGS CPT-SPT

CONE PENETROMETER TEST

INSTRUMENT: F5CK-230 SOUNDING: 88-C3

FIGURE A.36



PROJECT NO.:

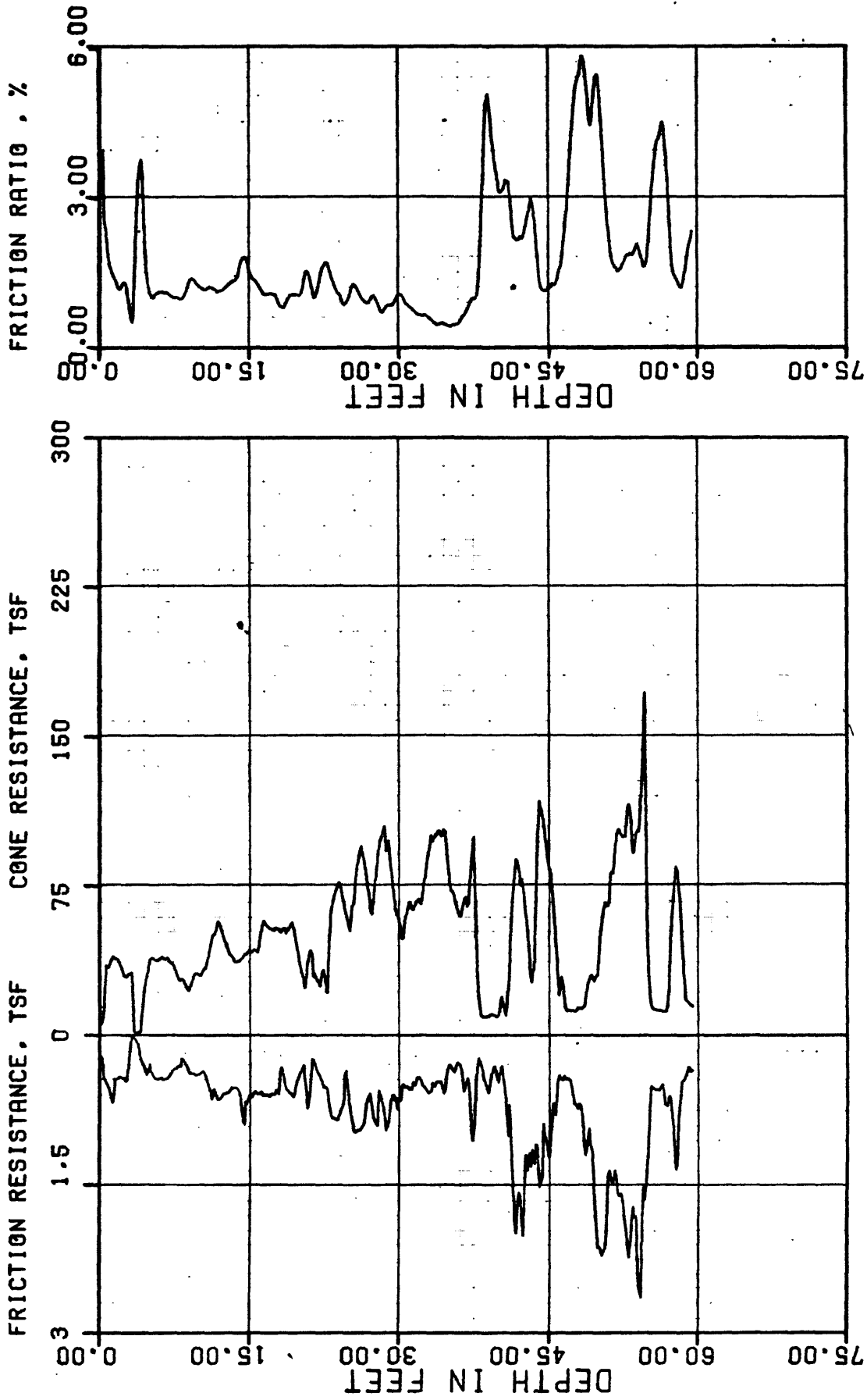
79-153

USGS CPT-SPT

CONE PENETROMETER TEST

INSTRUMENT: F5CK-230 SOUNDING: SS-C-9

FIGURE A.27



PROJECT NO.:

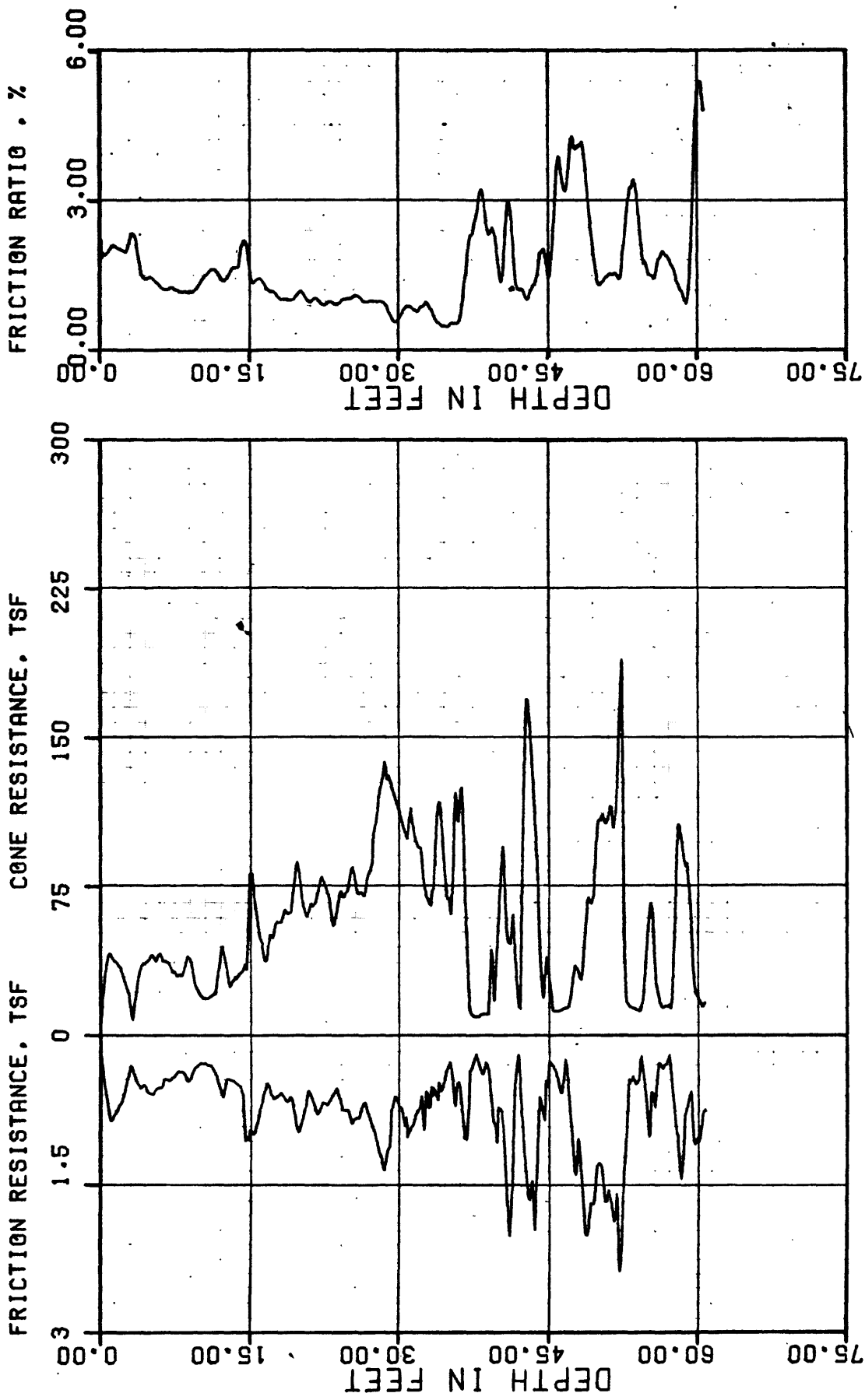
USGS CPT-SPT

79-153

CONE PENETROMETER TEST

INSTRUMENT: F5CK-230 SOUNDRING: SS-C-10

FIGURE A.28



PROJECT NO.:

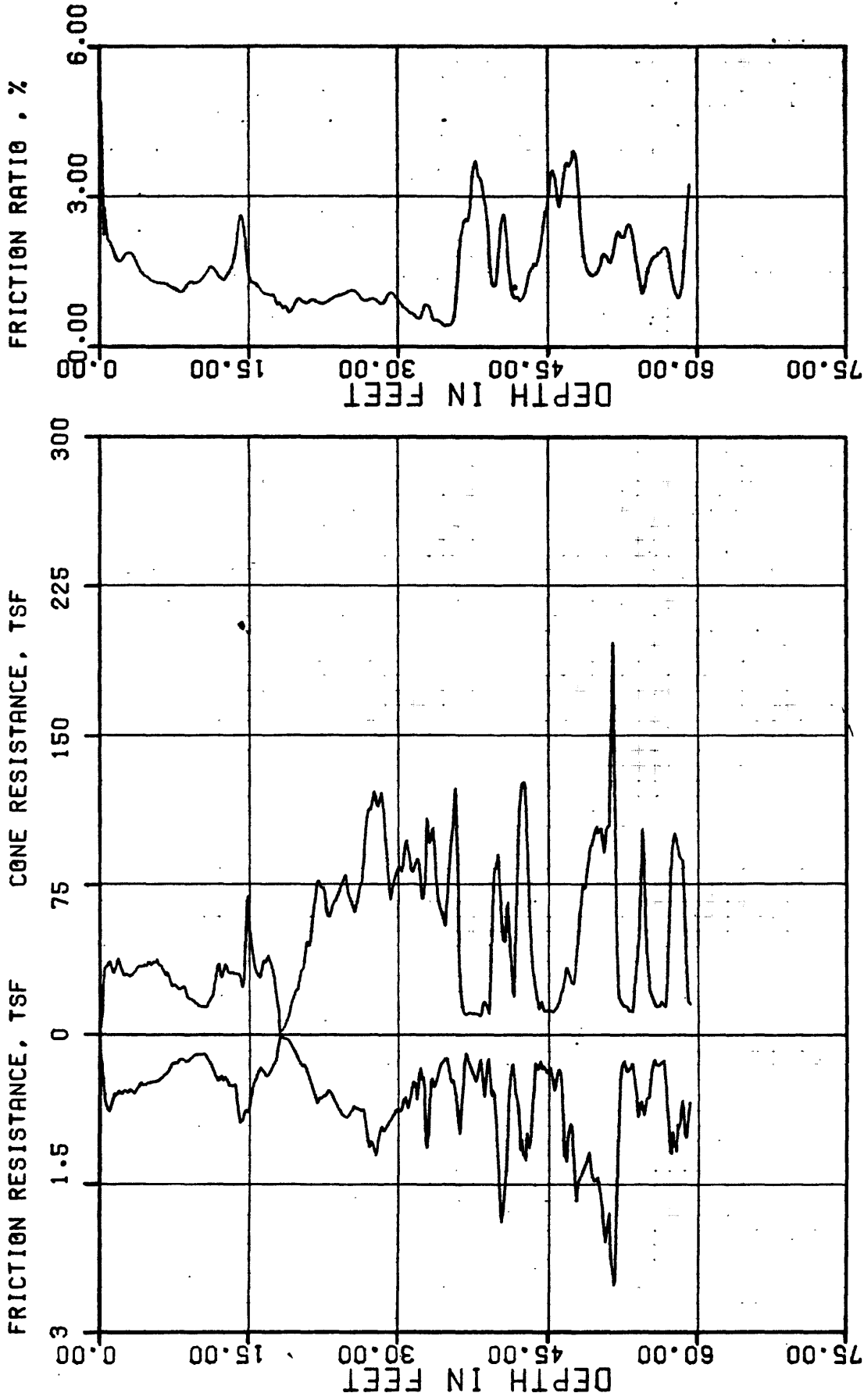
USGS CPT-SPT

79-153

CONE PENETROMETER TEST

INSTRUMENT: F5CK-230 SOUNDING: SS-C-11

FIGURE A.29



PROJECT NO.: 79-153

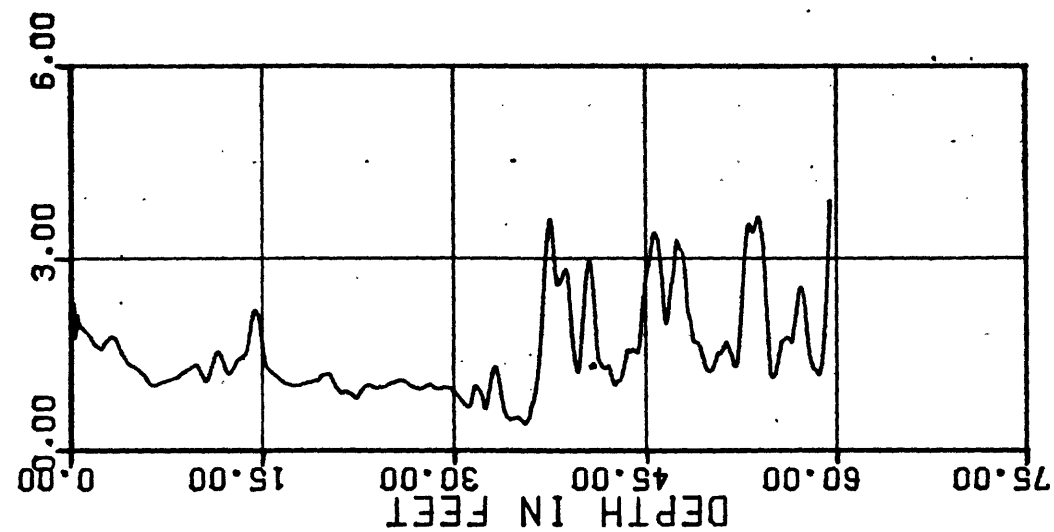
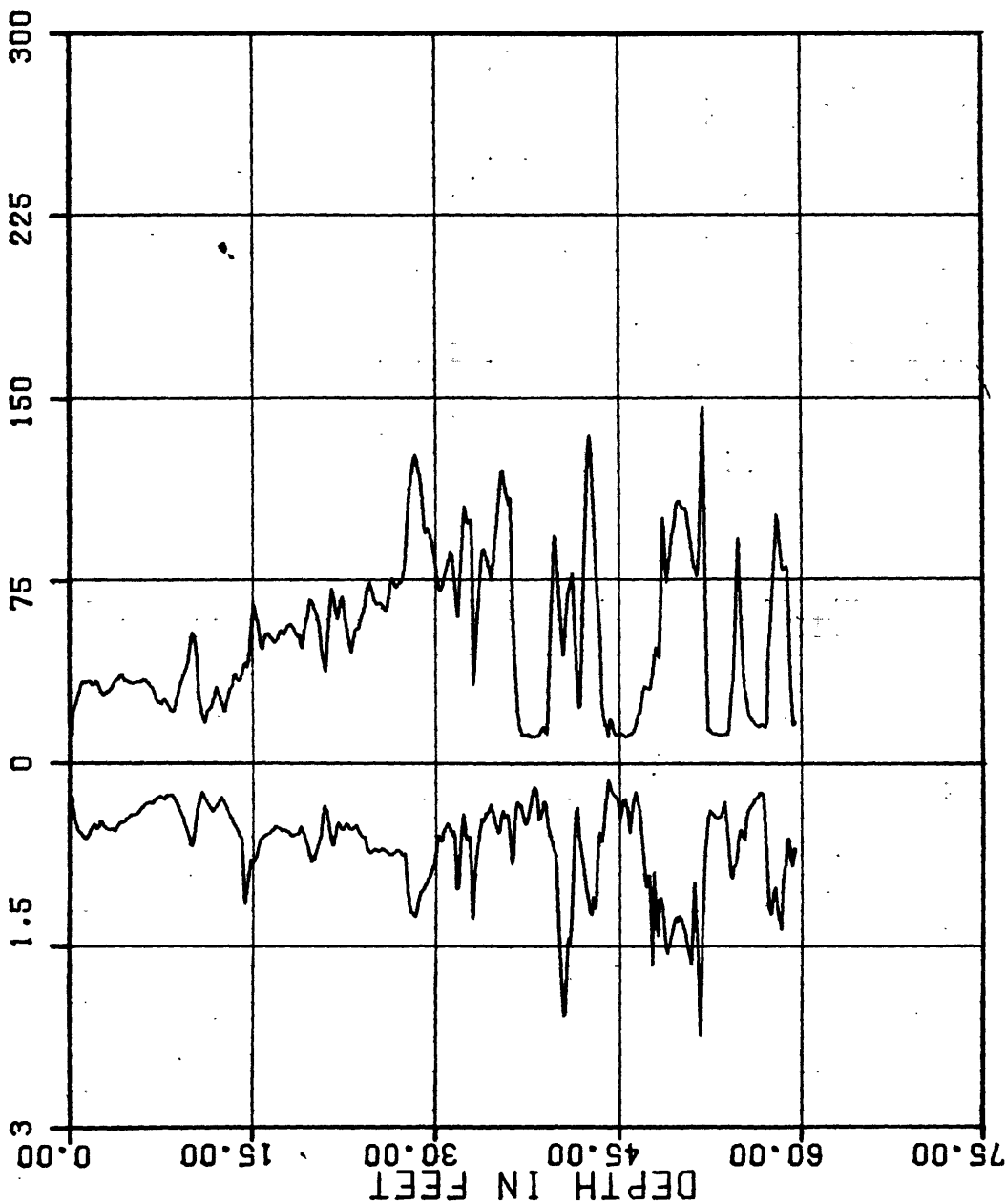
USGS CPT-SPT

CONE PENETROMETER TEST

INSTRUMENT: F5CK-230 SOUNDRING: SS-C-12 FIGURE A.30

FRICITION RESISTANCE, TSF

FRICITION RATIO, %



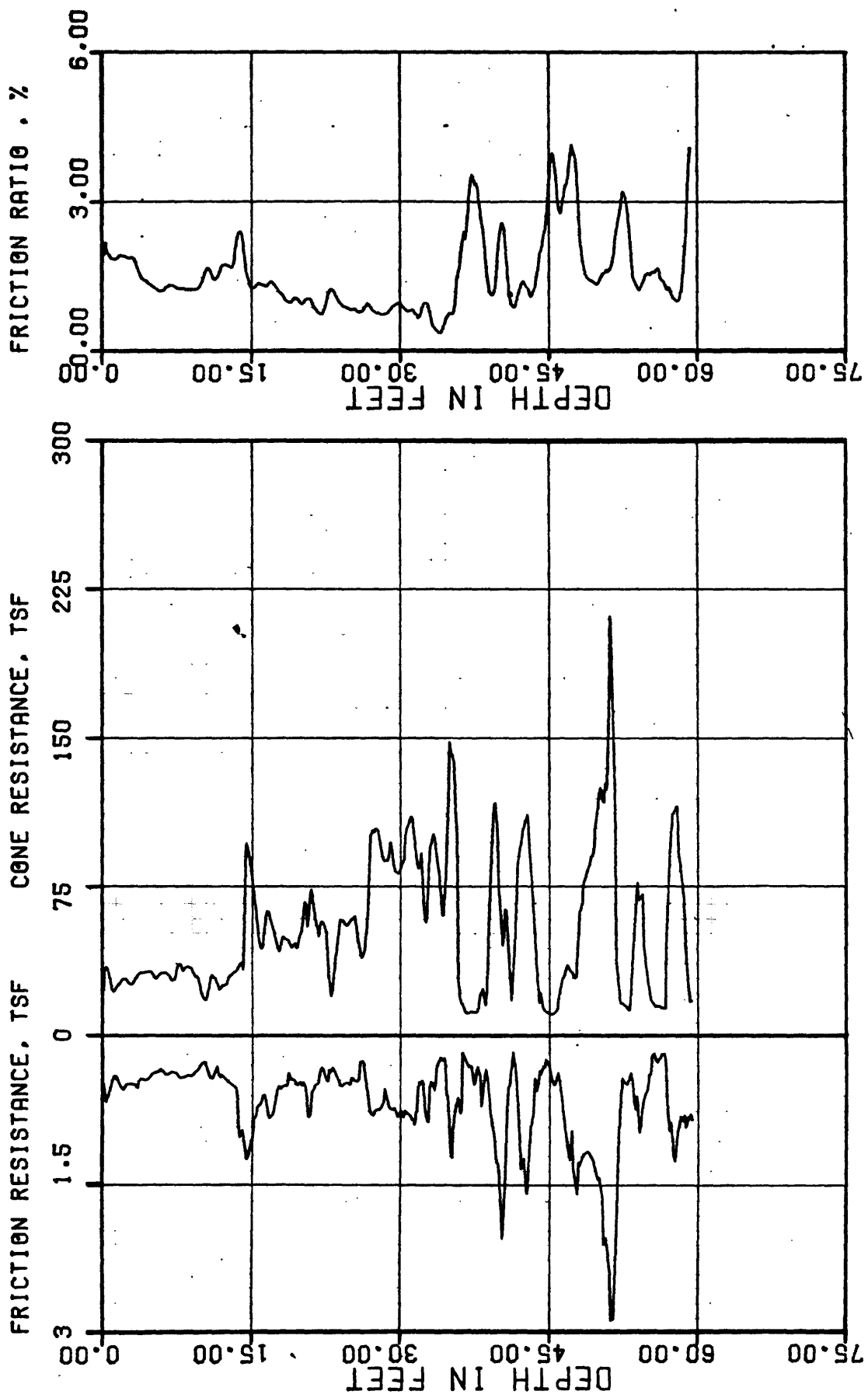
PROJECT NO.:

79-153

USGS CPT-SPT

CONE PENETROMETER TEST

INSTRUMENT: FBCK-230 SOUNDING: SS-C-13 FIGURE A.31



PROJECT NO.:

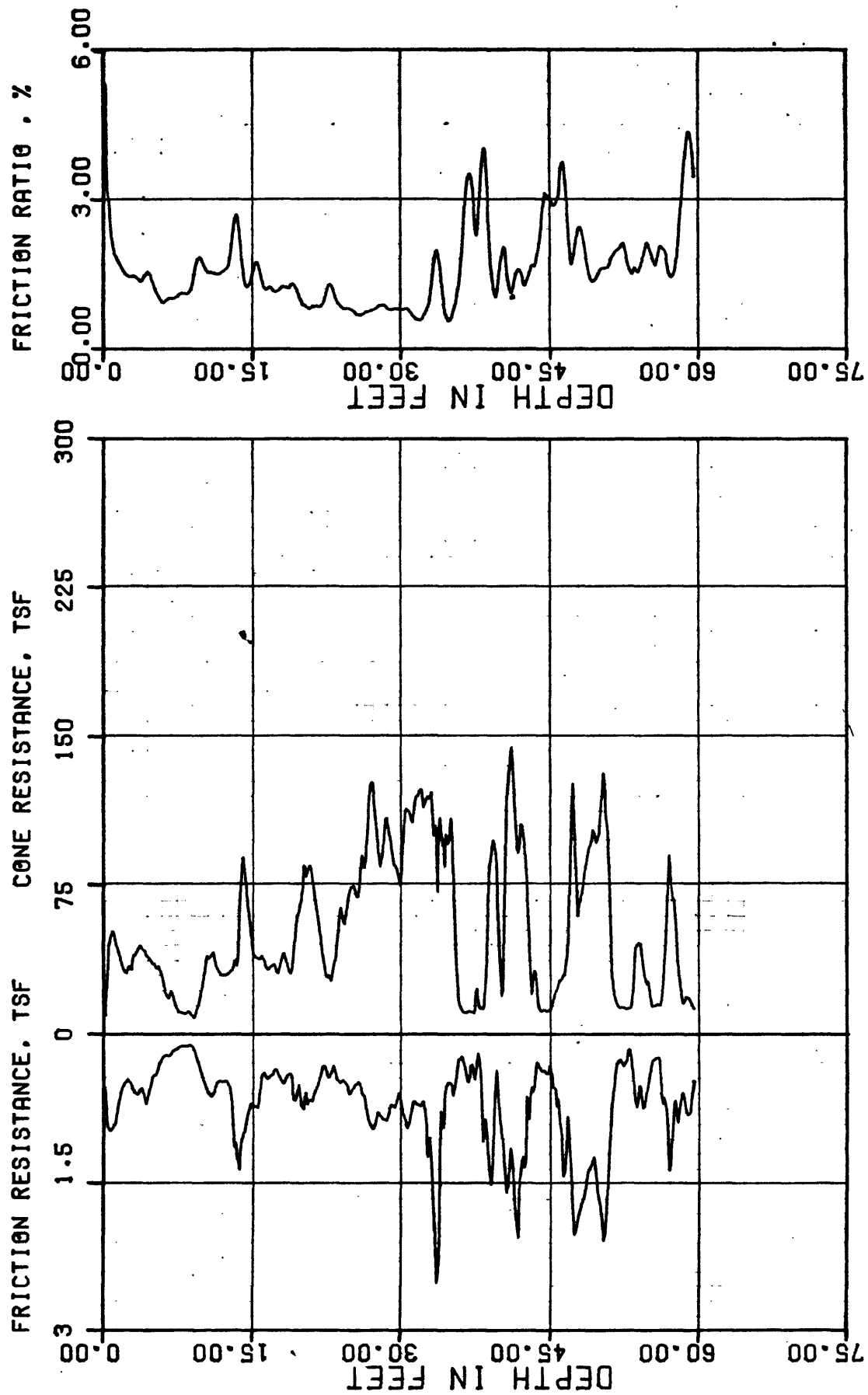
79-153

USGS CPT-SPT

CONE PENETROMETER TEST

INSTRUMENT: F5CK-230 SOUNDING: SS-C-14

FIGURE A.32



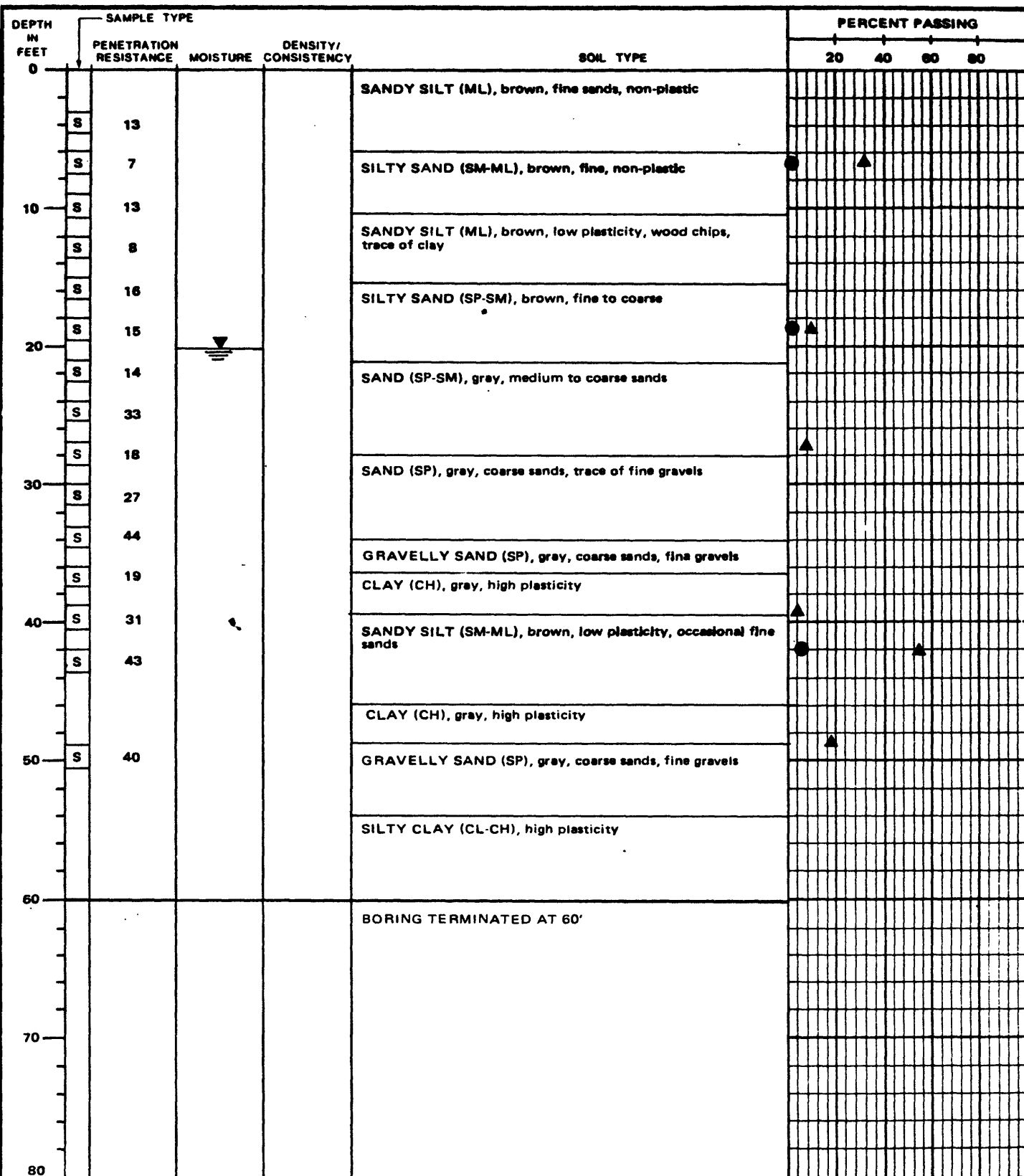
PROJECT NO.:

79-153

USGS CPT-SPT

CONE PENETROMETER TEST

INSTRUMENT: F5CK-230 SOUNDING: SS-C-15 FIGURE A.33



ELEVATION: DATE DRILLED: 11-7-79
 EQUIPMENT USED: 5 7/8" ROTARY WASH
 WATER LEVEL: 20'

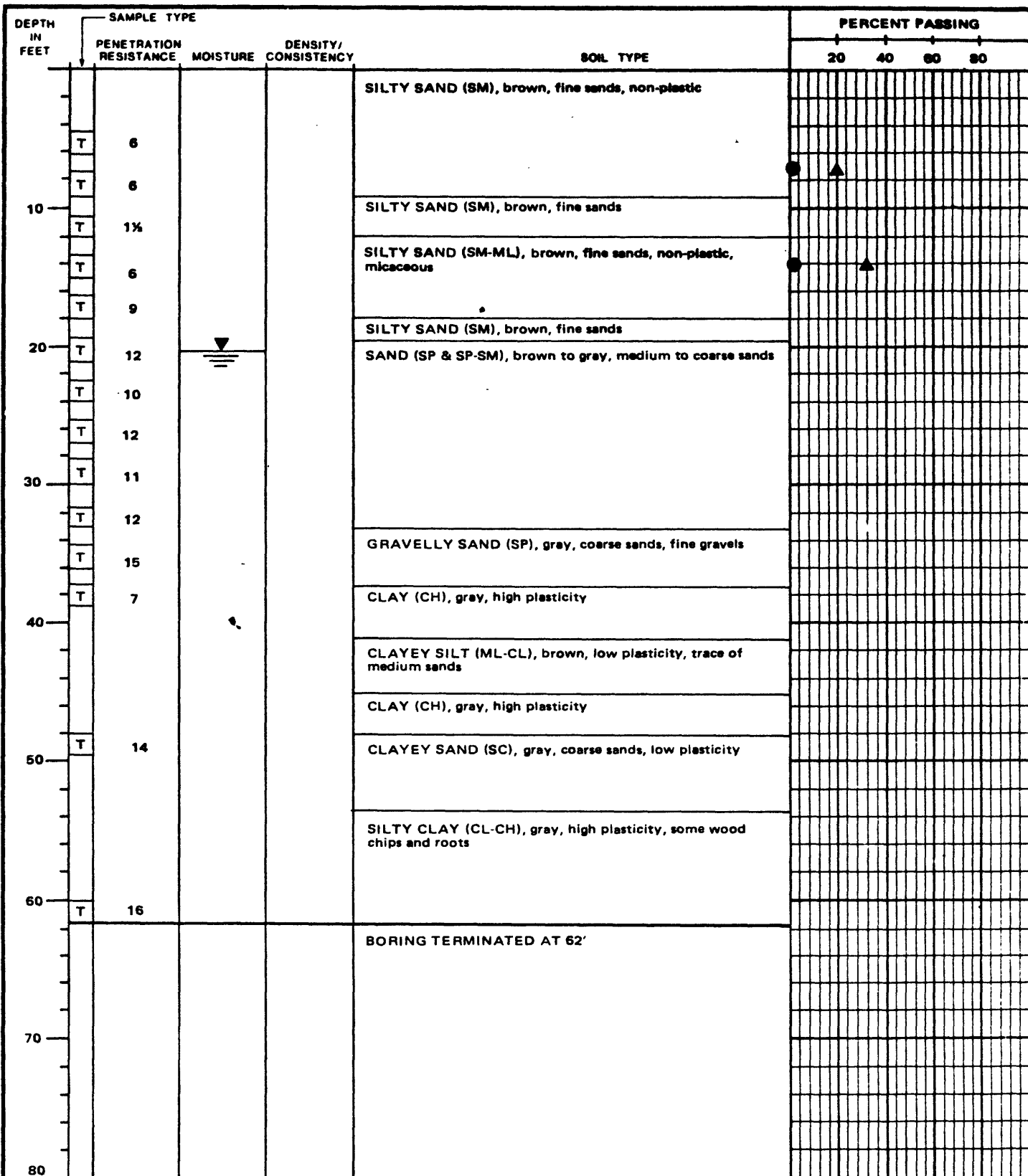
[S] STANDARD HAMMER SPLIT SPOON SAMPLE ▲ #200 SIEVE
 [T] TRIP HAMMER SPLIT SPOON SAMPLE ● 0.002 mm



PROJECT NO.: 79-153

USGS CPT-SPT

LOG OF BORING NO. 1
 SALINAS SITE



ELEVATION: DATE DRILLED: 11-6 & 7-79
 EQUIPMENT USED: 5 7/8" ROTARY WASH
 WATER LEVEL: 20'

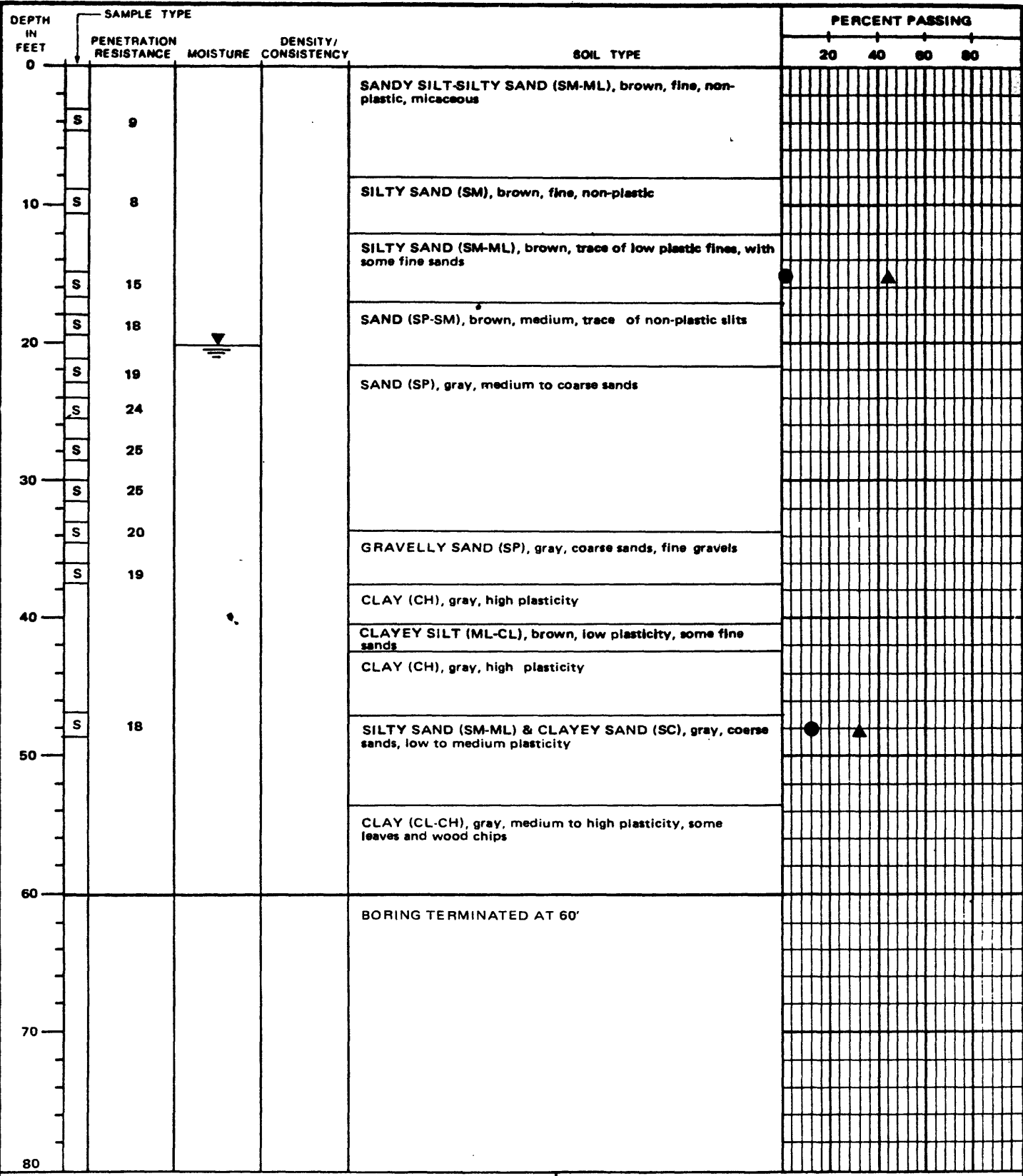
[S] STANDARD HAMMER SPLIT SPOON SAMPLE ▲ #200 SIEVE
 [T] TRIP HAMMER SPLIT SPOON SAMPLE ● 0.002 mm



PROJECT NO.: 79-153

USGS CPT-SPT

LOG OF BORING NO. 2
 SALINAS SITE



ELEVATION:
EQUIPMENT USED: 5 7/8" ROTARY WASH
WATER LEVEL: 20

DATE DRILLED: 11-B-79

S

STANDARD HAMMER SPLIT SPOON SAMPLE

T


TRIP HAMMER SPLIT SPOON SAMPLE

▲

#200 SIEVE

●

0.002 mm



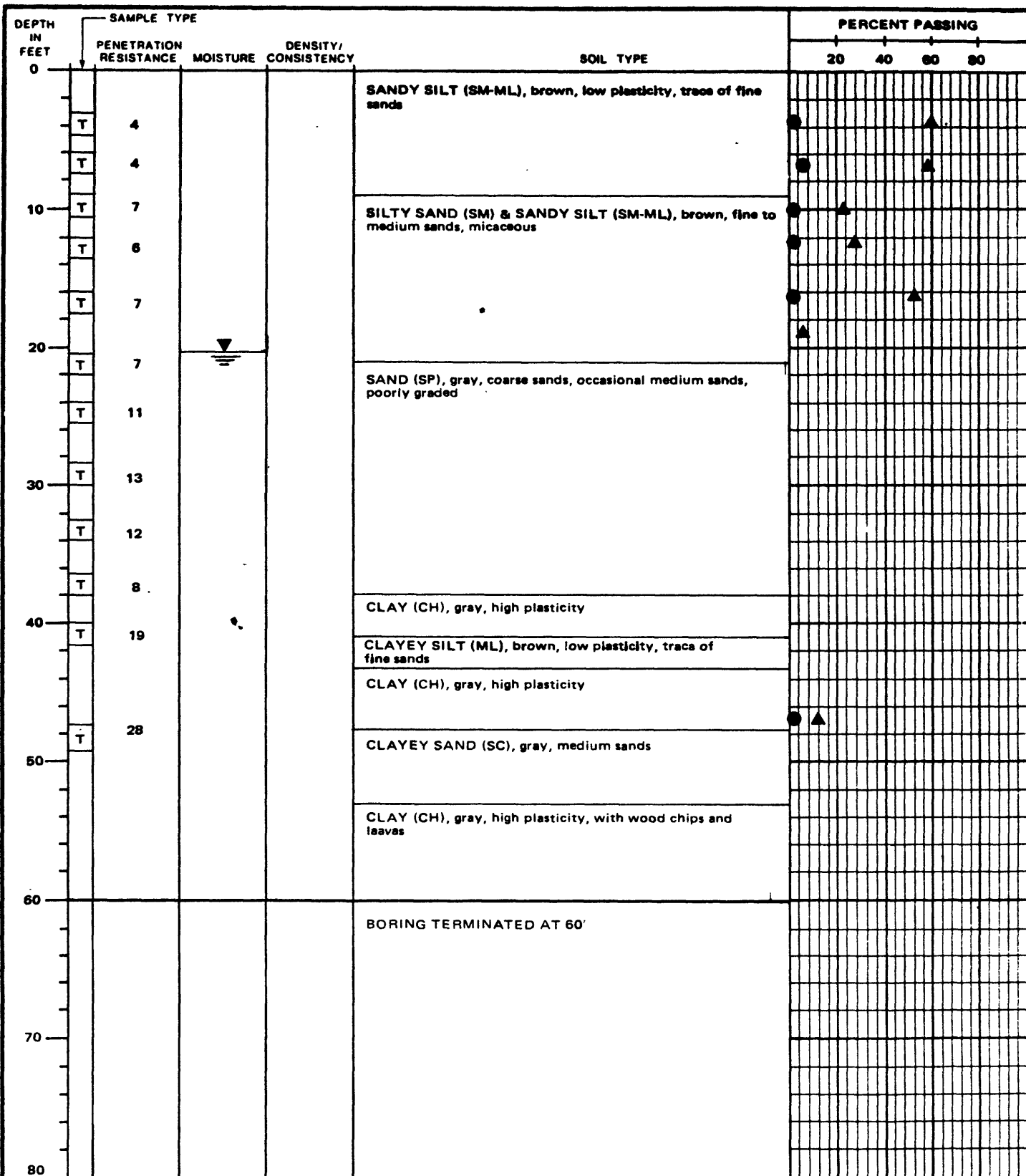
PROJECT NO.: 79-153

USGS CPT-SPT

LOG OF BORING NO. 3
SALINAS SITE

9-80

FIGURE A.36



ELEVATION: DATE DRILLED: 11-8-79
 EQUIPMENT USED: 5 7/8" ROTARY WASH
 WATER LEVEL: 20'

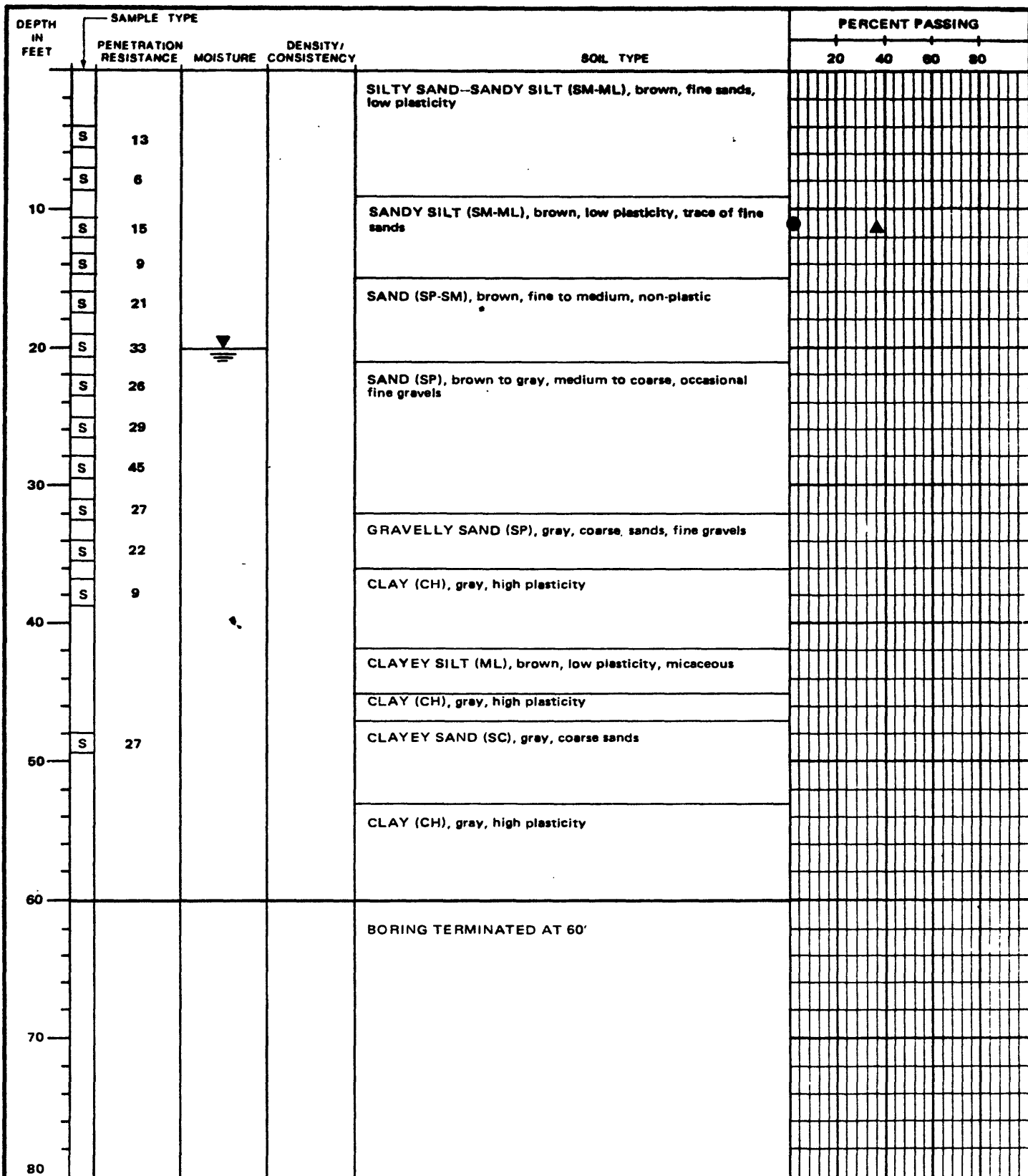
[S] STANDARD HAMMER SPLIT SPOON SAMPLE ▲ #200 SIEVE
 [T] TRIP HAMMER SPLIT SPOON SAMPLE ● 0.002 mm



PROJECT NO.: 79-153

USGS CPT-SPT

LOG OF BORING NO. 4
 SALINAS SITE



ELEVATION: DATE DRILLED: 11-9-79
 EQUIPMENT USED: 5 7/8" ROTARY WASH
 WATER LEVEL: 20'

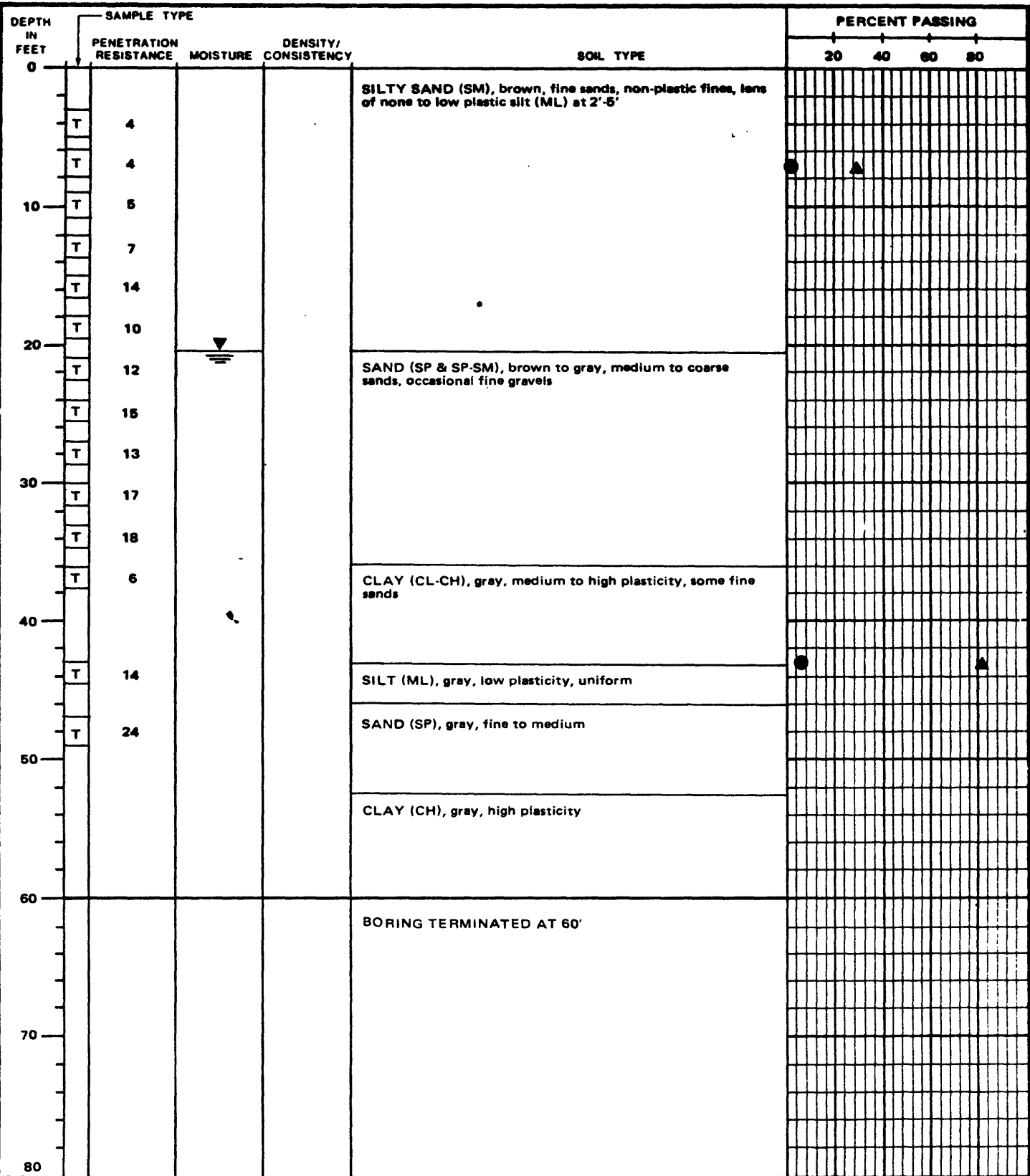
[S] STANDARD HAMMER SPLIT SPOON SAMPLE ▲ #200 SIEVE
 [T] TRIP HAMMER SPLIT SPOON SAMPLE ● 0.002 mm



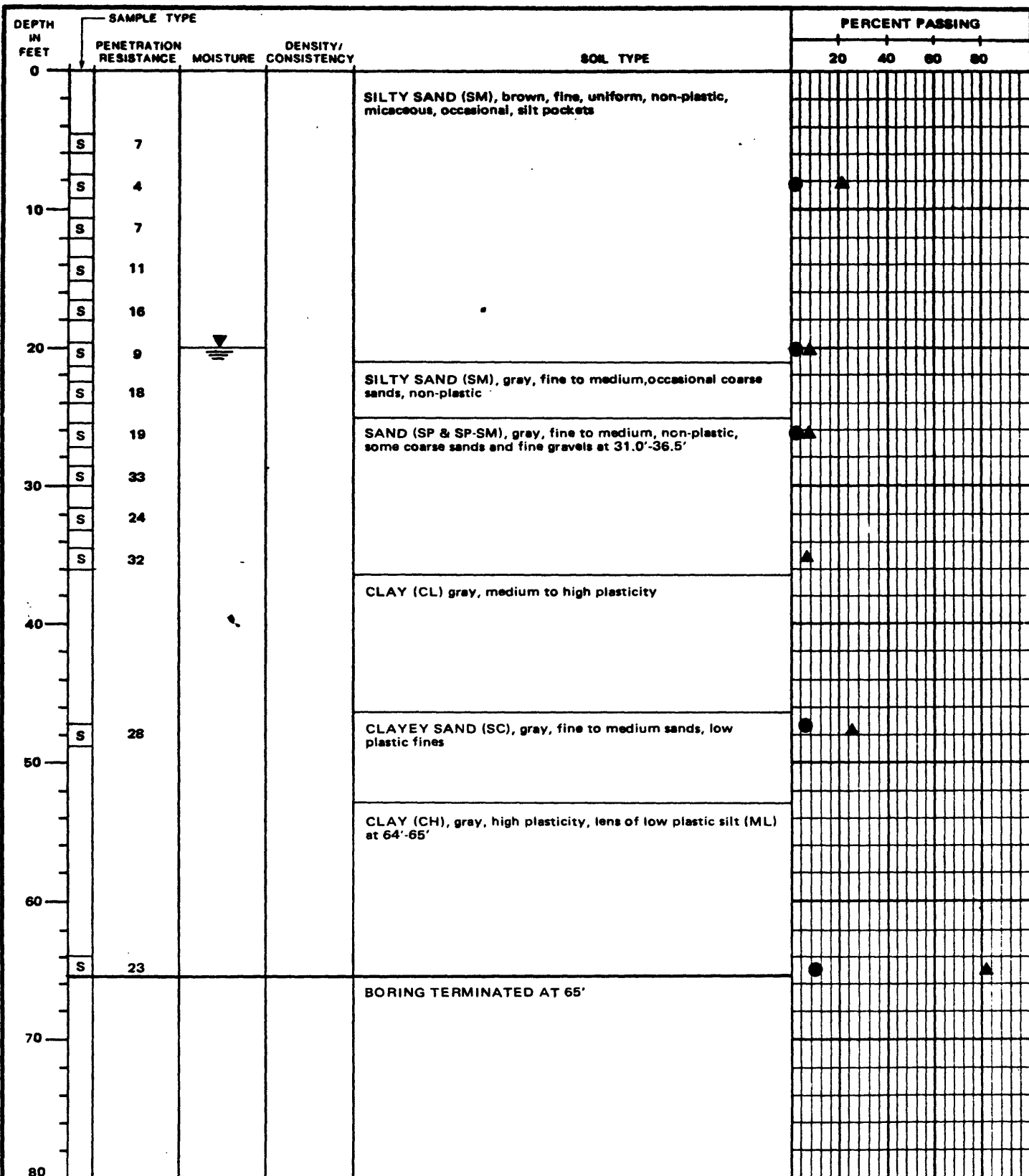
PROJECT NO.: 79-153

USGS CPT-SPT

LOG OF BORING NO. 5
 SALINAS SITE



ELEVATION:		DATE DRILLED: 11-9 & 12-79		PROJECT NO.:		79-153
EQUIPMENT USED: 5 7/8" ROTARY WASH				USGS CPT-SPT		
WATER LEVEL: 20'						
[S] STANDARD HAMMER SPLIT SPOON SAMPLE	▲ #200 SIEVE					
[T] TRIP HAMMER SPLIT SPOON SAMPLE	● 0.002 mm					
LOG OF BORING NO. 6 SALINAS SITE						
9-80						FIGURE A.39



ELEVATION: DATE DRILLED: 11-12-79
 EQUIPMENT USED: 5 7/8" ROTARY WASH
 WATER LEVEL: 20

[S] STANDARD HAMMER SPLIT SPOON SAMPLE ▲ #200 SIEVE
 [T] TRIP HAMMER SPLIT SPOON SAMPLE ● 0.002 mm

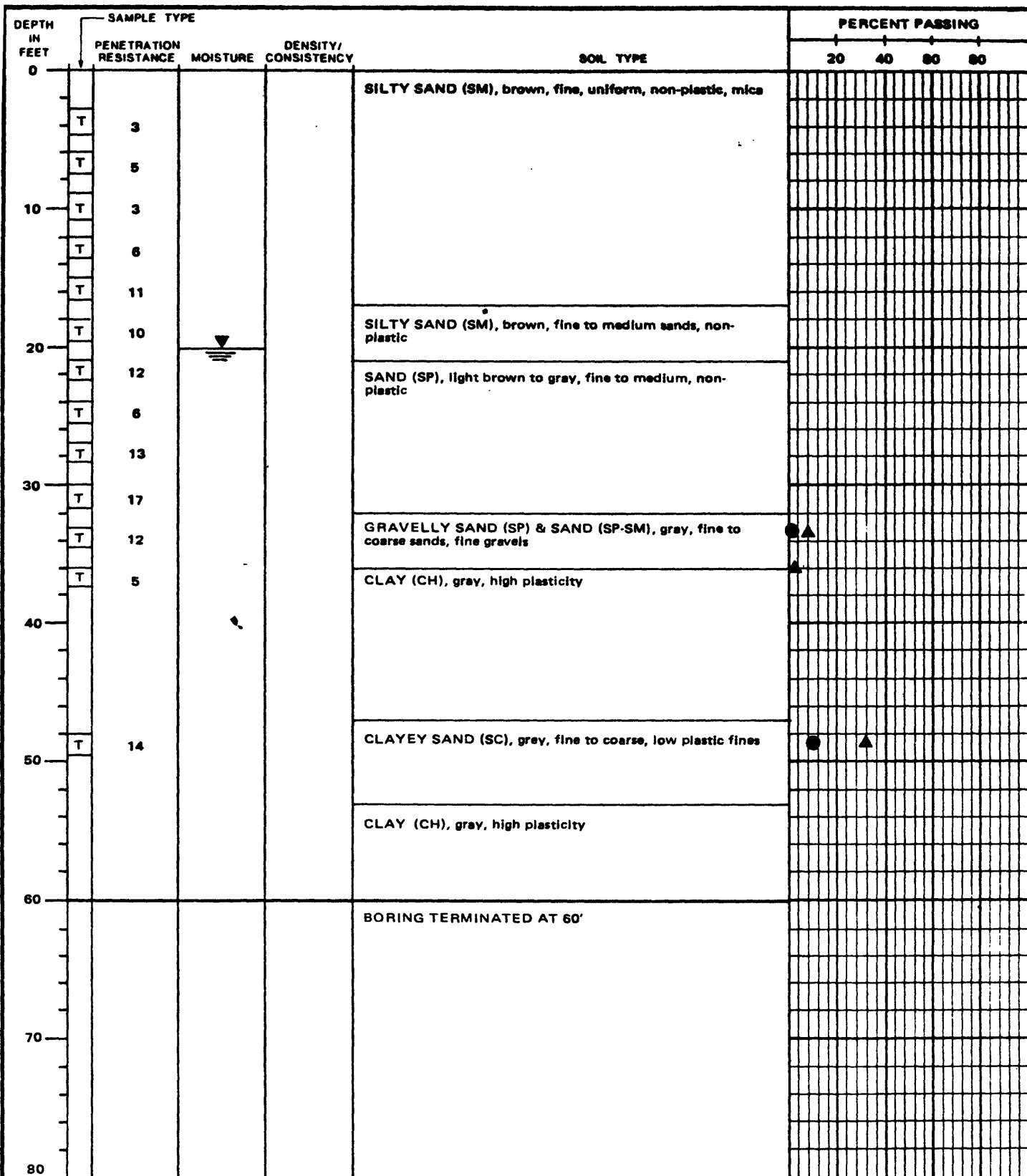


PROJECT NO.:

79-153

USGS CPT-SPT

LOG OF BORING NO. 7
 SALINAS SITE



ELEVATION: DATE DRILLED: 11-13-79
 EQUIPMENT USED: 5 7/8" ROTARY WASH
 WATER LEVEL: 20'

[S] STANDARD HAMMER SPLIT SPOON SAMPLE ▲ #200 SIEVE
 [T] TRIP HAMMER SPLIT SPOON SAMPLE ● 0.002 mm



PROJECT NO.:

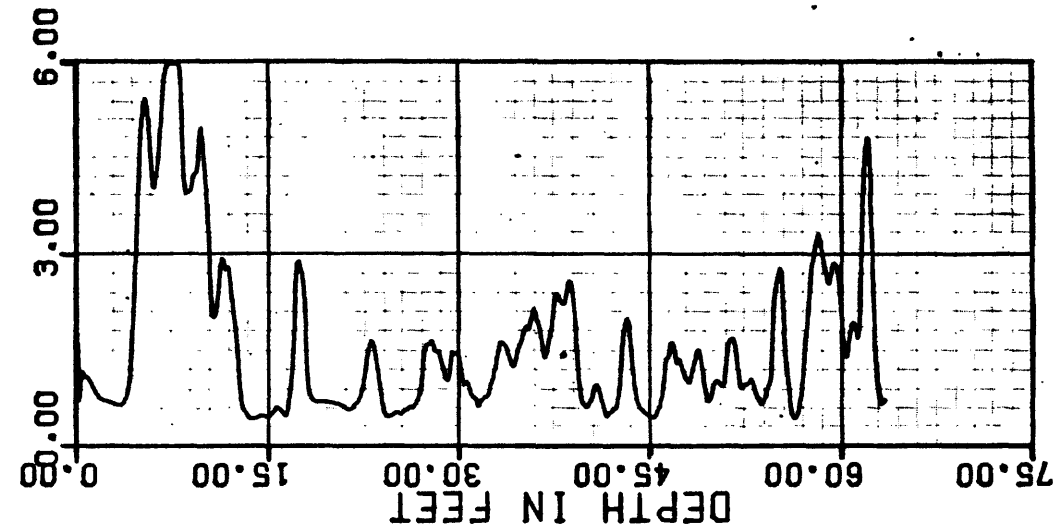
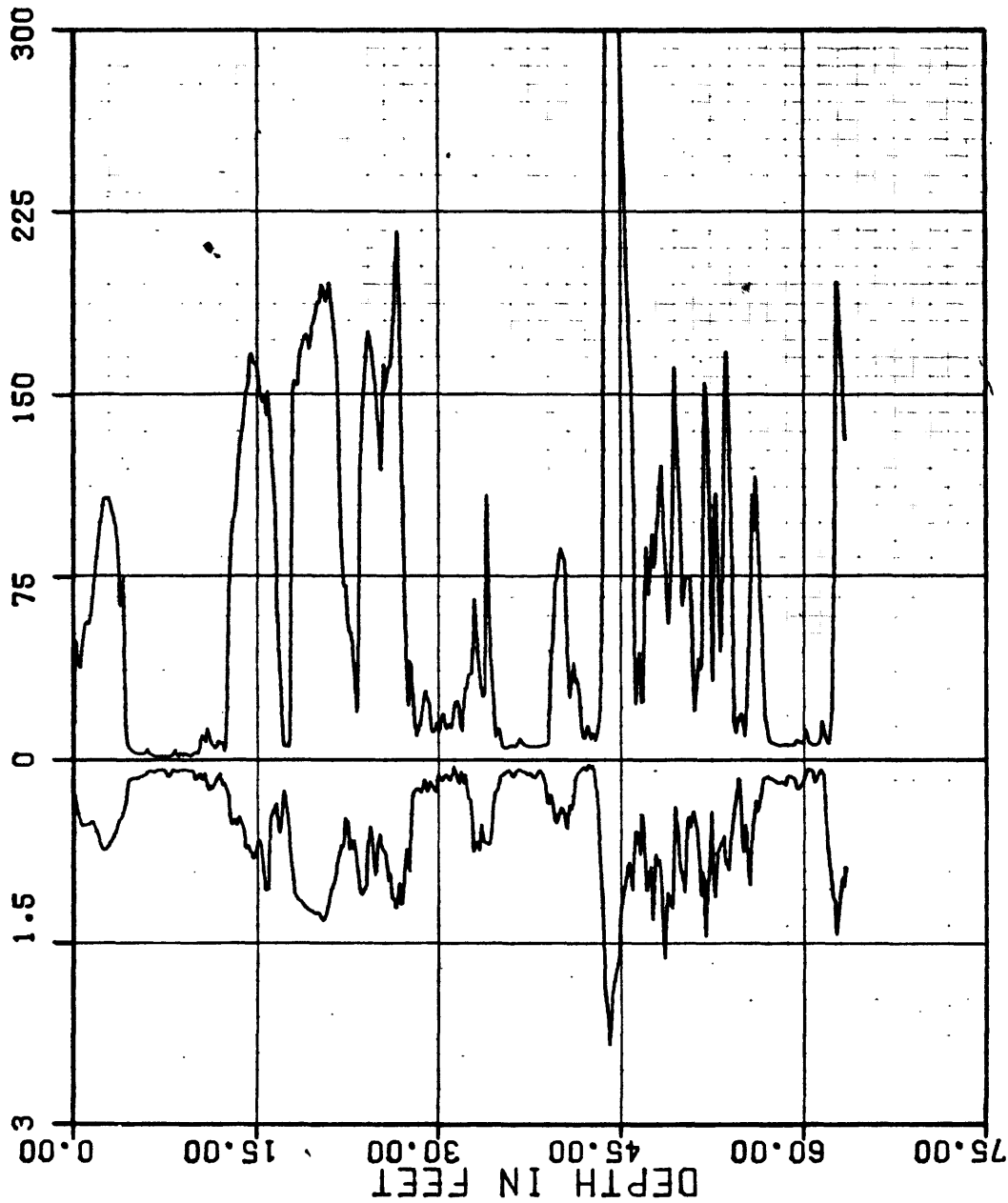
79-153

USGS CPT-SPT

LOG OF BORING NO. 8
 SALINAS SITE

FRICTION RESISTANCE, TSF

FRICTION RATIO, %



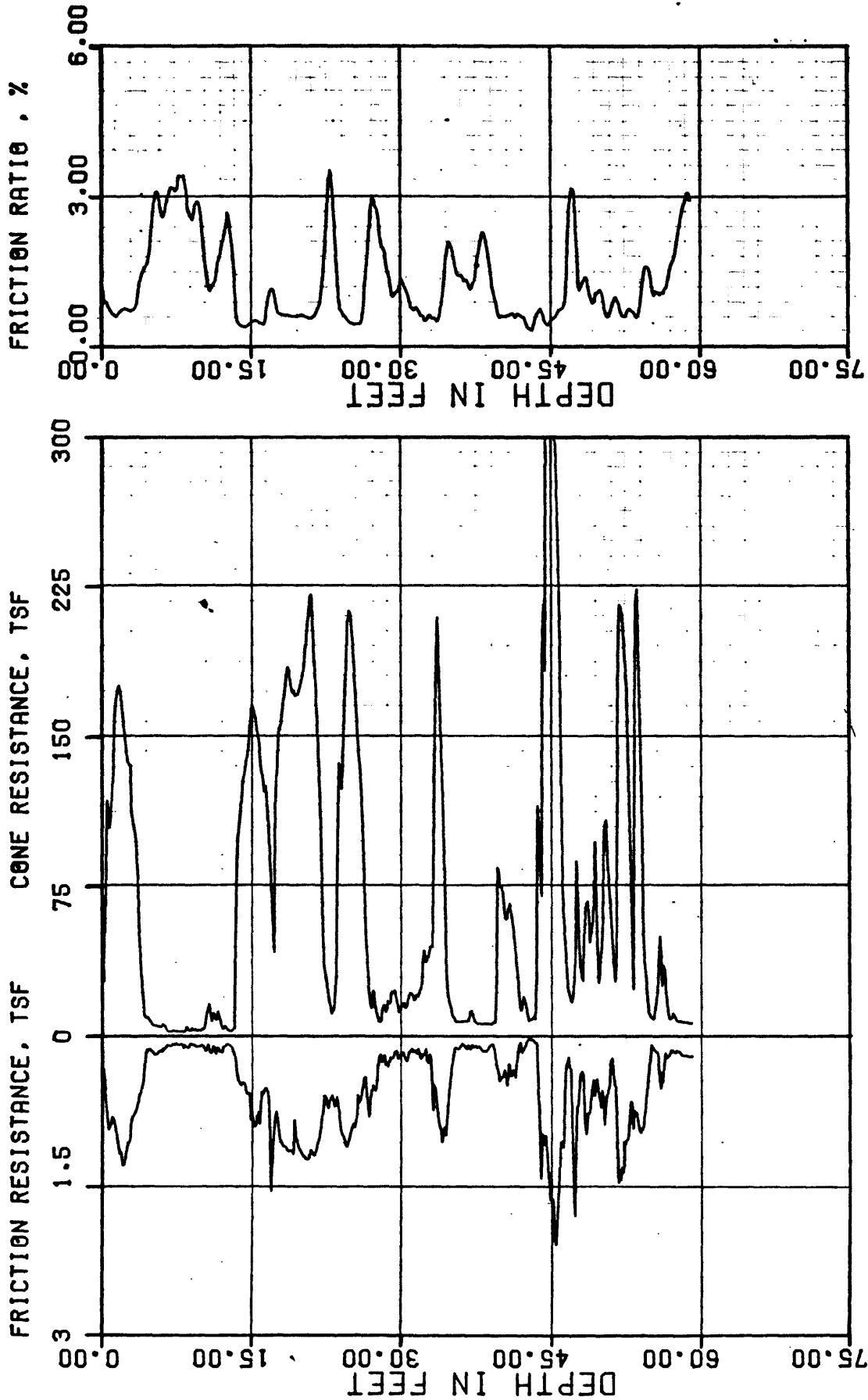
PROJECT NO.:

79-183

USGS CPT-SPT

CONE PENETROMETER TEST

INSTRUMENT: F5CK-230 SOUNDING: ML-C-1 FIGURE A.42



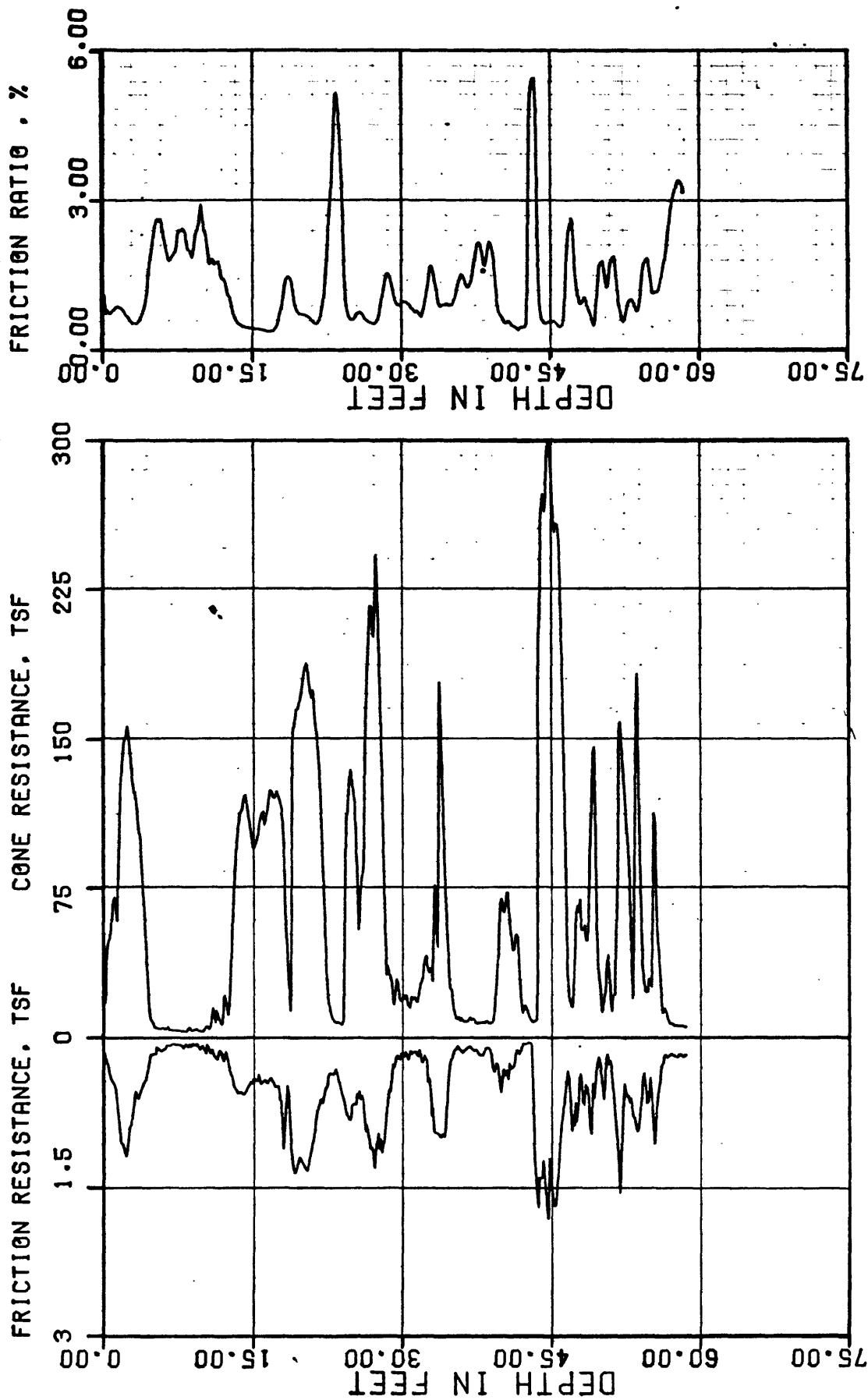
PROJECT NO.:

USGS CPT-SPT

79-153

CONE PENETROMETER TEST

INSTRUMENT: F5CK-230 SOUNDING: ML-C-2 FIGURE A.43



PROJECT NO.:

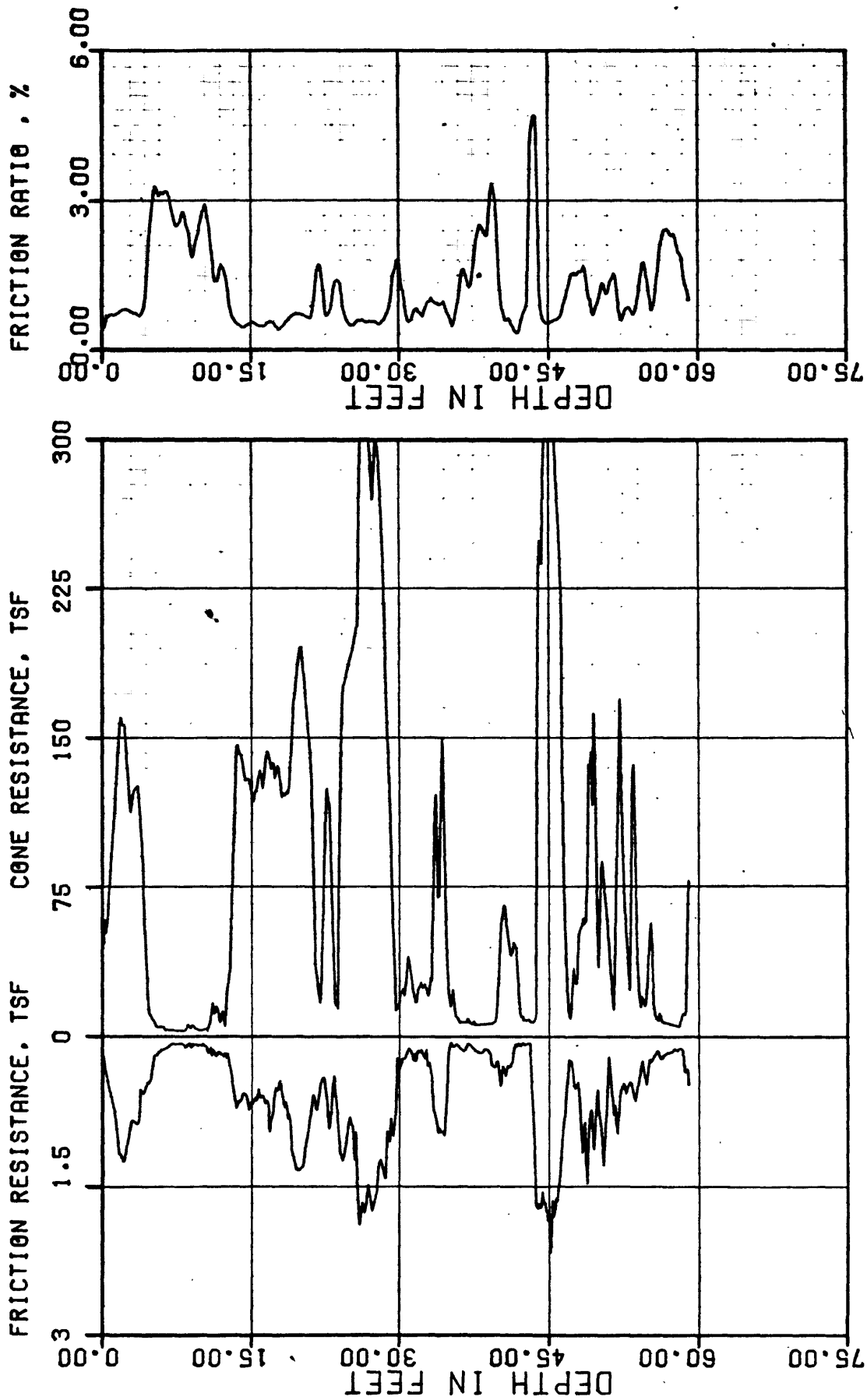
79-153

USGS CPT-SPT

CONE PENETROMETER TEST

INSTRUMENT: F5CK-230 SOUNDING: ML-C-3

FIGURE A.44



79-153

PROJECT NO.:



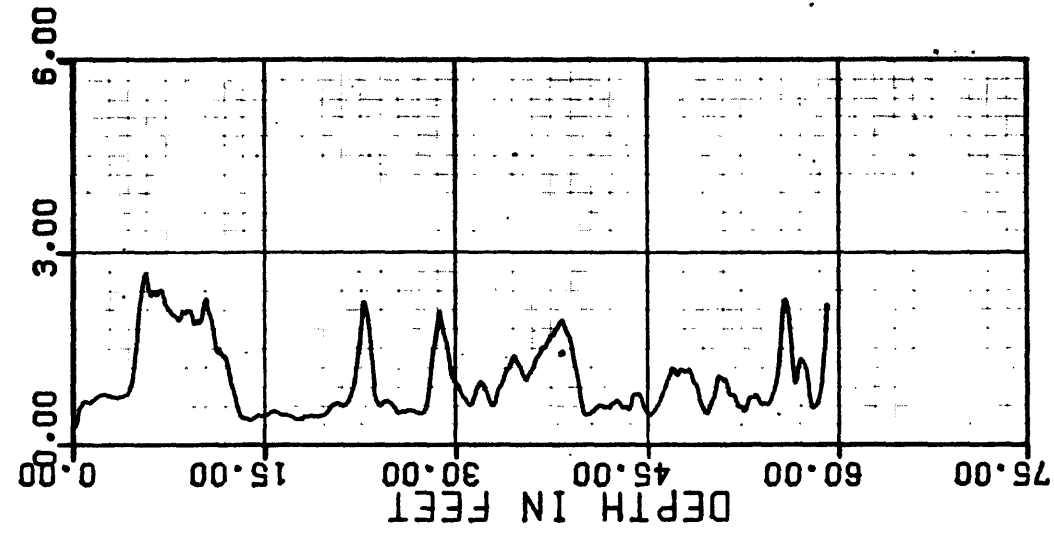
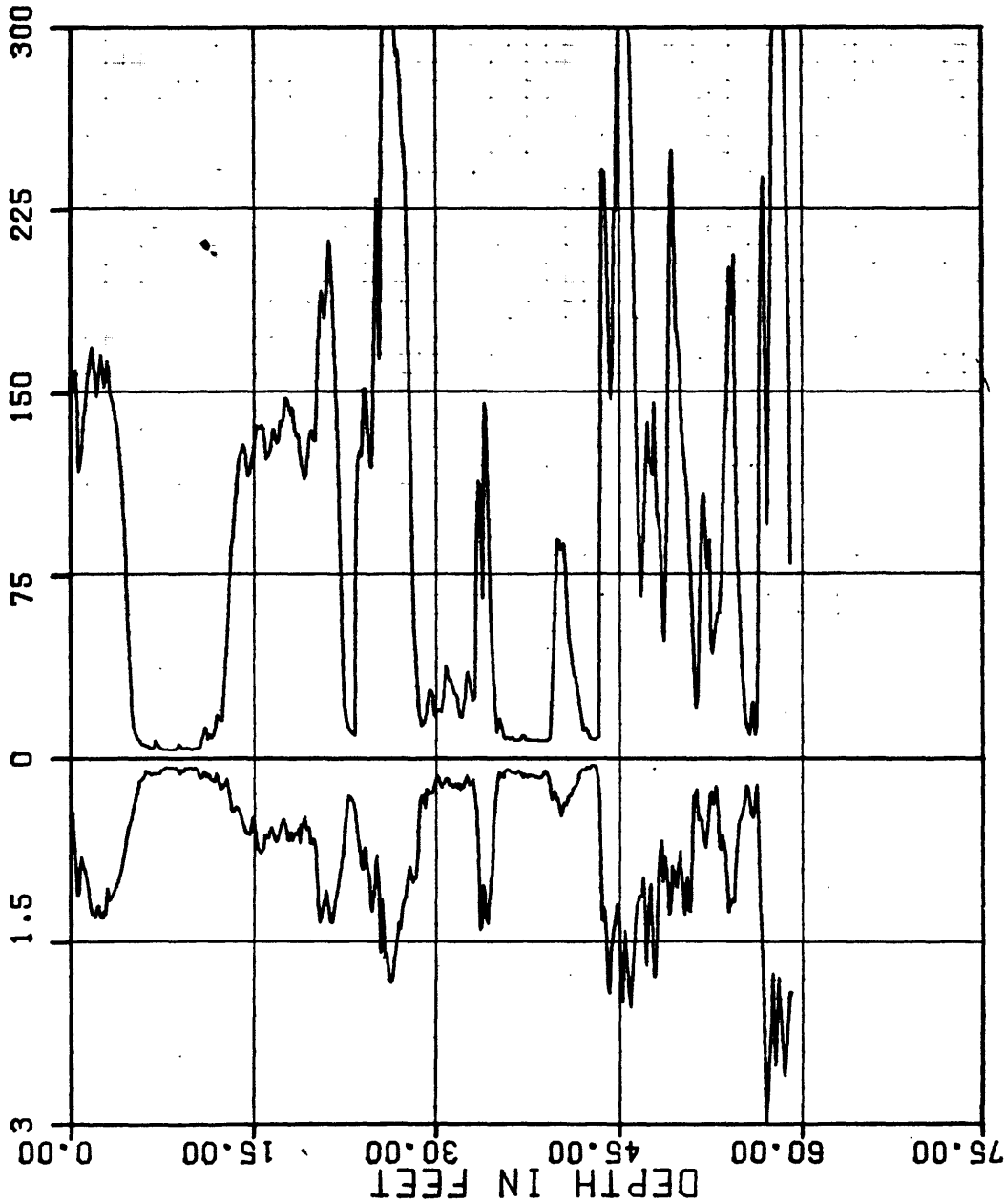
USGS CPT-SPT

CONE PENETROMETER TEST

INSTRUMENT: F5CK-230 SOUNING: ML-C4 FIGURE A.45

FRICTION RESISTANCE, TSF

FRICTION RATIO, %



PROJECT NO.:

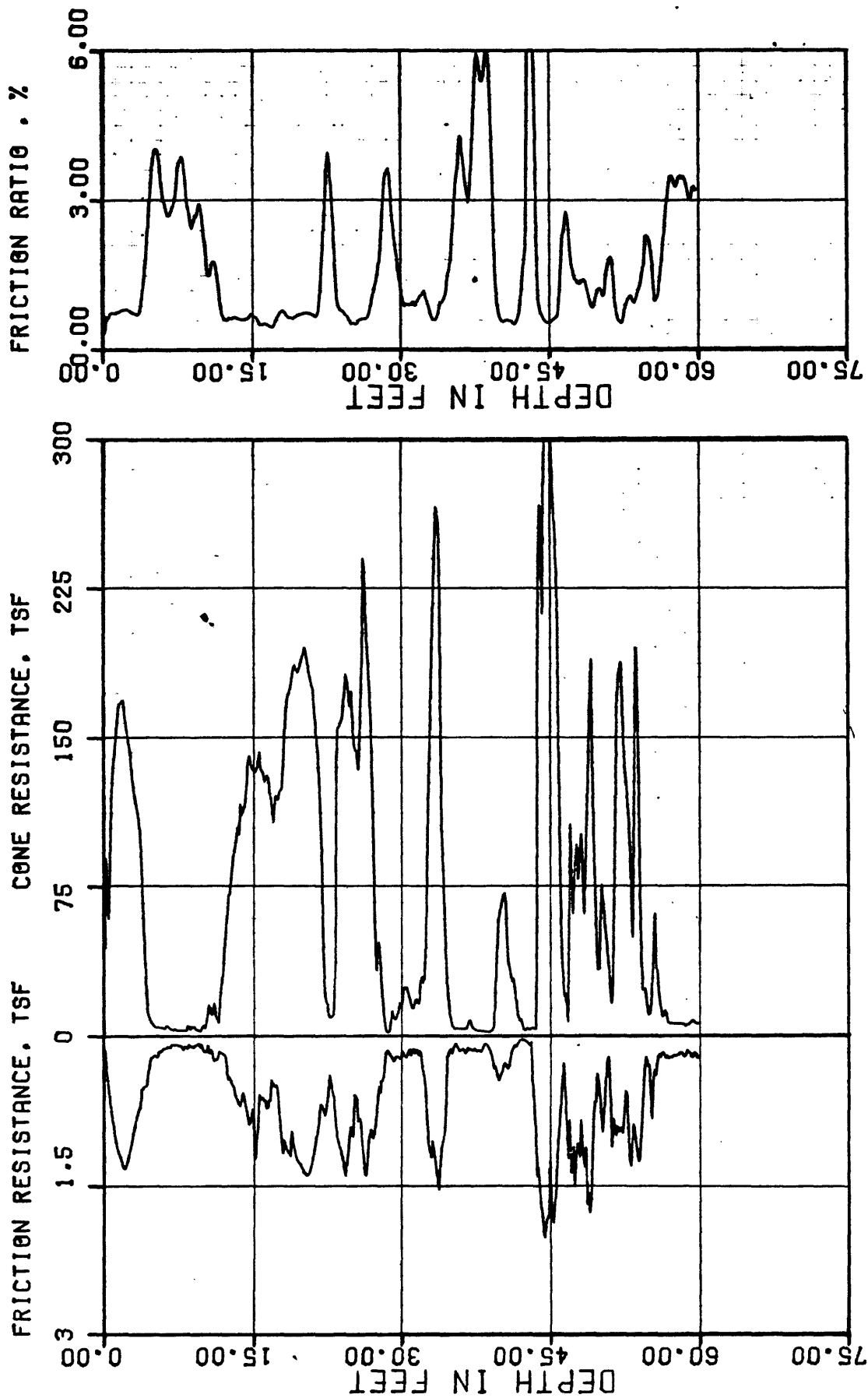
79-153

USGS CPT-SPT

CONE PENETROMETER TEST

INSTRUMENT: F5CK-230 SOUNING: ML-C-8

FIGURE A.46



PROJECT NO.:

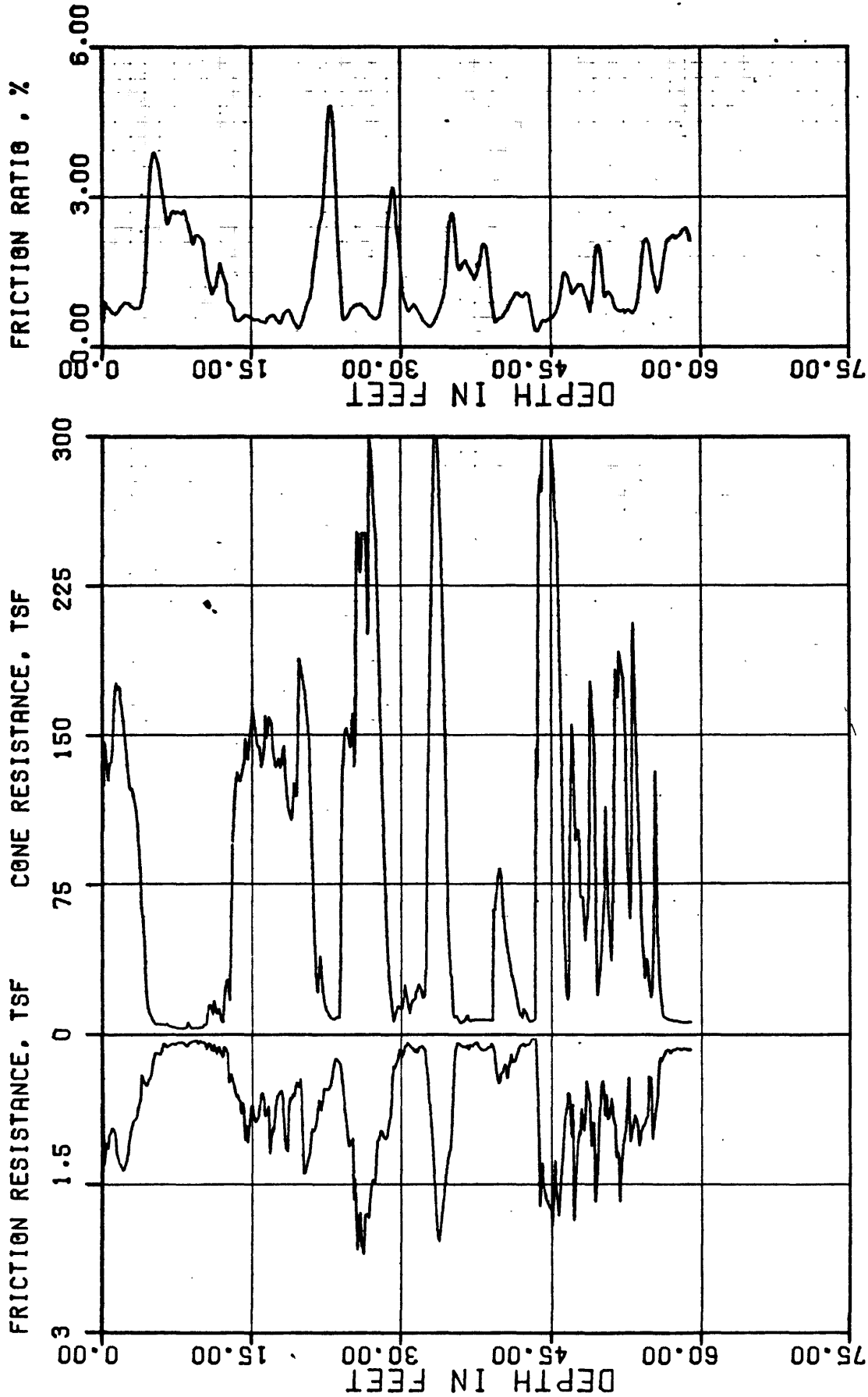
USGS CPT-SPT

79-153

CONE PENETROMETER TEST

INSTRUMENT: F5CK-230 SOUNDING: ML-C-6

FIGURE A.47



PROJECT NO.:

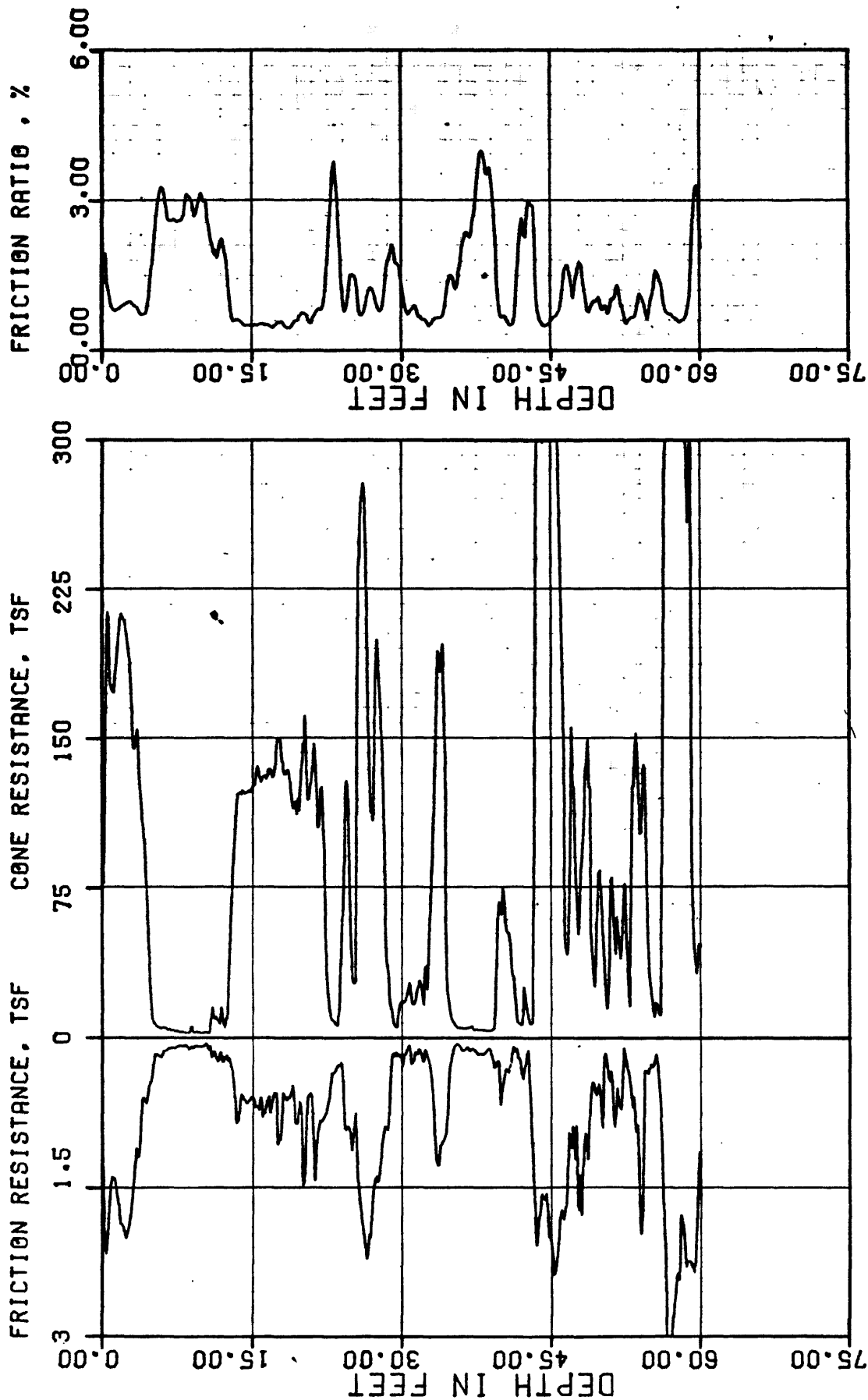
79-153

USGS CPT-SPT

CONE PENETROMETER TEST

INSTRUMENT: F5CK-230 SOUNDING: ML-C-7

FIGURE A.48



PROJECT NO.: 79-153



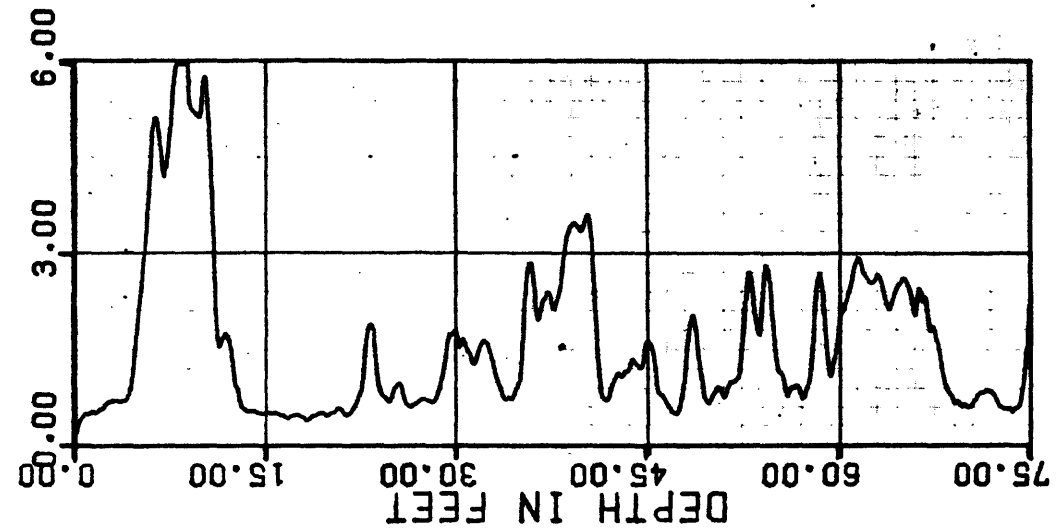
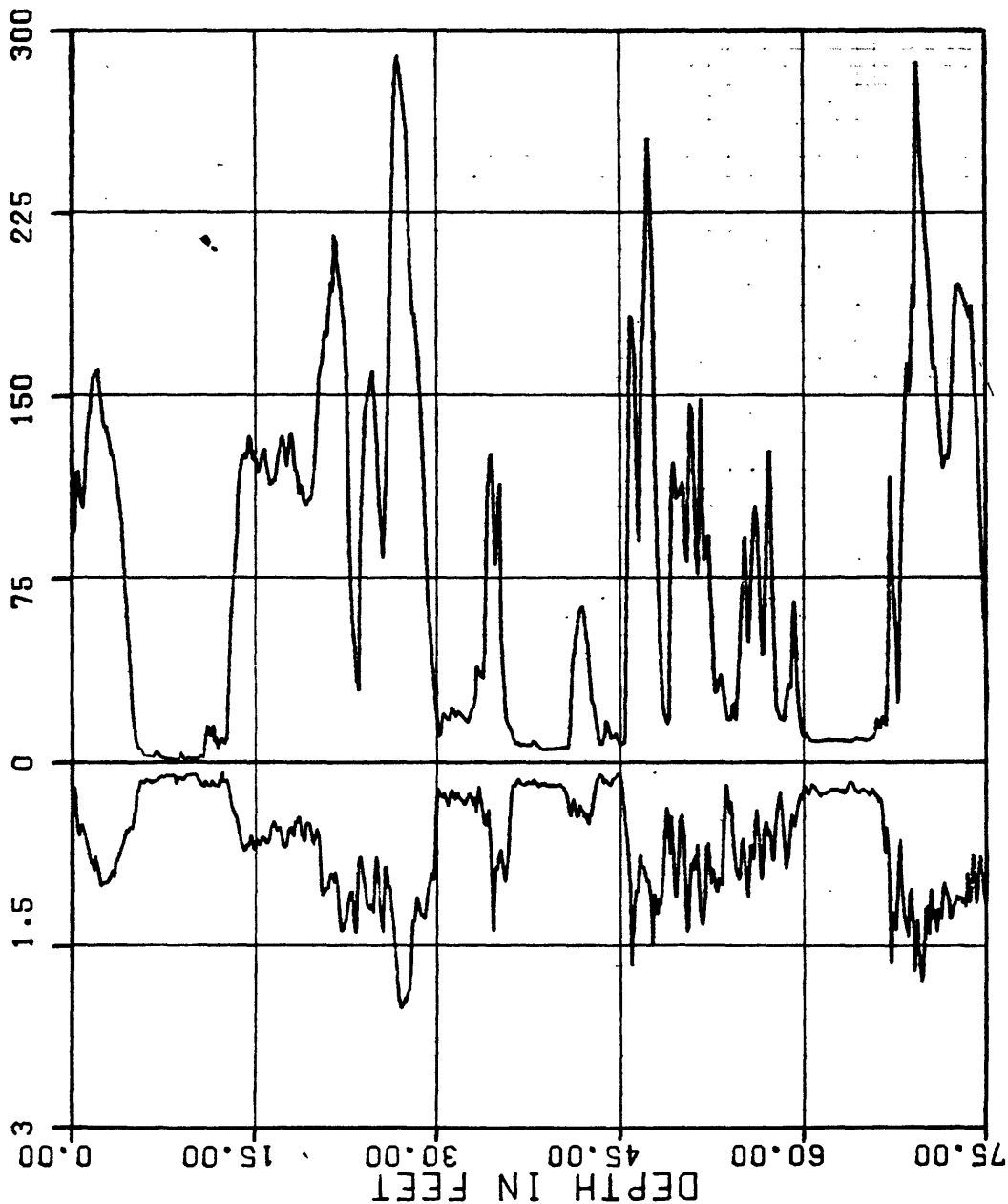
USGS CPT-SPT

CONE PENETROMETER TEST

INSTRUMENT: F5CK-230 SOUNDING: ML-C8 FIGURE A.49

FRICTION RESISTANCE, TSF

FRICTION RATIO, %



PROJECT NO.:

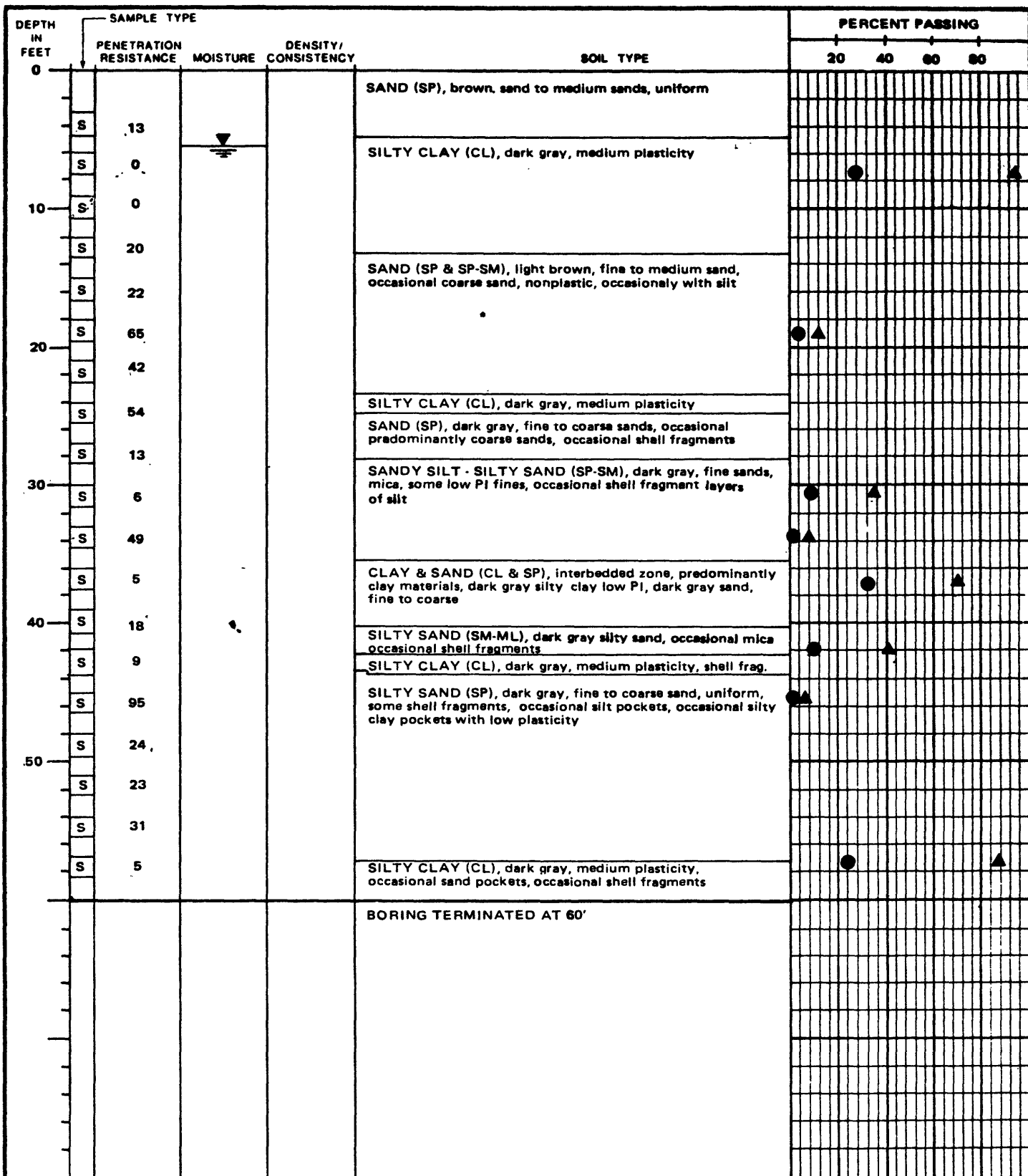
79-153

USGS CPT-SPT

CONE PENETROMETER TEST

INSTRUMENT: F15CKE-070A SOUNDING: ML-C-9

FIGURE A.80



ELEVATION: DATE DRILLED: 11-13-79
 EQUIPMENT USED: 5 7/8" ROTARY WASH
 WATER LEVEL: 5'

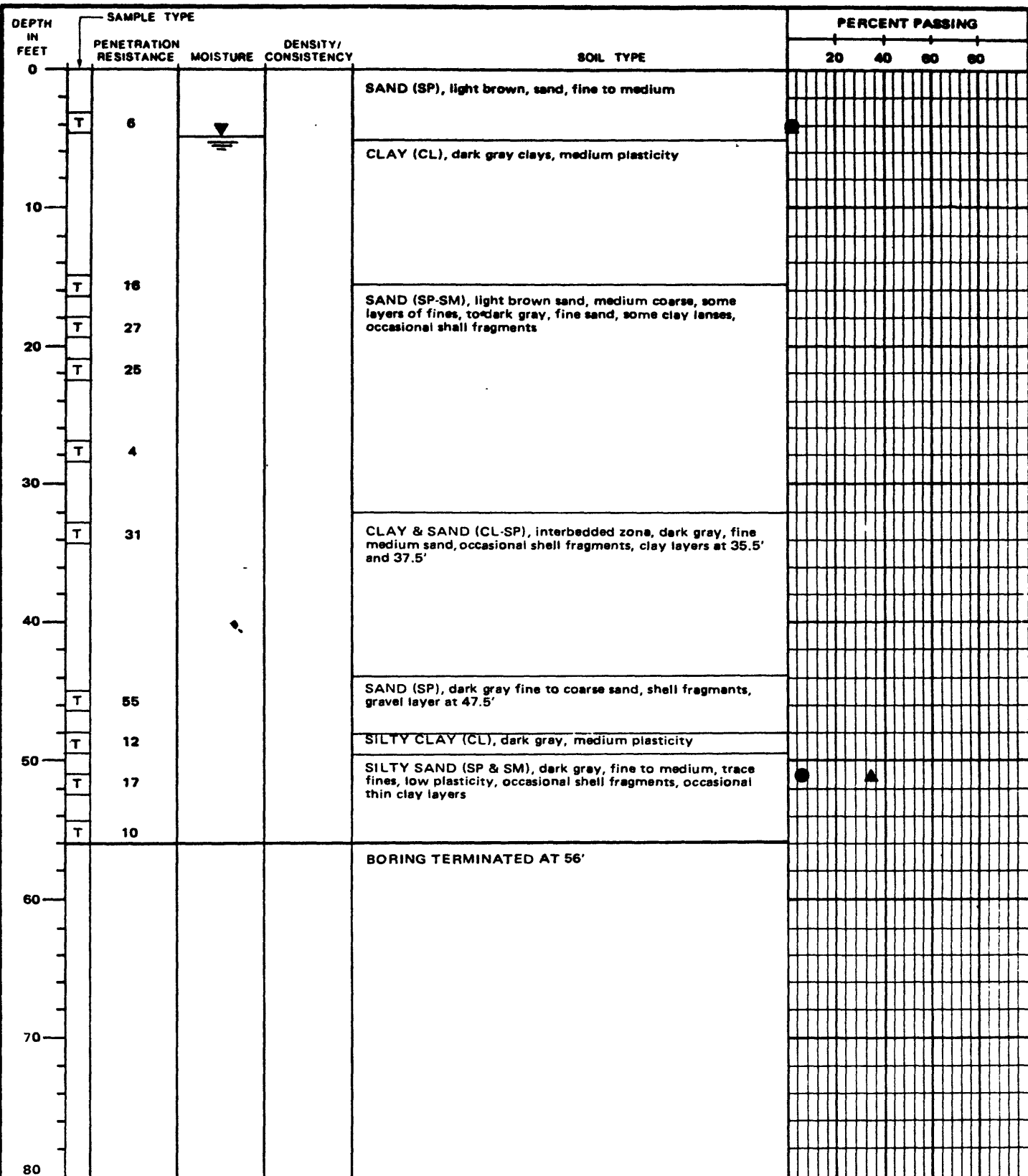
[S] STANDARD HAMMER SPLIT SPOON SAMPLE ▲ #200 SIEVE
 [T] TRIP HAMMER SPLIT SPOON SAMPLE ● 0.002 mm



PROJECT NO.: 79-153

USGS CPT-SPT

LOG OF BORING NO. 1
 MOSS LANDING SITE



ELEVATION:
DATE DRILLED: 11-14-79

EQUIPMENT USED: 5 7/8" ROTARY WASH
WATER LEVEL: 5'

S

STANDARD HAMMER SPLIT SPOON SAMPLE

T

TRIP HAMMER SPLIT SPOON SAMPLE


▲

200 SIEVE

●

0.002 mm

FUGRO



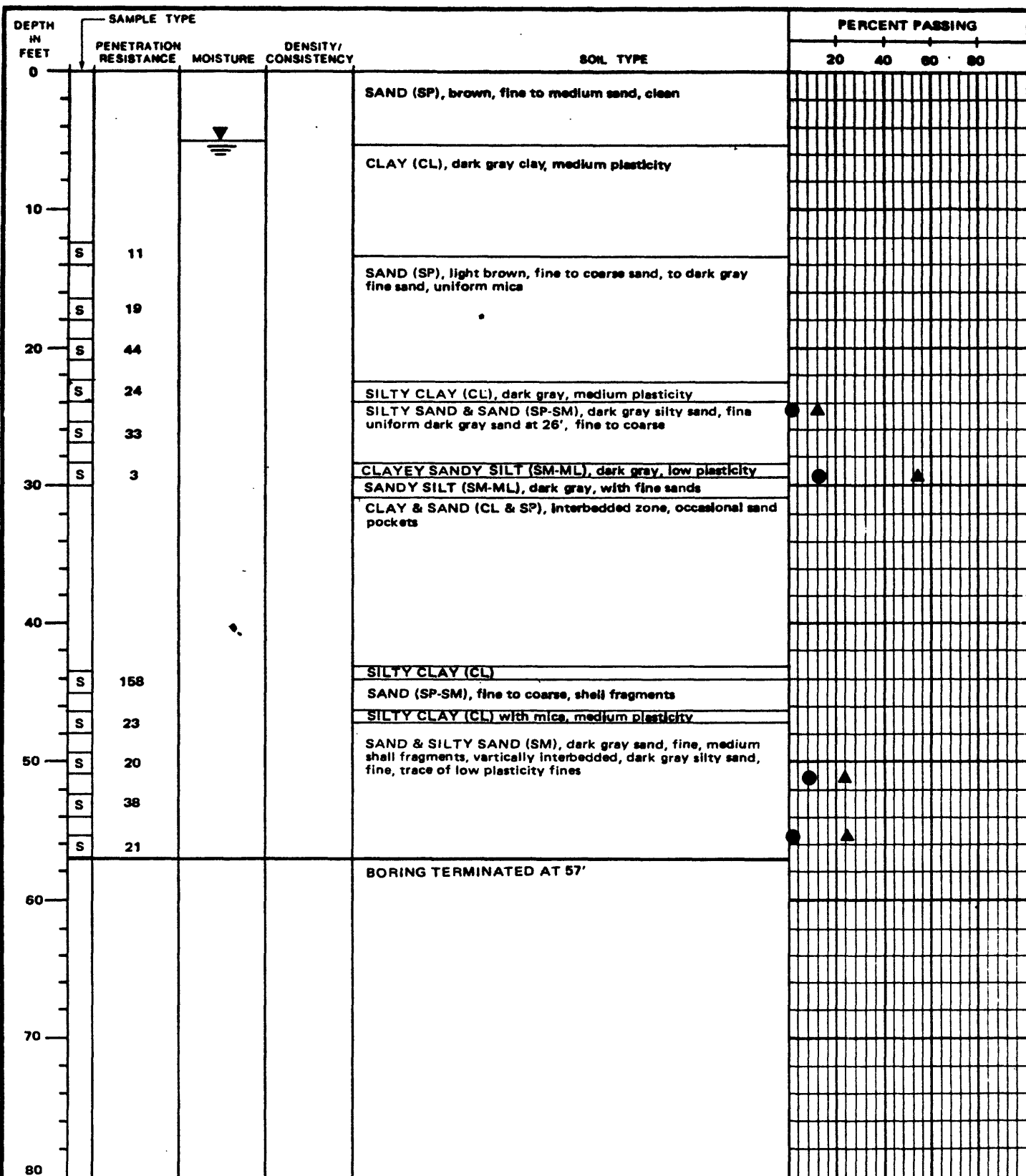
PROJECT NO.:
79-153

USGS CPT-SPT

LOG OF BORING NO. 2
MOSS LANDING SITE

9-80

FIGURE A.52



ELEVATION: DATE DRILLED: 11-13-79
 EQUIPMENT USED: 5 7/8" ROTARY WASH
 WATER LEVEL: 5'

[S] STANDARD HAMMER SPLIT SPOON SAMPLE ▲ #200 SIEVE
 [T] TRIP HAMMER SPLIT SPOON SAMPLE ● 0.002 mm

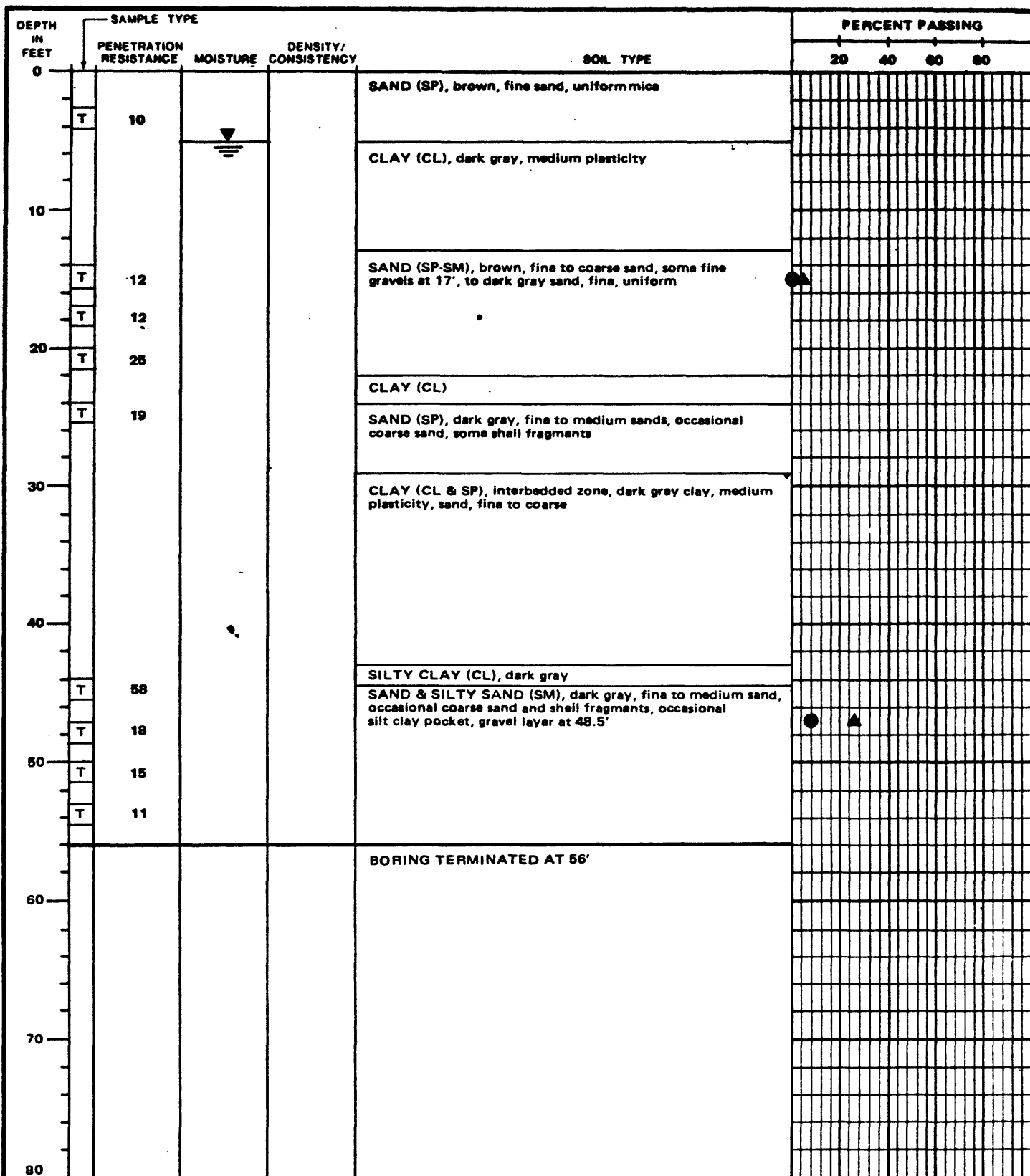


PROJECT NO.:

79-153

USGS CPT-SPT

LOG OF BORING NO. 3
 MOSS LANDING SITE



ELEVATION: DATE DRILLED: 11-14-79
 EQUIPMENT USED: 5 7/8" ROTARY WASH
 WATER LEVEL: 5'

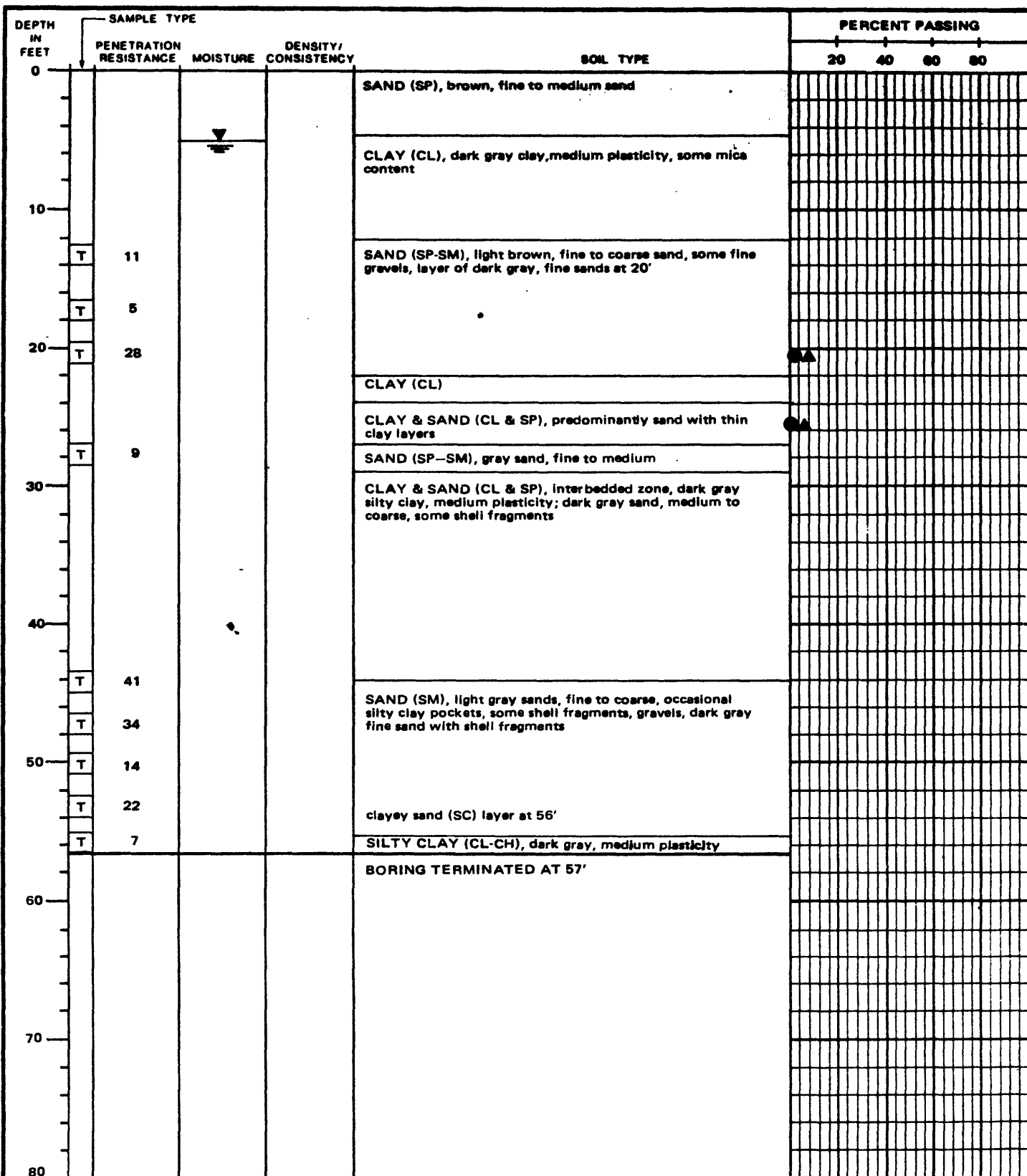
[S] STANDARD HAMMER SPLIT SPOON SAMPLE ▲ #200 SIEVE
 [T] TRIP HAMMER SPLIT SPOON SAMPLE ● 0.002 mm



PROJECT NO.: 79-153

USGS CPT-SPT

LOG OF BORING NO. 4
 MOSS LANDING SITE



ELEVATION: DATE DRILLED: 11-14-79
 EQUIPMENT USED: 5 7/8" ROTARY WASH
 WATER LEVEL: 5'

[S] STANDARD HAMMER SPLIT SPOON SAMPLE ▲ #200 SIEVE
 [T] TRIP HAMMER SPLIT SPOON SAMPLE ● 0.002 mm

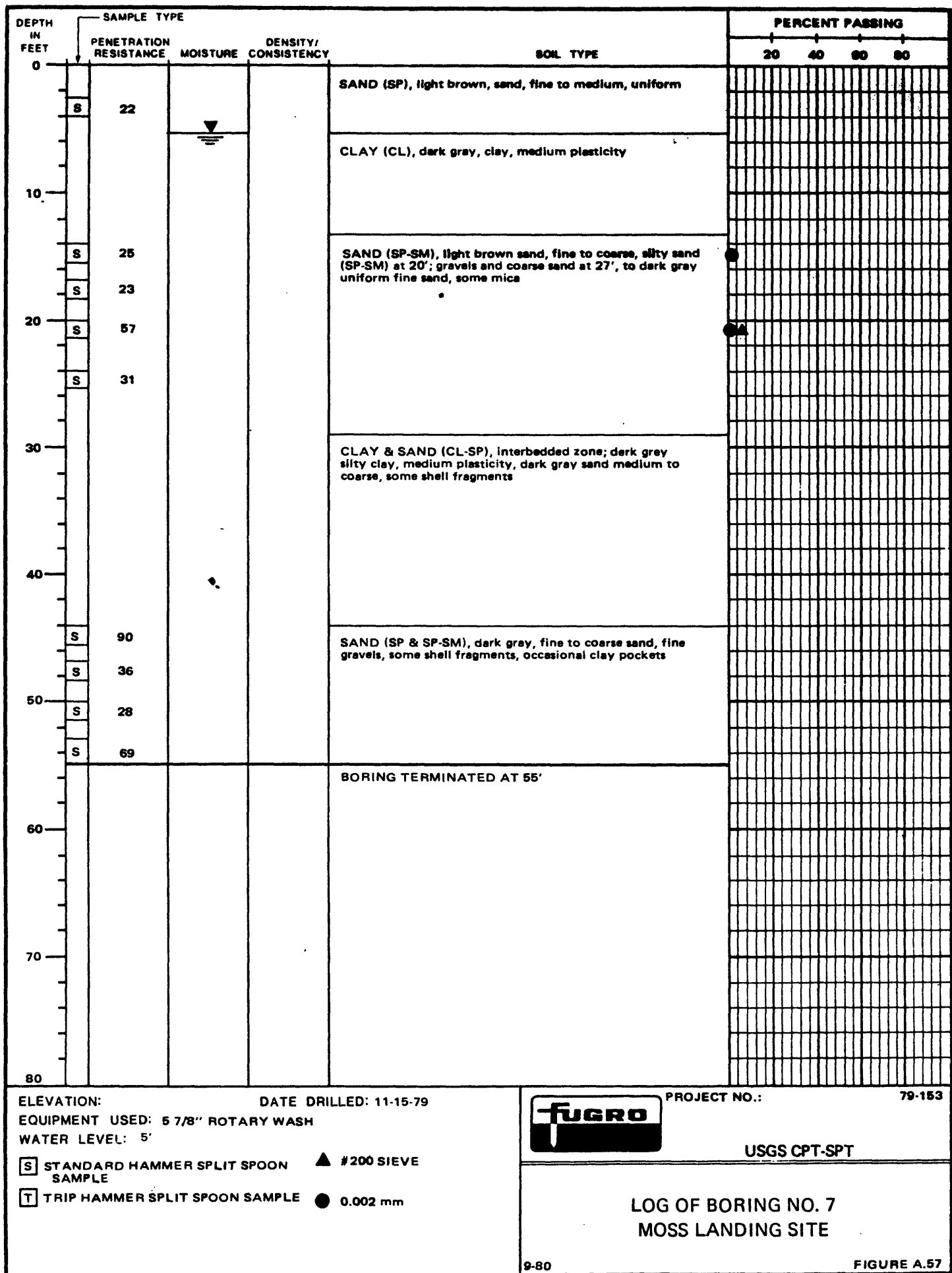


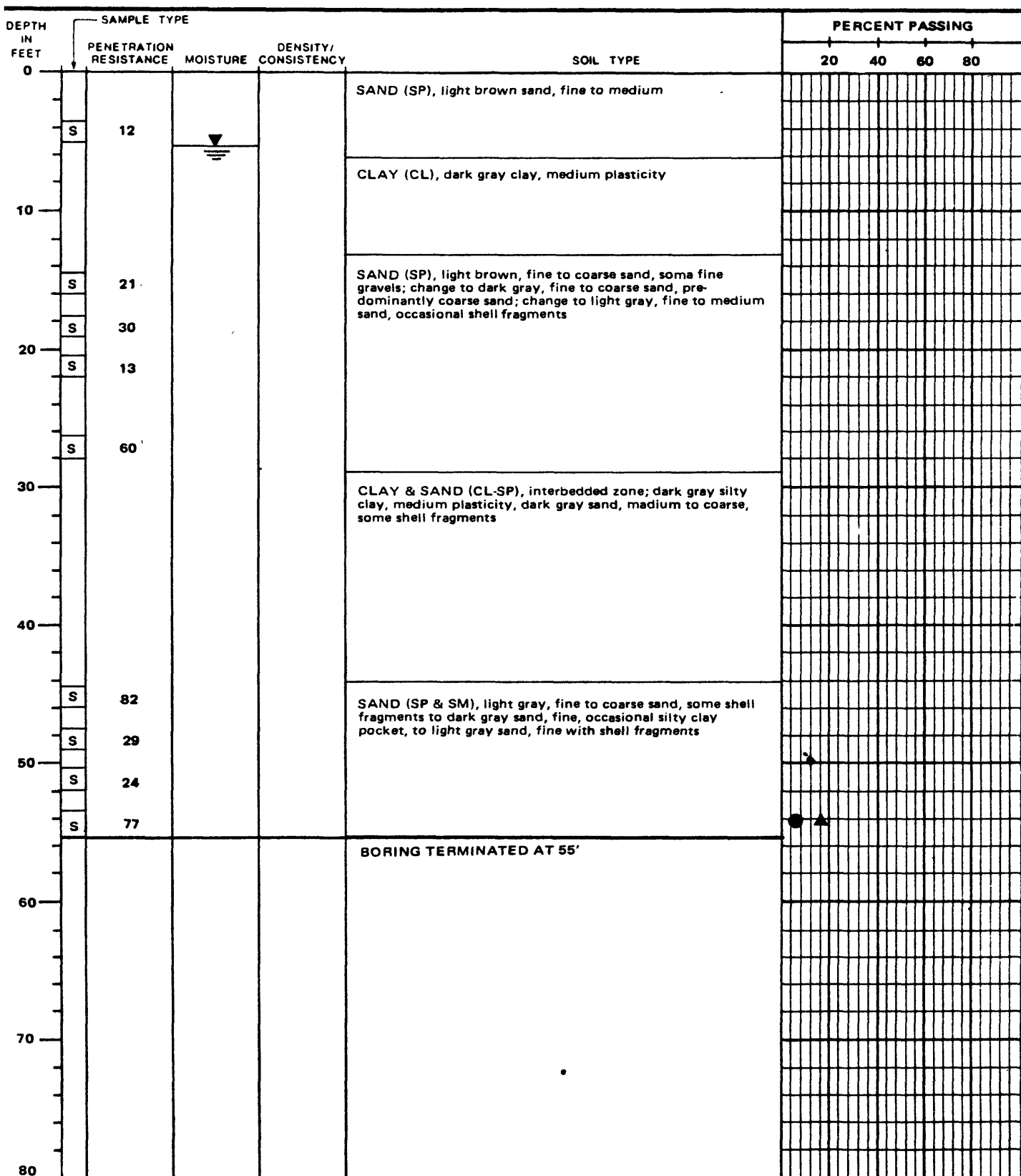
PROJECT NO.:

79-153

USGS CPT-SPT

LOG OF BORING NO. 6
 MOSS LANDING SITE





ELEVATION: DATE DRILLED: 11-15-79
EQUIPMENT USED: 5 7/8" ROTARY WASH
WATER LEVEL: 5'

[S] STANDARD HAMMER SPLIT SPOON SAMPLE ▲ #200 SIEVE
[T] TRIP HAMMER SPLIT SPOON SAMPLE ● 0.002 mm



PROJECT NO.:

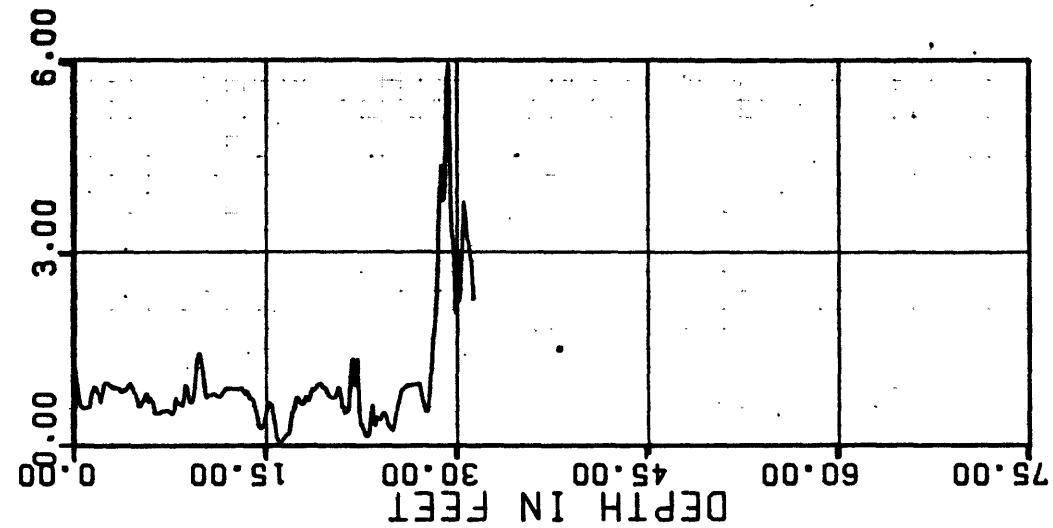
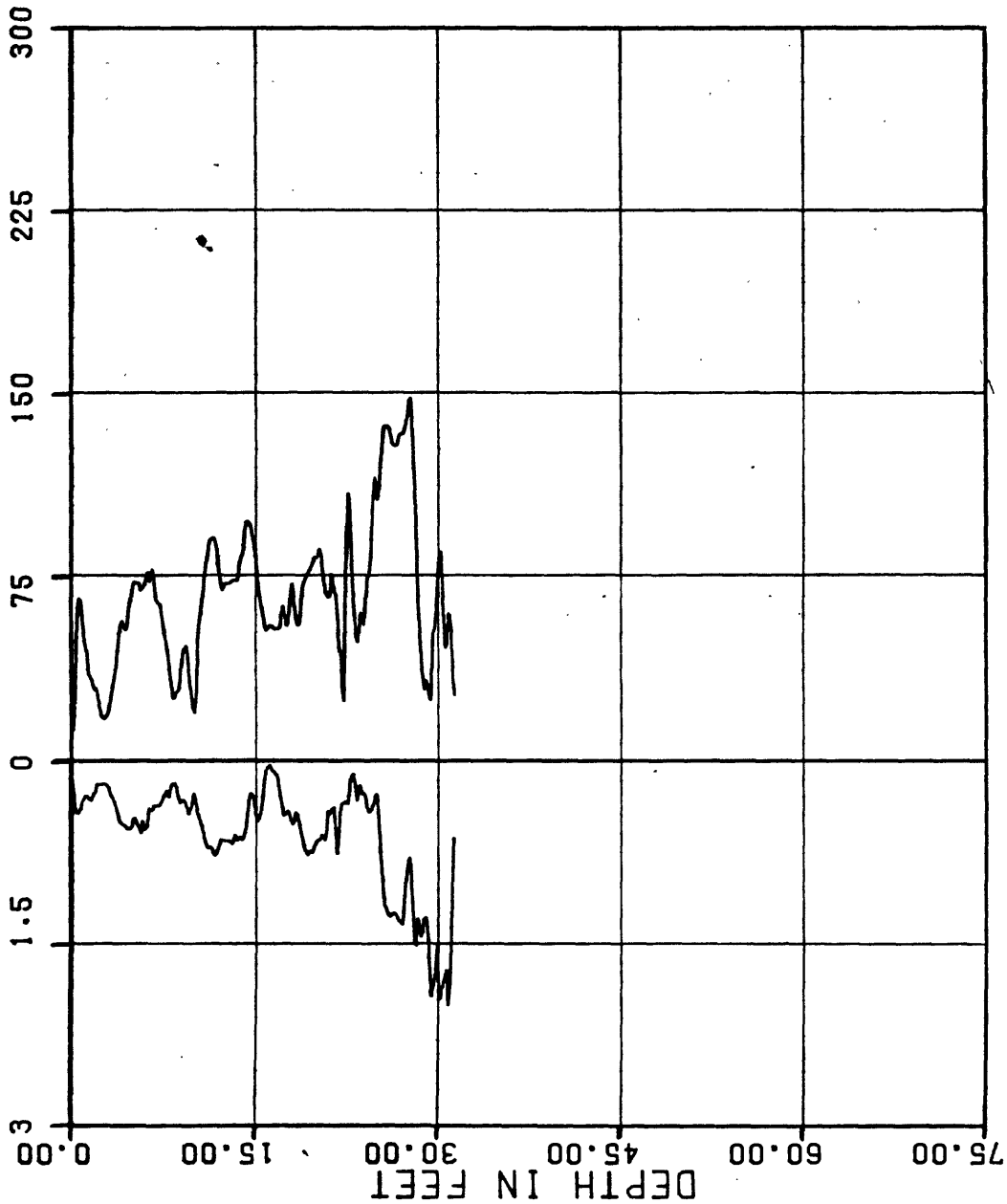
79-153

USGS CPT-SPT

LOG OF BORING NO. 8
MOSS LANDING SITE

FRICTION RESISTANCE, TSF

FRICTION RATIO, %



PROJECT NO.:

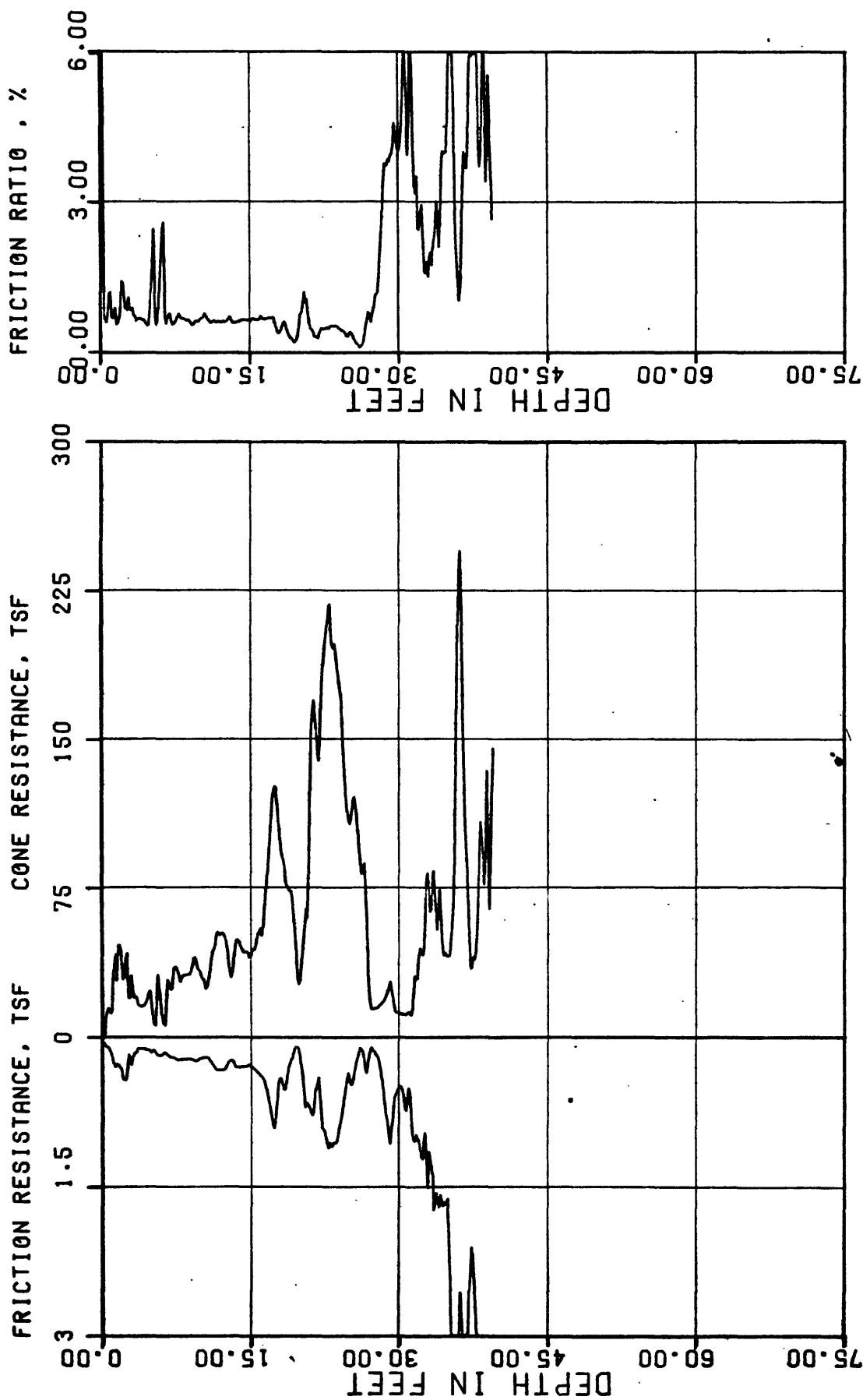
79-153

USGS CPT-SPT

CONE PENETROMETER TEST

INSTRUMENT: F15CKE-072 SOUNDING: SB-C-2

FIGURE A.89



PROJECT NO.:

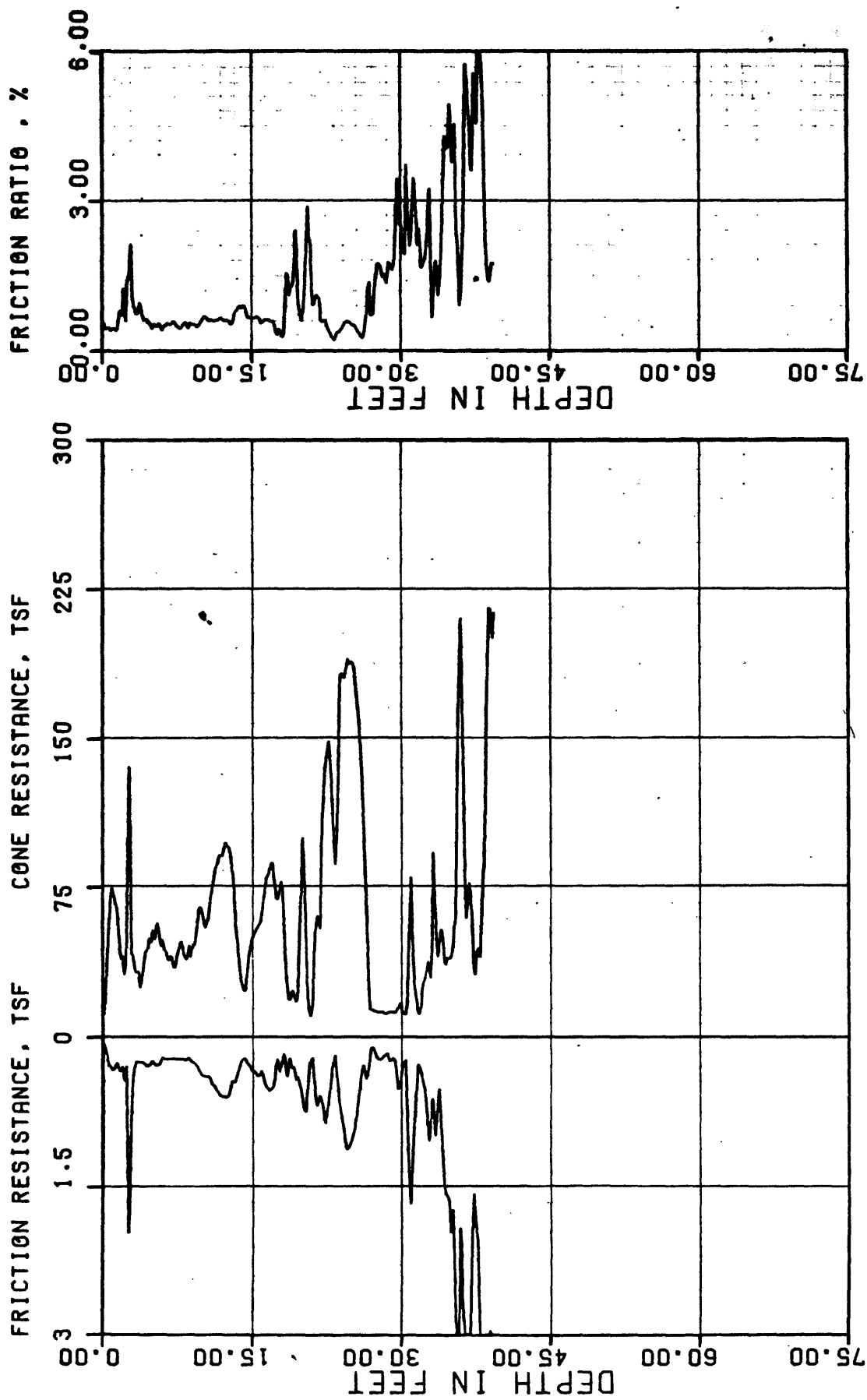
79-153

USGS CPT-SPT

CONE PENETROMETER TEST

INSTRUMENT: F5CK-230 SOUNDING: SB-C-3

FIGURE A.60



PROJECT NO.:

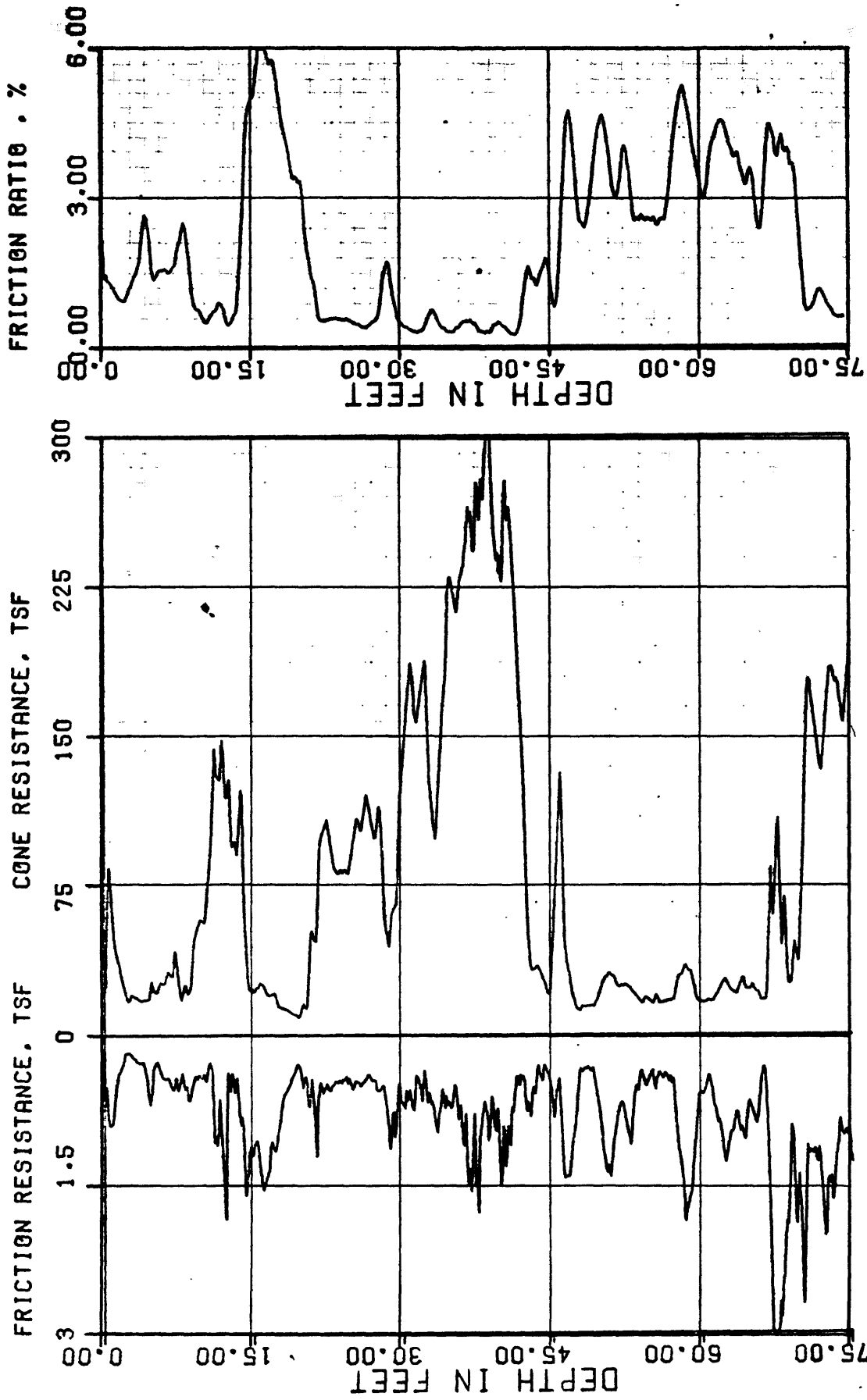
79-153

USGS CPT-SPT

CONE PENETROMETER TEST

INSTRUMENT: F5CK-230 SOUNDING: SB-C4

FIGURE A.61



PROJECT NO.: 79-163



USGS CPT-SPT

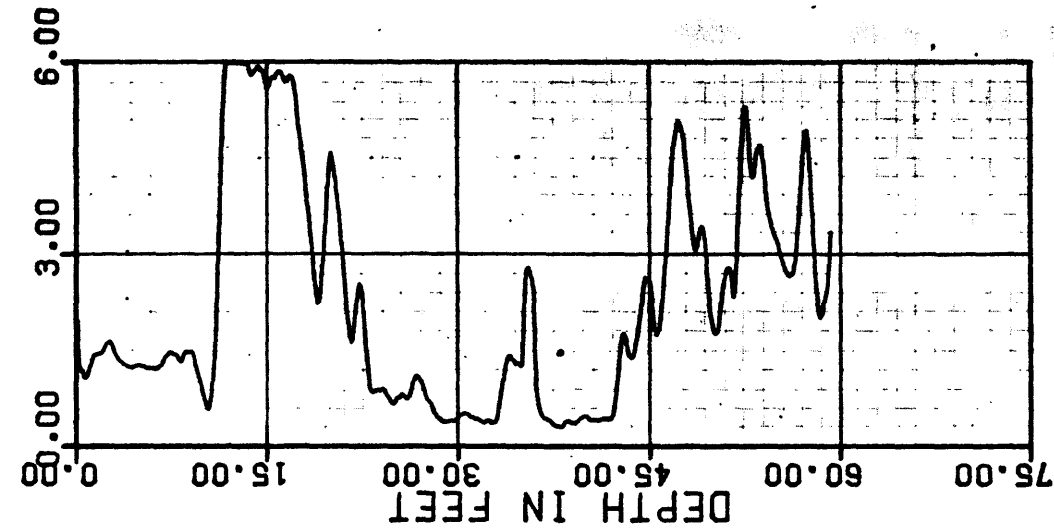
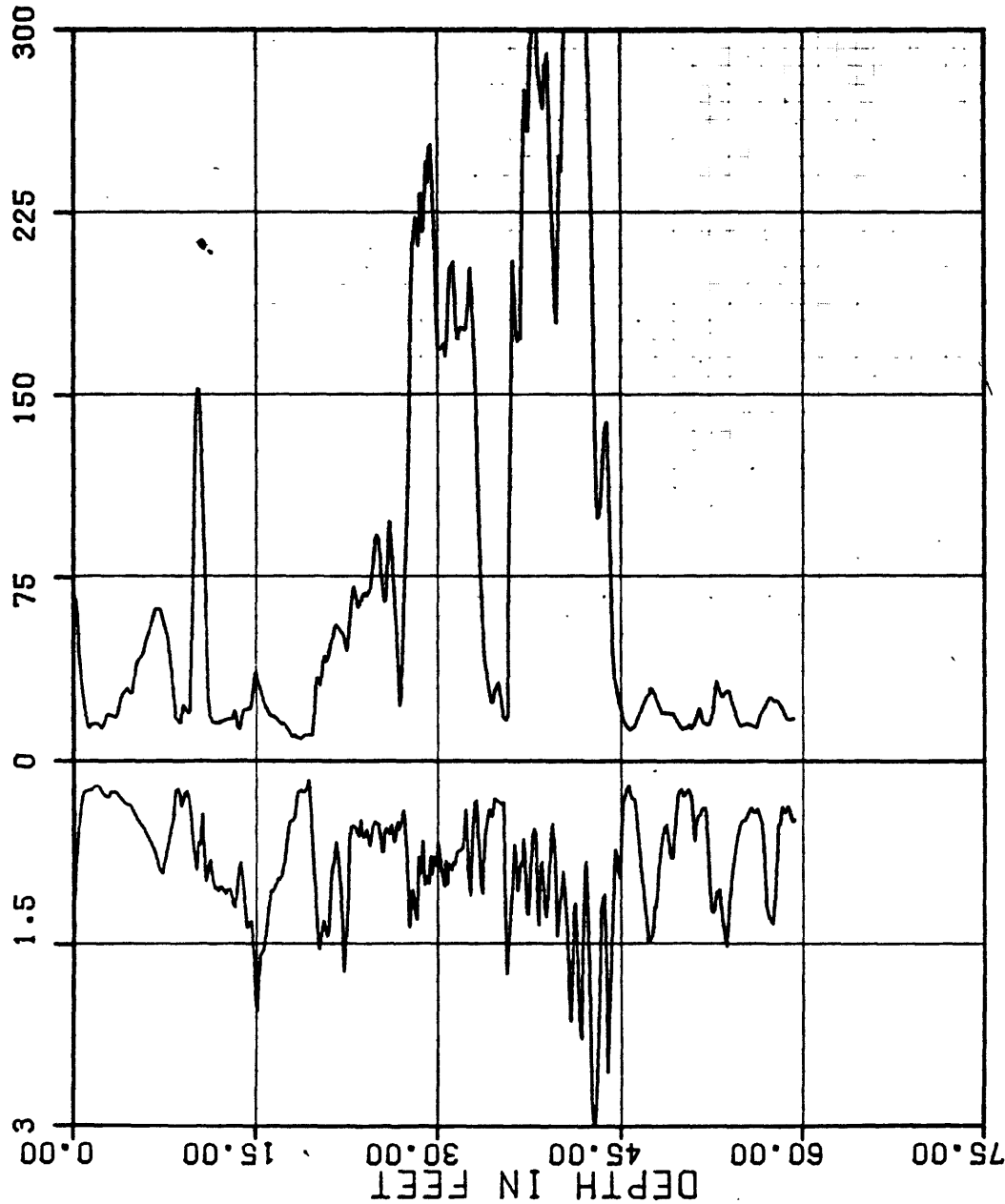
CONE PENETROMETER TEST

INSTRUMENT: F15CKE-070&OUNDING: CN-C-1

FIGURE A.62

FRICTION RESISTANCE, TSF

FRICTION RATIO, %



PROJECT NO.:

79-183

USGS CPT-SPT

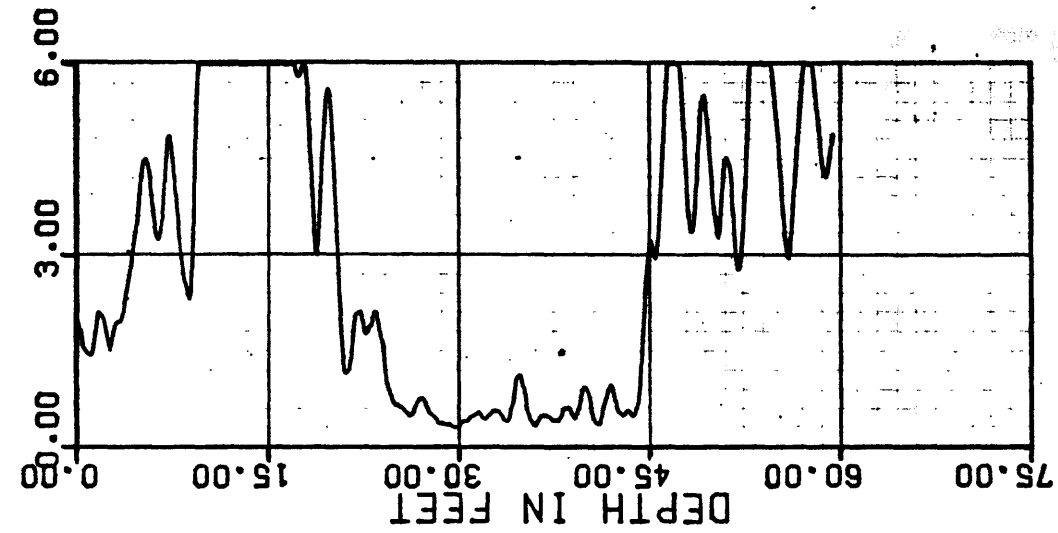
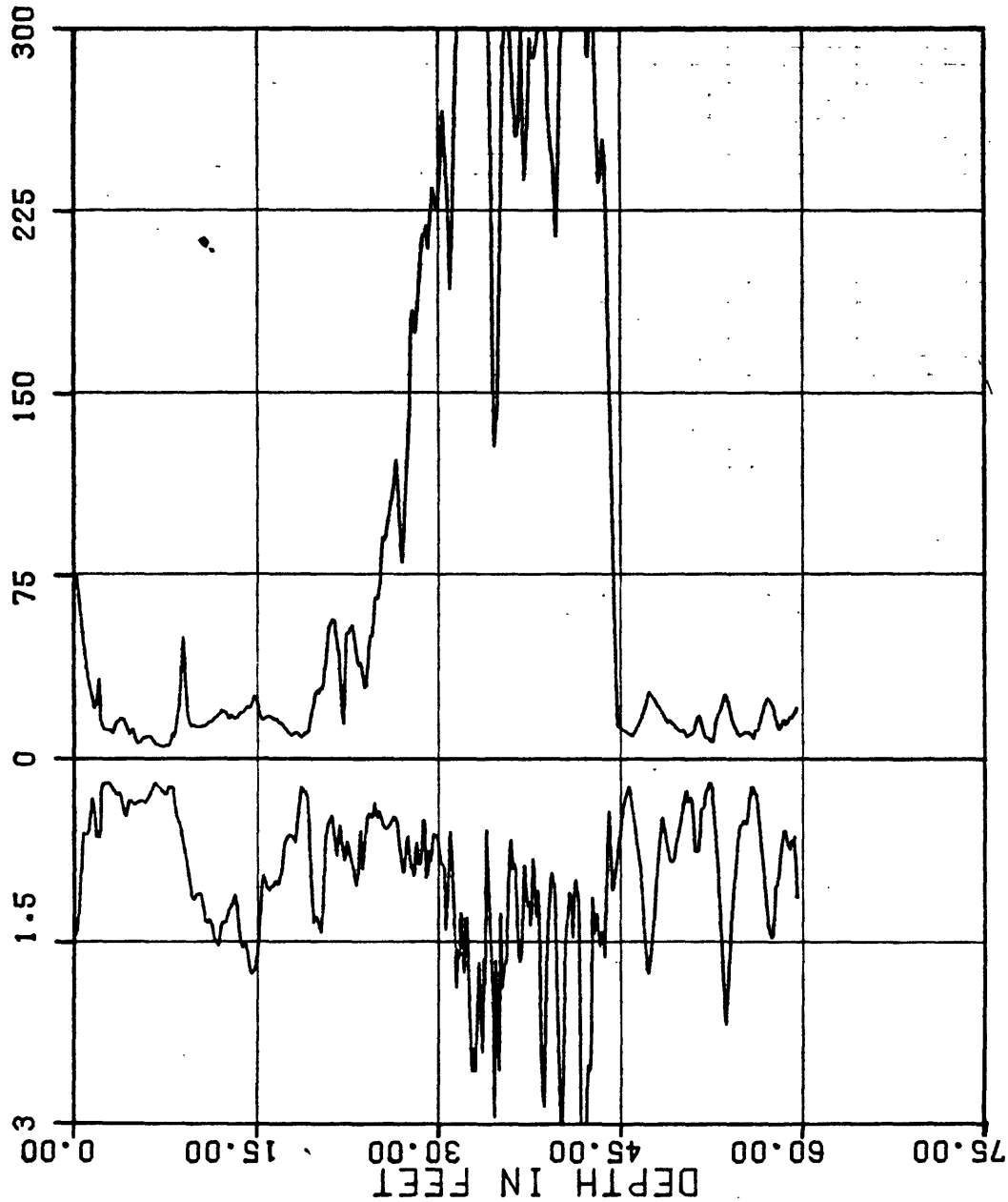
CONE PENETROMETER TEST

INSTRUMENT: F5CK-230 SOUNDING: CN-C-2

FIGURE A.63

FRICION RESISTANCE, TSF

FRICION RATIO, %



PROJECT NO.:

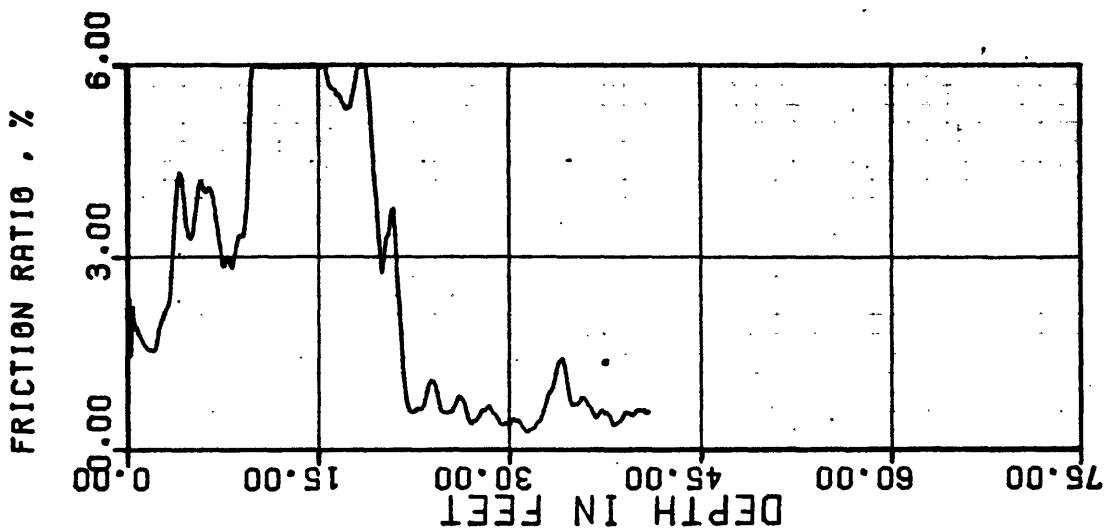
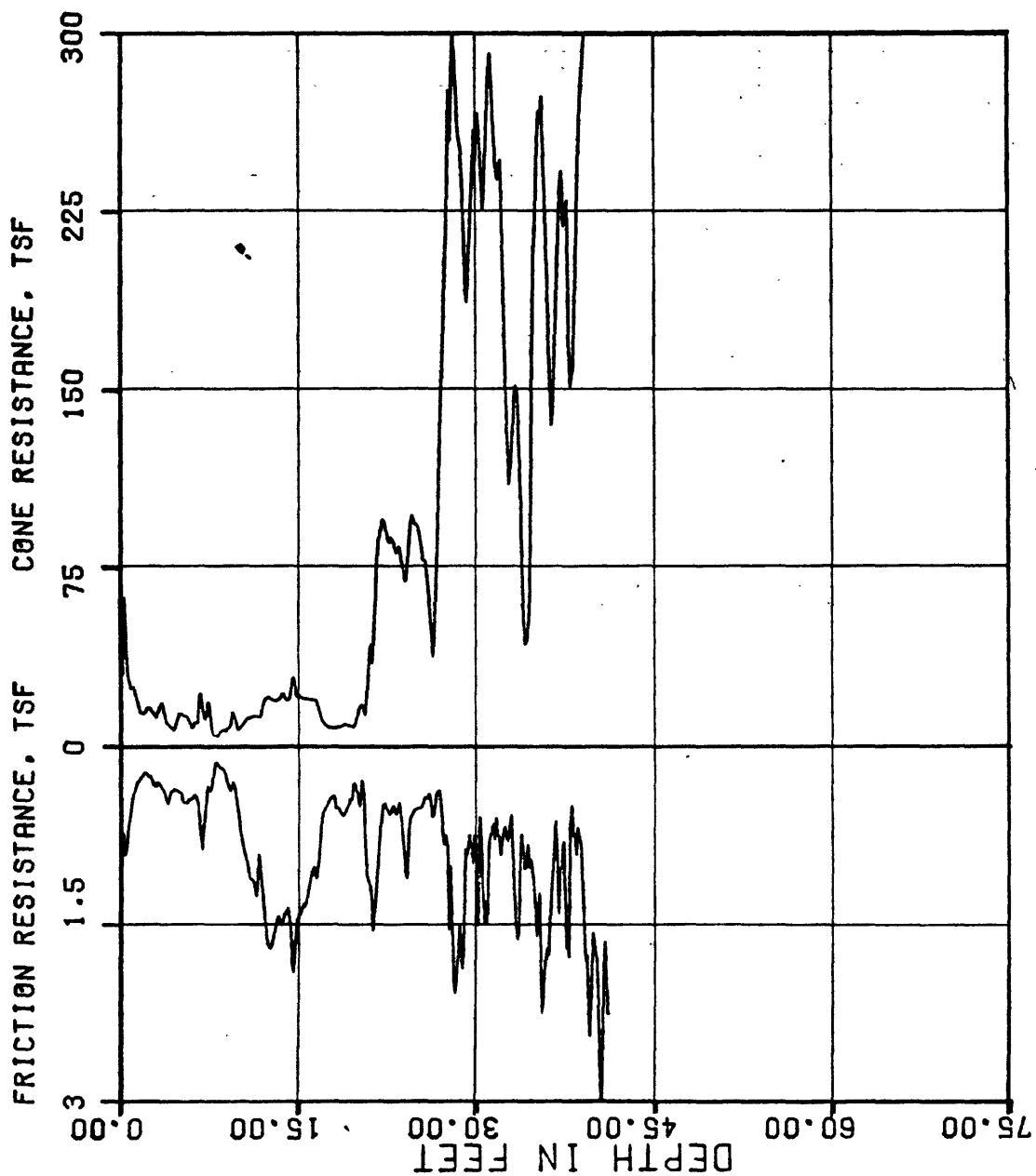
79-163

USGS CPT-SPT

CONE PENETROMETER TEST

INSTRUMENT: F5CK-230 SOUNDING: CN-C-3

FIGURE A.64



PROJECT NO.:

79-153

USGS CPT-SPT

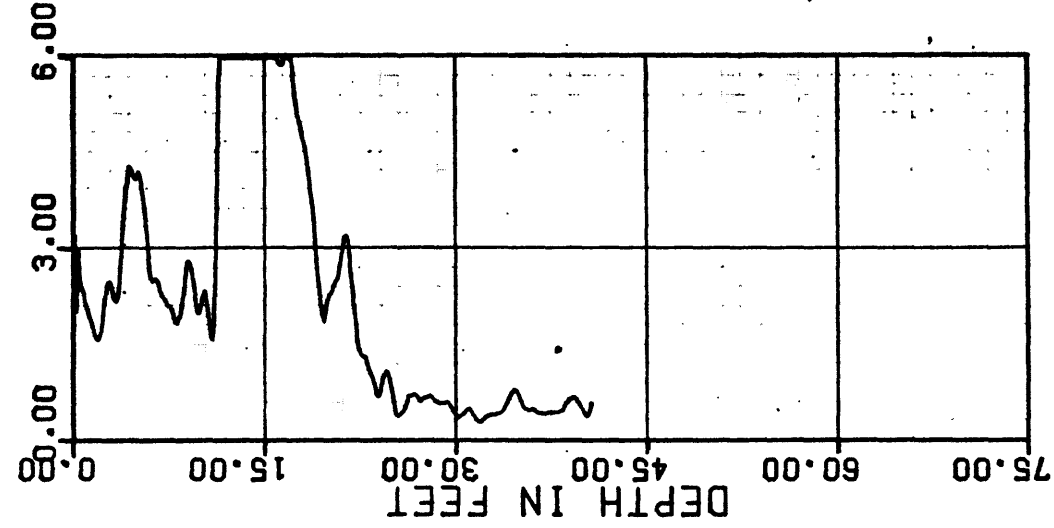
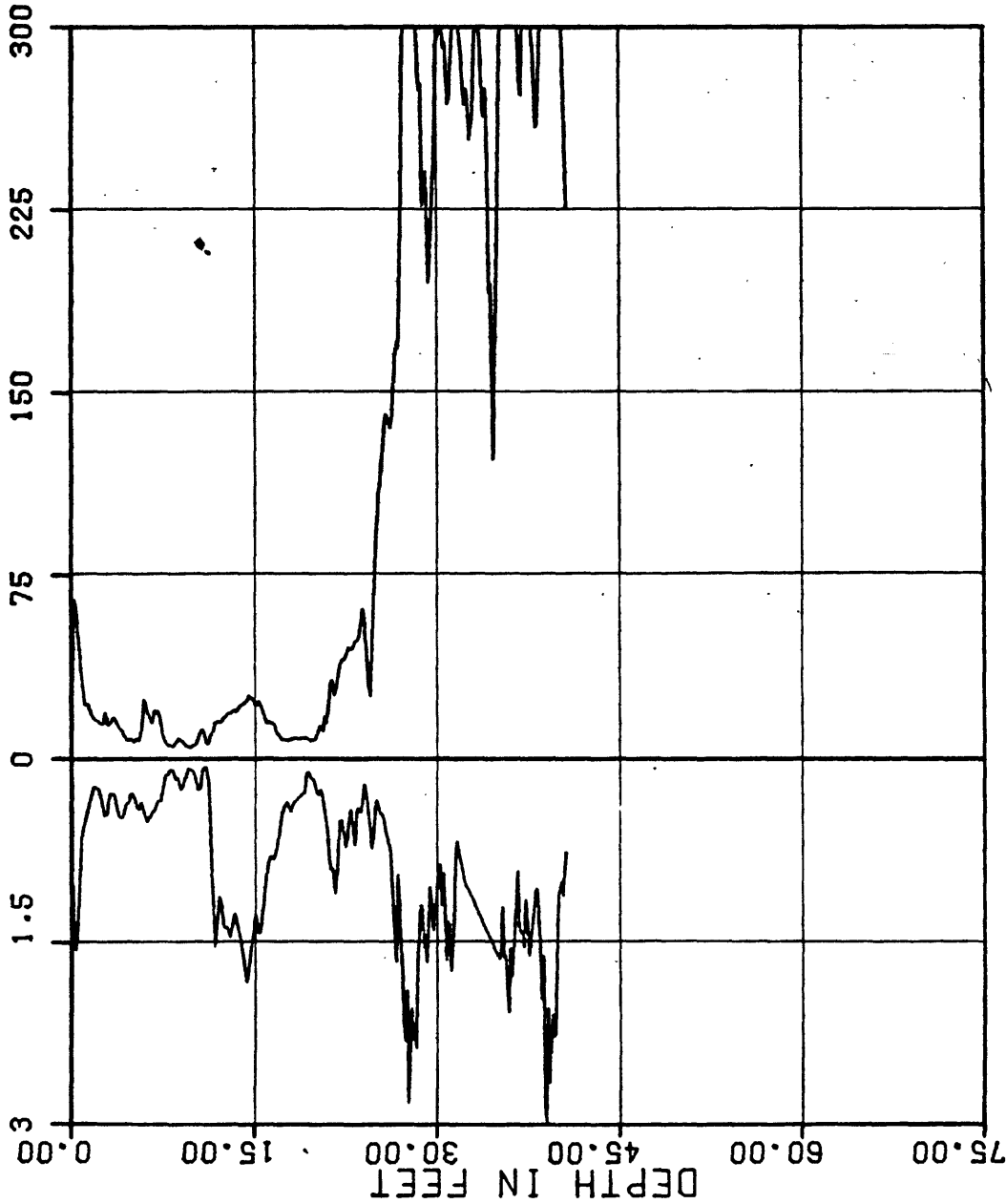
CONE PENETROMETER TEST

INSTRUMENT: F5CK-230 SOUNDING: CN-C-4

FIGURE A.06

FRICTION RESISTANCE, TSF

FRICTION RATIO, %



PROJECT NO.:

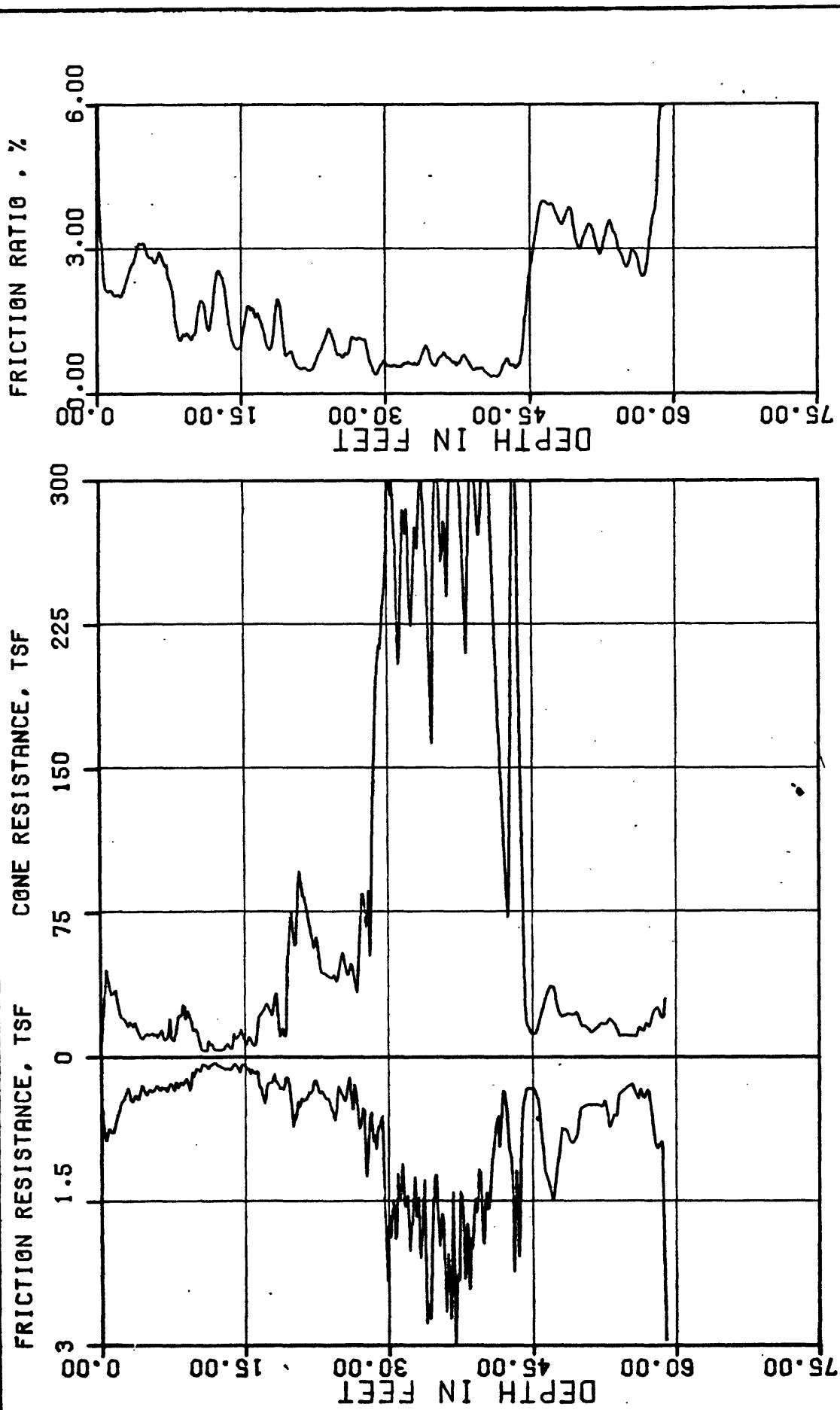
79-163

USGS CPT-SPT

CONE PENETROMETER TEST

INSTRUMENT: F5CK-230 SOUNDING: CN-C-6

FIGURE A.68



fugro PROJECT NO.: 79-153

USGS CPT-SPT

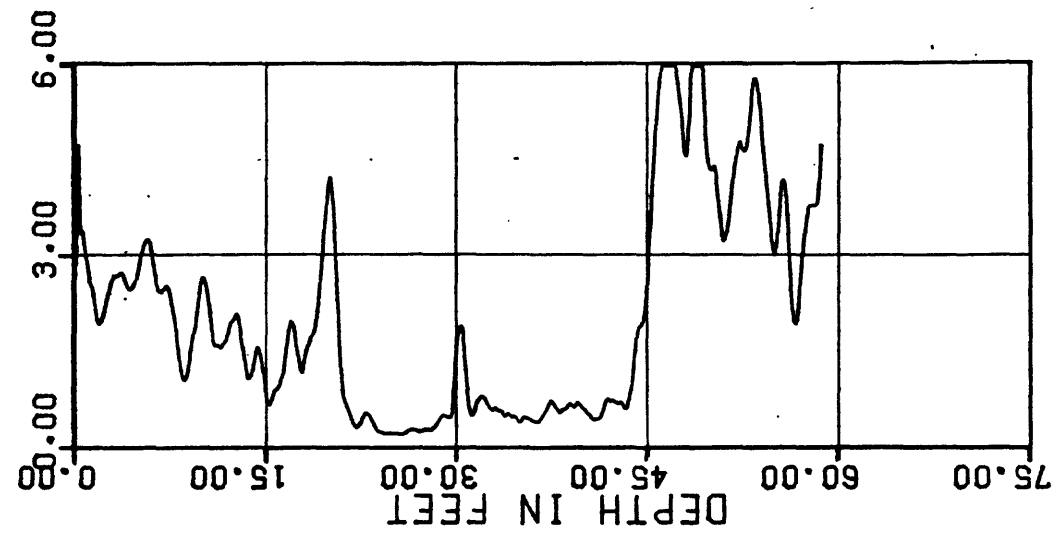
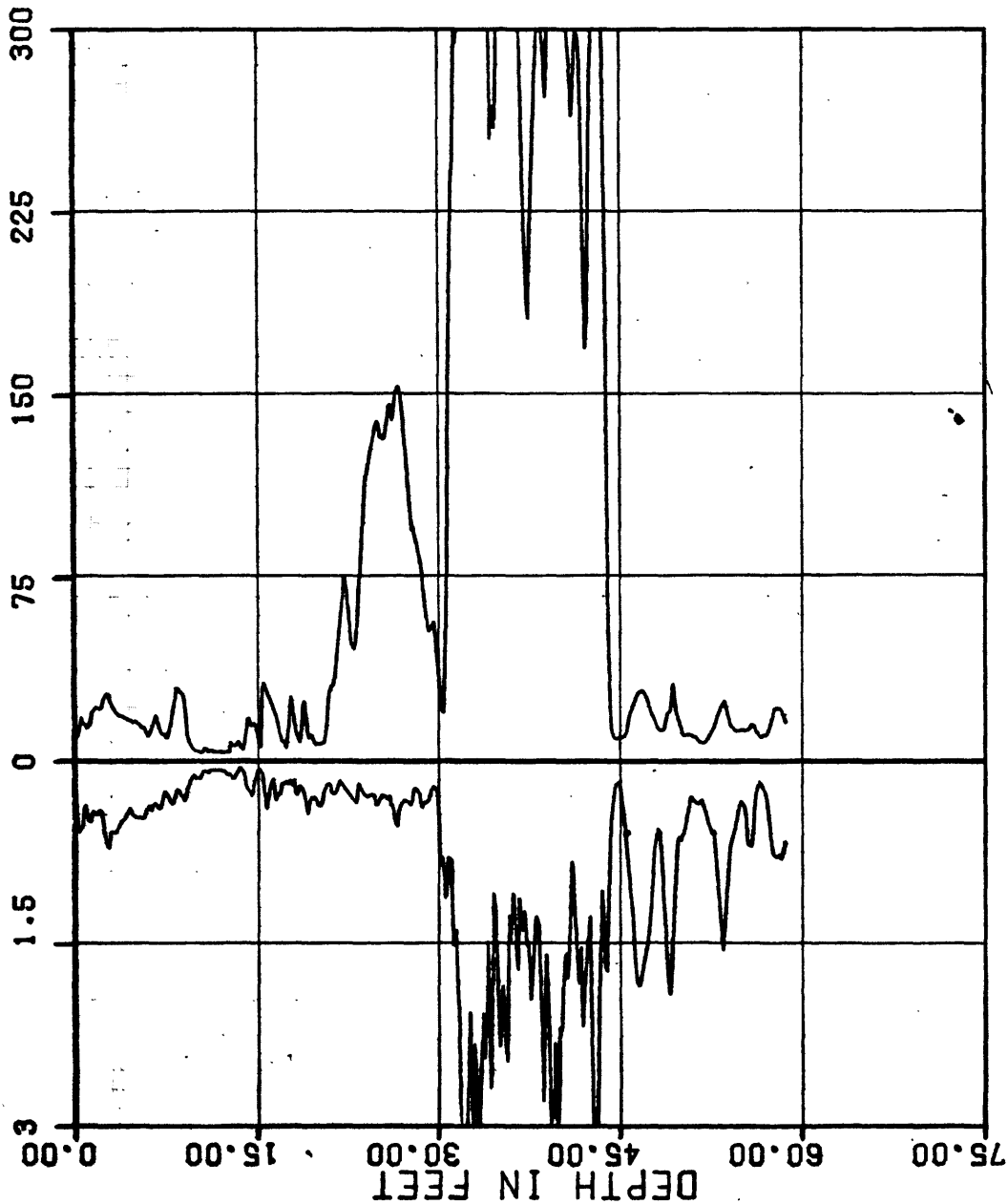
CONE PENETROMETER TEST

INSTRUMENT: F5CK-230 SOUNDING: CN-C-7 FIGURE A.67

FRICTION RESISTANCE, TSF

CONE RESISTANCE, TSF

FRICTION RATIO, %



PROJECT NO.:

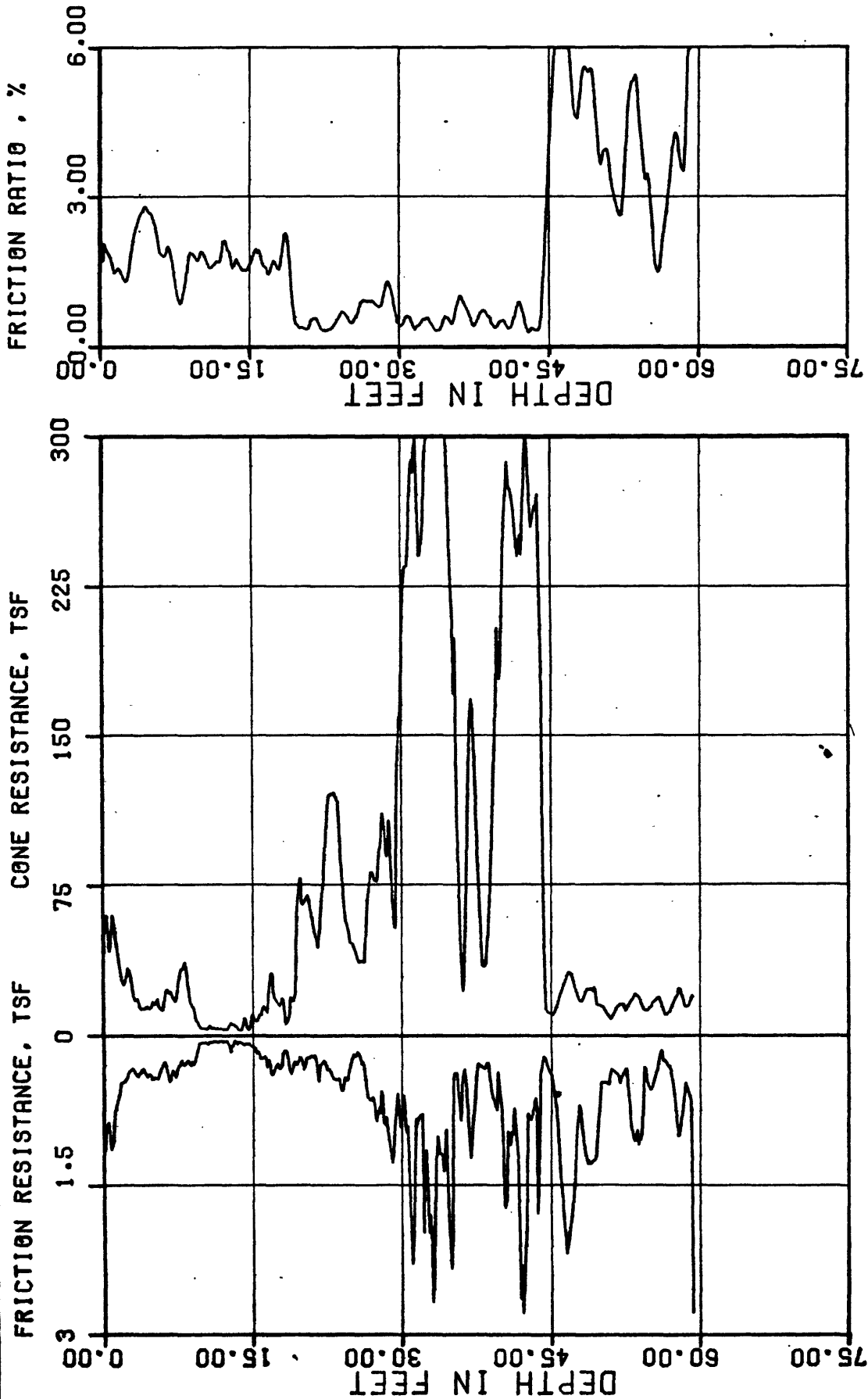
79-153

USGS CPT-SPT

CONE PENETROMETER TEST

INSTRUMENT: F5CK-230 SOUNDING: CN-C-9

FIGURE A.68



PROJECT NO.:

79 153

USGS CPT-SPT

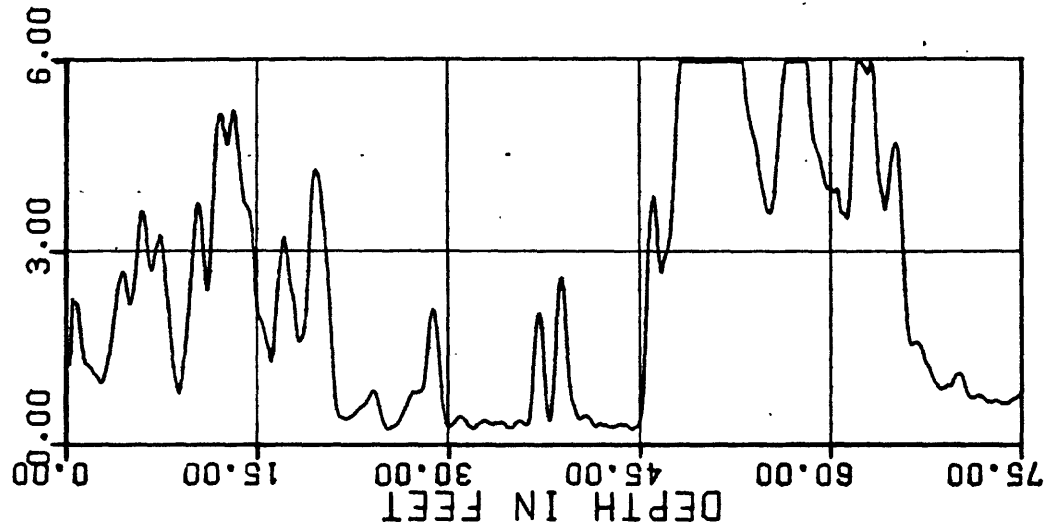
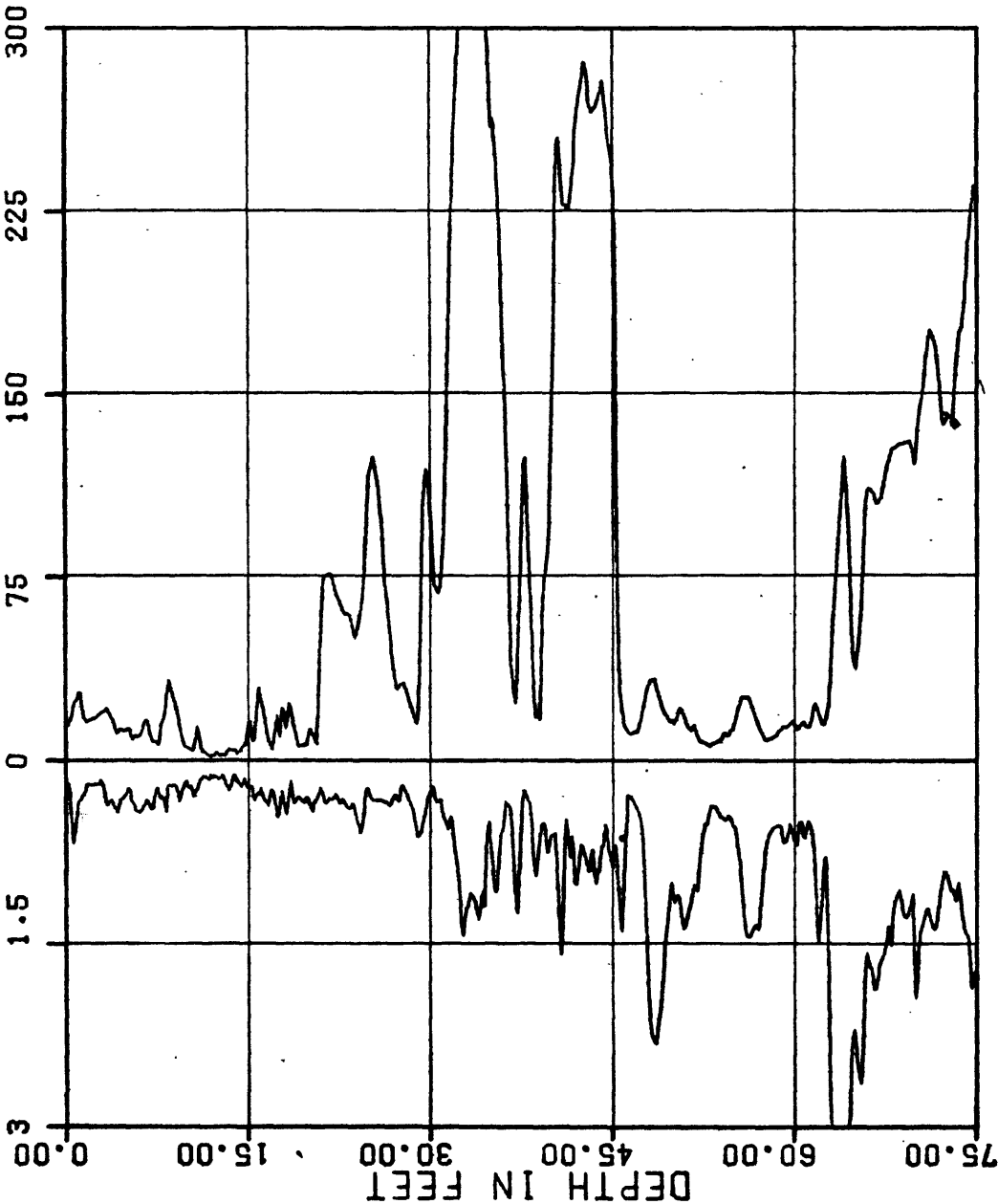
CONE PENETROMETER TEST

INSTRUMENT: F5CK-230 SOUNDING: CN-C-10 FIGURE A.69

FRICION RESISTANCE, TSF

CONE RESISTANCE, TSF

FRICION RATIO, %



PROJECT NO.:

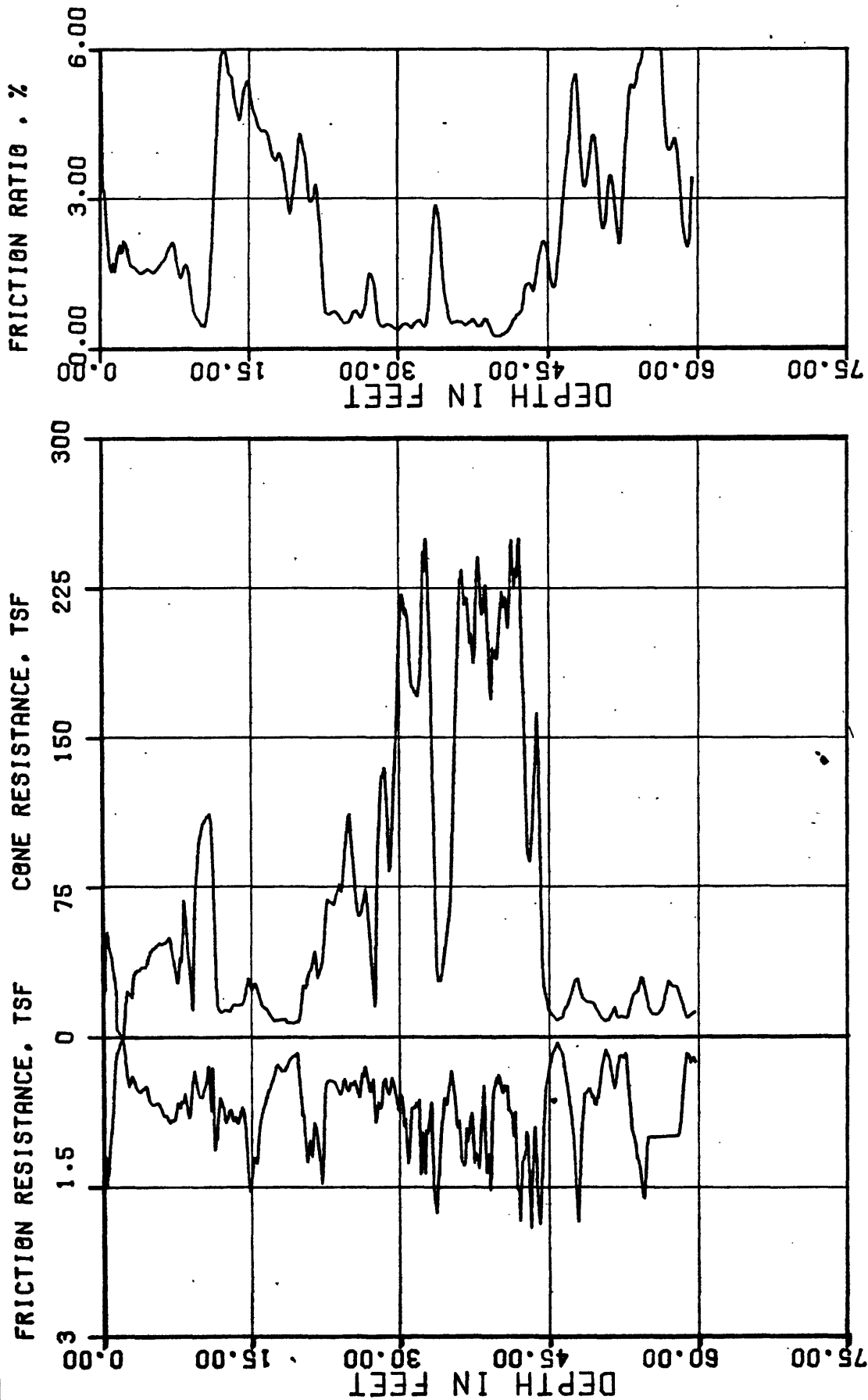
79-153

USGS CPT-SPT

CONE PENETROMETER TEST

INSTRUMENT: F15CKE-070ASOUNDING: CN-C-12

FIGURE A.70



PROJECT NO.:

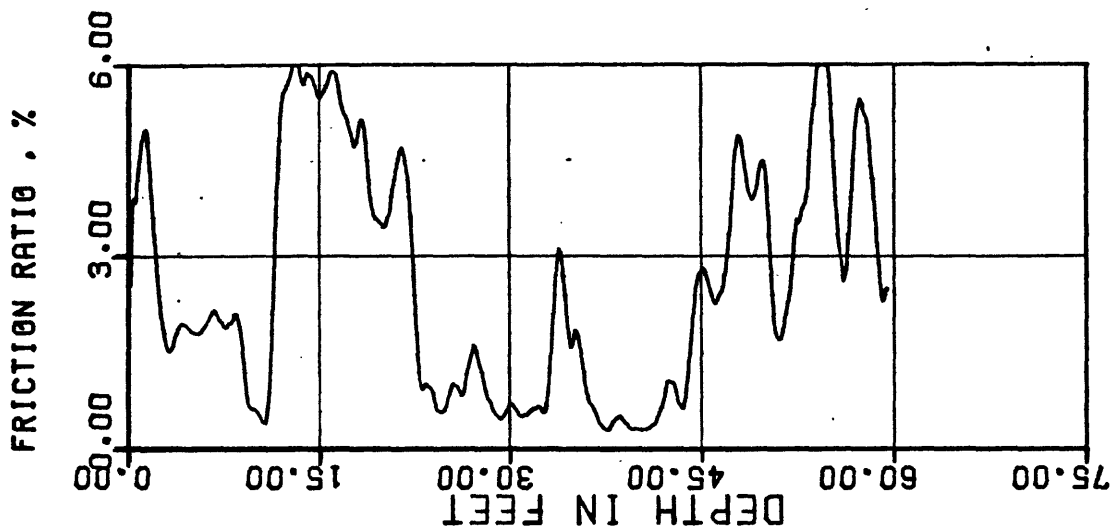
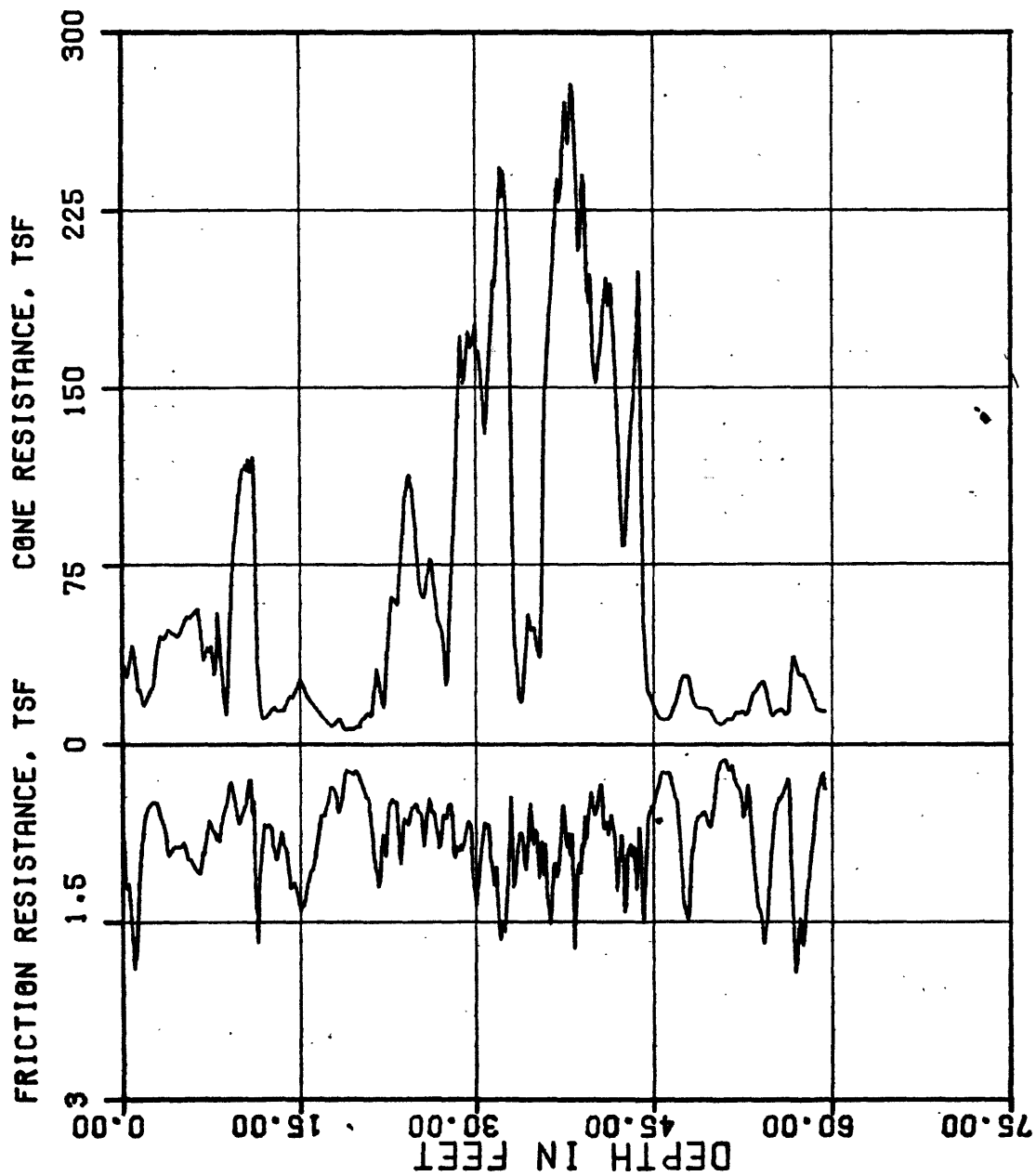
79-153

USGS CPT-SPT

CONE PENETROMETER TEST

INSTRUMENT: F5CK-230 SOUNDING: CN-C-13

FIGURE A.71



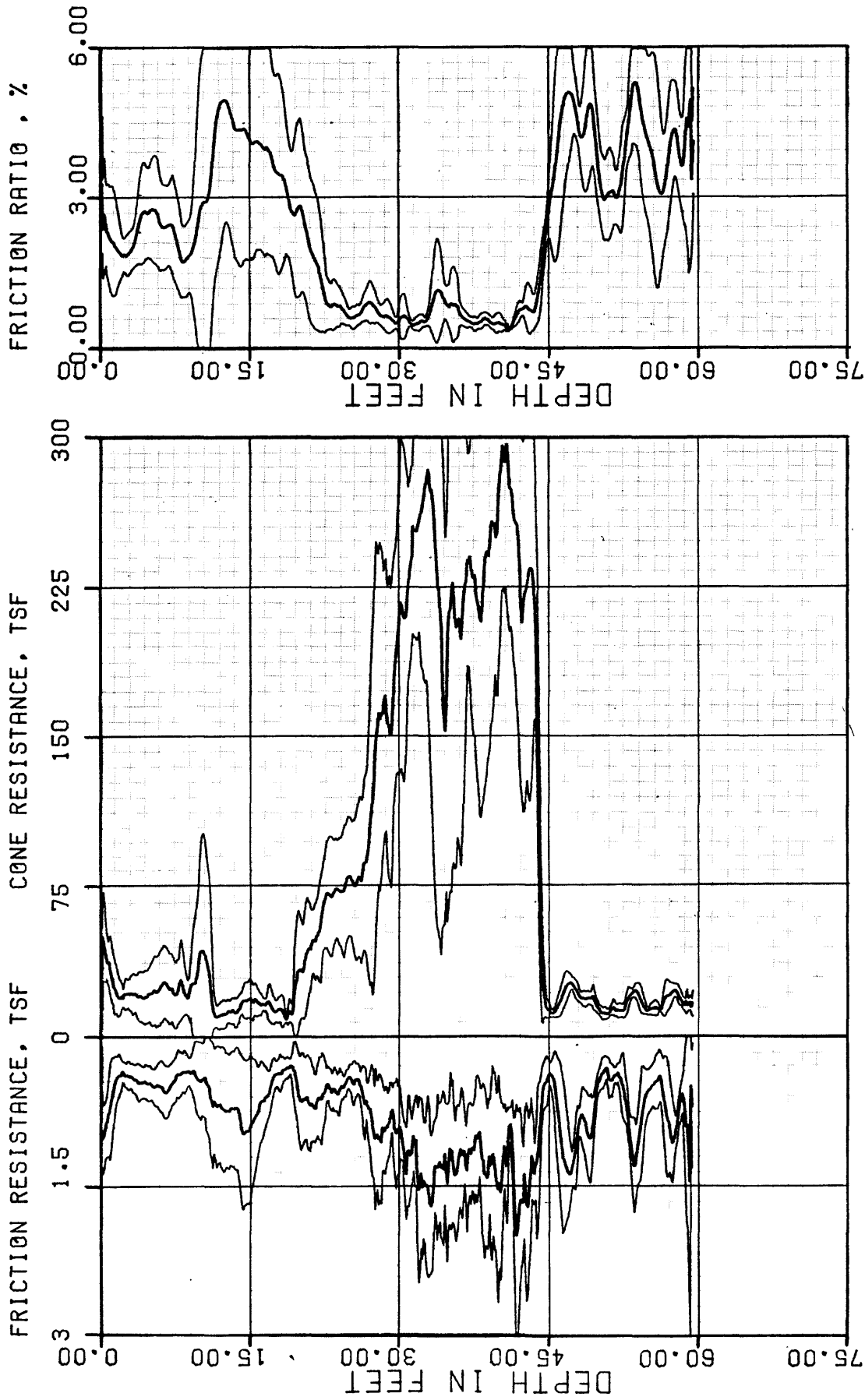
PROJECT NO.:

79-153

USGS CPT-SPT

CONE PENETROMETER TEST

INSTRUMENT: F5CK-230 SOUNDING: CN-C-14 FIGURE A.72



PROFILES REPRESENT AVERAGE AND \pm ONE STANDARD DEVIATION.



PROJECT NO.:

79-153

USGS CPT-SPT

PROFILE AVERAGE
CONE PENETROMETER TEST

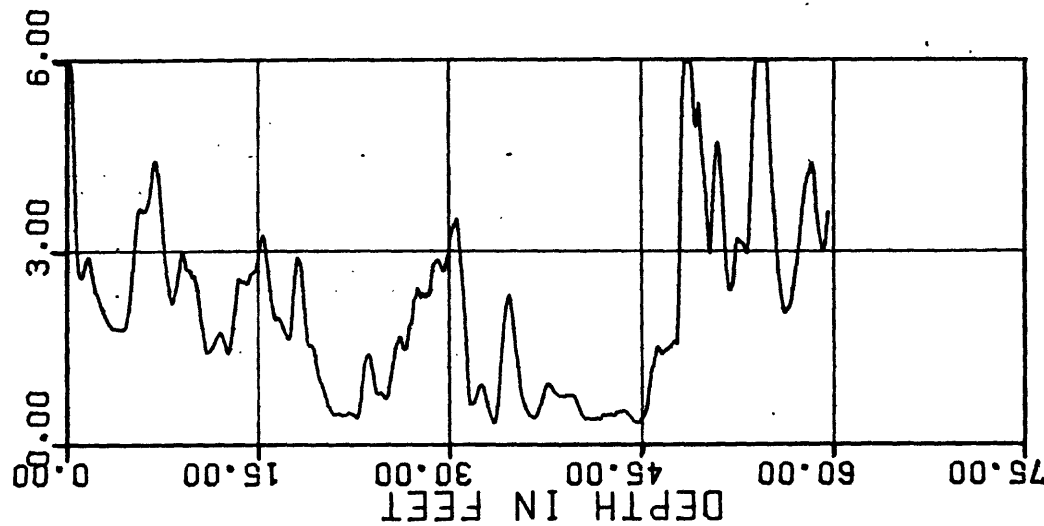
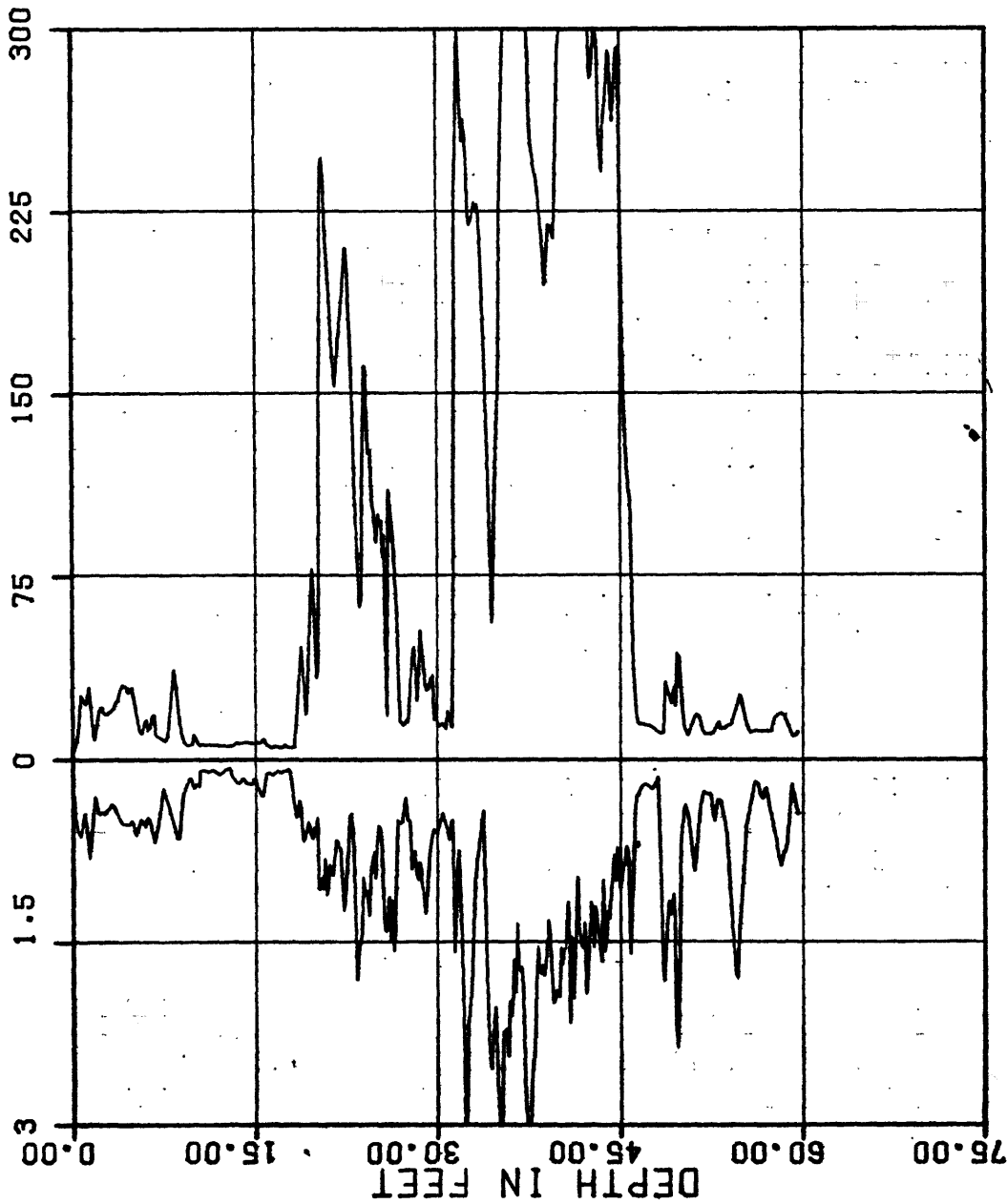
INSTRUMENT:

SOUNDING: SAN JOSECN FIGURE A.73

FRICITION RESISTANCE, TSF

CONE RESISTANCE, TSF

FRICITION RATIO, %



PROJECT NO.:

78-153

USGS CPT-SPT

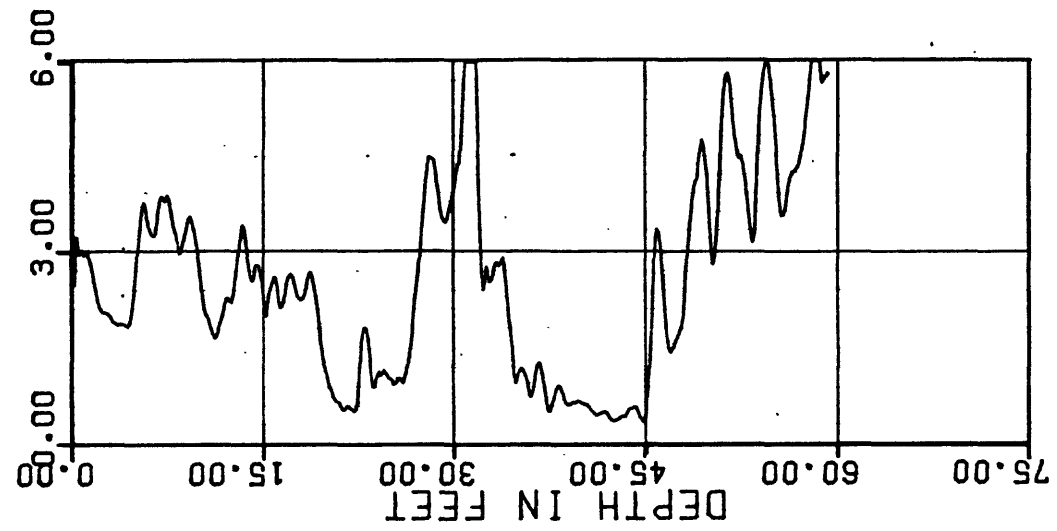
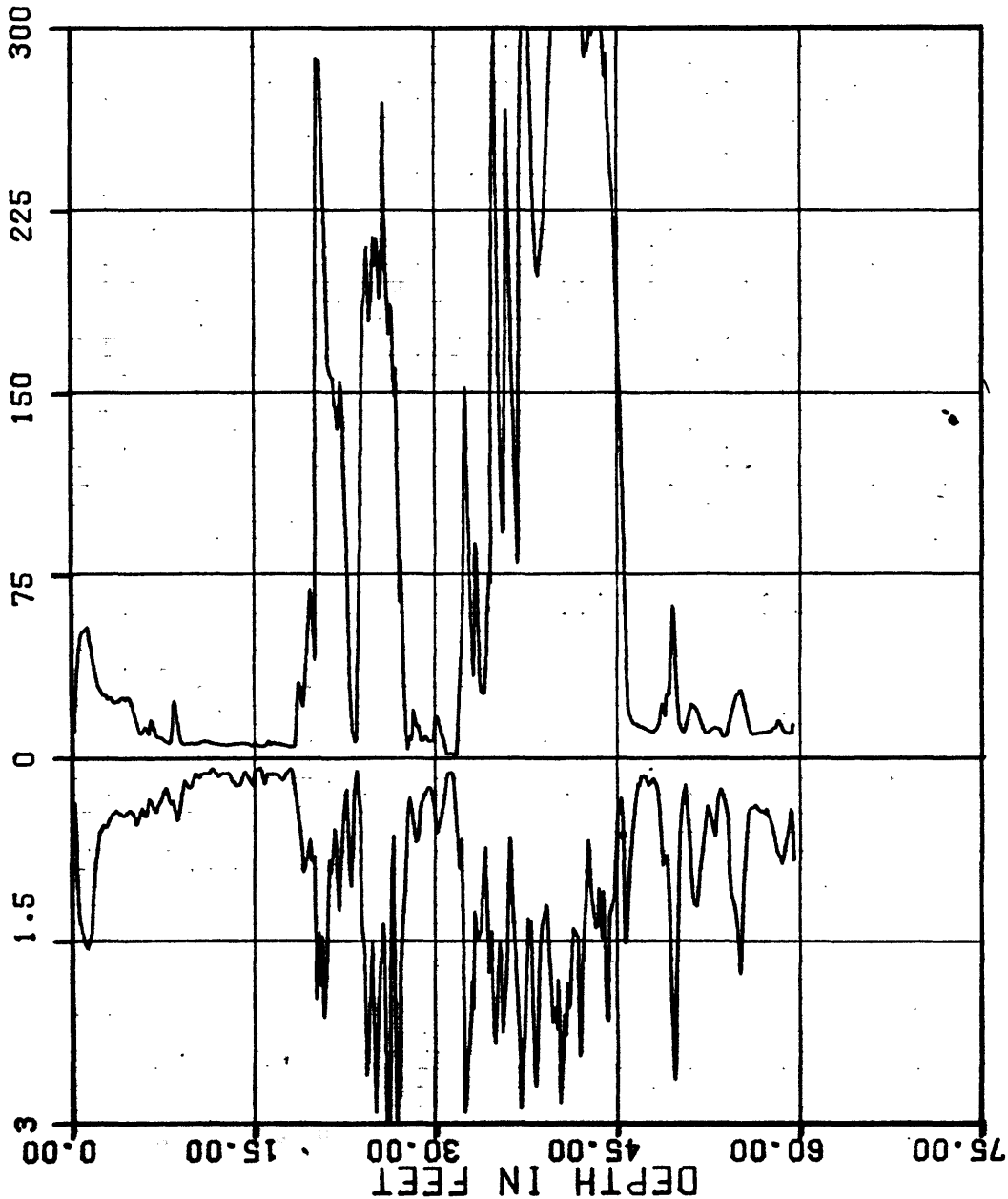
CONE PENETROMETER TEST

INSTRUMENT: F5CK-230 SOUNDING: CS-C-1

FIGURE A.74

FRICITION RESISTANCE, TSF

FRICITION RATIO, %



PROJECT NO.:

79-153

USGS CPT-SPT

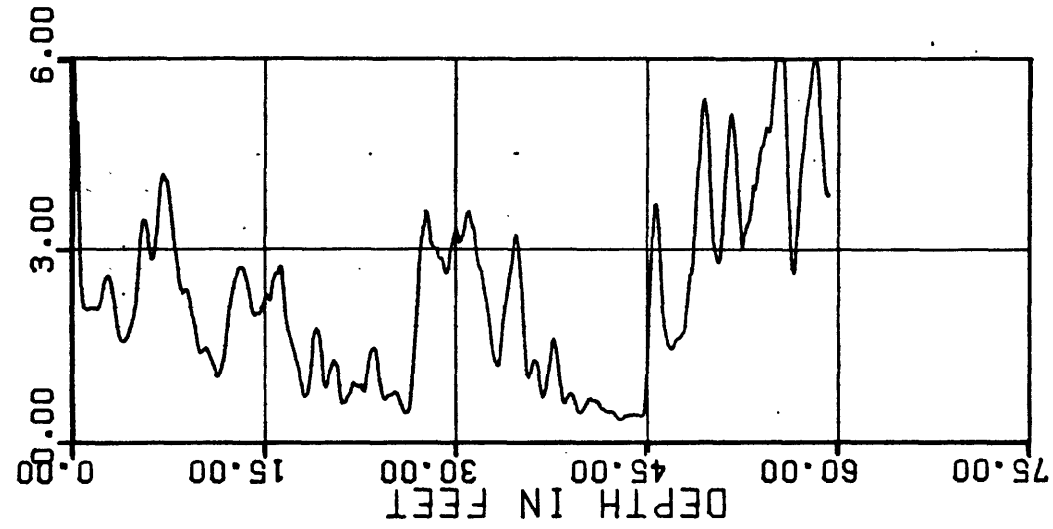
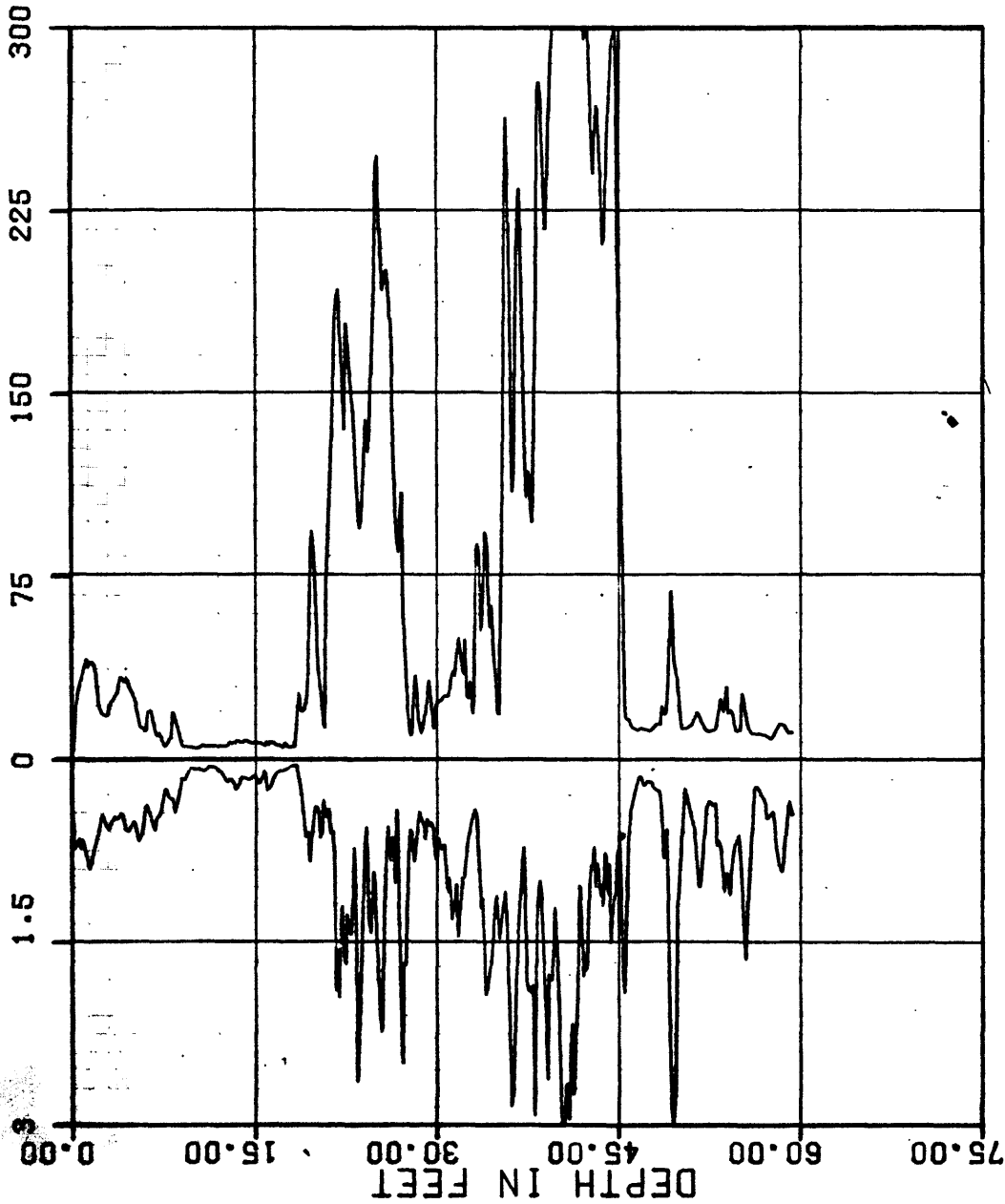
CONE PENETROMETER TEST

INSTRUMENT: F5CK-230 SOUNING: CS-C-2

FIGURE A.75

FRICION RESISTANCE, TSF

FRICION RATIO, %



PROJECT NO.:

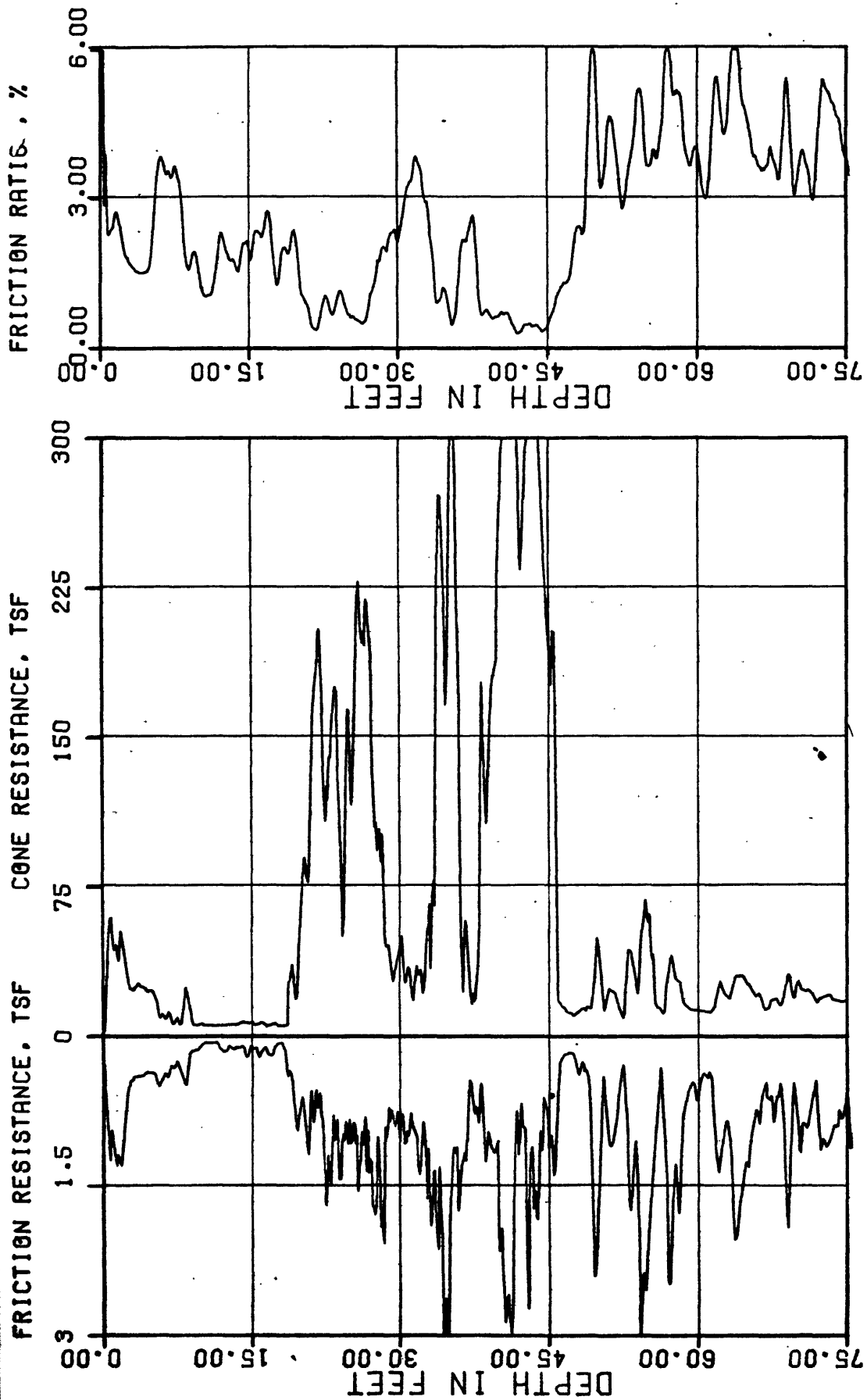
79 153

USGS CPT-SPT

CONE PENETROMETER TEST

INSTRUMENT: F5CK-230 SOUNING: CS-C3

FIGURE A.76



79-153

PROJECT NO.:



USGS CPT-SPT

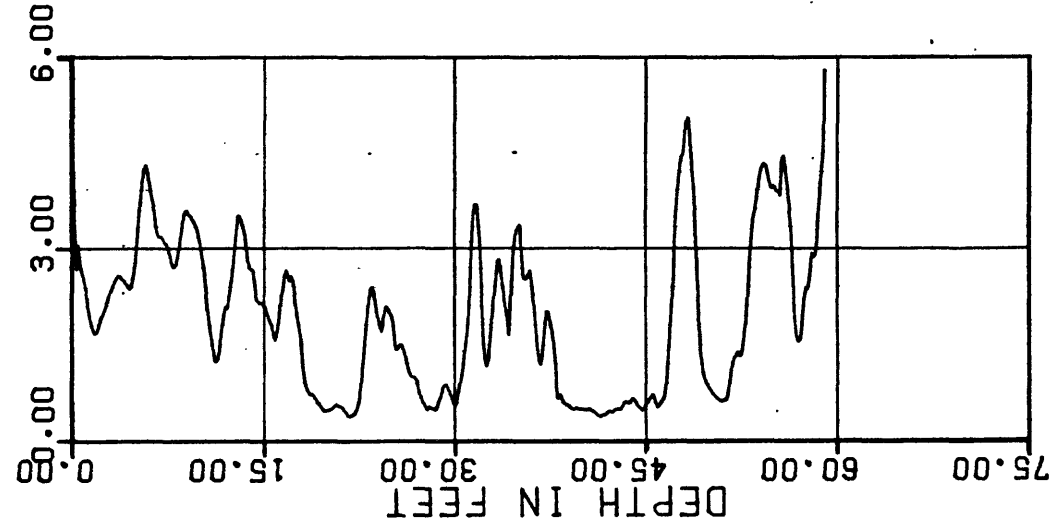
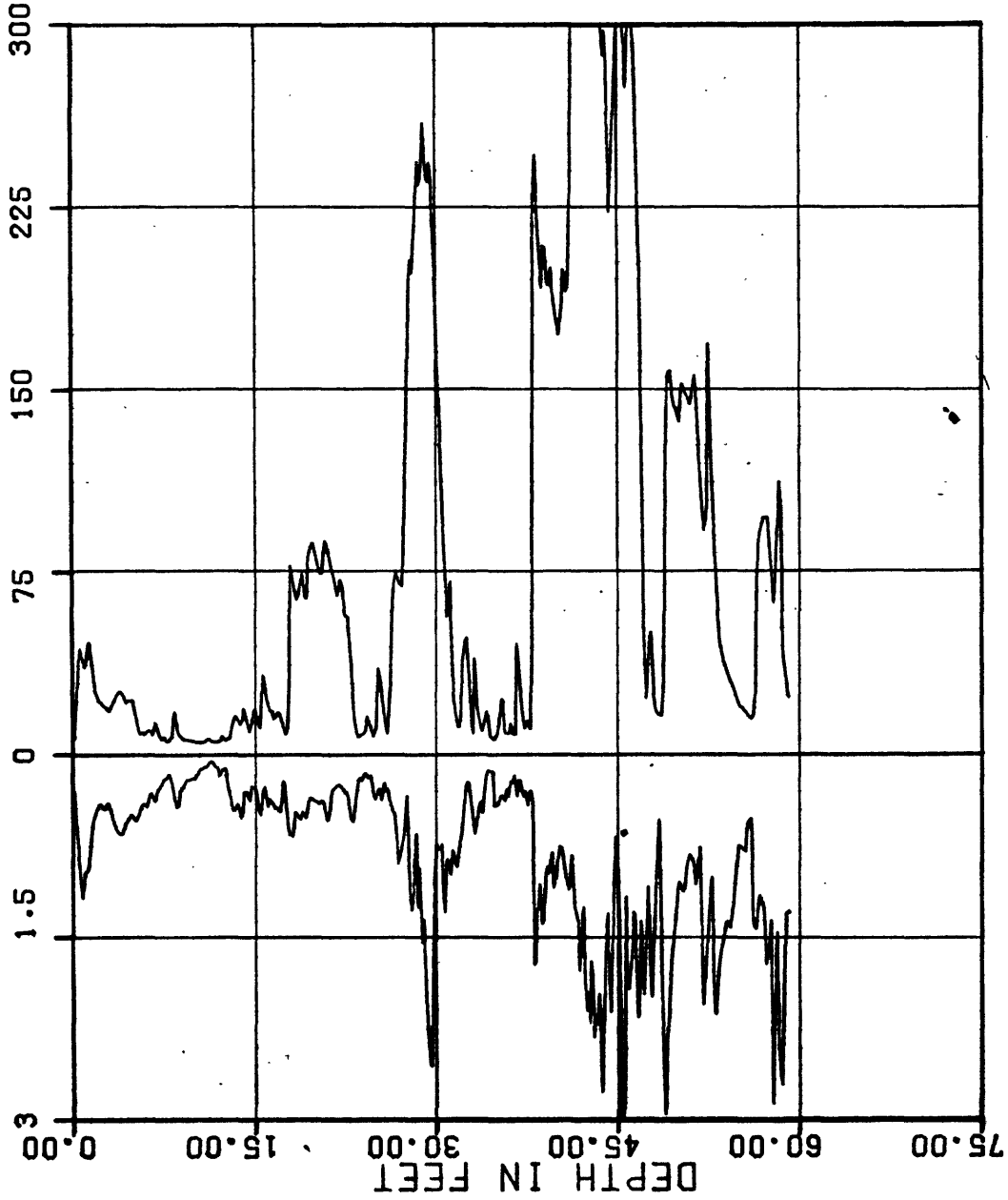
CONE PENETROMETER TEST

INSTRUMENT: F5CK-230 SOUNDING: CS-C-4

FIGURE A.77

FRICION RESISTANCE, TSF

FRICION RATIO, %



PROJECT NO.:

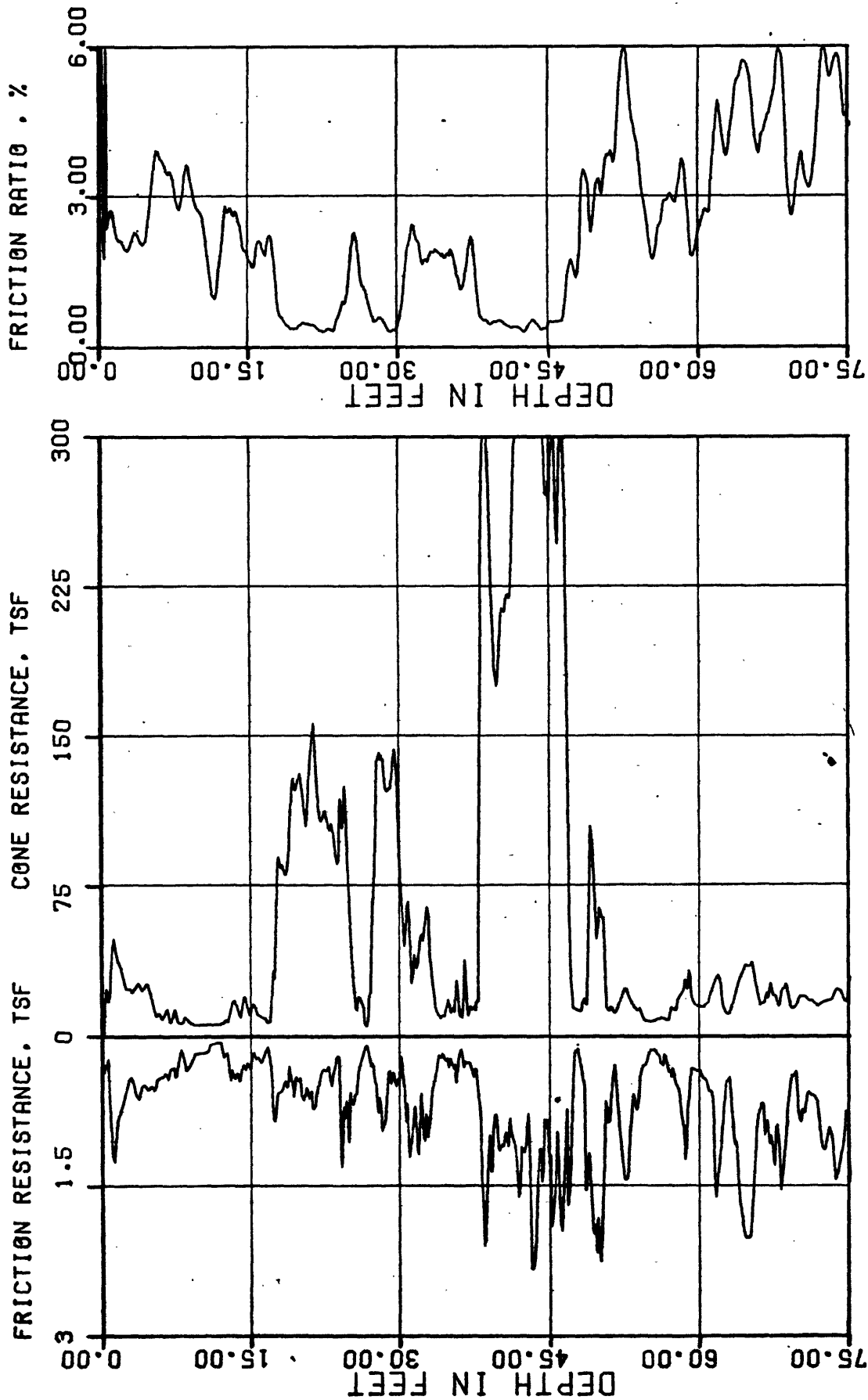
79-153

USGS CPT-SPT

CONE PENETROMETER TEST

INSTRUMENT: F5CK-230 SOUNING: CS-C-5

FIGURE A.78



79-153

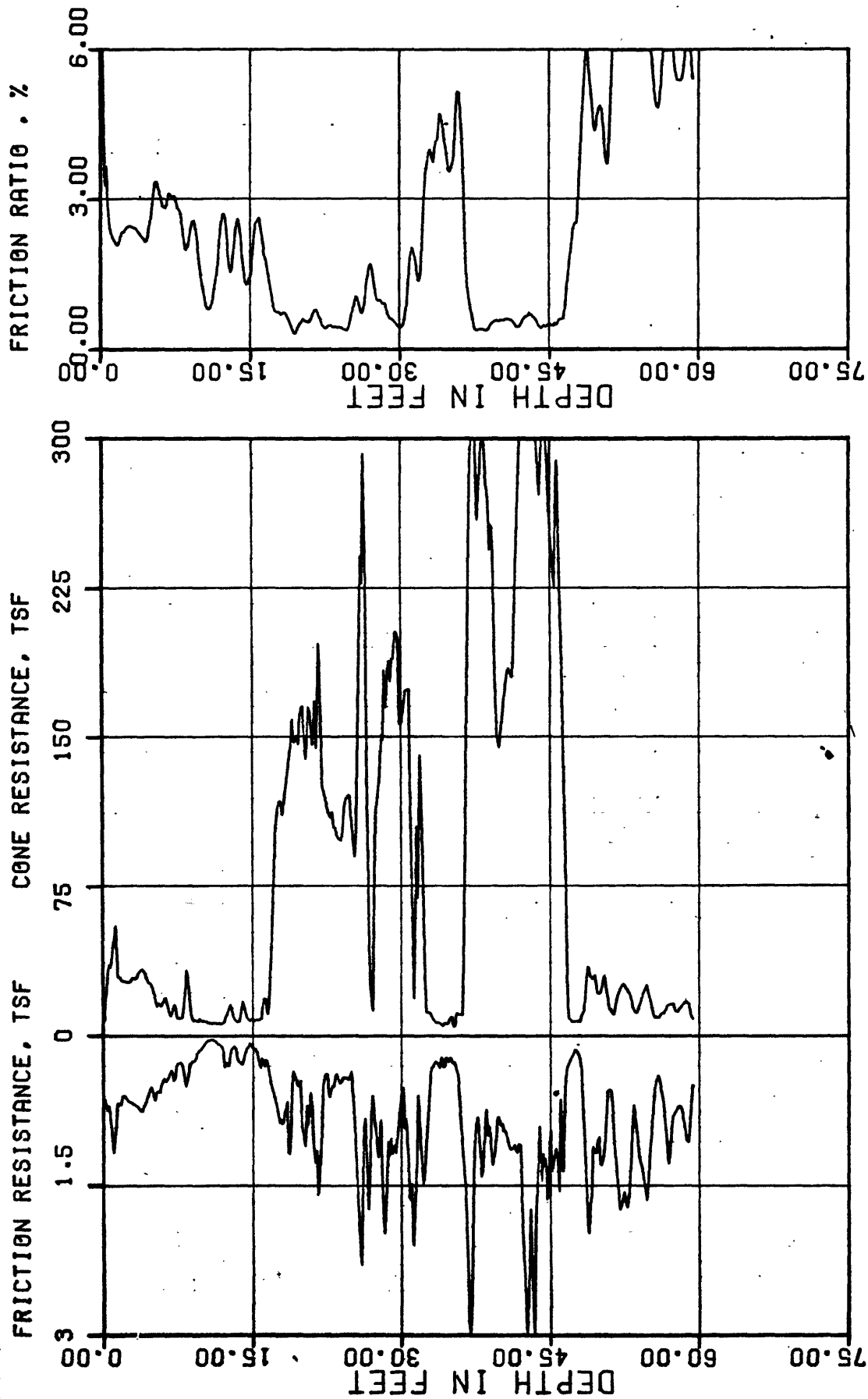
PROJECT NO.:



USGS CPT-SPT

CONE PENETROMETER TEST

INSTRUMENT: F5CK-230 SOUNDING: CS-C-6 FIGURE A.79



PROJECT NO.:

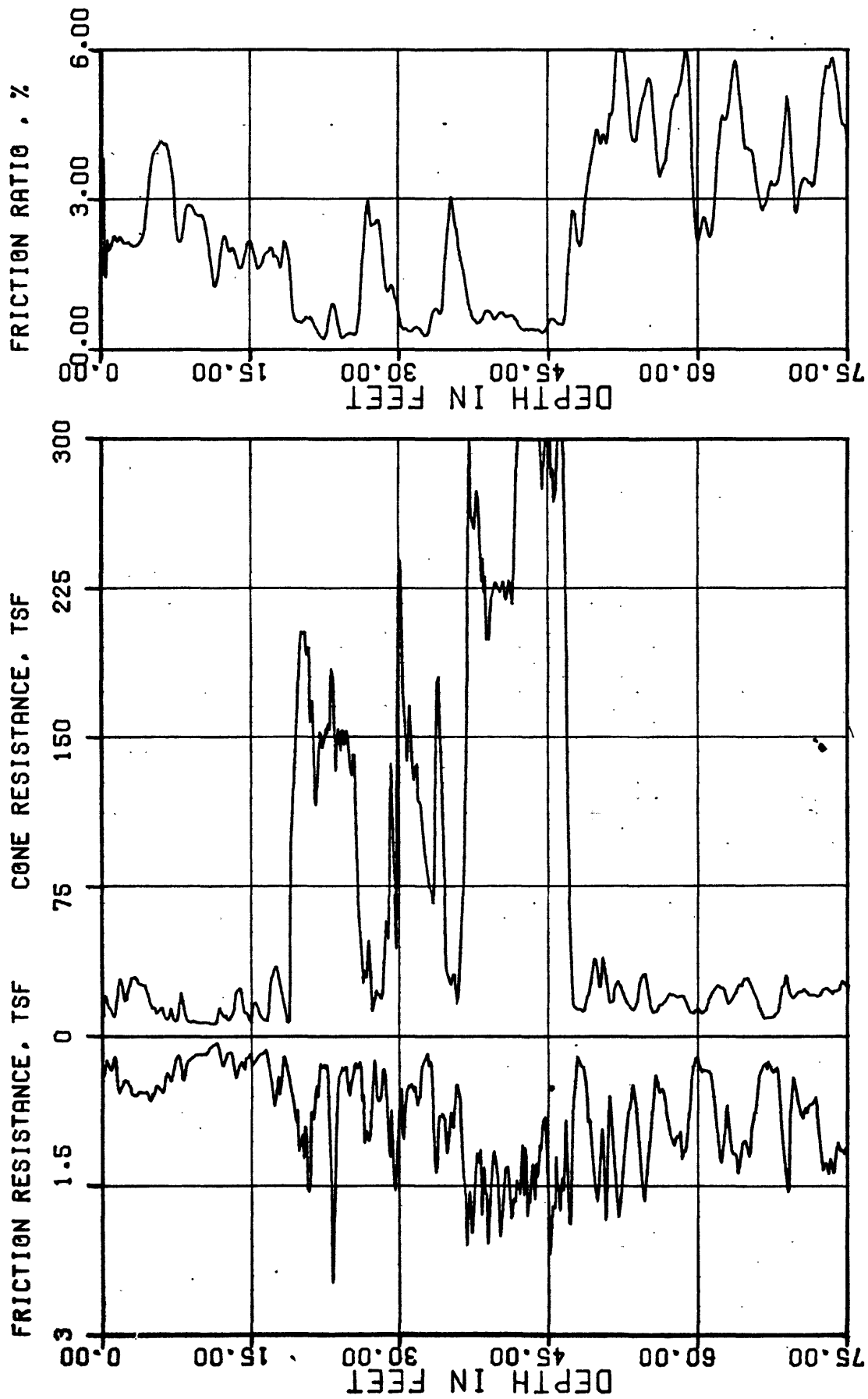
79-153

USGS CPT-SPT

CONE PENETROMETER TEST

INSTRUMENT: F5CK-230 SOUNING: CS-C-7

FIGURE A.80



PROJECT NO.:

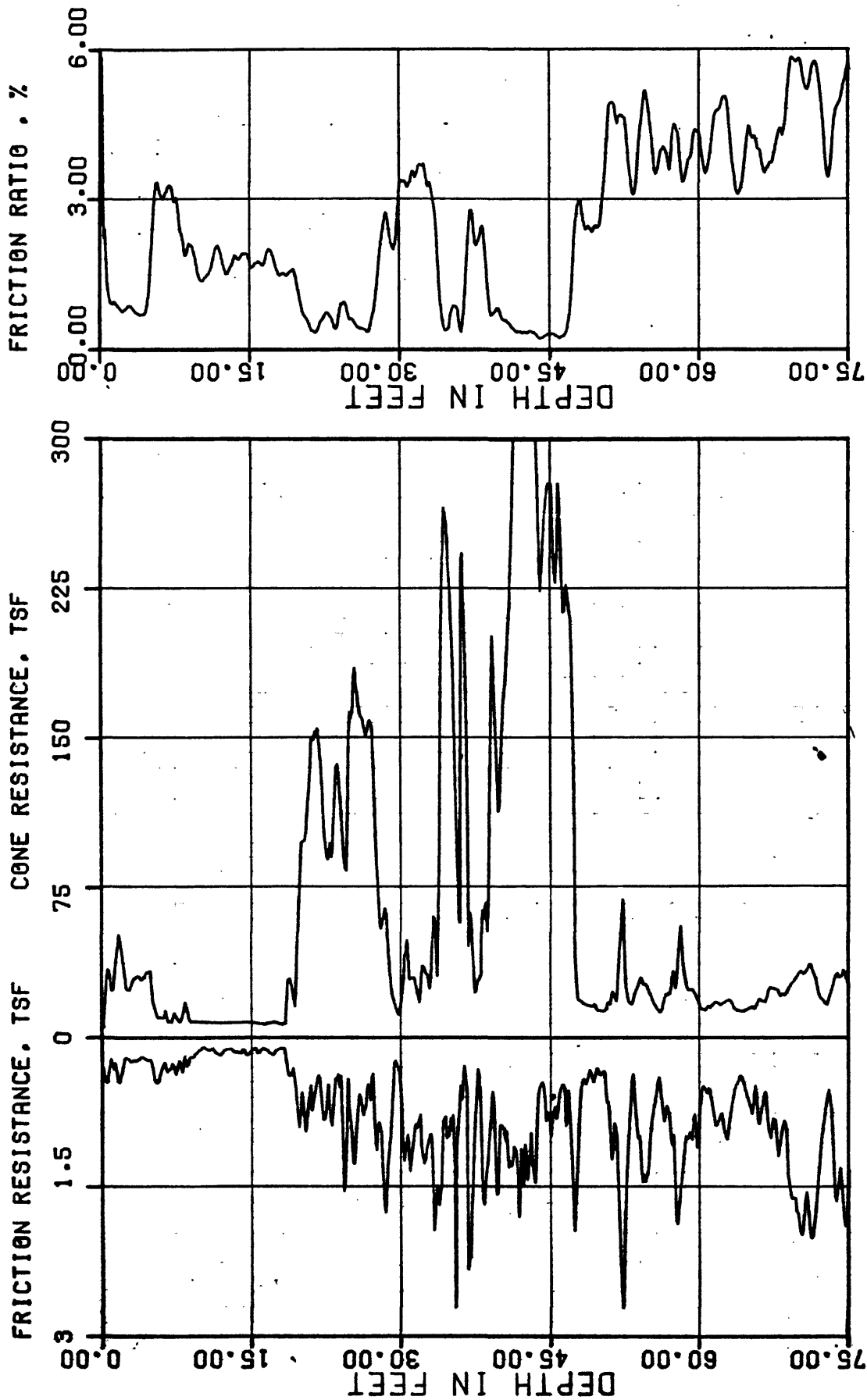
79-153

USGS CPT-SPT

CONE PENETROMETER TEST

INSTRUMENT: F5CK-230 SOUNDING: CS-C-8

FIGURE A.81



PROJECT NO.: 79-153

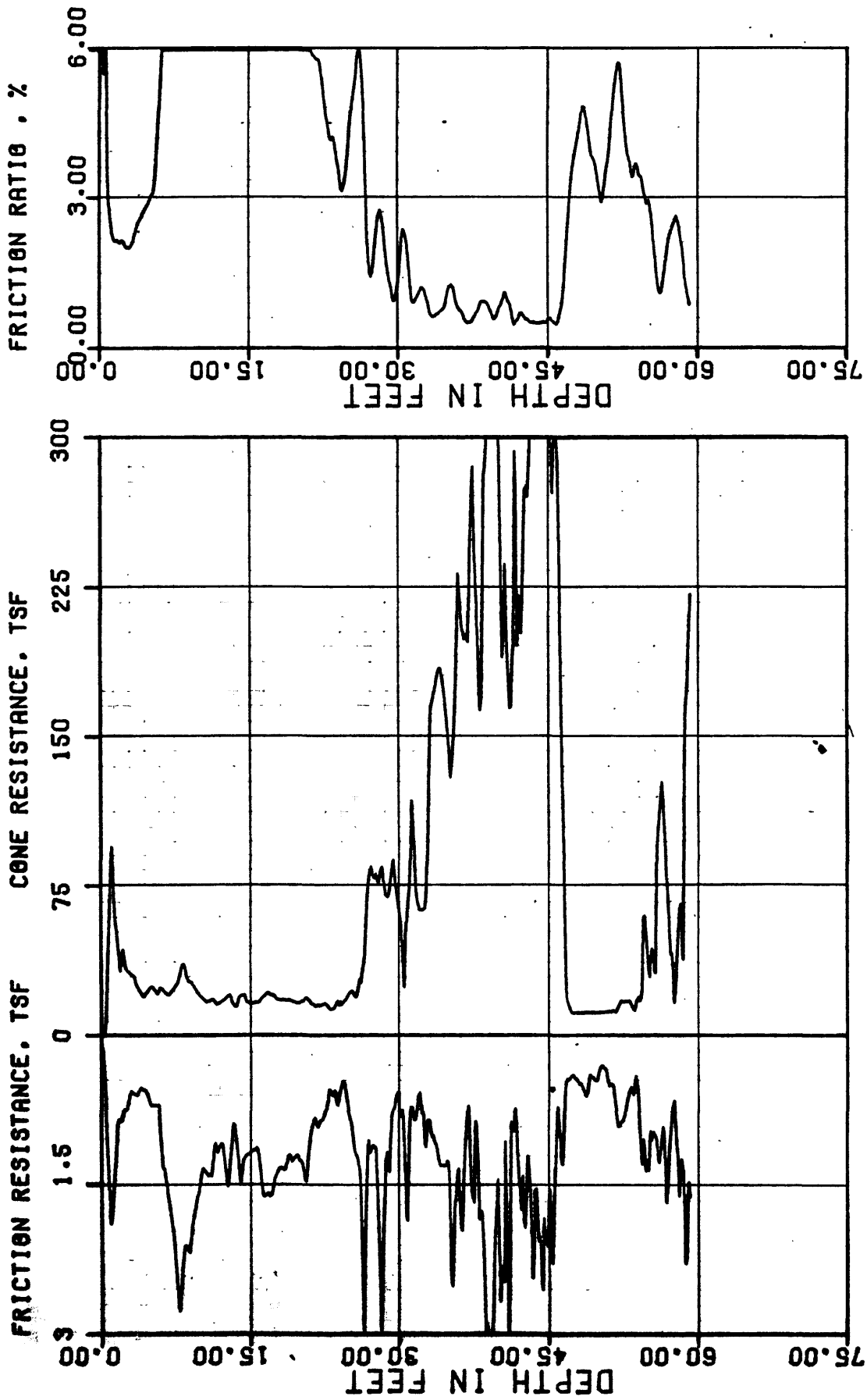


USGS CPT-SPT

CONE PENETROMETER TEST

INSTRUMENT: F5CK-230 SOUNDING: CS-C-9

FIGURE A.82

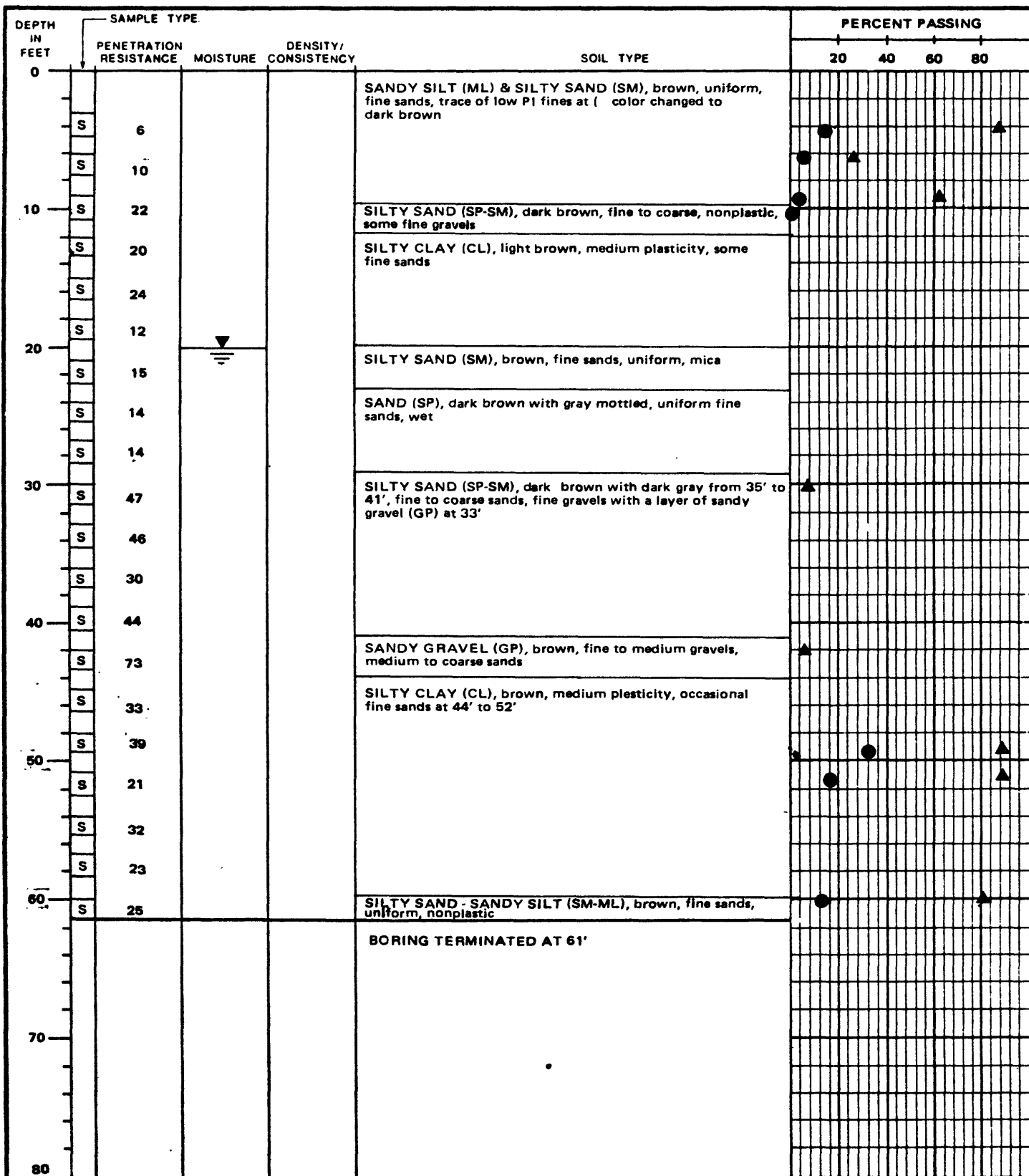


PROJECT NO.:

79-153

USGS CPT-SPT

CONE PENETROMETER TEST



ELEVATION: DATE DRILLED: 11-16-79
EQUIPMENT USED: 5 7/8" ROTARY WASH
WATER LEVEL: 20'

[S] STANDARD HAMMER SPLIT SPOON SAMPLE ▲ #200 SIEVE
[T] TRIP HAMMER SPLIT SPOON SAMPLE ● 0.002 mm

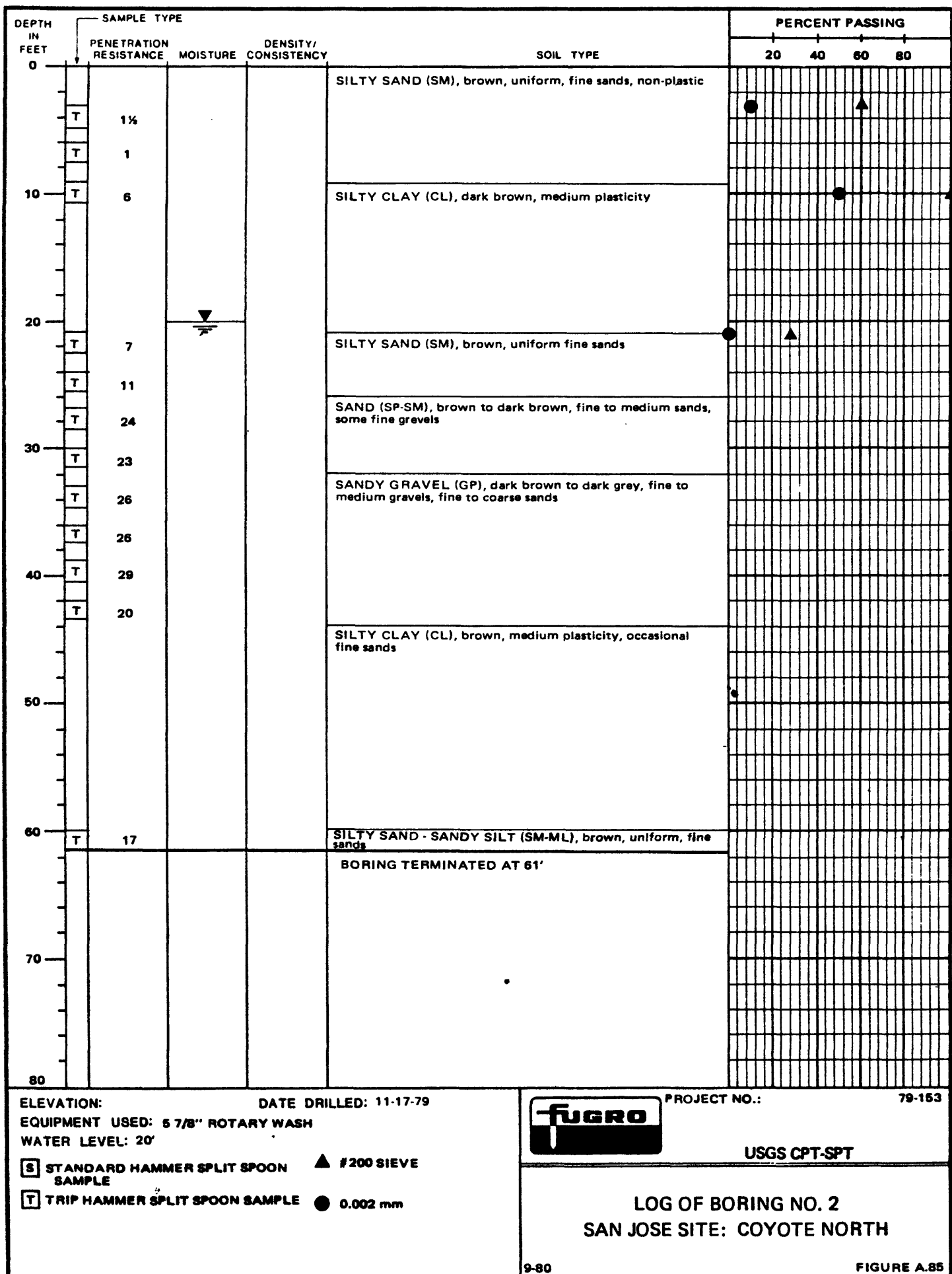


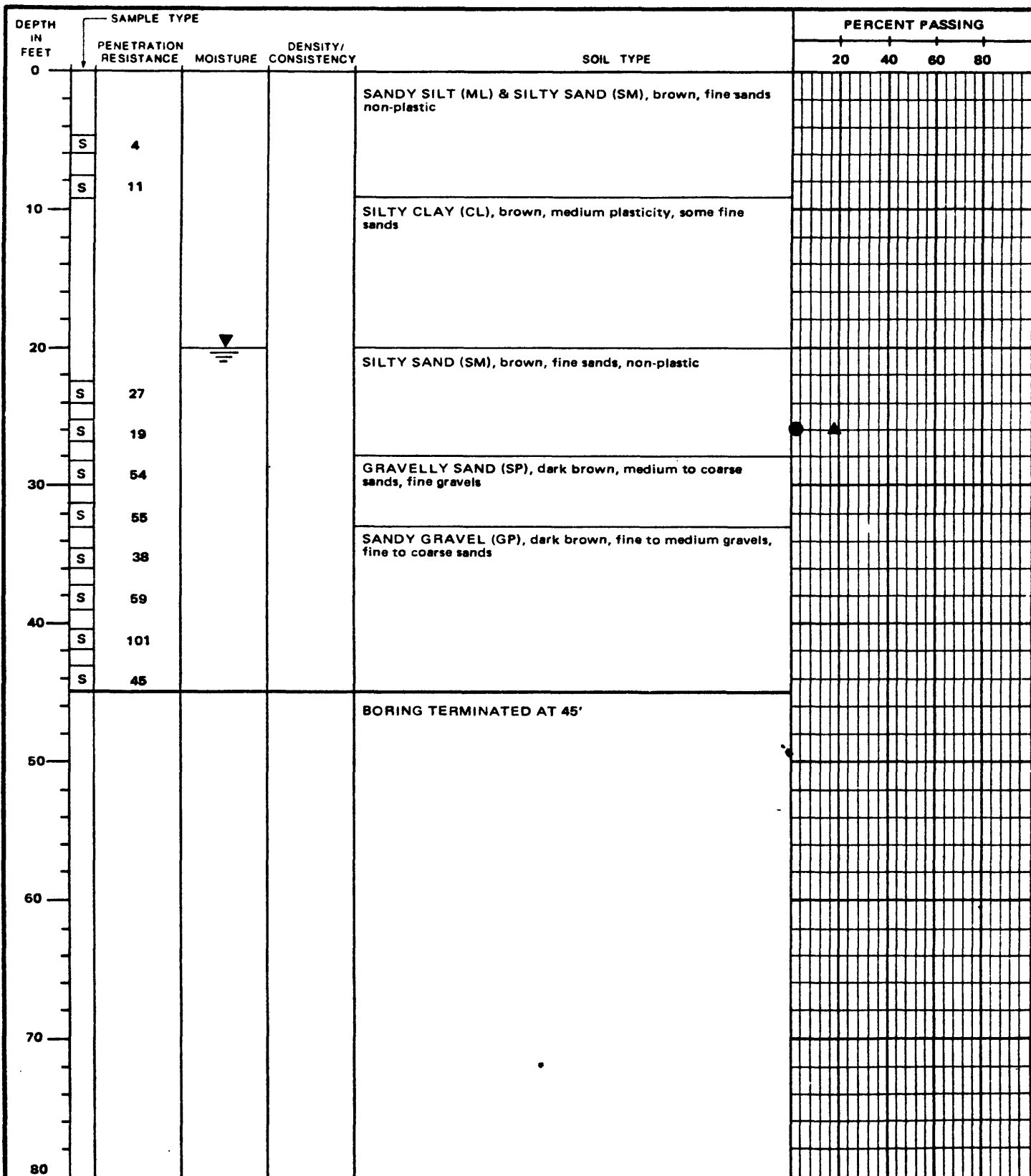
PROJECT NO.:

79-153

USGS CPT-SPT

LOG OF BORING NO. 1
SAN JOSE SITE: COYOTE NORTH





ELEVATION: DATE DRILLED: 11-17-79
 EQUIPMENT USED: 5 7/8" ROTARY WASH
 WATER LEVEL: 20'

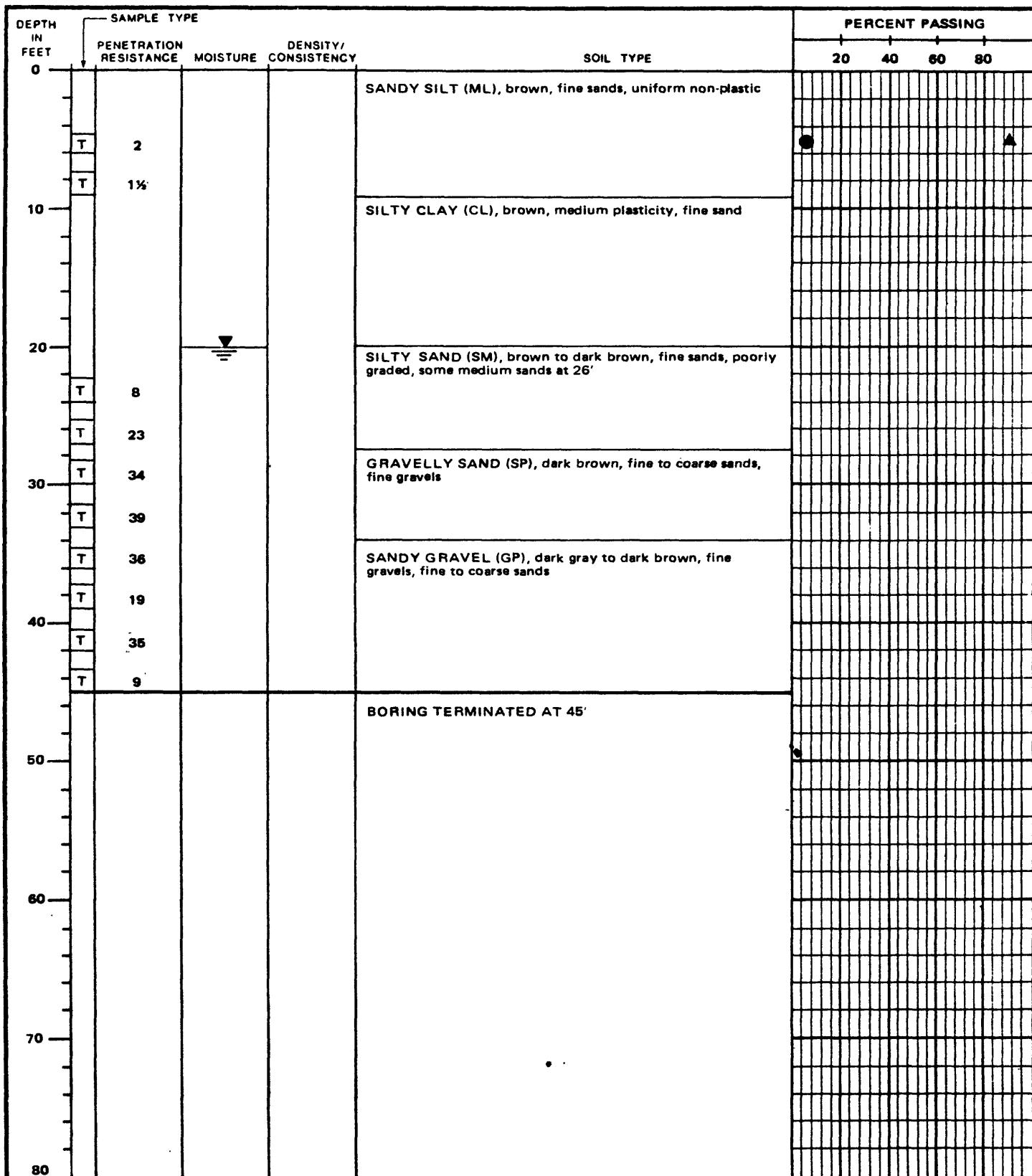
[S] STANDARD HAMMER SPLIT SPOON SAMPLE ▲ #200 SIEVE
 [T] TRIP HAMMER SPLIT SPOON SAMPLE ● 0.002 mm



PROJECT NO.: 79-153

USGS CPT-SPT

LOG OF BORING NO. 3
 SAN JOSE SITE: COYOTE NORTH



ELEVATION: DATE DRILLED: 11-15-79
EQUIPMENT USED: 5 7/8" ROTARY WASH
WATER LEVEL: 20'

[S] STANDARD HAMMER SPLIT SPOON SAMPLE ▲ #200 SIEVE
[T] TRIP HAMMER SPLIT SPOON SAMPLE ● 0.002 mm

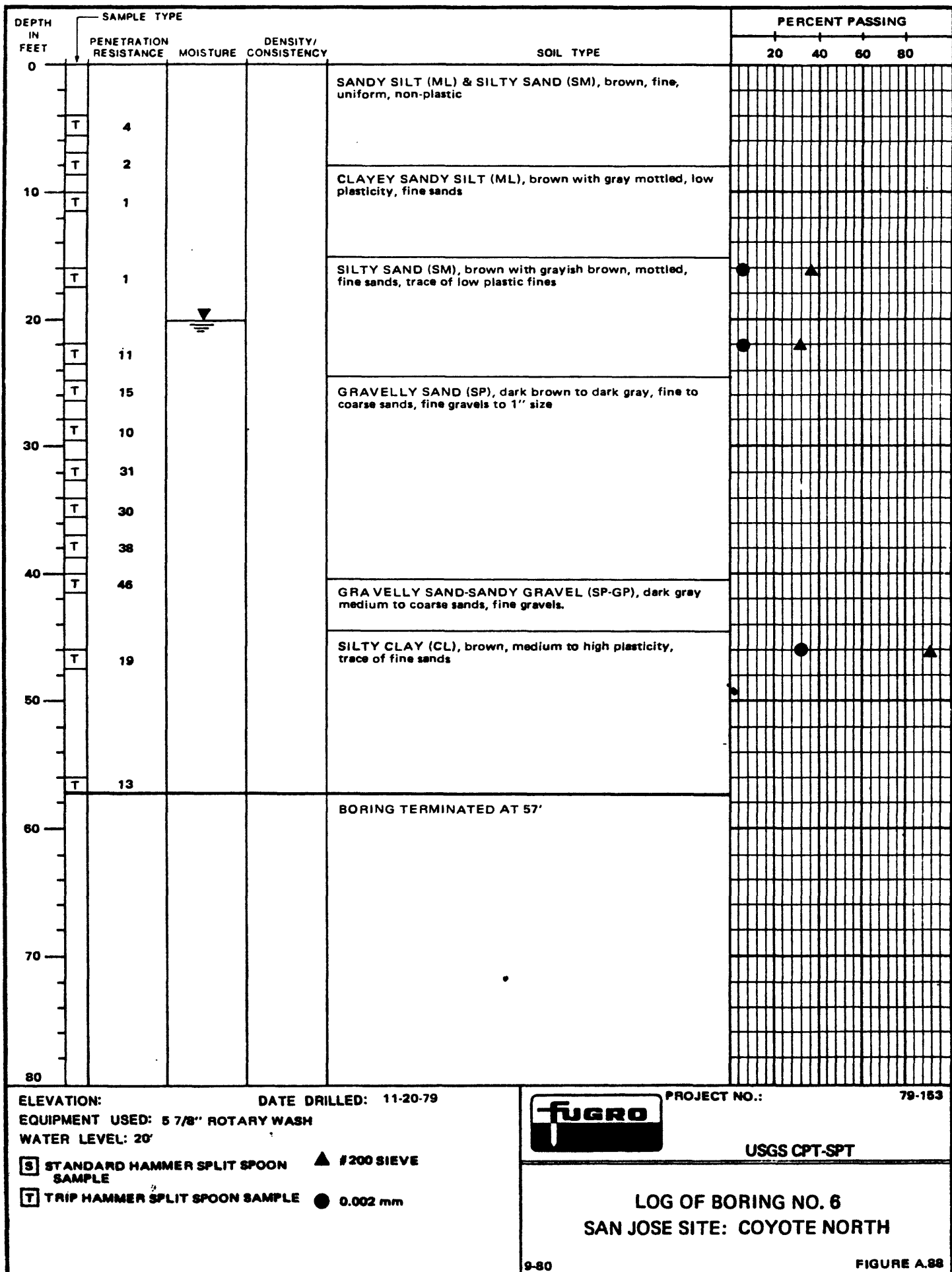


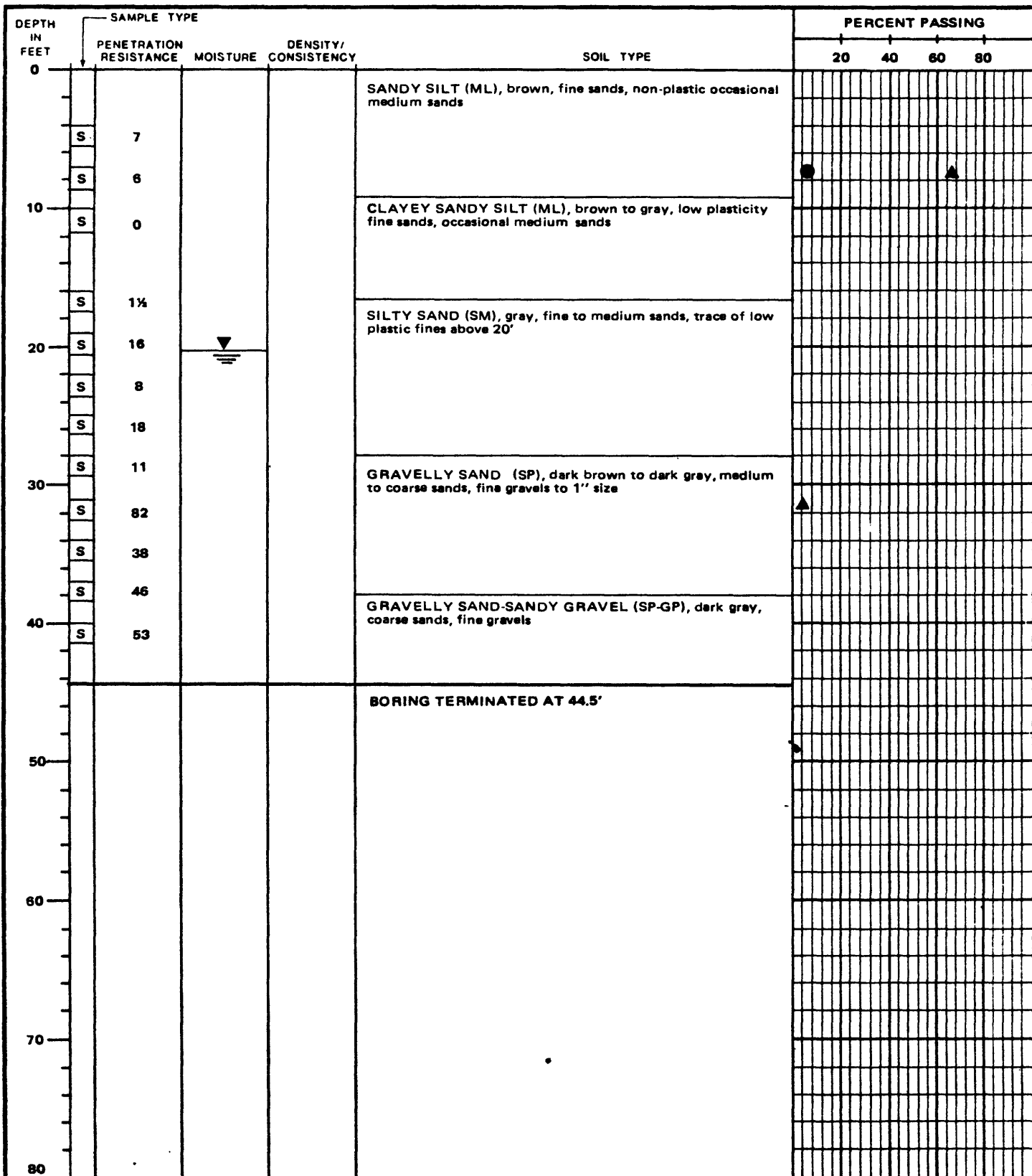
PROJECT NO.:

79-153

USGS CPT-SPT

LOG OF BORING NO. 4
SAN JOSE SITE: COYOTE NORTH





ELEVATION:

DATE DRILLED: 11-21-79

EQUIPMENT USED: 5 7/8" ROTARY WASH

WATER LEVEL: 20'

[S] STANDARD HAMMER SPLIT SPOON
SAMPLE

▲ #200 SIEVE

[T] TRIP HAMMER SPLIT SPOON SAMPLE

● 0.002 mm

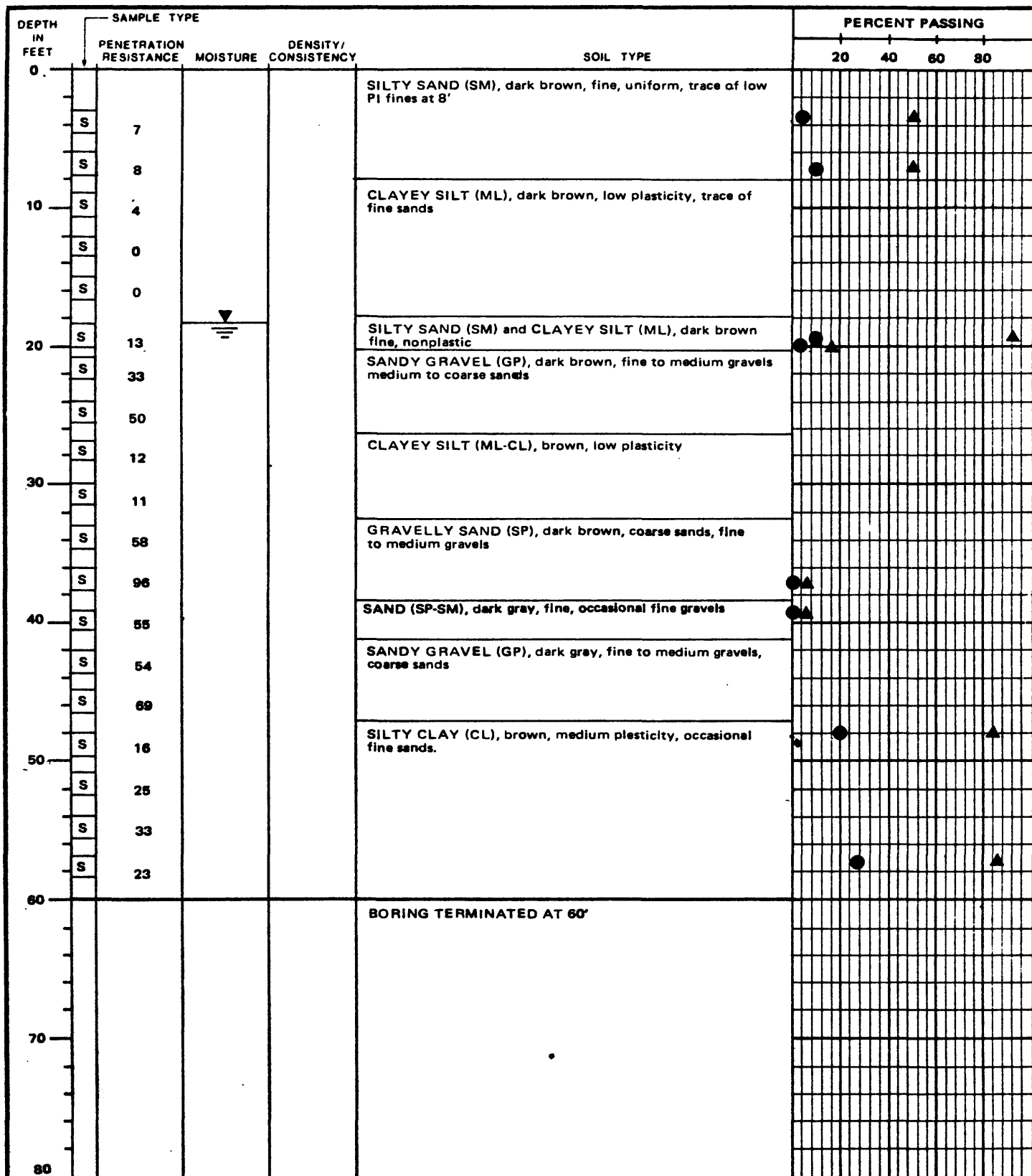


PROJECT NO.:

79-153

USGS CPT-SPT

LOG OF BORING NO. 8
SAN JOSE SITE: COYOTE NORTH



ELEVATION: DATE DRILLED: 11-19-79
EQUIPMENT USED: 8 7/8" ROTARY WASH
WATER LEVEL: 18'

[S] STANDARD HAMMER SPLIT SPOON SAMPLE ▲ #200 SIEVE
[T] TRIP HAMMER SPLIT SPOON SAMPLE ● 0.002 mm



PROJECT NO.:

79-153

USGS CPT-SPT

LOG OF BORING NO. 1
SAN JOSE SITE: COYOTE SOUTH

APPROVED BY: E-1 5-78
CHECKED BY:
DRAWN BY:

DEPTH IN FEET	SAMPLE TYPE			SOIL TYPE	PERCENT PASSING			
	PENETRATION RESISTANCE	MOISTURE	DENSITY/ CONSISTENCY		20	40	60	80
0				SILTY SAND (SM), dark brown, non-plastic, fine sands				
10	T	0		SILT (ML), brown with fine sands, low PI, color change to dark gray at 18'	●			▲
20	T	9	▼	SILTY SAND (SM), dark brown, fine, nonplastic				
	T	21		SANDY GRAVEL (GP), dark brown to dark gray, fine to medium gravel, medium to coarse sands				
	T	23						
30				CLAYEY SILT (ML-CL), brown, low plasticity				
	T	7		GRAVELLY SAND (SP), dark grayish brown, medium to coarse sands, fine gravels				
	T	25						
40	T	33		SAND (SP), dark gray, uniform fine to medium sands				
	T	43		SANDY GRAVEL (GP & GP-SP), dark grayish brown to dark gray, fine to medium gravels, medium to coarse sand				
	T	18						
50				BORING TERMINATED AT 46'				
60								
70								
80								

ELEVATION:
EQUIPMENT USED: 5 7/8" ROTARY WASH
WATER LEVEL: 18'


DATE DRILLED: 11-19-79

3 STANDARD HAMMER SPLIT SPOON SAMPLE

T TRIP HAMMER SPLIT SPOON SAMPLE

▲ #200 SIEVE

● 0.002 mm

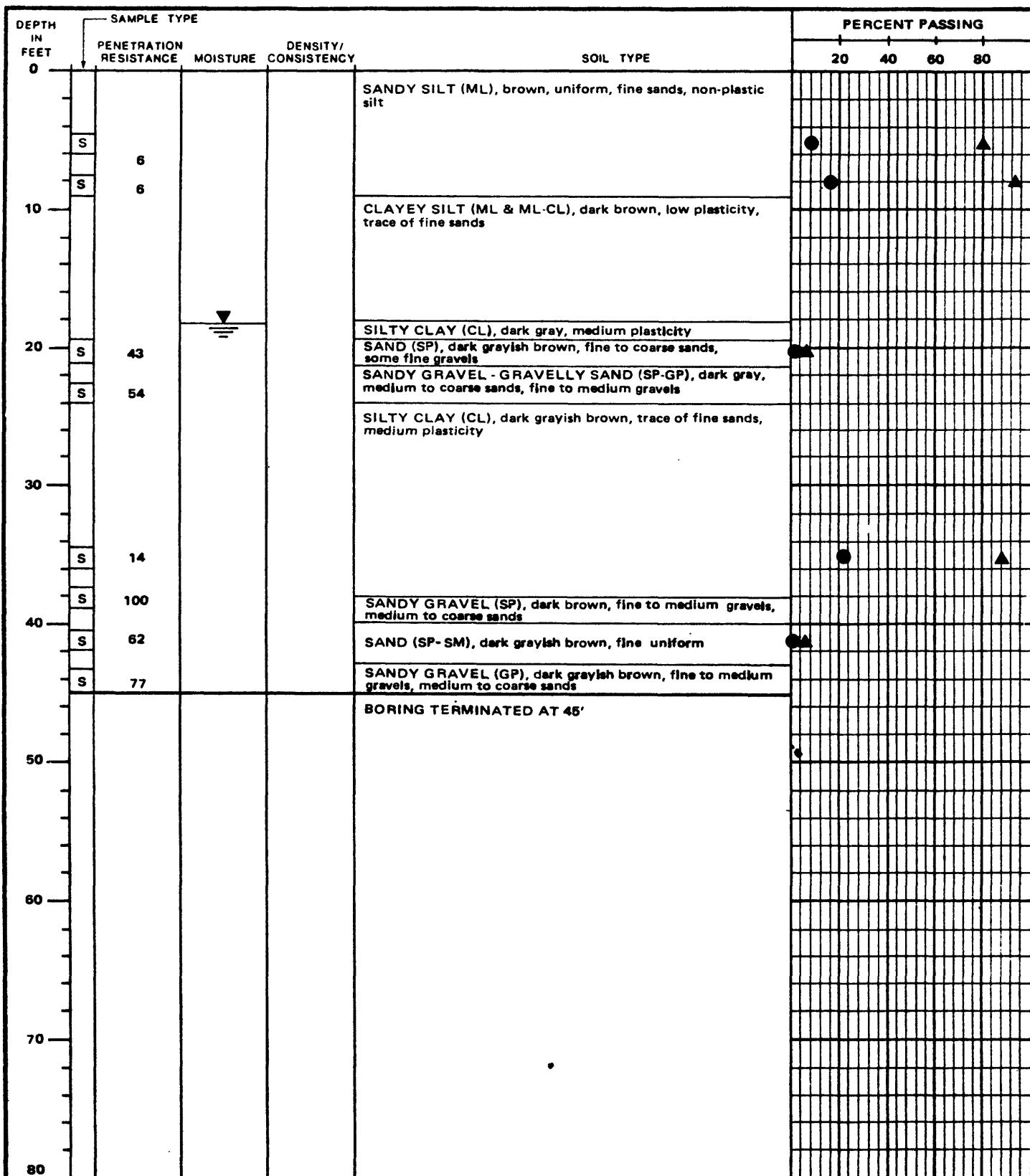
PROJECT NO.: 79-153

USGS CPT-SPT

LOG OF BORING NO. 2
SAN JOSE SITE: COYOTE SOUTH

9-80

FIGURE A.91



ELEVATION: DATE DRILLED: 11-19-79
 EQUIPMENT USED: 5 7/8" ROTARY WASH
 WATER LEVEL: 18'

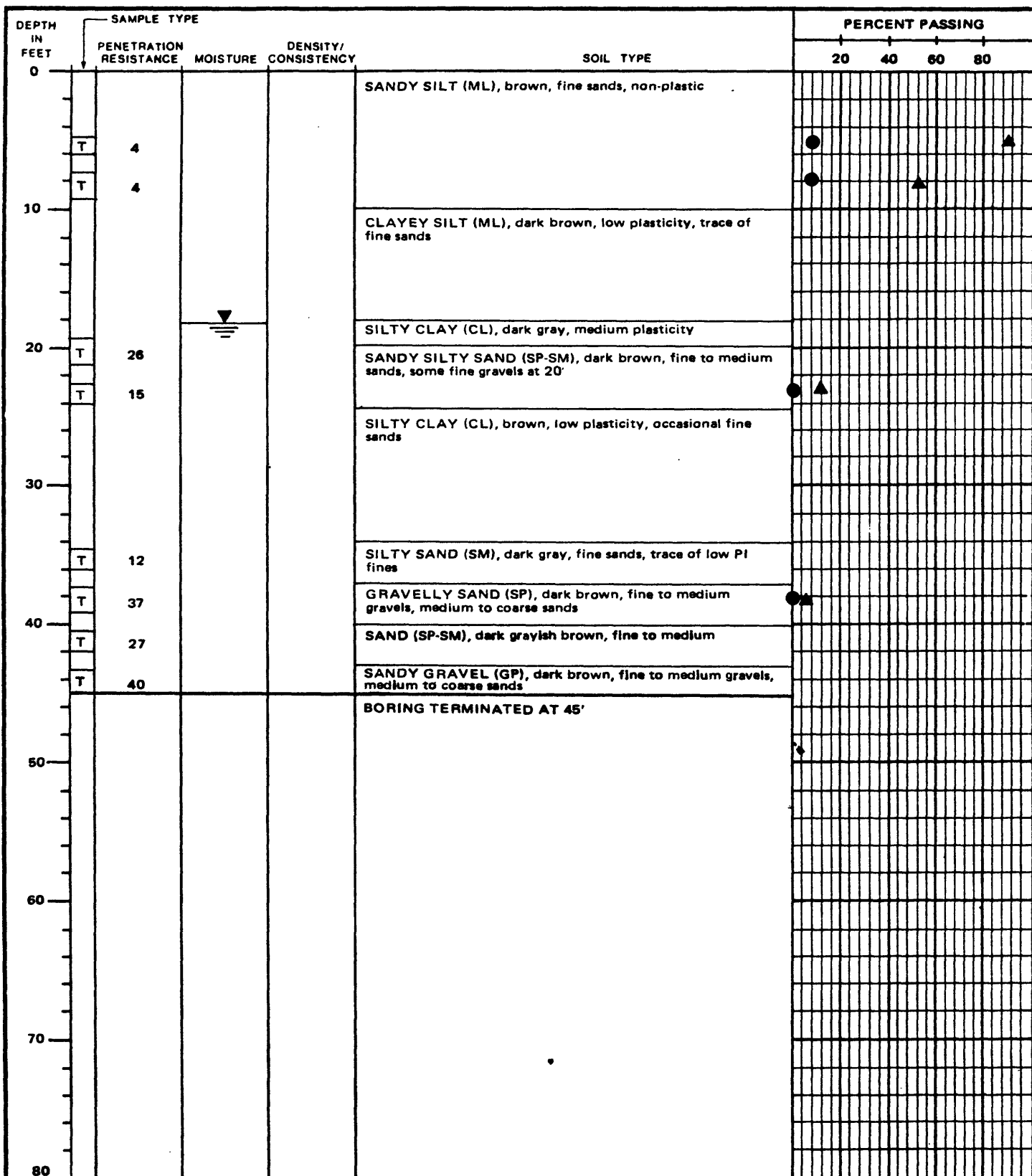
[S] STANDARD HAMMER SPLIT SPOON SAMPLE ▲ #200 SIEVE
 [T] TRIP HAMMER SPLIT SPOON SAMPLE ● 0.002 mm



PROJECT NO.: 79-153

USGS CPT-SPT

LOG OF BORING NO. 7
 SAN JOSE SITE: COYOTE SOUTH



ELEVATION: DATE DRILLED: 11-20-79
 EQUIPMENT USED: 5 7/8" ROTARY WASH
 WATER LEVEL: 18'

[S] STANDARD HAMMER SPLIT SPOON SAMPLE ▲ #200 SIEVE
 [T] TRIP HAMMER SPLIT SPOON SAMPLE ● 0.002 mm



PROJECT NO.:

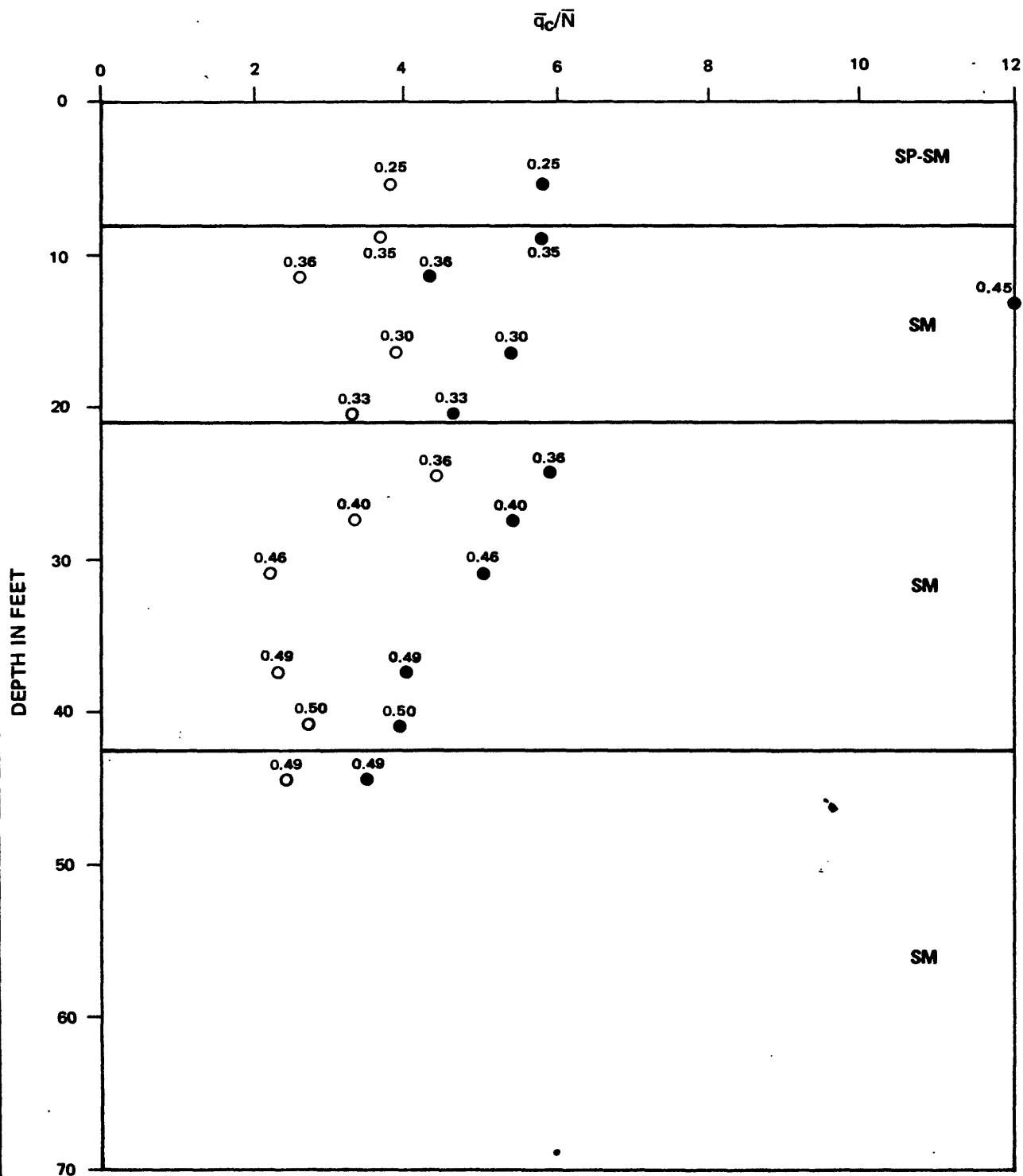
79-153

USGS CPT-SPT

LOG OF BORING NO. 8
 SAN JOSE SITE: COYOTE SOUTH

APPENDIX B

Approved by _____
Checked by _____
Drawn by _____
Compiled by _____



○ STANDARD

● TRIP

NUMBERS ON POINTS REPRESENT FRICTION RATIO, %



PROJECT NO.:

79-153

USGS CPT-SPT

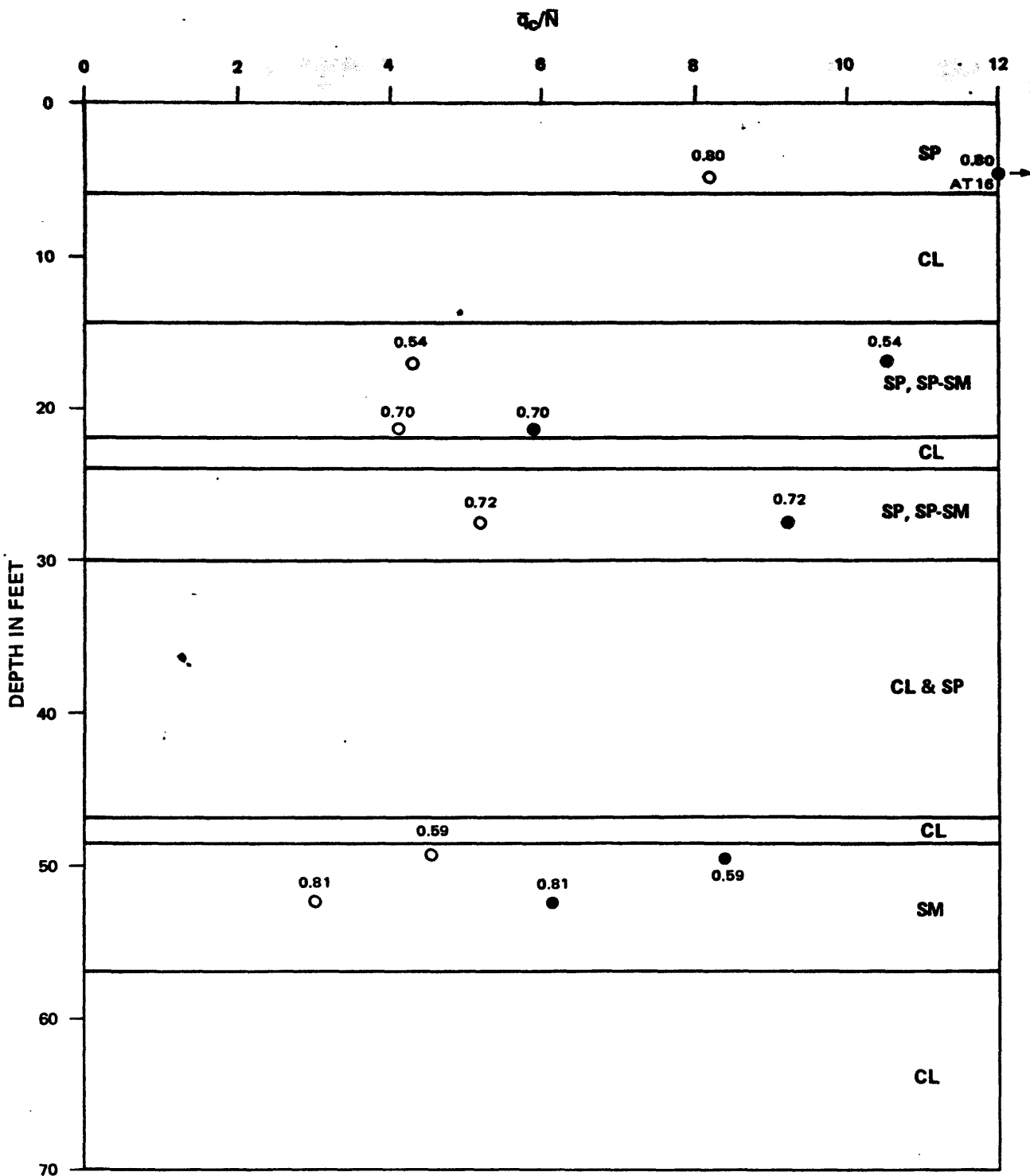
SAN DIEGO SITE: NAS NORTH ISLAND
 \bar{q}_c/\bar{N} VS DEPTH BY LAYER AVERAGES



79-153

SALINAS SITE
 \bar{q}_c/\bar{N} VS DEPTH BY LAYER AVERAGES

Approved by _____
Checked by _____
Drawn by _____
Compiled by _____

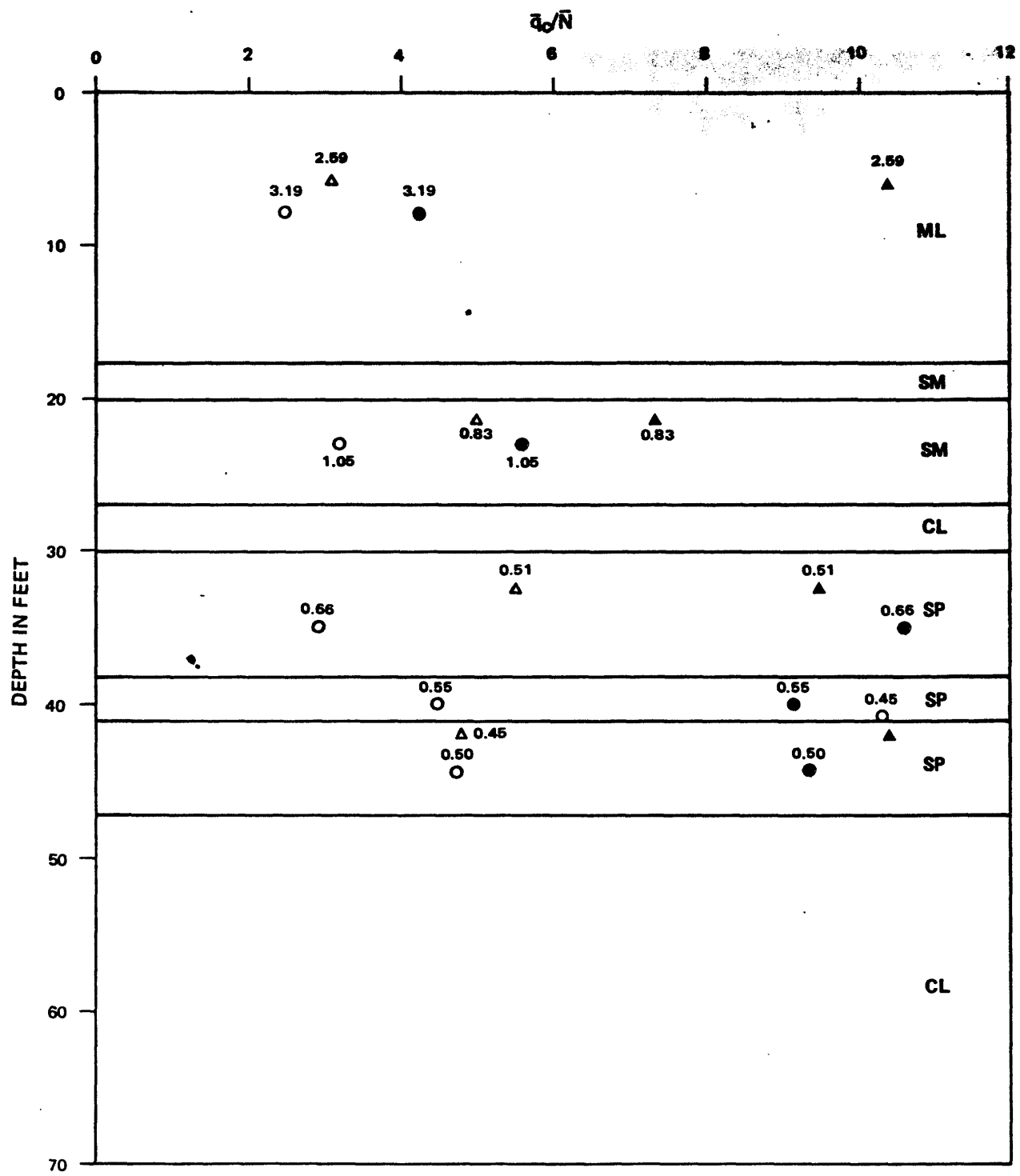


PROJECT NO.: 79-153

USGS CPT-SPT

MOSS LANDING SITE
 \bar{q}_c/N VS DEPTH BY LAYER AVERAGES


Approved by _____
Checked by _____
Drawn by _____
Compiled by _____



SOUTH NORTH

- STANDARD △
- TRIP ▲

NUMBERS ON POINTS REPRESENT FRICTION RATIO, %



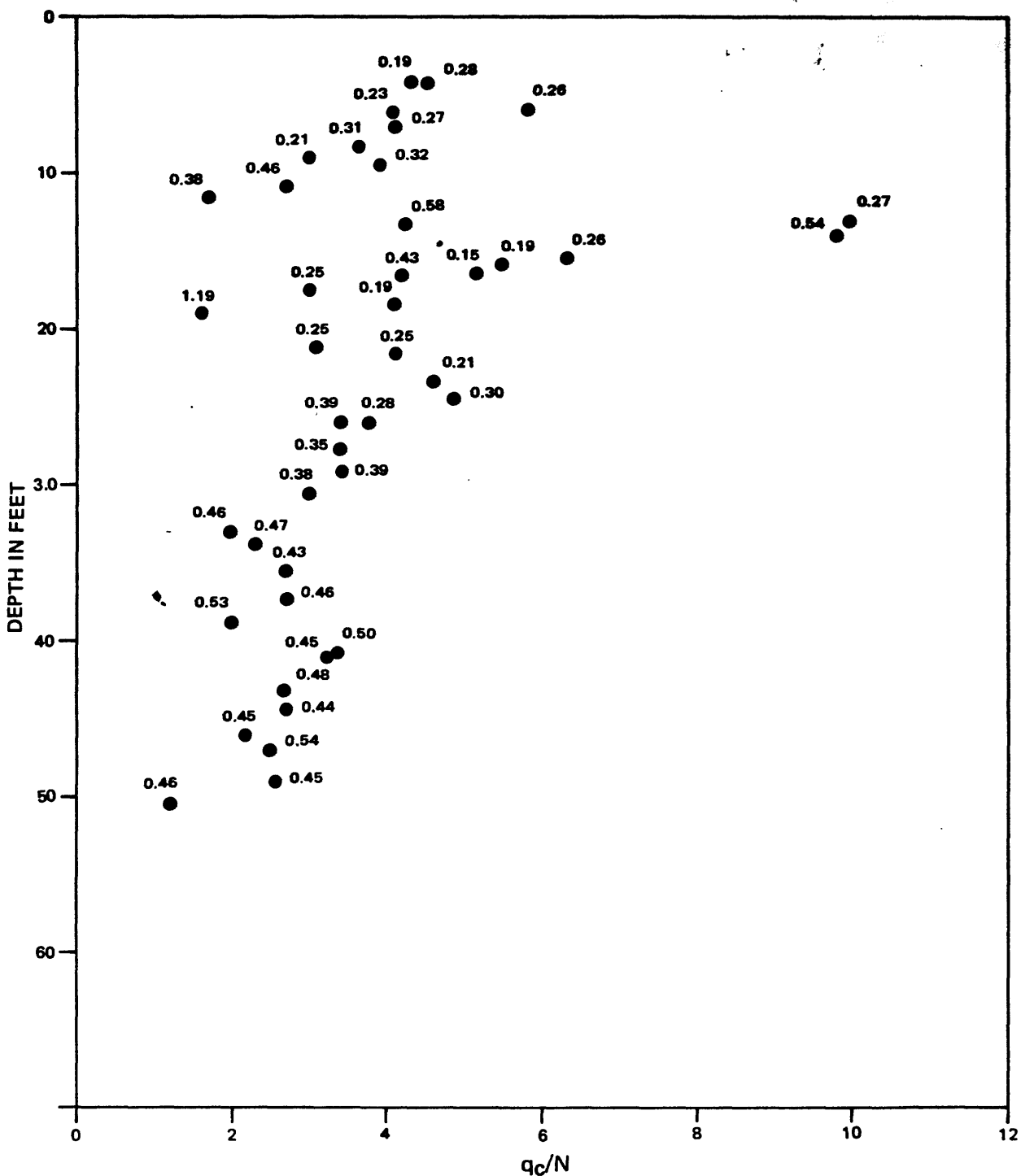
PROJECT NO.: 79-153

USGS CPT-SPT

SAN JOSE SITE:
COYOTE NORTH AND SOUTH
 q_c/N VS DEPTH BY LAYER AVERAGES

9-80

FIGURE B.4



NUMBERS ON POINTS REPRESENT FRICTION RATIO, %



PROJECT NO.:

79-153

USGS CPT-SPT

SAN DIEGO SITE: NAS NORTH ISLAND
 q_c/N VS DEPTH
 STANDARD HAMMER

9-80

FIGURE B.5

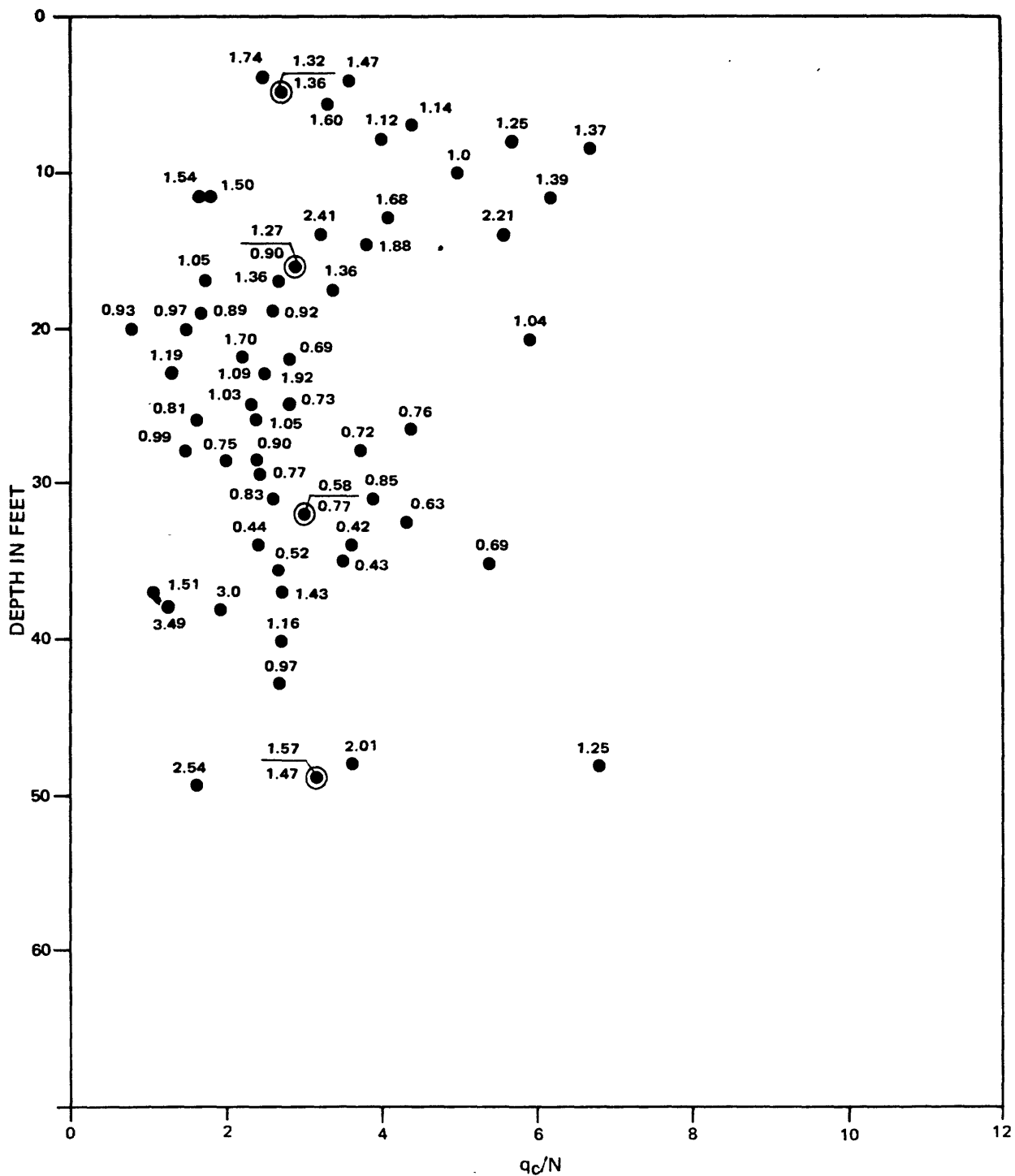
Approved by

Checked by

Drawn by

Compiled by

Approved by _____
Checked by _____
Drawn by _____
Compiled by _____



NUMBERS ON POINTS REPRESENT FRICTION RATIO, %



PROJECT NO.:

79-153

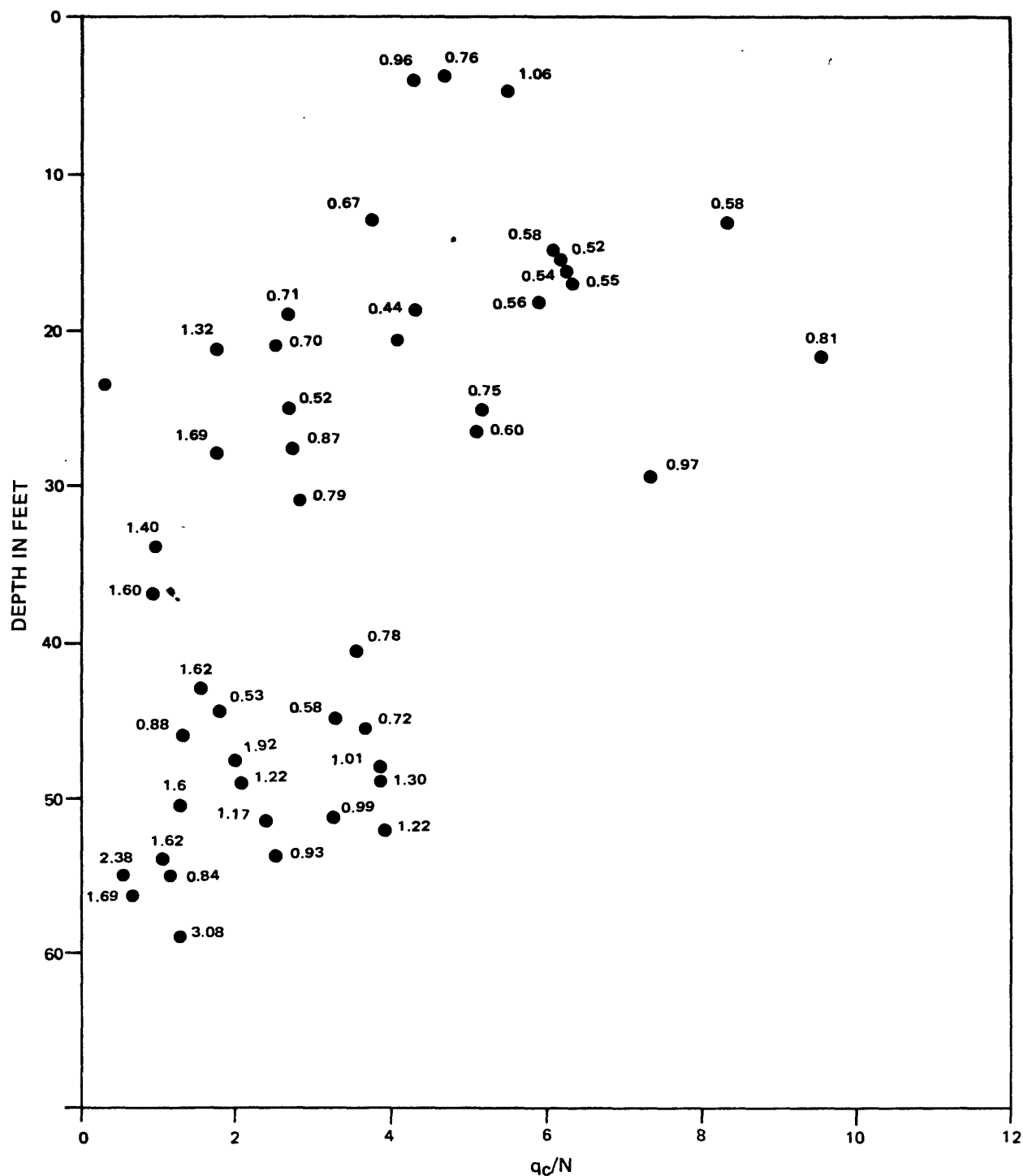
USGS CPT-SPT

SALINAS SITE
 q_c/N VS DEPTH
STANDARD HAMMER


9-80

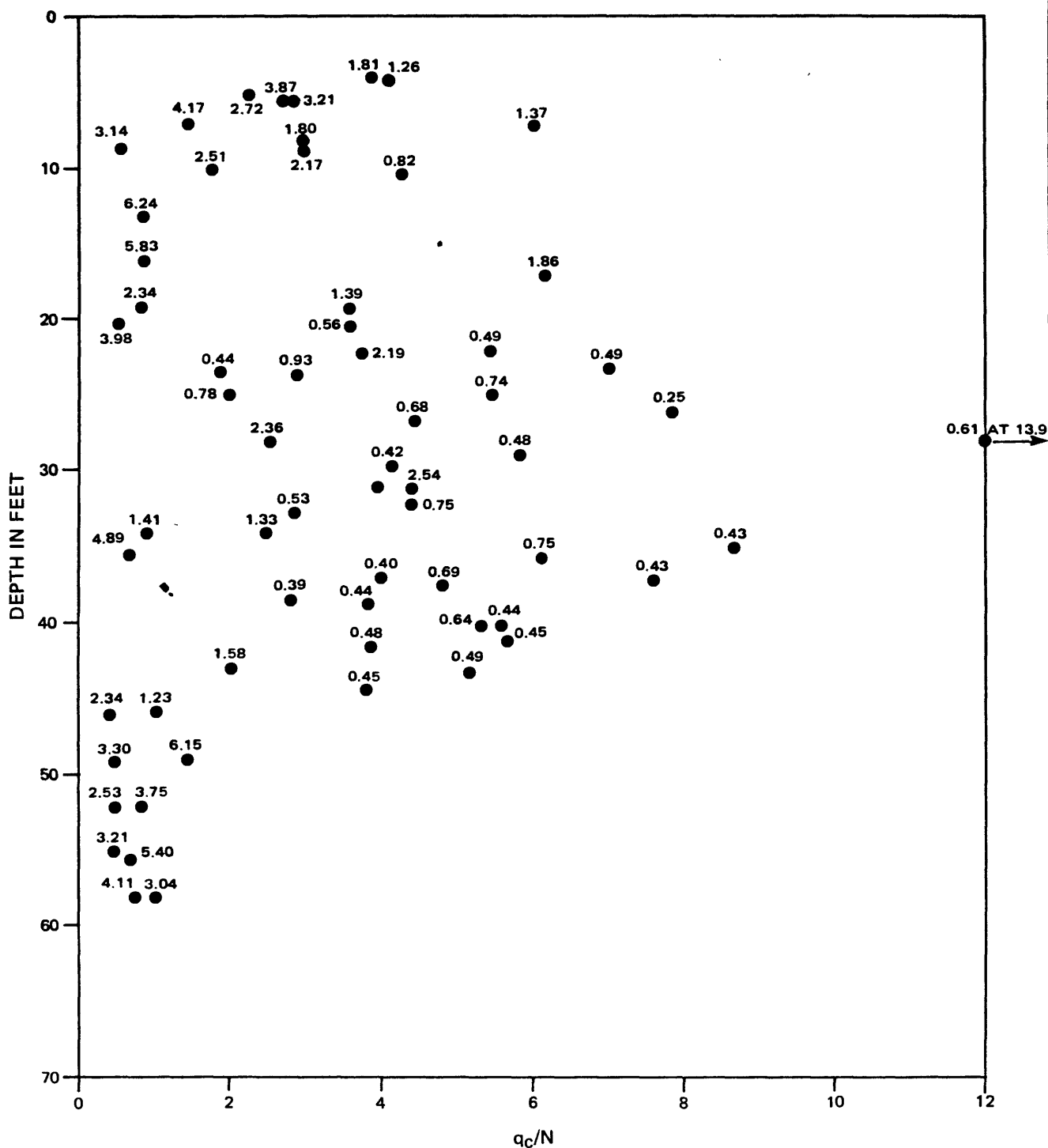
FIGURE B.6

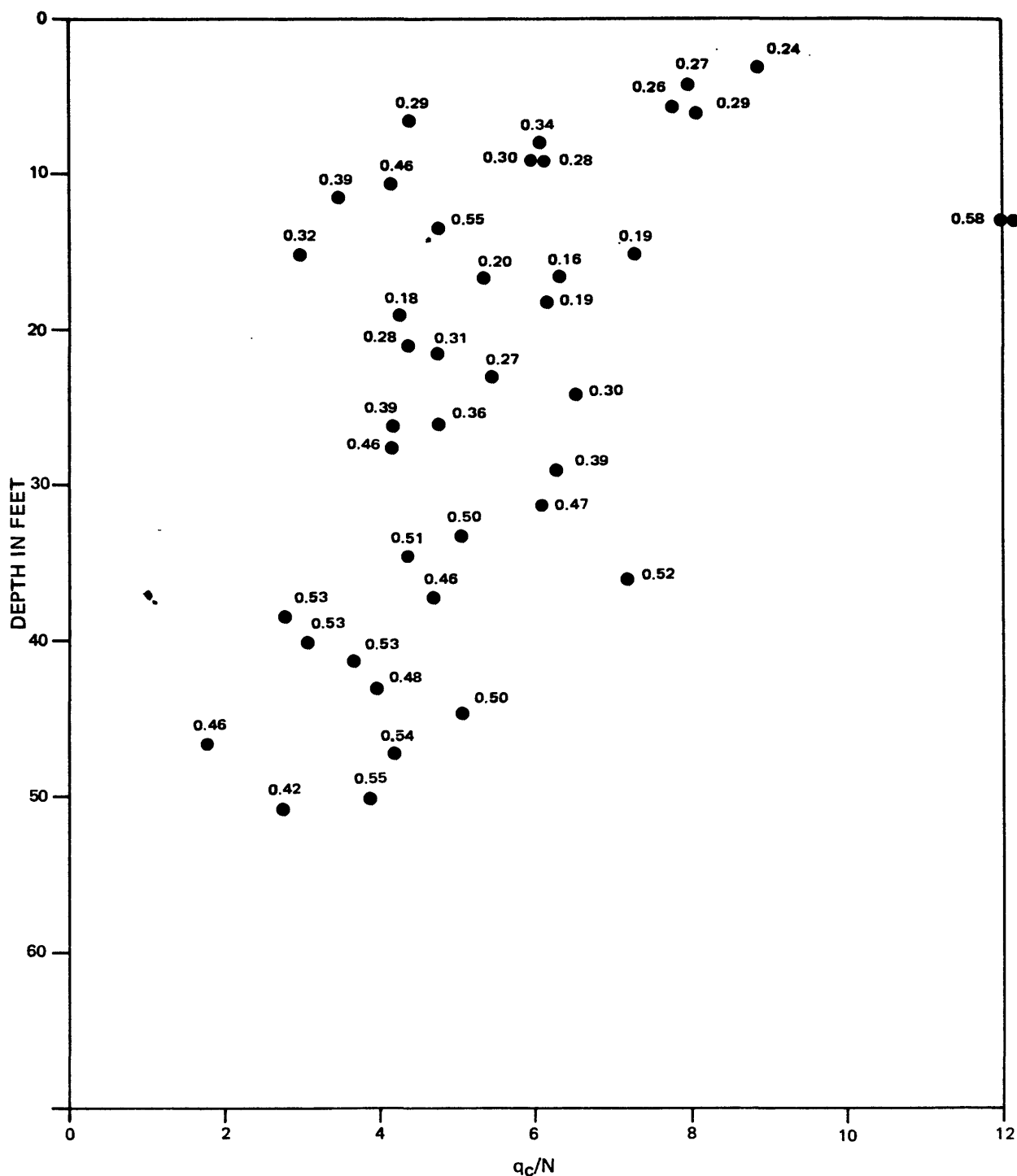
Approved by _____
Checked by _____
Drawn by _____
Compiled by _____



NUMBERS ON POINTS REPRESENT FRICTION RATIO, %

	PROJECT NO.:	79-153
	USGS CPT-SPT	
MOSS LANDING SITE q_c/N VS DEPTH STANDARD HAMMER		
9-80	FIGURE B.7	





NUMBERS ON POINTS REPRESENT FRICTION RATIO, %



PROJECT NO.:

79-153

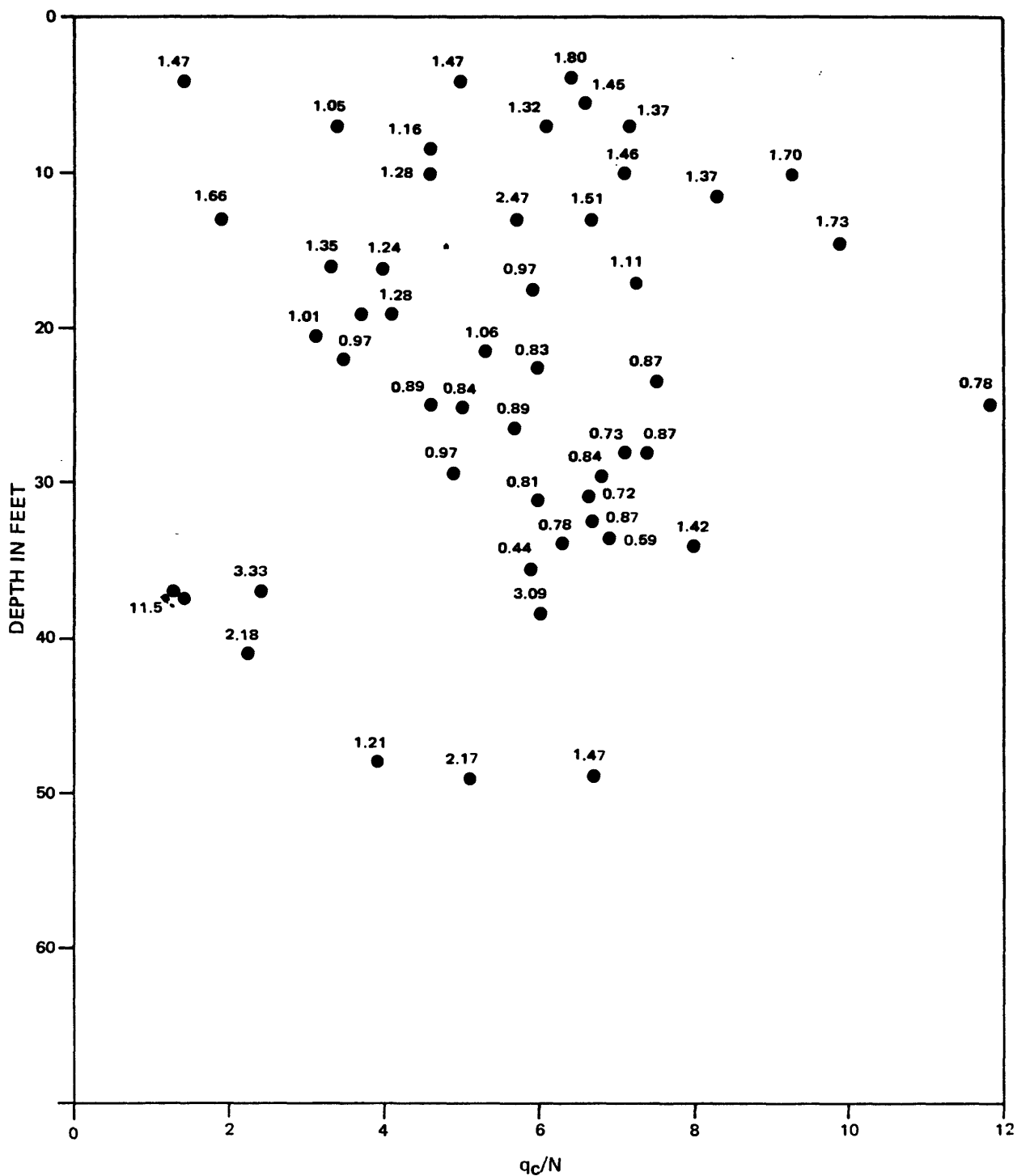
USGS CPT-SPT

SAN DIEGO SITE: NAS NORTH ISLAND
 q_c/N VS DEPTH
 TRIP HAMMER

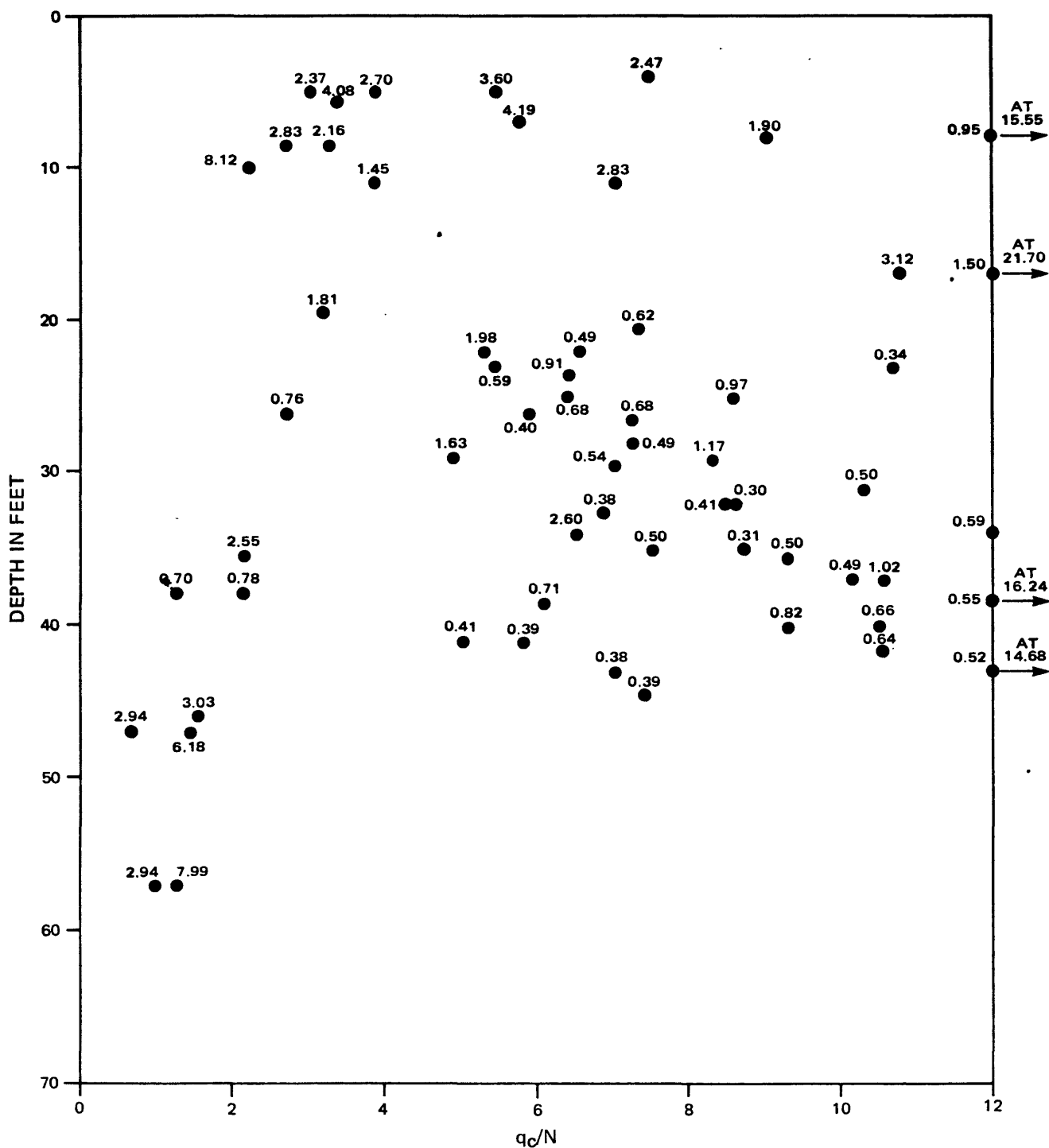
9-80

FIGURE 8.9

Approved by _____
Checked by _____
Drawn by _____
Compiled by _____



Approved by _____
Checked by _____
Drawn by _____
Compiled by _____



NUMBERS ON POINTS REPRESENT FRICTION RATIO, %



PROJECT NO.:

79-153

USGS CPT-SPT

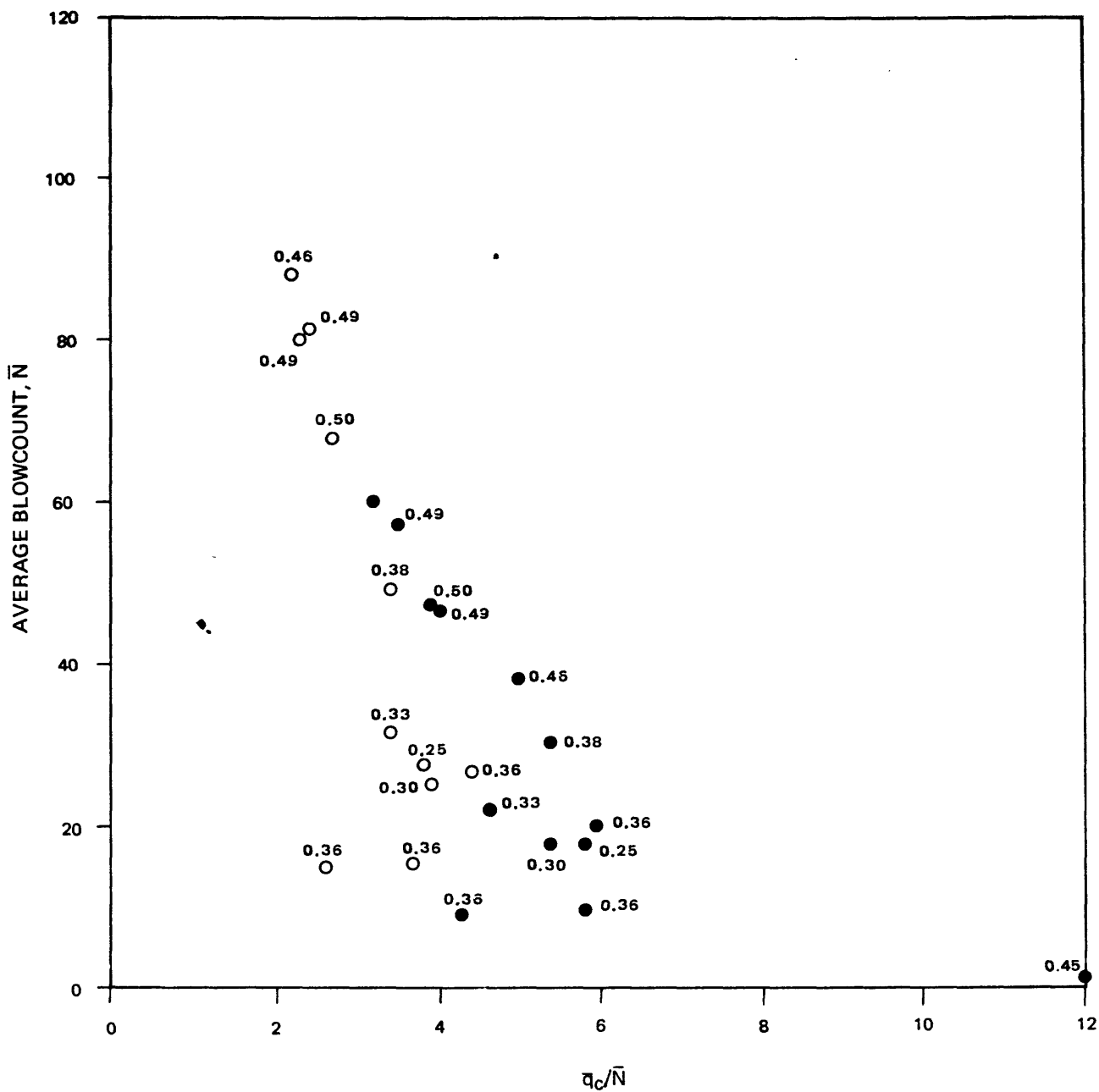
SAN JOSE SITE:
COYOTE NORTH & SOUTH
 q_c/N VS DEPTH
TRIP HAMMER

Approved by

Checked by

Drawn by

Compiled by



PROJECT NO.:

79-153

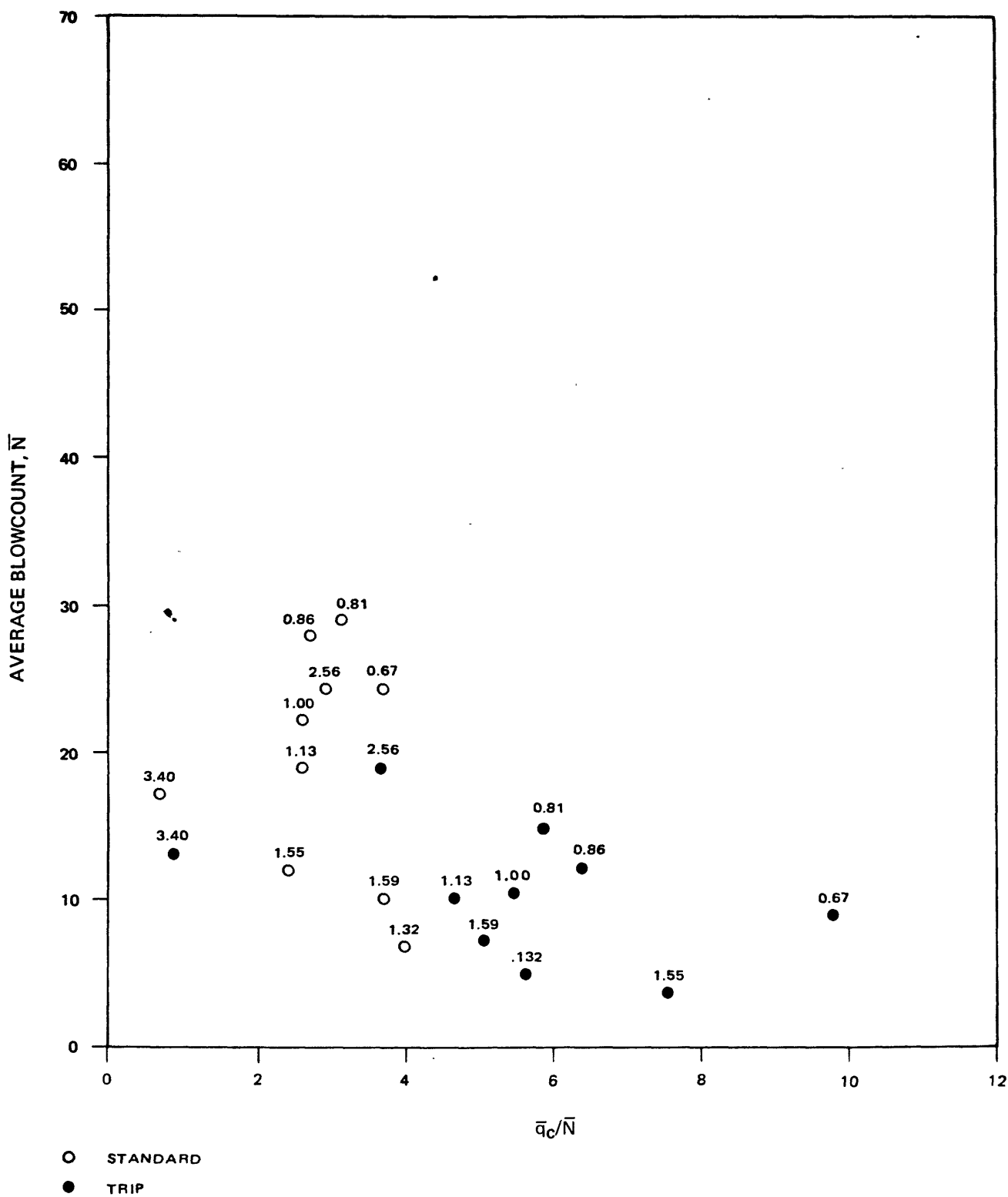
USGS CPT-SPT

SAN DIEGO SITE: NAS NORTH ISLAND
 q_c/\bar{N} VS \bar{N} BY LAYER AVERAGES

9-80

FIGURE B.13

Approved by _____
Checked by _____
Drawn by _____
Compiled by _____



PROJECT NO.:

79-153

USGS CPT-SPT

SALINAS SITE
 q_c/\bar{N} VS \bar{N} BY LAYER AVERAGES

9-80

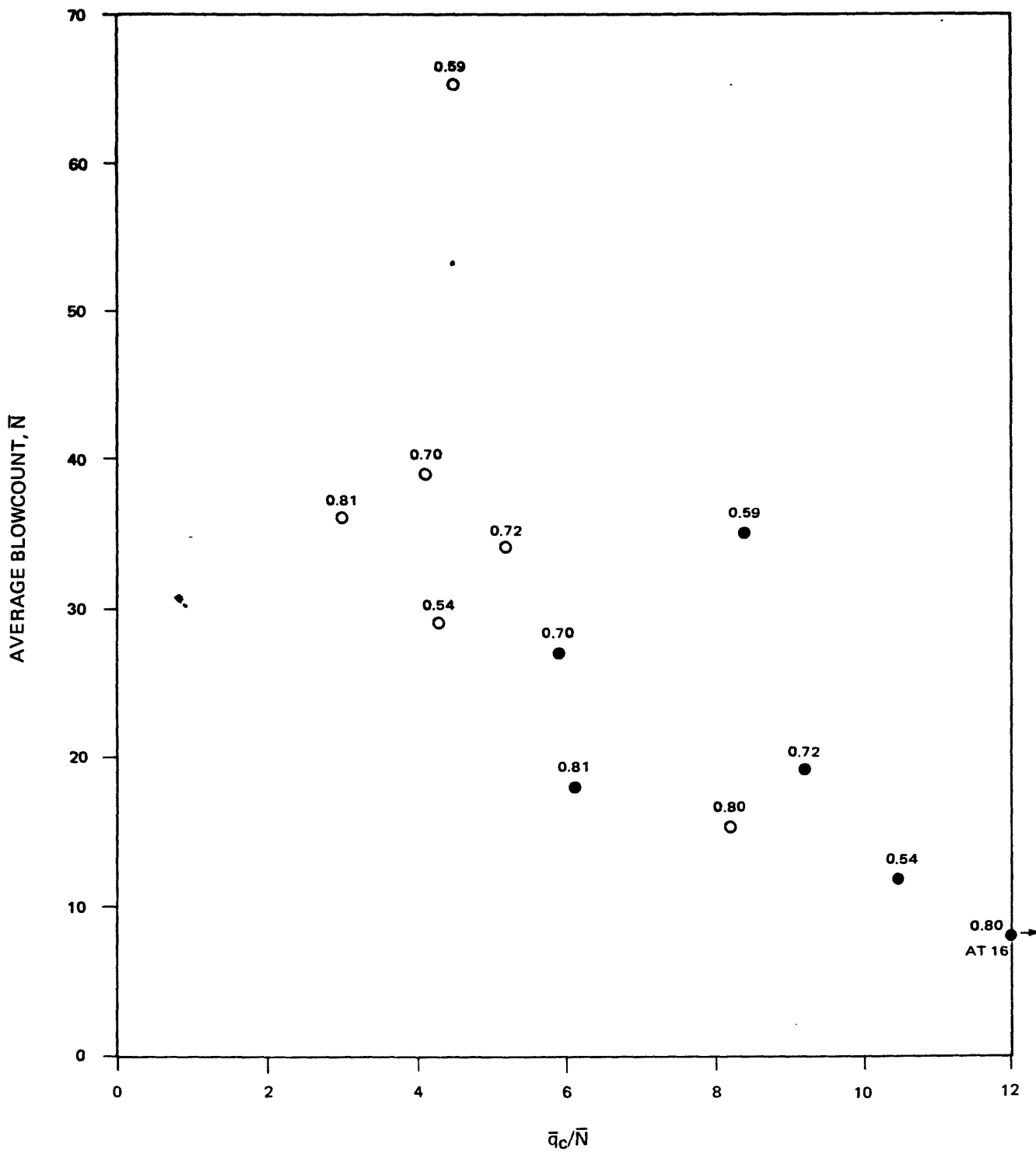
FIGURE B.14

Approved by

Checked by

Drawn by

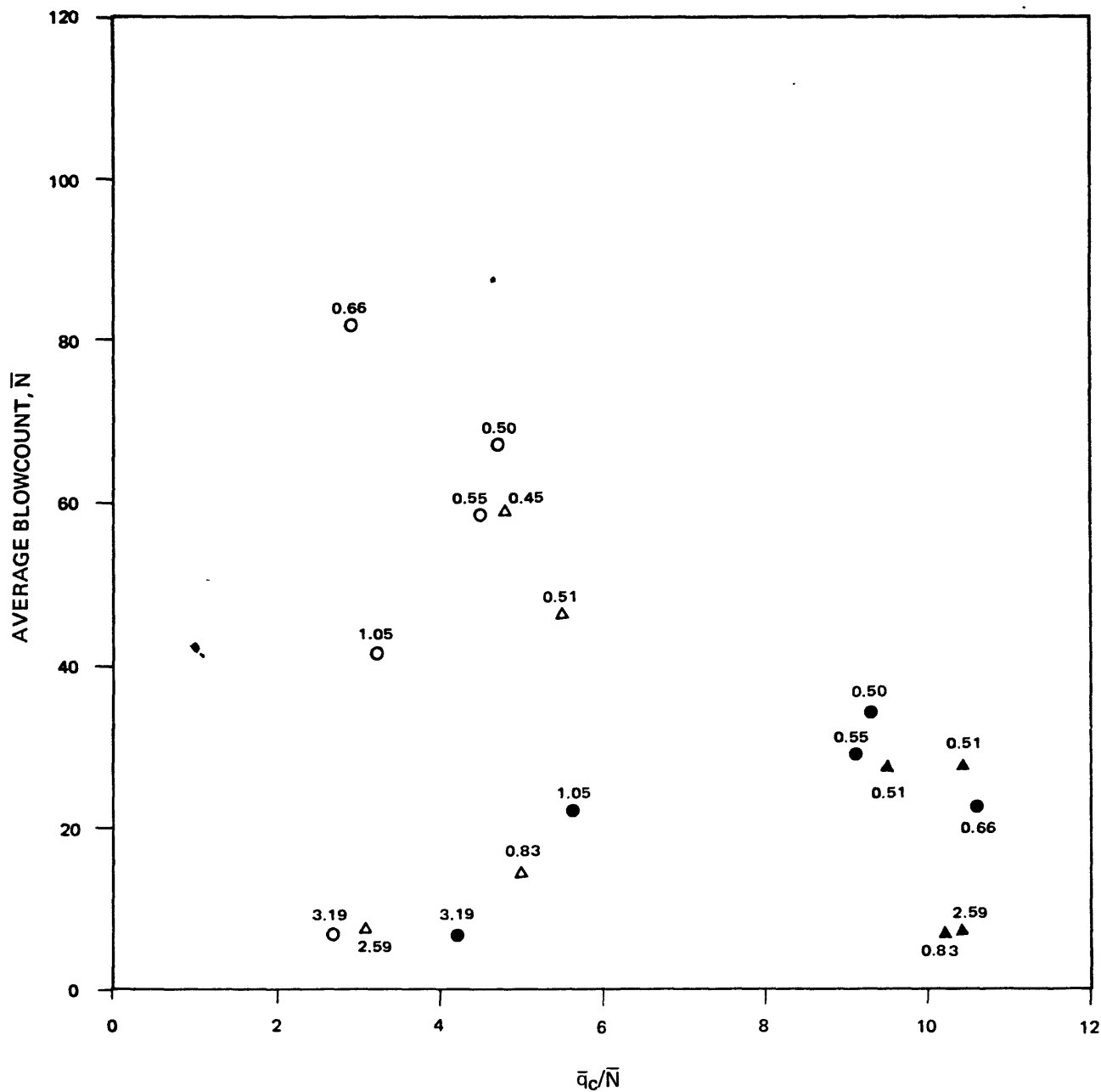
Compiled by



PROJECT NO.: 79-153

USGS CPT-SPT

MOSS LANDING SITE
 \bar{q}_c/\bar{N} VS \bar{N} BY LAYER AVERAGES



SOUTH

NORTH



STANDARD



TRIP



NUMBERS ON POINTS REPRESENT FRICTION RATIO, %

PROJECT NO.:

79-153

USGS CPT-SPT

SAN JOSE SITES:
COYOTE NORTH AND SOUTH
 q_c/\bar{N} VS \bar{N} BY LAYER AVERAGES

9-80

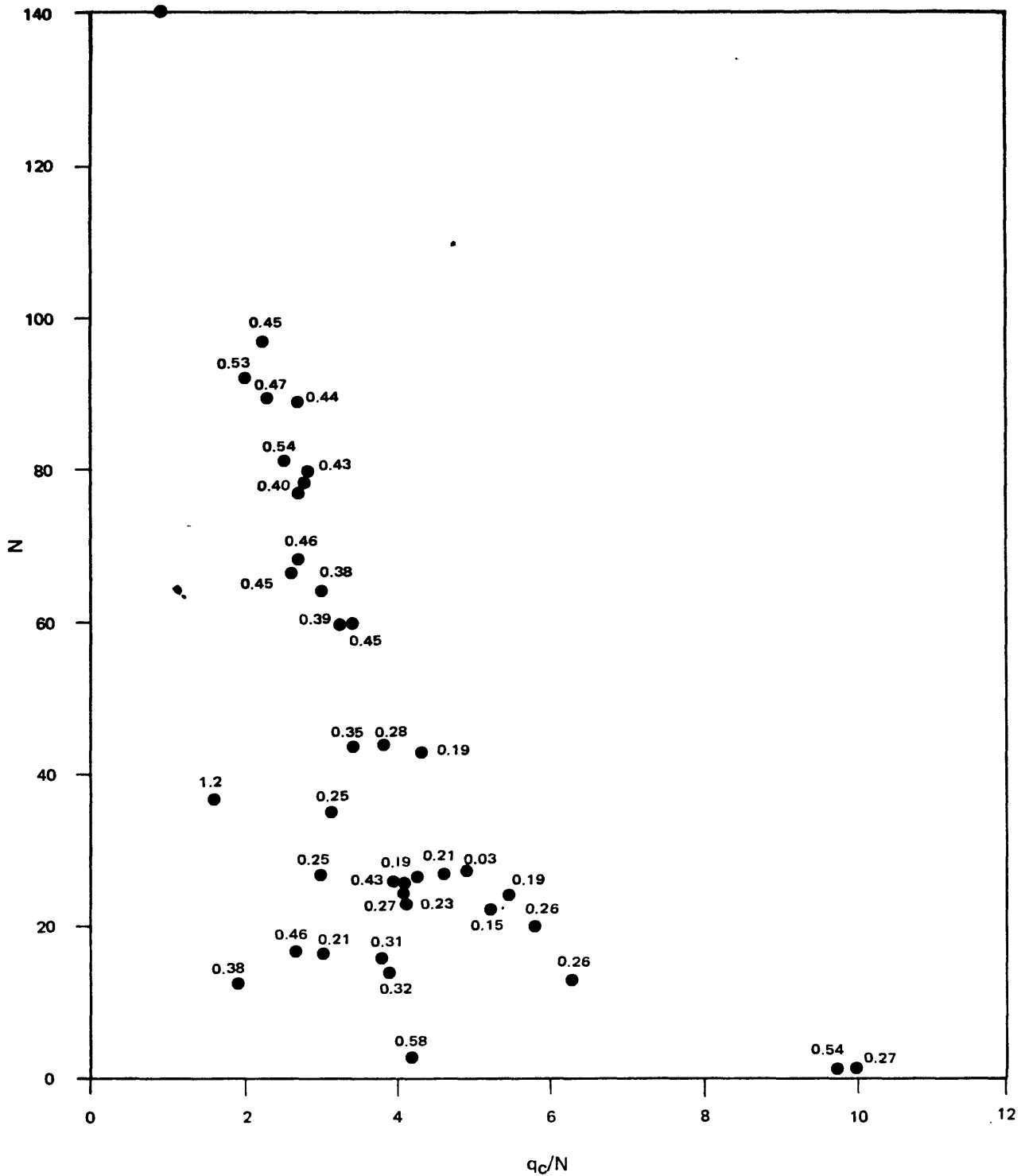
FIGURE B.16

Approved by

Checked by

Drawn by

Compiled by



NUMBERS ON POINTS REPRESENT FRICTION RATIO, %



PROJECT NO.:

79-153

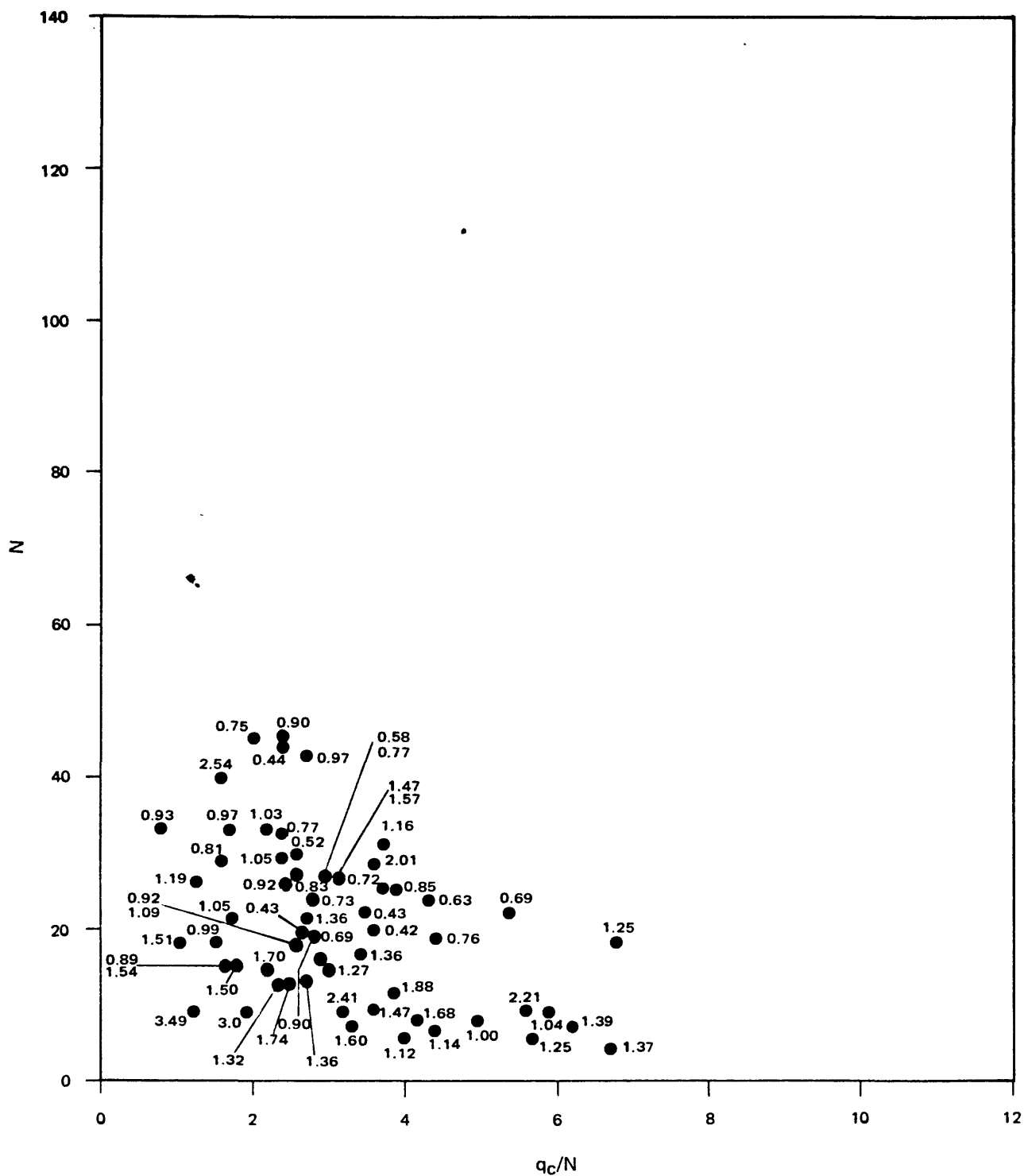
USGS CPT-SPT

SAN DIEGO SITE:
NAS NORTH ISLAND
qc/N VS N STANDARD HAMMER

9-80

FIGURE B.17

Approved by _____
Checked by _____
Drawn by _____
Compiled by _____



NUMBERS ON POINTS REPRESENT FRICTION RATIO, %



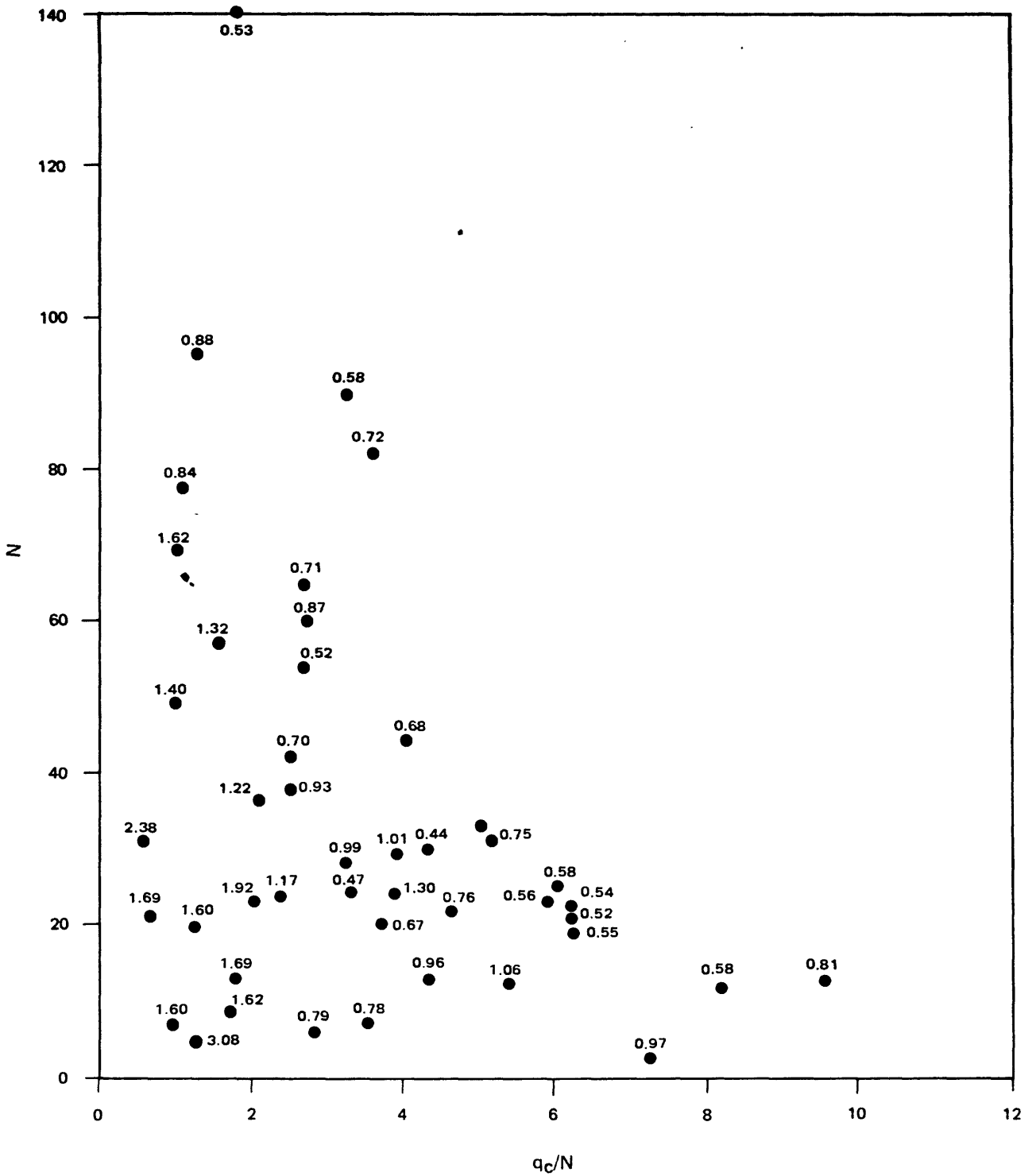
PROJECT NO.:

79-153

USGS CPT-SPT

SALINAS SITE
 q_c/N VS N STANDARD HAMMER

Approved by /
Checked by /
Drawn by /
Compiled by /



NUMBERS ON POINTS REPRESENT FRICTION RATIO, %



PROJECT NO.: 79-153

USGS CPT-SPT

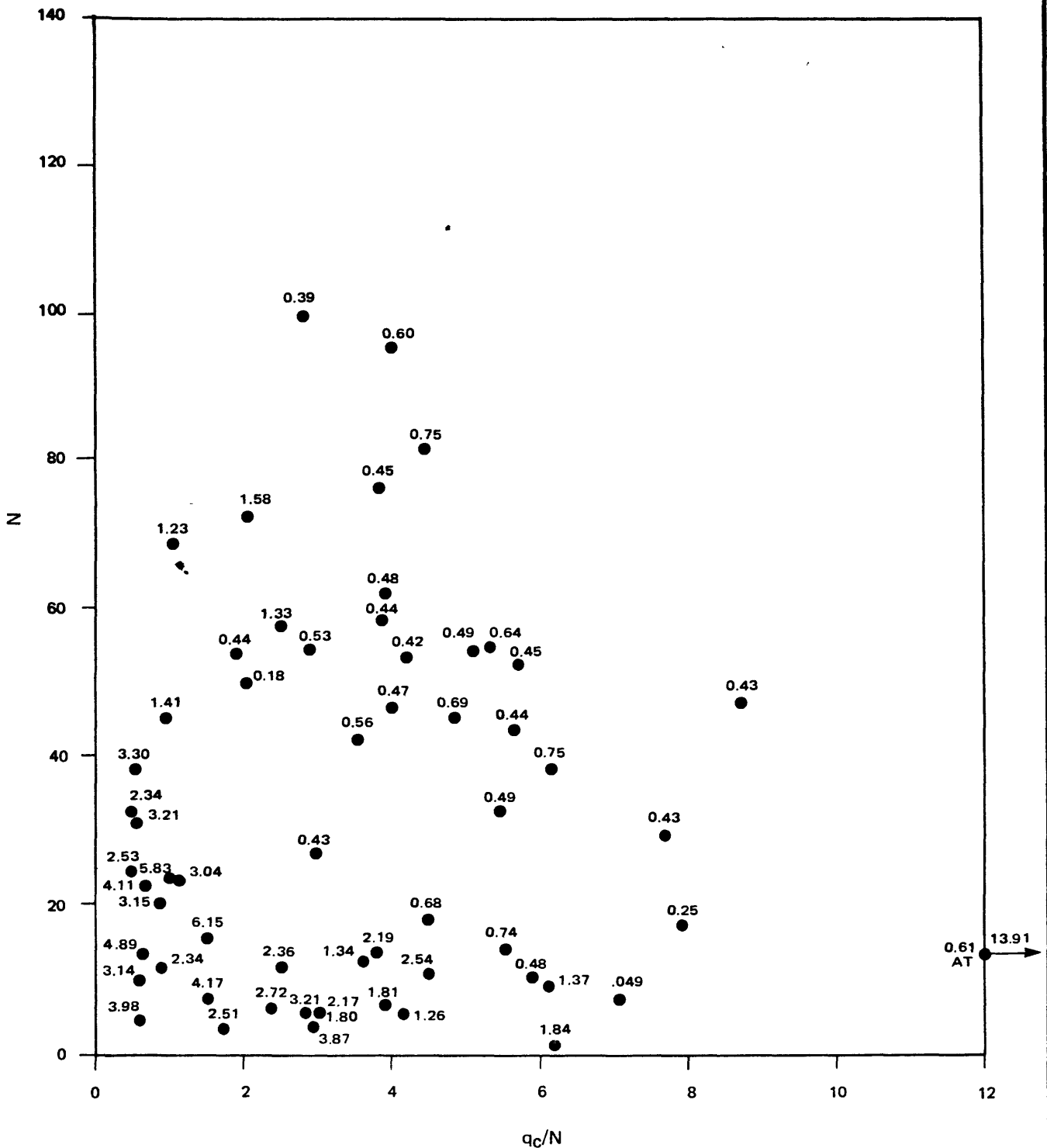
MOSS LANDING SITE
qc/N VS N STANDARD HAMMER

Approved by

Checked by

Drawn by

Compiled by



NUMBERS ON POINTS REPRESENT FRICTION RATIO, %



PROJECT NO.: 79-153

USGS CPT-SPT

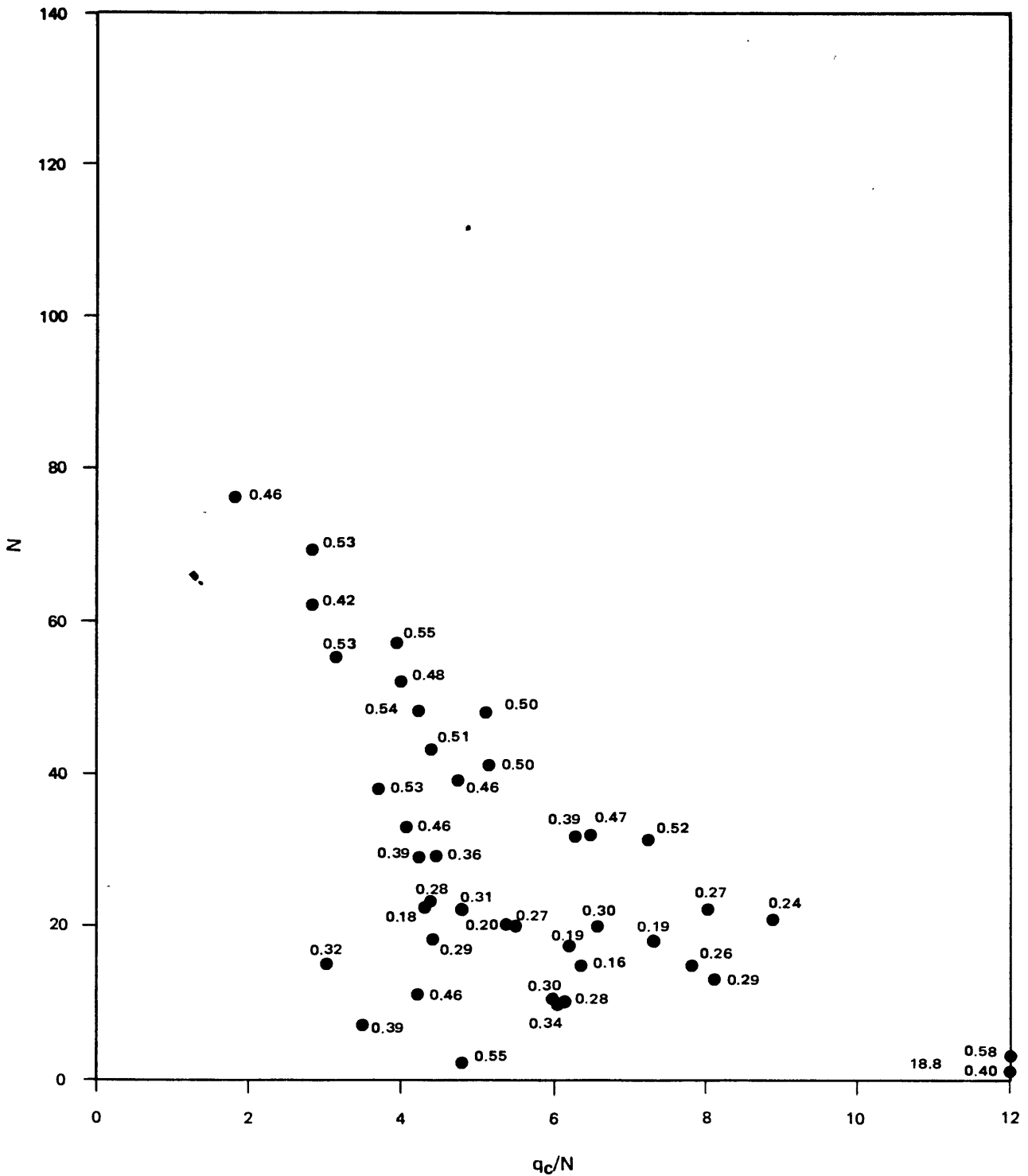
SAN JOSE SITE:
COYOTE NORTH & SOUTH
 q_c/N VS N STANDARD HAMMER

Approved by

Checked by

Drawn by

Compiled by



NUMBERS ON POINTS REPRESENT FRICTION RATIO, %



PROJECT NO.:

79-153

USGS CPT-SPT

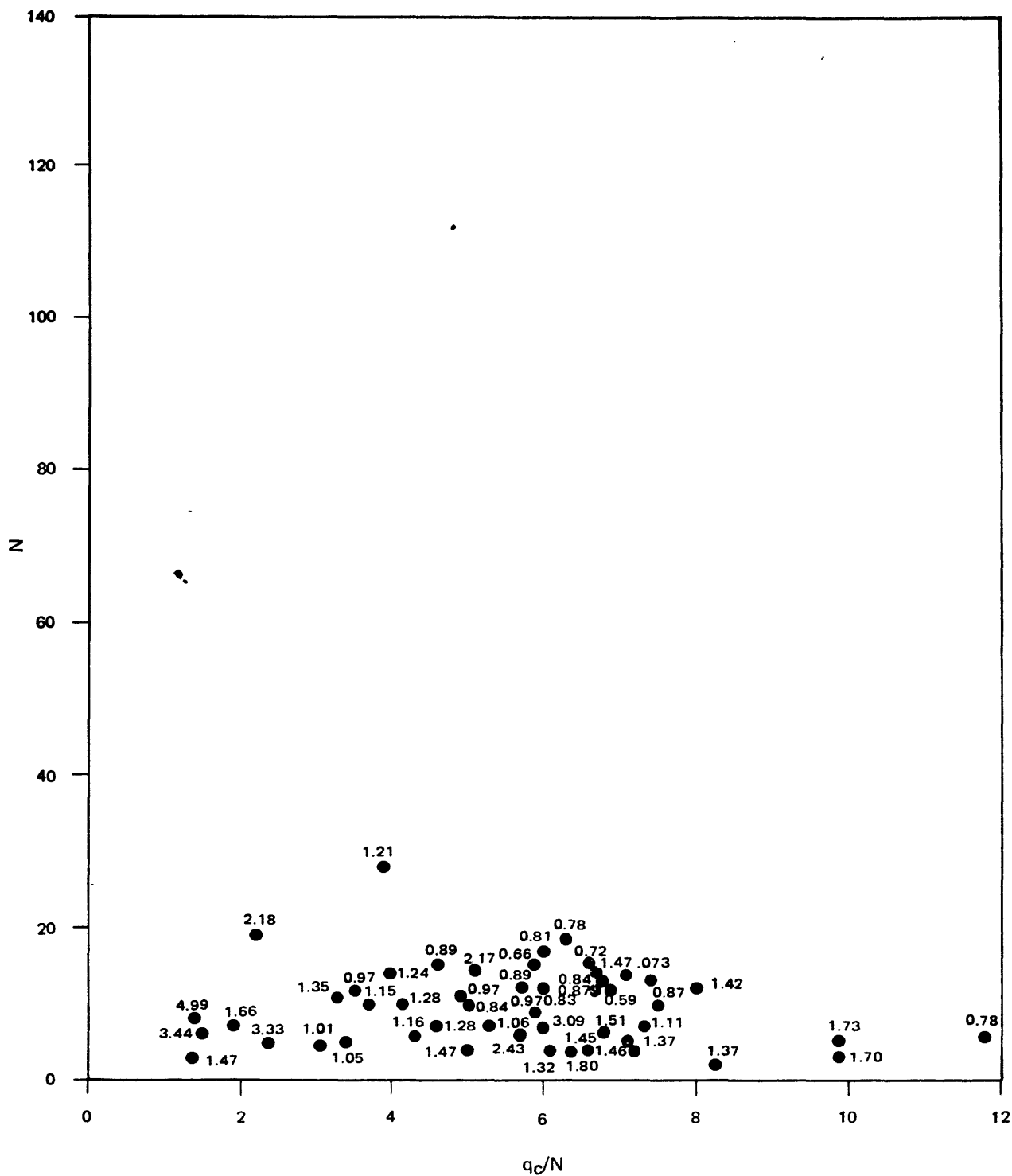
SAN DIEGO SITE:
NAS NORTH ISLAND
 q_c/N VS N TRIP HAMMER

Approved by

Checked by

Drawn by

Compiled by



NUMBERS ON POINTS REPRESENT FRICTION RATIO, %



PROJECT NO.:

79-153

USGS CPT-SPT

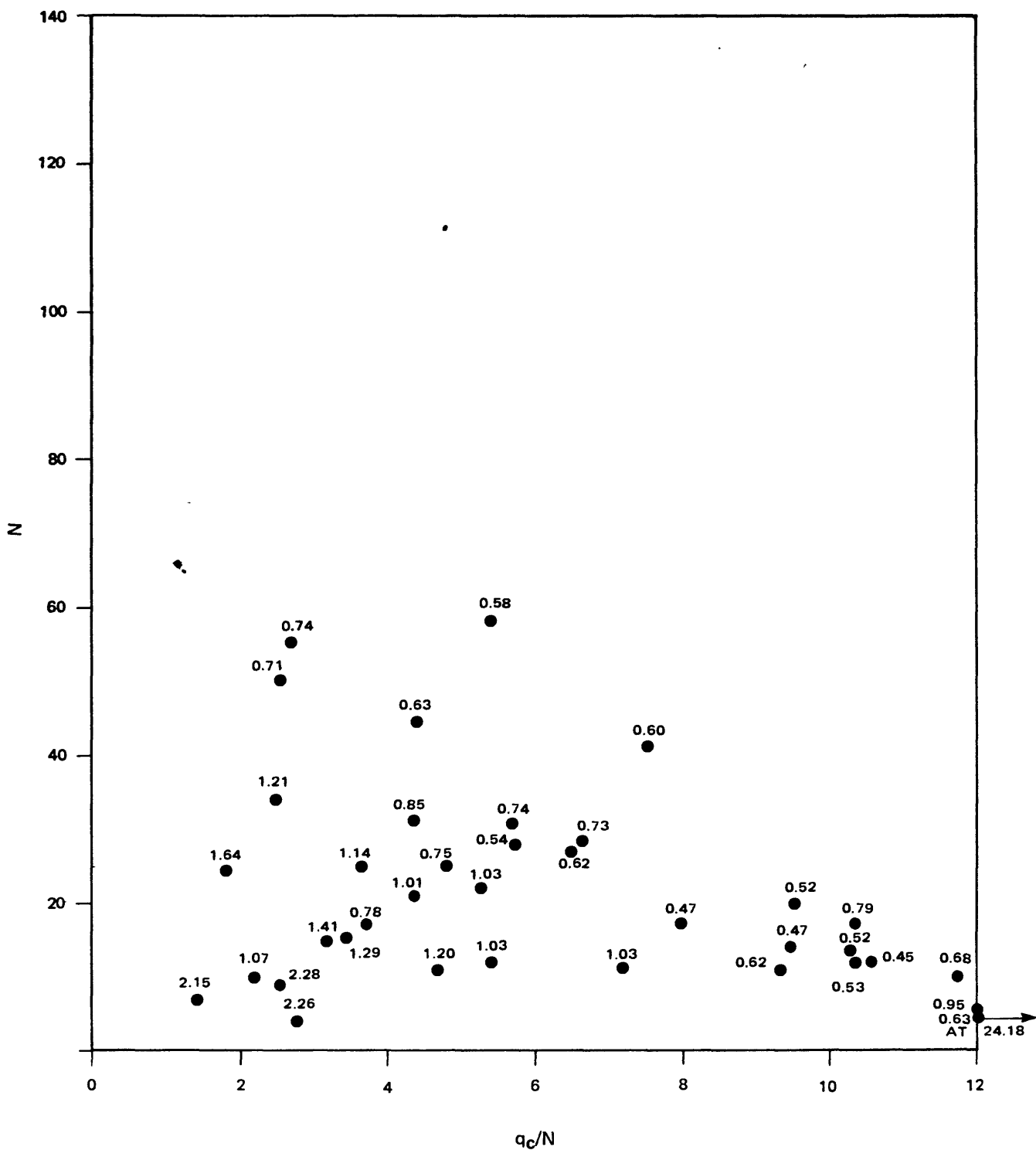
SALINAS SITE
 q_c/N VS N TRIP HAMMER

Approved by

Checked by

Drawn by

Compiled by



NUMBERS ON POINTS REPRESENT FRICTION RATIO, %



PROJECT NO.:

79-153

USGS CPT-SPT

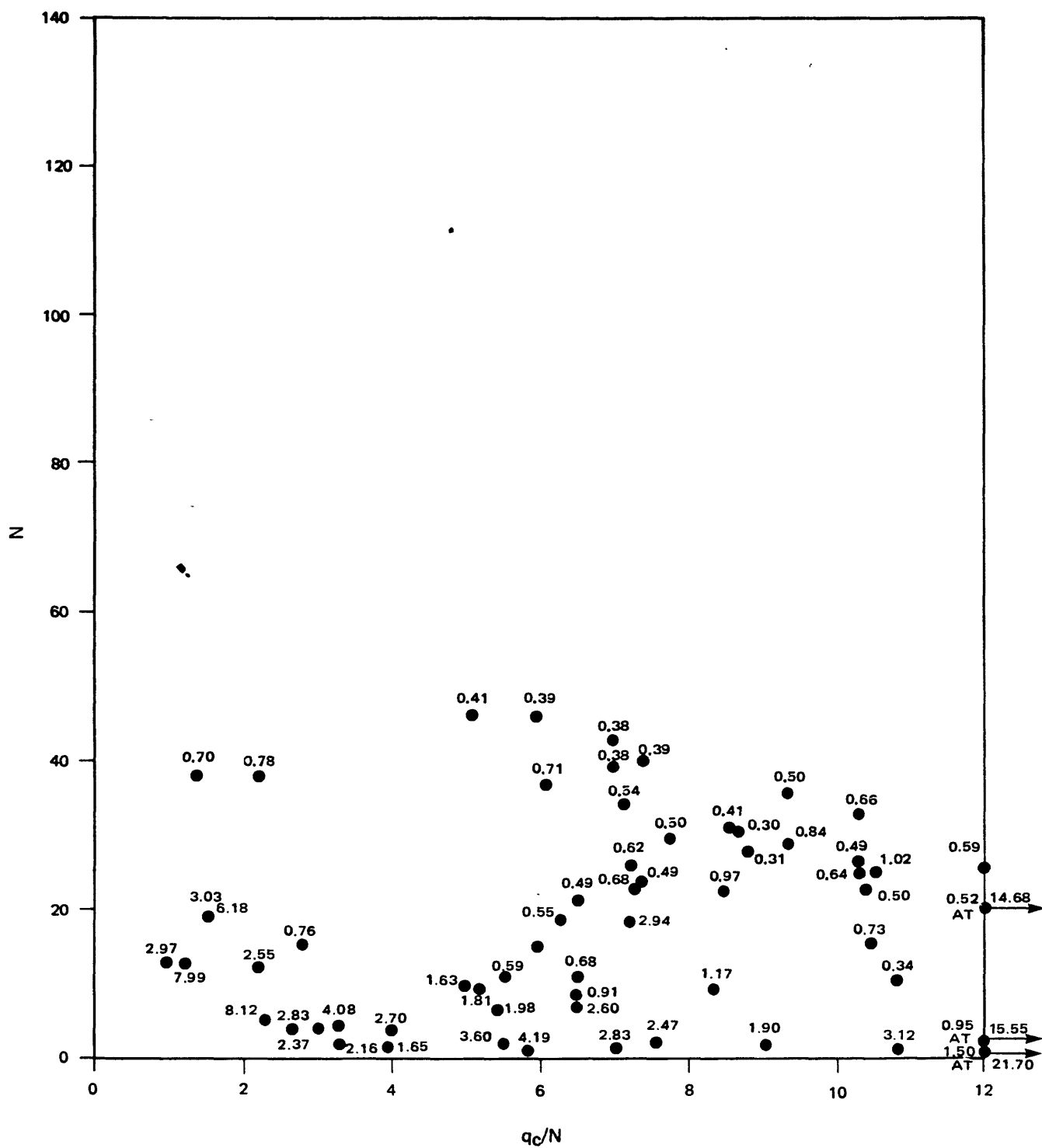
MOSS LANDING SITE
 q_c/N VS N TRIP HAMMER

Approved by

Checked by

Drawn by

Compiled by



NUMBERS ON POINTS REPRESENT FRICTION RATIO, %



PROJECT NO.:

79-153

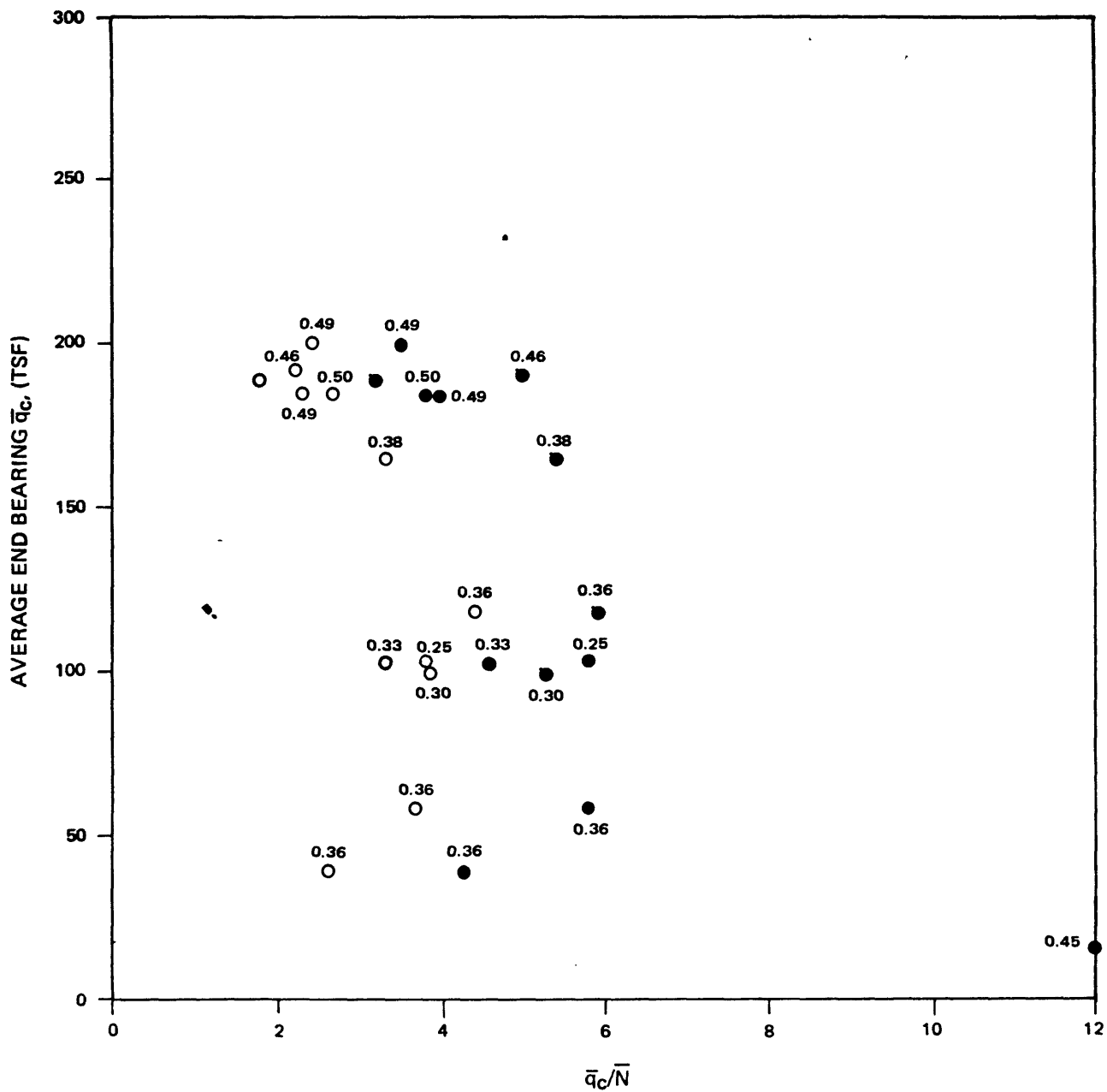
USGS CPT-SPT

SAN JOSE SITE:
COYOTE NORTH & SOUTH
 q_c/N VS N TRIP HAMMER

J-80

FIGURE B.24

Approved by _____
 Checked by _____
 Drawn by _____
 Compiled by _____



○ STANDARD

● TRIP

NUMBERS ON POINTS REPRESENT FRICTION RATIO, %



PROJECT NO.:

79-153

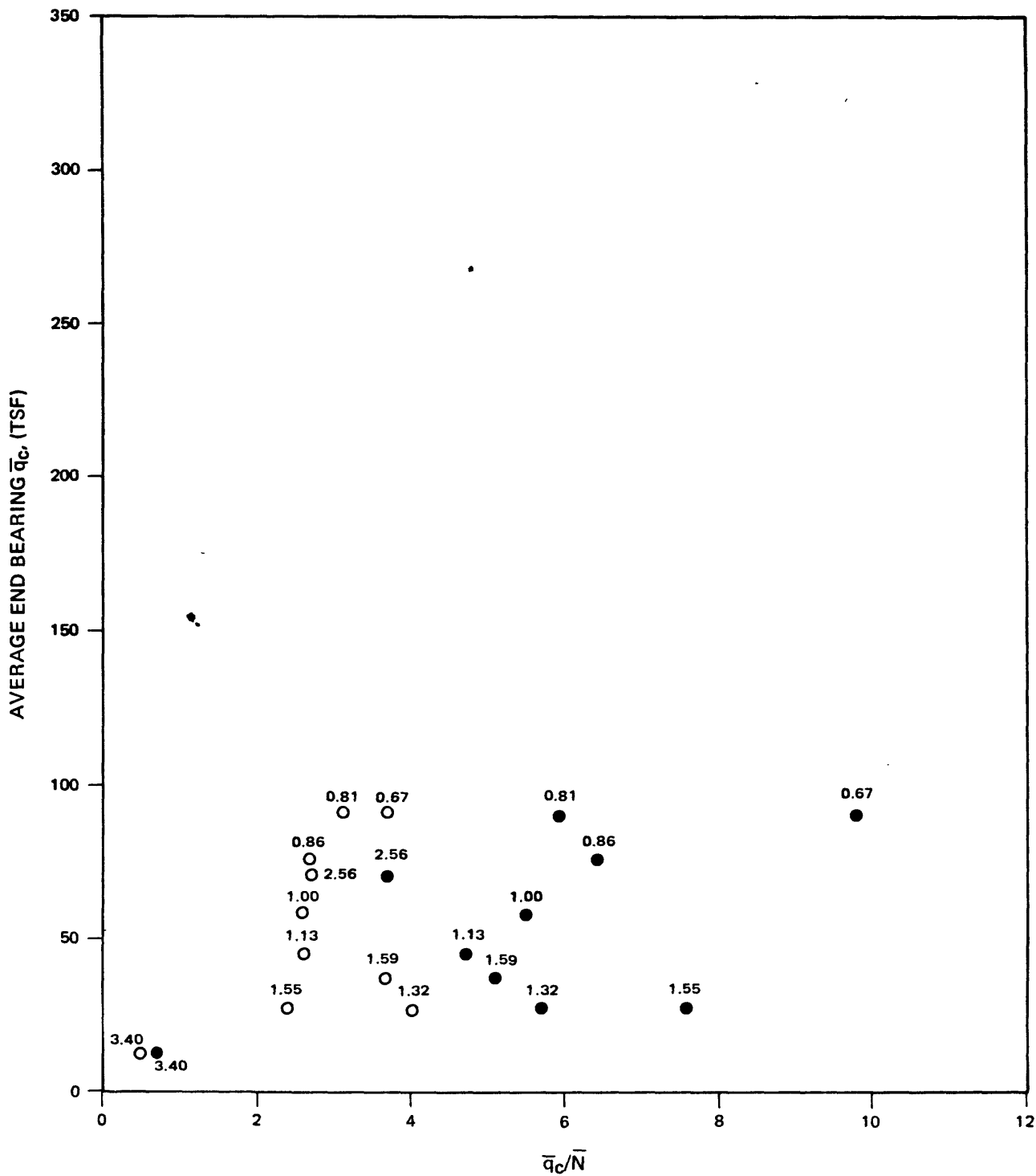
USGS CPT-SPT

SAN DIEGO SITE: NAS NORTH ISLAND
 \bar{q}_c/\bar{N} VS \bar{q}_c
 BY LAYER AVERAGES

9-80

FIGURE B.25

Approved by /
Checked by /
Drawn by /
Compiled by /



○ STANDARD

● TRIP

NUMBERS ON POINTS REPRESENT FRICTION RATIO, %



PROJECT NO.:

79-153

USGS CPT-SPT

SALINAS SITE
 \bar{q}_c/\bar{N} VS \bar{q}_c
BY LAYER AVERAGES

9-80

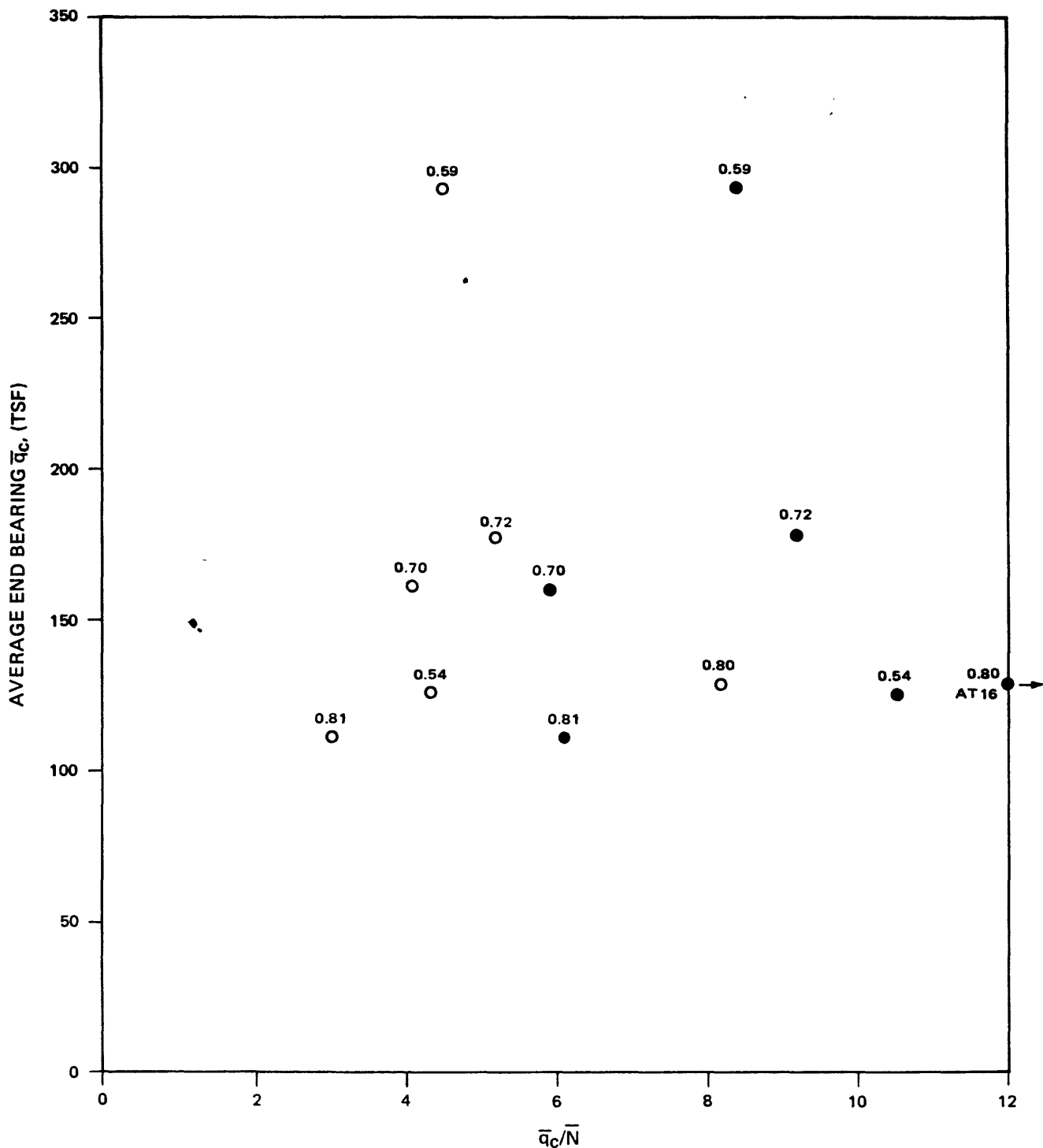
FIGURE B.26

Approved by

Checked by

Drawn by

Compiled by



○ STANDARD

● TRIP

NUMBERS ON POINTS REPRESENT FRICTION RATIO, %



PROJECT NO.:

79-153

USGS CPT-SPT

MOSS LANDING SITE
 \bar{q}_c/\bar{N} VS \bar{q}_c
BY LAYER AVERAGES

9-80

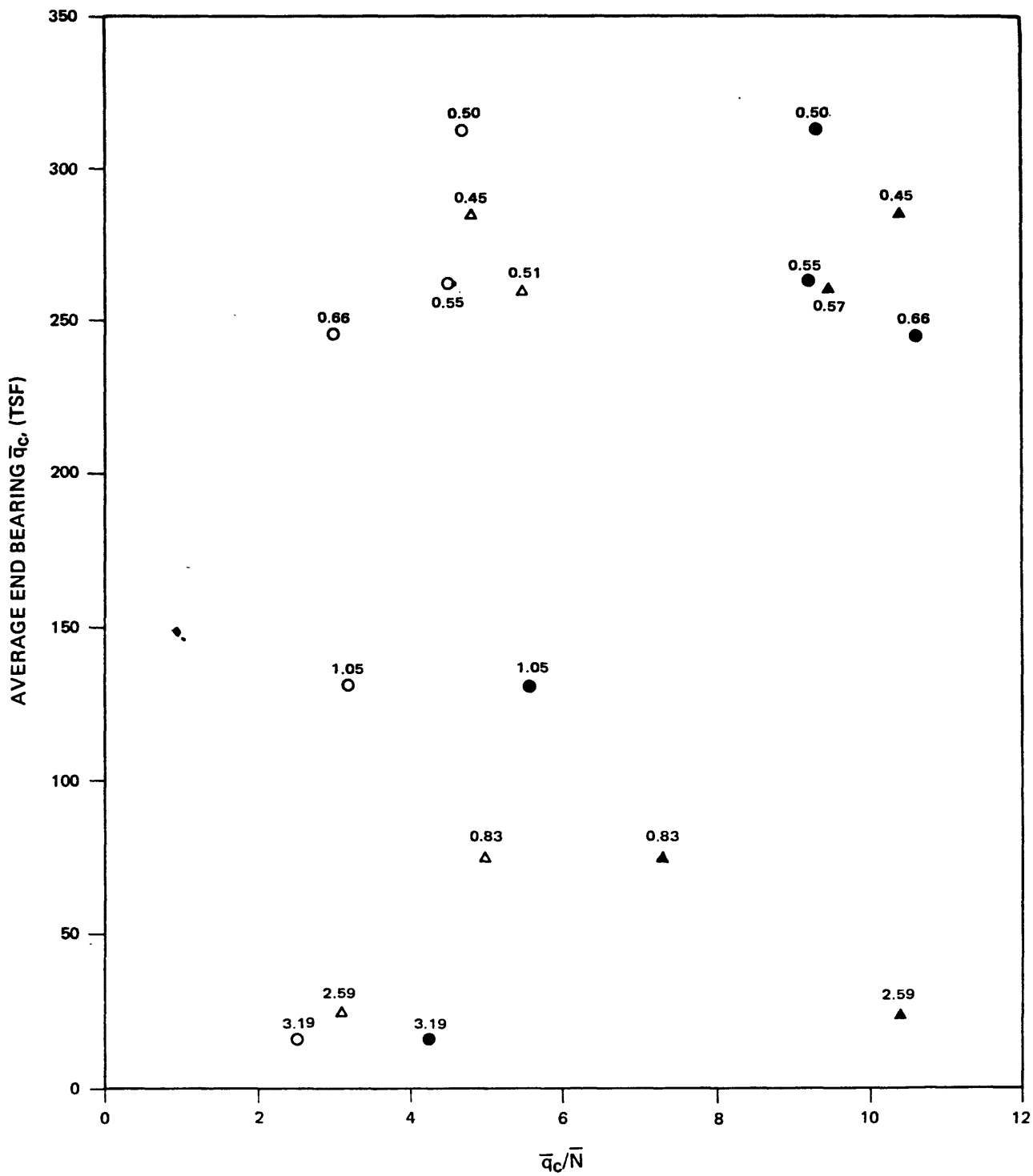
FIGURE B.27

Approved by


Checked by

Drawn by

Compiled by



○ STANDARD
● TRIP
NUMBERS ON POINTS REPRESENT FRICTION RATIO, %

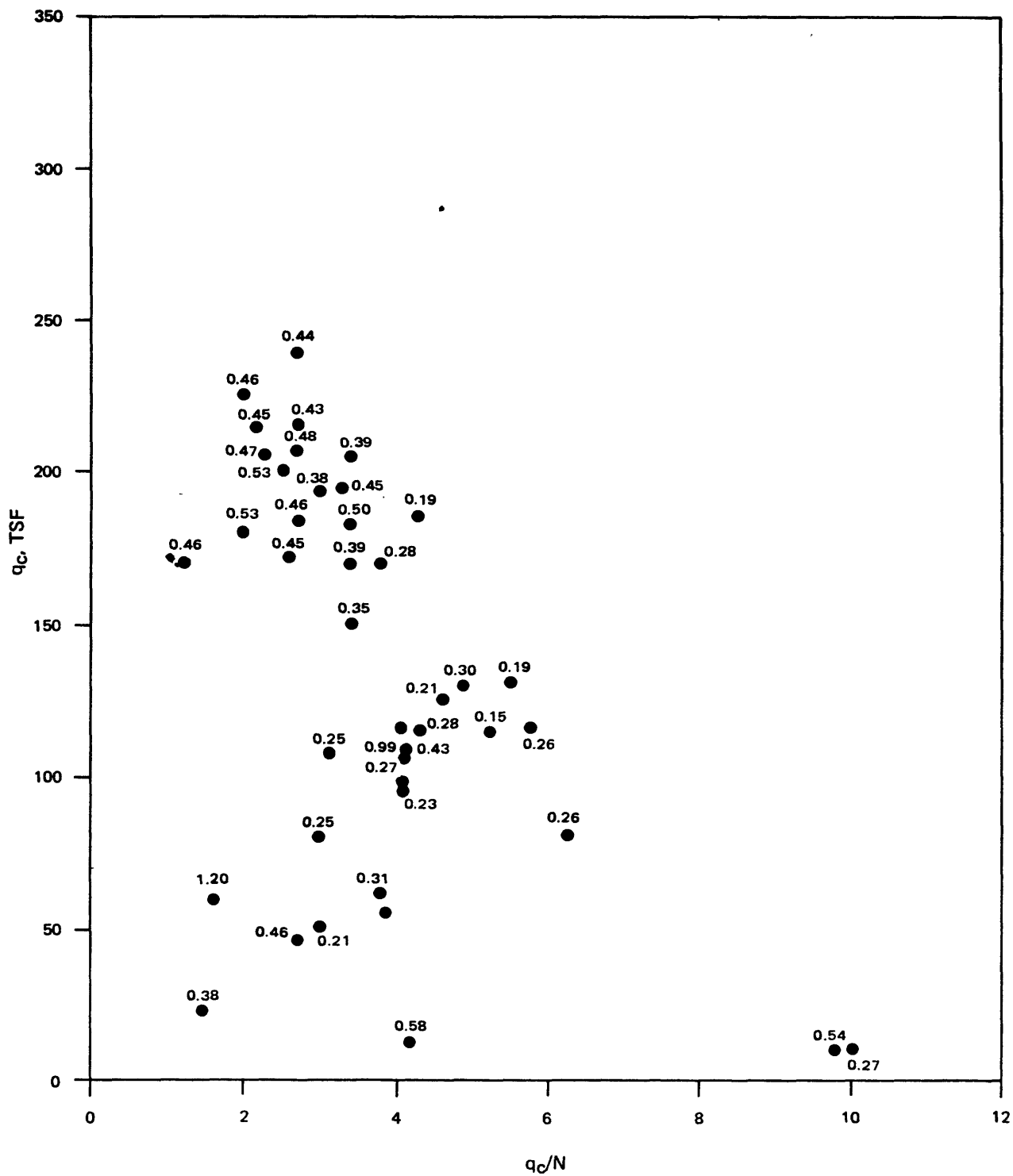
	PROJECT NO.:	79-153
	USGS CPT-SPT	
SAN JOSE SITE: COYOTE NORTH AND SOUTH \bar{q}_c / \bar{N} VS \bar{q}_c BY LAYER AVERAGES		
9-80	FIGURE B.28	

Approved by

Checked by

Drawn by

Compiled by



NUMBERS ON POINTS REPRESENT FRICTION RATIO, %



PROJECT NO.:

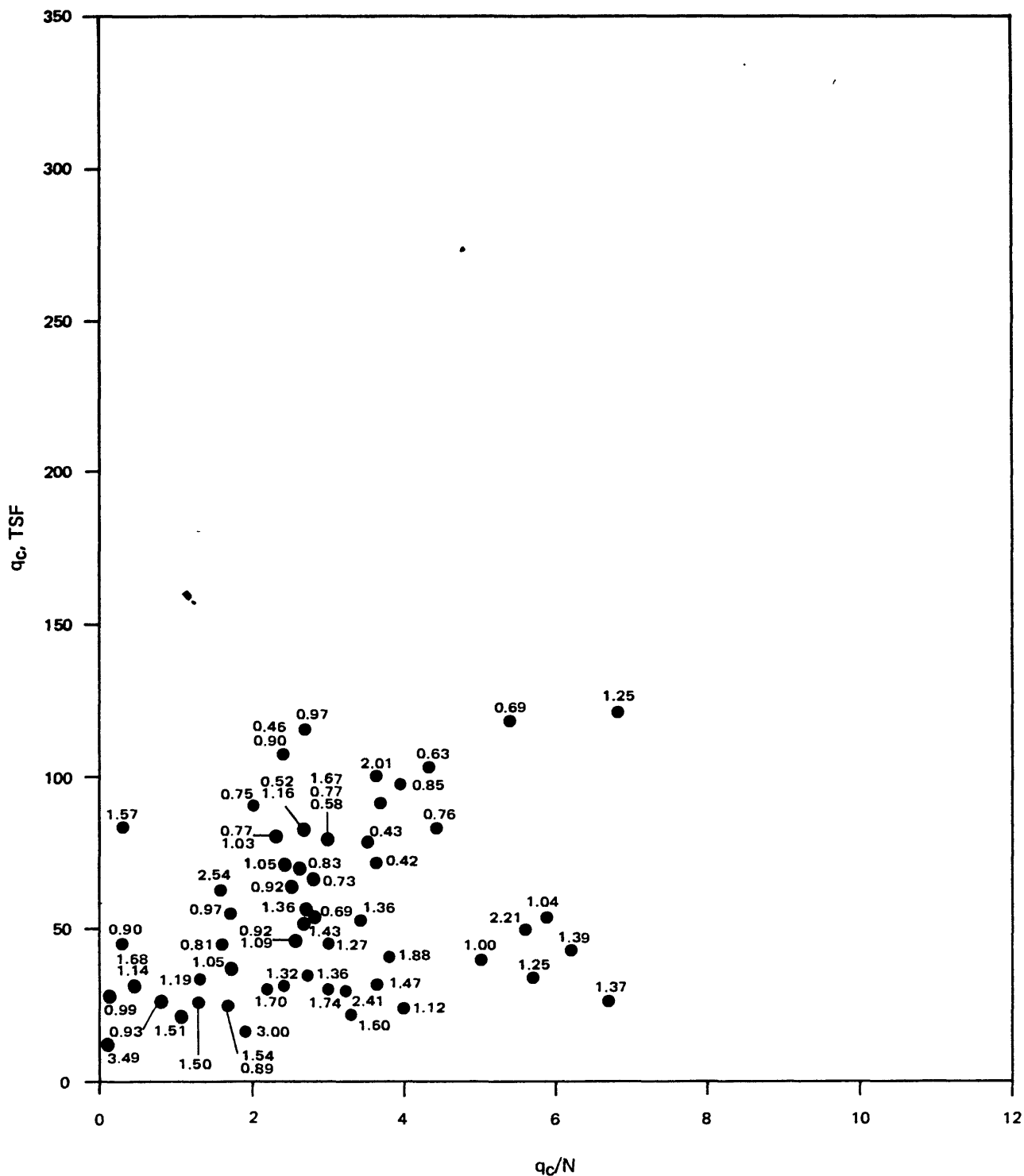
79-153

USGS CPT-SPT

SAN DIEGO SITE: NAS NORTH ISLAND
 q_c/N VS q_c
 STANDARD HAMMER

9-80

FIGURE B.29



NUMBERS ON POINTS REPRESENT FRICTION RATIO, %



PROJECT NO.:

79-153

USGS CPT-SPT

SALINAS SITE
 q_c/N VS q_c
 STANDARD HAMMER

9-80

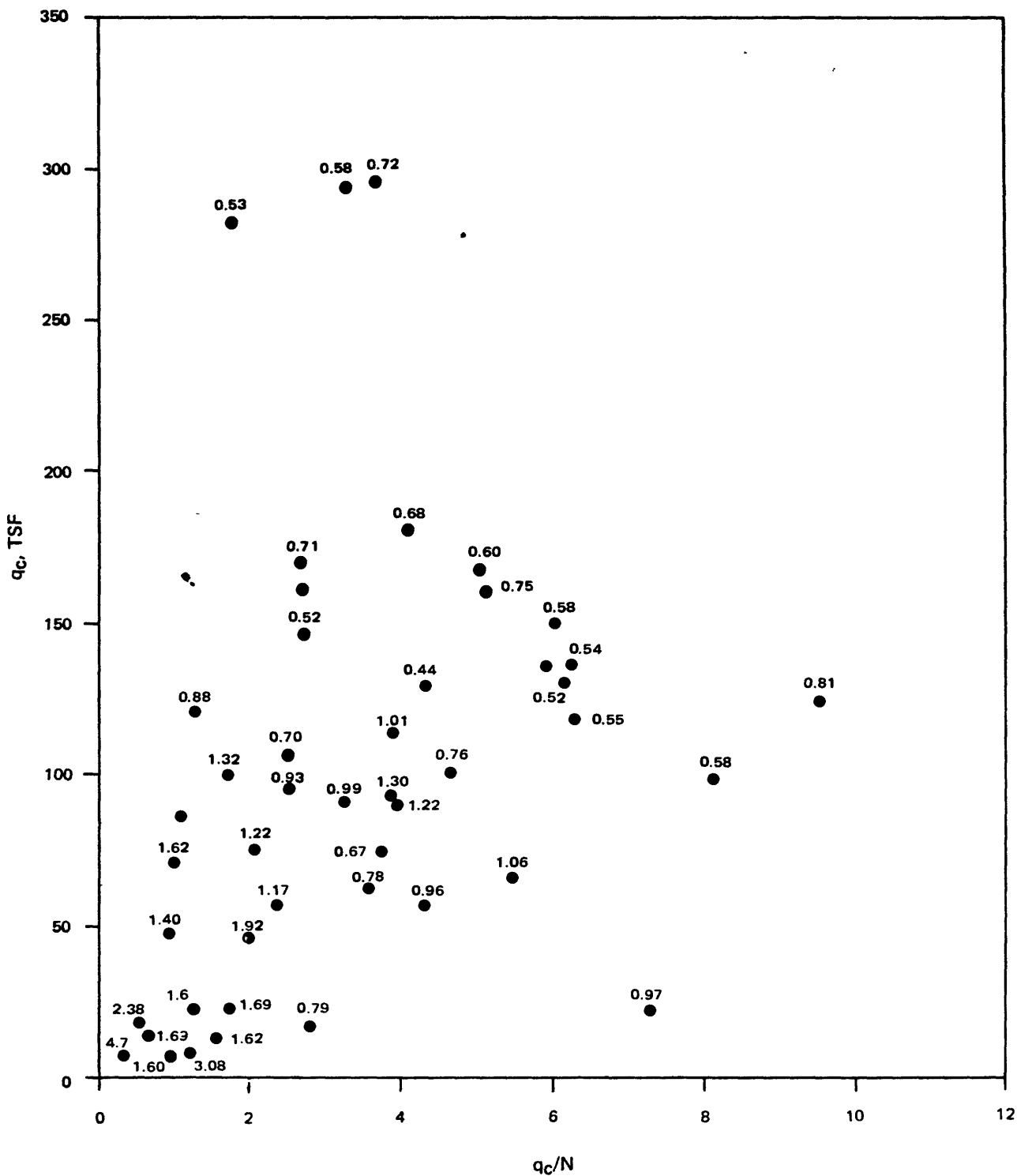
FIGURE B.30

Approved by

Checked by

Drawn by

Compiled by



NUMBERS ON POINTS REPRESENT FRICTION RATIO, %



PROJECT NO.:

79-153

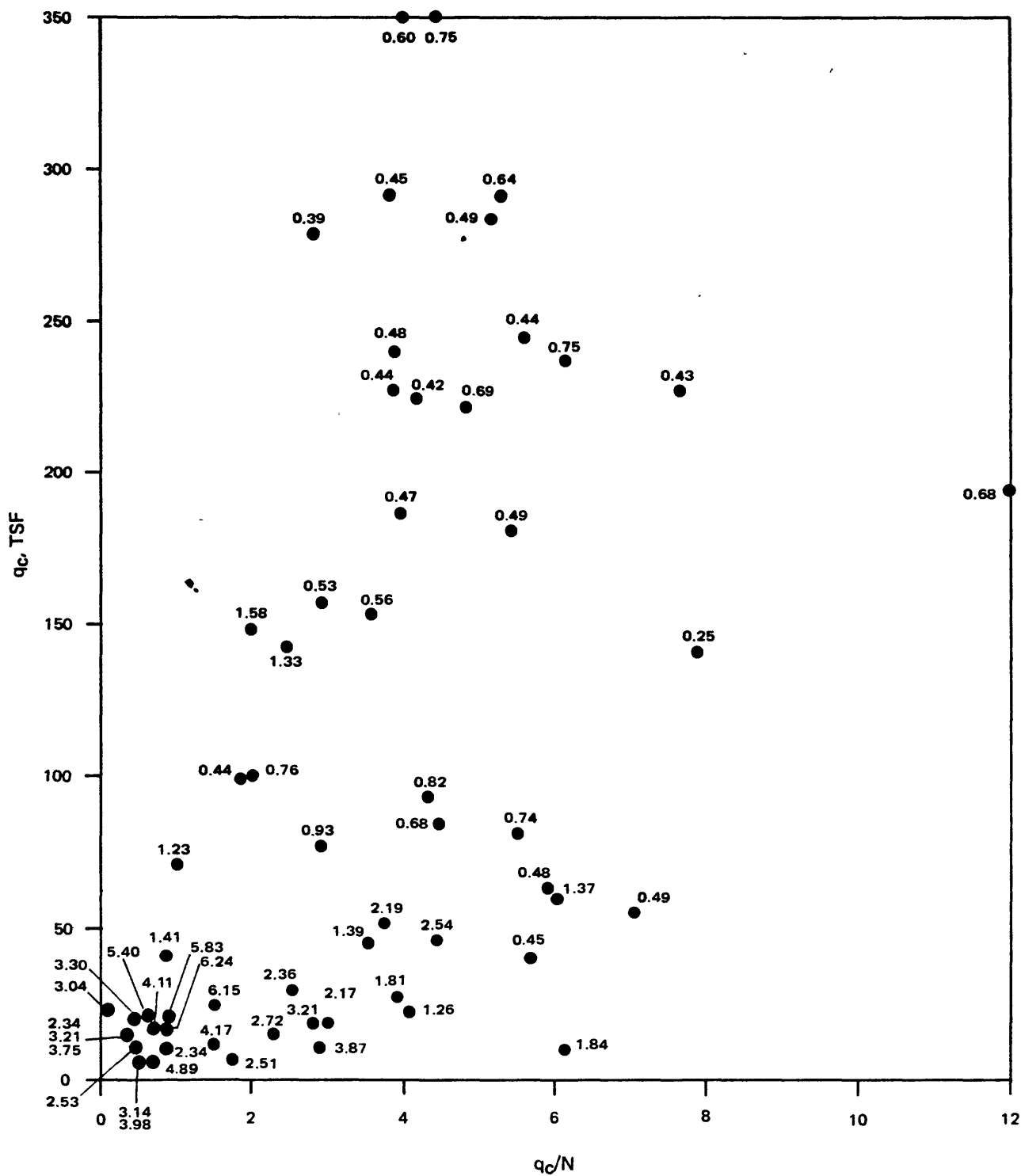
USGS CPT-SPT

MOSS LANDING SITE
 q_c/N VS q_c
STANDARD HAMMER

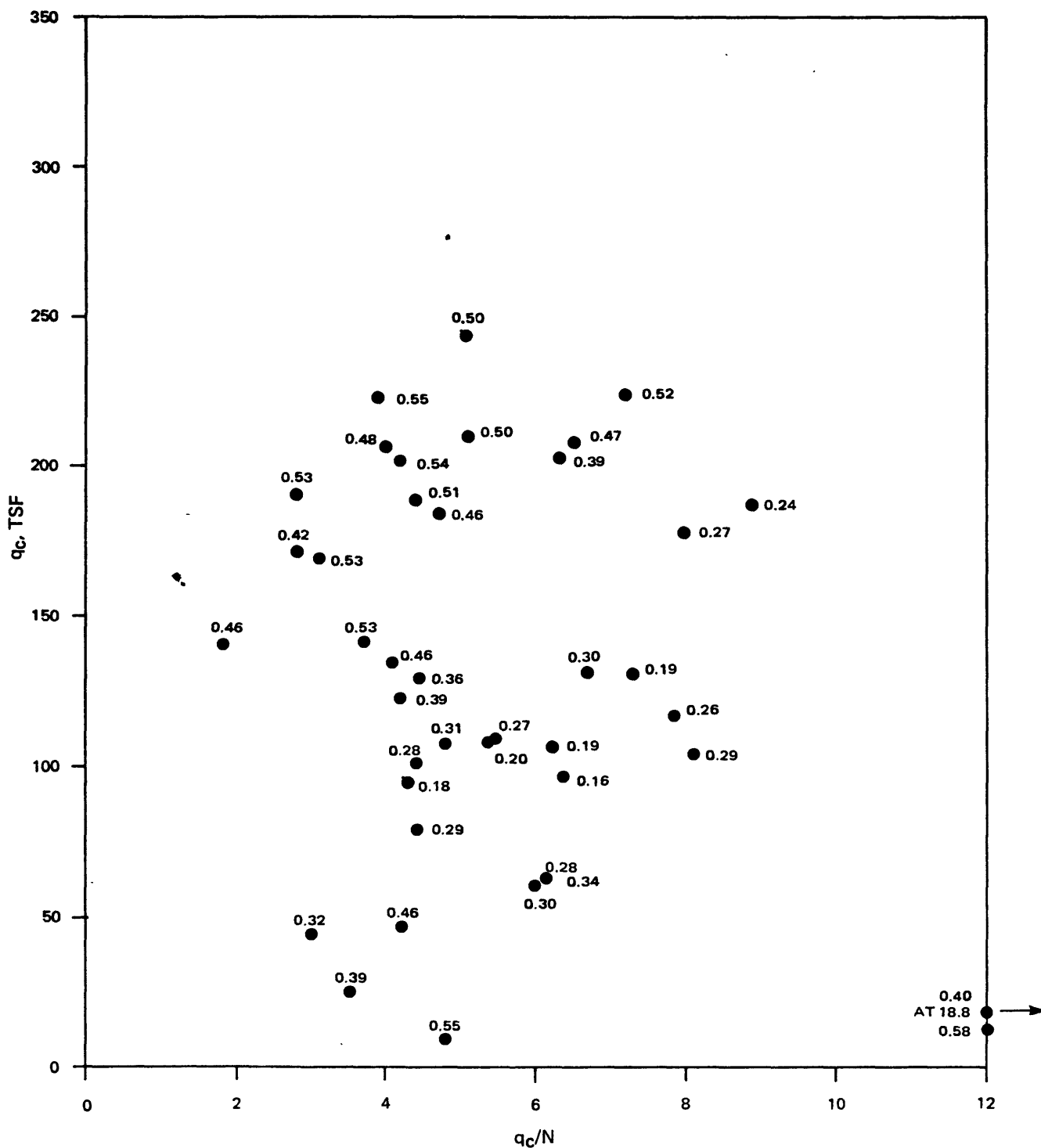
9-80

FIGURE B.31

Approved by /
Checked by /
Drawn by /
Compiled by /



Approved by
Checked by
Drawn by
Compiled by



NUMBERS ON POINTS REPRESENT FRICTION RATIO, %



PROJECT NO.:

70-153

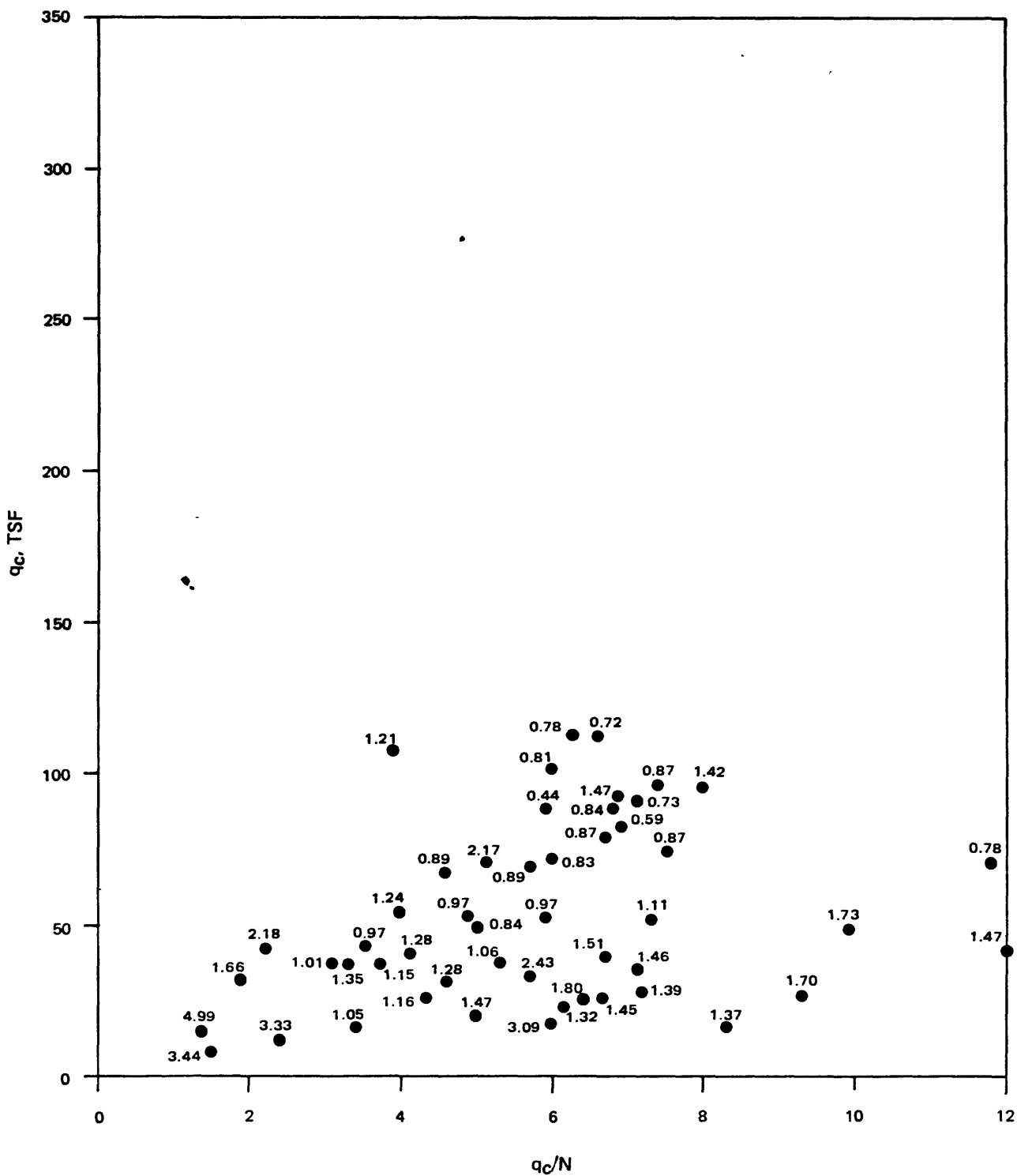
USGS CPT-SPT

SAN DIEGO SITE: NAS NORTH ISLAND
 q_c/N VS q_c
TRIP HAMMER

9-80

FIGURE B.33

Approved by /
Checked by /
Drawn by /
Compiled by /



NUMBERS ON POINTS REPRESENT FRICTION RATIO, %



PROJECT NO.:

79-153

USGS CPT-SPT

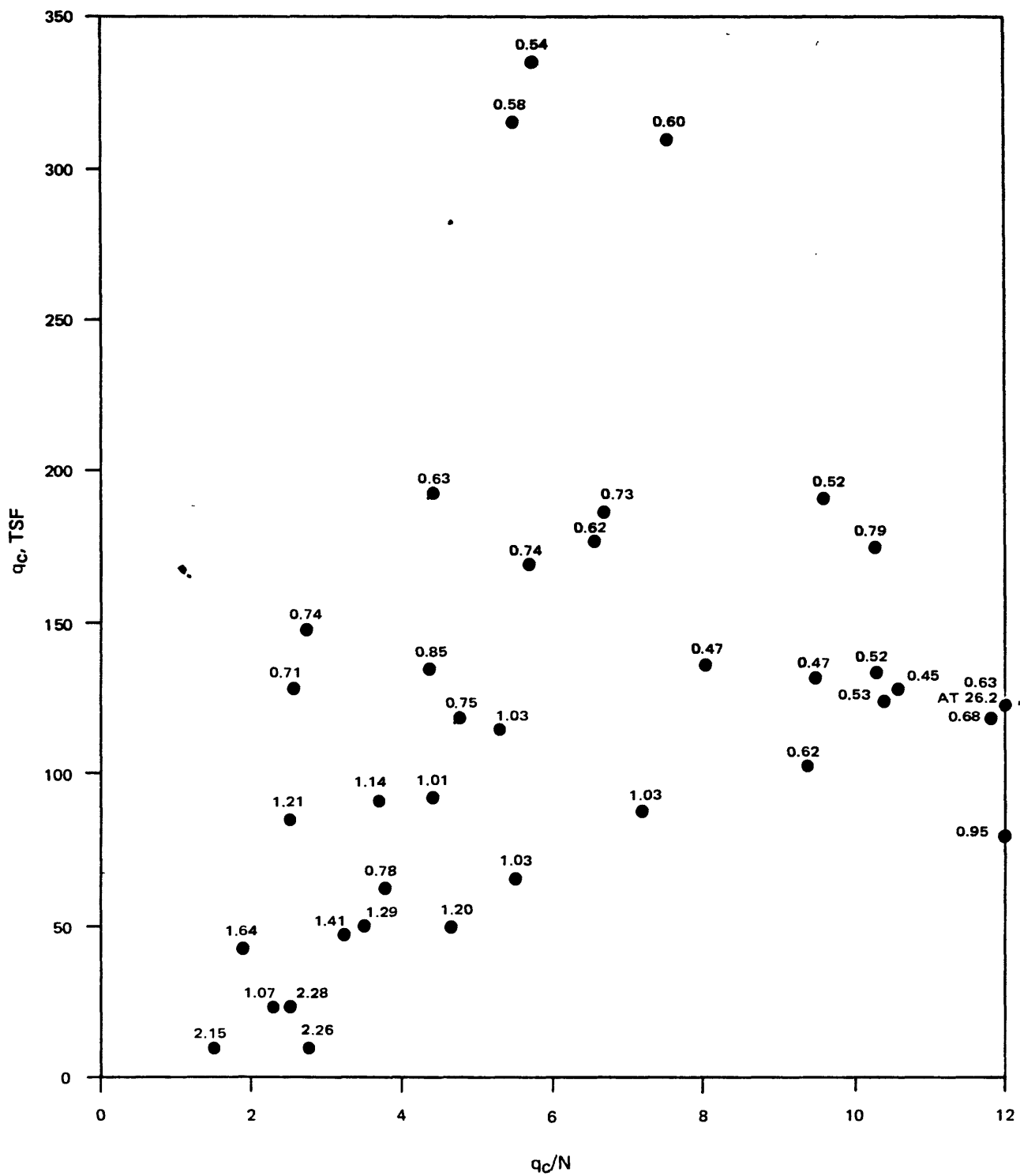
SALINAS SITE
 q_c/N VS q_c
TRIP HAMMER

Approved by

Checked by

Drawn by

Compiled by



NUMBERS ON POINTS REPRESENT FRICTION RATIO, %



PROJECT NO.:

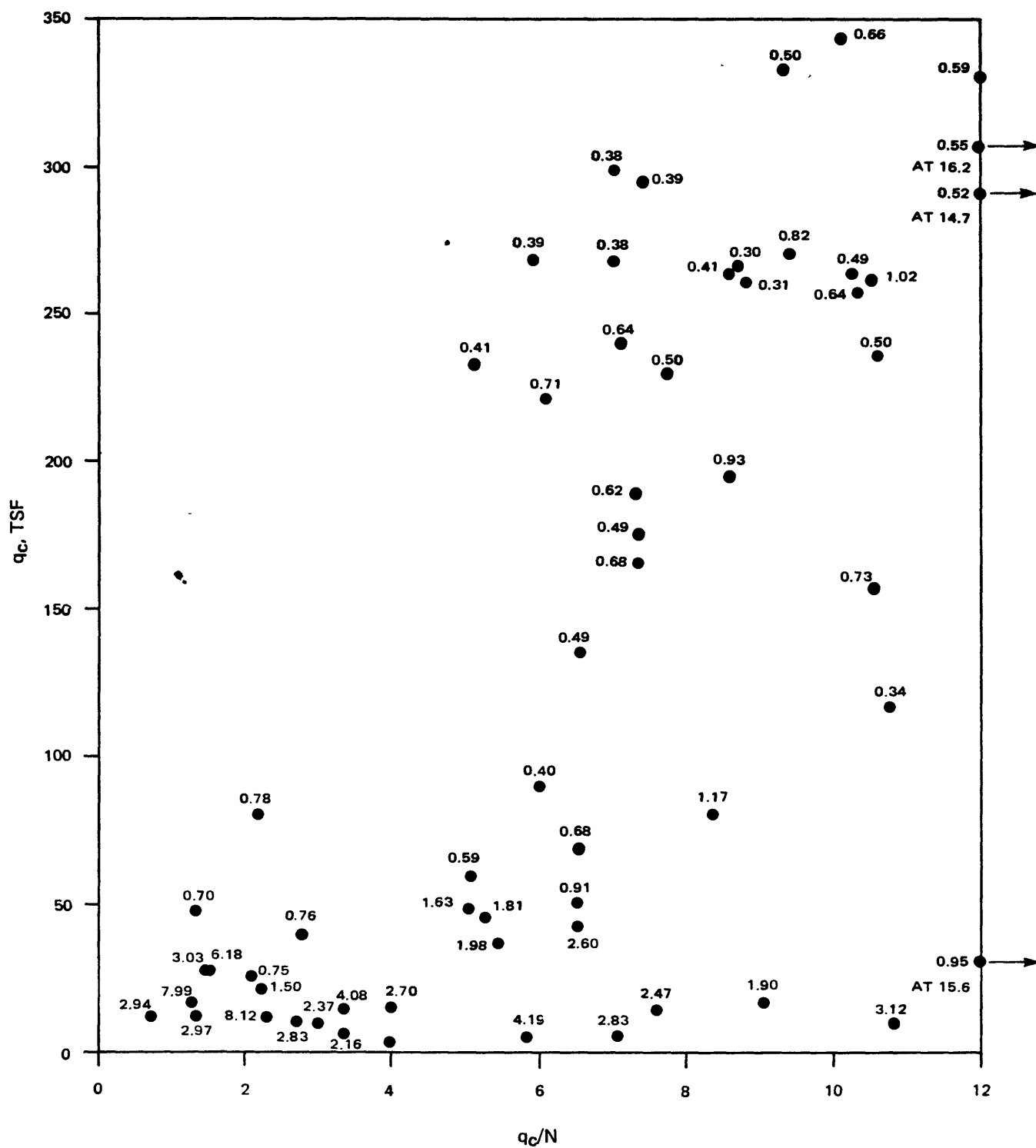
79-153

USGS CPT-SPT

MOSS LANDING SITE
 q_c/N VS q_c
TRIP HAMMER

9-80

FIGURE B.35



NUMBERS ON POINTS REPRESENT FRICTION RATIO, %



PROJECT NO.:

79-153

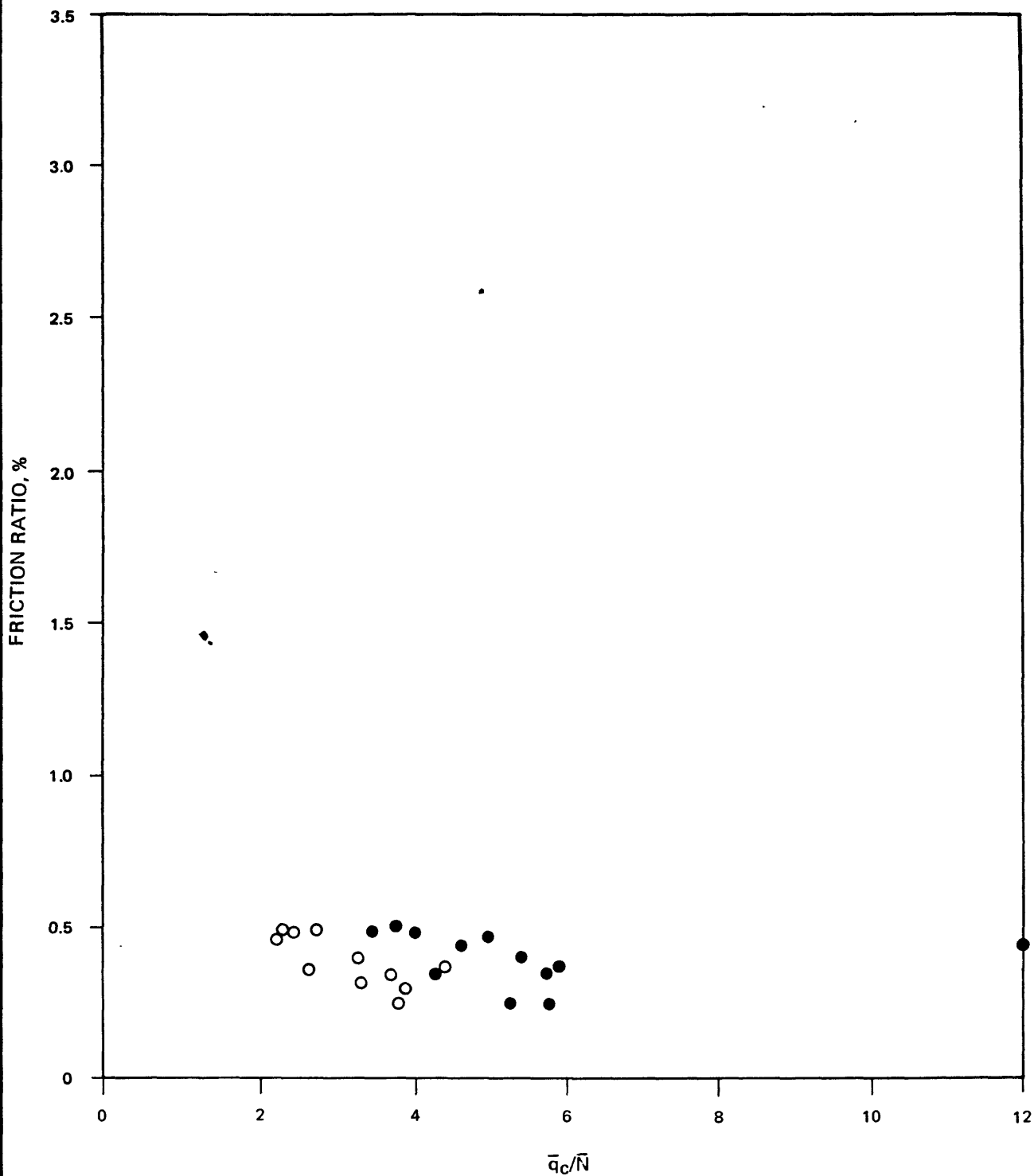
USGS CPT-SPT

SAN JOSE SITE:
COYOTE NORTH & SOUTH
qc/N VS qc
TRIP HAMMER

9-80

FIGURE B.36

Approved by _____
Checked by _____
Drawn by _____
Compiled by _____



○ STANDARD
● TRIP



PROJECT NO.:

79-153

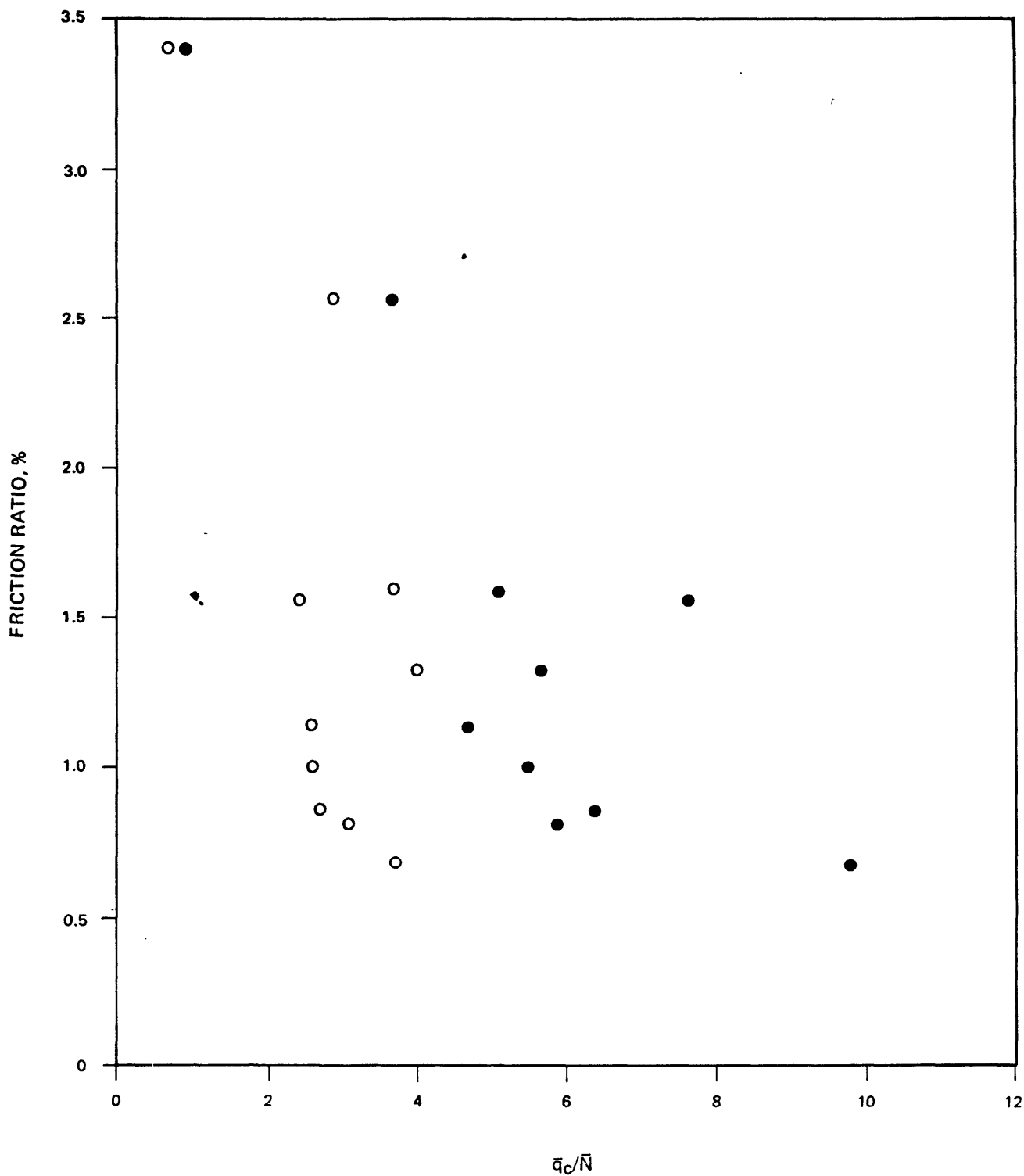
USGS CPT-SPT

SAN DIEGO SITE: NAS NORTH ISLAND
 \bar{q}_c/\bar{N} VS FRICTION RATIO
BY LAYER AVERAGES

9-80

FIGURE B.37

Approved by _____
Checked by _____
Drawn by _____
Compiled by _____



- STANDARD
- TRIP



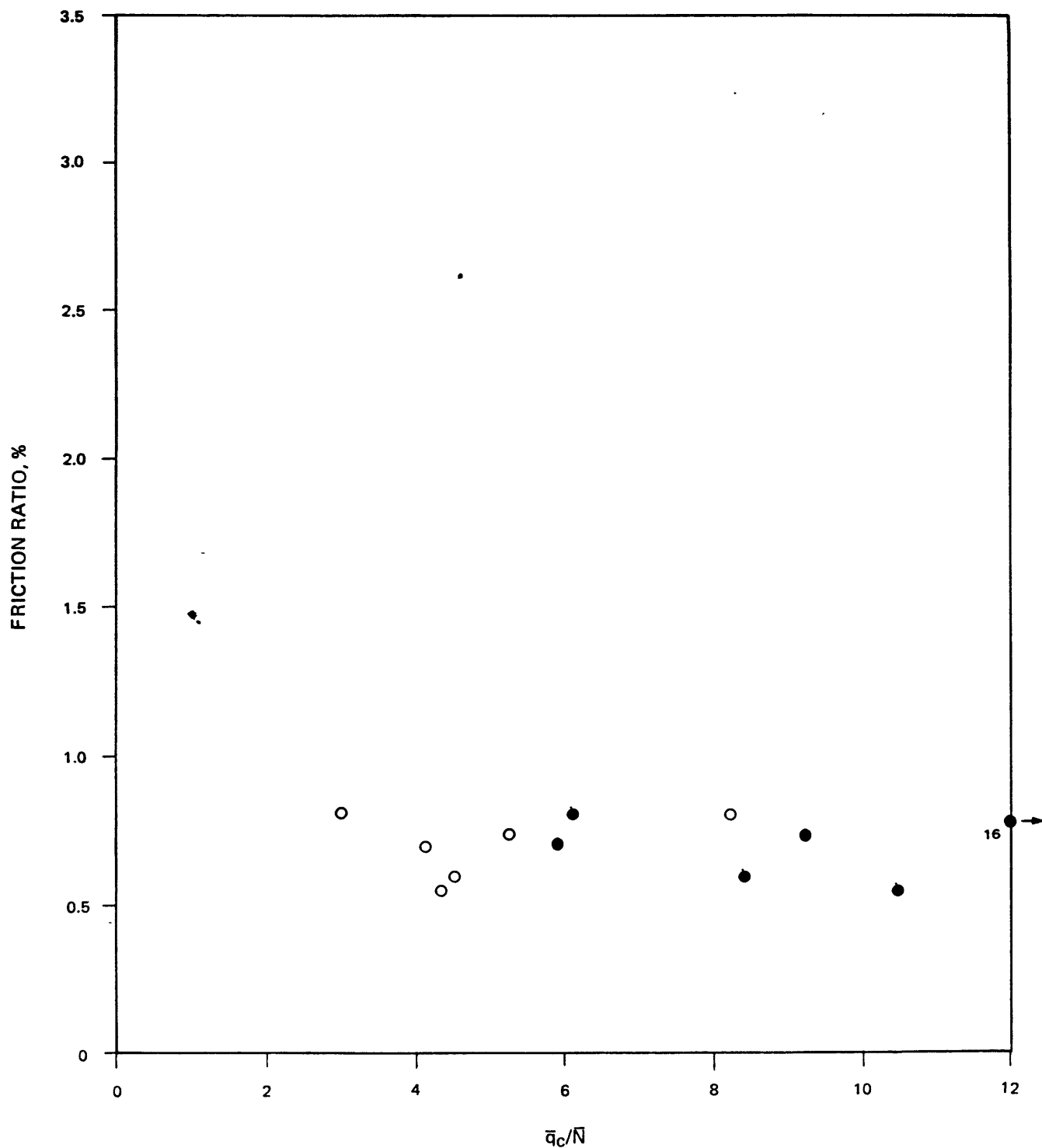
PROJECT NO.:

79-153

USGS CPT-SPT

SALINAS SITE
 q_c/\bar{N} VS FRICTION RATIO
BY LAYER AVERAGES

Approved by _____
Checked by _____
Drawn by _____
Compiled by _____



○ STANDARD
● TRIP



PROJECT NO.:

79-153

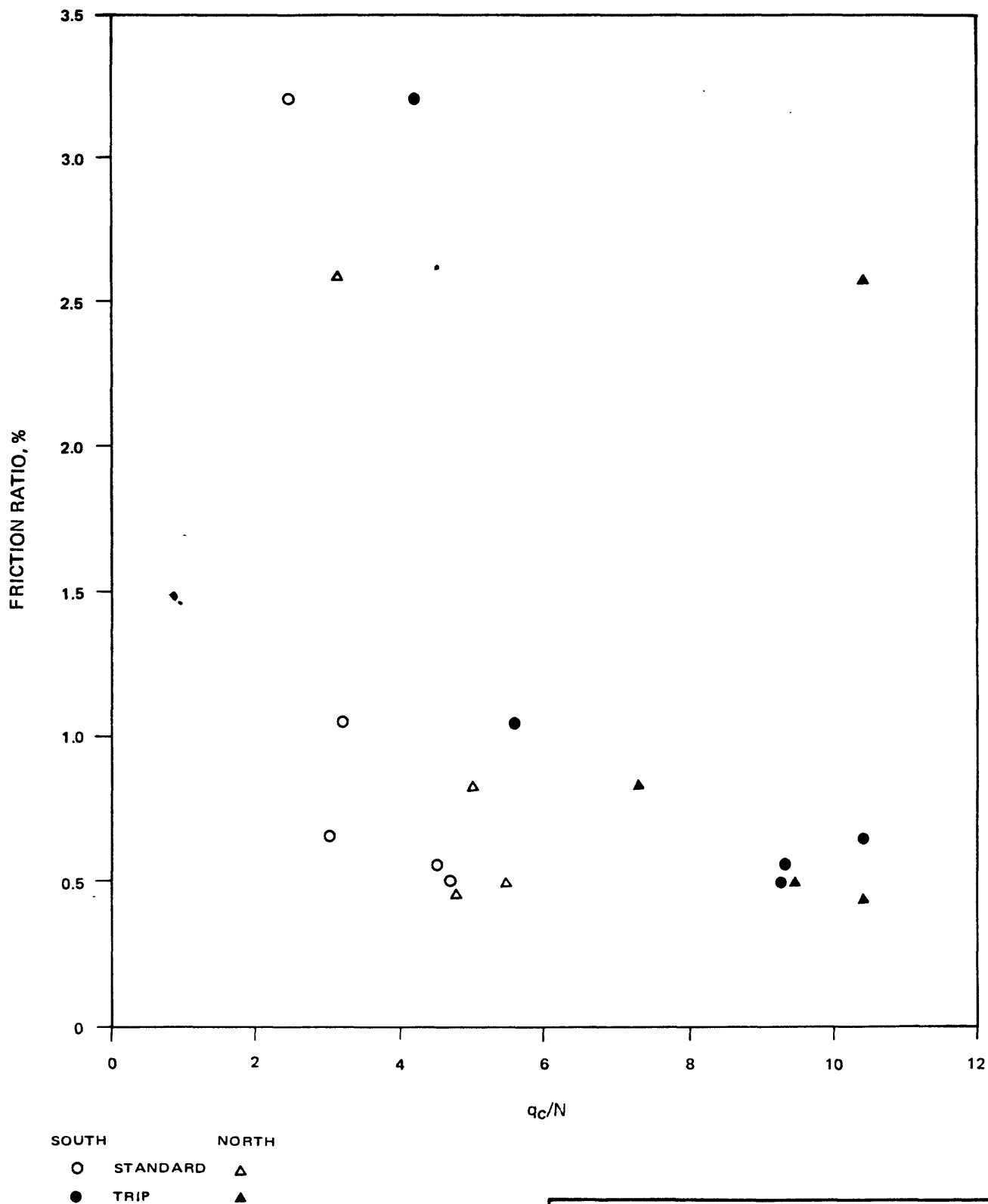
USGS CPT-SPT


MOSS LANDING SITE
 \bar{q}_c/\bar{N} VS FRICTION RATIO
BY LAYER AVERAGES

9-80

FIGURE B.39

Approved by _____
Checked by _____
Drawn by _____
Compiled by _____





PROJECT NO.: 79-153

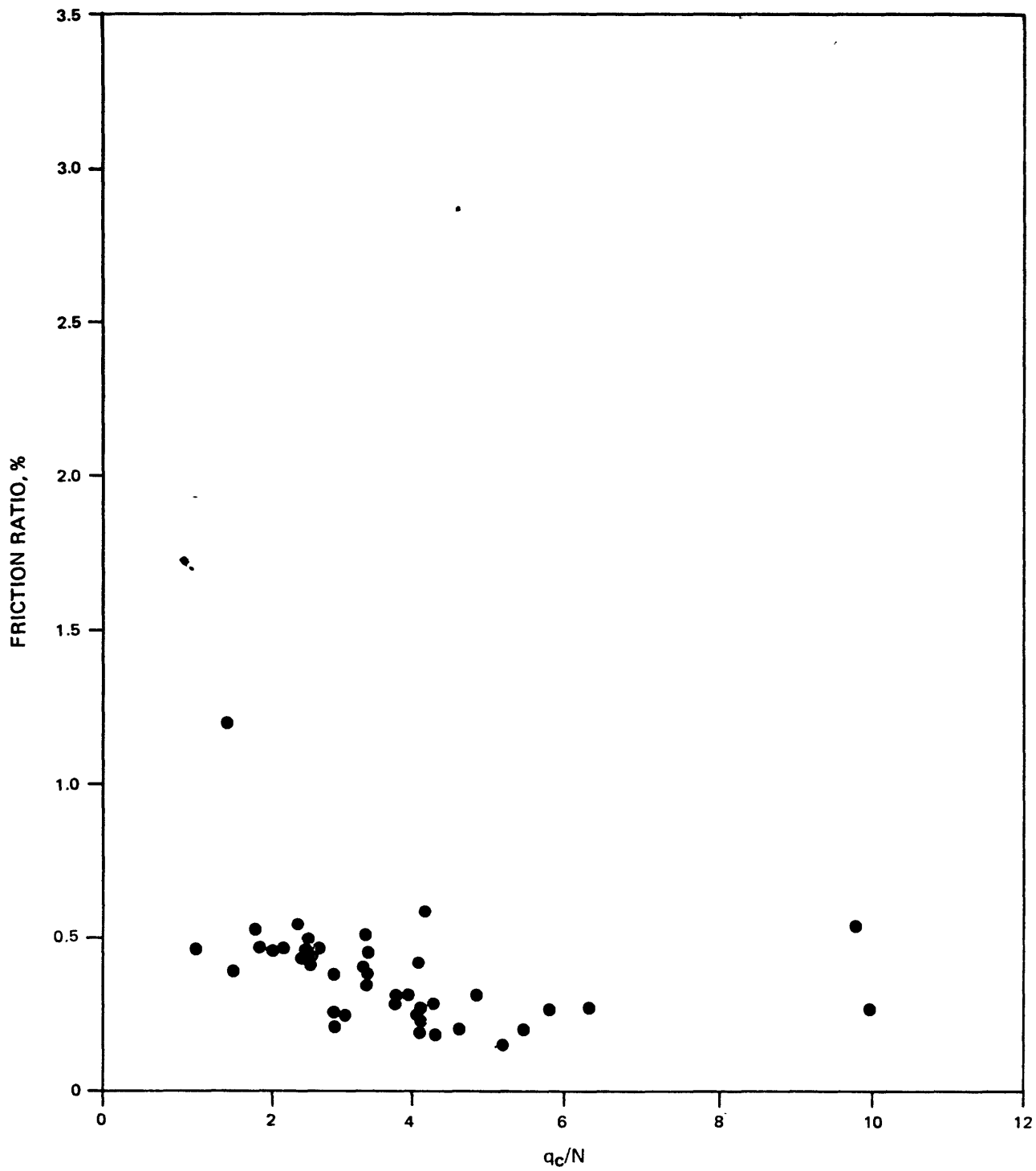
USGS CPT-SPT


SAN JOSE SITE:
COYOTE NORTH & SOUTH
qc/N VS FRICTION RATIO
BY LAYER AVERAGES

9-80

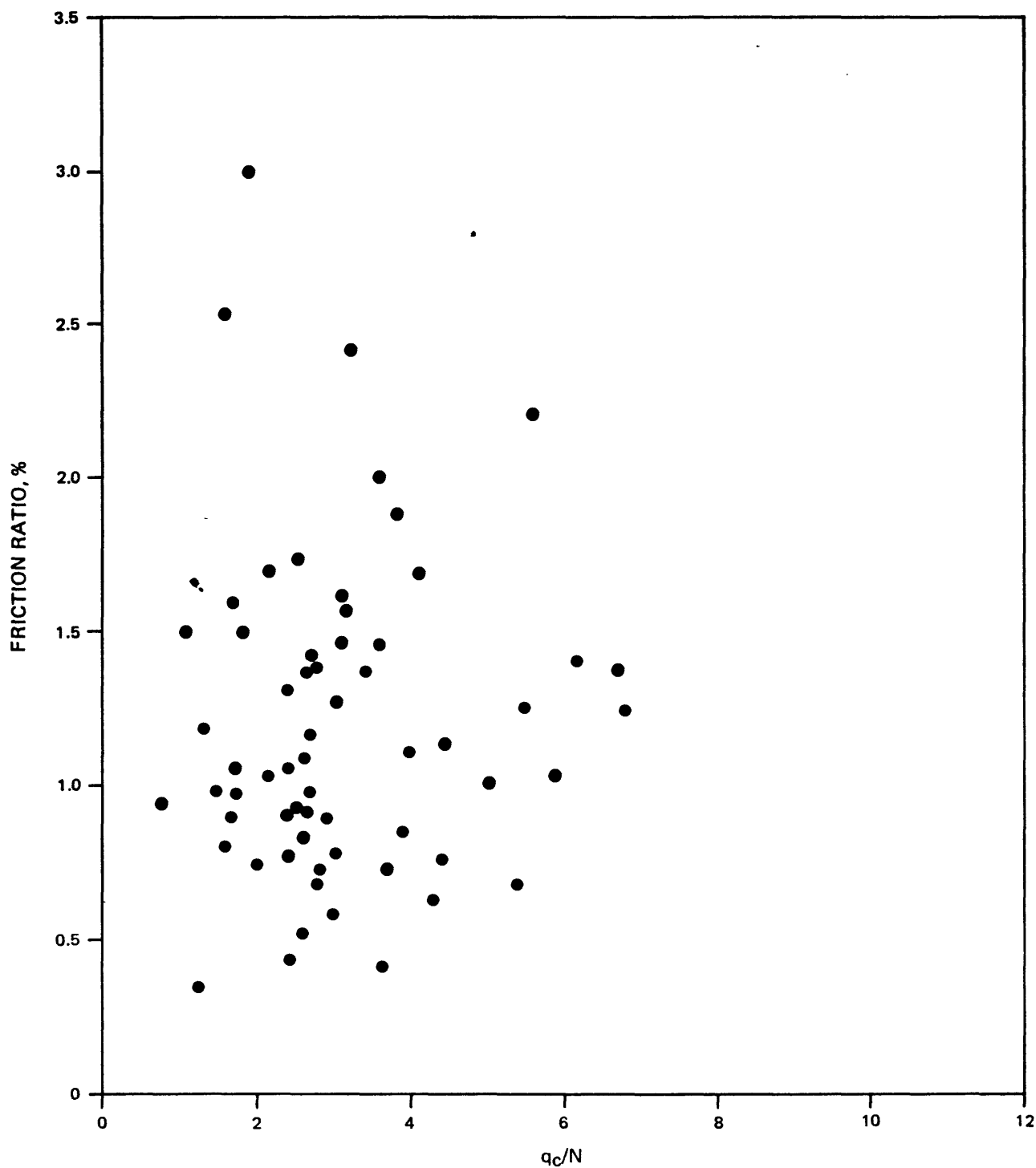
FIGURE B.40

Approved by _____
Checked by _____
Drawn by _____
Compiled by _____



	PROJECT NO.:	79-153
	USGS CPT-SPT	
SAN DIEGO SITE: NAS NORTH ISLAND		
q_c/N VS FRICTION RATIO		
STANDARD HAMMER		
9-80	FIGURE B.41	

Compiled by _____
Drawn by _____
Checked by _____
Approved by _____



PROJECT NO.:

79-153

USGS CPT-SPT

SALINAS SITE
 q_c/N VS FRICTION RATIO
STANDARD HAMMER

9-80

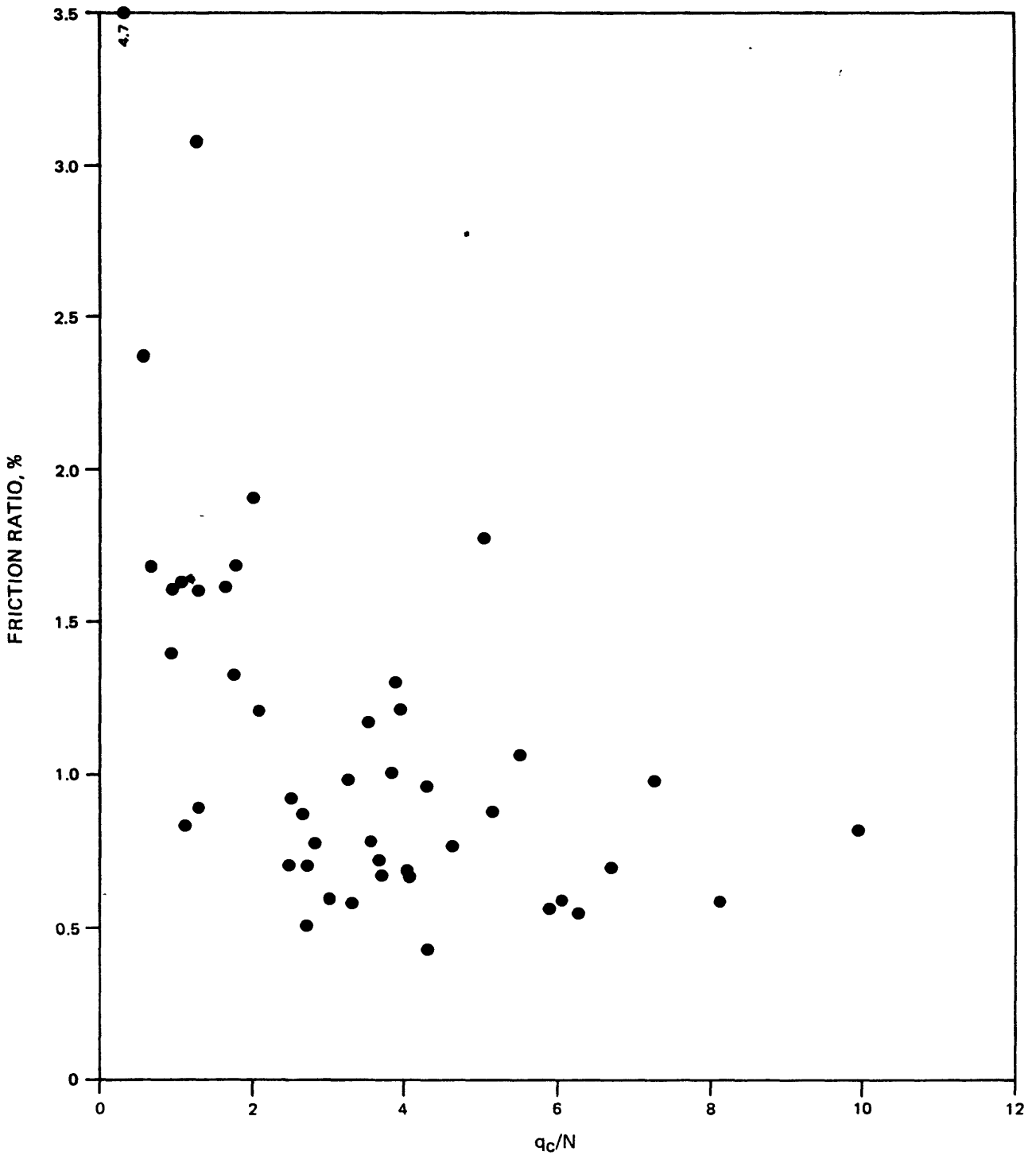
FIGURE B.42

Approved by

Checked by

Drawn by

Compiled by



PROJECT NO.:

79-153

USGS CPT-SPT

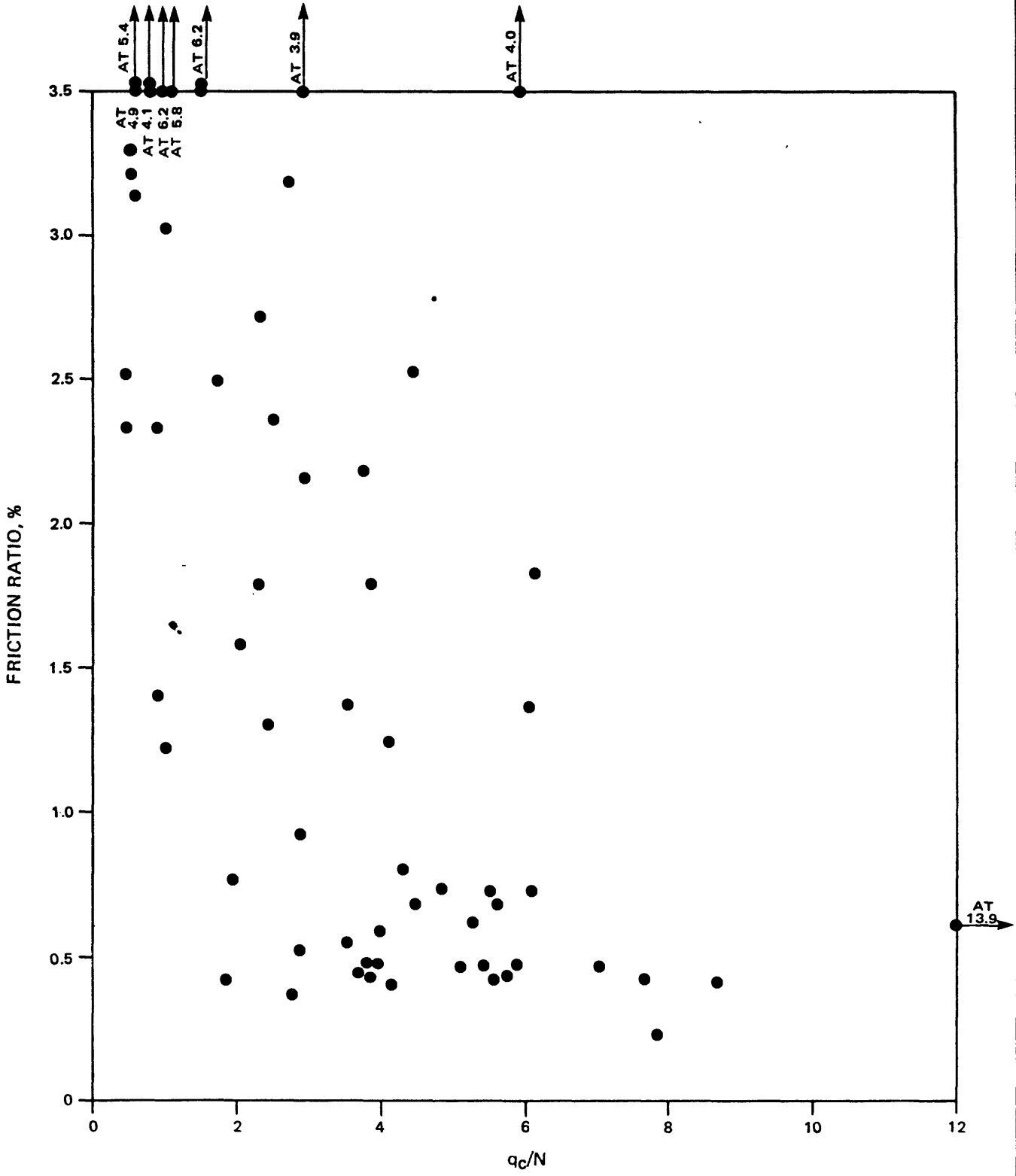
MOSS LANDING SITE
 q_c/N VS FRICTION RATIO
STANDARD HAMMER


Approved by

Checked by

Drawn by

Compiled by





PROJECT NO.: 79-153

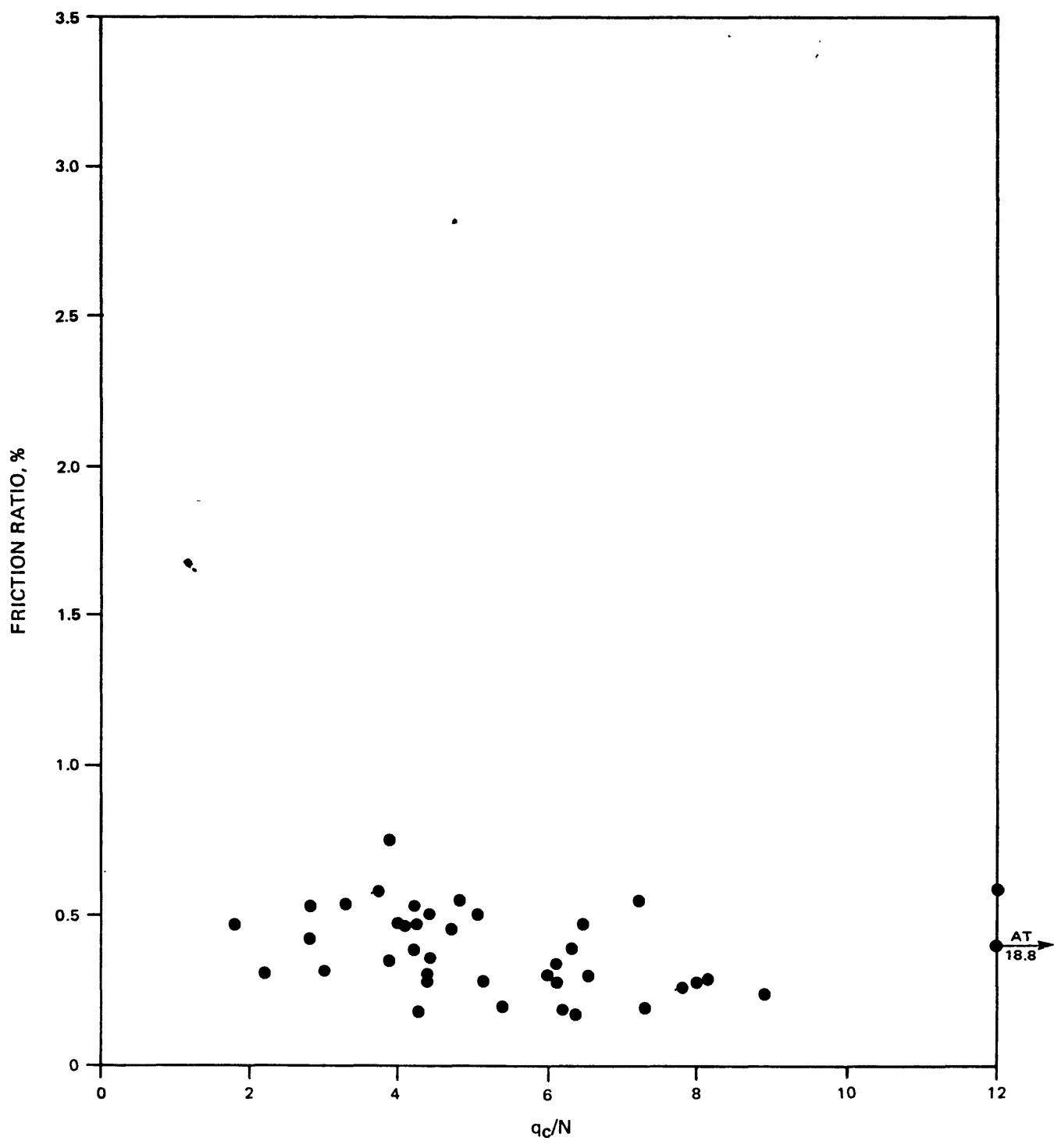
USGS CPT-SPT


SAN JOSE SITE:
COYOTE NORTH & SOUTH
 q_c/N VS FRICTION RATIO
STANDARD HAMMER

9-80

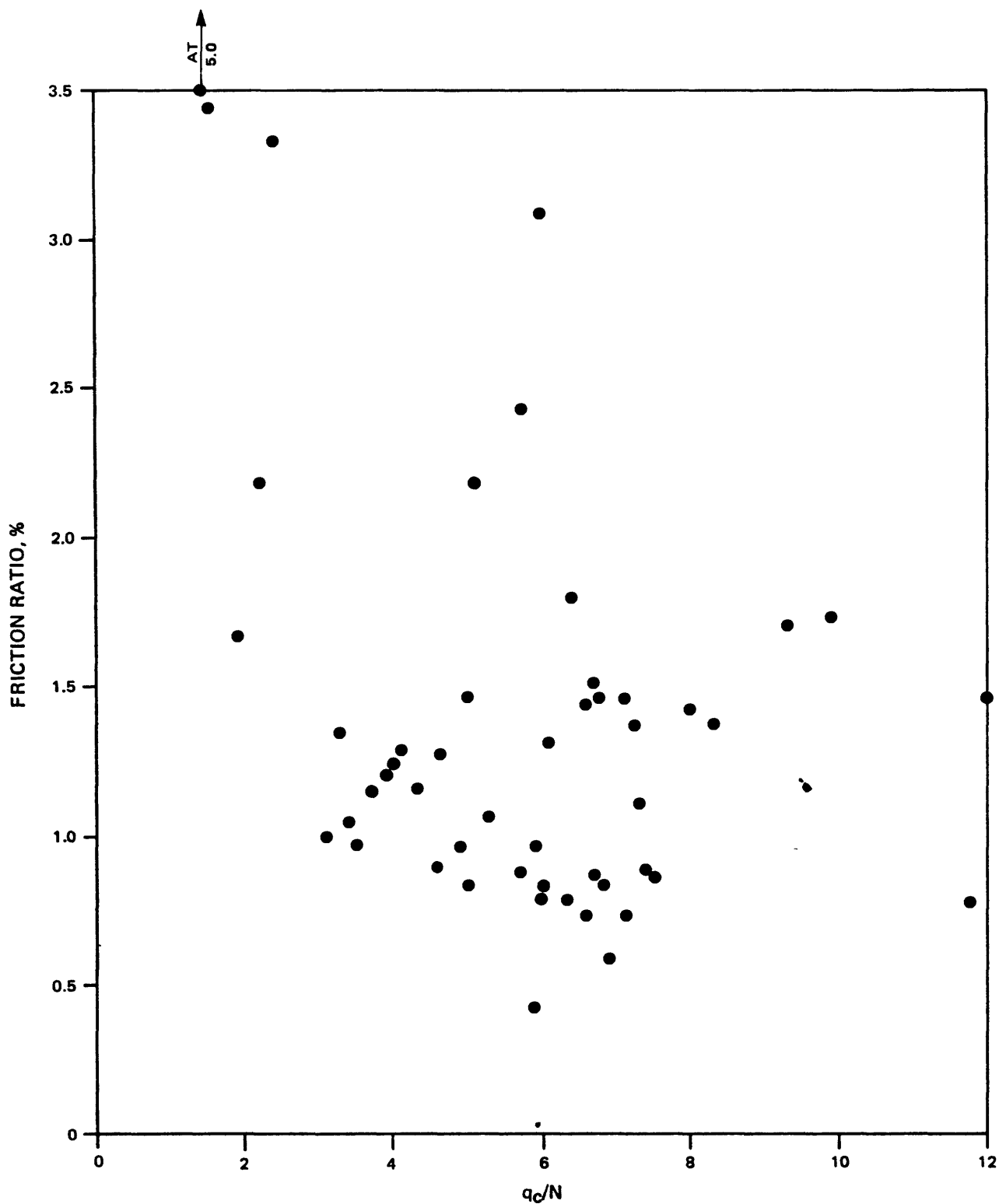
FIGURE B.44

Compiled by _____
Drawn by _____
Checked by _____
Approved by _____



	PROJECT NO.:	79-153
	USGS CPT-SPT	
SAN DIEGO SITE: NAS NORTH ISLAND		
q_c/N VS FRICTION RATIO		
TRIP HAMMER		
9-80	FIGURE B.45	

Approved by _____
Checked by _____
Drawn by _____
Compiled by _____



PROJECT NO.:

79-153

USGS CPT-SPT

SALINAS SITE
 q_c/N VS FRICTION RATIO
TRIP HAMMER

9-80

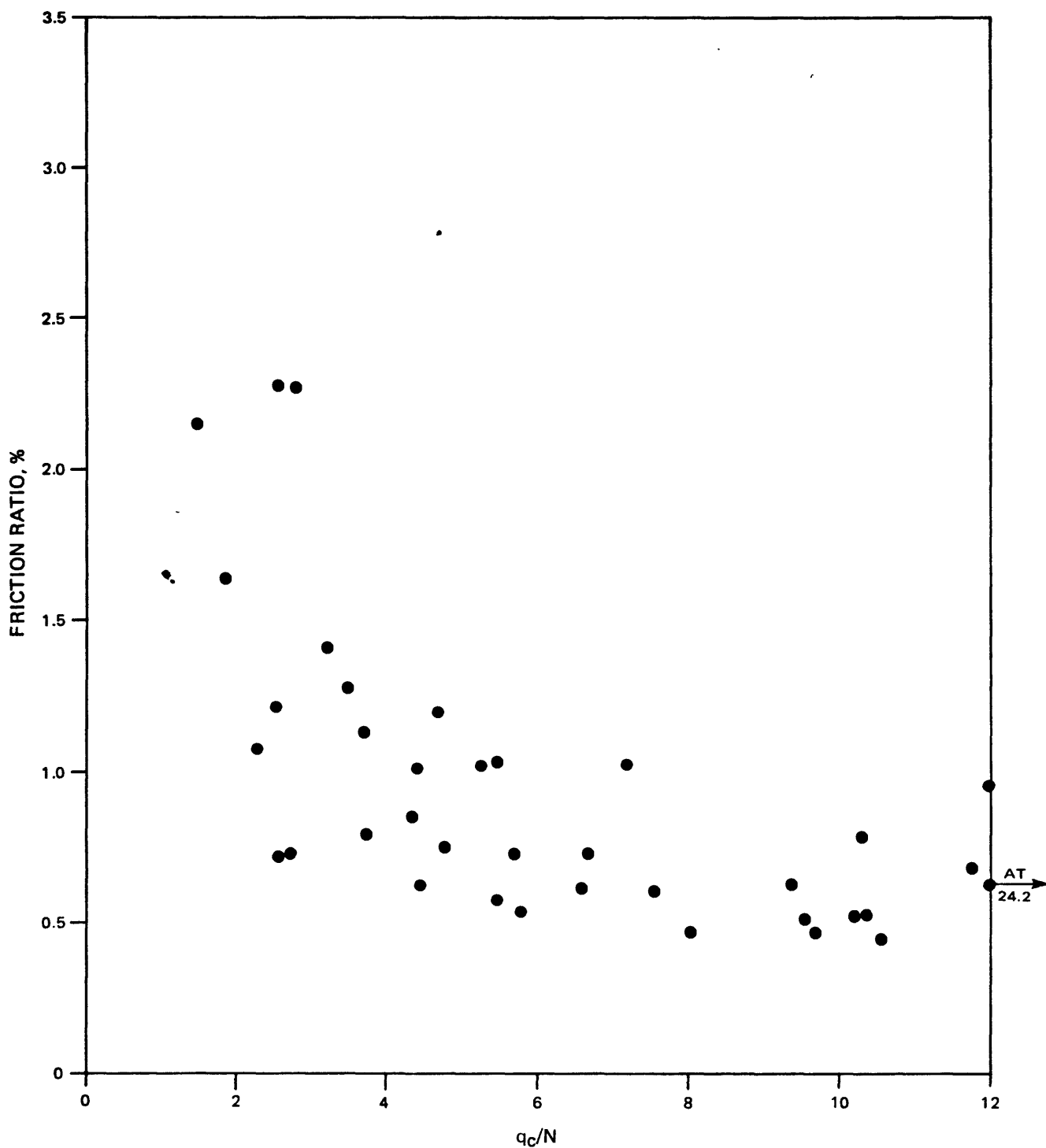
FIGURE B.46

Approved by

Checked by

Drawn by

Compiled by



PROJECT NO.:

79-153

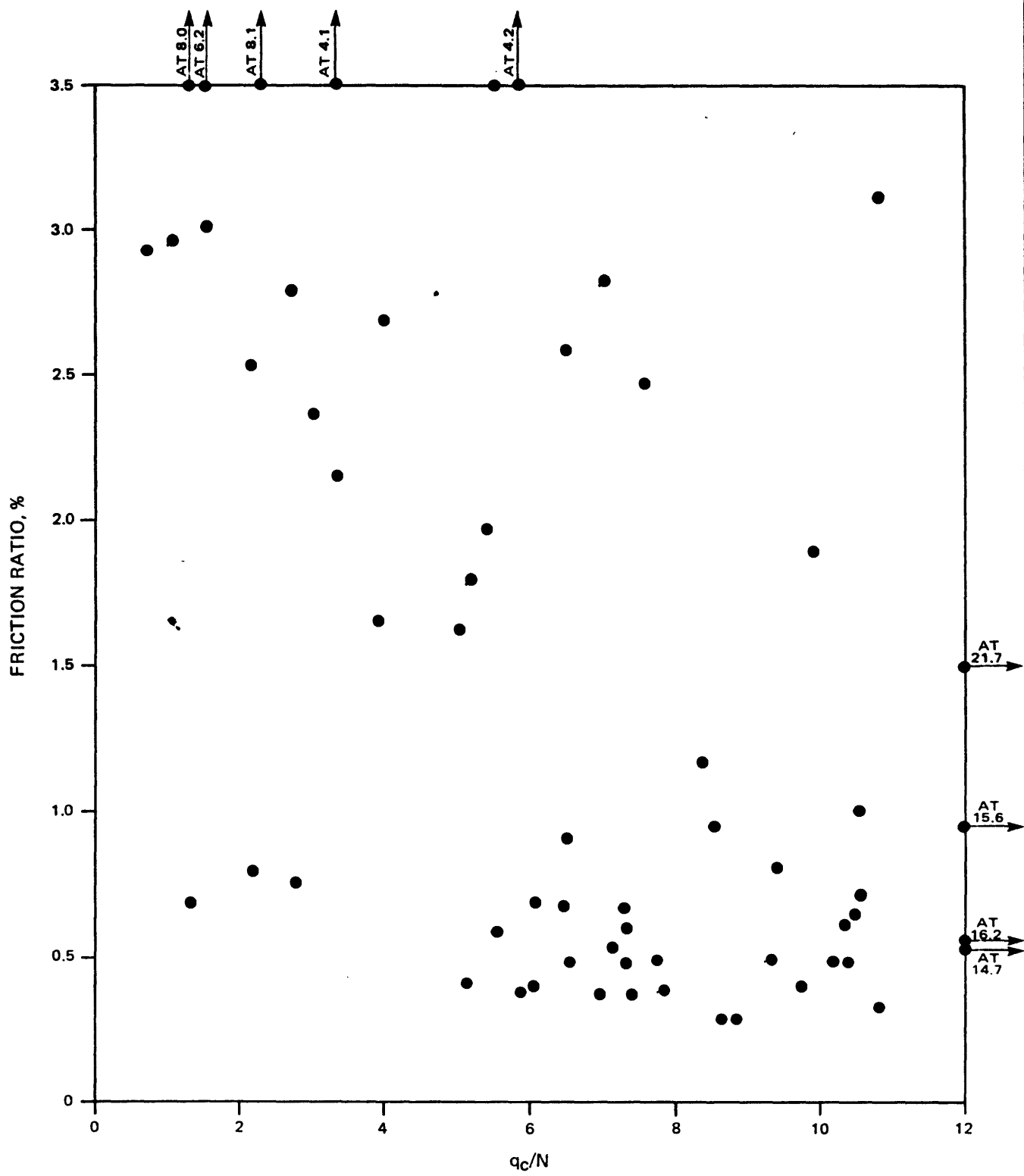
USGS CPT-SPT


MOSS LANDING SITE
 q_c/N VS FRICTION RATIO
TRIP HAMMER

9-80

FIGURE B.47

Approved by _____
Checked by _____
Drawn by _____
Compiled by _____





PROJECT NO.: 79-153

USGS CPT-SPT

SAN JOSE SITE:
COYOTE NORTH & SOUTH
 q_c/N VS FRICTION RATIO
TRIP HAMMER

9-80

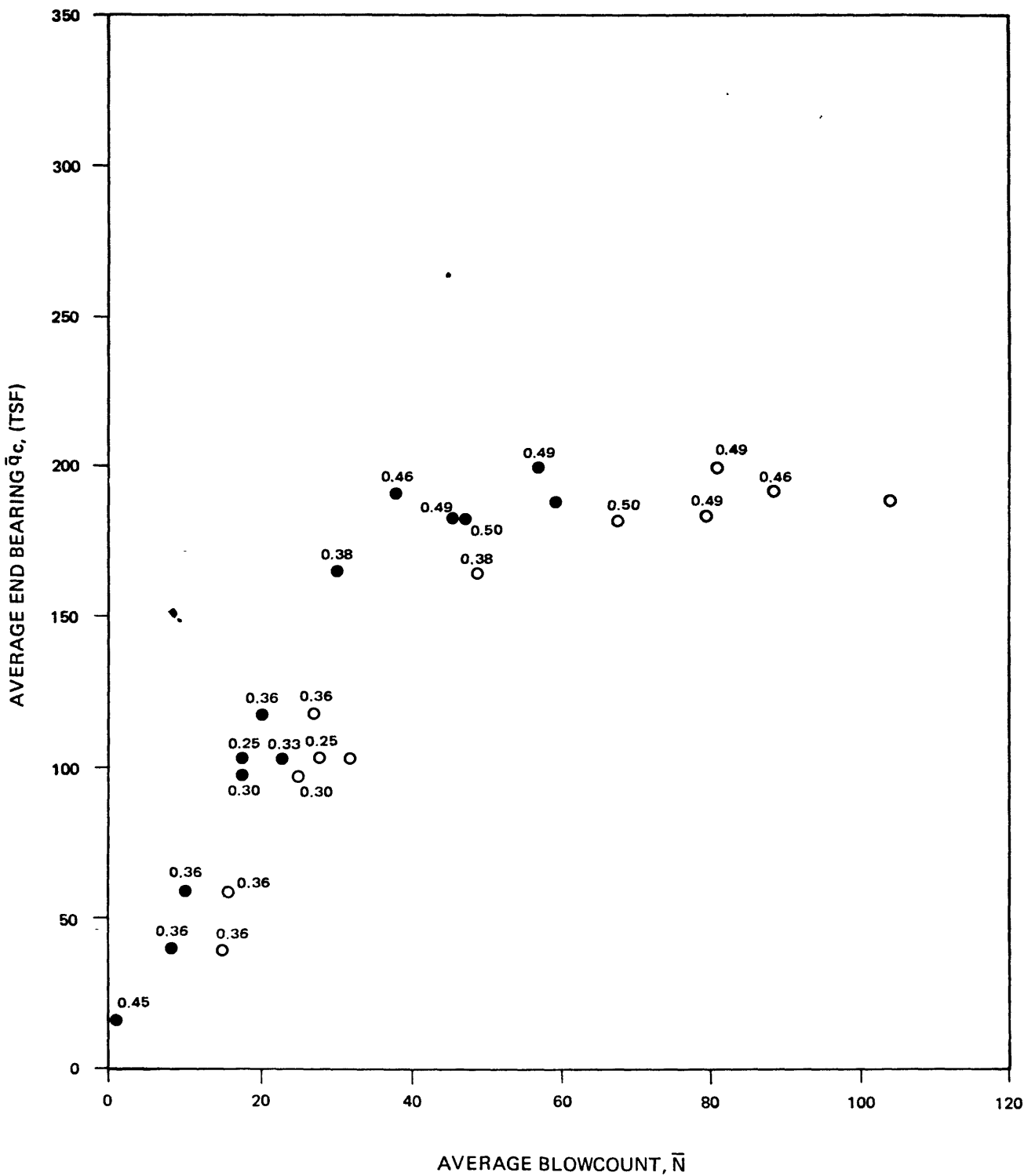
FIGURE B.48

Approved by

Checked by

Drawn by

Compiled by



O STANDARD

● TRIP

NUMBERS ON POINTS REPRESENT FRICTION RATIO, %



PROJECT NO.:

79-153

USGS CPT-SPT

SAN DIEGO SITE: NAS NORTH ISLAND
 \bar{q}_c VS \bar{N} BY LAYER AVERAGES

9-80

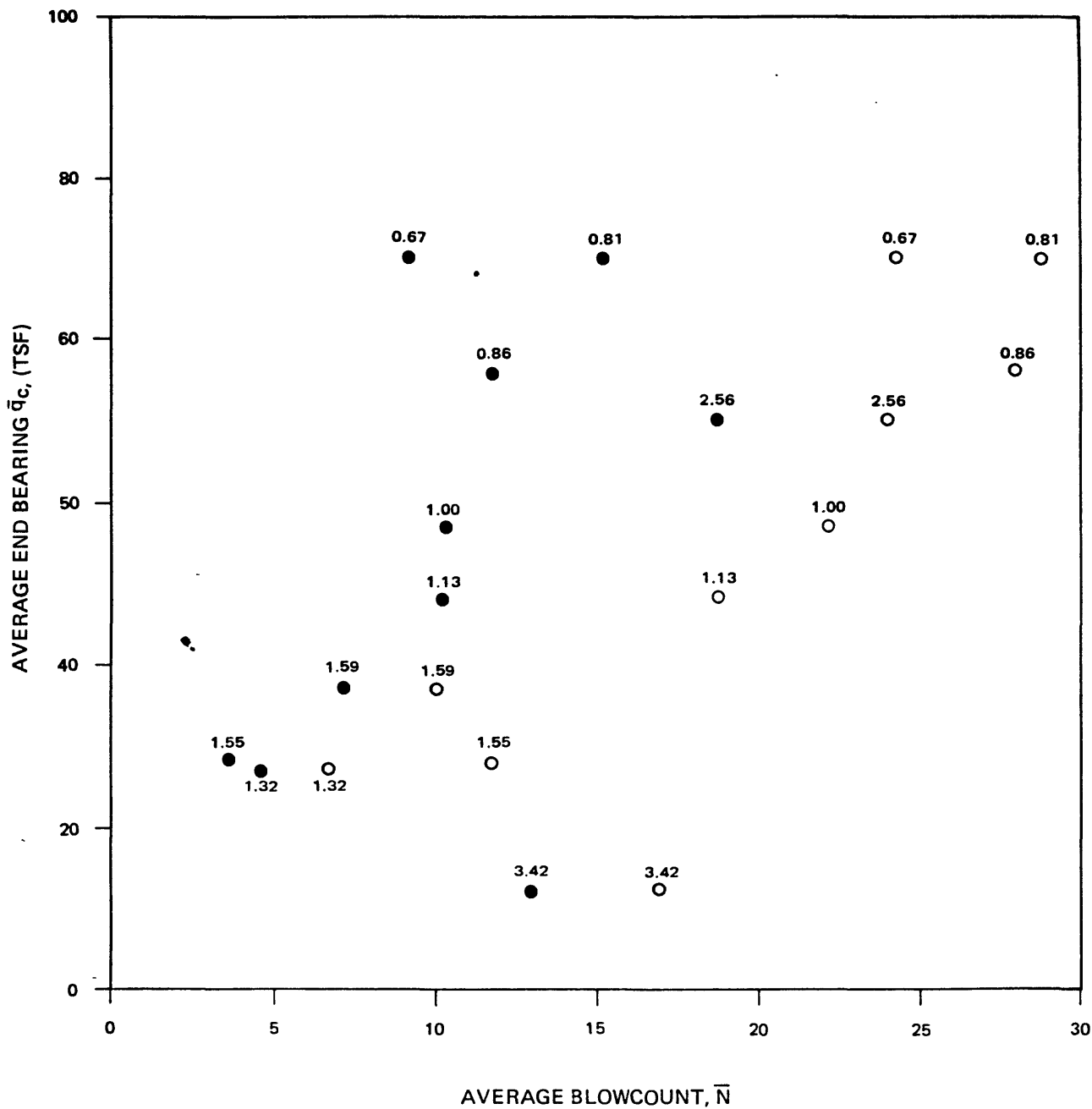
FIGURE B.49

Approved by

Checked by

Drawn by

Compiled by



○ STANDARD

● TRIP

NUMBERS ON POINTS REPRESENT FRICTION RATIO, %



PROJECT NO.:

79-153

USGS CPT-SPT

SALINAS SITE
 \bar{q}_c VS \bar{N} BY LAYER AVERAGES

9-80

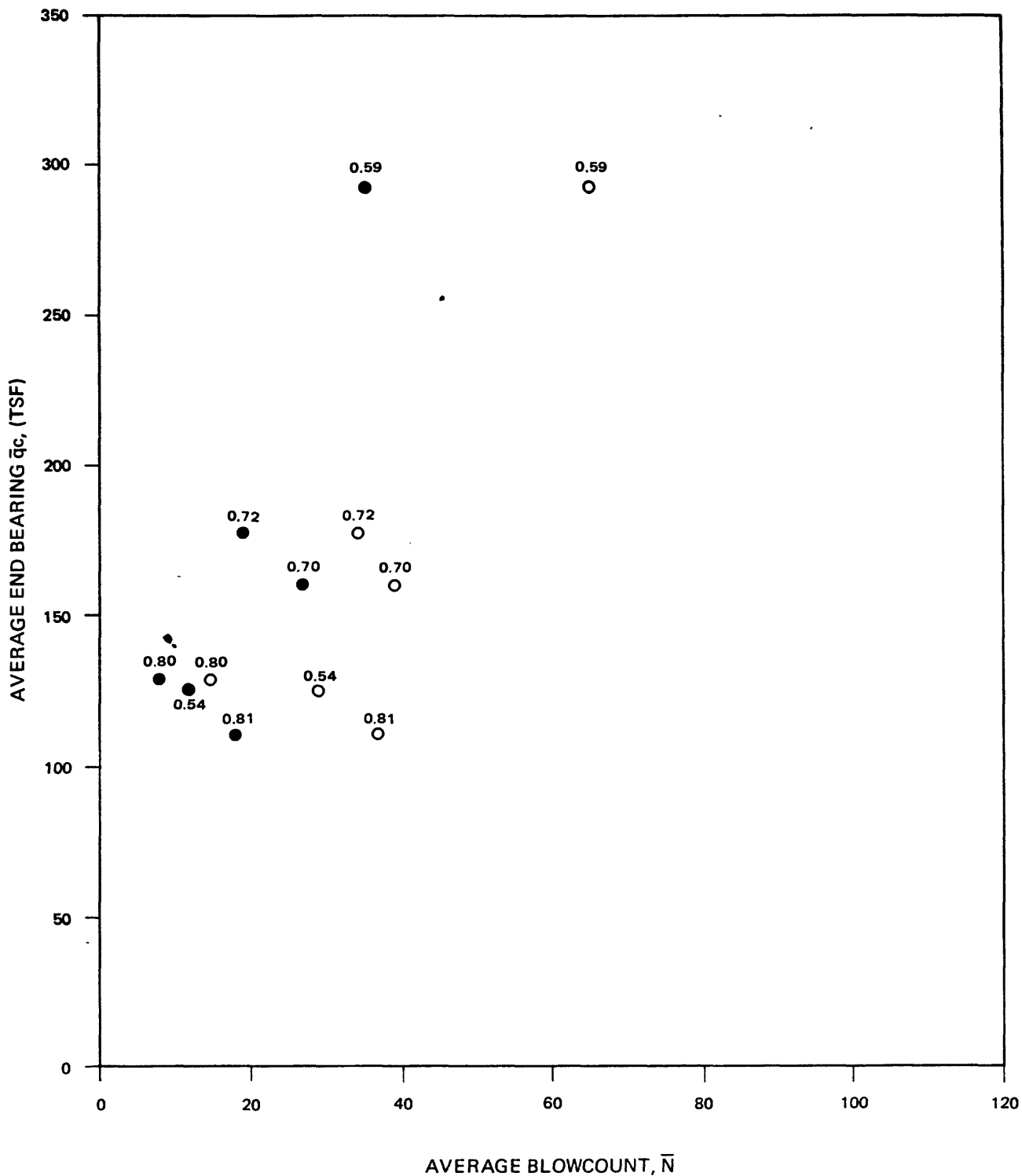
FIGURE 8.50

Approved by

Checked by

Drawn by

Compiled by



○ STANDARD

● TRIP

NUMBERS ON POINTS REPRESENT FRICTION RATIO, %



PROJECT NO.:

79-153

USGS CPT-SPT

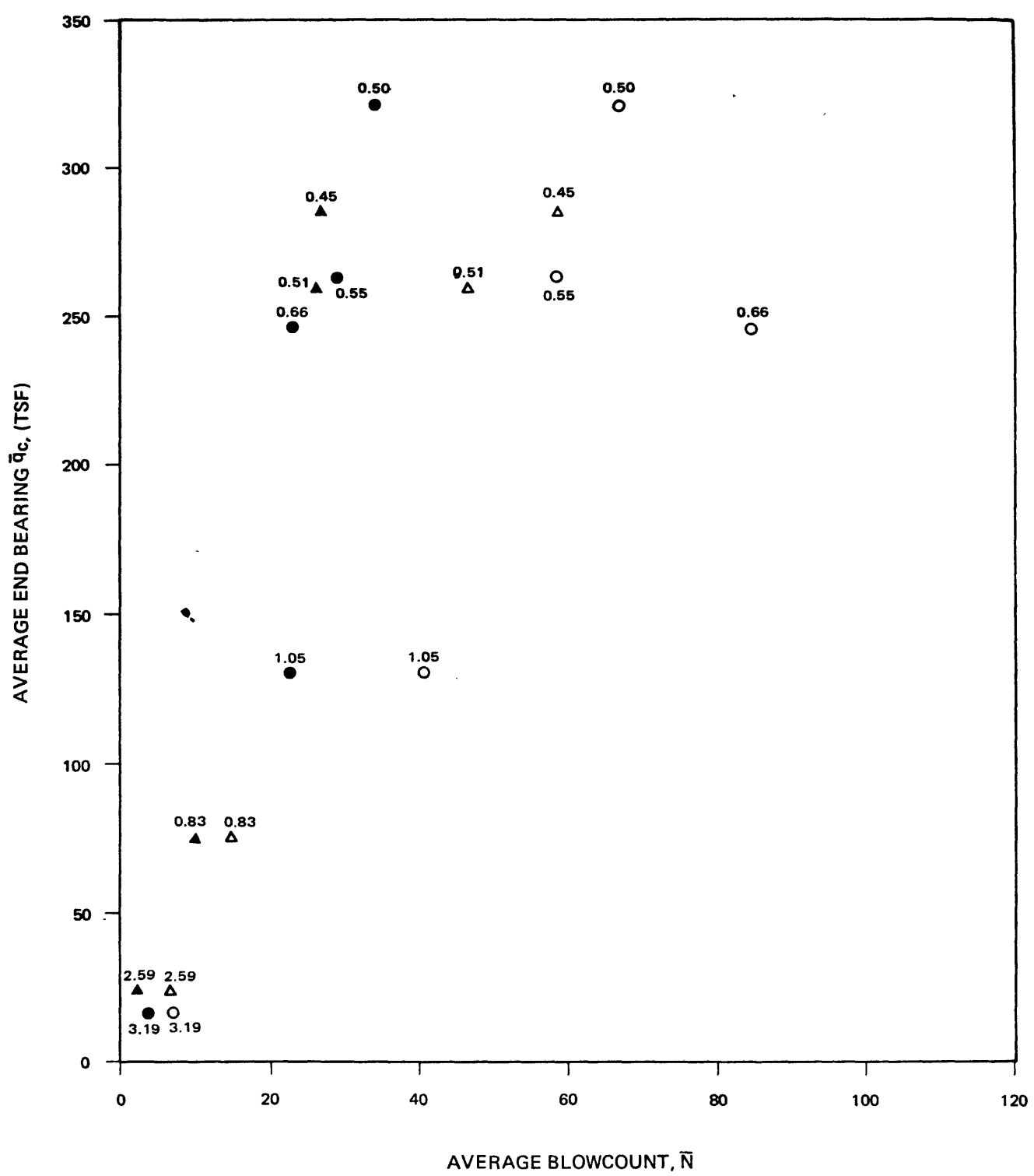
MOSS LANDING SITE
 \bar{q}_c VS \bar{N} BY LAYER AVERAGES

Approved by

Checked by

Drawn by

Compiled by




SOUTH NORTH

○ STANDARD △

● TRIP ▲

NUMBERS ON POINTS REPRESENT FRICTION RATIO, %



PROJECT NO.: 79-153

USGS CPT-SPT

SAN JOSE SITE:
COYOTE NORTH & SOUTH
 \bar{q}_c VS \bar{N} BY LAYER AVERAGES

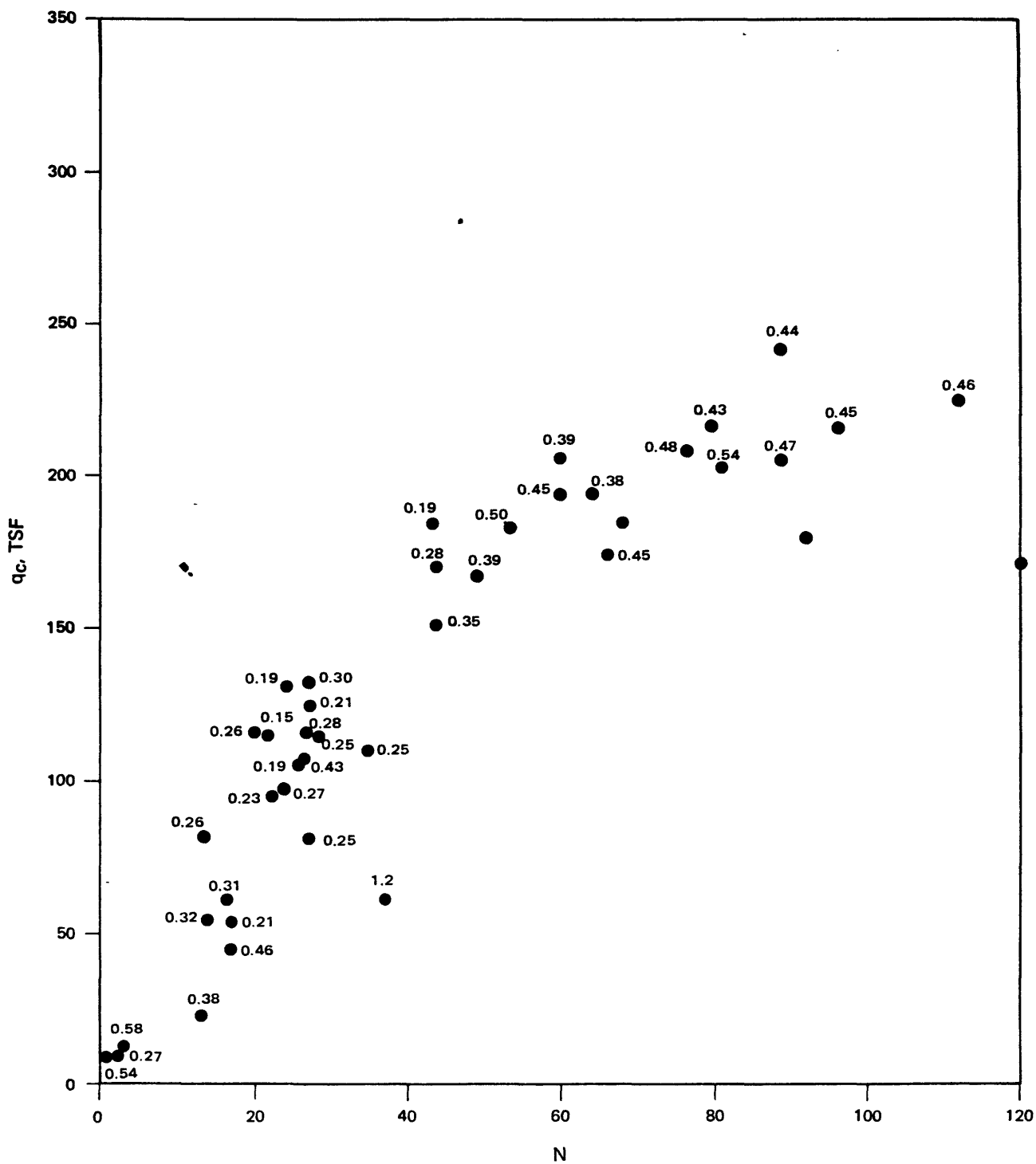
9-80 FIGURE B.52

Approved by

Checked by

Drawn by

Compiled by



NUMBERS ON POINTS REPRESENT FRICTION RATIO, %



PROJECT NO.:

79-153

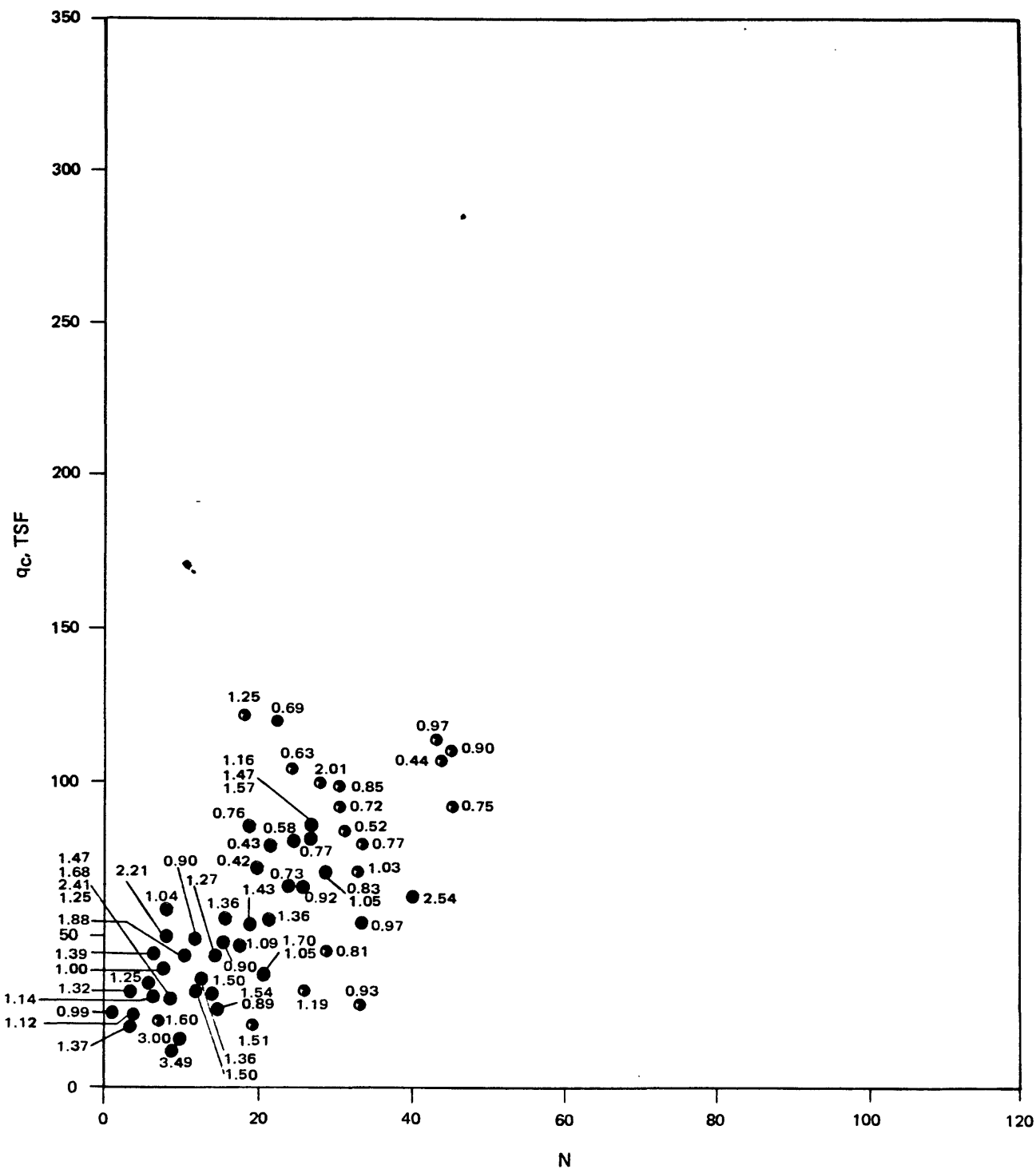
USGS CPT-SPT

SAN DIEGO SITE: NAS NORTH ISLAND
 q_c VS N
 STANDARD HAMMER


9-80

FIGURE B.53

Approved by _____
Checked by _____
Drawn by _____
Compiled by _____



NUMBERS ON POINTS REPRESENT FRICTION RATIO, %



PROJECT NO.: 79-153

USGS CPT-SPT

SALINAS SITE
qc VS N
STANDARD HAMMER

9-80

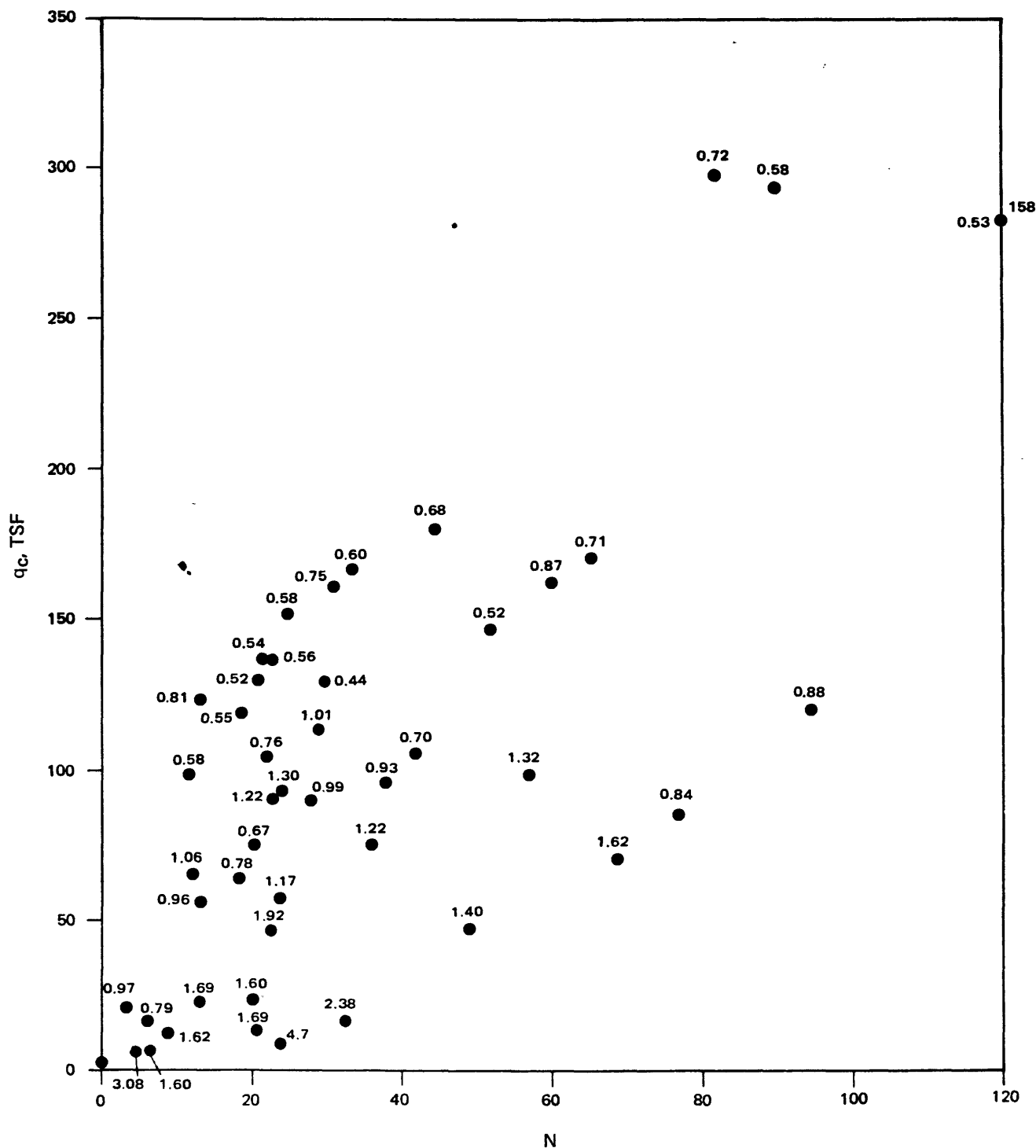
FIGURE B.54

Approved by

Checked by

Drawn by

Compiled by



NUMBERS ON POINTS REPRESENT FRICTION RATIO, %



PROJECT NO.:

79-153

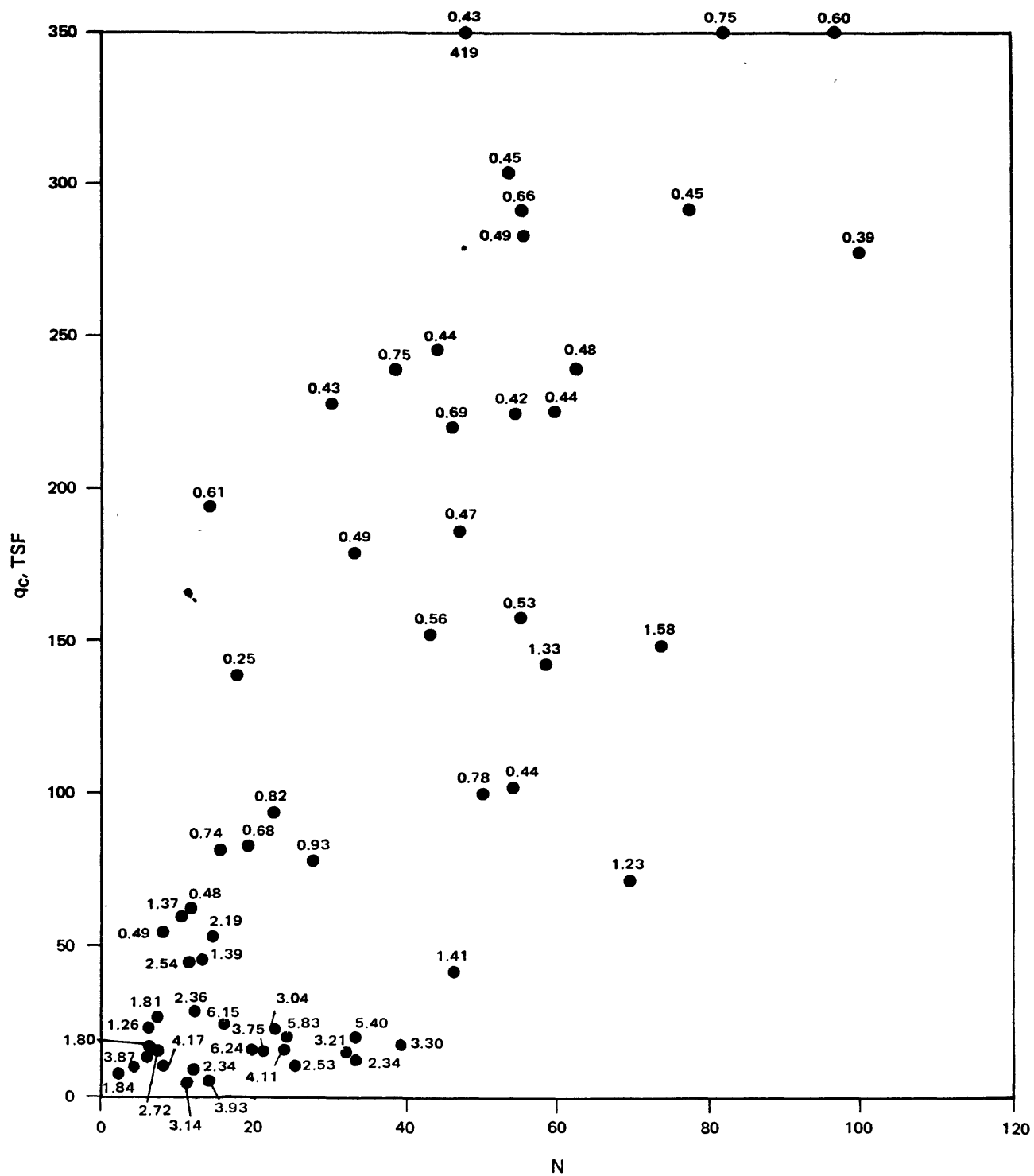
USGS CPT-SPT

MOSS LANDING SITE
 q_c VS N
STANDARD HAMMER


9-80

FIGURE B.55

Approved by _____
Checked by _____
Drawn by _____
Compiled by _____



NUMBERS ON POINTS REPRESENT FRICTION RATIO, %



PROJECT NO.: 79-153

USGS CPT-SPT

SAN JOSE SITE: COYOTE NORTH & SOUTH
 q_c VS N
STANDARD HAMMER

9-80

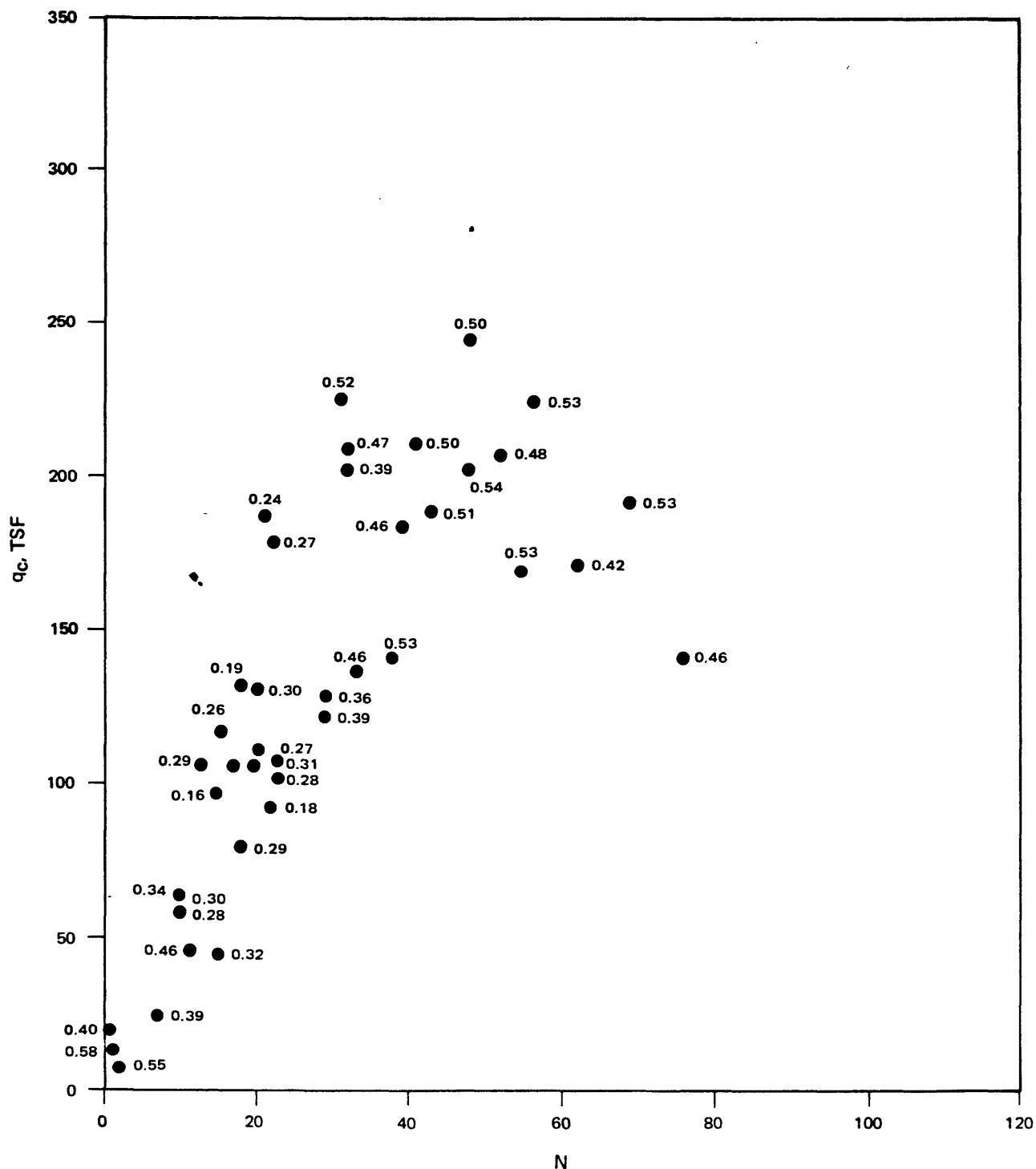
FIGURE B.56

Approved by

Checked by

Drawn by

Compiled by



NUMBERS ON POINTS REPRESENT FRICTION RATIO, %



PROJECT NO.:

79-153

USGS CPT-SPT

SAN DIEGO SITE: NAS NORTH ISLAND
 q_c VS N
TRIP HAMMER

9-80

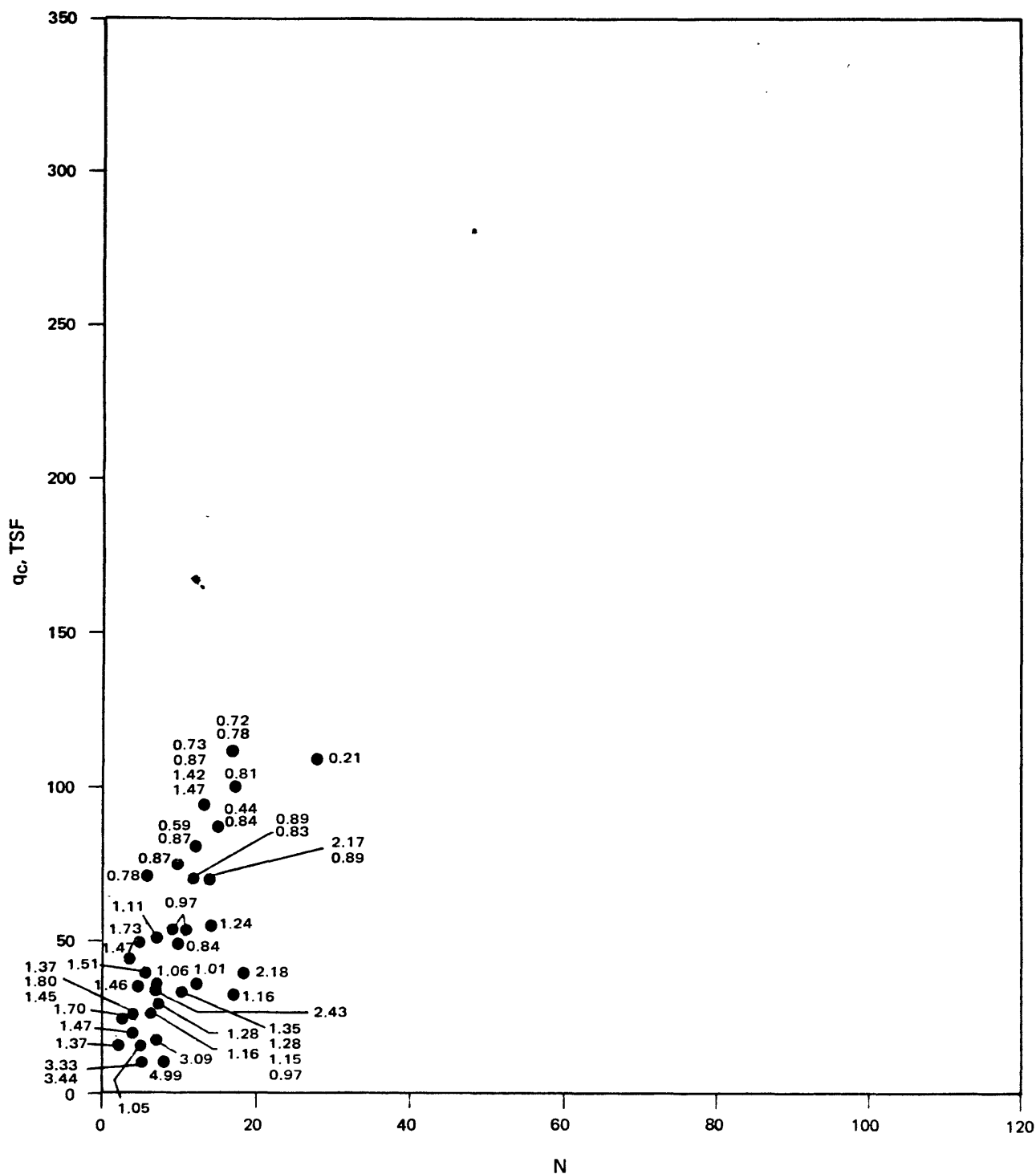
FIGURE B.57

Approved by

Checked by

Drawn by

Compiled by



PROJECT NO.:

79-153

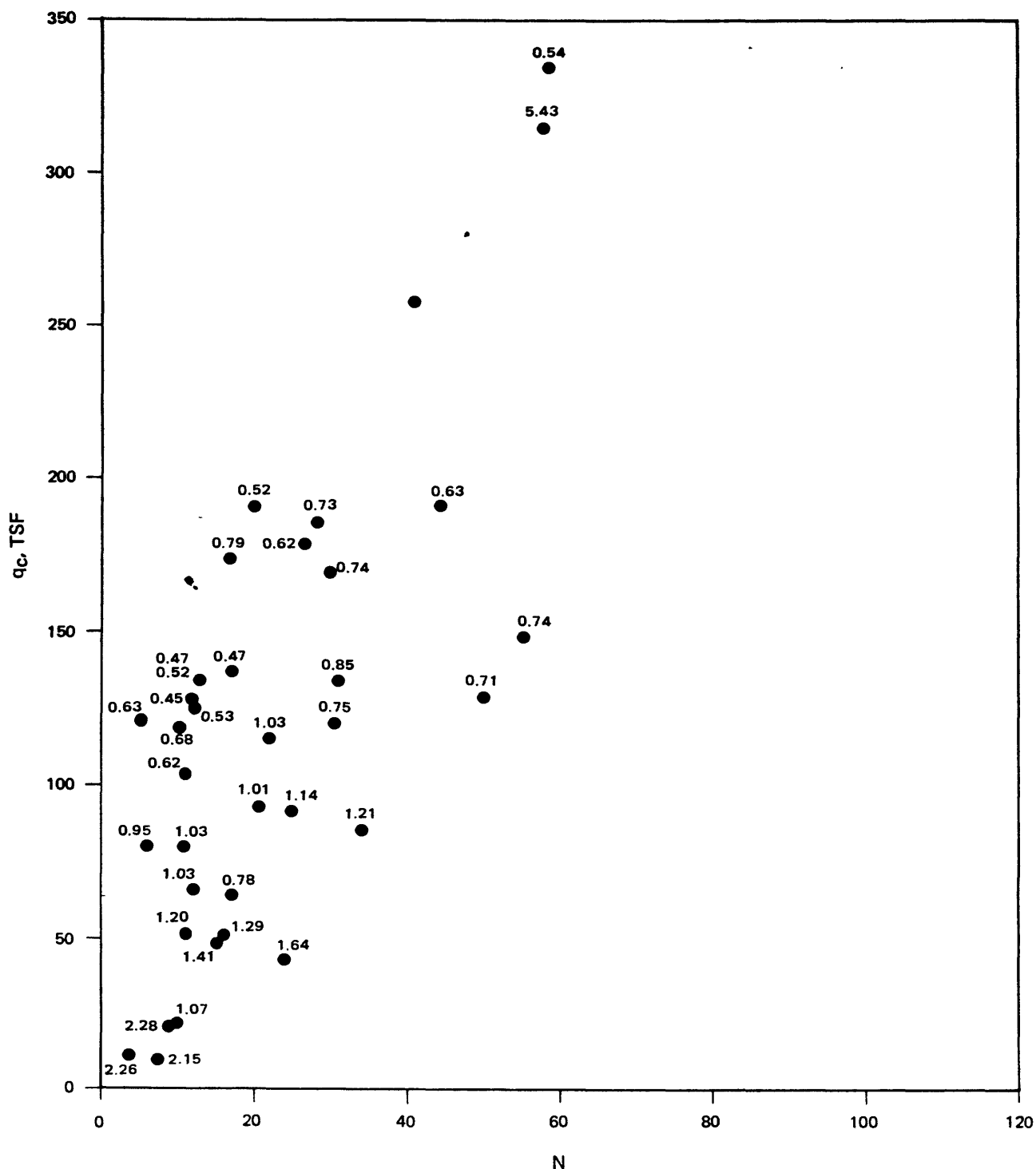
USGS CPT-SPT

SALINAS SITE
qc VS N
TRIP HAMMER

9-80

FIGURE B.58

Approved by _____
Checked by _____
Drawn by _____
Compiled by _____



NUMBERS ON POINTS REPRESENT FRICTION RATIO, %



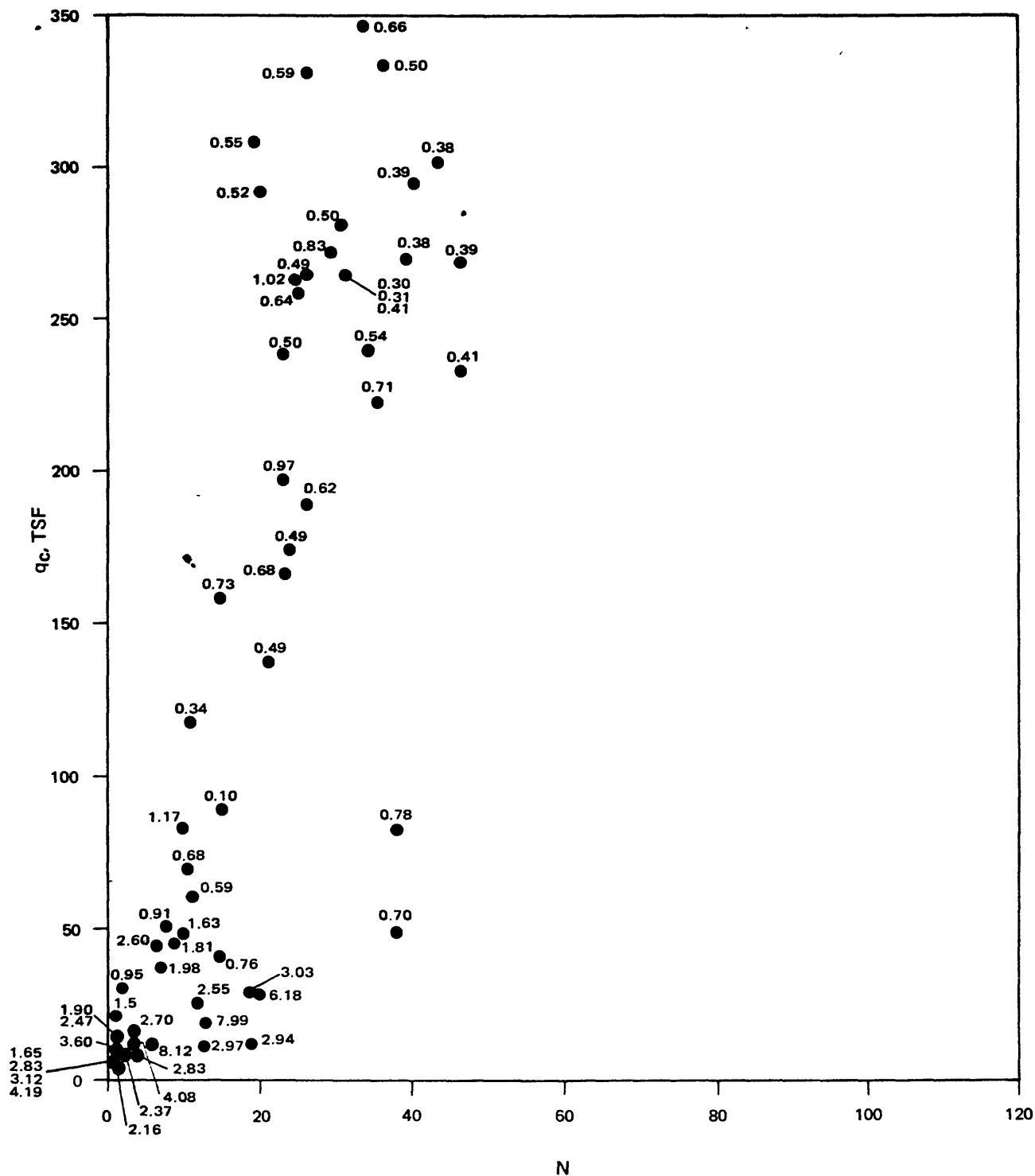
PROJECT NO.:


79-153

USGS CPT-SPT

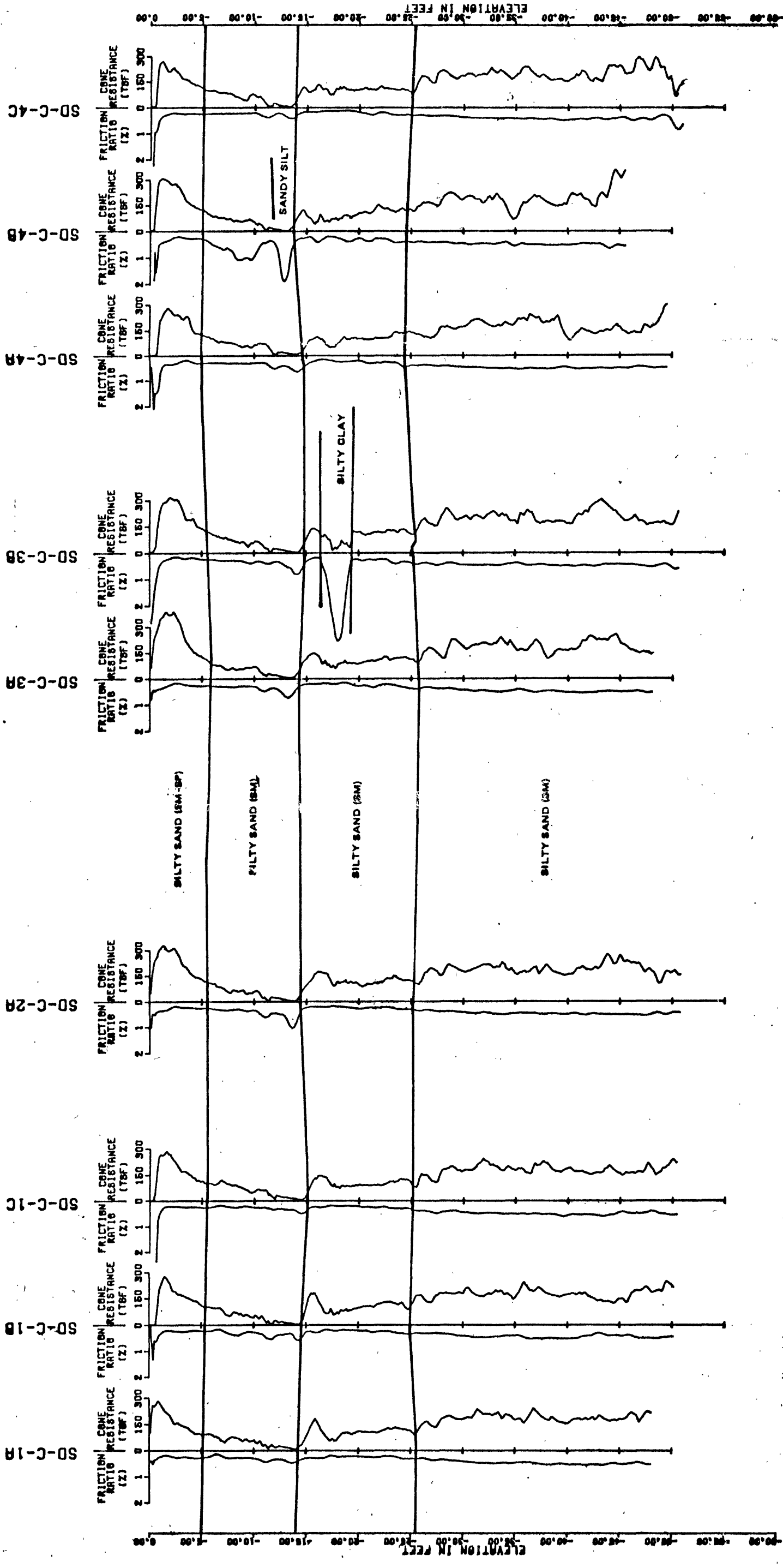
MOSS LANDING SITE
 q_c VS N
TRIP HAMMER

Approved by _____
Checked by _____
Drawn by _____
Compiled by _____



	PROJECT NO.: 79-153
	USGS CPT-SPT
SAN JOSE SITE: COYOTE NORTH & SOUTH	
qc VS N	
TRIP HAMMER	
9-80	FIGURE B.60

81-284



79-153

PROJECT NO.:



USGS CPT-SPT

SAN DIEGO SITE
CPT PROFILE

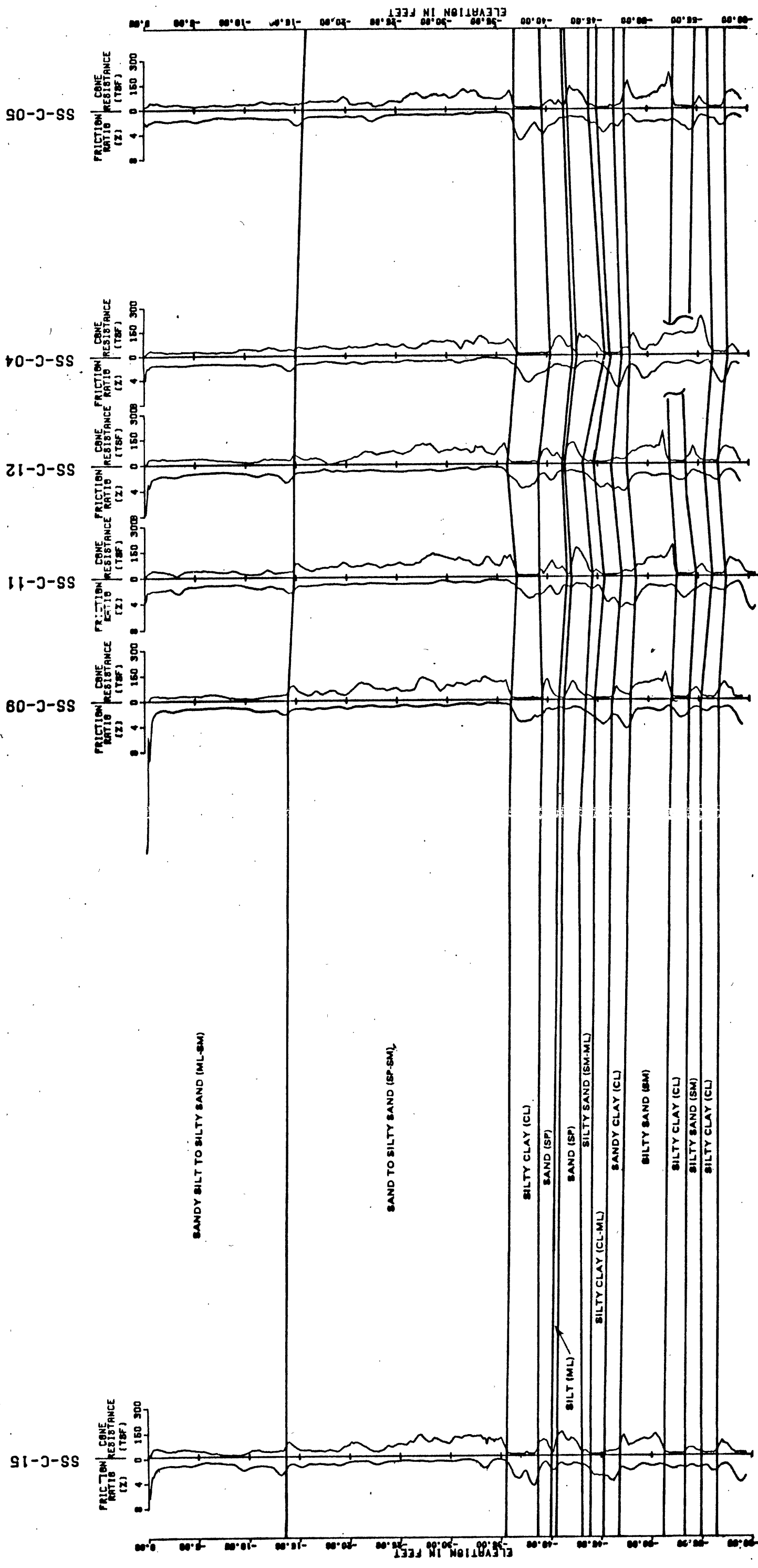
FIGURE 2.5

1-00

BORING LOGS												
DEPTH IN FEET	SD-S-1A SD-T-1B		SD-S-2A SD-T-2B SD-S-3A SD-T-3B		SD-T-4A SD-S-4B		AVERAGE CPT		AVERAGE BLOWCOUNT			
							q _c	FR	NS	NT		
0												
10								141.3	0.25	27.4	17.8	SAND (SP-SM), brown to dark brown, fine sands, nonplastic, micaceous, shell fragments
20								46.3	0.36	15.7	10.0	SILTY SAND (SM), grayish brown to brown, fine sands grading siltier with depth, nonplastic, micaceous
30								26	0.45	15.0	9.0	
40								100	0.30	1.3	1.3	
50								90	0.33	25.0	17.8	
60										31.5	22.5	
70								132	0.36	27.0	20.0	SILTY SAND (SM), yellowish brown, fine sands, nonplastic, occasional trace of low plasticity fines, local heavy mica content, occasional silt and sand pockets.
80								179.7	0.40	49.3	30.8	
90								200	0.46	88.3	38.5	
100								190.3	0.46			
110								190.3	0.49	79.6	46.3	
120								175.7	0.50	67.8	47.0	
130								201.7	0.49	81.3	57.0	SILTY SAND (SM), brown, fine sands, occasional medium sands, nonplastic, micaceous.
140								0	13	104.0	59.5	

EXPLANATION	
	SILTY AND SANDY CLAY (CL)
	CLAY (CH)
	SILT (ML, CL-ML)
	SILTY SAND (SM)
	UNIFORM SAND (SP, SP-SM)
	SANDY GRAVEL (GP, GM)
	CLAYEY SAND (SC)
	S - STANDARD HAMMER
	T - TRIP HAMMER

81-184



PROJECT NO.:

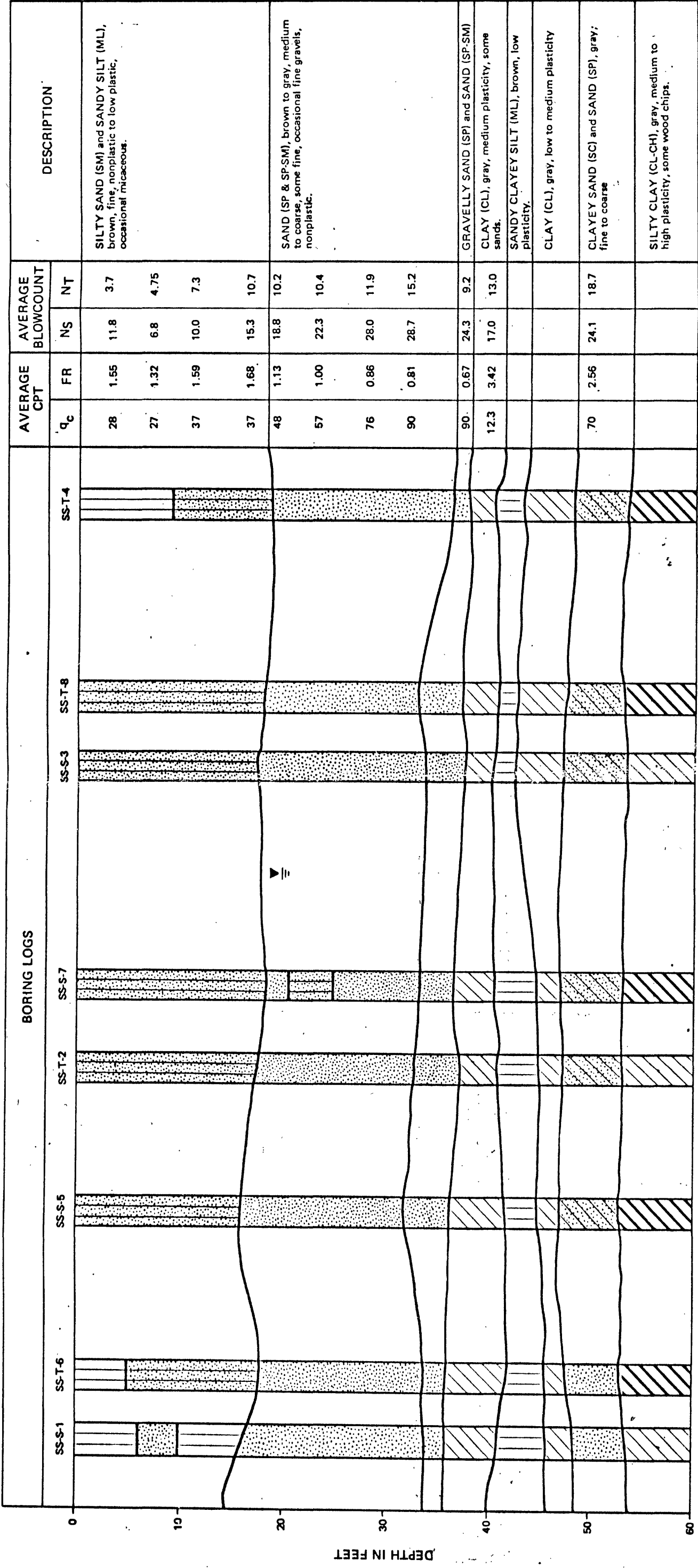
79-183

USGS CPT-SPT

SALINAS SITE
CPT PROFILE

9-00

FIGURE 2.9



EXPLANATION

- SILTY AND SANDY CLAY (CL)
- CLAY (CH)
- SILT (ML, CL-ML)
- SILTY SAND (SM)
- UNIFORM SAND (SP, SP-SM)
- SANDY GRAVEL (GP, GW)
- CLAYEY SAND (SC)
- S - STANDARD HAMMER
- T - TRIP HAMMER



PROJECT NO.:

78-153

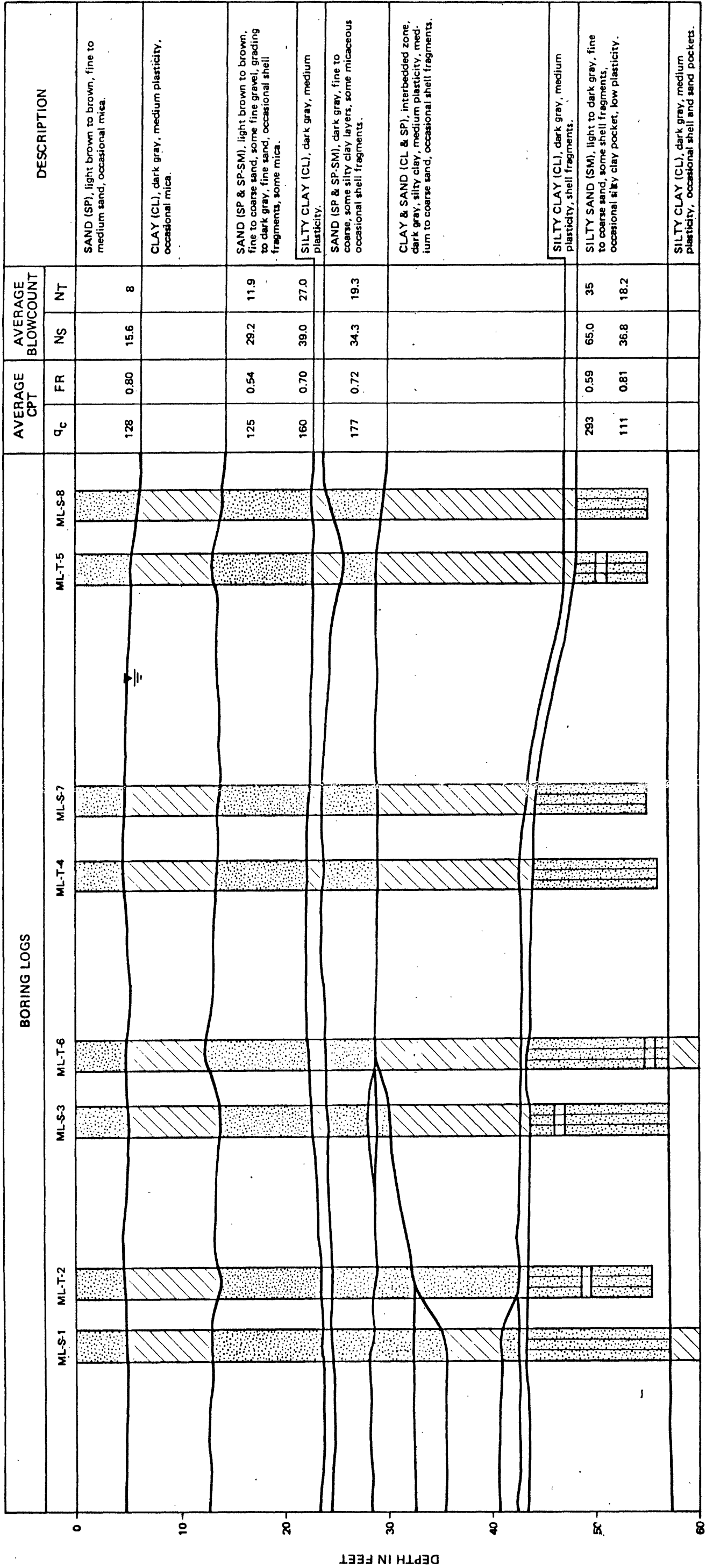
USGS CPT-SPT

SALINAS SITE
COMPOSITE SITE PROFILE










9-90

FIGURE 2.10

81-284



EXPLANATION

-  SILTY AND SANDY CLAY (CL)
-  UNIFORM SAND (SP, SP-SM)
-  CLAY (CH)
-  SANDY GRAVEL (GP, GW)
-  SILT (ML, CL-ML)
-  CLAYEY SAND (SC)
-  SILTY SAND (SM)
-  S - STANDARD HAMMER
-  T - TRIP HAMMER



PROJECT NO.:

79-153

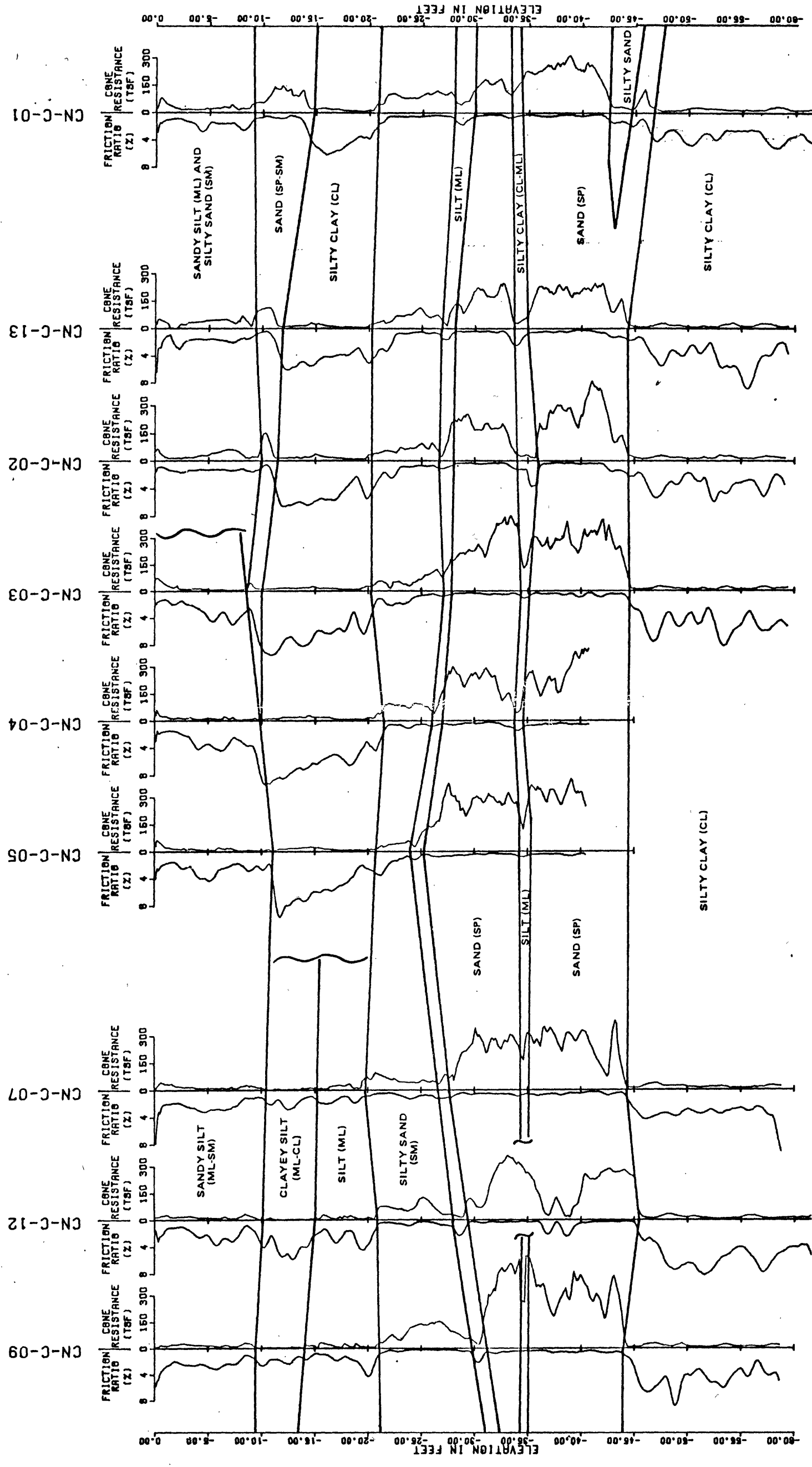
USGS CPT-SPT

**MOSS LANDING SITE
COMPOSITE SITE PROFILE**

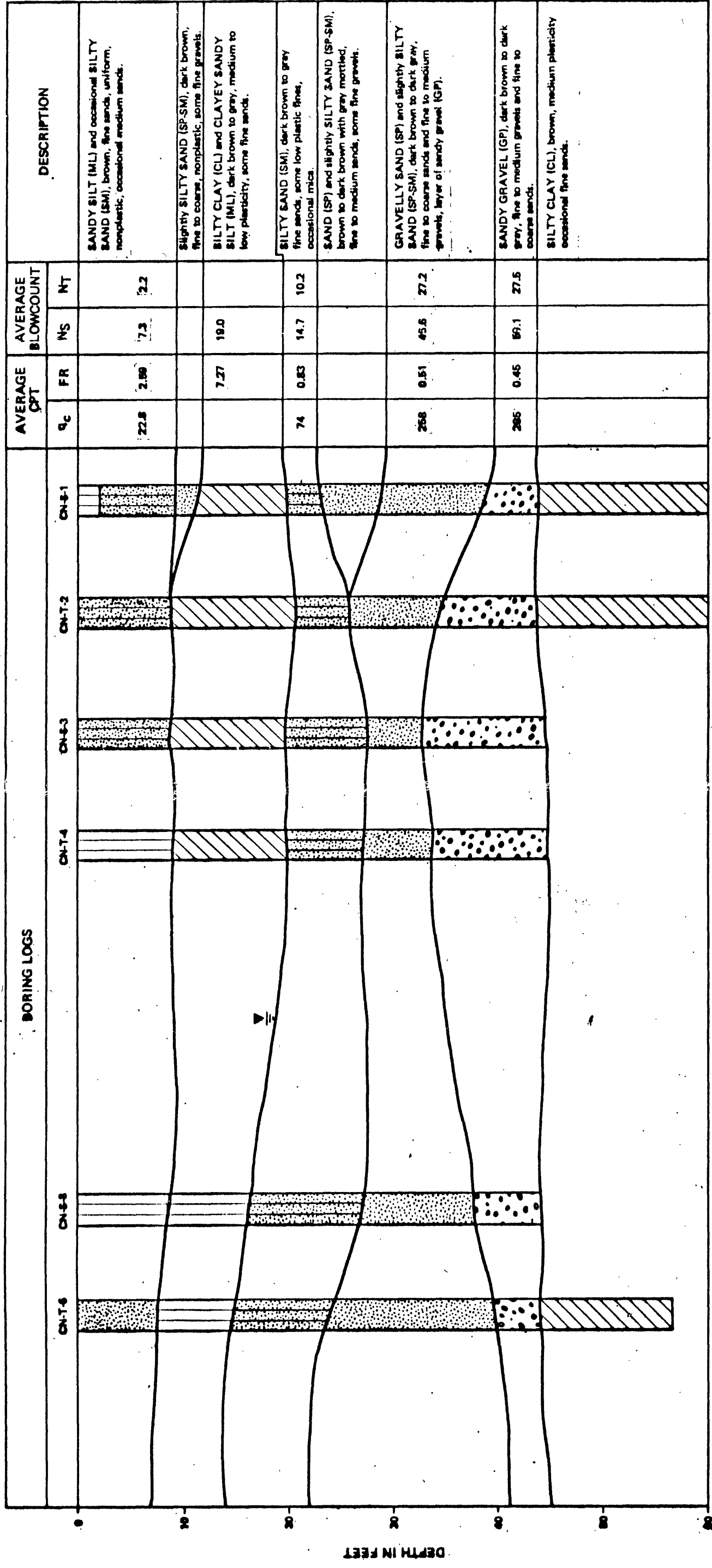
9-80

FIGURE 2.13

81-284



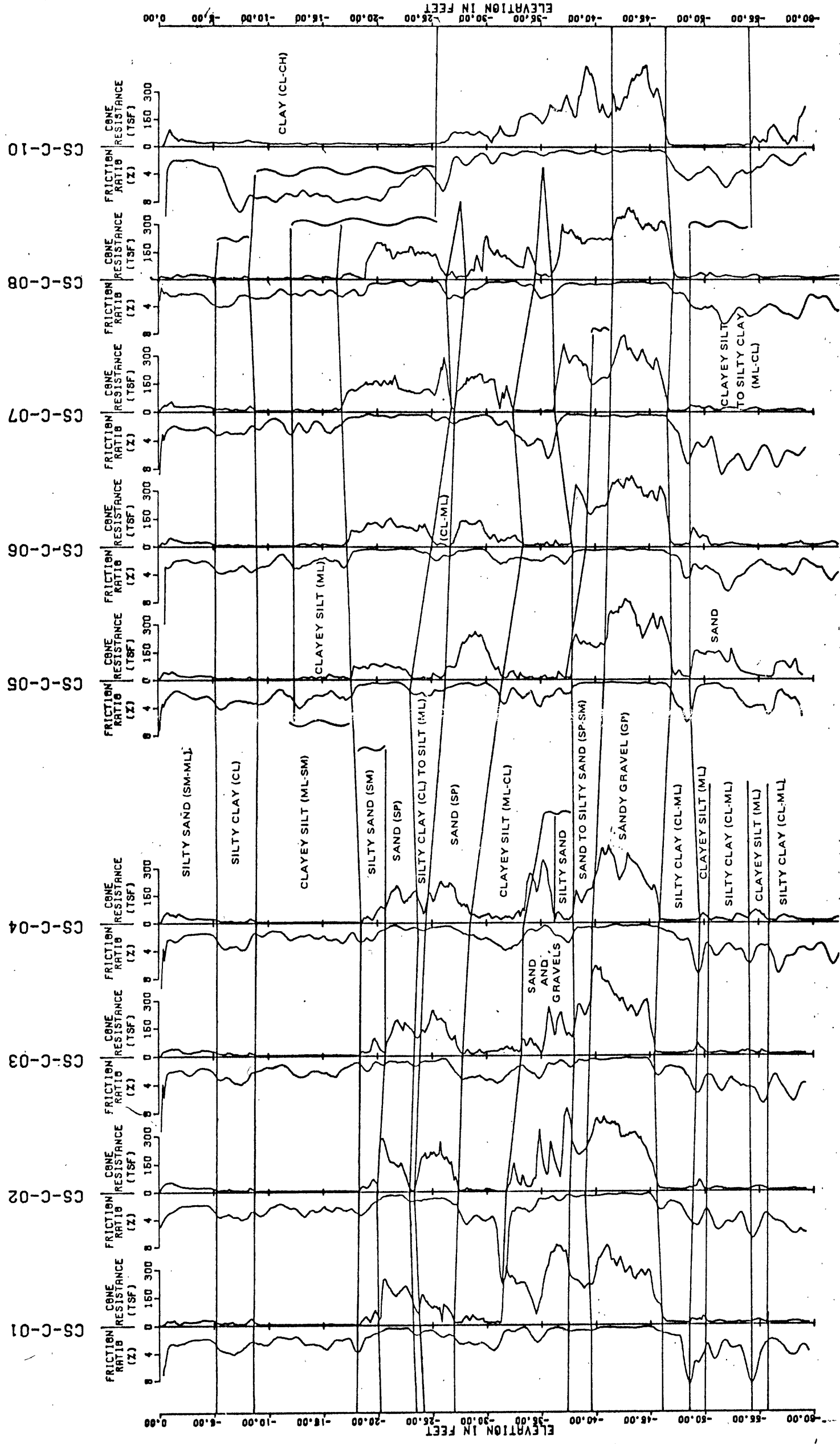
81-284



EXPLANATION

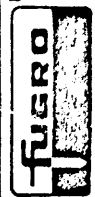
- | | | | |
|--|---------------------------|--|--------------------------|
| | SILTY AND SANDY CLAY (CL) | | UNIFORM SAND (SP, SP-SM) |
| | CLAY (CH) | | SANDY GRAVEL (GP, GW) |
| | SILT (ML, CL-ML) | | CLAYEY SAND (SC) |
| | SILTY SAND (SM) | | |
- S = STANDARD HAMMER
T = TRIP HAMMER

81284



79-153

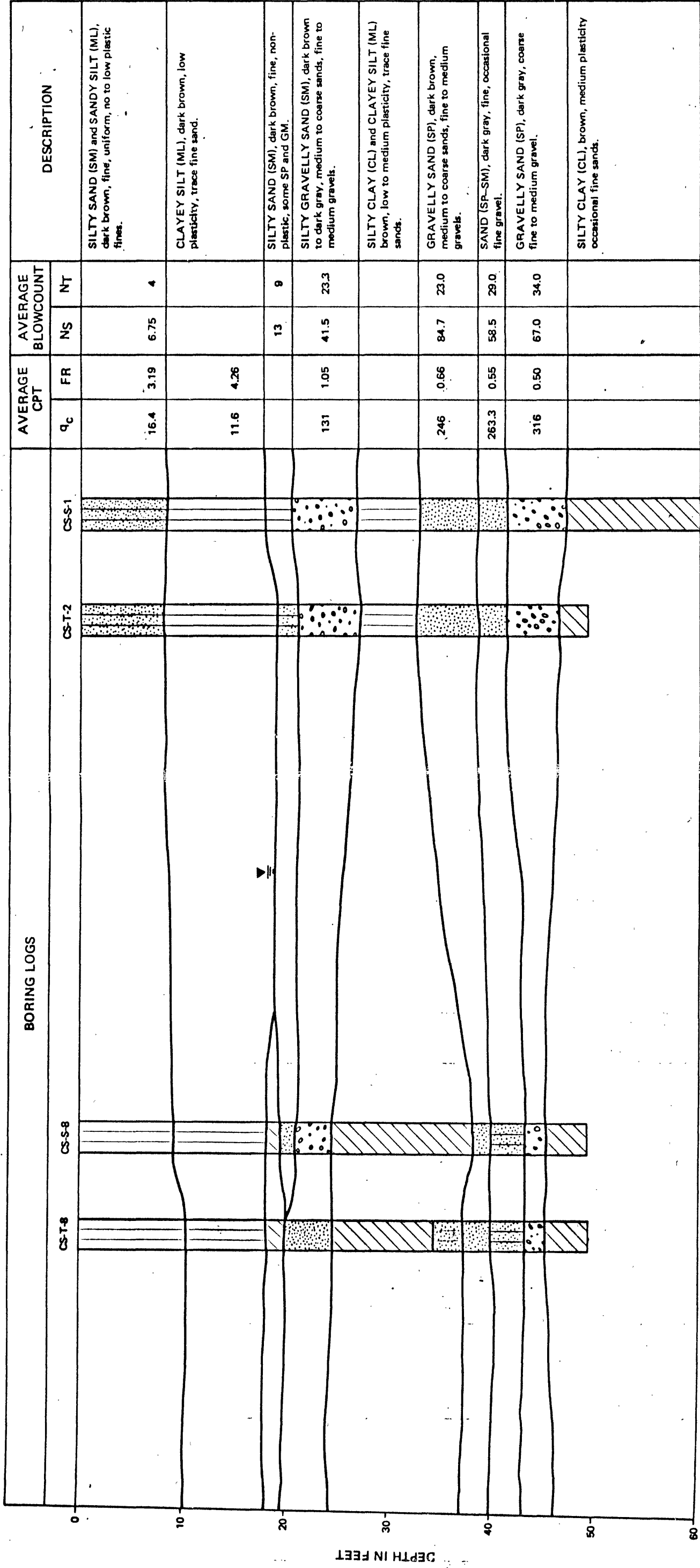
PROJECT NO.:



USGS CPT-SPT

SAN JOSE SITE: COYOTE SOUTH
CPT PROFILE

SL-284



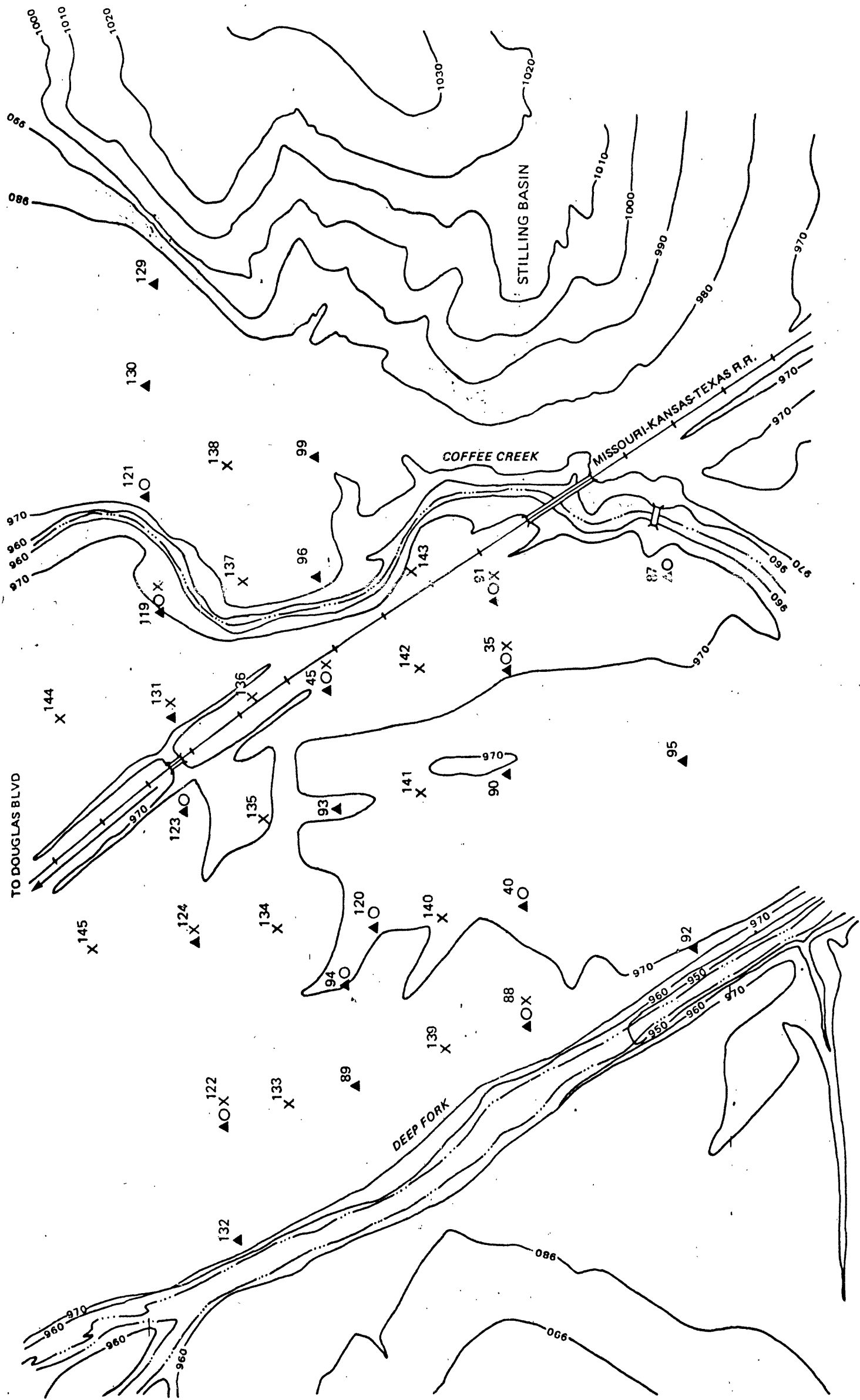
EXPLANATION

- SILTY AND SANDY CLAY (CL)
- CLAY (CH)
- SILT (ML, CL-ML)
- SILTY SAND (SM)
- UNIFORM SAND (SP, SP-SM)
- SANDY GRAVEL (GP, GW)
- CLAYEY SAND (SC)
- S - STANDARD HAMMER
- Y - TRIP HAMMER

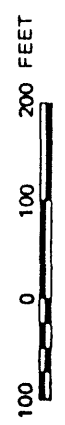
fugro PROJECT NO.: 79-153
USGS CPT-SPT

SAN JOSE SITE: COYOTE SOUTH
COMPOSITE SITE PROFILE

81-284



- EXPLANATION
- X FUGRO CONE SOUNDINGS
 - ▲ SPT BORINGS
 - O DENNISON BORINGS



PROJECT NO.:

79-153

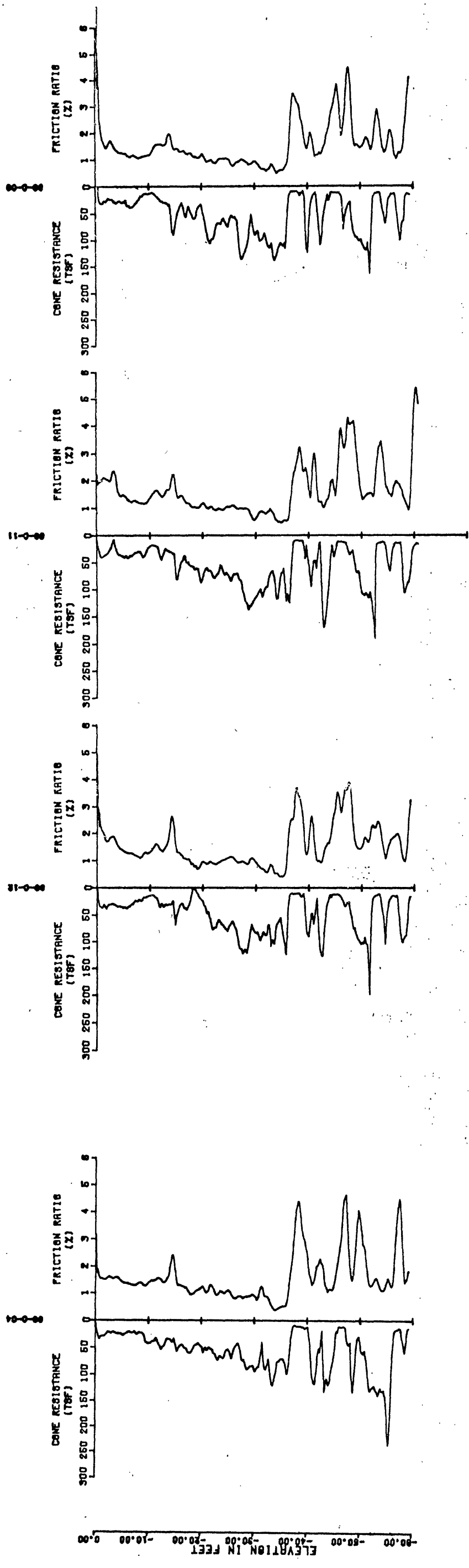
USGS CPT-SPT

OKLAHOMA SITE
CPT LAYOUT

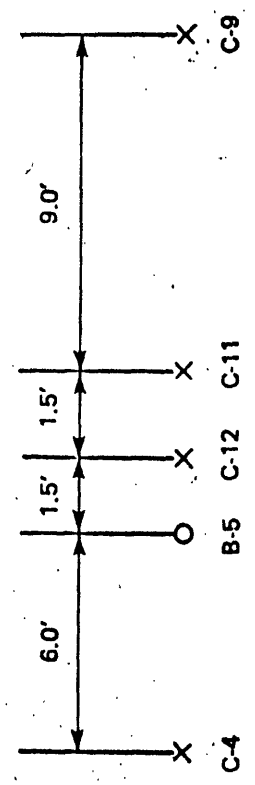
REFERENCE FIGURE 1 OF "CONE PENETROMETER INVESTIGATIONS OF THE ARCADIA DAM SITE, FUGRO, INC., AUGUST 1980



81-284



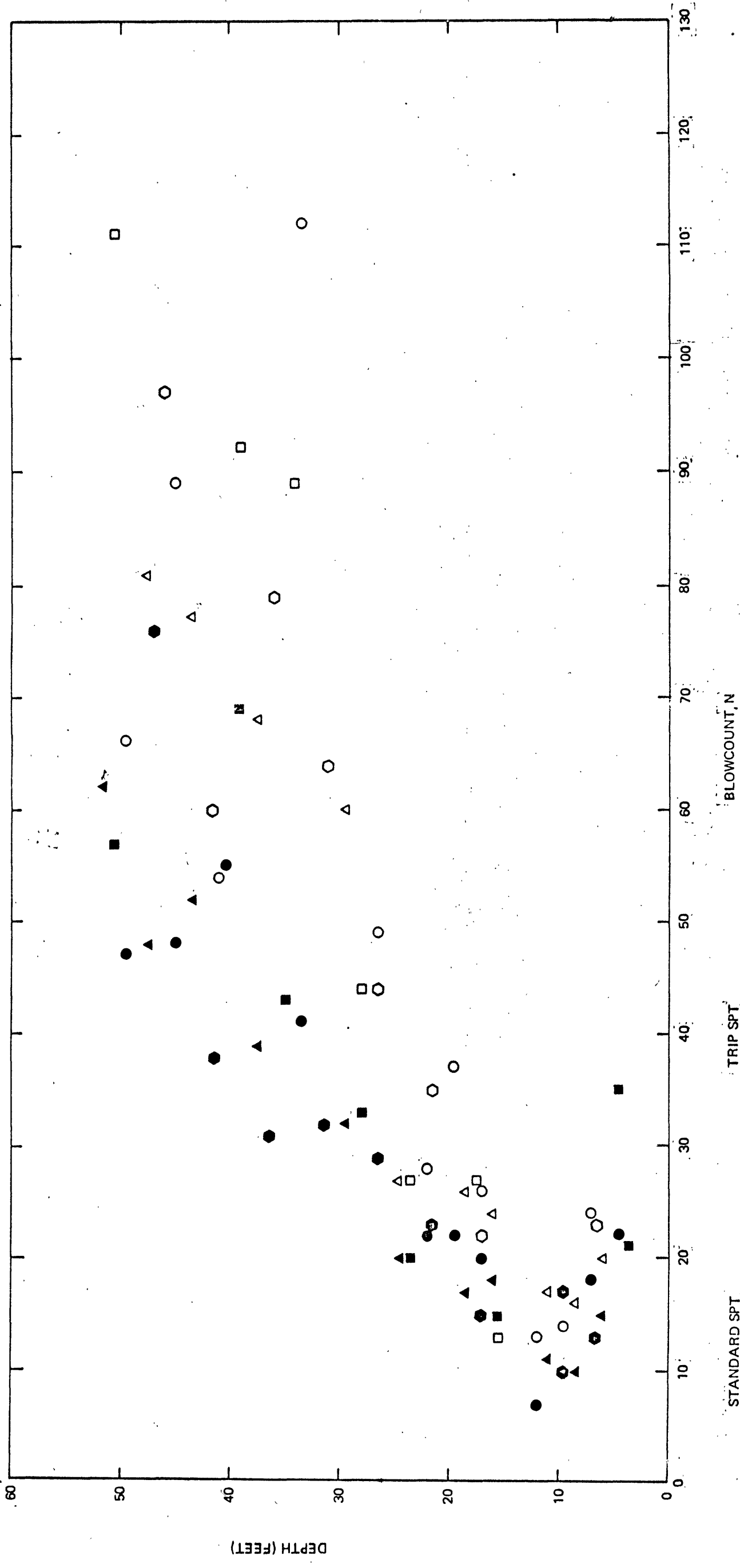
SITE LAYOUT




PROJECT NO.: 79-153
USGS CPT-SPT

EFFECT OF BOREHOLE ON
SUBSEQUENT ADJACENT CPT SOUNDINGS
SALINAS SITE

81-284





PROJECT NO.: 79-153

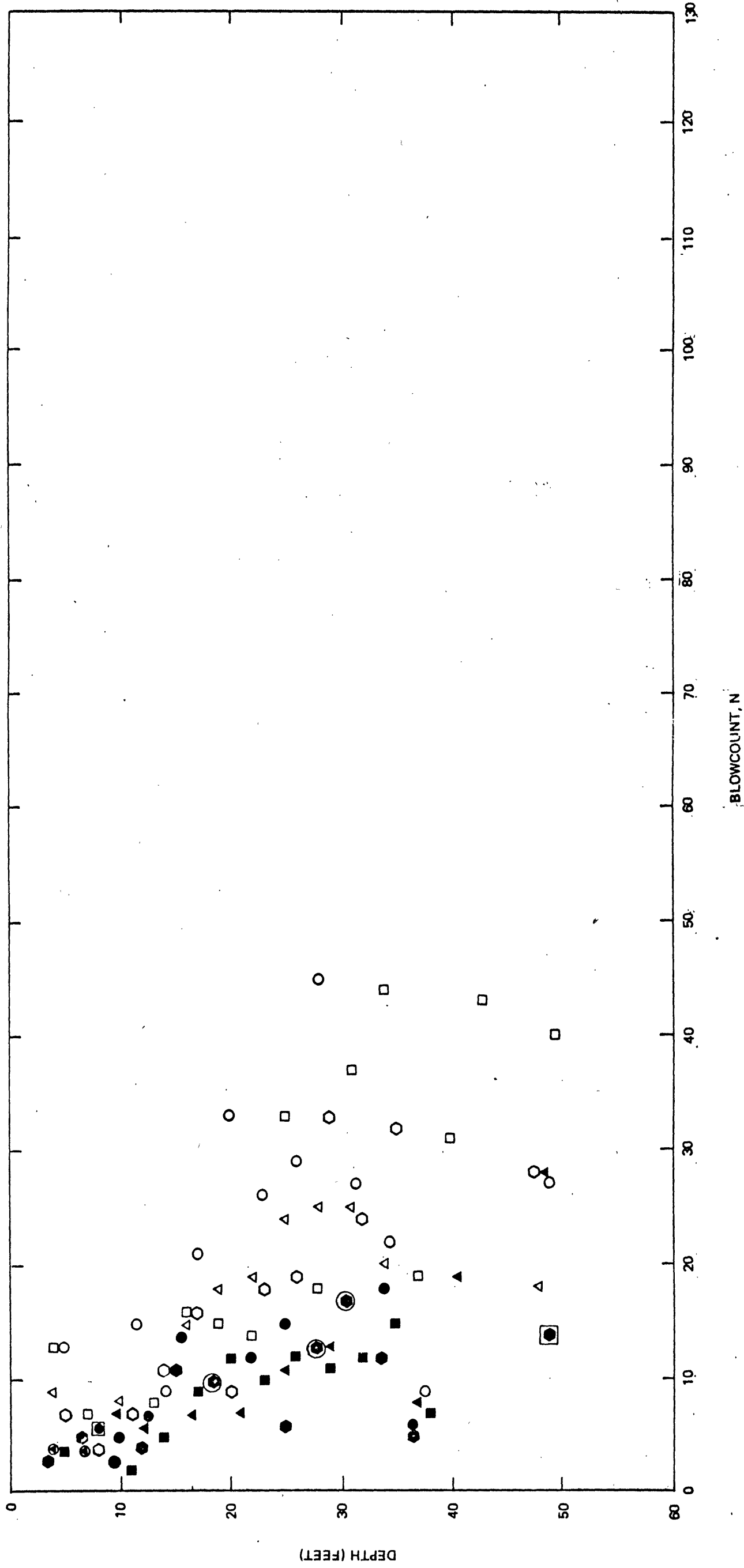
USGS CPT-SPT

COMPOSITE BLOWCOUNT VS DEPTH
SAN DIEGO SITE: NORTH ISLAND

9-80

FIGURE 3.31

81.284



PROJECT NO. 79-153

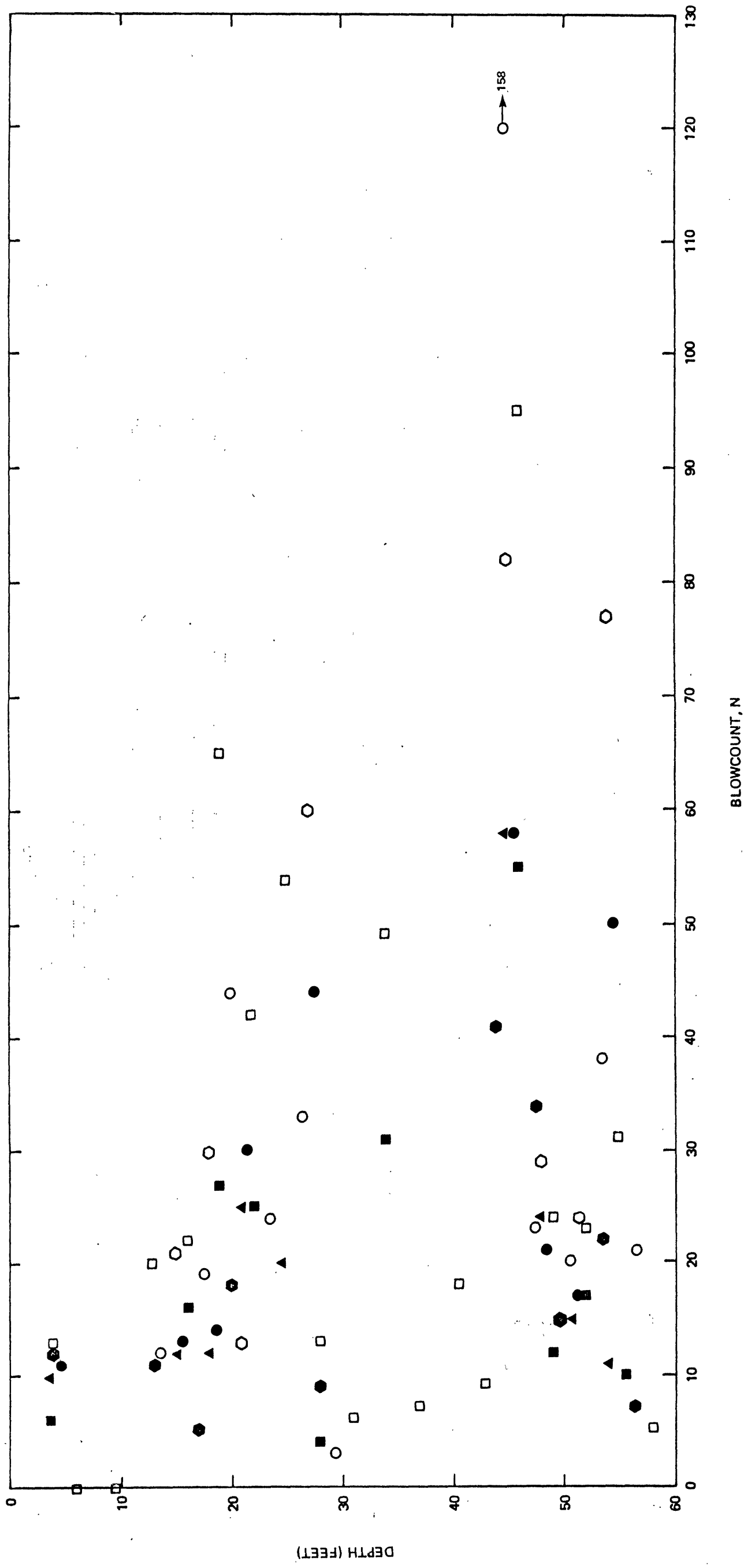
USGS CPT-SPT

COMPOSITE BLOWCOUNT VS DEPTH
SALINAS SITE

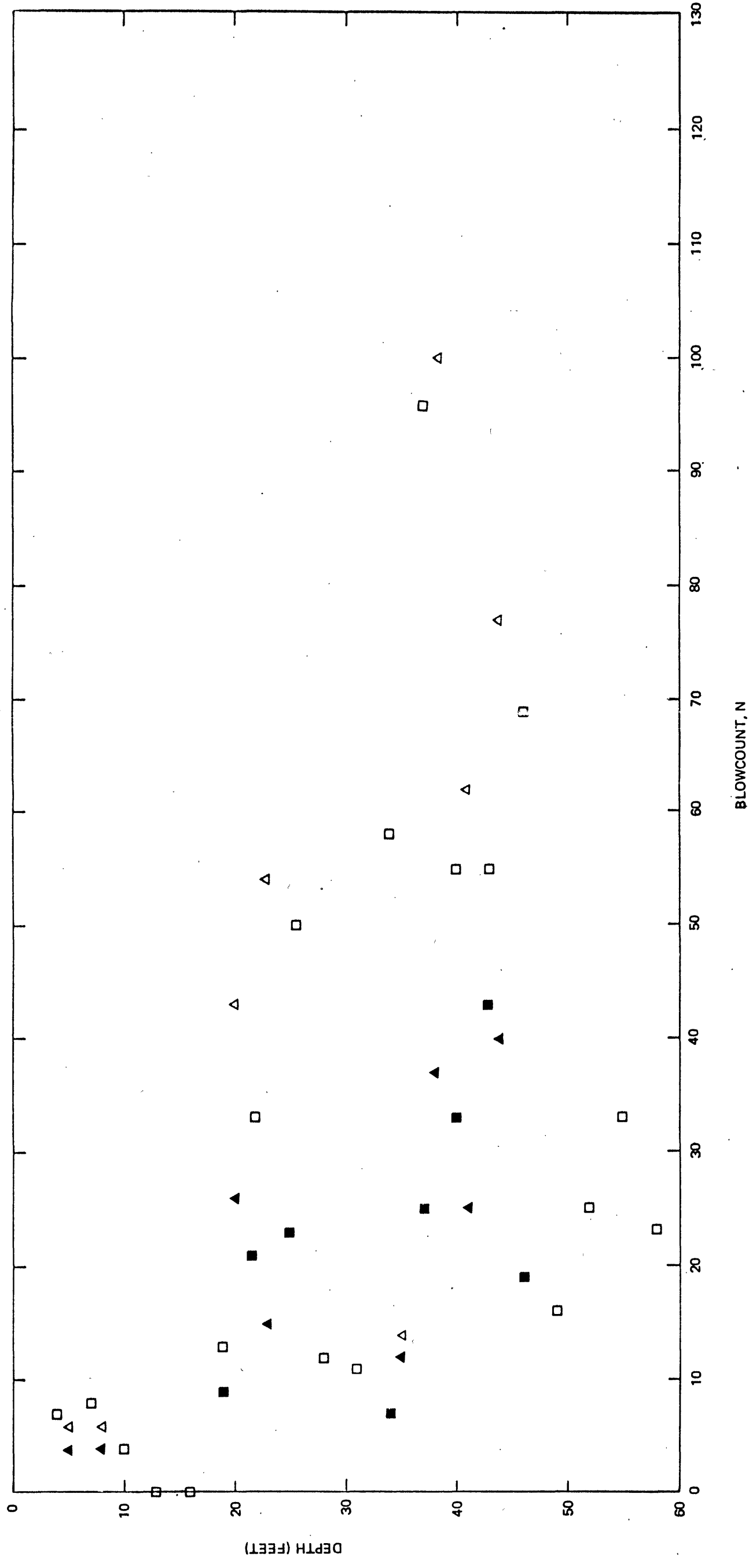
9-80


FIGURE 3.32

81.284




81-284





PROJECT NO.: 79-153



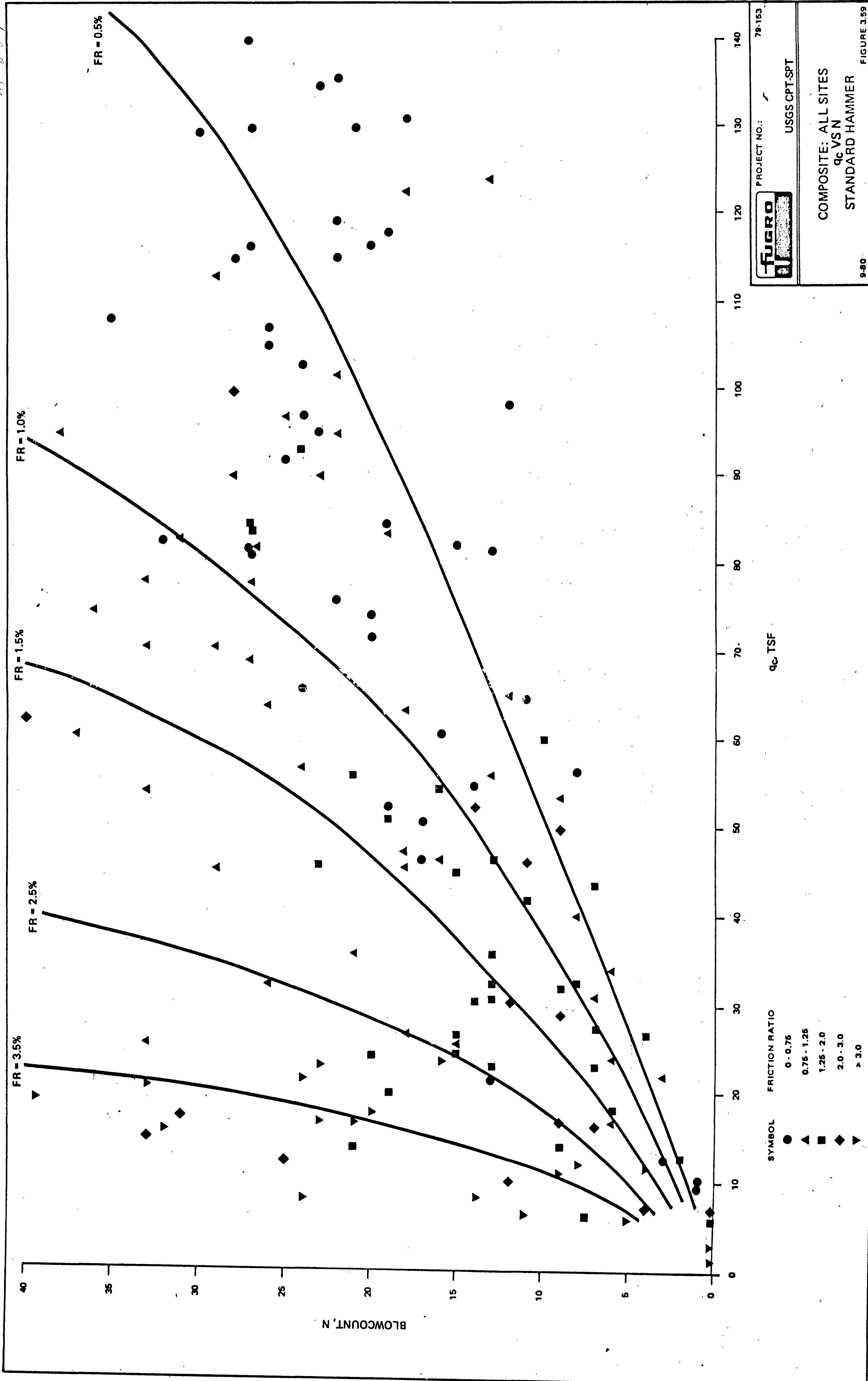
USGS CPT-SPT


COMPOSITE BLOWCOUNT VS DEPTH
SAN JOSE SITE: COYOTE NORTH

9-80

FIGURE 3.34

81-284





PROJECT NO.: 79-153

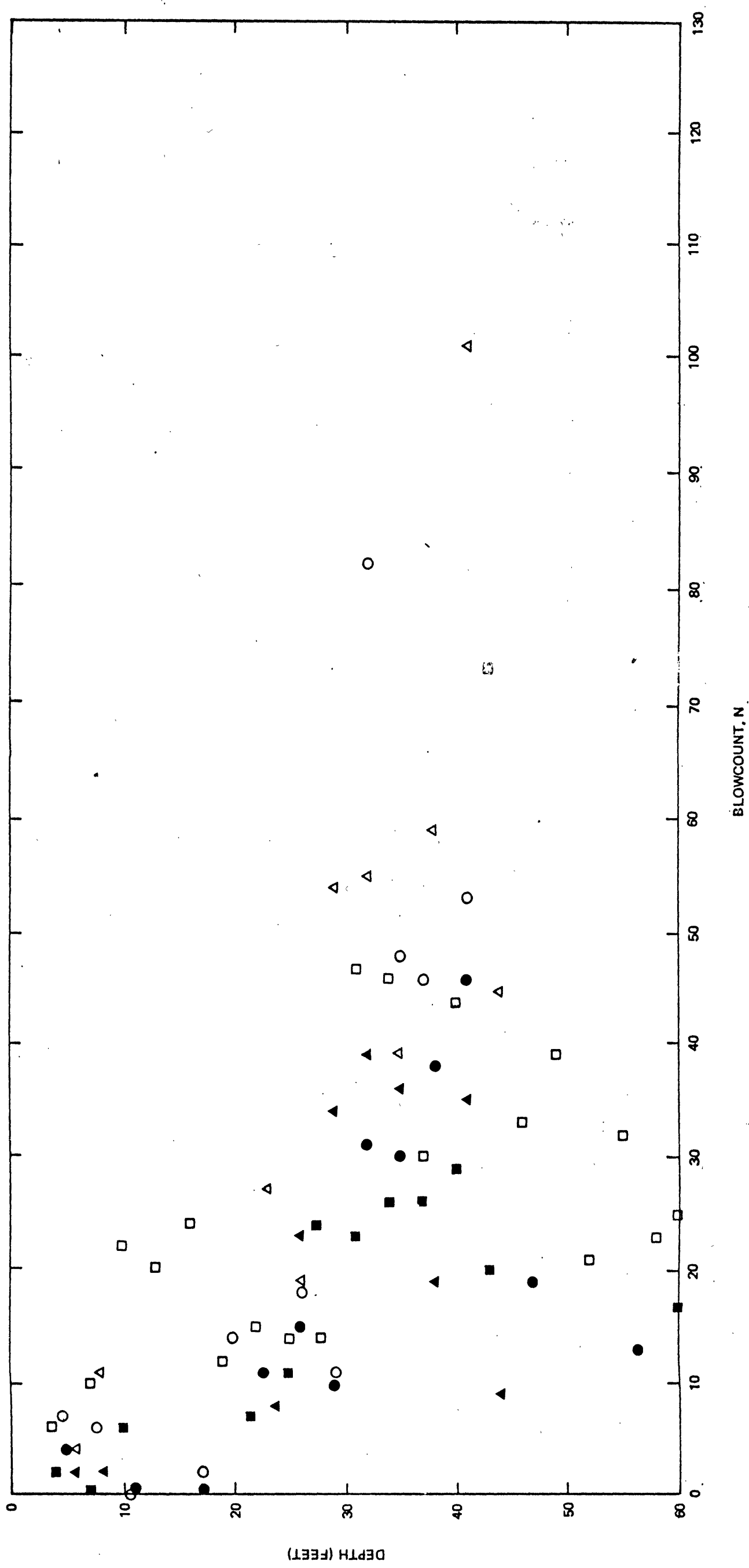
USGS CPT-SPT

COMPOSITE: ALL SITES
qc VSN
STANDARD HAMMER


9-80

FIGURE 359

81-284



- | STANDARD SPT | | TRIP SPT | |
|--------------|----------|----------|----------|
| □ | BORING 1 | ■ | BORING 2 |
| △ | BORING 3 | ▲ | BORING 4 |
| ○ | BORING 8 | ● | BORING 6 |



PROJECT NO.: 79-153

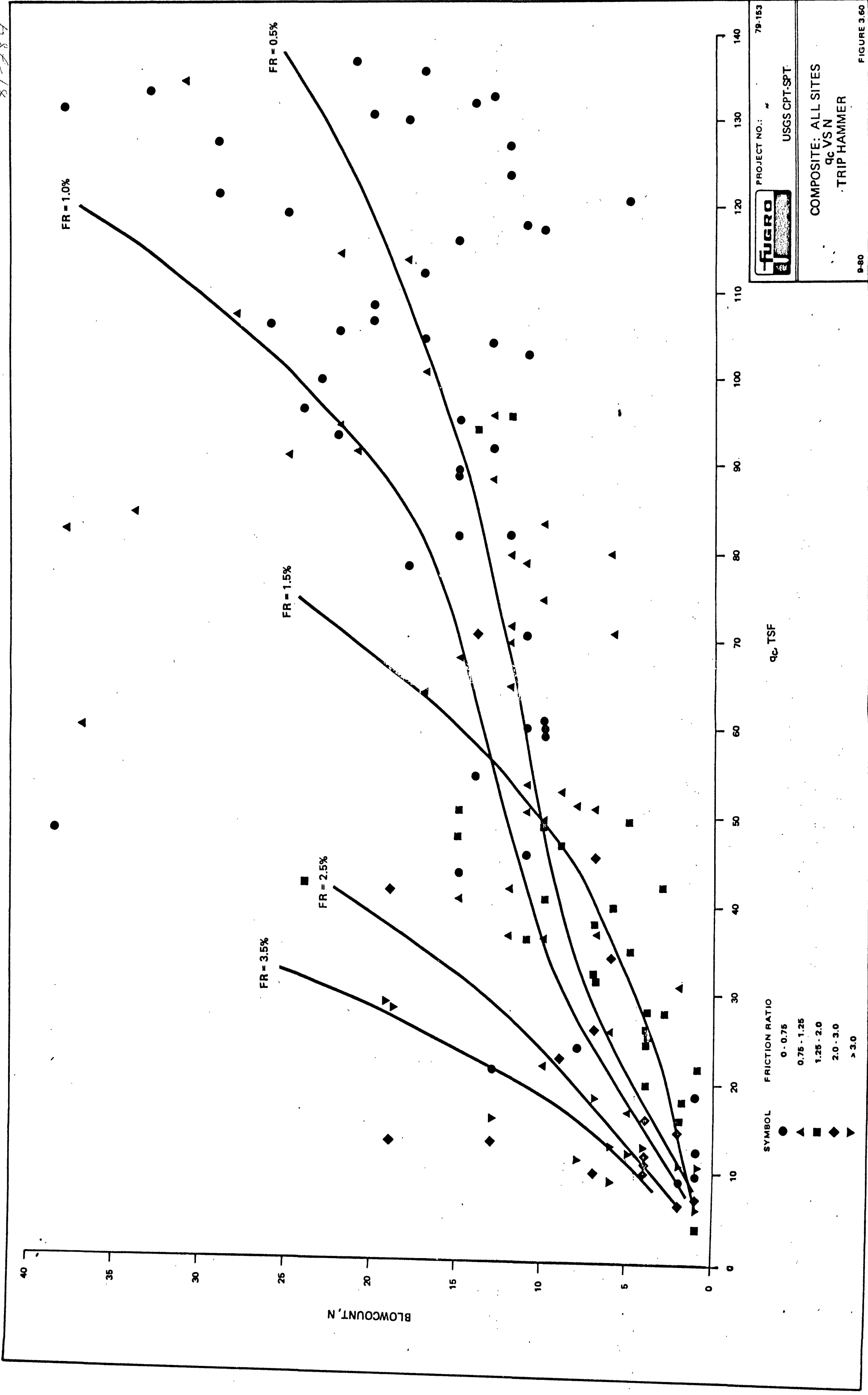
USGS CPT-SPT

COMPOSITE BLOWCOUNT VS DEPTH
SAN JOSE SITE: COYOTE SOUTH

9-80

FIGURE 3.35

81-184



PROJECT NO.: 79-153

USGS CPT-SPT

COMPOSITE: ALL SITES
qc VS N
TRIP HAMMER

9-80

FIGURE 3.60

81-284

